

2010-01-01

# Investigations of Grade Control, MacArthur Mine, Yerington, Nevada: an Oxidized Porphyry Copper System

Joseph Daniel Louis Lori

University of Texas at El Paso, josephlori@hotmail.com

Follow this and additional works at: [https://digitalcommons.utep.edu/open\\_etd](https://digitalcommons.utep.edu/open_etd)



Part of the [Geology Commons](#)

---

## Recommended Citation

Lori, Joseph Daniel Louis, "Investigations of Grade Control, MacArthur Mine, Yerington, Nevada: an Oxidized Porphyry Copper System" (2010). *Open Access Theses & Dissertations*. 2528.  
[https://digitalcommons.utep.edu/open\\_etd/2528](https://digitalcommons.utep.edu/open_etd/2528)

This is brought to you for free and open access by DigitalCommons@UTEP. It has been accepted for inclusion in Open Access Theses & Dissertations by an authorized administrator of DigitalCommons@UTEP. For more information, please contact [lweber@utep.edu](mailto:lweber@utep.edu).

**INVESTIGATIONS OF GRADE CONTROL, MACARTHUR MINE,  
YERINGTON, NEVADA:  
AN OXIDIZED PORPHYRY COPPER SYSTEM**

**JOSEPH DANIEL LOUIS LORI**

**Department of Geological Sciences**

**APPROVED:**

---

**Philip C. Goodell, Ph.D., Chair**

---

**José M. Hurtado, Jr., Ph.D.**

---

**David M. Borrok, Ph.D.**

---

**John C. Walton, Ph.D.**

---

**Patricia D. Witherspoon, Ph.D.  
Dean of the Graduate School**

**DEDICATION**

To my daughter Alyvia Jane...

My biggest motivation,

I love you so much,

Dad

**INVESTIGATIONS OF GRADE CONTROL, MACARTHUR MINE,  
YERINGTON, NEVADA:  
AN OXIDIZED PORPHYRY COPPER SYSTEM**

**by**

**JOSEPH DANIEL LOUIS LORI**

**THESIS**

**Presented to the Faculty of the Graduate School of  
The University of Texas at El Paso  
in Partial Fulfillment  
of the Requirements  
for the Degree of  
MASTER OF SCIENCE**

**Department of Geological Sciences**

**THE UNIVERSITY OF TEXAS AT EL PASO**

**December, 2010**

## **ACKNOWLEDGEMENTS**

I would first like to thank Eugene Spiering, V.P. of Quaterra Resources Inc. for the ongoing support in the completion of my thesis and continued employment. A very special thanks to Quaterra staff at the Yerington district office – George Eliopulos, Dave Heatwole, Todd Bonsall, and Taurus Massey for many geologic insights, figures, communications, and time. I would also like to thank Dr. Philip Goodell, my advisor, for letting me set my own path with my research. Together we learned about my project, interpreting data and looking forward to the next step. Of course I have to thank my parents Dan and Nancy Lori. Mom and Dad are patience, support, kind, loving, guidance, willing to go out of their way for their children, and funding; thank you and I love you. Lisa Arnold, thank you for putting up with me while working on this project, one day we will laugh about this, I promise. Last but never least, all who I have forgot to thank.

## ABSTRACT

Supergene enriched, low-grade oxidized porphyry copper deposits are of great economic value. Oxidized porphyry sections are economic targets because even low-grade prospects have the potential to produce low-cost copper in an environmentally friendly fashion due to easy leachability and high recovery rates of the oxide mineralization. The MacArthur Mine, in the historic Yerington mining district of Nevada, is the focus of this study. The MacArthur is a tilted oxidized porphyry deposit, partially mined by open pit methods, hosted in the Jurassic Bear Quartz Monzonite of the Yerington batholith. The objective of the study is to define controls of copper oxide mineralization within the open-pit mine. The objective is investigated through a multi-data study including rock descriptions, geochemistry, spectral radiometry, and fracture density. Multivariate factor score analysis of geochemical data defined potassic and sodic-calcic alteration as well as multiple elements (Co, Ni, Zn, As, Mo, Ag, Cd, U) absorbed in the mineral neotocite (Mn, Cu, Fe)SiO<sub>2</sub> x H<sub>2</sub>O. Finally, high geochemical associations were found in two groups 1 - Cu, Fe, Co, Mo, Ni, U, and 2 - Al, K, Rb, Na, Mn. The high correlations found in the groups represent the hydrothermal event at the MacArthur. Chlorite and epidote identified in spectra using Spectral Analyst tool in ENVI<sup>®</sup> demonstrate a propylitic alteration signature. Spectral Analysts identified several secondary iron and copper minerals produced in oxide zone geology. Fracture density studies defined 98.3% of all fractures in the MacArthur pit are associated with oxide zone produced copper and iron at a close to even distribution amongst fracture families.

## TABLE OF CONTENTS

	PAGE
ACKNOWLEDGMENTS .....	iv
ABSTRACT .....	v
TABLE OF CONTENTS .....	vi
LIST OF TABLES .....	x
LIST OF FIGURES .....	xiii
1. INTRODUCTION .....	1
2. GEOLOGY .....	4
2.1. Regional Geology .....	4
2.2. MacArthur Geology .....	9
2.2.1. MacArthur Rocks .....	9
2.2.2. MacArthur Faults .....	13
2.2.3. MacArthur Alteration .....	13
2.2.4. MacArthur Mineralization .....	17
3. HISTORIC EXPLORATION .....	19
3.1. District Exploration .....	19
3.2. MacArthur Exploration .....	20
4. RECENT EXPLORATION .....	22
4.1. District Exploration .....	22
4.2. MacArthur/Quaterra Exploration .....	23
5. OBJECTIVES .....	30
6. DATA .....	31
7. METHODS .....	35

	PAGE
8. GEOCHEMISTRY AND STATISTICAL ANALYSES .....	37
8.1. Introduction .....	37
8.2. Data .....	37
8.2.1. Field Methods .....	38
8.3. Processing .....	39
8.4. Analysis .....	41
8.4.1. Descriptive Statistics .....	41
8.4.2. Univariate Analysis .....	42
8.4.3. Bivariate Analysis .....	47
8.4.4. Multivariate Analysis .....	50
8.4.5. Spatial Analysis .....	51
8.5. Results .....	53
8.5.1. Univariate .....	53
8.5.2. Bivariate .....	55
8.5.3. Multivariate .....	57
8.5.4. Spatial .....	63
8.6. Initial Interpretations .....	67
9. SPECTRAL RADIOMETRY .....	71
9.1. Introduction .....	71
9.2. Data .....	72
9.3. Methods .....	74
9.3.1. Lab Methods .....	74
9.3.2. Field Methods .....	74
9.4. Processing .....	75
9.5. Analysis .....	75
9.5.1. Spectral Analyst of 52 rock sample spectrums vs. USGS and JPL spectral libraries .....	76
9.5.2. Spectral Analyst of 35 homogeneity spectrums .....	76
9.5.3. Analysis of 52 rock samples; relationship to copper grade .....	77
9.6. Results .....	77
9.6.1. Spectral Analyst of 52 rock sample spectrums vs. USGS and JPL spectral libraries .....	77
9.6.2. Spectral Analyst of 35 homogeneity spectrums .....	82
9.6.3. Analysis of 52 rock samples; relationship to copper grade .....	90
9.7. Initial Interpretations .....	95

	PAGE
10. FRACTURE DENSITY .....	97
10.1. Introduction .....	97
10.2. Data .....	97
10.3. Field Methods.....	98
10.4. Processing.....	100
10.5. Analysis.....	101
10.5.1. Stereonets .....	101
10.5.2. % Density and % Oxides.....	102
10.5.3. Statistical Analysis .....	103
10.5.4. Spatial Analysis.....	104
10.6. Results .....	104
10.6.1. Stereonets .....	104
10.6.2. % Density and % Oxides.....	106
10.6.3. Statistical Analysis .....	109
10.6.4. Spatial Analysis.....	114
10.7. Initial Interpretations .....	116
11. DISCUSSION AND INTERPRETATIONS.....	119
11.1. Introduction .....	119
11.2. Hydrothermal.....	119
11.3. Alteration.....	120
11.4. Oxidation.....	121
11.5. Fracture Density .....	123
12. CONCLUSIONS .....	125
13. RECOMMENDATIONS .....	126
13.1. Geochemistry.....	126
13.2. Spectral Radiometry as Grade Control Method .....	127
14. REFERENCES.....	128
15. APPENDIX 1 – GEOCHEMICAL DATA.....	133
15.1. Appendix 1.1. Geochemical Data Tables.....	134
16. APPENDIX 2 – STATISTICAL ANALYSES TABLES AND FIGURES.....	153
16.1. Appendix 2.1. Descriptive Statistics .....	154
16.2. Appendix 2.2. Univariate Analysis .....	160
16.3. Appendix 2.3. Bivariate Analysis.....	193
16.4. Appendix 2.4. Multivariate Factor Analysis .....	202
16.5. Appendix 2.5. Spatial Distribution of Factor Scores.....	210

	PAGE
17. APPENDIX 3 – ELEMENT ABUNDANCE .....	214
17.1. Appendix 3.1. Element Abundance Contour Maps.....	215
18. APPENDIX 4 – SPECTRAL PROFILES.....	220
18.1. Appendix 4.1. Spectral Profiles of 52 Geochemical Samples.....	223
18.2. Appendix 4.2. Spectral Profiles of QMP-4780 .....	249
18.3. Appendix 4.3. Spectral Profiles of QMP-4750 .....	251
18.4. Appendix 4.4. Spectral Profiles of QMP-4600 .....	254
18.5. Appendix 4.5. Spectral Profiles of RHY-4700.....	259
18.6. Appendix 4.6. Spectral Profiles of RHY-4675.....	264
18.7. Appendix 4.7. Spectral Profiles from USGS Spectral Library.....	269
18.8. Appendix 4.8. Spectral Profiles from JPL Spectral Library.....	279
19. APPENDIX 5 – FRACTURE DENSITY .....	289
19.1. Appendix 5.1. Bench Interval UTM Locations and Total Density .....	290
19.2. Appendix 5.2. Bench Interval Fracture Density Variables .....	292
19.3. Appendix 5.3. Steronets with % Cu and % Fe in Fractures .....	299
19.4. Appendix 5.4. Fracture Density Bivariate Analyses .....	324
19.5. Appendix 5.5. Spatial Distribution of Fracture Density Data .....	327
20. APPENDIX 6 – DATA INTEGRATION FIGURES .....	331
20.1. Appendix 6.1. Data Integration Figures .....	332
21. CURRICULUM VITA.....	336

## LIST OF TABLES

	PAGE
Table 3.1 ..... Previous exploration drilling programs operated by companies involved in exploration of the MacArthur prospect.	20
Table 4.1 ..... Estimated copper resources in the Yerington district.	22
Table 4.2 ..... MacArthur project indicated and inferred copper resources.	23
Table 6.1 ..... Available data for study.	31
Table 6.2 ..... Rock descriptions of surface samples collected in the MacArthur pit.	33
Table 8.1 ..... Actlabs analytical methods and detection limits of Ultratrace 2 method.	40
Table 8.2 ..... List of elements used in surface analysis. Surface data total 63 samples.	41
Table 8.3 ..... List of elements used in subsurface analysis. Subsurface data total 1000 samples.	41
Table 8.4 ..... Correlation frequencies from analysis of surface data correlation matrices.	56
Table 8.5 ..... Correlation frequencies from analysis of subsurface data correlation matrices.	56
Table 8.6 ..... Pairwise correlations from analysis of surface data.	57
Table 8.7 ..... Pairwise correlations from analysis of subsurface data.	57
Table 8.8 ..... Surface factor score coefficients from Factor analysis.	59
Table 8.9 ..... Subsurface factor score coefficients from Factor analysis.	60

	PAGE
Table 8.10 ..... Factor Analysis results of Surface Samples.	61
Table 8.11 ..... Factor Analysis results of Subsurface Samples.	61
Table 9.1 ..... Rock samples used in Spectral Analysis.	72
Table 9.2 ..... Field samples used in spectral analysis.	73
Table 9.3 ..... Bench 4800 Spectral Analyst matches with USGS and JPL spectral libraries.	78
Table 9.4 ..... Bench 4700 Spectral Analyst matches with USGS and JPL spectral libraries.	79
Table 9.5 ..... Bench 4675 Spectral Analyst matches with USGS and JPL spectral libraries.	79
Table 9.6 ..... Bench 4600 Spectral Analyst matches with USGS and JPL spectral libraries.	80
Table 9.7 ..... Spectral Analyst results from QMP-4780.	82
Table 9.8 ..... Spectral Analyst results from QMP-4750.	82
Table 9.9 ..... Spectral Analyst results of a continuous porphyry dike.	82
Table 9.10 ..... Spectral Analyst results from QMP-4600.	83
Table 9.11 ..... Spectral Analyst results from RHY-4700.	84
Table 9.12 ..... Spectral Analyst results from RHY-4675.	84

	PAGE
Table 9.13 ..... Spectral Analyst results of a continuous rhyolite dike.	85
Table 9.14 ..... RHY-4675 Spectral Analyst matches from USGS and JPL spectral libraries.	86
Table 9.15 ..... Spectral Analyst matches of geochemical samples with associated percent copper below 0.18 with- rock type, and visible copper oxide color.	91
Table 9.16 ..... Spectral Analyst matches of geochemical samples with associated percent copper above 0.18 with- rock type, and visible copper oxide color.	93
Table 10.1 ..... Table shows how data was recorded at each bench interval measurement.	99
Table 10.2 ..... Demonstration of how fracture density ( $\rho$ ) is calculated for this study.	100
Table 10.3 ..... Red numbers indicate 20 variables used in statistical analysis for F1, F2, F3, and Totals.	103
Table 10.4 ..... Resulting correlation scores from bivariate analysis of fracture density data scores $> 0.9$ .	109
Table 10.5 ..... Resulting correlation scores from bivariate analysis of fracture density data scores 0.9-0.7.	110
Table 10.6 ..... Resulting correlation scores from bivariate analysis of fracture density data scores 0.7-0.5.	110
Table 11.1 ..... Pure neotocite vs. mean value of surface sample data for selected elements in the MacArthur pit.	122
Table 11.2 ..... Correlation coefficient scores for F1, F2, and F3 CuOx and FeOx vs. total iron and copper in fractures at the MacArthur pit.	123

## LIST OF FIGURES

	PAGE
Figure 1.1..... Geographic location of Yerington, NV and the MacArthur prospect.	1
Figure 1.2..... Quaterra Resources current claim status, Yerington District, Nevada.	2
Figure 2.1..... Basin and Range province.	4
Figure 2.2..... North-south cross section of the Yerington Batholith.	8
Figure 2.3..... Surface geology of Quaterra Resources MacArthur property.	10
Figure 2.4..... Alteration and mineral assemblages of the San Manuel / Kalamazoo porphyry copper deposit.	15
Figure 2.5..... Alteration zone map of the MacArthur property.	16
Figure 4.1..... Extent of copper oxides identified in phase 1 drilling by Quaterra Resources. From: Bonsall, Unpublished (2010).	24
Figure 4.2..... Extent of chalcocite defined in phase 1 drilling by Quaterra Resources.	25
Figure 4.3..... North-south cross section line A-A'.	26
Figure 4.4..... Phase 2 of drilling by Quaterra Resources at the MacArthur prospect. December 2009 – April 2010.	27
Figure 4.5..... Phase 2 of drilling by Quaterra Resources at the MacArthur prospect. April 2010 – September 2010.	28
Figure 7.1..... Surface sample location map.	35

	PAGE
Figure 8.1..... Location of QMT series diamond drill holes with multi-element analysis.	38
Figure 8.2..... Histogram, outlier box plot, and normal quantile plot for aluminum.	43
Figure 8.3..... Raw data univariate analysis for % Ca.	44
Figure 8.4..... Outlier removed univariate analysis for % Ca.	45
Figure 8.5..... Log data univariate analysis for % Ca.	46
Figure 8.6..... An example of the scatter plot from surface data showing Al, Cu, Fe, Mg, Ni, U, and V.	48
Figure 8.7..... An example of the Pairwise correlations of surface data.	49
Figure 8.8..... Surface factor analysis factor 5 at the MacArthur Mine.	51
Figure 8.9..... Contour map of surface Cu abundance at the MacArthur Mine.	52
Figure 8.10..... Spatial distribution of multivariate analysis factor 5 at the Macarthur Mine.	52
Figure 8.11..... Proposed alteration zones of the MacArthur pit.	70
Figure 9.1..... Spectral field test locations.	73
Figure 9.2..... Spectral profile of sample 44 (white) from bench 4800 with - goethite (yellow) and jarosite (red) from USGS spectral library.	78

	PAGE
Figure 9.3..... Spectral profile of sample 74 (white) from bench 4700 with - riebeckite (yellow) from JPL spectral library.	80
Figure 9.4..... Spectral profile of sample 57 (white) from bench 4600 with - atacamite (yellow) from JPL spectral library.	81
Figure 9.5..... Spectral profile of sample R-4675.3 (white) with - atacamite (yellow) from JPL spectral library.	87
Figure 9.6..... Spectral profile of sample R-4675.7 (white) with – glauconite from USGS (yellow) and JPL (red) spectral libraries.	89
Figure 9.7..... Spectral profile of sample R-4675.9 (white) with - copiapite (yellow) from USGS spectral library.	89
Figure 10.1..... Fracture density measurement locations.	98
Figure 10.2..... Stereonet of interval 4675_00 showing F1 (red), F2 (blue), and F3 (black) orientation, number of fractures (n), and density ( $\rho$ ).	101
Figure 10.3..... Stereonet of interval 4675_00 showing orientation, number of fractures, fracture density, and copper and iron occurring in each fracture family.	102
Figure 10.4..... Stereonets showing orientations and ranges of fracture families in the MacArthur pit.	105
Figure 10.5..... Percent occurrence of fracture family in the MacArthur pit from 99 fracture density measurements.	107
Figure 10.6..... Pie charts displaying percent oxides (copper and iron) in fracture families.	108

Figure 10.7.....	111
Fracture density factor 1.	
Figure 10.8.....	112
Fracture density factor 2.	
Figure 10.9.....	113
Fracture density factor 3.	
Figure 10.10.....	114
Fracture density factor 4.	

## 1. INTRODUCTION

The MacArthur copper prospect in Yerington, NV, is located approximately 50 miles southeast of Reno, NV (figure 1). The MacArthur prospect is an oxidized copper porphyry deposit, partially mined by open pit methods, hosted in Jurassic aged quartz monzonite (Heatwole 1978). The MacArthur prospect is located on the northern edge of the historic Yerington District, a district known for several copper deposits in a variety of mineralization styles. Today, inferred copper reserves of the district are greater than 20 billion pounds, more than 5 billion of which are in deposits currently owned by Quaterra Resources Inc (Quaterra) (<http://www.quaterraresources.com/>). The MacArthur prospect is unique in that it is the only known copper deposit in the district to have mineralization occurring entirely as acid-soluble copper oxides and sulfides.

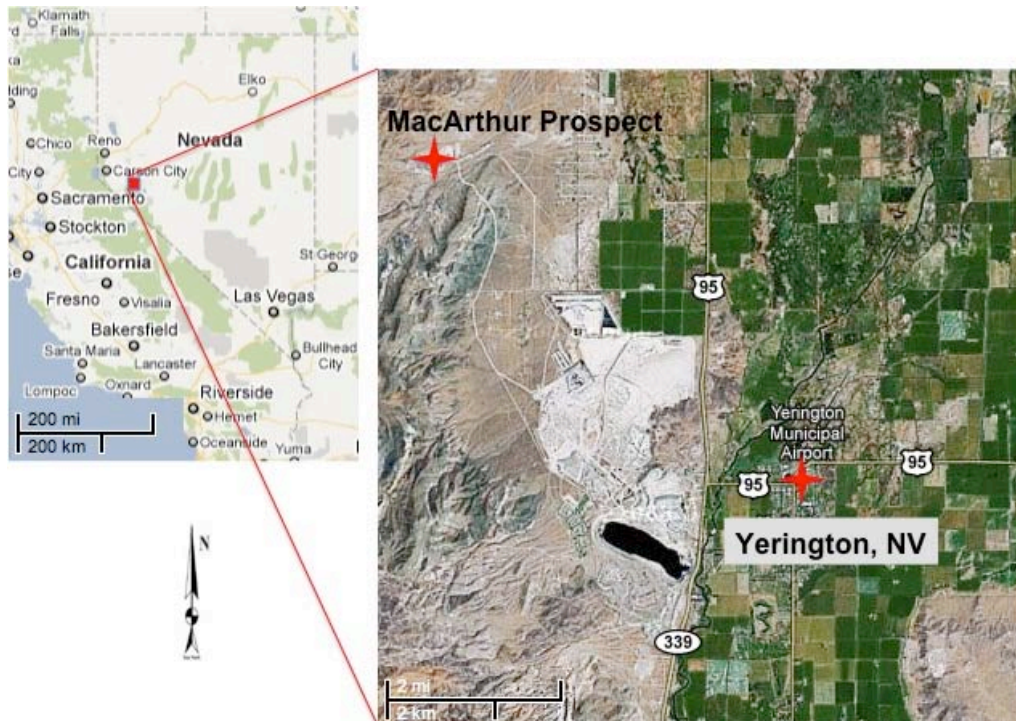


**Figure 1.1.** Geographic location of Yerington, NV and the MacArthur prospect.

The Yerington district is geographically in the western edge of the Great Basin and Range province (figure 2.1) therefore, characterized by extensional tectonics. Due to the complexity of tilting, faulting, and oxidation events at the MacArthur, high-grade copper oxide zones are poorly defined and difficult to project. A detailed study of the oxidation and enrichment environments in the open pit has assisted in understanding the geological parameters controlling mineralization.

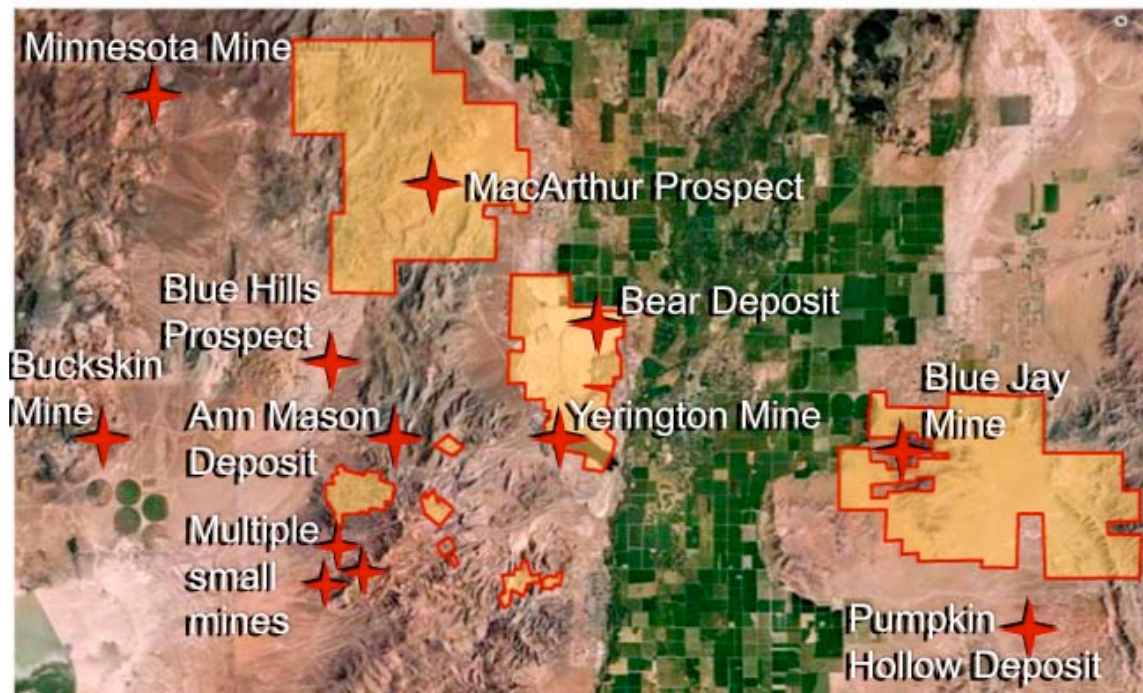


**Figure 1.2.** Red stars indicate known deposits and yellow boxes indicate Quaterra Resources current claim status, Yerington District, Nevada. (From Quaterra Resources)

From 1971 – 1973 the Anaconda Company developed a copper oxide reserve for the MacArthur prospect indicating 11.5 million tons of 0.42% Cu using data from 280 drill holes (Heatwole 1972). The source of the copper oxide is thought to be derived from in-situ oxidation of primary copper sulfides and from exotic copper from the peripheral phyllic zones (Heatwole, 1978). Current drilling of the MacArthur prospect commissioned by Quaterra indicates

mineralization occurs as surface copper oxides, an underlying chalcocite blanket, and deep primary copper sulfide.

Since April 2010, Quaterra has drilled a total of 21,143 feet in 37 reverse circulation holes to expand the known copper resource at MacArthur and the outer margins of the deposit have not yet been delineated (Spiering, 2010). Quaterra Resources are the 100% owners of the MacArthur prospect and one of the largest claim holders in the Yerington District.

## 2. GEOLOGY

### 2.1. Regional Geology

The state of Nevada lies almost entirely in the Great Basin province (Figure 2.1), a region characterized by internal drainage due to a series of generally north-trending mountain ranges separated by alluviated valleys (Stewart and Carlson, 1978). Nevada has a well-documented, long, and complex geologic history with major episodes of sedimentation, igneous activity, orogenic deformation, and continental rifting (Stewart, 1980).



**Figure 2.1.** Basin and Range province. (From <http://rst.gsfc.nasa.gov/Sect6>).

The present discussion of Yerington district geology is largely from Dilles et al., (2000) as well as Todd Bonsall (unpublished work) and Dave Heatwole, Quaterra Resources geologists. The detailed geologic description is the result of extensive work in the area performed by Anaconda geologists and the ongoing efforts of John H. Dilles, John M. Proffett, and James E. Wright.

The numerous deposits, of varying mineralization types that occur in the Yerington district are associated with Yerington batholith intrusion, estimated in size to be 1325 km<sup>3</sup> (Dilles, 1987). More recent work by Dilles et al, (2000) indicates that hydrothermal alteration has affected more than 100 km<sup>3</sup> of rock in the Yerington batholith and was produced by a similar volume of hydrothermal fluids. Four major intrusions of Jurassic age form the Yerington batholith: (1) The McLeod Hill quartz monzodiorite, (2) Bear quartz monzonite, (3) Luhr Hill granite, and (4) Quartz Monzonite Porphyry Dikes. Age constraints using U/Pb zircon dating show the emplacement of the Yerington batholith to take place over a one million year period from 169.4 Ma to 168.5 Ma (Dilles and Wright, 1985).

The oldest rocks in the Yerington district are middle to late Triassic volcanic, sedimentary, and plutonic rocks (Dilles and Wright, 1988). Triassic and Jurassic marine sedimentary and volcanoclastic unconformably overlie the volcanic and plutonic rocks in a sequence consisting of limestone and black argillite, tuffaceous and limy beds, a dacitic tuff, limestone, tuffaceous siltstones and argillites, a thin marble, evaporite gypsum, and an aeolian sandstone (Dilles et al., 2000). These rocks are also overlain by a sequence of intermediate to silicic lavas, tuffs, and volcanoclastic rocks and together make up the Artesia Lake Volcanics (Dilles et al., 2000).

The Artesia Lake Volcanic group is intruded by the Yerington batholith (Proffett and Dilles, 1984), and is thought to represent the extrusive counterpart of the Yerington batholith (Dilles et al., 2000). The oldest intrusion of the Yerington batholith is the McLeod Hill quartz monzodiorite defined by biotite and hornblende occurring in a fine to medium-grained groundmass.

The next igneous event is the Bear quartz monzonite and is intruded into the McLeod Hill quartz monzodiorite and locally the Artesia Lake Group (Dilles et al., 2000). The Bear quartz monzonite is compositionally zoned, consisting of a fine-grained contact phase grading into a hornblende rich, medium to coarse-grained texture (Dilles et al., 2000). The fine-grained contact phase is locally called the Border Phase Bear quartz monzonite.

The youngest rock representing the Yerington batholith emplacement is the Luhr Hill granite. The Luhr Hill granite is described as “a deeply emplaced, medium to coarse-grained K-feldspar megacryst-bearing hornblende-biotite granite,” resulting in multiple granite porphyry dike swarms (Dilles et al., 2000). The dike swarms display 40-60 volume percent phenocrysts of quartz, K-feldspar, with hornblende and biotite in an aphanitic to aplitic matrix of quartz, K-feldspar, and plagioclase (Dilles et al., 2000). Proffett (1979) identified five separate dike intrusions in the Yerington mine with slight variations in composition.

Following the Yerington Batholith emplacement the next group of rocks is the Fulstone Spring Volcanics consisting of subareal intermediate- to silicic lavas, domes, ignimbrite, and volcaniclastic sedimentary rocks (Dilles et al., 2001). Dilles and Wright (1988) used U/Pb zircon dating to obtain an age of 165.5 Ma from a dome in the upper Fulstone. Intruding the Fulstone volcanics is a series of monzodiorite porphyry dikes with an U/Pb zircon age of 165 Ma (Dilles et al., 2000). Lying south of the Yerington district is the Shamrock batholith. It consists

of a large body of hornblende-biotite granite and U/Pb zircon dating showed the batholith to be 165 Ma.

Jurassic intrusive dikes of rhyolite and andesite occur throughout the Yerington district. Age dating of the dikes has not been completed but work by Proffett and Dilles (1984), and observed by Quaterra Resources geologists are cross cutting relationships of dikes indicating the andesite and rhyolite dikes are the youngest Jurassic intrusives.

Volcanic activity ceased in the mid to-late Jurassic and resumed in the Tertiary with and a series of twelve Oligocene ash flow tuff units mapped by Proffett and Proffett (1976). The final stage of rock forming activity occurred in the middle Miocene consisting of andesitic lavas (Dilles et al., 2000). The onset of Basin and Range (17 to 18 Ma) marks the end of the volcanic deposition in the Yerington district (Proffett, 1977). Figure 2 is a model of the Yerington district from Dilles (1987). Extensive mapping work in the district by Proffett and Dilles identified three episodes of normal faulting all dipping to the east and the youngest of which includes the active system bounding the modern day basin and ranges of the district (Dilles et al., 2000). Proffett (1977) recognized the extensive east-dipping normal faulting caused Tertiary and pre-Tertiary rocks in the district to tilted to the west by 70-90° exposing the Yerington porphyry copper deposit in horizontal cross section.



## **2.2. MacArthur Geology**

MacArthur geology is described based on surface and subsurface mapping by Quaterra Resources and Anaconda and Heatwole (1978), summarized in unpublished work by Todd Bonsall for a presentation at Geologic Society of Nevada (GSN) 2010 Symposium.

Geology of the MacArthur area includes two members of the Artesia Lake Volcanics, the McLeod Hill quartz monzodiorite, the Bear quartz monzonite, Jurassic intrusives, and Tertiary flows. The McLeod Hill quartz monzodiorite and the Bear quartz monzonite are the dominant rock of the MacArthur area and are intruded by at least five varieties of granite porphyry dikes of Jurassic age. Rocks associated with mineralization at the MacArthur deposit are described below and Figure 2.3 shows a geologic map of the MacArthur area mapped by Quaterra Resources.

### **2.2.1. MacArthur Rocks**

*McLeod Hill quartz monzodiorite (GD).*

Fine to medium-grained consisting of 15-20% and up to 50% biotite and hornblende commonly altered to chlorite or sericite, hornblende-biotite ratio around 5:5. Magnetite is common, 1-5 percent in unaltered rock. The monzodiorite makes up the hanging wall of the MacArthur fault (Figure 2.3) and is heavily stained with limonite from in-situ oxidation of pyrite and alteration of mafic minerals. As identified by Heatwole (2010), in the western portions of the property, the monzodiorite locally contained up to 10 percent sulfide mineralization before oxidation based on residual boxworks texture.

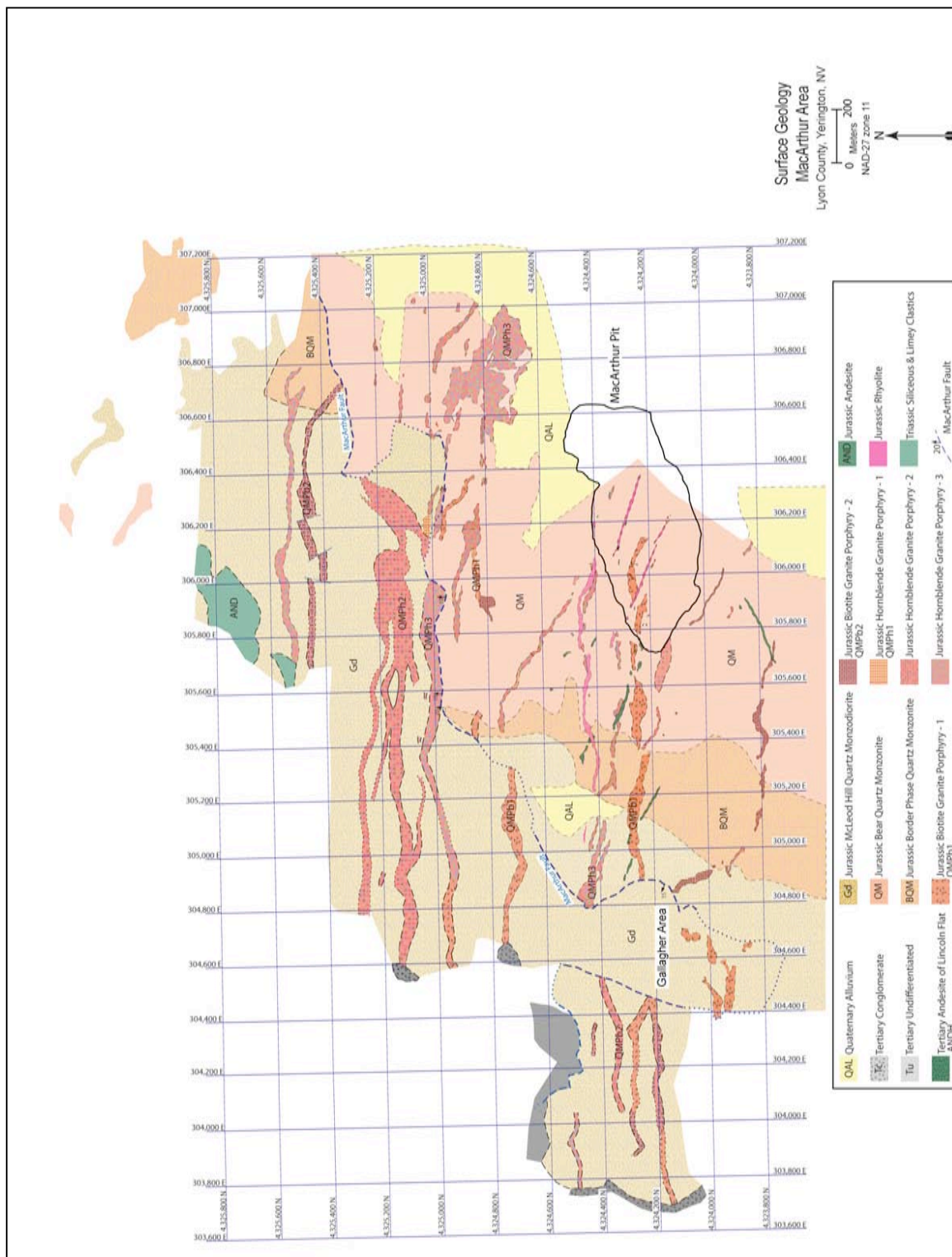


**Figure 2.3.** Surface geology of Quaterra Resources MacArthur property.  
(From Quaterra Resources, 2010).

### *Bear quartz monzonite (QM)*

Medium to coarse-grained consisting of 10-15 percent hornblende and less biotite; hornblende-biotite ratio around 8:2. Unaltered quartz monzonite commonly contains minor ( $\approx 1\%$ ) sphene. Hornblendes can be large, 3-5 mm phenocrysts and are often altered to chlorite and sericite. The historic MacArthur ore body is hosted in the Bear quartz monzonite (Figure 2.3), which often displays alteration of hornblende to secondary biotite.

### *Quartz Monzonite Porphyry Dikes*

The quartz monzonite porphyry dikes at the MacArthur prospect are classified by Todd Bonsall and Dave Heatwole based on rock forming minerals. The porphyry dikes are classified this way due to no age relationships or dating of the dikes but Heatwole (1978) established the biotite porphyry is younger as it cuts the hornblende porphyry. The following groupings of porphyry dikes may be subject to change when further age relationships are developed.

### *Biotite granite porphyry-1 (QMPb-1)*

QMPb-1 was originally described by Heatwole (1978) and updated by Bonsall (2010) as a series of north dipping ( $30^\circ$  to vertical), northwest-trending dikes consisting of abundant (5%) quartz eyes, 3-5 mm K-feldspar phenocryst, and black biotite phenocrysts (2-3 mm) in an aphanitic texture. Occasionally, the dike displays 2-3 percent disseminated pyrite and chalcopyrite.

### *Biotite granite porphyry-2 (QMPb-2)*

QMPb-2 is defined by Bonsall (2010) as black biotite phenocrysts occurring with hornblende phenocrysts, 3-5 mm K-feldspar phenocrysts and abundant (5%) quartz eyes in an aphanitic texture. Occasionally, the dike displays 2-3 percent disseminated pyrite and chalcopyrite.

#### *Hornblende granite porphyry-1 (QMPH-1)*

QMPH-1 is defined by Bonsall (2010) as abundant (3-5%) quartz eye phenocrysts, abundant hornblende needles, 3-5 mm K-feldspar phenocrysts occurring with 3 percent or more pyrite phenocrysts up to 5 mm. To date, no chalcopyrite or copper oxide mineralization has been observed with the dike and is also the least common porphyry on the property.

#### *Hornblende granite porphyry-2 (QMPH-2)*

QMPH-2 is described by Bonsall (2010) as abundant (2-5%) quartz eye phenocrysts, abundant hornblende needles, 2-5 mm K-feldspar phenocrysts commonly occurring with 3 percent pyrite and chalcopyrite oxidizing to copper oxides.

#### *Hornblende granite porphyry-3 (QMPH-3)*

QMPH-3 is originally described by Heatwole (1978) and updated by Bonsall (2010) as abundant hornblende needles occurring with large (up to 3-4 cm), epidotized K-feldspar phenocrysts. The porphyry contains rare (<1%) quartz eye phenocrysts and pyrite and is often enriched with exotic copper oxides.

#### *Jurassic andesite (AND)*

Jurassic andesites are black fine-grained rocks that vary from hornblende rich phenocrysts bodies to bodies with a negligible amount of identifiable minerals. Heatwole, (1978) noticed the andesite dikes commonly display propylitic alteration.

#### *Jurassic rhyolite (RHY)*

Fine grained aphanitic texture, rare (<1%) 1-3 mm needle like hornblende phenocrysts. The rhyolite dikes in the MacArthur pit display strong exotic copper oxide mineralization due to feldspars “buffering” effects of copper rich acidic solutions.

### **2.2.2. MacArthur Faults**

Multiple faults are seen in drill cuttings at the MacArthur property and the largest of which, the MacArthur fault (Fig. 3) cuts the property in a northwest strike, dipping to the north (15-30°). Proffett and Dilles (1984) believe the fault moved in late Jurassic and later during Basin and Range extension in the Tertiary. This is based from observations of west-to-east 1200 meter displacement of the contact of the Jurassic border quartz monzonite and McLeod hill monzodiorite while only a 600 meter displacement of the base of the Tertiary.

Geologic contacts seen in drill cuttings by Quaterra Resource geologists show that in the western portions of the property the MacArthur fault has McLeod hill in both the footwall and hanging wall. In the north and northeast of the MacArthur property, The McLeod hill monzodiorite is the hanging wall of the fault while the Bear quartz monzonite is the footwall. Recent drilling in the summer of 2010 indicates a possible McLeod hill – Bear quartz monzonite border phase contact in the west-northwest of the property. The MacArthur fault is commonly a high-grade zone of copper mineralization hosting oxides, chalcocite, and chalcopyrite.

### **2.2.3. MacArthur Alteration**

At least five alteration types associated with porphyry deposits have been identified on the MacArthur property. Weak to strong phyllic, propylitic, sodic-calcic, and potassic alteration are present, as well as minor amounts of skarn developed along the northwest margins associated with Triassic limestone and associated sedimentary rocks. Figure 2.4 shows idealized alteration zones and primary mineralization zones associated with porphyry system as described by Guilbert and Park (1986) and Figure 2.5 shows a plan view map of alterations mapped at the MacArthur from unpublished work by Dilles 1992-1995 and updated by Quaterra Resources

throughout 2010. Figure 2.4 by Guilbert and Park is idealized and makes no mention of the sodic-calcic zone unique to porphyry deposits in the Yerington district.

Sodic-calcic alteration is defined in the MacArthur pit by the partial to complete alteration of K-feldspar to albite and significant increases in the titanite content (Bonsall, 2010, unpublished). Weak to moderate sodic-calcic alteration is seen in the eastern portion of the MacArthur pit. Strength increases in an easterly direction resulting in complete replacement of K-feldspar by albite while hornblende is replaced by actinolite. The alteration to the east of the MacArthur pit is interpreted as being structurally deep in the porphyry copper system, now exposed due to westerly tilting (Bonsall, 2010 unpublished).

Potassic alteration involves the introduction or recrystallization of K-feldspars by means of hydrothermal alteration in the central deep portions of a porphyry copper system (Guilbert and Park 1986). At the MacArthur, potassic alteration is recognized by the biotization of hornblende. This is a hydrothermal process that replaces hornblendes with secondary biotite. Weak potassic alteration is seen in the central core of the MacArthur pit and has been identified in deep drill cuttings by Quaterra Resources in the northern margins of the property.

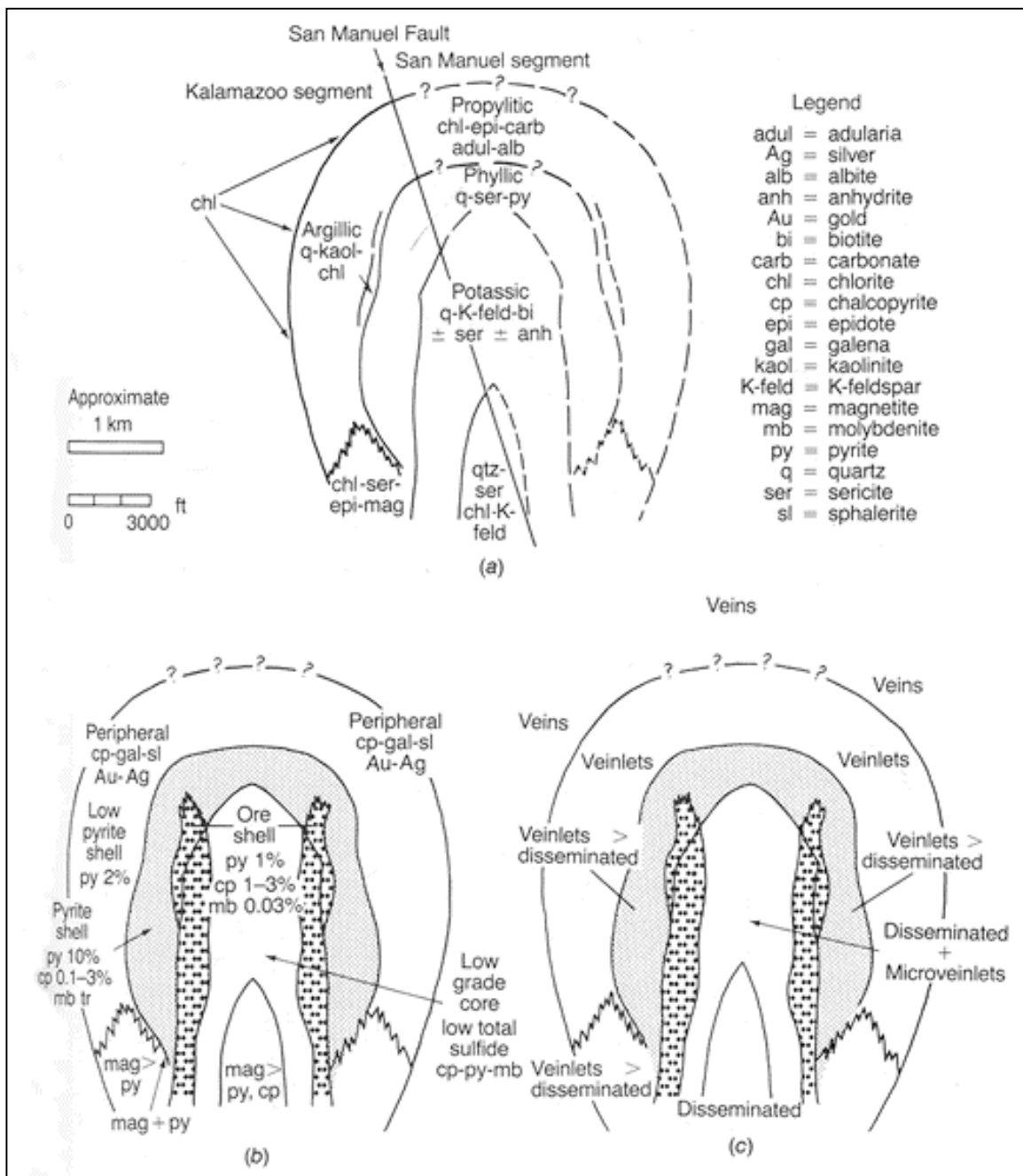


**Figure 2.4.** Alteration and mineral assemblages of the San Manuel / Kalamazoo porphyry copper deposit (From Guilbert and Park, 1987).

Phyllic alteration is the removal of sodium, calcium, and magnesium and the replacement of silicates by micas (Guilbert and Park, 1986). The zone is characterized by quartz-sericite-pyrite assemblages and is considered to be the shell that surrounds potassic alteration in a porphyry system (Lowell and Guilbert, 1970).

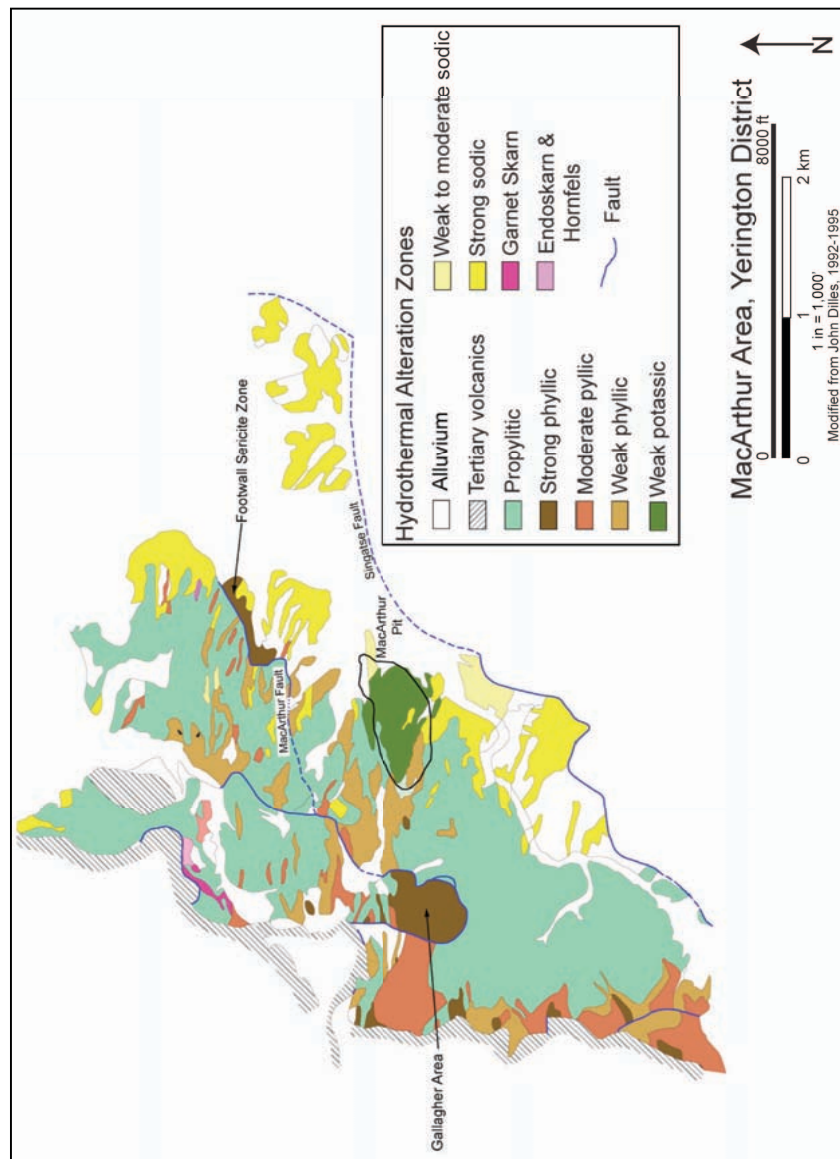


**Figure 2.5.** Alteration map of the MacArthur property. Modified by Quaterra Resources from unpublished work by Dilles (1992-1995).

Strong phyllic alteration is mapped in the Gallagher area and tends to weaken in a easterly direction and also occurs west and north of the MacArthur pit. The phyllic zone in the western part of the MacArthur pit, as described by Heatwole (1978), is defined by the partial alteration of plagioclase and K-feldspar to sericite, and strong alteration of mafic minerals to sericite or clay.

Propylitic alteration is the replacement of plagioclase and hornblende-biotite by chlorite and epidote due to the alteration of epidote, chlorite, and carbonate minerals (Guilbert and Park, 1986). Propylitic alteration is wide spread on the MacArthur property and is recognized by the partial to complete alteration of hornblende to chlorite. Propylitic alteration occurs at low temperature-pressure in the outer shell of a porphyry system (Guilbert and Park, 1986).

#### **2.2.4. MacArthur Mineralization**

Three types of Cu mineralization have been identified at the MacArthur property by Quaterra Resources through extensive drilling programs. They include copper oxide, supergene chalcocite, and hypogene sulfides. Chalcopyrite mineralization was indentified through deep exploration drilling for porphyry style mineralization in the Gallagher area. Drilling defined discontinuous vein like chalcopyrite zones in unaltered to propylitically-altered monzodiorite (Bonsall, 2010, unpublished). In 2010, drilling in the north resulted in the discovery of chalcopyrite mineralization ranging 10 – 95 feet thick with a continuous strike length of over 4600 feet. This zone may represent the fringe of a porphyry deposit (Spiering, 2010).

Copper oxides at the MacArthur pit, first described by Heatwole (1978), occur as (1) green copper oxides, (2) black copper wad, and (3) dark-brown iron oxides. Green copper oxides occur predominately as chrysocolla with less malachite and azurite and very sporadic turquoise. Black copper wad occurs in the MacArthur pit as neotocite, a secondary silicate mineral comprised of manganese, iron, and copper in an uncertain formula (Anthony et al.,

1995). That last group is the dark-brown iron oxides. Heatwole (1978) found that goethite rich rocks with fresh feldspars could contain up to 0.3% Cu. Heatwole today, demonstrates this in the field by plating copper on a nail using weak hydrochloric acid.

Copper oxides dominate the upper 300 ft of rocks in MacArthur pit region and are found in chlorite rich chalcopyrite veins southeast of the Gallagher area. Heatwole, (1978) noticed high-grade copper oxide zones are difficult to define and project because recognizable grade controls of primary mineralization were “washed out” as the result of supergene processes. Small sporadic copper oxide minerals are found across the entire MacArthur property within the oxide zone geology.

Chalcocite mineralization occurs in the MacArthur property as a partially oxidized, predominately flat zone commonly coating pyrite and chalcopyrite at the interchange of the oxidation/reduction boundary (Bonsall, 2010, unpublished). Chalcocite is commonly intercepted in up to 150 feet thick zones north of the MacArthur pit thinning to the west and south under the pit. Quaterra Resources drilling continues to expand the extent of chalcocite mineralization. Sporadically perched sections of oxidized chalcocite are also encountered throughout the MacArthur property suggesting multiple oxidation-reduction-enrichment cycles.

### 3. HISTORIC EXPLORATION

#### 3.1. District Exploration

Copper of economic value in the Yerington district was first produced in the early 1900s (<http://www.minemarket.com/yerington.htm>) Because of the recognized mineralization potential, many major companies and government agencies began exploration in the district including: Anaconda, US Steel Corp, Superior Oil Company, and US Bureau of Mines. In the early 1940s, a subsidiary of the Anaconda Company delineated a reserve of 60 million tons of ore at 0.90% to 0.95% Cu consisting of 40 million tons of oxide ore and a deeper 20 million tons of sulfide ore (<http://www.minemarket.com/yerington.htm>) hosted in porphyry style mineralization. The Yerington Mine began operations in 1953 and produced oxide and sulfide ore through 1978 totaling 162 million tons at an average grade of 0.55% Cu producing approximately 1.75 billion pounds of copper from the open pit mine (<http://www.minemarket.com/yerington.htm>).

As an ongoing effort to identify new deposits, US Steel Corp commissioned an airborne magnetic survey of the district in 1959 (<http://www.nevadacopper.com> 1) identifying a large magnetic anomaly southeast of Yerington, the Pumpkin Hollow deposit. Later magnetic surveys and drilling efforts defined several magnetite rich skarns with 40% plus iron. Other companies, including the Anaconda Company intercepted copper grades of 20% in drilling efforts to define a host body (<http://www.nevadacopper.com> 1). However, production of the Pumpkin Hollow deposit has never occurred.

### 3.2. MacArthur Exploration

Mineralization at the MacArthur prospect was recognized in the early 1930s. During this time, mining claims were staked by a local prospector and several small shipments of hand-cobbed, high-grade ore were made (Heatwole, 1978). Beginning in 1950 and until 1971, the property was explored by the U.S. Bureau of Mines and later optioned by at least four major mining companies including The Anaconda Company (Heatwole, 1978). Table 3.1 shows drilling operations completed by various companies involved in exploration at the MacArthur prospect.

**Table 3.1.** Previous exploration drilling programs operated by companies involved in exploration of the MacArthur prospect.

(From Tetra Tech Inc. MacArthur copper project NI 43-101, 2009).

<b>Table 3.1 - Previous Drill Operations at MacArthur Prospect</b>			
<b>Operator</b>	<b>Years Drilled</b>	<b># of Holes</b>	<b>Feet Drilled</b>
US Bureau of Mines	1947-50	8	3,414
The Anaconda Company	1955-57	14	3,691
Beer Creek Mining Company / Kennecott Mining	1963-?	14	???
Superior Oil Company	1967-68	11	13,117
The Anaconda Company	1971-73	280	55,807
Pangea Explorations Inc.	1987-90	15	2,110
Arimetco International Inc	1990-1997	???	???

In 1972, geologists with the Anaconda Company developed a reserve estimation for the MacArthur deposit totaling 11.5 million tons of 0.42% Cu acid-soluble using data from over 280 drill holes (Heatwole, 1972). Arimetco Inc. later mined the MacArthur deposit, beginning in 1995, with a drill proven resource of 29 million tons of 0.28% Cu (<http://www.minemarket.com/Arimetco.htm>). Arimetco Inc. developed an open pit mine

producing in three years about 5.5 million tons of heap-leach (acid-soluble) ore at an average grade of 0.28% Cu. However, in 1997 Arimetco Inc. shut down operations due to financial difficulties and excessive haulage costs (<http://www.minemarket.com/yerington.htm>). As indicated by drill proven resources, Arimetco Inc. only mined about 19% of the known deposit.

## 4. RECENT EXPLORATION

### 4.1. District Exploration

Because of the inferred 20 billion pounds of copper in the ground, and a current average \$3.00/lb copper price (<http://www.mineweb.com/>), the Yerington district is busy with exploration activity. Besides Quaterra Resources, Nevada Copper (<http://www.nevadacopper.com>), and Entrée Gold Inc. (<http://www.entreegold.com>) are currently operating exploration programs in various locations in the district. Quaterra Resources continues to peruse the acquisition of the Yerington Mine site and the development of other prospects in and near the Yerington district. Today, three major porphyry systems are recognized in the district along with several small deposits related to skarn and vein type mineralization. Table 4.1 shows estimated Cu resource and property ownership for some of the larger deposits in the Yerington District.

**Table 4.1.** Estimated copper resources in the Yerington district.

<b>Table 4.1. Resources of Deposits in the Yerinton District</b>					
<b>Deposit</b>	<b>Est. Resource (mt)</b>	<b>% Cu</b>	<b>lbs (billion)</b>	<b>Claim Holder</b>	<b>Source</b>
Yerington Mine	126	0.34	0.86	Arimecto	<a href="http://www.minemarket.com">http://www.minemarket.com</a>
Bear	500	0.44	4.4	Quaterra Resources	<a href="http://www.minemarket.com">http://www.minemarket.com</a>
MacArthur	140	0.26	0.702	Quaterra Resources	<a href="http://www.quaterraresources.com">http://www.quaterraresources.com</a>
Ann Mason	810	0.4	7.1	Entrée Gold	<a href="http://www.entreegold.com">http://www.entreegold.com</a>
Pumpkin Hollow	780	0.5	9.3	Nevada Copper	<a href="http://www.nevadacopper.com">http://www.nevadacopper.com</a>
<b>Totals</b>	<b>2356</b>		<b>22.362</b>		

## 4.2. MacArthur/Quaterra Exploration

Quaterra Resources Inc. acquired the MacArthur prospect in 2006 and exploration drilling has substantially increased reserve estimations in and adjacent to Arimetco's pit. Quaterra completed 80,137 feet of drilling in 124 reverse circulation and 49 diamond core holes (<http://www.quaterraresources.com>) through December 2008. This stage of drilling defined a 1.5 square mile area of mineralization in and around the MacArthur pit and the program resulted in the discovery of an underlying supergene enriched chalcocite zone. New resource estimation, using a 0.18% Cu cut-off grade, was developed consisting of 140 million tons of copper ore with an average grade of 0.26% Cu, or about 700 million pounds (<http://www.quaterraresources.com>). Resource estimates of acid-soluble copper with increasing grade cut-offs are found in Table 4.2.

**Table 4.2.** MacArthur project indicated and inferred copper resources.  
(From Quaterra Resources)

<b>MacArthur Copper Project</b> <i>Oxide and Chalcocite Material</i>			
<b>Cutoff Grade</b> (%TCu)	<b>Tons</b> (x1000)	<b>Average Grade</b> (%TCu)	<b>Contained Copper</b> (lbs x 1000)
<i>Measured and Indicated Copper Resources</i>			
0.18	57,365	0.239	273,653.15
0.20	39,078	0.262	204,462.69
0.25	14,617	0.332	96,964.08
<i>Inferred Copper Resources</i>			
0.18	75,832	0.283	429,335.65
0.20	57,484	0.313	359,765.78
0.25	29,287	0.401	234,916.85

The Quaterra drilling program indicated mineralization occurs dominantly as acid soluble copper oxides and underlying chalcocite blankets. The program began in and around the historic MacArthur pit to delineate the parameters of oxide mineralization, and to test for underlying supergene chalcocite enrichment. The program identified oxide/chalcocite mineralization in up to a 6000-foot, east-west strike that remains open to the south and the west (Figure 4.1) and identified an underlying chalcocite blanket.

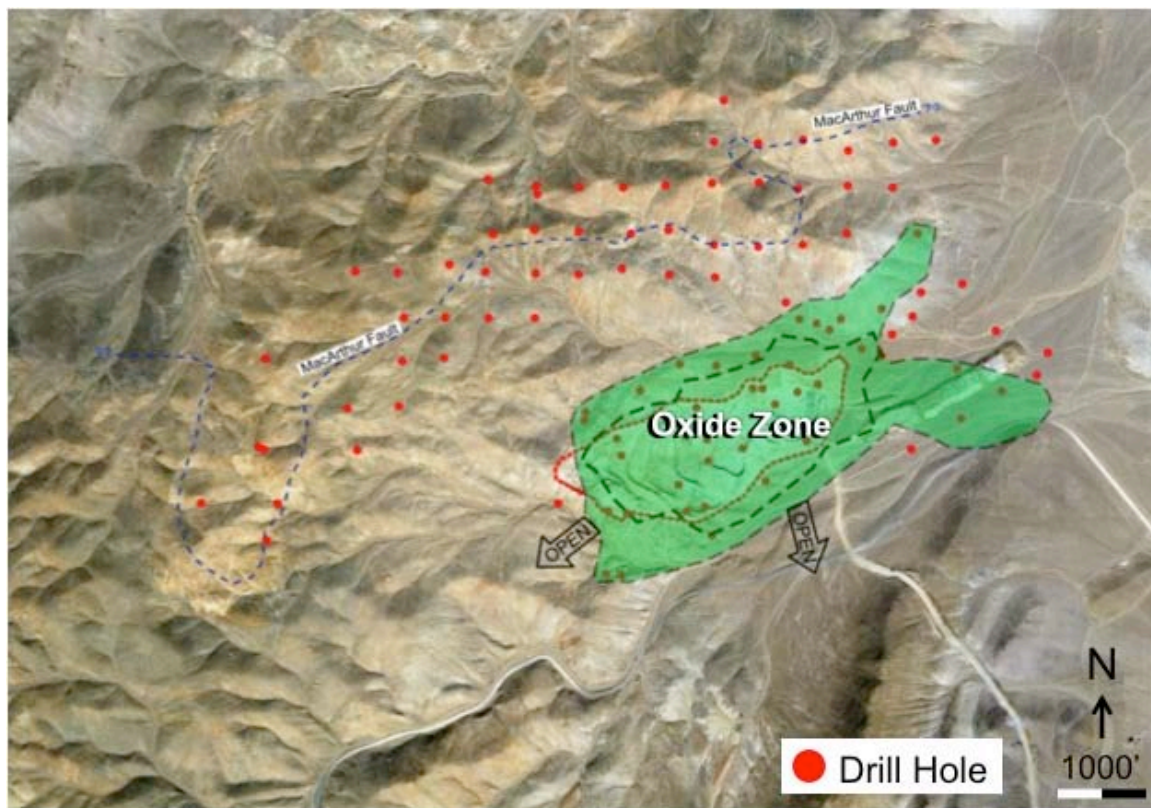


**Figure 4.1.** Extent of copper oxides identified in phase 1 drilling by Quaterra Resources. (From Bonsall, Unpublished 2010).

The drilling program expanded to the east, north, and west of the MacArthur pit to begin to define parameters of chalcocite mineralization. Chalcocite mineralization occurs in greater than 6000 feet of strike length to the north of the MacArthur pit and is encountered in what is

known as the Gallagher area on the property (Figure 4.2). Chalcocite mineralization remains open to the north, west, and south.

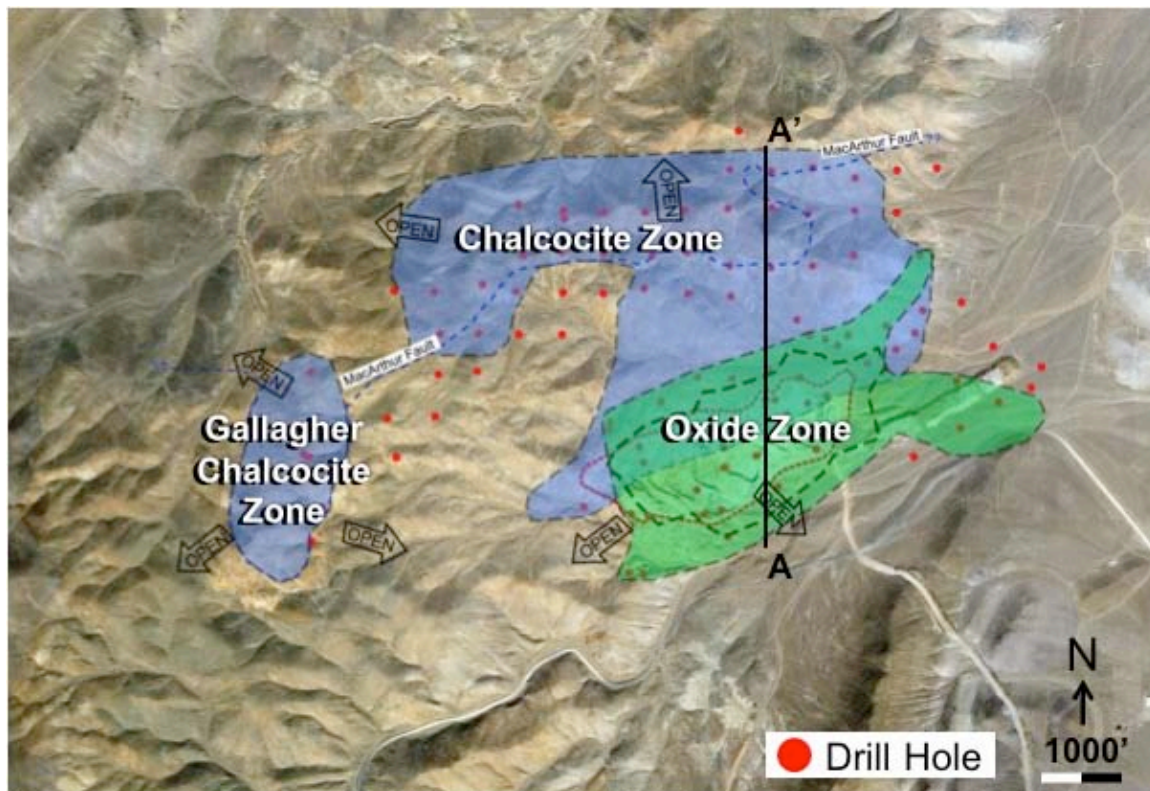


**Figure 4.2.** Extent of chalcocite defined in phase 1 drilling by Quaterra Resources. (From Bonsall, Unpublished 2010).

Cross section A-A' (Figure 4.2) along Quaterras drill line 19420 E (Figure 4.3) includes data by Quaterra, Anaconda, and US Bureau of Mines drilling and demonstrates a continuous 4000 foot long, 57 foot thick supergene enriched chalcocite blanket with an average grade of 0.36% Cu. The cross section also outlines the increased oxide resource around the historic oxide resource showing a 1800 foot long, 147 foot thick intersection with an average grade at 0.20% Cu. The cross section also shows 60 feet of 0.82% deep primary chalcopyrite mineralization in the north. Continued drilling in 2010 explored the northern margins of the property in effort to define primary porphyry type mineralization.

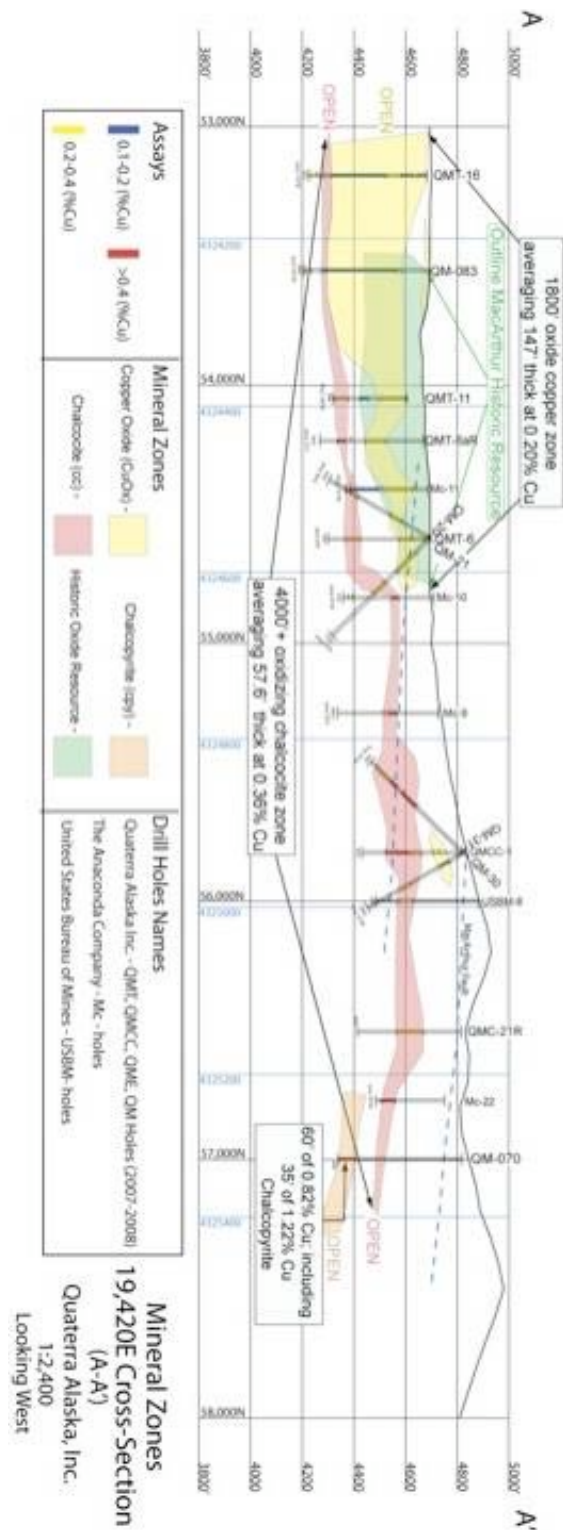


**Figure 4.3.** North-south cross section line A-A'. (From Bonsall, Unpublished 2010).

In December 2009, Quaterra Resources recommenced drilling at the MacArthur prospect (<http://www.quaterraresources.com>) in effort to expand oxide and chalcocite potential. Target areas included the Gallagher area, northwest area, and infill drilling north and west of the MacArthur pit to delineate chalcocite boundaries. Quaterra also planned to target deep primary porphyry style mineralization in the northern areas encountered in three holes during the previous drill program. In search of primary mineralization, Quaterra conducted an Induced-Potential Resistivity (IPR) in the fall of 2009 identifying five potential targets to the north and northwest of primary mineralization encountered in drilling. From December 2009 to April of 2010, Quaterra Resources completed 19,110 feet of drilling (Figure 4.4) in 32 reverse circulation holes and three deep diamond core holes (<http://www.quaterraresources.com>).

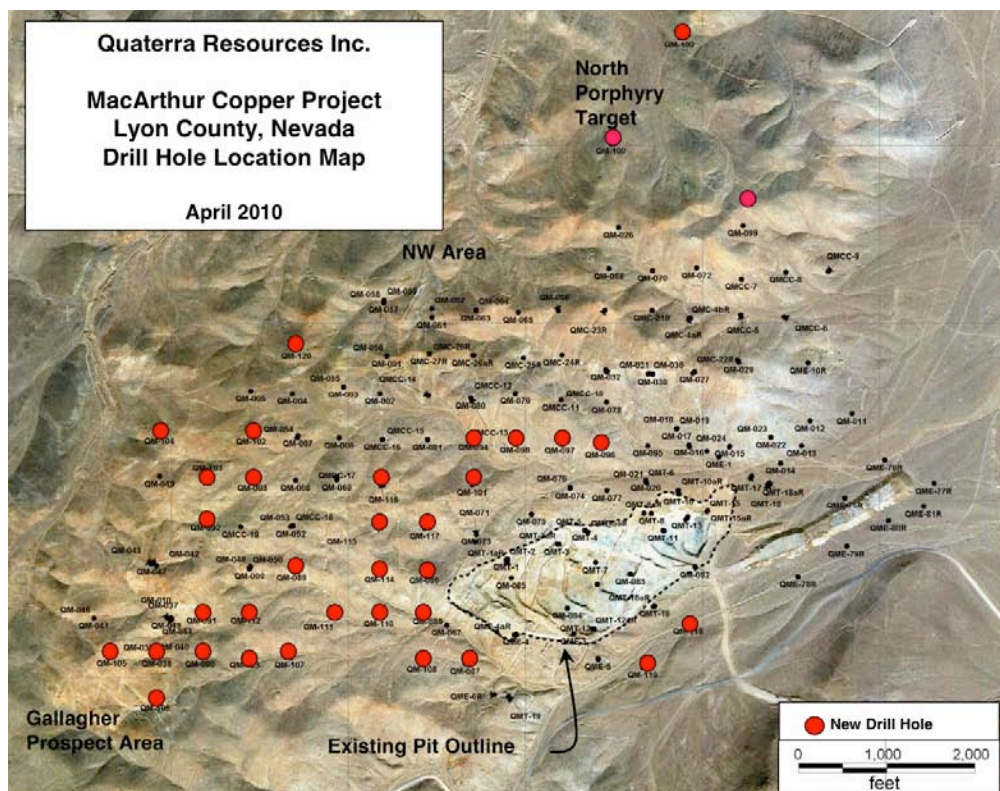


**Figure 4.4.** Phase 2 of drilling by Quaterra Resources at the MacArthur prospect. Red circles indicate holes drilled from December 2009 – April 2010. (From Quaterra Resources).

Since April 2010, Quaterra has drilled an additional 21,143 feet in 37 reverse circulation holes to expand the known oxide and chalcocite copper resource at the MacArthur. Chalcocite mineralization occurs in greater than 7500 feet of strike length to the north of the MacArthur pit and the outer limits of which have not yet been delineated (Spiering, 2010). Quaterra continued drilling with investigation around the Gallagher area (Figure 4.5) as well as drilling the northwest area for deeper primary sulfide porphyry type mineralization.

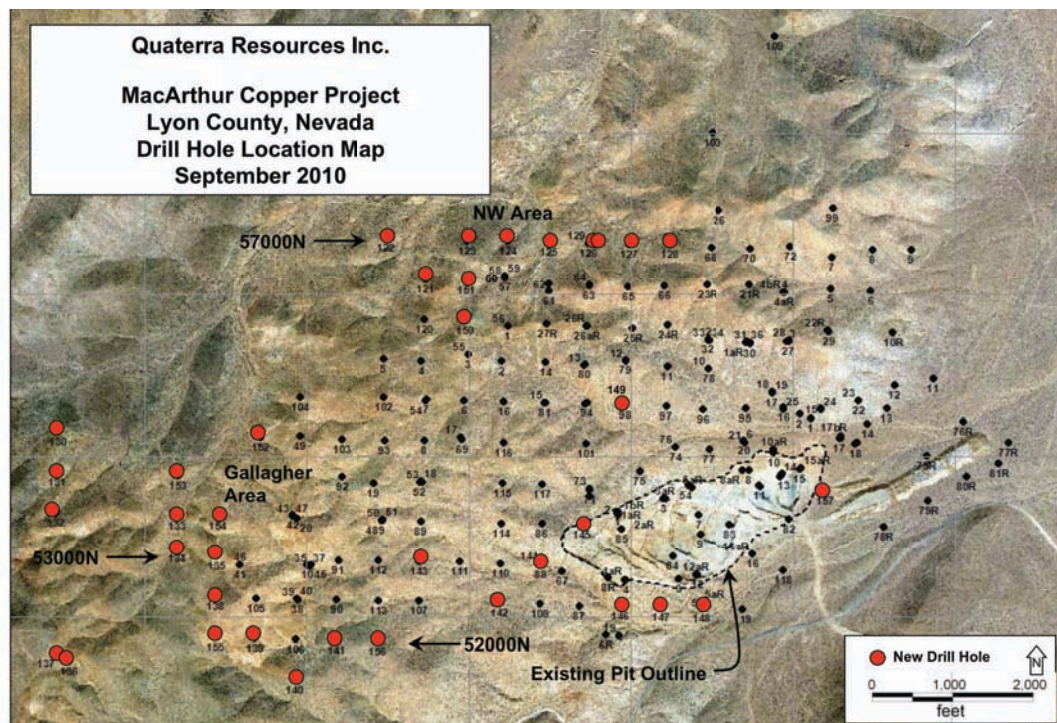


**Figure 4.5.** Phase 2 of drilling by Quaterra Resources at the MacArthur prospect. Red circles indicate holes drilled from December 2009 – April 2010. (From Quaterra Resources).

Drilling between the Gallagher area and the MacArthur pit confirmed continuity in acid-soluble copper and will substantially increase reserves. Drilling toward the northwest resulted in the discovery of primary chalcopyrite mineralization ranging 10 – 95 feet thick with a continuous strike length of over 4600 feet. This intercept may represent the fringe of porphyry style mineralization (<http://www.quaterraresources.com>). New resource estimations in the range of 1

billion pounds of copper will be released in late 2010 in Quaterra's updated N-43-101 technical compliant report to be completed by Tetra Tech Inc (<http://www.tetrattech.com/>). Quaterra Resources has plans to further explore and continue drilling the MacArthur prospect through 2010 and into 2011.

## **5. OBJECTIVES**

The main objective of this study is developing an understanding of controls of copper oxide mineralization and enrichment at the MacArthur pit, NV. The objective is investigated through the use of (1) rock descriptions, (2) multi-element geochemical data, (3) spectral radiometry data, and (4) fracture orientation and density data. A brief description of each follows:

- (1) Rock descriptions document alteration, rock type types, and mineralogy of oxide occurrences.
- (2) Statistical analyses of multi-element geochemistry data define element associations and geologic processes.
- (3) Spectral Analyst tool in ENVI (Environment for Visualizing Images) compares spectral reflectance data between study samples and samples in spectral libraries to determine mineralogy.
- (4) Fracture density distribution, oxide occurrence in fractures, and statistical analyses define relationships between oxide mineralogy and fracture systems.

This study also uses the integration of spectral reflectance data and geochemistry data as a new way to define zones of economic interest in oxidized deposits. From this test, mine geologists may find hand-held spectral radiometers a cost-effective and useful tool in the identification of mineralization above a cutoff grade.

## 6. DATA

Data used in this study are presented in the Table 6.1. Rock descriptions as a data type in Table 6.1 are presented in Table 6.2. A detailed description of data types for multi-element, spectral reflectance, and fracture density will be presented in later sections. Quaterra Resources provided complete access to updated maps, figures, geology, analyses, personal communications, and funding.

**Table 6.1.** Available data for study. Data provided by Quaterra Resources includes: 13 diamond core drill holes analyzed for 62 elements on 5 foot sections totaling 1000 samples, and access to maps and figures. The author collected remaining data with funding from Quaterra Resources.

<b>Table 6.1 - Data used in study</b>			
<b>Data Type</b>	<b>Source</b>	<b>Description</b>	<b>Uses</b>
Maps and Figures	Quaterra Resources Inc.	Current up to date: geologic maps, personal communications	Geologic parameters, data integration
Digital Images	Joe Lori	Digital images of bench face geology	Displaying: geologic parameters, data integration
Rock Descriptions	Joe Lori	63 samples describing: rock type, alteration, and oxide mineralization	Geologic parameters, alteration assemblages, data integration
ICP/MS 62-element	Quaterra Resources Inc / Joe Lori	Multi-element analysis of: 63 surface samples, 1000 subsurface samples	Geochemical environments, copper pathfinders, data integration
Spectral Reflectance	Joe Lori	Spectral reflectance data of: 52 surface sample spectra, 35 field collected spectra	Alteration, mineralogy, grade control, data integration
Fracture Density	Joe Lori	99 bench face interval fracture density measurements	Fracture orientation, fracture mineralization, data integration

Rock description data type consists of 63 samples described using a binocular microscope in terms of feldspar alteration, mafic alteration, and oxide mineralogy, as shown in table 6.2, a shortened version of a Quaterra Resources standard logging form. Oxide mineralization is

shown as copper oxides (CuOx) and iron oxides (FeOx). All copper produced by means of chemical weathering in the oxide zone of the MacArthur porphyry copper system is referred to as copper oxides (CuOx) regardless of chemical composition; the same rule applies to iron.

Following is a list which defines symbols used in the 63 sample descriptions and UTM locations can be found in Appendix 1.

- #.** Sample ID number
- Bench #.** Column describes bench locations of samples.  
Number indicates the average elevation of each bench floor.
- RX.** Host rock type.  
QM = Quartz Monzonite, GD = Monzodiorite, RHY = Rhyolite,  
AND = Andesite, QMPH = Quartz Monzonite Hornblende Porphyry,  
QMPb = Quartz Monzonite Biotite Porphyry
- 2d Kf.** Column describes replacement of primary plagioclase by secondary k-feldspar.  
This indicates potassic alteration.  
W=weak, M=moderate, S=strong
- 2d Plag.** Column describes replacement of primary plagioclase and K-feldspar by secondary oligoclase or albite. This indicates sodic alteration.  
W=weak, M=moderate, S=strong
- 2d bi/hb.** Column describes alteration of mafic minerals to secondary biotite.  
W=weak, M=moderate, S=strong
- mf alt.** Column describes alteration of any mafics (primary or secondary) to chlorite, sericite or other late alteration minerals.  
F=fresh, PC=partial to chlorite, DC=destroyed to chlorite, PS=partial to sericite, DS=destroyed to sericite
- CuOx.** Column describes CuOx mineralization.  
B=black (neotocite), G= green (malachite and chrysocolla), BL=blue (azurite)
- int.** Column describes strength of CuOx mineralization.  
T=trace, W=weak, M=moderate, S=strong
- oc.** Column describes occurrence of CuOx mineralization.  
FX=fracture control, D=disseminated, C=coating
- FeOx.** Column describes FeOx mineralization.  
G=goethite, H=hematite, J=jarosite
- int.** Column describes strength of FeOx mineralization.  
T=trace, W=weak, M=moderate, S=strong
- oc.** Column describes occurrence of FeOx mineralization.  
T=transported, F=filled sulfide cavities, P=partially filled sulfide cavities, E=empty sulfide cavities
- GL.** Column describes presence of glass limonite.  
W=weak, M=moderate, S=strong

**Table 6.2.** Descriptions of surface samples collected in the MacArthur pit. This table is a shortened version of Quaterra Resources standard logging form.

<b>Table 6.2 - Rock Descriptions</b>														
#	Bench #	RX	2d Kf	2d Plag	Fd alt	2d bi/hb	mf alt	CuOx	int	oc	FeOx	int	oc	GL
1	4730	QM			F	W	PC F				GH	S	TP	
2	4730	QM			F	W	PC F				GH	S	TP	
3	4730	QM			F	W	PC F	B	W	C	GH	M	TP	
4	4730	QM			F	W	PC F				GH	M	TP	
5	4730													
6	4600	QMPH		M	F		PC DC	G	M	D FX	G	T	T	
7	4600	QMPH		M	F		PC DC	G	M	D FX	G	T	T	
8	4600	QM		S	F		DC DS	G	W	D	G	T	T	
9	4600	QM		S	F		DC DS	G	W	D	G	T	T	
10	4730													
11	4730													
12	4730													
17	4600	GGE												
19	4675	QM		M	F	M	DS	G BL	S	D FX	G	W	T	
21	4700	QMPH		M	F	M	PC F	G	M	C	G	W	TF	
22	4780	QM			F	W	F PC	G B	W	D	G	M	TF	
26	4800	QMPb			F		DS DC				GH	S	TE	
27	4800	QM			F		PC PS	G B	T	FX C	G	W	TF	
28	4600	GGE												
29	4780	QMPb			F		DS PC				G	W	TE	
30	4675	QM		M	F	M	DS	G BL	S	D	G	T	T	
31	4700	QM		M	P	W	DS PC	G	W	D	G	T	TF	
32	4700	QM		M	P	W	DS PC	B	W	C	G	T	TF	
33	4800	QMPb			F		DC DS	B	T	FX	GH	M	TE	
38	4800	QM			F	W	PC PS				GH	M	TP	
39	4800	QMPb			F	W	PS PC	G	T	D	G	W	TP	
40	4800	QM		M	F		DS PC				G	M	TP	
41	4800	QM			F	W	PC PS	B	T	C	GH	M	TP	W
42	4800	QM			F	W	PC PS				G	W	TP	
43	4800	QM			F	W	PC PS	B	T	C	G	W	TP	

**Table 6.2.** (cont.) Descriptions of surface samples collected in the MacArthur pit.

<b>Table 6.2 cont. - Rock Descriptions</b>														
#	Bench #	RX	2d Kf	2d Plag	Fd alt	2d bi/hb	mf alt	CuOx	int	oc	FeOx	int	oc	GL
44	4800	QM			F	W	PC PS	B	T	C	GH	M	TP	
45	4780	QM			F	M	PS F				G	M	TF	
46	4780	QM	M		F	W	PS PC	G B BL	S	D FX	GJ	M	TP	
47	4780	QM	W		F		PS PC	B G	W	D C	GJ	M	TP	
48	4780	QM			F	W	PC PS				GH	M	TP	W
49	4780	QMPb			F		PS PC	B	M	C	GH	M	TP	
51	4750	QM			F		PC PS				GH	M	TF	
52	4750	QM			F		PC PS	B	T	C	GH	M	T	
53	4750	QM			F	W	PC F				G	W	T	
54	4750	QM			F		PC				G	T	F	
55	4750	QMPb			F		PC				GH	M	TF	
56	4750	QMPb			F		PC				GH	M	TP	
57	4600	QM		M	F	W	PC DC	G BL B	S	D FX	G	T	T	
58	4600	QM		S	F		PC DC	G B	W	D C	G	T	T	
59	4600	QM		W	F	W	PC PS	B	W	C	GH	S	TP	
60	4600	QM		M	P	W	PC DC	B G	S	C D	G	M	T	
61	4600	QM		W	F	W	PC DC	G	W	D	GH	M	TP	
62	4600	QM		S	F		PC DC	G B BL	S	D C	GH	M	T	
63	4600	QM		W	F	W	PC	B	T	C	GH	M	TP	
64	4600	QM		S	F		DC DS	G	T	D	G	T	T	
65	4630	QM		W	F	W	PS DS	B G	W	C D	G	W	T	
66	4630	QM		W	F	W	PC DC				GH	M	T	
67	4700	QM		M	P		DS				GH	M	TF	
68	4700	QM		M	P		DS	B	W	C	G	M	TP	
69	4700	RHY			F		DS	G B	S	D C	G	T	T	
70	4700	AND			F		DS				G	M	T	
71	4700	AND			F		PC				G	W	T	
72	4700	QMPh			F		PC F	G	T	D	G	W	TP	
73	4675	QM		W	F	W	PS F	G	T	D	GH	M	TF	
74	4675	QMPh		W	F		PS DS	B	T	C				
75	4675	QMPh		W	F		PS DS	B	T	C	GH	M	TP	

## 7. METHODS

This project utilizes four major methods of study: (1) Rock alteration descriptions, (2) Geochemistry, (3) Spectral Radiometry, and (4) Fracture Density. A complete, detailed explanation of methods for 2, 3, and 4 are found in the corresponding chapters.

(1) Rock descriptions are used to strengthen interpretations regarding geochemistry, spectral radiometry, and fracture density data. A total of 63 samples were collected in the geologic units exposed in the MacArthur bench faces (Figure 7.1) and represent the basis for much of this study. Table 6.2 describes rock type, alteration, and oxide mineralization associated with each sample.

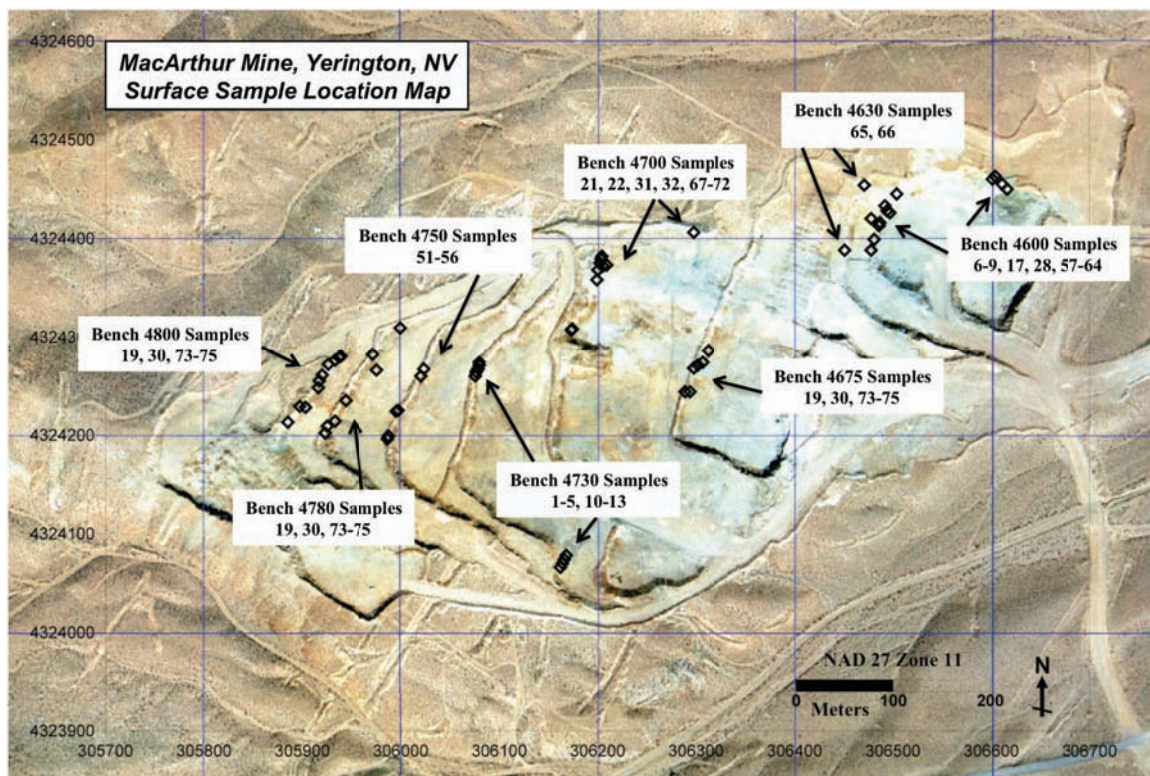


**Figure 7.1.** Surface sample locations. UTM location data can be found in Appendix 2.2.

(2) Geochemistry is used in this study to understand geochemical environments associated with the oxide zone at the MacArthur pit. Geochemical data consist of a multi-element ICP/MS analysis for 63 surface samples and 1000 samples from thirteen diamond core drill holes in the MacArthur pit. Data are analyzed using univariate, bivariate, and multivariate statistical methods.

(3) Spectral radiometry is used for the identification of minerals in the oxide zone, thus interpreting alteration assemblages. Spectral reflectance was measured for each of the surface rock samples in the lab and a field test was performed to test for homogeneity of oxide mineralization. Spectral reflectance data of surface rock samples is also used to investigate relationships between spectral reflectance and percent Cu as a new method of grade control in oxidized sections.

(4) A total of 99 bench interval fracture density measurements were collected along the MacArthur bench faces to determine fracture orientation and density. Density measurements were collected on 25-foot centers in the MacArthur documenting fracture orientation strength and transported oxide occurrences in fractures. Variables collected in density measurements are analyzed using stereonet, bar charts displaying percent Cu and Fe in fractures, and pie graphs to display percent mineralization per fracture orientation. Bivariate and multivariate statistical analyses are also used to test for relationships between oxide occurrences and fracture orientation.

## **8. GEOCHEMISTRY AND STATISTICAL ANALYSES**

### **8.1. Introduction**

Statistical analysis and interpretation of geochemical data are the primary focus of this chapter. Data are analyzed in an effort to understand primary source rock and oxide enriched host-rock distribution at the MacArthur pit. The development of oxide assemblages (Fe & Cu) in the geochemical environment of the leaching zone is a function of primary source-rock and host-rock mineralogy (Chavez, 1990). A statistical analysis of geochemical data is used to recognize geochemical patterns and anomalies related to mineralization (Rose 1979, Levinson 1974, Zumlot, 2006). Statistical analysis in this chapter includes univariate, bivariate and multivariate methods, which indicate deviation from normality, correlations between two elements, and multi-element correlation families respectively. Statistical analyses also aid in the identification of geochemical families. The ultimate goal of these geochemical analyses is to relate grade control to physical and chemical characteristics of exposed faces.

### **8.2. Data**

Two major data families are used for this study. Geochemical data includes (1) surface samples collected from vertical bench faces, (2) subsurface samples from the “QMT” diamond core drill hole series.

(1) A geochemical data set from 63 surface samples (Fig. 7.1) was collected within the MacArthur pit; rock and fault gouge samples are represented. Actlabs analyzed samples for 62 elements and results are shown in Appendix 1. Also shown in Appendix 1 is data from a single sample of pure neotocite (sample # 99). This sample will be discussed in final interpretations.

(2) The second data set comes from subsurface samples and includes 13 diamond core drill holes labeled, QMT-1 – QMT-13, completed in 2006. Figure 8.1 also shows location and total depth (TD) of each of the drill holes. Sample analyses was commissioned by Quaterra Resources for the 13 drill holes and analyzed for 62 elements in five foot sections totaling 1000 samples. This original data set is displayed in Appendix 1. Field collection and processing methods are as follows.

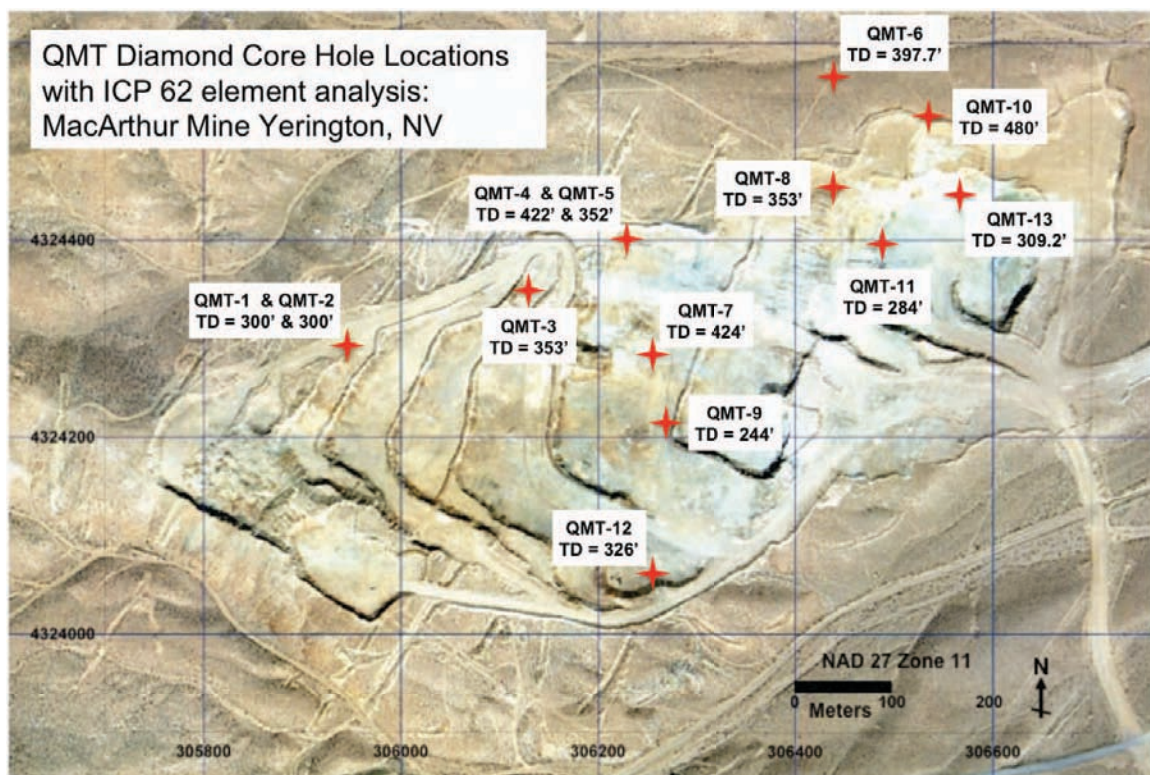


**Figure 8.1.** Location of drill holes in and near the MacArthur pit with multi-element analysis commissioned by Quaterra Resources Inc.

### 8.2.1. Field Methods

Field methods describe surface sample data set (1), data set (2) is provided by Quaterra Resources. A total of 63 samples were collected along the bench faces of the MacArthur pit to determine oxide mineralogy (Fe and Cu families) and alteration zones (Fig. 3.5). These samples

may be subdivided into families as either whole rock or fault gouge samples. Fault gouge samples were collected in order to help understand what elements were mobile during hydrothermal/oxidation phase(s), as faulting at the MacArthur provided conduits for fluid movement and element enrichment based on observations of drill cuttings. Some fault gouge samples will not be found in rock descriptions (Table 6.2) due to the absence of an identifiable hard rock host. Samples were collected in each lithology to thoroughly investigate oxide mineralogy, sulfide mineralogy and alteration types. These descriptions are found in Table 8.1. Surface samples represent oxide zone mineralogy.

### **8.3. Processing**

Surface sample geochemical data, analyzed by Actlabs (<http://www.actlabs.com/>), was completed using aqua regia extraction ICP/ICP-MS ultra-trace II method. Table 8.1 shows the elements reported, analytical method, and detection limits of this technique. The first step in data processing was the complete removal of elements below the detection limit and those that showed little to no variation. These elements provide limited to no information in statistical analysis.

Elements removed from the surface data set include: Au, Bi, Ge, Hf, In, Lu, Nb, Pb, Re, Ta, Te, Tl, Tm, and W. Elements removed from the subsurface data set include: B, Bi, Br, Cd, Cs, Ge, Hf, Hg, Ho, I, In, Ir, Os, Pd, Pt, Re, Rh, Ru, Sb, Ta, and Tb. Table 8.2 shows a list of elements from the surface sample data set used in this study, and Table 8.3 shows the subsurface elements.

**Table 8.1.** Actlabs Code Ultratrace-2 Elements and Detection Limits (ppm) Note:

\* May not be total. Unaltered silicates and resistates may not be dissolved.

Element	Detection Limit	Upper Limit	Reported By
Ag*	0.002	50	ICP/MS
Al*	0.01%	10%	ICP/MS
As*	0.1	10,000	ICP/MS
Au*	0.5 ppb	10,000 ppb	ICP/MS
B*	1	5,000	ICP/MS
Ba*	0.5	6,000	ICP/MS
Be*	0.1	1,000	ICP/MS
Bi	0.02	2,000	ICP/MS
Ca*	0.01%	50%	ICP/MS
Cd	0.01	-	ICP/MS
Ce*	0.01	10,000	ICP/MS
Co	0.1	5,000	ICP/MS
Cr*	0.5	5,000	ICP/MS
Cs*	0.02	-	ICP/MS
Cu	0.01	10,000	ICP/MS
Dy	0.1	-	ICP/MS
Er	0.1	-	ICP/MS
Eu*	0.1	-	ICP/MS
Fe*	0.01%	50%	ICP/MS
Ga*	0.02	500	ICP/MS
Ge*	0.1	500	ICP/MS
Gd	0.1	-	ICP/MS
Hf*	0.1	500	ICP/MS
Ho	0.1	-	ICP/MS
In	0.02	-	ICP/MS
K*	0.01%	5%	ICP/MS
La*	0.5	1,000	ICP/MS
Li	0.1	-	ICP/MS
Lu*	0.1	100	ICP/MS
Mg*	0.01%	10%	ICP/MS
Mn*	1	10,000	ICP/MS

Element	Detection Limit	Upper Limit	Reported By
Mo	0.01	10,000	ICP/MS
Na*	0.001%	5%	ICP/MS
Nb*	0.1	500	ICP/MS
Nd*	0.02	-	ICP/MS
Ni*	0.1	10,000	ICP/MS
P	0.001%	10%	ICP
Pb*	0.01	10,000	ICP/MS
Pr	0.1	-	ICP/MS
Rb*	0.1	500	ICP/MS
Re	0.001	100	ICP/MS
S	0.001%	20%	ICP
Sb	0.02	500	ICP/MS
Sc	0.1	-	IPC/MS
Se*	0.1	10,000	ICP/MS
Sm*	0.1	100	ICP/MS
Sn*	0.05	200	ICP/MS
Sr*	0.5	1,000	ICP/MS
Ta*	0.05	50	ICP/MS
Tb*	0.1	100	ICP/MS
Te	0.02	500	ICP/MS
Th*	0.1	200	ICP/MS
Ti*	0.01%	20%	ICP
Tl*	0.02	500	ICP/MS
Tm	0.1	-	IPC/MS
U*	0.1	10,000	ICP/MS
V*	1	1,000	ICP/MS
W*	0.1	200	ICP/MS
Y*	0.01	-	ICP/MS
Yb*	0.1	200	ICP/MS
Zn*	0.1	5,000	ICP/MS
Zr*	0.1	5,000	ICP/MS

**Table 8.2.** Elements used in surface analysis. Surface data set is 63 samples.

<b>Table 8.2</b> <b>Elements used in Surface Study</b>
<b>Ag, Al, As, B, Ba, Be, Ca, Cd, Ce, Co, Cr, Cs, Cu, Dy, Er, Eu, Fe, Ga, Gd, Ho, K, La, Li, Mg, Mn, Mo, Na, Nd, Ni, P, Pr, Rb, S, Sb, Sc, Se, Sm, Sn, Sr, Tb, Th, Ti, U, V, Y, Yb, Zn, Zr</b>

**Table 8.3.** Elements used in subsurface analysis. Subsurface data set is 1000 samples.

<b>Table 8.3</b> <b>Elements used in Subsurface Study</b>
<b>Ag, Al, As, Au, Ba, Be, Ca, Ce, Co, Cr, Cu, CuOx, Dy, Er, Eu, Fe, Ga, Gd, K, La, Li, Lu, Mg, Mn, Mo, Na, Nd, Ni, P, Pb, Pr, Rb, S, Sc, Se, Si, Sm, Sn, Sr, Te, Th, Ti, Tl, Tm, U, V, W, Y, Yb, Zn, Zr</b>

## 8.4. Analysis

All data are analyzed using JMP<sup>®</sup> V.4 (<http://www.jmp.com/index.shtml>) software and methods include descriptive statistics, univariate, bivariate, and multivariate analyses. Contour maps showing element abundance for the surface data are created using Surfer by Golden Software (<http://www.goldensoftware.com/>). Data for the following statistical methods will be displayed in the results section.

### 8.4.1. Descriptive Statistics

Descriptive statistics for this study include (1) percentiles, (2), median, (3) mean, (4) standard deviation, (5) skewness, and (6) kurtosis. A brief discussion of each follows and is taken from JMP<sup>®</sup> V.4 help directory and user guide as well as Davis (2002).

- (1) Percentile is based on a scale of one hundred that shows the percent of a distribution that is equal to or below it. The 25<sup>th</sup> percentile is called the 1<sup>st</sup> quartile, 50<sup>th</sup> percentile is the median, and the 75<sup>th</sup> percentile is called the 3<sup>rd</sup> quartile.
- (2) Median reflects the middle value where 50% of the data is greater than and 50% of the data is less than the middle value.
- (3) Mean indicates the average value of a set of data. It is calculated by summing all data points for a particular variable and dividing by the number of values.
- (4) Standard deviation is a measure of dispersion around the mean value. It shows how much variation there is around the mean value using a numerical value. Low values indicate the standard deviation to be close to the mean while large values indicate data is spread out or deviates from the mean value.
- (5) Skewness is a measure of asymmetry of the distribution shape. Skewness can be positive, negative, or undefined.
- (6) Kurtosis is a measure of peakedness of the distribution shape. High kurtosis indicates variance is the result of large deviations.

#### **8.4.2. Univariate Analysis**

Univariate analyses for this study result in (1) histograms, (2) normal quantile plots, and (3) outlier box plots (Fig. 3). Data is represented in graphs, and groups of these graphs for each element are developed for (1.1) raw data, (1.2) outliers removed data, and (1.3) log transformed data with no outliers. The following descriptions of statistical analyses are from JMP<sup>®</sup> V.4 help directory and users guide as well as Davis (2002).

(1) The use of the histogram is a way to display frequency distributions divided into classes. The frequency of each class is what determines the shape of the curve. Data with normal distribution will have a symmetric bell curve while a curve with a tail to the right indicates the data is positively skewed. Figure 8.2 shows an example of a positively skewed histogram for aluminum from surface data.

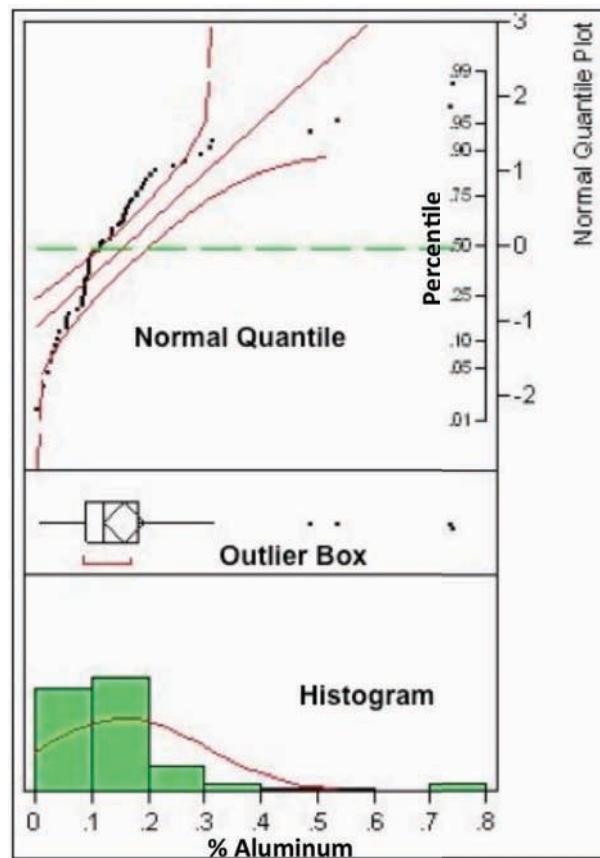


**Figure 8.2.** Histogram, outlier box plot, and normal quantile plot for aluminum. X-axis values are % Al and y-axis is percentile.

(2) Normal quantile plots are graphs used to show interval variables. Data that is close to normal distribution will plot as a straight diagonal line along the y- and x-axis. Changes in the slope of this line represent interval variables and can be related to geochemical families. Figure 8.2 shows a quantile plot of aluminum deviated from normality.

(3). The outlier box is a method of showing element distribution with anomalous values located outside the whiskers connected to the box plot, the outliers. Outliers can be positive or negative. The box contains data that falls within the 25<sup>th</sup> and 75<sup>th</sup> percentile and the vertical line in the box represents the median. Figure 8.2 shows an outlier box for aluminum and dots to the right of the whiskers are outlier data.

(1.1) The first step in analysis of the raw data is in the form of tables and graphs consisting of histograms, normal quantile plots and outlier box plots. Figure 8.3 shows the results of this first step for calcium from surface data.

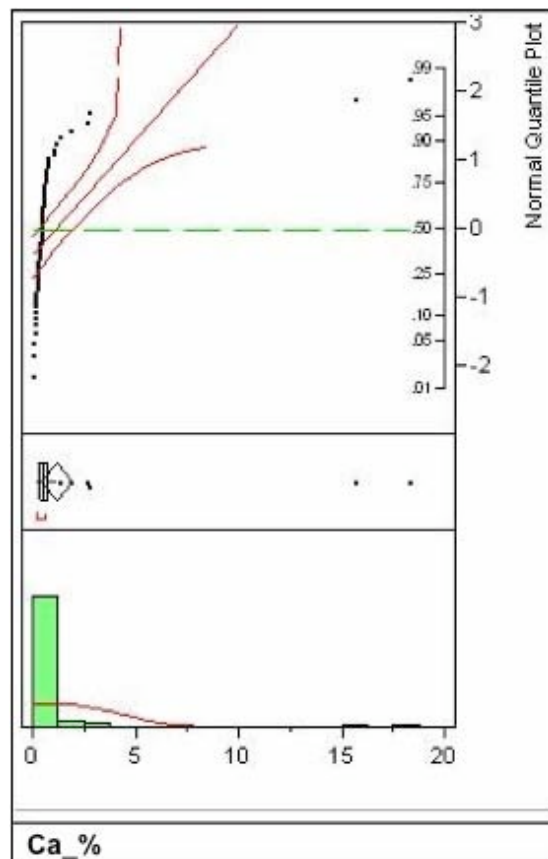


**Figure 8.3.** Raw data univariate analysis for % Ca. Histogram shows positive skewed data with anomalous values to the far right of the box plot.

Concentrations of anomalous high values are reflected in the histograms with data concentrated to the left. These anomalous values are visualized past a specific concentration and are located outside the whiskers in box plots. These are identified as outliers and may be regarded as evidence of mineralization processes (Zumlot, 2006). The normal quantile diagrams show the most deviation from normality at the highest values located on the right side of the normal distribution line. Normal quantile diagrams also provide useful information on populations or geochemical families identified by changes in slope for the elements.

(1.2) The next step was to remove the outliers from the data set and repeat the analysis for histograms and normal quantile plots. Figure 8.4 shows the result of this for calcium.

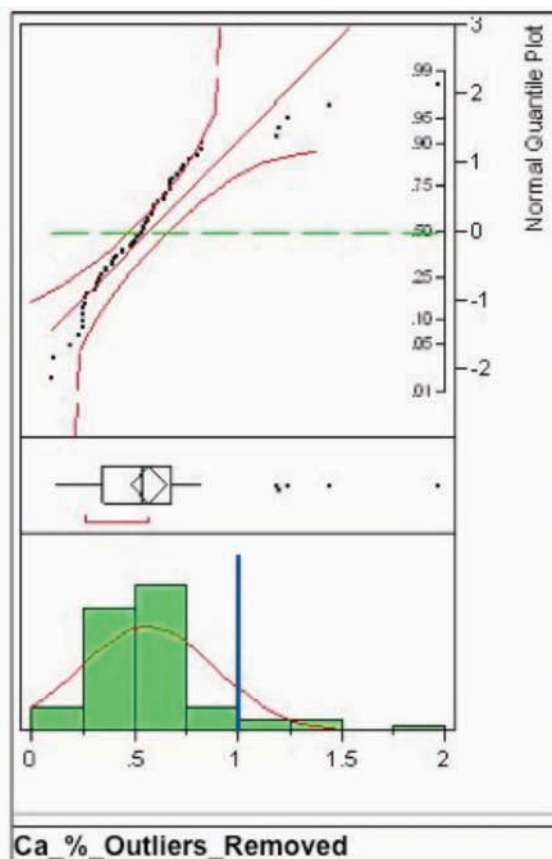


**Figure 8.4.** Outlier removed univariate analysis for % Ca. Histogram shows data is closer to normality with a close to symmetric bell curve and data points that are closer to the diagonal axis of the quantile plot.

Outliers are removed in statistical analysis to avoid distortion in data concerning the original geochemical background values (Shuyun, X., *et al.*, 2008). As a comparison for normality conditions in element concentrations, average elemental concentrations (Mason, B., and Moore, C.B., 1982) of granitic rocks in the earth's crust are imposed as blue lines on the raw data or outlier removed histograms as seen in Figure 8.4. The results of this will be discussed later.

(1.3) The final step for univariate analysis is to log-transform the data. Log-transformed geochemical data more readily behaves closer to normality conditions. An example of this can be seen in Figure 8.5 showing calcium close to normal conditions.

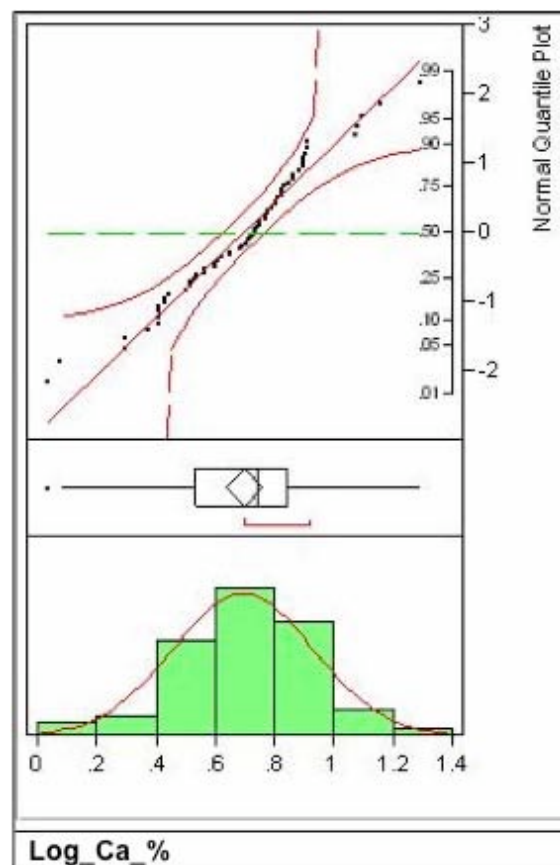


**Figure 8.5.** Log data univariate analysis for % Ca. Histogram and normal quantile shows data is close to normality conditions.

Data becomes easier to visualize and interpret because it corrects skewness in the data. The end result is symmetric bell curves on histograms and s-shape curves for many elements in normal quantile plots. The changes in slope in the log-transformed quantile plots again are a result from the several geochemical families and their identification may prove to be a challenge.

#### **8.4.3. Bivariate Analysis**

Bivariate analyses for this study are (1) correlation coefficient matrix, (2) correlation scatter plot, and (3) pairwise correlations. A brief description of each follows and comes from the JMP<sup>®</sup> V.4 help directory and users guide as well as Davis (2002).

(1) The correlation coefficient (Appendix 2) is a way to test for linear relationships between a pair of variables. Elements are arranged in a matrix so they are listed on both rows and columns and the relationship (coefficient) is displayed as a value. A diagonal row of 1's indicates where the element is analyzed against itself. In strong relationships, values tend towards 1 and -1, positive and negative, while weak correlations tend towards zero. This result determines which elements behave the same.

(2) The correlation scatter plot is a graphical way to visualize correlations between two variables. Figure 8.6 is a small selection of elements present in the matrix.

Data are displayed in a matrix arrangement with an imposed 95% bivariate density ellipse. This means 95% of data fall within this ellipse. When ellipses are compressed along the diagonal axis, it represents a positive correlation between two variables. If the ellipse is large and round or not diagonally oriented, correlation does not exist between the variables.

(3) The pairwise correlation (Fig 8.7) is another way to view correlations between two variables based on the correlation coefficient. In this method, data is displayed on a bar chart with correlations trending towards 1 and -1 and weak correlations trending toward zero.

Correlations							
	Al	Cu	Fe	Mg	Ni	U	V
Al	1.0000	0.3898	0.6765	0.7824	0.5200	0.1388	0.6690
Cu	0.3898	1.0000	0.1383	0.4285	0.7347	0.6280	0.3430
Fe	0.6765	0.1383	1.0000	0.5584	0.2447	-0.0031	0.6931
Mg	0.7824	0.4285	0.5584	1.0000	0.6761	0.1756	0.7256
Ni	0.5200	0.7347	0.2447	0.6761	1.0000	0.4021	0.5612
U	0.1388	0.6280	-0.0031	0.1756	0.4021	1.0000	0.2221
V	0.6690	0.3430	0.6931	0.7256	0.5612	0.2221	1.0000

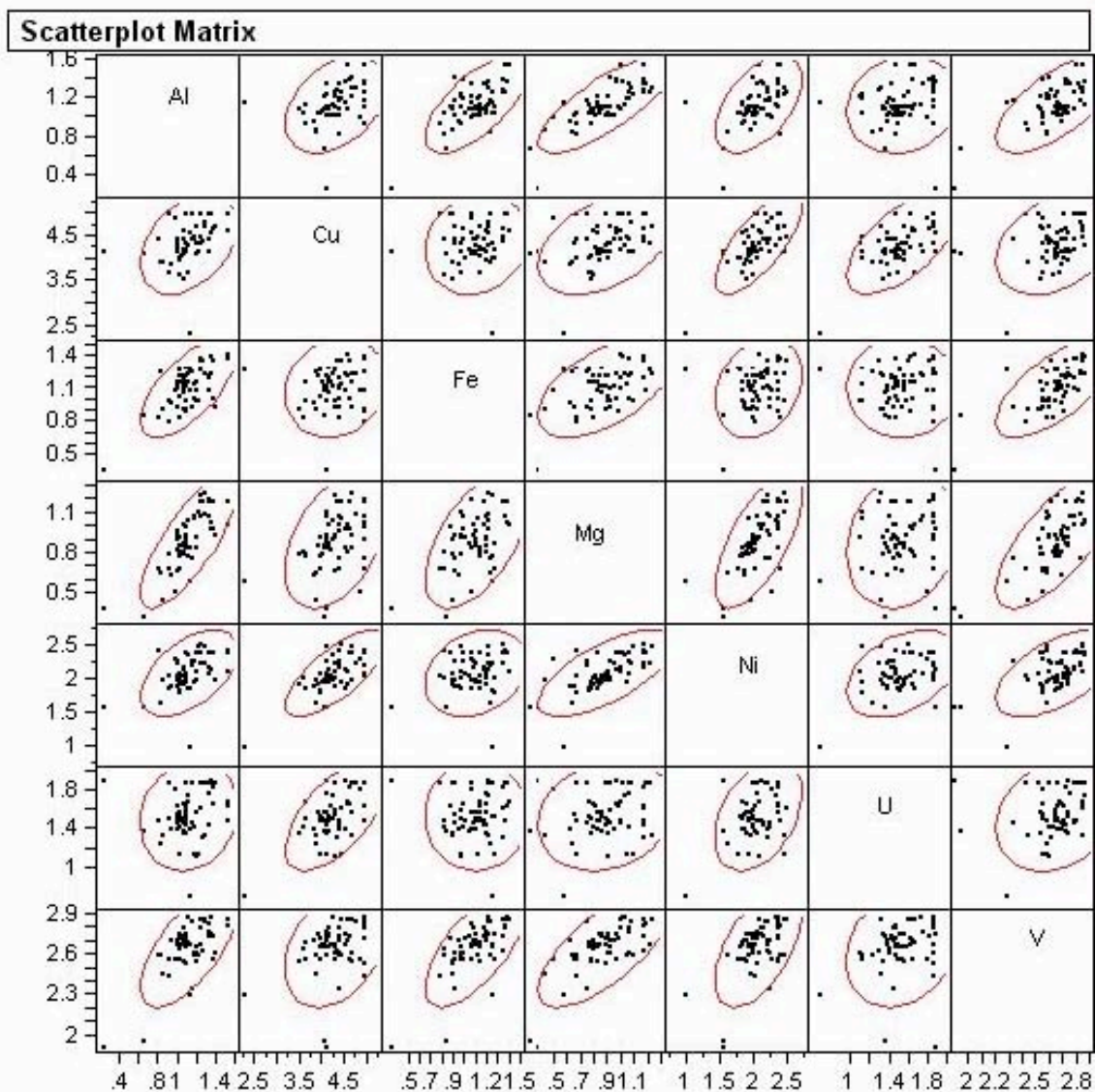


**Figure 8.6.** A section of the scatter plot from surface data showing Al, Cu, Fe, Mg, Ni, U, and V. The strongest correlation here is seen between Al and Mg (0.782), followed closely by Cu and Ni (0.735). The x and y-axis indicate data ranges for the element listed in box. A correlation score is seen in the correlation matrix above the scatter matrix.

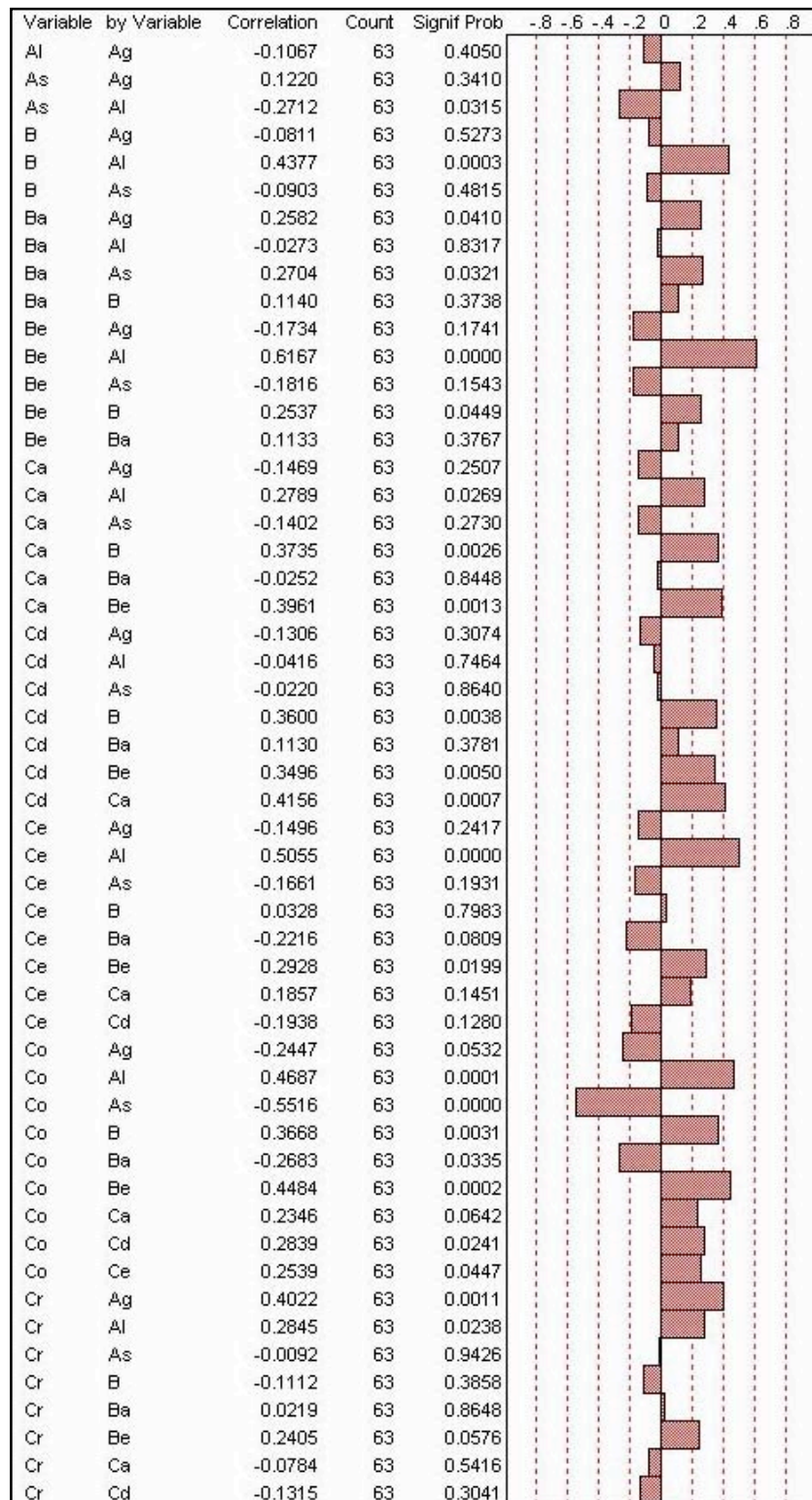


**Figure 8.7.** Pairwise correlations of surface data. A positive correlation with a score of 0.6 is seen between Al and Be and a negative correlation with a score of -0.53 is seen between Co and As.

Before the data is processed for bivariate analyses, the outlier values removed from the original data input are replaced. Missing outliers are replaced with a value from the 95<sup>th</sup> percentile for high outliers and 5th percentile for low outliers. This method of data replacement maintains the closest representation of the original data. Because the bivariate method analyses compares variable by variable in a linear fashion, missing data points cannot be present in the data set (JMP<sup>®</sup> V.4 directory). Bivariate analysis is performed using log-transformed data because it is used to test for normality and log-transformed data behave closer to normality conditions.

#### **8.4.4. Multivariate Analysis**

Principal component analysis (PCA) is used as the multivariate analysis for this study. The following discussion is from JMP<sup>®</sup> V.4 help directory and users guide as well as Darlington, R.B., (1997). Multivariate analysis is performed using the log-transformed data set because principal components are calculated by linear combinations of an eigenvector of the correlation matrix with a standardized original variable (JMP<sup>®</sup> V.4 directory). PCA seeks a linear combination of variables such that the maximum variance is extracted from the variables. It then removes this variance and seeks a second linear combination, which explains the maximum proportion of the remaining variance, and so on. This is called the principal axis method and results in orthogonal (uncorrelated) factors (<http://en.wikipedia.org>). The result of this calculation is “Factors,” a way to view positive and negative relationships or commonalities between a set of elements. The factors reflect a geochemical family of elements that can lead to a statement regarding a single geologic process. Factors are represented first in a matrix, then in a bar chart and factors with coefficients greater than 0.2 are interpreted to be part of the factor. Figure 8.8 shows an example of a factor graph.

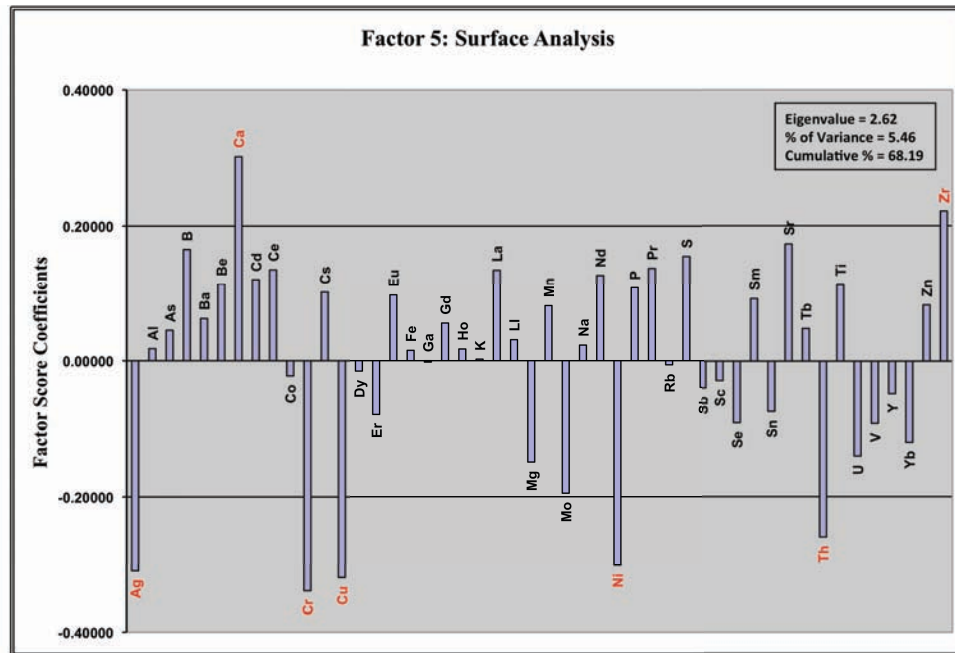


**Figure 8.8.** Surface analysis factor 5. This figure shows a relationship between Ca and Zr, and between Ag, Cr, Cu, Ni, and Th. The positive and negative elements have a negative relationship with each other.

#### 8.4.5. Spatial Analysis

Spatial analyses consist of (1) spatial distribution of elements and (2) spatial distribution of factor scores. Spatial analysis is only used for the surface samples since it describes patterns and distributions of surface data.

(1) Spatial distribution of the elements documents where concentrations of relevant elements are located in the MacArthur pit and how they spatially correlate with other elements. Spatial distribution is in the form of contour maps showing concentrations in ppm and %. The contour maps were created using the original data set and with the outliers removed. Most contour maps shown in this study are from the original data, and only when extreme values made the contours close to a solid color are outlier-removed contours shown. Figure 8.9 is an example contour of spatial distribution of Cu.

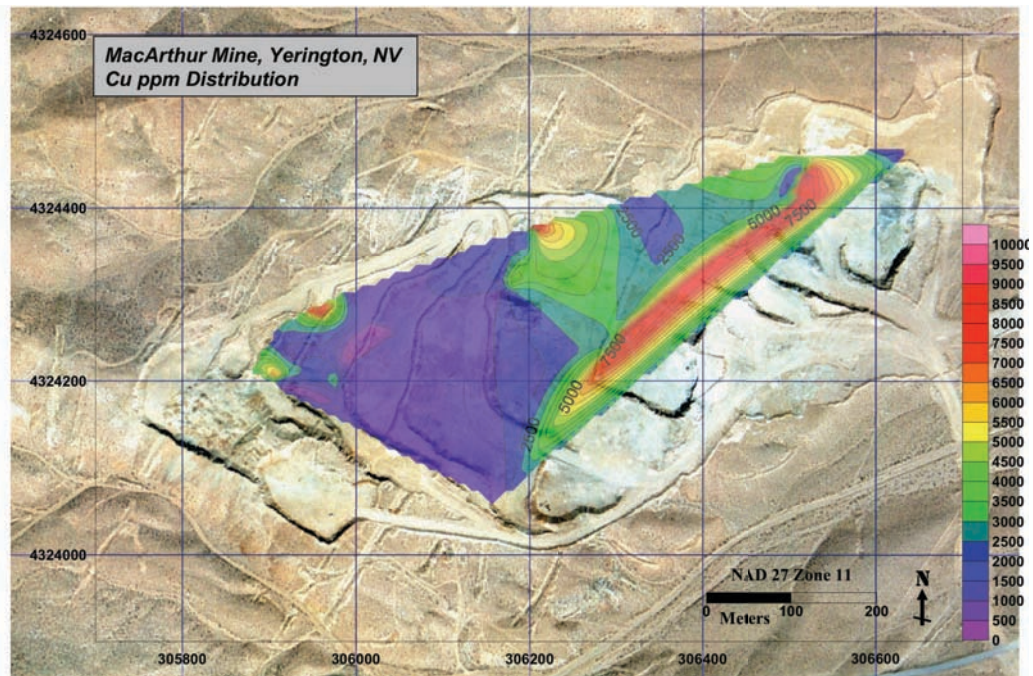


Figure 8.9. Contour map of surface Cu abundance at the MacArthur Mine.

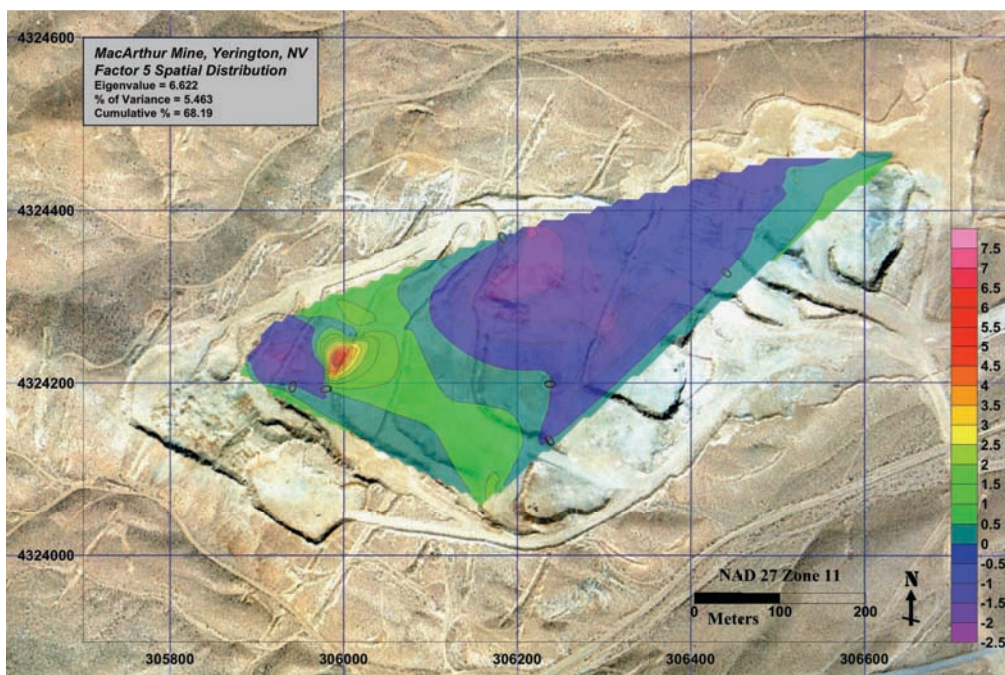


Figure 8.10. Spatial distribution of factor 5 at the Macarthur Mine.

(2) Spatial distribution of factor score coefficients is used to document where in the MacArthur pit geochemical families identified in factors scores are present (Fig. 8.10). Since the factors will be interpreted as geochemical events, a temporal evolution of such events may be established.

## **8.5. Results**

The results of statistical analyses and spatial analyses are presented in this section.

A complete list of elements used in this study for the surface and subsurface can be found in Table 6.1 and 6.2 respectively. Surface data consists of 63 samples and statistical analyses may not be traditionally carried out on populations this small. The analyses of the subsurface data of 1000 samples is used to help interpret and support the results of the same analyses performed to the surface data.

### **8.5.1. Univariate**

Histograms for all elements used in this study are shown in Appendix 2. These figures show, from left to right, raw data, outlier removed data, and log-transformed data. The red bell curves on the histograms show most elements approach a log-normal distribution. The exceptions to log-normal distributions show normal distributions for outlier-removed data but never for raw data. These elements include Ba, Cr, Ga, Gd, La, P, Pr, Sm, and V.

Raw data histograms show frequency distributions for every element except Th to be positively skewed. Th is shown to be negatively skewed by a longer tail on the bell curve to the left of raw, outlier removed, and log-transformed data. This is due to Th having more frequencies of high values compared to low values, without producing outliers.

Outliers are seen in the raw data represented by dots to the left and right (lower and upper) of the whiskers attached to the box plots (Appendix 2). The box plots of positively skewed raw data include some very high values for elements like As, Ca, Co, Cr, Gd, Li, Mn,

Mo, Ni, Sr, U, Y, and Zn. These extreme values appear to be separated from the majority of the samples and may be interpreted as evidence of mineralization at the MacArthur and may serve as pathfinder elements.

Normal quantile diagrams are also shown in Appendix 2. Raw data quantile plots support raw data histograms by showing the majority of the data on the left side of the diagonal axis, while extreme high values are visualized to far right of the diagonal axis. These plots show that most elements depart from normality at these high values, or in the mineralization process. Due to the steepness and sudden changes in slopes of many of these lines, it is hard to make statements concerning geochemical families.

The log-transformed quantile plots show that most elements approach a log-normal distribution. These elements are in exact correlation with histograms and are visualized by data points tightly clustered along the diagonal axis. Some quantile plots show repetitive concentration values for elements represented by vertically stacked values along the diagonal axis. This is especially true for rare earth elements (REE's), and is due to the precession and accuracy of analytical methods. For most elements log-transformed quantile plots show values approaching an S-shaped curve along the diagonal axis. This is very helpful in determining geochemical families. In the case of iron (Fe), at least five changes in slope can be identified. Five different mineral families containing iron can represent this in the MacArthur pit: iron oxides, iron sulfides, mica group, hornblende group, and iron rich alteration clay minerals found in fault gouge.

### 8.5.2. Bivariate

Bivariate analyses used in this study comprise of correlation coefficients, correlation scatter plots, and pairwise correlation. Bivariate analyses are performed using log-transformed data with no outliers. The log-transformed data set is used because most elements show close approach to normality, which is required for correlation analyses. Due to the lack of precision in analytical methods, rare earth elements are highly correlated with each other in both data sets.

The correlation coefficient matrix for surface and subsurface samples is shown in Appendix 2. The correlation matrix shows a total of 48 variables for surface samples and 52 variables for subsurface samples. This matrix reports a value between 1 and -1 describing positive and negative relationships between two variables or elements. Generally correlation interpretations state that correlations less than 0.3 are weak, between 0.3 and 0.7 are moderate, and those above 0.7 are considered highly correlative ([www.visualstatistics.net](http://www.visualstatistics.net)). Besides showing relationships between two elements, detailed analysis of correlation matrices can give us correlation frequencies.

Correlation frequencies display a variety of element associations. Correlation frequencies are considered high when elements correlate with 10 or more other elements. The results for surface data are displayed in Table 8.4 and subsurface data is displayed in Table 8.5. Frequencies are shown for elements that correlate with 10 or more other elements, those with frequencies between 5-9, those that have correlation frequencies of less than 5, and those that have no correlations. The surface data set uses a correlation coefficient greater than 0.4 and the subsurface data set uses a correlation coefficient greater than 0.35 to be used in correlation frequencies.

**Tables 8.4.** Correlation frequencies of surface data from correlation coefficient scores greater than 0.4.

<b>Table 8.4 - Surface Data: Coefficient Scores &gt; 0.4</b>	
Number of Correlations	Group of Elements
> 10	Al, Be, Co, Cs, Cu, Fe, Ga, Li, Mg, Ni, P, Th, V, Y, Zn, and all REE
5 to 9	B, Cr, Fe, Mn, Rb, Sb, Sn, K
Less than 5	Ag, As, Ba, Ca, Mo, S, Sr, Ti, U, Zr
No Correlations	Cd, Na, Sc, Se

**Tables 8.5.** Correlation frequencies of subsurface data from correlation coefficient scores greater than 0.35.

<b>Table 8.5 - Subsurface Data: Coefficient Scores &gt; 0.35</b>	
Number of Correlations	Group of Elements
> 10	Al, Ba, Be, Ca, Co, Ga, Mg, Rb, Sc, Sr, V, Y, and all REEE
5 to 9	Fe, K, Li, Mn, Th, Ti, Zr
Less than 5	Ag, As, Cr, Cu, CuOx, Lu, Na, Ni, P, S, Se, Si, Sn, Te, U, Zn
No Correlations	Au, Mo, Pb, Tm

A small section of the correlation scatter plot for the surface is shown in Figure 8.6.

Scatter plots (described above) are a graphical way to view the correlation coefficient matrix.

The complete scatter plot matrix can be found in Appendix 2.

The pairwise correlation (Appendix 2, Fig. 8.7) shows correlations for all pair of variables using available data. Pairwise correlations are represented as bar charts and correlations with a score greater than 0.5 and greater than 0.7 are shown in Table 8.6 for surface data and Table 8.7 for subsurface data. All correlations are not shown in this table, however, common correlations that may indicate copper mineralization are displayed. The pairwise correlation shows the same high correlation between the REE suite.

**Table 8.6.** Pairwise correlations from surface data.

<b>Table 8.6 - Pairwise Correlation: Surface Data</b>		
Element	Scores > 0.7	Scores > 0.5
Al	Ga, Dy, Li, Mg	Be, Ce, Cs, Er, Eu, Gd, Ho, V, Zn
K	Rb	Ba, Fe
Cu	Ni	Co, U, Y, Yb
Ni	Cu	V, Y, Yb, Fe
Fe	Ga	K, Rb, V, Mg
Mn	Co	Zn
Mg	Li, V	Cs, Dy, Er, Eu, Fe, Ni, Y, Yb

**Table 8.7.** Pairwise correlations from subsurface data.

<b>Table 8.7 - Pairwise Correlation: Subsurface Data</b>		
Element	Scores > 0.7	Scores > 0.5
Al	Ga, Mg	Ba, Ca, Eu, K, Sc, V
K	Ba	Mg, Rb, Al
Cu	CuOx	
CuOx	Cu	
Fe		Gd
Mn		Co
Mg	Al	Ba, Ga, K, Li, Rb, Sc, V

### 8.5.3. Multivariate

Multivariate analysis for this study consists of a principal component analysis (PCA). Eight principal components (PCs) are used with eigenvalues larger than 1 to help understand geochemical families at the MacArthur pit. The eight surface sample factors describe 79.01% of the total variance while the eight subsurface factors describe 61.4% of the total variance. PCA results are shown as data, graphs and tables. Table 8.8 shows the factor score coefficients from PCA analysis for surface data and Table 8.9 for subsurface data. Bar charts (Appendix 2) show elements that are associated with each factor and Tables 8.10 and 8.11 describe geochemical families for surface and subsurface factors respectively. The following discussion uses Rose, (1979) and Levinson, (1974) as a basis for geologic/geochemical environments.

*Surface factor 1* accounts for 35.14% of the total variance and includes Al, Y and REE. This group can be described as a heavy and light rare earth factor with a clay component. REE are likely a strong factor due to stability of rare earth bearing minerals.

*Subsurface factor 1* accounts for 23.16% of the total variance and includes Al, Dy, Eu, Ga, Sc, V, and Y. Al and Ga have a general association in plutonic rocks. The subfamily Sc and V is representative of mafic igneous rocks but is considered unexplained at the MacArthur pit. Subsurface factor 1 is very similar to surface factor 1 and represents a rare earth factor with a clay component.

*Surface factor 2* accounts for 11.33% of the total variance and includes high loadings of K and Rb with weaker As, Ba, Fe, Se, Sn, Sr, and Ti. This factor includes a potassium feldspar signature containing K, Ba, and Rb and weak epithermal influence containing As and Se.

*Subsurface factor 2* accounts for 8.61% of the total variance and includes positive correlations between Ag, Li, Pr, Rb, and Th and negative correlations with Er, Gd, and Lu. This factor is best interpreted the same as surface factor 2.

*Surface factor 3* accounts for 9.27% of the total variance and includes positive correlations between B, Cd, Cs, and S and negative correlations between Ce, La, Pr, Sn, and Ti. The correlations between Cd, and S likely represent chalcogenides and Cs and B suggest a weak pegmatitic signature, with a weak REE anti-association.

**Table 8.8.** Surface factors from PCA analysis. Elements shaded in grey have factor score coefficients greater than 2 or -2 and are interpreted as geochemical families.

Table 8.8 - Surface Factors from PCA Analysis								
	Factor 1	Factor 2	Factor 3	Factor 4	Factor 5	Factor 6	Factor 7	Factor 8
Ag	-0.00995	0.14214	0.00795	0.20132	-0.31018	-0.15123	-0.09740	-0.01847
Al	0.20132	0.04481	0.12690	-0.16661	0.01783	0.08927	-0.10196	-0.03388
As	-0.07583	0.20910	-0.03743	0.02890	0.04497	-0.17088	0.05445	-0.20047
B	0.08320	-0.03705	0.33049	0.08073	0.16525	-0.16993	-0.04821	-0.01541
Ba	-0.03740	0.27010	0.16293	0.02724	0.06242	-0.04848	0.08363	0.17820
Be	0.13064	0.08181	0.11234	0.02906	0.11333	0.37235	0.02282	0.00298
Ca	0.08917	-0.04290	0.11174	0.17779	0.30221	0.11045	0.11701	-0.33473
Cd	-0.00455	-0.07551	0.20378	0.23428	0.12048	0.25235	0.30927	-0.11492
Ce	0.19125	0.00102	-0.22160	-0.02003	0.13519	-0.06932	0.10284	0.14370
Co	0.12958	-0.19804	0.17517	0.05371	-0.02248	0.23701	-0.03894	0.24029
Cr	0.08802	0.14466	-0.06887	0.14435	-0.33949	0.14146	-0.23546	-0.11350
Cs	0.14971	0.14494	0.20568	-0.16071	0.10160	-0.14687	0.07029	-0.09404
Cu	0.13025	-0.13831	0.14153	0.11283	-0.31997	0.01825	0.09289	0.09605
Dy	0.22980	-0.04192	-0.09057	0.02981	-0.01527	-0.01162	-0.05919	-0.03084
Er	0.22085	-0.07609	-0.02284	0.12135	-0.07895	-0.04727	0.00342	-0.05068
Eu	0.22323	-0.00746	-0.11390	0.00355	0.09695	-0.08658	-0.08548	-0.00430
Fe	0.13532	0.22408	0.08119	-0.15883	0.01522	0.14531	-0.02713	0.18658
Ga	0.19368	0.08554	0.03448	-0.24545	0.00005	0.04391	-0.05883	-0.02915
Gd	0.22754	-0.04759	-0.11083	0.03091	0.05539	-0.07597	-0.05012	0.01159
Ho	0.18084	-0.12300	0.00259	0.12899	0.01721	-0.08589	0.03877	-0.18643
K	0.05899	0.35806	0.00582	-0.15968	0.00229	0.02208	0.09552	-0.05118
La	0.18877	-0.00329	-0.22184	-0.03457	0.13464	-0.04444	0.13051	0.14332
Li	0.14423	-0.00711	0.18605	-0.25968	0.03089	-0.04729	-0.03343	-0.27322
Mg	0.17324	0.07507	0.15795	-0.16187	-0.14901	-0.00669	-0.06943	-0.23278
Mn	0.11706	-0.08645	0.15918	-0.12848	0.08116	0.31758	0.13279	0.29813
Mo	0.05497	0.18116	0.14541	-0.00339	-0.19478	-0.00519	0.01240	0.25601
Na	0.07652	-0.01526	0.13165	-0.06781	0.02295	-0.02684	-0.37423	0.20142
Nd	0.20967	0.00663	-0.19803	-0.02174	0.12669	-0.06589	0.03488	0.07076
Ni	0.15469	-0.08493	0.12237	0.05029	-0.30168	0.12303	-0.02085	-0.19214
P	0.14352	-0.00689	0.08203	0.17817	0.10789	-0.10510	-0.12011	-0.22965
Pr	0.19872	0.00952	-0.21075	-0.00354	0.13724	-0.07369	0.08907	0.09467
Rb	0.08231	0.34284	0.04922	-0.12943	-0.00607	-0.05218	0.09672	-0.08497
S	-0.01984	0.16166	0.23680	0.13573	0.15503	-0.25503	-0.12805	0.16508
Sb	0.09468	-0.00824	0.18460	0.11413	-0.03925	-0.25952	-0.03861	0.23398
Sc	0.03002	0.12301	0.07078	-0.13216	-0.02822	-0.07296	0.33304	-0.08646
Se	0.02212	0.25360	0.04859	0.16696	-0.09039	0.01575	0.26421	0.13332
Sm	0.21850	0.00056	-0.17393	-0.00700	0.09269	-0.09105	-0.02078	0.02387
Sn	0.08449	0.21970	-0.20756	0.09580	-0.07366	0.26912	-0.07570	0.06873
Sr	0.01128	0.24967	0.08544	0.30765	0.17308	-0.07474	-0.05806	0.08821
Tb	0.21661	-0.05967	-0.05069	0.07681	0.04845	-0.13577	-0.00866	0.09235
Th	0.11228	0.03167	-0.18382	-0.02933	-0.25894	-0.02647	0.32810	0.02802
Ti	0.00610	0.21466	-0.21193	0.19675	0.11324	0.19508	-0.08753	-0.08638
U	0.08642	-0.04102	0.12960	0.33106	-0.13999	-0.14287	0.26971	0.05441
V	0.18139	0.18608	0.04182	0.02960	-0.09154	0.13058	-0.09245	-0.11937
Y	0.22573	-0.09459	-0.00453	0.07824	-0.04767	-0.03351	-0.04242	0.02579
Yb	0.21756	-0.05530	-0.04001	0.12655	-0.11970	-0.01154	-0.02416	-0.04886
Zn	0.13212	-0.19406	0.17724	-0.10437	0.08338	0.04411	0.13221	0.05411
Zr	-0.00810	0.10230	0.00034	0.30515	0.22176	0.23473	-0.14644	-0.02567
Eigenvalue	16.86821914	5.439898205	4.451075603	3.349033799	2.622394862	2.124985706	1.604714317	1.461163089
Percent	35.14212321	11.33312126	9.273074173	6.977153748	5.463322629	4.427053554	3.343154828	3.044089768
Cum Percent	35.14212321	46.47524447	55.74831865	62.72547239	68.18879502	72.61584858	75.9590034	79.00309317

*Subsurface factor 3* accounts for 7.13% of the total variance and includes positive correlations between Ba, Cr, K, Ni, Sn, and Ti and negative correlations with Ce and Dy. K is considered part of potassic alterations while Ba, Cr, and Ni could represent andesite dikes at the MacArthur pit. Sn and Ti are not understood.

**Table 8.9.** Subsurface factors from PCA analysis. Elements shaded in grey have factor score coefficients greater than 2 or -2 and are interpreted as geochemical families.

Table 8.9 - Subsurface Factors from PCA Analysis								
	Factor 1	Factor 2	Factor 3	Factor 4	Factor 5	Factor 6	Factor 7	Factor 8
Ag	0.07811	0.24599	0.02897	0.07072	0.12826	0.03304	0.06351	-0.02253
Al	0.24249	-0.08310	0.05576	-0.07527	-0.05053	-0.11489	-0.14062	0.01800
As	0.13688	0.12754	-0.10505	-0.06043	0.22562	0.16399	0.00292	-0.04180
Au	0.02528	0.05031	0.04319	0.03815	-0.04163	0.01997	-0.05278	-0.05046
Ba	0.17138	-0.00199	0.21178	-0.10731	-0.19439	-0.09760	-0.01103	0.05729
Be	0.15109	-0.00071	-0.10816	-0.18919	0.21649	-0.05654	0.06803	0.00931
Ca	0.18240	-0.04948	0.02594	0.11555	0.04072	0.03442	-0.08790	-0.26142
Ce	0.19439	0.01625	-0.23021	0.06845	-0.05238	0.08420	-0.12347	0.10583
Co	0.14700	-0.12475	0.00489	-0.21115	0.15467	0.06434	0.08559	-0.22510
Cr	0.09372	-0.10542	0.30624	0.11190	0.14263	0.09091	-0.07195	0.13914
Cu	0.06641	-0.11258	-0.13397	0.02281	0.04640	-0.31811	0.23226	0.10353
CuOx	0.02576	-0.16279	-0.12116	0.13774	0.10559	-0.39786	0.14686	0.15811
Dy	0.21181	0.06806	-0.23009	0.05434	-0.02285	-0.05117	0.03463	-0.12836
Er	0.13382	-0.22396	-0.16445	0.12093	-0.09941	-0.02001	0.06707	0.14148
Eu	0.23525	0.04447	-0.17664	-0.03597	-0.03849	0.02393	-0.02319	0.00150
Fe	0.14042	-0.07512	0.15005	-0.24263	0.11440	0.14534	0.12197	-0.03029
Ga	0.20889	-0.06591	0.07290	-0.14413	-0.06992	-0.04988	-0.08261	-0.00619
Gd	0.15588	-0.30447	-0.00567	-0.16927	0.00737	0.15595	-0.03025	0.06389
K	0.15454	0.07615	0.20014	-0.14238	-0.26670	-0.21173	-0.00776	0.08511
La	0.19110	0.13420	-0.13903	0.07328	0.07808	0.17236	-0.04261	0.16979
Li	0.13086	0.24744	0.04699	-0.07793	0.12198	-0.21706	-0.17980	-0.15896
Lu	0.08628	-0.20925	-0.12412	0.08862	-0.14703	0.08427	0.35202	-0.13246
Mg	0.18274	0.04023	0.12329	-0.17098	-0.03298	-0.29358	-0.04342	0.03259
Mn	0.09941	-0.18252	0.12885	-0.07275	0.30206	-0.05368	-0.00617	-0.14766
Mo	0.05675	0.03782	-0.01493	-0.08838	-0.10866	0.01300	0.20162	0.34195
Na	0.12299	0.07529	0.14397	0.29256	0.03281	0.00679	-0.17422	0.10846
Nd	0.16703	0.07768	-0.15977	0.08470	-0.04964	0.09578	0.23075	-0.08885
Ni	0.08243	-0.09275	0.27267	0.07570	0.25746	-0.04959	0.09990	0.18555
P	0.14775	0.02501	-0.00944	0.01492	0.11951	-0.15441	0.08752	-0.06620
Pb	0.03196	0.12291	0.01466	-0.08317	0.14367	0.19233	-0.18097	0.23621
Pr	0.12528	0.34905	-0.05557	0.01585	0.12351	-0.04789	-0.04720	-0.08777
Rb	0.14984	0.22974	0.12488	-0.02923	-0.18662	-0.17494	0.16895	0.02928
S	0.06711	0.14799	0.09275	-0.24309	-0.19620	0.29343	0.06721	0.02787
Sc	0.20462	-0.07705	0.03919	-0.09048	0.00711	0.03889	-0.07828	0.06184
Se	0.07505	0.08756	-0.00832	-0.09660	-0.12455	0.22423	0.27624	0.21526
Si	0.10351	0.07304	0.12171	0.31765	0.06422	-0.02639	0.04213	0.29038
Sm	0.12015	-0.00280	-0.17817	0.02746	-0.00189	0.11562	-0.07278	0.12418
Sn	0.04093	0.04309	0.20402	0.10536	0.21736	0.04047	0.10126	0.24148
Sr	0.15369	-0.09708	0.08759	0.06264	-0.26303	0.21391	-0.13588	-0.02163
Tb	0.09884	0.03788	0.19670	0.18338	-0.08191	-0.02580	0.14833	-0.18718
Te	0.11359	0.18191	0.10008	0.06344	0.11864	0.11585	0.22421	-0.17488
Th	0.11335	0.29316	-0.11613	0.14715	-0.02870	-0.10494	-0.05326	-0.10068
Ti	0.14658	-0.11586	0.20607	0.18014	-0.16445	0.03856	-0.08804	-0.17510
Tl	0.02407	-0.03176	0.03100	0.13169	-0.20221	-0.04118	0.04931	-0.21286
Tm	0.04985	0.11619	0.03015	0.06133	-0.10058	0.08420	0.34058	-0.05115
U	0.07244	0.17149	-0.01272	0.08377	0.01578	0.10122	-0.07008	0.06112
V	0.20477	-0.05618	0.08172	-0.13633	-0.12784	-0.09820	-0.02374	0.06524
W	0.07593	-0.08975	-0.01912	0.26170	0.08360	0.03580	0.20533	0.02701
Y	0.21244	-0.11523	-0.21791	0.03285	0.04505	-0.02951	-0.16752	-0.01573
Yb	0.17761	-0.14032	-0.25378	0.07661	-0.00501	0.01551	-0.14033	0.08526
Zn	0.07278	-0.05357	0.01657	-0.17884	0.27803	0.06340	0.19448	-0.12720
Zr	0.10727	-0.18147	0.16708	0.29544	0.04384	0.17200	-0.07813	-0.16418
Eigenvalue	12.0452931	4.47779694	3.70884363	2.96573727	2.7399018	2.29232575	1.93587159	1.76033886
Percent	23.1640252	8.61114796	7.1323916	5.70334091	5.26904192	4.40831876	3.72282998	3.38526703
Cum Percent	23.1640252	31.7751732	38.9075648	44.6109057	49.8799476	54.2882664	58.0110963	61.3963634

Surface factor 4 accounts for 6.98% of the total variance and includes positive correlations between Ag, Cd, Sr, U, and Zr and negative correlations between Ga and Li. This factor is best interpreted as zircon and a weak chalcogenide signature.

**Table 8.10.** Factor Analysis of Surface Samples. Factor analyses are in part interpreted to known minerals and alteration documented in the MacArthur pit.

Table 8.10 - Factor Analysis: Surface Samples							
		Factor Families		Geochemical Interpretations			
Factor	% Variance	Positive	Negative	Positive	Negative	Not Explained	MacArthur Relation
1	35.14%	Al, Dy, Er, Eu, Gd, Nd, Sm, Tb, Y, Yb		clay alteration REE bearing accessory			clay and fault gouge
2	11.33%	As, Ba, Fe, K, Rb, Se, Sn, Sr, Ti		potassic alteration epithermal		Fe, Sn, Ti	potassic alteration
3	9.27%	B, Cd, Cs, S	Ce, La, Pr, Sn, Ti	pegmatitic chalcogenide	REE bearing accessory	Sn, Ti	
4	6.98%	Ag, Cd, Sr, U, Zr	Ga, Li	zircon chalcogenide		Sr, Ga, Li	
5	5.46%	Ca, Zr	Ag, Cr, Cu, Ni, Th	caliche zircon?	???	Zr	surface weathering ?
6	4.43%	Be, Cd, Co, Mn, Sn, Zr	S, Sb	Mn oxides adsorbed on Mn oxides	sulfide leaching	Be, Sn, Zr	neotocite
7	3.43%	Cd, Sc, Se, Th, U	Cr, Na	mafic, chalcogenide zircon, monazite ?	sodium removal		sodic alteration
8	3.04%	Co, Mn, Mo, Na, Sb	As, Ca, Li, Mg, P	neotocite ?	???	Na, Sb	oxide limonites

**Table 8.11.** Factor Analysis of Subsurface Samples. Factor analyses are in part interpreted to known minerals and alteration documented in the MacArthur pit.

Table 8.11 - Factor Analysis: Subsurface Samples							
		Factor Families		Geochemical Interpretations			
Factor	% Variance	Positive	Negative	Positive	Negative	Not Explained	MacArthur Relation
1	23.16%	Al, Dy, Eu, Ga, Sc, V, Y		clay alteration REE bearing accessory		Sc, V	clay and fault gouge
2	8.61%	Ag, Li, Pr, Rb, Th	Er, Gd, Lu	potassic alteration epithermal	REE bearing accessory	Li, Pr, Th	potassic alteration
3	7.13%	Ba, Cr, K, Ni, Sn, Ti	Ce, Dy, Y, Yb	potassic alteration andesite ?	REE bearing accessory	Sn, Ti	potassic alteration andesite dikes ?
4	5.70%	Na, Si, W, Zr	Co, Fe, S	sodic metasomatism	sulfide leaching		sodic alteration
5	5.26%	As, Be, Mn, Ni, Sn, Zn	K, Sr, Ti	Mn oxides adsorbed on Mn oxides	potassium leaching	Be, Sn, Sr, Ti	neotocite
6	4.40%	S, Se, Sr	Cu, CuOx, K, Li, Mg	sulfide		Sr	
7	3.72%	Cu, Lu, Mo, Nd, Se, Te, Tm, W		chalcogenide REE bearing accessory			porphyry ?
8	3.39%	Mo, Pb, Se, Si, Sn	Ca, Co	weak Mo porphyry ?		Se	

*Subsurface factor 4* accounts for 5.7% of the total variance and includes positive correlations between Na, Si, W, and Zr and negative correlations between Co, Fe, and S. This factor represents sodic metasomatism with tungsten introduced magmatically with strong sodic fluids in a sulfide leaching environment.

*Surface factor 5* accounts for 5.46% of the total variance and includes a positive correlation between Ca and Zr and a negative correlation between Ag, Cr, Cu, Ni, and Th. This factor is interpreted caliche associated with possible surface weathering. The negative elements are mobile and in this case leached due to surface weathering affects.

*Subsurface factor 5* accounts for 5.26% of the total variance and includes positive correlations between As, Be, Mn, Ni, Sn, and Zn and negative correlations with K, Sr, Tl. Positive correlations suggest this factor may be related to manganese oxide with other adsorbed elements. This factor would indicate neotocite at the MacArthur pit.

*Surface factor 6* accounts for 4.43% of the total variance and includes positive correlations between Be, Cd, Co, Mn, Sn, and Zr and a negative correlation between S and Sb. This factor is interpreted as manganese oxides with absorbed elements and weak sulfide leaching indicated by Sb and S. Again, this could represent neotocite in the MacArthur pit.

*Subsurface factor 6* accounts for 4.4% of the total variance and includes positive correlations between S, Se, and Sr and negative correlations between Cu, CuOx, K, Li, and Mg. This factor indicates sulfides with an anti-relationship with oxide minerals.

*Surface factor 7* accounts for 3.43% of the total variance and includes positive correlations between Cd, Sc, Se, Th, and U and negative correlation between Na and Cr. This factor represents sodium leaching with resistive accessory zircon or monazite minerals.

*Subsurface factor 7* accounts for 3.72% of the total variance and includes positive correlations between Cu, Lu, Mo, Nd, Se, Te, Tm, and W. A weak porphyry signature is seen in this factor with Cu, Mo, and W with distinctive rare earth accessory mineral precipitation (Lu, Nd, Tm).

*Surface factor 8* accounts for 3.04% of the total variance and includes positive correlations between Co, Mn, Mo, Na, and Sb and negative correlations between As, Ca, Li, Mg, and P. This factor is interpreted as neotocite due to high presence of positive elements found in pure neotocite element analysis, discussed in final interpretations.

*Subsurface factor 8* accounts for 3.39% of the total variance and includes positive correlations between Mo, Pb, Se, Si, and Sn and negative correlations between Ca, Co, and Tl. Mo, Pb, and Se all show hydrothermal sulfide ore associations (Levinson, 1974) and suggest a weak Mo-porphyry signature.

#### **8.5.4. Spatial**

Spatial analyses for this study are (1) spatial distribution of factor scores and (2) spatial distribution of elements. The results of each are described below.

(1) The eight surface factors described above are used here to show spatial distribution of the factor score coefficient. JMP V.4 calculates spatial data by summing the factor scores and multiplying them by the original geochemical values. Contour maps of factor scores are created using Golden Software Surfer, interpolated using the natural neighbor method. Many interpolation methods were tried and natural neighbor fit the data best based on element distribution contours. The contour maps are colored with purple representing low values and pink representing the high values. An example can be seen for factor 5 in Figure 8.10, and the complete set is in Appendix 2.

*Factor 1* is dominated by REE, Al and Y. Low values are seen in the northern most sections of the upper benches and the highest values are seen along the southern edge of the pit and in the lower benches. This factor shows a close correlation to REE abundance contours and tends to occur strongest in areas with known sodic alteration.

*Factor 2* shows strong potassium feldspar signature interpreted from K, Rb, and Ba. Spatial distribution of this factor shows it is strongest in the middle and western areas of the MacArthur pit. A patch of low separates the two strong high areas and the eastern most part of the pit also contains very low values. This factor distribution correlates well with element distribution contours for K, Rb, and Ba.

*Factor 3* was interpreted as weak pegmatitic and chalcogenides. The spatial distribution map shows two strong high values along the northern section of the pit and a smaller high in the lower benches. A strong low occurs in the very middle of the pit. This distribution shows correlation with abundance contours for B and S and weaker correlations with REE abundance.

*Factor 4* was interpreted as zircon with a weak chalcogenide signature. Spatial distribution shows 3 segregated lows surrounded by high values. The low values occur in the west, middle, and east sections of the pit. This distribution correlates with abundance contours for Sr and Cd and shows weak anti-correlations with contours for Ga and Li.

*Factor 5* is interpreted as caliche associated with surface weathering. Spatial distribution shows only one high located in the western part of the pit surrounded by low values. This spatial distribution shows a weak anti-correlation with abundance contours for Cr, Cu, and Ni.

*Factor 6* is interpreted as manganese oxide minerals signature with sulfide leaching (Sb and S). Spatial distribution shows the strongest values occurring along the southern edge of the pit with lows in the northwest and south-central regions. This distribution shows weak correlation with abundance contours for Be, Cd, Mn, and Sn, with a weak anti-correlation with Sb.

*Factor 7* was interpreted as sodium leaching. The distribution of this factor shows high values bordering the southern edge of the pit and in the northwest-central regions and lows to the west and northeast. This distribution moderately correlates with abundance contour of U and weakly correlates with Cd, Se, and Th. It also shows a weak anti-correlation with Na.

*Factor 8* was interpreted as neotocite. This would indicate strong limonite occurrence in the oxide zone. The spatial distribution shows two strong highs in the northwest and east, and two moderate highs in the central and north-central of the pit. This distribution moderately correlates with the abundance contour of Co and weakly correlates with Mn, Mo, and Sb. It also shows weak anti-correlations with Li and P.

(2) A complete list of elements used in this study for the surface at the MacArthur pit is shown in Table 8.2. Contour maps of element abundance are created using Golden Software Surfer interpolated using the natural neighbor method. Many interpolation methods were tried and natural neighbor fit the data best based on element distribution contours. The contour maps are colored with purple representing low values and pink representing the high values (Fig. 8.9). A complete set of figures for element abundance can be found in Appendix 3. The following discussion is focused on elements that are associated with porphyry style mineralization and observed in statistical analysis.

*Silver (Ag)* shows the strongest value in the QMPb-1 dike located on bench 4800 followed by the QMPb-2 dike on bench 4680. It correlates weakly with Mo, Rb, V, and moderately correlates with Ti.

*Aluminum (Al)* occurs the strongest in the eastern (lower) half of the MacArthur pit and is associated with gouge samples. Al shows the best correlations with Ga and Li and weak correlations with Mg, Ni, and V.

*Calcium (Ca)* has the strongest occurrence in two locations along the northern edge of the pit. Ca shows a moderate correlation with S and weak correlations with B and Na.

*Copper (Cu)* has the strongest occurrence along the south and east of the MacArthur pit. The strength in the east of the pit correlates with gouge samples and with black copper (neotocite) along the southeast. Cu has a strong correlation with U and moderately correlates with Mn and Mo. Cu also shows weak correlations with Co, Ga, Mg, Ni, and Th.

*Iron (Fe)* occurs in the northwestern region of the MacArthur pit and has been identified to occur in the QMPb-1 dike on bench 4800 and 4780. Fe shows weak correlations with Ag, K, Mg, Sc, and V. It also shows a very weak correlation with REE.

*Potassium (K)* has the strongest occurrence in the west and decreases in value as you move east. K only shows a weak correlation with Rb.

*Magnesium (Mg)* shows the two strongest areas to be in the northwest and central portions of the MacArthur. Mg shows a weak correlation with Ga and V and a moderate correlation with Al.

*Manganese (Mn)* shows to have the strongest values in the southeast and eastern regions of the MacArthur. It also shows a small strong section on the north end of bench 4700, related to a rhyolite dike. The high Mn values correlate with those samples collected in fault gouge and are representative of regions with strong neotocite. Mn correlates best with Cu and shows weak correlations with Be, Co, Li, Mo, Ni, and U.

*Molybdenum (Mo)* has its strongest occurrence in three isolated areas to the north and south central as well as the western margin of the MacArthur. Mo is best correlated with Mn and shows weak correlations with Co, Cu, Li, Ni, and U.

*Sodium (Na)* has its strongest occurrence in the northeast regions of the MacArthur pit. Na shows weak correlations with Ca, Cs, and Zr.

*Uranium (U)* shows concentration along south and eastern regions of the MacArthur pit. Samples show high levels of U associated with fault gouge samples. Uranium correlates best with Cu and moderately correlates with Mn and Mo. U also shows weak correlations with Co, Ga, Mg, Ni, and Th.

## **8.6 Initial Interpretations**

Key elements in porphyry copper exploration include, but are not limited to: Cu, Mo, Au, and Ag. At the Pulang porphyry copper deposit in China (Yongqing, 2008), factor analysis indicated that Zn, Ag, Cu, Au, W, and Mo could all be regarded as pathfinder elements for prospecting new ore bodies at depth. The analysis of geochemical data at the MacArthur pit has provided clues as to the nature of Cu mineralization in the oxide zone while raising some questions. For example, a clue in the surface data set shows Cu is highly correlated with U at a correlation score of 0.628, second only to Ni at 0.735. Element distribution contours show Cu and U to behave correlative on the surface, therefore demonstrating that U could act as a pathfinder element for Cu. Statistical and spatial analysis of surface data indicates that U, Mn, Mo, Co, and Ni may serve as pathfinder elements in locating sections of secondary Cu mineralization. A question is now raised as to why subsurface data shows Cu and U have a negative correlation with a score of -0.018 and Ni correlates positively with a score of 0.099.

Univariate analyses provide clues as to the nature of alteration at the MacArthur pit (Appendix 2). When results are compared to average element abundance for granites in the crust, (Mason, B., and Moore, C.B., 1982) the MacArthur pit shows an overall depletion in abundance of many elements and enrichment that is dominated by metals. For the case of U, it

shows an average value compared to granites in the surface, but in the subsurface shows to be 5x lower than the average value. For both surface and subsurface data, the elements Al, Ca, Ga, K, Li, Na, and Th all show at least a 3x depletion factor and elements Co, Cu, Mg, Ni, and S all show at least a 3x enrichment factor. This may be interpreted as early hydrothermal processes enriching metals. Later tilting and exposure at the MacArthur resulted in strong oxidation and enrichment overprinting potassic and sodic style alterations.

Bivariate analyses demonstrate relationships between two elements for multi-element data at the MacArthur. Several of the same elements observed as enriched in univariate analysis are observed to have relationships in bivariate analysis and depleted elements show relationships as well. Some of the major relationships observed are in two groups.

The first group shows the strongest relationships and includes Al, Ga, Mg, K, Ba, and Rb. The second group includes Cu, Ni, Co, U, and Y. The strongest of the groups represent primary K-feldspar and mafic minerals found in the quartz monzonite. This group may also be related to a clay component found in clay and fault gouge. The second group represents the oxide enrichment zone at the MacArthur. These elements become mobile during strong oxidation and can be interpreted as having similar behaviors in the oxidizing environment at the MacArthur pit. Hydrothermal magmatic aqueous fluid associated with the Luhr Hill granite was rich in Cl, Na, K, Fe, S, and Cu (Dilles, 1987, Dilles and Proffett, 1995), and the two groups together may represent a geochemical environment of primary hydrothermal alteration.

Multivariate analyses show relationships between a set of elements (factor) for data collected in the MacArthur pit. Again, the same groups which are seen in univariate and bivariate analysis show relationships in multivariate analysis. Together these groups represent

several geological processes associated with oxidized porphyry copper deposits identified by factor score coefficients. A clay component factor dominates both surface and subsurface data. This indicates that strong alteration and transport have occurred in the oxidation zone of the MacArthur as well as late surface weathering. The clay component may also represent phyllic alteration. For the case of Cu, it is seen in factors to have relationships with elements Ni, Co, Mo, U and in subsurface factor 6 Cu, CuOx, and Mg have a negative relationship with S. This indicates that the oxide zone Cu is dominantly in oxide mineralogy demonstrating oxide zone geology.

Spatial analysis of factor score coefficients show spatial distribution of factor families in the MacArthur pit. One possible model of alteration zones (Fig. 8.11) is sodic alteration to the east - northeast, a central western potassic zone and a phyllic zone in the north - northwestern areas of the pit (Heatwole, 2009). Element abundance contours of Na, K, Ca, and Mg support this observation, as does spatial distribution of factor families interpreted as sodic and potassic alteration. Rock descriptions (Table 6.2) also support this model of alteration showing strong sodic alteration in the eastern rock samples.

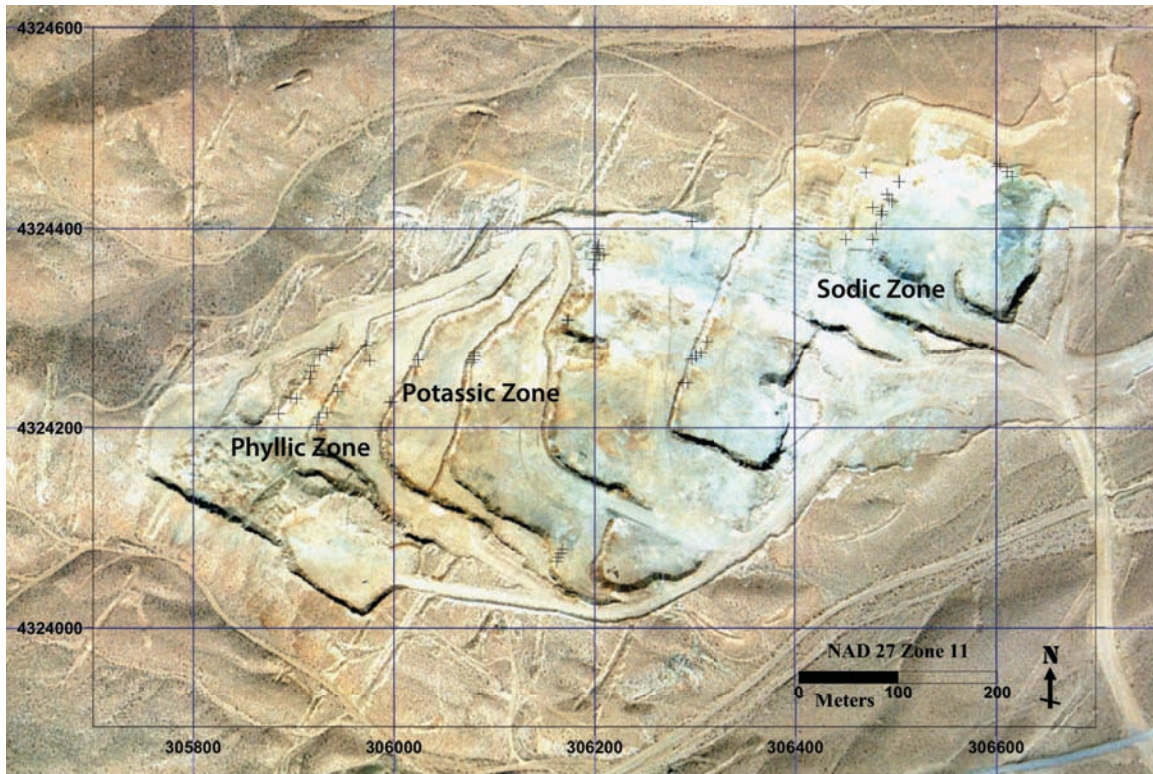


**Figure 8.11.** Proposed alteration zones of the MacArthur pit.

Sodic alteration tends to destroy or “flush” large masses of metals (Barton, 2001).

Bivariate analysis shows Na to have no correlations on the surface and moderately correlates with Si and Zr, 0.549 and 0.455 respectively in the subsurface. This likely represents zircon, which tends to be resistant to weathering and alteration. The elevated CuOx in the eastern portion of the MacArthur is precipitated over a strong sodically altered zone, suggesting CuOx at the MacArthur has been introduced from peripheral sulfide zones.

## **9. SPECTRAL RADIOMETRY**

### **9.1. Introduction**

Analysis of spectral radiometry data has many documented uses in identification of materials on earth and in space. In space, emission features seen in the electromagnetic spectrum reflect composition of stars. On Earth, absorbance features in the electromagnetic spectrum relate to materials from plant life, soils, liquids, and minerals. Spectral reflectance data is used in this study for the identification of alteration and oxide zone mineralogy of the MacArthur pit. An understanding of spatial distribution of alteration in a porphyry system gives clues as to where to locate possible additional mineralization. It also provides clues as to the series of events or the evolution of the system.

This study also attempts to apply spectral data to percent copper value, in effort to test the use of reflectance data as a method of grade control. When an element of interest drops below a certain percent, mine operators lose money and no longer want to spend time moving and processing the material. This initiates a cut-off grade; at the MacArthur pit the cut-off grade for copper in the oxidized sections is .18% Cu (<http://www.quaterraresources.com>). When copper drops below this value, it is no longer economic to extract and process. Using the Spectral Analyst tool in ENVI® (Environment for Visualizing Images) reflectance data will be tested in the identification of oxide rich rocks that contain value and those that do not. If a relationship can be developed, spectral radiometry would be save time and money as a grade control method in oxidized sections.

## 9.2. Data

Data for this study includes a total of 87 spectral profiles collected using the GER 3700 spectral radiometer. Data collected includes two studies:

- (1) Spectral analysis of 52 rock samples (Table 9.1)
- (2) Spectral homogeneity study (35 measurements in Table 9.2)

**Table 9.1.** Sample numbers used in Spectral Analysis. Descriptions of rock samples are found in Table 6.2.

Table 9.1 - Rock Samples used in Spectral Analysis						
Bench 4800	Bench 4780	Bench 4750	Bench 4730	Bench 4700	Bench 4675	Bench 4600
26	22	51	1	21	30	6
27	29	52	2	31	73	7
33	45	53	3	32	74	8
38	46	54	4	67	75	9
39	47	55		68		57
40	48	56		69		58
41	49			70		59
42				71		60
43				72		61
44						62
						63
						64

Spectrum of rock samples were obtained in a laboratory environment. These samples are the same samples from geochemical analysis. Some of the original geochemical rock samples were not spectrally analyzed due to an insignificant amount of material. Table 9.1 shows samples used in the spectral analysis.

The spectral homogeneity study includes 35 spectral profiles measured in the field along the MacArthur bench faces. The 35 profiles represent 5 study areas in the MacArthur pit that appear to contain a homogenous oxide type, iron and/or copper. The five homogeneity tests include two rhyolite dikes and three porphyry dikes from five different bench faces (Fig. 9.1). A list of sample numbers from homogeneity tests is found in Table 9.2.

**Table 9.2.** Field samples used in spectral analysis. QMP indicates porphyry dike samples and RHY indicates rhyolite dike samples.

Table 9.2 - Field Samples used in Spectral Analysis				
QMP-4780	QMP-4750	QMP-4600	RHY-4700	RHY-4675
Q-4780.1	Q-4750.1	Q-4600.1	R-4700.1	R-4675.1
Q-4780.2	Q-4750.2	Q-4600.2	R-4700.2	R-4675.2
Q-4780.3	Q-4750.3	Q-4600.3	R-4700.3	R-4675.3
	Q-4750.4	Q-4600.4	R-4700.4	R-4675.4
	Q-4750.5	Q-4600.5	R-4700.5	R-4675.5
		Q-4600.6	R-4700.6	R-4675.6
		Q-4600.7	R-4700.7	R-4675.7
		Q-4600.8	R-4700.8	R-4675.8
		Q-4600.9	R-4700.9	R-4675.9

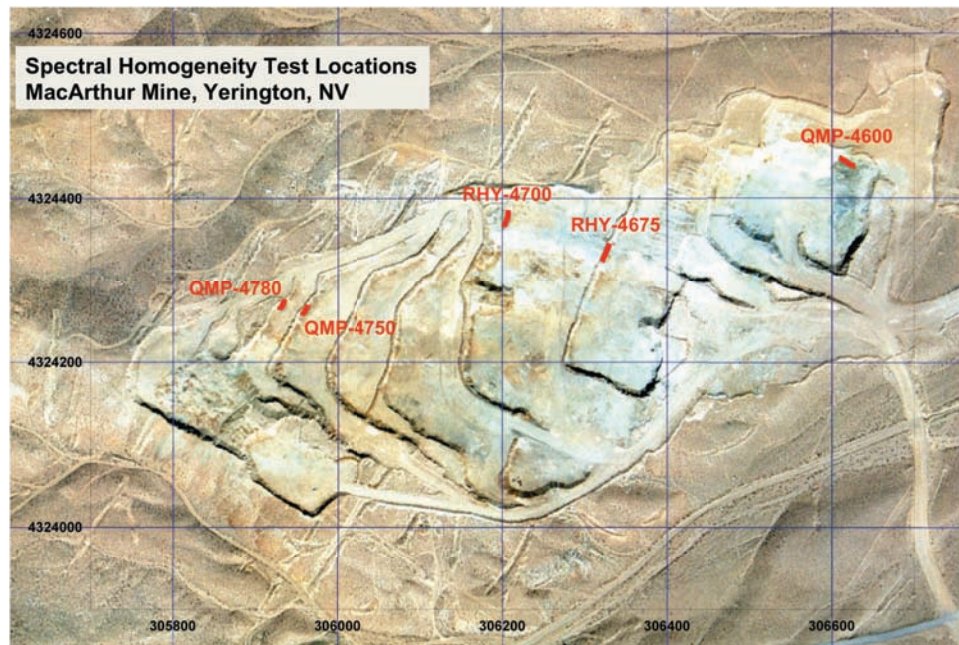


**Figure 9.1.** Spectral homogeneity test locations. QMP-4780 and 4750 are a continuous porphyry dike and both RHY locations are a continuous dike.

### **9.3. Methods**

#### **9.3.1. Lab Methods**

Spectral profiles obtained in the lab were measured using the GER 3700 (<http://www.spectravista.com>). The GER 3700 has a spectral range of 350nm – 2500nm, sampling on 704 channels. Sample preparation consisted of crushing rock samples with a jaw crusher to the size of ½ inch and collecting samples to measure spectrally in a labeled Petri dish. The first step in measuring the data is to calibrate the GER 3700. This is done using a white 100% reflection calibration plate and is repeated after every fifth measurement. Upon collection of the data, processing is needed to display and analyze the data and will be discussed in processing.

#### **9.3.2. Field Methods**

Spectral profiles obtained from the MacArthur bench faces were measured using the GER 3700. Field homogeneity locations were selected on basis of visual inspection of oxide content and rock type. Five locations were chosen, with two varieties of porphyry dikes and a rhyolite dike, (Fig 9.1) since in the MacArthur pit the dikes act as sponges for oxide iron and copper mineralization. They also provide an opportunity to sample a single outcropping that can reflect a single alteration type in more than one location, testing homogeneity spatially. The five homogeneity tests are as follows:

- (1) Biotite porphyry-1 dike, bench 4780 (QMP-4780)
- (2) Biotite porphyry-1 dike, bench 4750 (QMP-4750)
- (3) Rhyolite dike, bench 4700 (RHY-4700)
- (4) Rhyolite dike, bench 4675 (RHY-4675)
- (5) Hornblende porphyry-3 dike, bench 4600 (QMP-4600)

A total of nine spectrums are collected from QMP-4600 and both RHY locations. Five spectrums are collected at QMP-4750 and three at QMP-4780. Spectrums are all collected within a homogenous body within 100 square feet of each other.

#### **9.4. Processing**

The data is processed into two variables, wavelength and spectra (% reflectance). The GER 3700 saves data as three variables: wavelength, unknown reflectance, and illumination reflectance. These represent spectral range 350nm – 2500nm, sample reflectance, and calibration reflectance respectively. Spectra are achieved by dividing the unknown by illumination. The last step in data processing is to change wavelength from nanometers to microns ( $\mu\text{m}$ ). This step scales the x-axis (wavelength) to match spectral libraries from the U.S. Geological Survey (USGS) (<http://www.usgs.gov/>) and NASA Jet Propulsion Laboratory (JPL) (<http://www.jpl.nasa.gov/>). Data is saved as a Microsoft excel sheet (.xls) and text files (.txt). Text files are used to import data into ENVI for spectral analysis.

#### **9.5. Analysis**

Analysis of spectral data is performed using ENVI 4.6.1 ([www.idl-  
envi.com/ENVIOverview](http://www.idl-<br/>envi.com/ENVIOverview)) Spectral Analyst tool. The use of Spectral Analyst is to help identify materials based on their spectral characteristics. The Spectral Analyst tool uses ENVI techniques such as Binary Encoding, Spectral Angle Mapper (SAM), and Spectral Feature Fitting (SFF) <sup>TM</sup> in a hybrid identification tool to compare symmetry of spectra absorption features of an unknown spectrum to the materials in a spectral library (Kruse and Lefkoff, 1999). The result of Spectral Analyst is a list of matching minerals from a known spectral library with a similarity score from 0 to 1. The scores provide a basis as to what minerals might be present, but it is up to the user to

make positive identifications based on absorbance features between spectral profiles and geologic reason. Three analyses were performed on the data available for this study using ENVI:

- (1) Spectral Analyst of 52 geochemical spectrums vs. USGS and JPL spectral libraries.
- (2) Spectral Analyst of 35 homogeneity spectrums
- (3) Analysis of 52 geochemical samples; relationship to copper grade.

#### **9.5.1. Spectral Analyst of 52 geochemical spectrums vs. USGS and JPL spectral libraries.**

In this analysis, spectral data was imported by bench number (Table 9.1) into ENVI and saved as spectral library files. Each sample was analyzed using the Spectral Analyst tool comparing to the USGS and JPL spectral libraries. In this study, the complete spectral range was analyzed in this method. An option in Spectral Analyst is to only compare spectral ranges of known absorbance features for associated minerals (ENVI help menu). Results were recorded and spectral profiles of matching minerals from USGS and JPL were obtained. A list of mineral matches and scores can be found in Tables 9.3 -9.6 and spectral profiles of geochemical samples can be found in Appendix 4.

#### **9.5.2. Spectral Analyst of 35 homogeneity spectrums.**

Analysis of spectrum measured in the field was completed as described above for the geochemistry samples. In this study, analysis was carried further to determine if homogeneity of oxide mineralization could be determined by spectrum. Using the Spectral Analyst tool each homogeneity test was analyzed against spectrum from its own family. Finally, QMP-4780 and QMP-4750 were analyzed against each other to see how a spectrum varies spatially in a homogenous body. The same was completed for the rhyolite dikes (Appendix 4).

### **9.5.3. Analysis of 52 geochemical samples; relationship to copper grade.**

The basis of this analysis is to determine if absorbance features in spectrum have a relationship with copper grade. In this analysis a single spectral library was used representing the 52 geochemical samples and analyzed against itself using ENVI Spectral Analyst. A maximum of five scores were recorded from each sample with a value over 0.7 (Tables 9.15 and 9.16). Added to this data table is %Cu, rock type, and color of copper oxide of each sample from rock descriptions (Table 6.2). The purpose of this analysis is to use spectra reflectance data as a method of grade control in an oxidized section of active mines.

## **9.6. Results**

The results of spectral analysis are presented in this section. Results of Spectral Analyst are dominated by matches from minerals produced in oxidation zones associated with primary copper and iron. Mineralogy of oxides indicates hydrothermal, propylitic, and silicification alteration types. Tables are presented in text and a complete set of spectral profiles from samples (geochemical and field) and correlating matches with USGS and JPL can be seen in Appendix 4.

### **9.6.1. Spectral Analyst of 52 geochemical spectrums vs. USGS and JPL spectral libraries.**

Table 9.3 shows Spectral Analyst results for samples on bench 4800. All matches suggest the bench is dominated by oxide limonite; jarosite, goethite, and hematite. Rock descriptions as well as field mapping aid in support. The presence of plumbojarosite also supports oxidizing environments of pyrite, with accompanying lead, (Anthony J.W. et al, 2005) and nontronite suggest a weak hydrothermal signature (Anthony J.W. et al, 1995). Figure 9.2 shows jarosite and goethite spectral profiles from USGS library with sample 44, a strong iron sample. Matching absorbance features can be seen at 1.44 $\mu$ m and 1.85 $\mu$ m.

**Table 9.3.** Bench 4800 Spectral Analyst matches with USGS and JPL spectral libraries.

Table 9.3 - Bench 4800 Spectral Analyst Matches					
Bench	Sample #	USGS Library Matches	Score	JPL Library Matches	Score
4800	38	hematit2.spc	0.009		
	40	hematit2.spc	0.067	hematite synthetic O	0.058
		ferrihyd.spc	0.031		
	41	hematit2.spc	0.021		
	44	jarosit9.spc	0.26	goethite OH-2A	0.179
		lepidocr.spc	0.254	hematite synthetic O	0.169
		jarosit5.spc	0.214	natrojarosite SO-7C	0.144
		goethit1.spc	0.201	nontronite PS-6B	0.114
		goethit3.spc	0.198	plumbojarosite SO-7B	0.075
		jarosit2.spc	0.188	jarosite SO-7A	0.071
		jarosit7.spc	0.17		
		hematit2.spc	0.161		

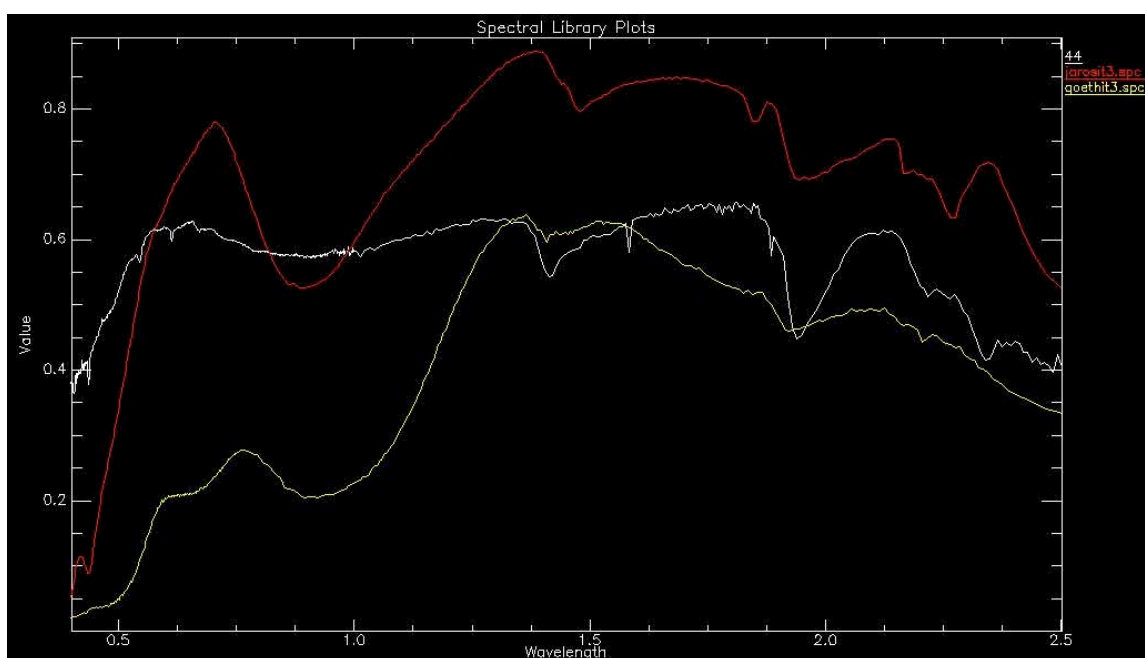


**Figure 9.2.** Spectral profile of sample 44 (white) from bench 4800 with - goethite (yellow) and jarosite (red) from USGS spectral library. Matching absorbance features can be seen at 1.44µm and 1.85µm.

Table 9.4 shows Spectral Analyst results for samples on bench 4700. Spectral Analyst matches from this bench also indicate a domination of secondary iron minerals formed in the oxidation process of primary iron sulfides. Comparison of praseodymium spectrum shows common absorption features at 1.61µm and 2.36µm as sample 32 however; there is no geologic reason for its presence at the MacArthur pit.

**Table 9.4.** Bench 4700 Spectral Analyst matches with USGS and JPL spectral libraries.

Table 9.4 - Bench 4700 Spectral Analyst Matches					
Bench	Sample #	USGS Matches	Score	JPL Matches	Score
4700	31	praseody.spc	0.113		
		h20-ice.spc	0.074		
	32	hematit2.spc	0.265		
		ferrihyd.spc	0.262		
		maghemit.spc	0.144		
		praseody.spc	0.123		
		lepidocr.spc	0.117		
		hematitb.spc	0.09		
		goethit1.spc	0.071		
		jarosit9.spc	0.043		
	68	hematit2.spc	0.108		
		ferrihyd.spc	0.054		

Maghemite suggest surface weathering or low-temperature oxidation containing ferrous-iron, commonly derived from magnetite (Anthony J.W. et al, 1997). The spectrum matches on this bench indicate oxidation processes and weak argillic alteration or surface weathering phenomena.

Table 9.5 shows Spectral Analyst results for samples on bench 4675. These samples demonstrate secondary iron minerals formed from the oxidation of primary iron minerals. Riebeckite and sample 74 have a common absorption at 2.33 $\mu$ m (Fig. 9.4). Riebeckite is not seen at the MacArthur pit; however, actinolite is found in and near the pit suggesting propylitic alteration. Actinolite and riebeckite are both amphibole group minerals and have similar properties (Anthony J.W. et al, 1995) suggesting riebeckite cannot be ruled out.

**Table 9.5.** Bench 4675 Spectral Analyst matches with USGS and JPL spectral libraries.

Table 9.5 - Bench 4675 Spectral Analyst Matches					
Bench	Sample #	USGS Matches	Score	JPL Matches	Score
4675	30	praseody.spc	0.089		
	74	praseody.spc	0.094	riebeckite IN-7A	0.037
		hematit2.spc	0.047		
	75	hematit2.spc	0.051		
		ferrihyd.spc	0.039		

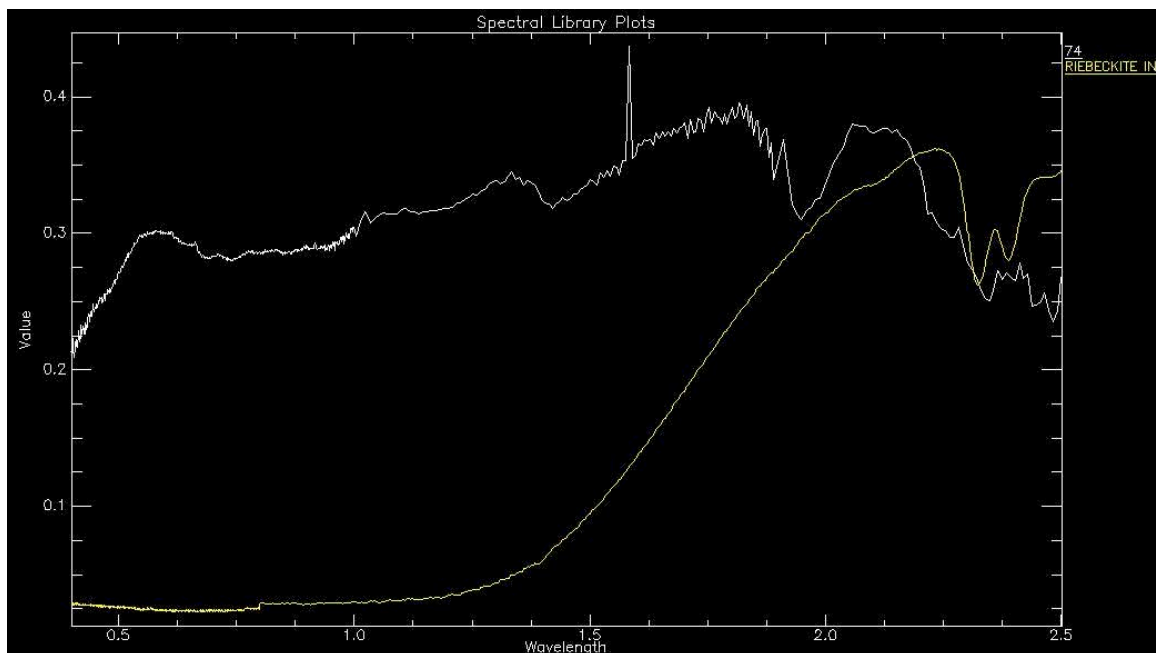


**Figure 9.3.** Spectral profile of sample 74 (white) from bench 4700 with - riebeckite (yellow) from JPL spectral library. Matching absorbance features can be seen at 1.61 $\mu$ m.

**Table 9.6.** Bench 4600 Spectral Analyst matches with USGS and JPL spectral libraries

Table 9.6 - Bench 4600 Spectral Analyst Matches					
Bench	Sample #	USGS Matches	Score	JPL Matches	Score
4600	57	chrysoco.spc	0.032	malachite C-7A	0.088
				azurite C-12A	0.07
				atacamite H-44	0.038
	58	hematit2.spc	0.023		
		ferrihyd.spc	0.014		
	62	hematit2.spc	0.07		
		ferrihyd.spc	0.051		
		lepidocr.spc	0.048		
		jarosit9.spc	0.032		
		goethit1.spc	0.004		
	64	jarosit9.spc	0.169	natrojarosite SO-7C	0.042
		hematit2.spc	0.144	jarosite SO-7A	0.007
		jarosit5.spc	0.129		
		lepidocr.spc	0.125		
		jarosit2.spc	0.119		
		goethit3.spc	0.115		
		jarosit7.spc	0.113		
		ferrihyd.spc	0.11		

Table 9.6 shows Spectral Analyst results for samples on bench 4600. Bench 4600 shows oxidation processes through secondary copper and iron minerals. Common secondary copper minerals azurite, malachite, and chrysocolla all occur in the oxidation zone and have been identified in the MacArthur pit on bench 4600.

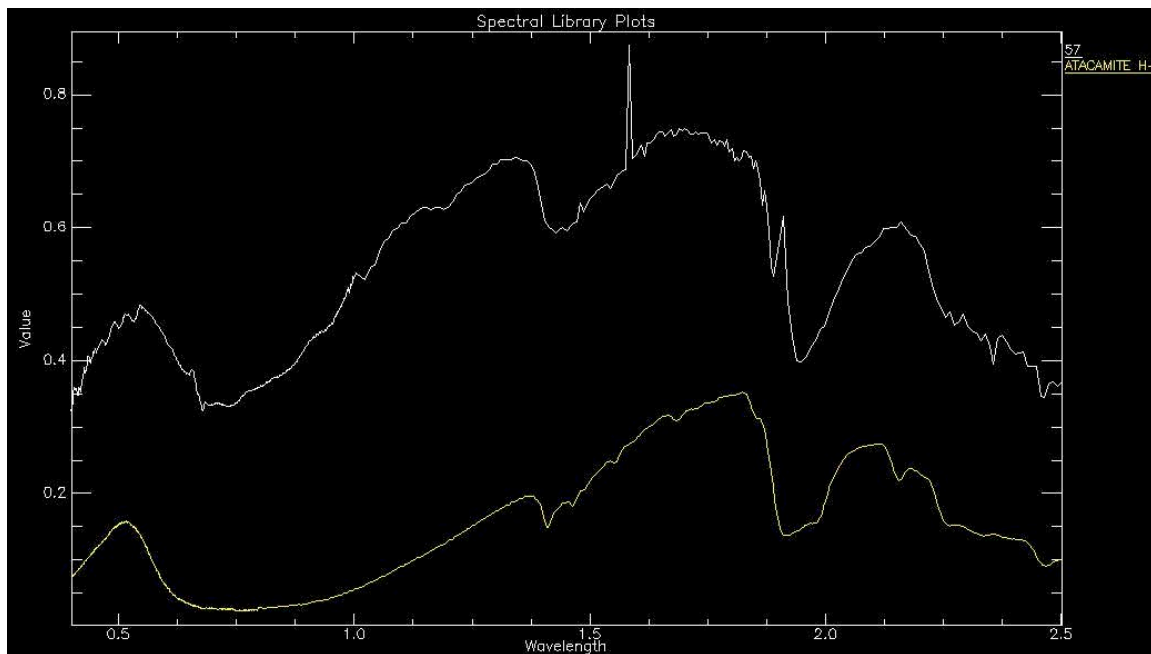


**Figure 9.4.** Spectral profile of sample 57 (white) from bench 4600 with - atacamite (yellow) from JPL spectral library. A similar line shape is seen but correlating absorption features are weak.

Atacamite, more rare and associated with oxidation under arid, saline conditions (Anthony J.W. et al 1997) is seen as a Spectral Analyst match in sample 57. Comparison of the spectra lines (Fig. 9.5) shows an overall similar line shape but weak correlations of absorbance features. Atacamite should not be ruled out as occurring at the MacArthur. The remaining Spectral Analyst matches all show secondary iron minerals and limonites that have associations with oxidation zones.

### 9.6.2. Spectral Analyst of 35 homogeneity spectrums.

Score ranges of Spectral Analyst matches are presented here by sample numbers. QMP-4780 and QMP-4750 homogeneity tests both resulted in low Spectral Analyst scores demonstrating a variability in alteration minerals (tables 9.7 and 9.8 respectively). When the spectrum of the both sites were compared against each other the results showed all scores to be below 0.2 (table 9.9).

**Table 9.7.** Spectral Analyst results from QMP-4780. An overall lack of spectral homogeneity suggests a mix of oxide minerals.

<b>Table 9.7 - QMP-4780 Homogeneity Test</b>				
<b>Sample #</b>	<b>Spectral Analyst matches and score range</b>			
	<b>0.6 - 0.4</b>	<b>0.4 - 0.2</b>	<b>0.2 - 0.1</b>	<b>&lt; 0.1</b>
Q-4780.1		Q-4780.3		
Q-4780.3		Q-4780.1		

**Table 9.8.** Spectral Analyst results from QMP-4780. An overall lack of spectral homogeneity suggests a mix of oxide minerals.

<b>Table 9.8 - QMP-4750 Homogeneity Test</b>				
<b>Sample #</b>	<b>Spectral Analyst matches and score range</b>			
	<b>0.6 - 0.4</b>	<b>0.4 - 0.2</b>	<b>0.2 - 0.1</b>	<b>&lt; 0.1</b>
Q-4750.2			Q-4750.4	
			Q-4750.3	
Q-4750.3	Q-4750.4		Q-4750.2	
Q-4750.4		Q-4750.3		Q-4750.2

**Table 9.9.** Spectral Analyst results show a weak overall correlation between sites of a continuous porphyry body.

<b>Table 9.9 - QMP-4750 &amp; QMP-4780 Homogeneity Test</b>				
<b>Sample #</b>	<b>Spectral Analyst matches and score range</b>			
	<b>0.6 - 0.4</b>	<b>0.4 - 0.2</b>	<b>0.2 - 0.1</b>	<b>&lt; 0.1</b>
Q-4750.1			Q-4780.2	
Q-4750.2			Q-4780.2	
Q-4750.3				Q-4780.1

QMP-4600 homogeneity test shows the highest Spectral Analyst scores for the three porphyry tests between samples 5, 8, and 9. These samples represent the best matches in the family (Table 9.10) with scores between 0.4 – 0.2. An overall lack in homogeneity represents a variety of minerals in the spectrum.

**Table 9.10.** Spectral Analyst results from QMP-4600. The relationship between samples 5, 8, and 9 indicates the strongest homogeneity in the family.

<b>Table 9.10 - QMP-4600 Homogeneity Test</b>				
<b>Sample #</b>	<b>Spectral Analyst matches and score range</b>			
	<b>0.6 - 0.4</b>	<b>0.4 - 0.2</b>	<b>0.2 - 0.1</b>	<b>&lt; 0.1</b>
Q-4600.4			Q-4600.1	
				Q-4600.5
				Q-4600.9
Q-4600.5		Q-4600.9		Q-4600.2
		Q-4600.8		Q-4600.7
		Q-4600.6		
Q-4600.7	Q-4600.8	Q-4600.9	Q-4600.5	Q-4600.1
				Q-4600.2
				Q-4600.6
Q-4600.8		Q-4600.9	Q-4600.6	Q-4600.2
		Q-4600.7		
		Q-4600.5		
Q-4600.9		Q-4600.8	Q-4600.6	
		Q-4600.5		

RHY-4700 homogeneity test shows two strong family relationships with spectrum 3 and 4 as well as spectrum 7 and 8. The scores for the relationship are between 0.6 - 0.4 (table 9.11). RHY-4675 homogeneity test shows a spectral relationship with 1, 9 and 7 with scores between 0.6 – 0.4 (table 9.12).

**Table 9.11.** Spectral Analyst results from RHY-4700. The relationship between samples 3 & 4 and 7 & 8 indicate the strongest homogeneity in the family.

<b>Table 9.11 - RHY-4700 Homogeneity Test</b>				
<b>Sample #</b>	<b>Spectral Analyst matches and score range</b>			
	<b>0.6 - 0.4</b>	<b>0.4 - 0.2</b>	<b>0.2 - 0.1</b>	<b>&lt; 0.1</b>
R-4700.1		R-4700.2	R-4700.5	R-4700.9
R-4700.2	R-4700.1	R-4700.9	R-4700.4	R-4700.8
	R-4700.5	R-4700.3	R-4700.7	
R-4700.3	R-4700.4		R-4700.7	R-4700.2
			R-4700.6	R-4700.8
R-4700.4	R-4700.3		R-4700.6	R-4700.8
			R-4700.7	R-4700.9
R-4700.5			R-4700.2	
R-4700.7	R-4700.8	R-4700.3	R-4700.2	R-4700.9
		R-4700.4	R-4700.5	
R-4700.8	R-4700.7		R-4700.3	R-4700.2
			R-4700.4	R-4700.5
R-4700.9				R-4700.2

**Table 9.12.** Spectral Analyst results from RHY-4675. The strongest relationship is between samples 1, 7, and 9.

<b>Table 9.12 - RHY-4675 Homogeneity Test</b>				
<b>Sample #</b>	<b>Spectral Analyst matches and score range</b>			
	<b>0.6 - 0.4</b>	<b>0.4 - 0.2</b>	<b>0.2 - 0.1</b>	<b>&lt; 0.1</b>
R-4675.1	R-4675.9	R-4675.4		R-4675.6
	R-4675.7	R-4675.5		
		R-4675.8		
		R-4675.3		
		R-4675.2		
R-4675.3			R-4675.7	
			R-4675.6	
R-4675.4		R-4675.5		R-4675.8
		R-4675.1		
		R-4675.9		
R-4675.5		R-4675.4		R-4675.7
		R-4675.9		R-4675.2
		R-4675.1		
		R-4675.8		
R-4675.6				R-4675.3
R-4675.7	R-4675.3	R-4675.2	R-4675.5	
	R-4675.9	R-4675.8		
	R-4675.1	R-4675.6		
R-4675.8		R-4675.9		
R-4675.9	R-4675.1	R-4675.3		
	R-4675.8	R-4675.4		
	R-4675.7	R-4675.6		
	R-4675.5			
	R-4675.2			

When the spectrum from both RHY test sites was compared against each other using Spectral Analyst (Table 9.13), the results indicate a relationship between R-4675.1, .9, and .7 with R-4700.7 and .8. These are the same variables from relationships at each location. This suggests a common alteration and oxide mineral occurrence in the rhyolite dikes.

**Table 9.13.** Spectral Analyst results show a correlation with RHY-4675.1, .9, and .7, with RHY-4700.7 and .8. This demonstrates spectral homogeneity in rhyolite mineralogy.

<b>Table 9.13 RHY-4675 &amp; RHY-4700 Homogeneity Test</b>				
<b>Sample #</b>	<b>0.6 - 0.4</b>	<b>0.4 - 0.2</b>	<b>0.2 - 0.1</b>	<b>&lt; 0.1</b>
R-4675.1	R-4700.7	R-4700.5		R-4700.6
	R-4700.8	R-4700.2		
		R-4700.1		
		R-4700.3		
		R-4700.9		
		R-4700.4		
R-4675.3	R-4700.4	R-4700.2	R-4700.9	
	R-4700.3	R-4700.6	R-4700.1	
		R-4700.7	R-4700.8	
			R-4700.5	
R-4675.5				R-4700.7
				R-4700.8
R-4675.6				R-4700.1
R-4675.7	R-4700.7	R-4700.6		
	R-4700.2			
	R-4700.3			
	R-4700.9			
	R-4700.1			
	R-4700.4			
	R-4700.8			
	R-4700.5			
R-4675.9	R-4700.2	R-4700.3	R-4700.6	
	R-4700.7	R-4700.4		
	R-4700.5			
	R-4700.8			
	R-4700.1			
	R-4700.9			

Spectral Analyst of homogeneity spectrum vs. USGS and JPL returned results for RHY-4675 samples 1, 3, 4, 7, and 9. Spectrum matches from this analysis represent minerals associated with three alteration types found in oxidized porphyry copper deposits: hydrothermal, propylitic, and oxidation (Table 9.14).

**Table 9.14.** RHY-4675 Spectral Analyst matches from USGS and JPL spectral libraries.

<b>Table 9.14 - RHY-4675 Homogeneity Spectral Analyst Matches</b>				
<b>Sample #</b>	<b>USGS Matches</b>	<b>Score</b>	<b>JPL Matches</b>	<b>Score</b>
R-4675.1	jarosit5.spc	0.317	natrojarosite SO-7C	0.273
	jarosit4.spc	0.305	jarosite SO-7A	0.257
	jarosit9.spc	0.3	plumbojarosite SO-7B	0.237
	jarosit7.spc	0.292	chlorite PS-12C	0.22
	jarosit2.spc	0.289	johannsenite IN-12A	0.213
	jarosit3.spc	0.264	tourmaline D-S	0.204
	goethit3.spc	0.253	chlorite T	0.202
	copiapit.spc	0.25	epidote SS-1A	0.196
	jarosit1.spc	0.246	chlorite R	0.194
	limonite.spc	0.243	chlorite P	0.192
R-4675.3	chrysoco.spc	0.044	azurite C-12A	0.141
			malachite C-7A	0.135
			atacamite H-4A	0.092
			antlerite SO-11A	0.028
R-4675.4	erionitm.spc	0.137	nontronite PS-6B	0.068
	sauconit.spc	0.104	mimetite A-1A	0.061
	mascagn2.spc	0.091	natrojarosite SO-7C	0.053
	goethit1.spc	0.06	sulfur E-2A	0.051
	nontron.spc	0.052	plumbojarosite SO-7B	0.05
	maghemit.spc	0.048	realgar S-3A	0.016
	sulfur.spc	0.046	jarosite SO-7A	0.013
	jarosit8.spc	0.045		
	jarosit2.spc	0.039		
	jarosit3.spc	0.038		
R-4675.7	malachit.spc	0.299	azurite C-12A	0.293
	acmite.spc	0.273	malachite C-7A	0.291
	plimonit.spc	0.267	chlorite P	0.276
	cchlore5.spc	0.259	glauconite PS-19A	0.273
	pyroxene.spc	0.257	chlorite R	0.268
	chrysoco.spc	0.242	atacamite H-4A	0.268
	glauconi.spc	0.24	antlerite SO-11A	0.259
	chlorit2.spc	0.233	chlorite T	0.246
	hornble2.spc	0.224	chlorite PS-12C	0.245
	azurite.spc	0.224	tourmaline D-S	0.227
R-4675.9	copiapit.spc	0.305	tourmaline D-S	0.302
	acmite.spc	0.297	glauconite PS-19A	0.272
	jarosit5.spc	0.228	johannsenite IN-12A	0.267
	jarosit4.spc	0.274	chlorite R	0.26
	jarosit9.spc	0.27	chlorite T	0.259
	jarosit7.spc	0.263	chlorite PS-12C	0.254
	glauconi.spc	0.262	chlorite P	0.25
	pyroxene.spc	0.259	ferroxinite CS-4A	0.248
	jarosit2.spc	0.253	enstatite IN-10B	0.234
	cchlore5.spc	0.246	malachite C-7A	0.226

Spectral Analyst matches from RHY-4675 sample 1 indicate minerals from oxidation and propylitic alteration. USGS matches indicate strong pyrite oxidation signature while the JPL matches indicate both pyrite oxidation and propylitic alteration. The oxidation of pyrite was accompanied by sodium and lead as indicated by natrojarosite and plumbojarosite respectively (Anthony J.W., 2003) while propylitic alteration is indicated by the strong presence of chlorite and epidote. Propylitic alteration is associated with low temperatures occurring in the distal regions (Fig. 2.4) of a porphyry system (Guilbert J.M., 1986).

Spectral Analyst matches from RHY-4675 sample 3 indicate oxidation of primary copper minerals. The presence of atacamite and antlerite suggest oxidation occurred under highly acidic conditions, especially in arid regions (Anthony J.W., 1997). When the spectral profile of R-4675.3 is compared to atacamite spectrum they show similar line shape and absorbance features at  $1.41\mu\text{m}$  and  $2.43\mu\text{m}$  (Fig 9.5).

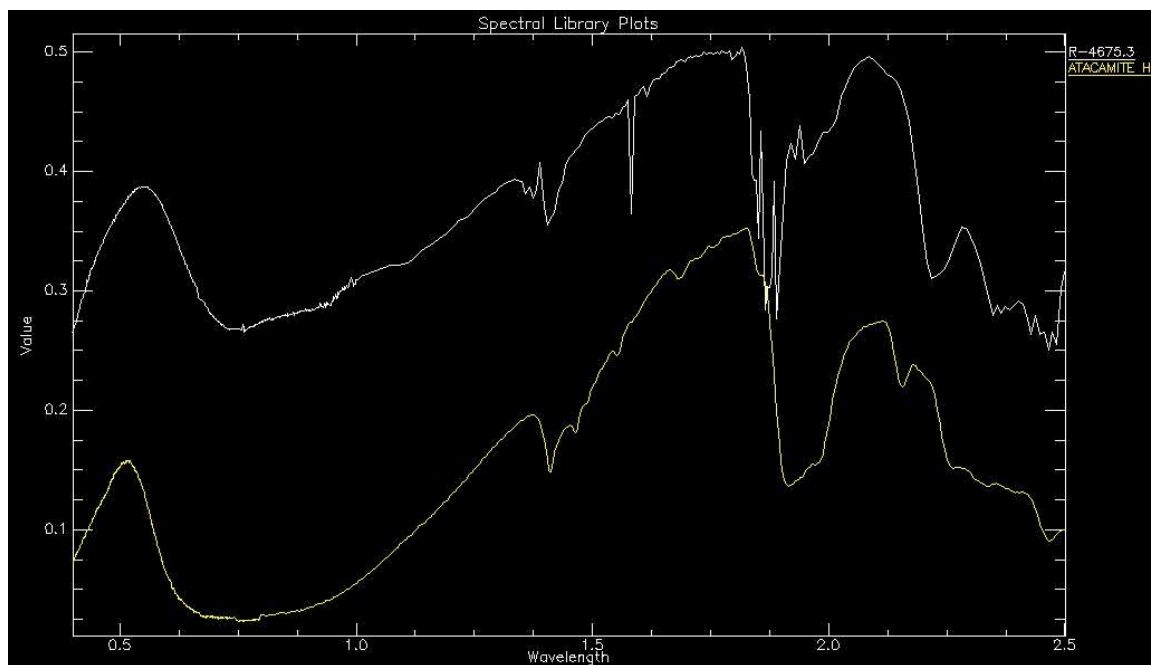


**Figure 9.5.** Spectral profile of sample R-4675.3 (white) with - atacamite (yellow) from JPL spectral library. A similar line shape is seen with matching absorption features at  $1.41\mu\text{m}$  and  $2.43\mu\text{m}$ .

Spectral Analyst matches from RHY-4675 sample 4 indicate hydrothermal alteration and oxidation. Hydrothermal alteration is indicated by the presence of nontronite, sulfur, and realgar (Anthony J.W., 2005). Hydrothermal alteration likely introduced other primary sulfide minerals such as magnetite, pyrite, and less galena. Today, oxidation products are seen as maghemite, limonites, and plumbojarosite respectively. The presence of sulfur in the spectrum from both USGS and JPL libraries suggests the system is partially oxidized. Sauconite is a zinc silicate mineral that also supports partial oxidation due to an association with water tables in copper oxide deposits (Anthony, J.W., 1995).

Spectral Analyst matches from RHY-4675 sample 7 indicate oxidation and propylitic alteration. The presence of glauconite indicates alteration of biotite and the spectrum shows a weak common absorption at 2.36 $\mu$ m with both USGS and JPL spectrum (Fig. 9.6) for glauconite, but its presence at the MacArthur is doubtful. Propylitic alteration is indicated by strong chlorite occurrences while oxidation is indicated by strong occurrences of secondary copper oxide minerals.

Spectral Analyst matches from RHY-4675 sample 9 indicate oxidation and propylitic alteration with weak sillication. Sillication is indicated by tourmaline and johannsenite, while propylitic alteration is indicated by the strong presence of chlorite group minerals. Secondary copper minerals and limonites along with copiapite, an iron sulfate, are part of obvious oxidation. The spectral profile of sample 9 compared to USGS copiapite is seen in Figure 9.7. A weak common absorption feature is seen at 1.93 $\mu$ m suggesting the presence of copiapite at the MacArthur should not be ruled out.

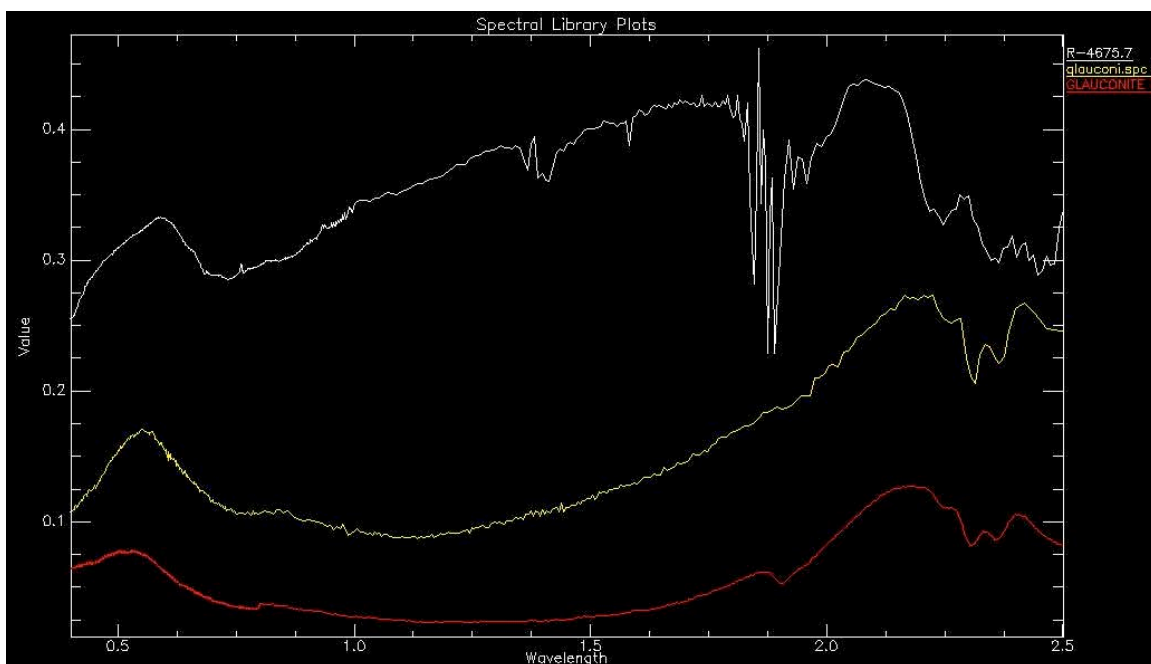


**Figure 9.6.** Spectral profile of sample R-4675.7 (white) with – glauconite from USGS (yellow) and JPL (red) spectral libraries. A weak common absorption is seen 2.36μm.

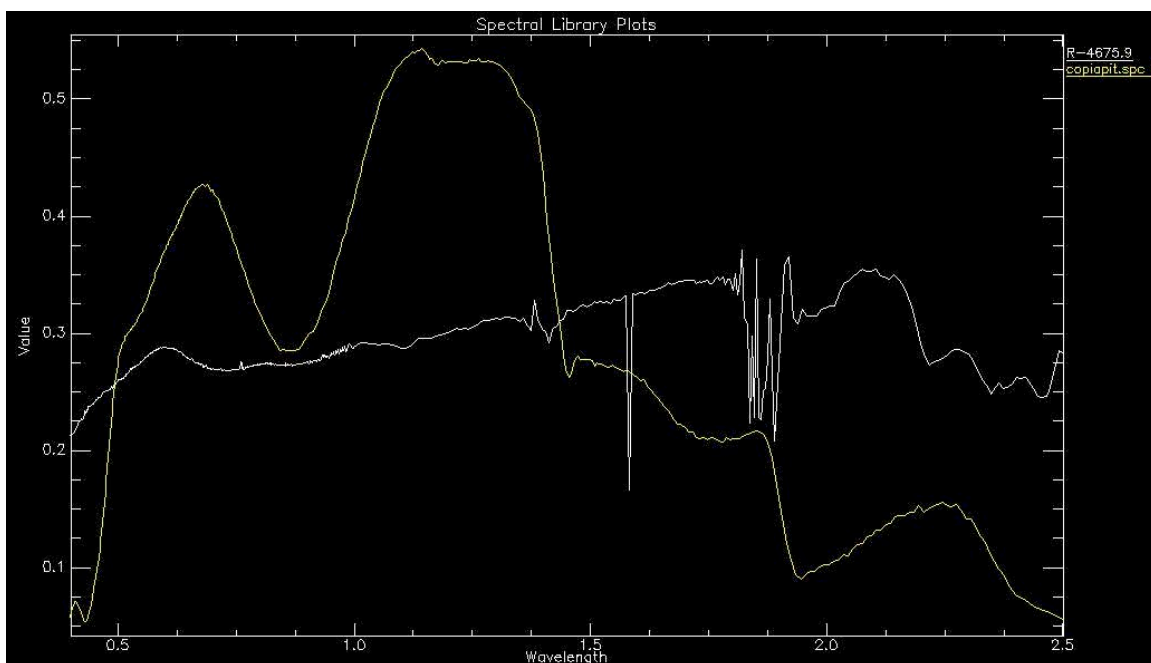


**Figure 9.7.** Spectral profile of sample R-4675.9 (white) with - copiapite (yellow) from USGS spectral library. A weak matching absorption feature is located at 1.93μm.

### 9.6.3. Analysis of 52 geochemical samples; relationship to copper grade.

Spectral Analyst in this study was used to test for homogeneity between spectra of geochemical samples and copper grade (%Cu). Quaterra Resources uses 0.18% Cu as a cut-off grade (<http://www.quaterraresources.com/>) in the oxide zone at the MacArthur and data presented here is in two tables, one representing samples below 0.18% Cu and one representing samples at or above 0.18% Cu (table 9.15 and 9.16 respectively). The tables show in the first column the test sample number and % Cu followed by column two displaying matching Spectral Analyst sample numbers and score. Added to column two from rock descriptions and geochemical analysis is % Cu, rock type, and visible copper color.

Table 9.15 shows 19 geochemical samples with percent Cu less than 0.18 that have Spectral Analyst matches with other samples. A maximum of five top matches are used with scores above 0.7 totaling 67 spectral matches. Of the 67 matches, 53 matches contain less than 0.18% Cu. Two of the samples, 39 and 63, have copper equal or greater than 0.18%, and appear several times as spectral matches. Sample 39 matches samples 41, 45, 56, and 59 while sample 63 matches samples 9, 29, 32, and 43.

Table 9.16 shows 20 samples with Cu equal to or greater than 0.18% that have spectral matches with other samples. A maximum of five top matches are used with scores above 0.7 totaling 74 spectral matches. Of the 74 matches, 60 matches contain equal to or greater than 0.18% Cu. Two of the samples, 29 and 32, with copper less than 0.18% appear several times as spectral matches. Sample 29 matches samples 33, 39, and 37 while sample 32 matches samples 40, 63, 68, and 75.

**Table 9.15.** Spectral Analyst matches of geochemical samples with associated percent copper below 0.18% with- rock type, and visible copper oxide color.

<b>Table 9.15 - Sample Spectrum with copper below cutt-off grade: 0.18%, Spectral Analyst Matches</b>						
<b>Sample Spectrum</b>		<b>Spectral Analyst Matches</b>				
<b>Sample #</b>	<b>% Cu</b>	<b>Sample #</b>	<b>Score</b>	<b>% Cu</b>	<b>RX type</b>	<b>V_CuOx</b>
1	0.08	42	0.772	0.14	QM	
		56	0.751	0.1	QMPb	
		55	0.749	0.07	QMPb	
		59	0.743	0.14	QM	B
		29	0.735	0.13	QMPb	
2	0.05	53	0.71	0.15	QM	
6	0.03	67	0.755	0.14	QM	
		51	0.744	0.12	QM	
		38	0.73	0.09	QM	
		32	0.703	0.15	QM	B
		43	0.7	0.09	QM	B
9	0.14	63	0.703	0.18	QM	B
29	0.14	41	0.799	0.16	QM	B
		63	0.789	0.18	QM	B
		38	0.759	0.09	QM	
		1	0.753	0.08	QM	
		67	0.751	0.14	QM	
32	0.15	67	0.837	0.14	QM	
		58	0.833	0.26	QM	G, B
		75	0.826	0.52	QMPh	B
		41	0.822	0.16	QM	B
		63	0.807	0.18	QM	B
38	0.09	45	0.772	0.05	QM	
		59	0.76	0.14	QM	B
		42	0.735	0.14	QM	
41	0.16	45	0.783	0.05	QM	
		59	0.781	0.14	QM	B
		55	0.748	0.08	QMPb	
		39	0.747	0.21	QMPb	G
42	0.14	54	0.777	0	QM	
		51	0.7	0.12	QM	

**Table 9.15 cont.** Spectral Analyst matches of geochemical samples with associated percent copper below 0.18% with- rock type, and visible copper oxide color.

<b>Table 9.15 cont - Sample Spectrum with copper below cutt-off grade: 0.18%, Spectral Analyst Matches</b>						
<b>Sample Spectrum</b>		<b>Spectral Analyst Matches</b>				
<b>Sample #</b>	<b>% Cu</b>	<b>Sample #</b>	<b>Score</b>	<b>% Cu</b>	<b>RX type</b>	<b>V_CuOx</b>
43	0.1	29	0.784	0.13	QMPb	
		9	0.768	0.14	QM	G
		63	0.738	0.18	QM	B
		41	0.737	0.16	QM	B
		32	0.735	0.15	QM	B
45	0.05	42	0.773	0.14	QM	
		39	0.772	0.21	QMPb	G
		59	0.74	0.14	QM	B
		55	0.733	0.08	QMPb	
51	0.12	43	0.74	0.1	QM	B
		54	0.731	0	QM	
		68	0.716	0.26	QM	B
		67	0.709	0.14	QM	
		7	0.71	0.05	QMPh	G
53	0.15	2	0.756	0.05	QM	
54	0	43	0.814	0.1	QM	B
		51	0.733	0.12	QM	
55	0.08	42	0.73	0.14	QM	
		45	0.728	0.05	QM	
		59	0.7	0.14	QM	B
56	0.1	1	0.767	0.08	QM	
		55	0.758	0.08	QMPb	
		39	0.733	0.21	QMPb	G
		45	0.732	0.05	QM	
		29	0.718	0.13	QMPb	
59	0.14	42	0.773	0.14	QM	
		39	0.762	0.21	QMPB	G
		45	0.742	0.04	QM	
		55	0.707	0.08	QMPb	
67	0.13	32	0.819	0.15	QM	B
		38	0.81	0.09	QM	
		29	0.786	0.13	QMPb	
		41	0.783	0.16	QM	B
		68	0.775	0.26	QM	B
72	0.13	69	0.812	0.99	RHY	G, B
		30	0.702	0.28	QM	

**Table 9.16.** Spectral Analyst matches of geochemical samples with associated percent copper above 0.18% with- rock type, and visible copper oxide color.

<b>Table 9.16 - Sample Spectrum with copper above cutt-off grade: 0.18%, Spectral Analyst Matches</b>						
<b>Sample Spectrum</b>		<b>Spectral Analyst Matches</b>				
<b>Sample #</b>	<b>% Cu</b>	<b>Sample #</b>	<b>Score</b>	<b>% Cu</b>	<b>RX type</b>	<b>V_CuOx</b>
22	0.99	69	0.782	0.99	RHY	G, B
		46	0.716	0.93	QM	G, B
		48	0.728	0.15	QM	
		63	0.725	0.18	QM	B
27	0.35	60	0.725	0.99	QM	B, G
		61	0.718	0.22	QM	G
30	0.28	69	0.765	0.99	RHY	G, B
		22	0.764	0.99	QM	G, B
		72	0.762	0.13	QMPH	G
		47	0.739	0.38	QM	B, G
		57	0.719	0.99	QM	G, BL
31	0.48	58	0.7	0.26	QM	G, B
33	0.22	67	0.822	0.14	QM	
		70	0.819	0.2	AND	
		68	0.816	0.26	QM	B
		29	0.806	0.13	QMPb	
		75	0.788	0.52	QMPH	B
39	0.21	38	0.83	0.1	QM	
		67	0.807	0.14	QM	
		56	0.804	0.1	QMPb	
		29	0.774	0.13	QMPb	
		6	0.766	0.04	QMPH	G
40	0.66	63	0.849	0.18	QM	B
		68	0.823	0.26	QM	B
		58	0.811	0.26	QM	G, B
		32	0.801	0.15	QM	B
		62	0.798	0.99	QM	G
44	0.26	42	0.774	0.14	QM	
		59	0.735	0.14	QM	B
		39	0.714	0.21	QMPb	G
46	0.93	69	0.712	0.99	RHY	G, B
47	0.38	30	0.705	0.28	QM	G, BL
58	0.26	62	0.838	0.99	QM	G, B
		60	0.821	0.99	QM	B, G
		64	0.789	0.51	QM	G
		61	0.785	0.22	QM	G
		31	0.775	0.48	QM	G

**Table 9.16 cont.** Spectral Analyst matches of geochemical samples with associated percent copper above 0.18% with- rock type, and visible copper oxide color.

<b>Table 9.16 cont - Sample Spectrum with copper above cutt-off grade: 0.18%, Spectral Analyst Matches</b>						
<b>Sample Spectrum</b>		<b>Spectral Analyst Matches</b>				
<b>Sample #</b>	<b>% Cu</b>	<b>Sample #</b>	<b>Score</b>	<b>% Cu</b>	<b>RX type</b>	<b>V_CuOx</b>
60	0.99	62	0.814	0.99	QM	G, B
		58	0.807	0.26	QM	G, B
		61	0.791	0.22	QM	G
		64	0.744	0.51	QM	G
		33	0.723	0.22	QM	B
61	0.22	60	0.777	0.99	QM	B, G
		30	0.759	0.28	QM	G, BL
		64	0.753	0.51	QM	G
		58	0.752	0.26	QM	G, B
		62	0.736	0.99	QM	G, B
62	0.99	58	0.849	0.26	QM	G, B
		60	0.838	0.99	QM	B, G
		75	0.793	0.52	QMPh	B
		61	0.785	0.22	QM	G
		64	0.778	0.51	QM	G
63	0.18	41	0.827	0.16	QM	B
		29	0.79	0.13	QMPh	
		9	0.769	0.29	QM	
		68	0.757	0.26	QM	B
		32	0.752	0.15	QM	B
64	0.51	58	0.796	0.26	QM	G, B
		61	0.793	0.22	QM	G
		62	0.771	0.99	QM	G, B
		60	0.77	0.99	QM	B, G
		30	0.754	0.28	QM	G, BL
68	0.26	41	0.821	0.16	QM	B
		75	0.815	0.52	QMPh	B
		63	0.786	0.18	QM	B
		40	0.779	0.66	QM	
		32	0.775	0.15	QM	B
69	0.99	46	0.726	0.93	QM	G, B
70	0.2	38	0.771	0.09	QM	
75	0.52	62	0.813	0.99	QM	G, B
		68	0.794	0.26	QM	B
		58	0.783	0.26	QM	G, B
		32	0.782	0.15	QM	B
		60	0.759	0.99	QM	B, G

## 9.7. Interpretations

Spectral radiometry provides means for the identification of uncommon and rare minerals in oxidized sections, and the results of analyses performed in this chapter give strong clues into the alteration styles in the MacArthur pit. Interpreted from Spectral Analyst, three alteration types associated with porphyry copper deposits can be identified: hydrothermal, propylitic, and oxidation. RHY-4675 homogeneity test shows all of the above-mentioned alterations in a single rhyolite dike and reflect an overall process in the MacArthur pit.

Chemistry of minerals identified in Spectral Analyst, indicate the hydrothermal event at the MacArthur was rich in metals Fe and Cu. Three major alteration types: potassic, sodic, and sericitic are seen in field studies at the MacArthur, but are not identified in spectral data. Sericitic alteration is seen in hand samples of quartz monzonite. Late argillic alteration and surface weathering phenomena have overprinted the sericitic alteration with Cu and Fe oxides so that other spectra are not detected.

Propylitic alteration is seen in three of the spectra from the field homogeneity test and field observations with rock descriptions support this in the lower benches of the MacArthur pit. The lower benches show hornblende and biotite altering to chlorite, while in the upper benches strong sericite is encountered. This likely reflects a transition zone from the outer propylitic shell to start of the phyllic zone (Guilbert and Park, 1986). The phyllic zone is recognized at the MacArthur pit by the increase of sericite with destruction of feldspars, and abundant iron oxides from strong oxidation of primary pyrite (Tables 9.3 and 9.4). The mineral occurrences and alteration styles here suggest the MacArthur pit is near the outer shell of porphyry system.

Oxidation is the last alteration at the MacArthur, occurring late, likely with and post-Basin and Range. Tables 9.3 – 9.6 and 9.14 demonstrate that Spectral Analyst matches are dominated by oxide zone-product mineralogy. Because oxidation is strong and last to occur, it may prevent spectral data from detecting earlier alteration minerals and other rock minerals by dominant copper and iron coatings. However, because oxide zone mineralogy is strong it provides an opportunity to test for relationships between spectral absorption features and percent copper.

Initial results in the study of spectral radiometry, as related to copper grade in the MacArthur pit, indicate spectral reflectance data has validity in the identification of rocks associated with value in oxide zone mineralogy. Finding wavelengths associated with copper mineralization and removing the rest of the spectrum may achieve tighter control on results. In this method, Spectral Analyst uses only the wavelength that contains the diagnostic absorption features related to the material of interest (Kruse and Lefkoff, 1999). The refinement of this study will be discussed in recommendations (Chapter 13).

## **10. FRACTURE DENSITY**

### **10.1. Introduction**

Studies related to the origin and evolution of porphyry systems indicates large masses of fluid flow through fractured host rocks and intrusive stock works (Haynes and Titley, 1980). Titley et al., (1986) used fracture density at the Sierrita-Esperanza porphyry deposit in Arizona to define the limits of the hydrothermal system through the distribution, abundance, and mineralization of fracture systems. Fractures in the MacArthur pit show varying physical orientations and mineralization characteristics for three major families of fractures. Fracture families are found not to be random, but similarly oriented throughout the span of the pit area. The aim of this study is to use fracture density to understand transport pathway orientations related to copper grade control in the oxide zone of the Macarthur pit.

### **10.2. Data**

Data for this fracture density study includes 99 sites (Fig. 10.1) collected in 25ft intervals from the MacArthur bench faces. Each interval can be broken into several variables including (Table 10.1):

- (1) Fractures that contain only transported copper
- (2) Fractures that contain only transported limonite
- (3) Fractures that contain a mix of transported copper and limonite
- (4) Fractures that have no association with mineralization, fresh fractures.

Three major fracture orientation families represent the above data:

Family 1 (F1): A west-northwest orientation that dips north/northeast.

Family 2 (F2): A southeast-northwest orientation that dips to the southwest.

Family 3 (F3): A close to vertical east-west orientation dipping north or south.

Appendix 5 shows the bench interval, UTM location, and total fracture density of each sample location. Appendix 5 also shows data for the above-mentioned variables per bench for each individual site. These variables will be further discussed in methods.

### 10.3. Field Methods

A total of 99 bench interval density measurements were collected along the MacArthur bench faces to determine fracture orientation and density (Fig. 10.1). Fracture density mapping consists of using a 2x2 foot frame, placing it on a bench face at set 25-foot intervals (Eliopulos and Heatwole, 2009), and measuring fracture orientation and length as well as observing where transported (oxide) copper and iron occur within the fracture system. Set 25-foot intervals were used to prevent un-intended bias in density measurements.

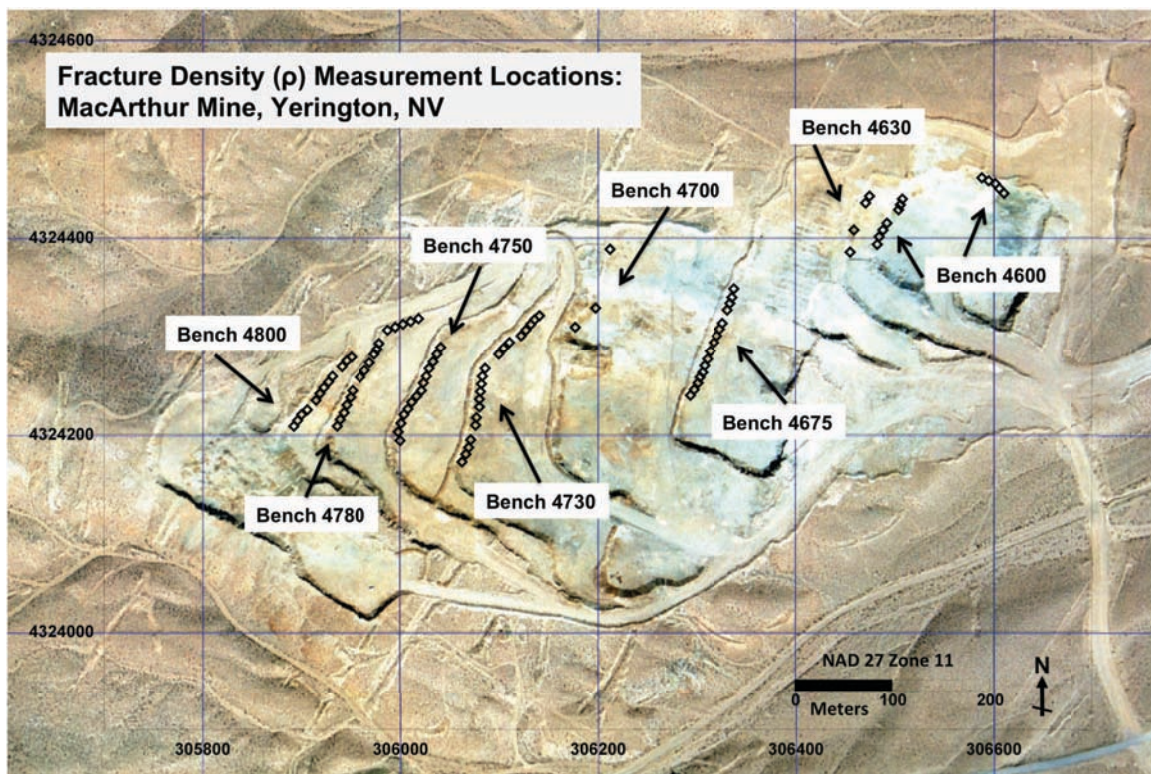


**Figure 10.1.** Fracture density measurement locations. Interval labeling starts in the north and moves south in 25-foot intervals along the MacArthur bench faces. Missing locations are due to bench face collapse or covered interval.

Field observations show the pit area to have three major families of fracture orientations; the strongest of which strikes approximately west to northwest, and dips to the north, northeast. Heatwole (1972) tested the northwest fractures in Anaconda trenches to see if they could be used to project grade zones. He discovered that although the northwest fracture pattern is well developed all orientations are equally mineralized. To gain an understanding regarding distribution of oxides in fractures, the three most abundant fracture families F1, F2, and F3 were recorded.

Once orientations were recorded the next step was to record the length of each individual fracture per orientation. Fractures were measured with a standard tape measure and the length of each fracture in inches was recorded in the column thus denoting what secondary transport mineralogy it carried or if it was a fresh fracture. Each fracture was listed as its own length thus providing an “n” number of how many fractures in each orientation are present as well as a density measurement. Table 10.1 shows an example of the how the data was recorded in the field.

**Table 10.1.** Table shows how data was recorded at each bench interval measurement. Each number in the boxes represents a single fracture.

<b>Table 10.1 - Fracture Density Interval 4675-00'</b>				
<b>Cu_Only</b>	<b>Fe_Only</b>	<b>Cu + Fe</b>	<b>Fresh</b>	<b>Orientation</b>
	12, 8, 6	14, 18, 23, 13, 26, 30, 8, 15, 20, 15, 7	3, 16, 4, 14, 6	104°, 64° <sup>N</sup> (Family 1)
		25, 18, 26		164°, 37° <sup>SW</sup> (Family 2)
		6, 4, 7, 11	8, 9, 6	291°, 82° <sup>S</sup> (Family 3)

## 10.4. Processing

The first step in data processing was to transfer all field recorded data into digital format. A total of three spreadsheets were created using Microsoft Excel, one sheet for each fracture family.

The next step was to solve fracture density for each bench interval. This was performed by summing the fracture lengths for all families and dividing by the area of the frame (Titley, 1986). In this study, inches are the units. An example of this for bench interval 4675-00' is seen in Table 10.2. As well as solving total density, each fracture family density was solved. Appendix 5 shows data from Table 10.2 for all bench intervals.

The final step in data processing was to calculate percent (%) densities. First, percent density was solved for the three fracture families, then for each family percent Cu, Fe, Cu + Fe, and fresh fractures were calculated per interval. Percent densities of these variables are described further in analysis.

**Table 10.2.** Demonstration of how fracture density ( $\rho$ ) is calculated for this study.

<b>Table 10.2 - Bench Interval 4675-00' Density (<math>\rho</math>)</b>					
<b># 4675-00</b>	<b>Cu</b>	<b>Fe</b>	<b>Fe + Cu</b>	<b>Fresh</b>	<b><math>\rho = \text{in}^{-1}</math></b>
Family 1	0	26	189	43	0.448
Family 2	0	0	69	0	0.120
Family 3	0	0	28	23	0.089
<b>Total Fx Length =</b>			378 in		
<b>Total Frame Area =</b>		24*24	576 in <sup>2</sup>		
<b>Total <math>\rho</math> =</b>		<b>378 in</b> <b>576 in<sup>2</sup></b>	<b>0.656 in<sup>-1</sup></b>		

## 10.5. Analysis

When data processing was complete it became evident that several analysis options could represent the data. Analysis techniques performed on the data set encompass stereonet, % density and % oxides, statistical analysis, and spatial analysis.

### 10.5.1. Stereonets

The first step in analysis was to make stereonet for each fracture family to test for homogeneity in orientation and then stereonet were made for the 50 bench intervals. This was accomplished using *Stereonet 6.3.3X*, (Allmendinger, 2006). The bench interval stereonet show orientation, number of fractures per family (n), and density ( $\rho$ ) of each family (Fig. 10.2). Stereonets are color coordinated with red, blue, and black representing fracture family 1, family 2, and family 3 respectively.

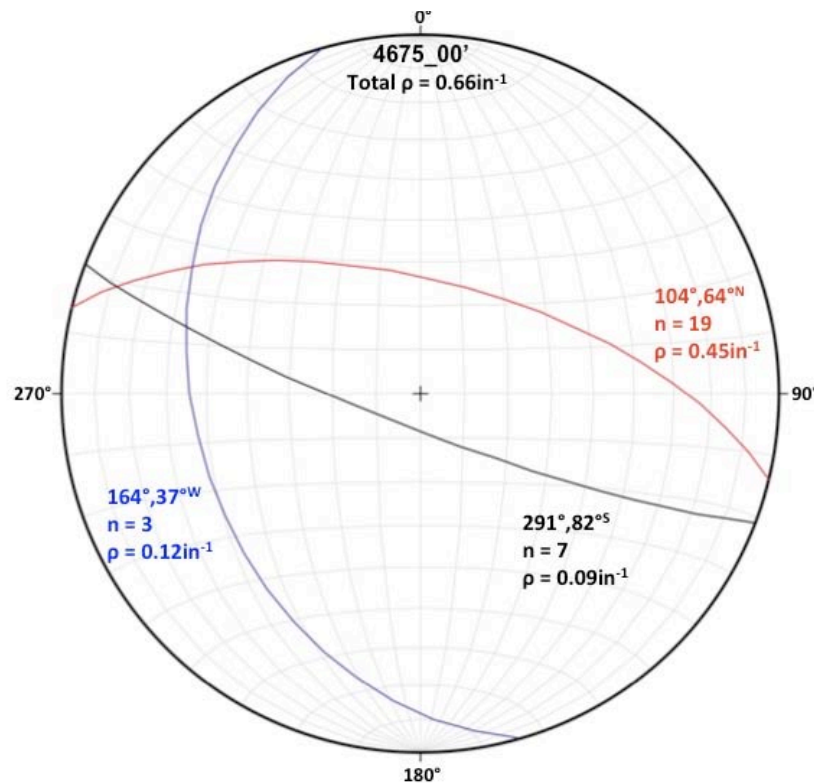


**Figure 10.2.** Stereonet of interval 4675\_00 showing F1 (red), F2 (blue), and F3 (black) orientation, number of fractures (n), and density ( $\rho$ ).

### 10.5.2. % Density and % Oxides:

Percent density is calculated to determine what fracture family is the dominant orientation. This data is represented in a pie chart (fig 10.5, pg 108.). Three pie charts show for each fracture family percent Fe, Cu, Cu + Fe, and fresh fractures and another pie chart represents total occurrence of each percent for all density interval measurements (fig 10.6, pg 109.). The last step in percent analysis uses bar graphs to represent percent total Fe and Cu per fracture family for bench intervals. This was completed for the 50 bench interval measurements with stereonet. The bar graphs are color coordinated the same as stereonet and combined on stereonet figures. Figure 7.3 shows the “updated” stereonet figures and all 50 figures may be found in Appendix 5.

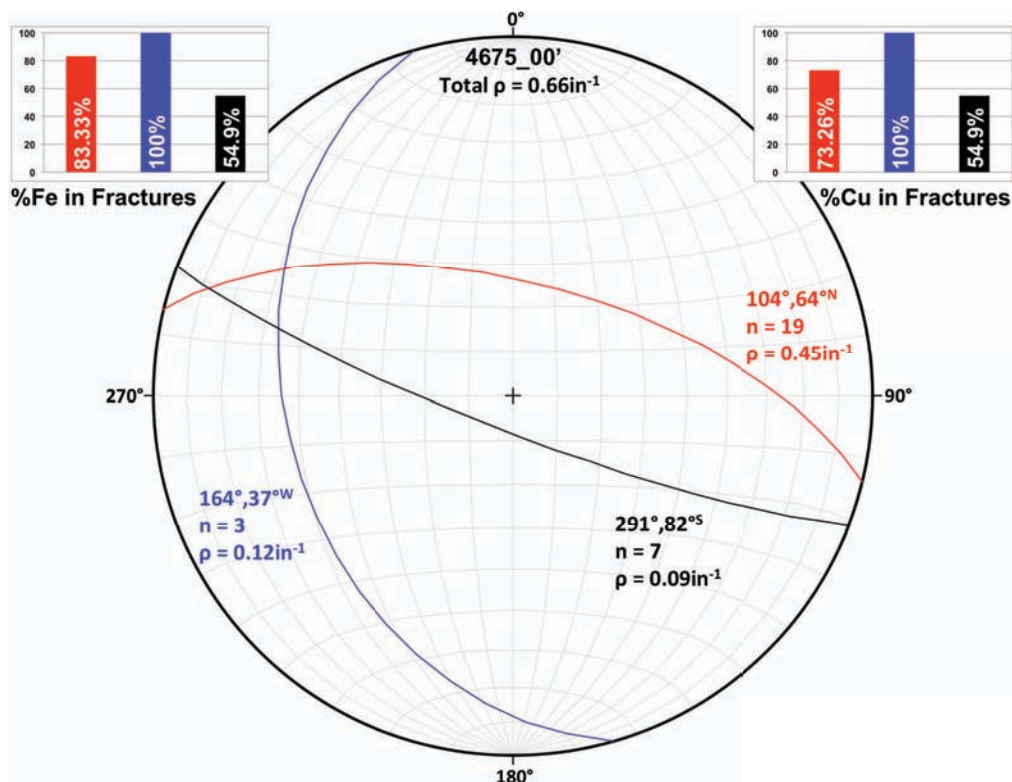


**Figure 10.3** Stereonet of interval 4675\_00 showing orientation, number of fractures, and fracture density as well as percent copper and iron occurring in each fracture family.

### 10.5.3. Statistical Analysis

Statistical analyses for this study include bivariate and multivariate analysis. Bivariate analysis includes correlation coefficient matrix and correlation scatter plot matrix. The correlation coefficient matrix and correlation scatter plot are used to investigate linear relationships between variables. Principal component analysis (PCA) is the multivariate analysis for this study. PCA seeks a linear combination in variables and results in factor score coefficients. Factors are a way to view positive and negative relationships or commonalities between a set of variables that can lead to a statement regarding a single geologic process or substance.

In this study, multivariate analysis is used to determine relationships between fracture density and transported oxide mineralogy for all 99-bench interval measurements (Appendix 5). The 20 variables used in this study include: for F1, F2, and F3 – copper oxides (CuOx), iron oxides (FeOx), total oxides (t-Ox), number of fractures (n), and fracture density ( $\rho$ ). The remaining 5 variables are totals of variables described above, T-CuOx, T-FeOx, T-Ox, T-n, and T- $\rho$ . Table 10.3 demonstrates the variable values for bench interval 4675-00.

**Table 10.3.** Red numbers indicate 20 variables used in statistical analysis for; F1, F2, F3, and Totals.

<b>Table 10.3 - Variables for Statistical Analysis: 4675-00'</b>							
<b>Family</b>	<b>Total Ox</b>	<b>Cu</b>	<b>Fe</b>	<b>Fe + Cu</b>	<b>Fresh</b>	<b>n</b>	<b><math>\rho = \text{in}^{-1}</math></b>
F1	215	0	26	189	43	19	0.448
F2	69	0	0	69	0	3	0.120
F3	28	0	0	28	23	7	0.089
<b>Variables</b>	<b>t-Ox</b>	<b>CuOx = Cu + (Fe + Cu)</b>		<b>FeOx = Fe + (Fe + Cu)</b>		<b>n</b>	<b><math>\rho</math></b>
F1	215	189		215		19	0.448
F2	69	69		69		3	0.120
F3	28	28		28		7	0.089
<b>Totals:</b>	<b>T-Ox</b>	<b>T-CuOx</b>		<b>T-FeOx</b>		<b>T-n</b>	<b>T-<math>\rho</math></b>
F1+F2+F3	312	286		312		29	0.656

#### **10.5.4. Spatial Analysis**

Spatial analysis used in this study is density data from bench interval measurements.

Spatial analysis of density is used to understand the distribution of fracture patterns and associated oxide occurrence in the MacArthur pit.

Contour maps are made for eight variables:

- (1) Family 1 density ( $\rho$ -F1)
- (2) Family 2 density ( $\rho$ -F2)
- (3) Family 3 density ( $\rho$ -F3)
- (4) Total interval density ( $\rho$ -T)
- (5) CuOx density ( $\rho$ -CuOx)
- (6) FeOx density ( $\rho$ -FeOx)
- (7) CuOx and FeOx density ( $\rho$ -Cu-FeOx)
- (8) Fresh fracture density ( $\rho$ -Fr).

#### **10.6. Results**

The results of fracture density analysis are summarized in this section. Quantitative data from the oxide zone of the MacArthur pit leads to an understanding of behavior and distribution of fractures and associated oxide occurrences in the MacArthur pit. A complete list of figures and data can be found in Appendix 5.

##### **10.6.1. Stereonets**

The four stereonet in Figure 10.4 are used to demonstrate ranges of orientation in fracture families. Family 3 is represented in two stereonet, one to show north dipping fractures and one showing south dipping fractures. Fracture family 1 has a strike range of 84-121° with 4 fractures that deviate up to 135°. This orientation dips moderately to the north – northeast between 39-75°. Fracture family 2 has a strike range 131-171° with only two fractures that deviate to 124°. Family 2 has a moderate southwest - west dip ranging 31-68°. South dipping fractures in family 3 show a tight clustering with a strike range of 280-294° with four fractures

that deviate up to  $305^\circ$ . They dip steeply south with a range of  $77-89^\circ$ . North dipping fractures in family 3 have a strike range of  $267-309^\circ$ , dipping steeply north with a range of  $80-89^\circ$ . The ranges in strike for F1, F2, and F3:  $51^\circ$ ,  $47^\circ$ , and  $42^\circ$  respectively, show there is continuity in fracture families. The south dipping fractures in family 3 show the best continuity clustering within  $14^\circ$  of each other while the north dipping fractures show the most variability over the largest range -  $42^\circ$ . Excluding fractures that deviate from clustered groups, families 1 and 2 show an overall tighter clustering than the north dipping fracture of family 3.

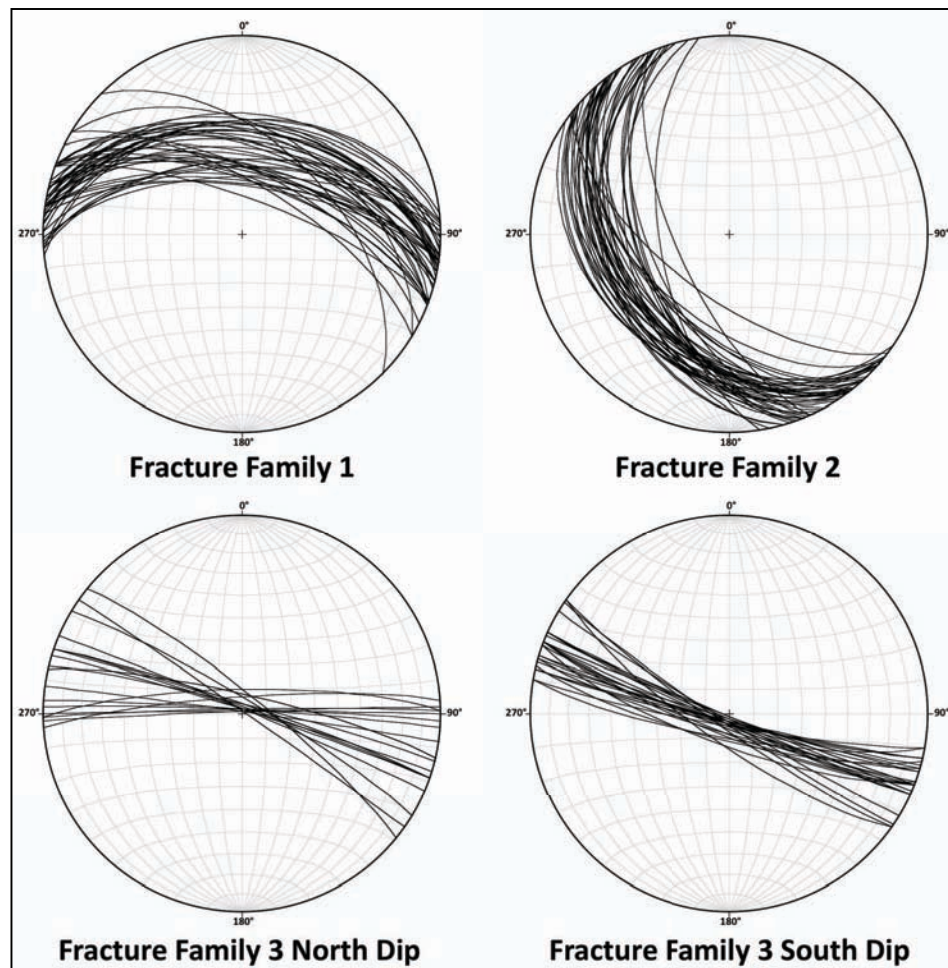


**Figure 10.4.** Stereonets showing orientations and ranges of fracture families in the MacArthur pit.

Appendix 5 shows stereonet created for 50 bench intervals with orientation, number of fractures, and density for each fracture family as well as total interval density. The figures include bar charts showing percent Cu and Fe oxides in each fracture family and will be discussed together. The figures show a variety of density behaviors and associated oxide behavior. The percent Cu graphs show an overall trend of Cu increasing in F2 while decreasing in F1 and F3 from north to south along the bench faces. An exception to this is bench 4600 where F3 is associated with the strongest oxides.

For two of the upper benches (4800 and 4750), the increase of transported Cu in F2 is associated with an increase in fracture density, but not necessarily an increase in number of fractures. Bench 4730 and 4700 show high values ( $< 0.4$ ) for density in F1 and F3 while bench 4675 shows an overall increase in total density. The number of fractures seen for each interval shows a weak association with density and will be discussed further in bivariate analysis.

#### **10.6.2. % Density and % Oxides**

Five pie charts are used in this section to discuss the results of percent densities of fracture families and transported oxides found in fractures. Figure 10.5 represents all 99-bench interval measurements and shows total percent density of each fracture family. Results indicate that F1 is the dominant fracture family and accounts for 39.1% of all fractures in the MacArthur pit, followed by F2 and F3 respectively.

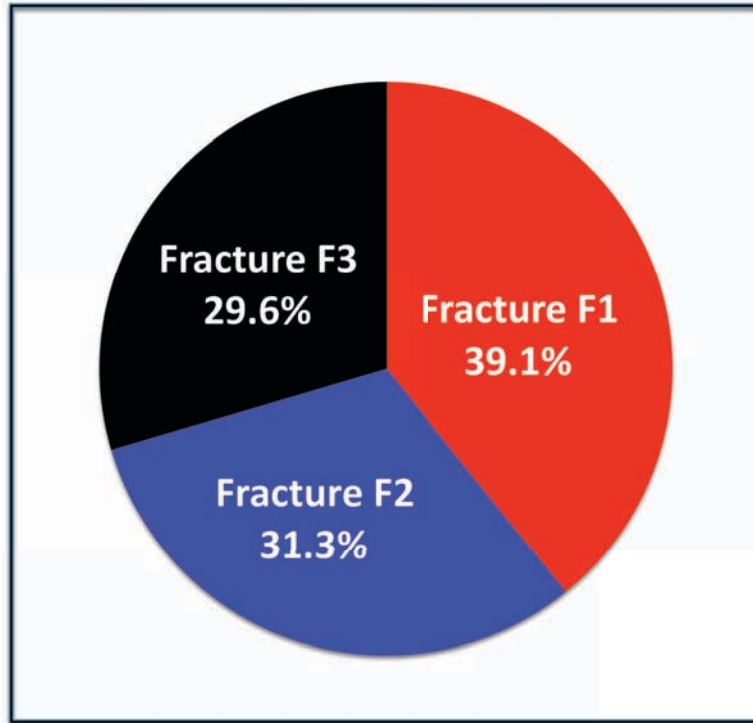


**Figure 10.5.** Percent occurrences of fracture families in the MacArthur pit from 99 fracture density measurements.

Figure 10.6 shows four pie charts displaying total percent oxides in fracture families and all fractures together from 99 bench interval measurements. Results of Figure 10.6 show that F2 contains the highest values for Cu only fractures, fresh fractures, and total Cu, but contains the least amount of total transported oxides by 0.1%. Results also show that F3 contains no Cu only fractures and 2% fresh fractures. Fracture F1 is the strongest occurrence of Fe only fractures, and oxides occur in 98.6% of all fractures in F1. The results of this test demonstrate that 98.3% of all fractures in the MacArthur pit are associated with oxide zone produced copper and iron at a close to even distribution amongst fracture families.

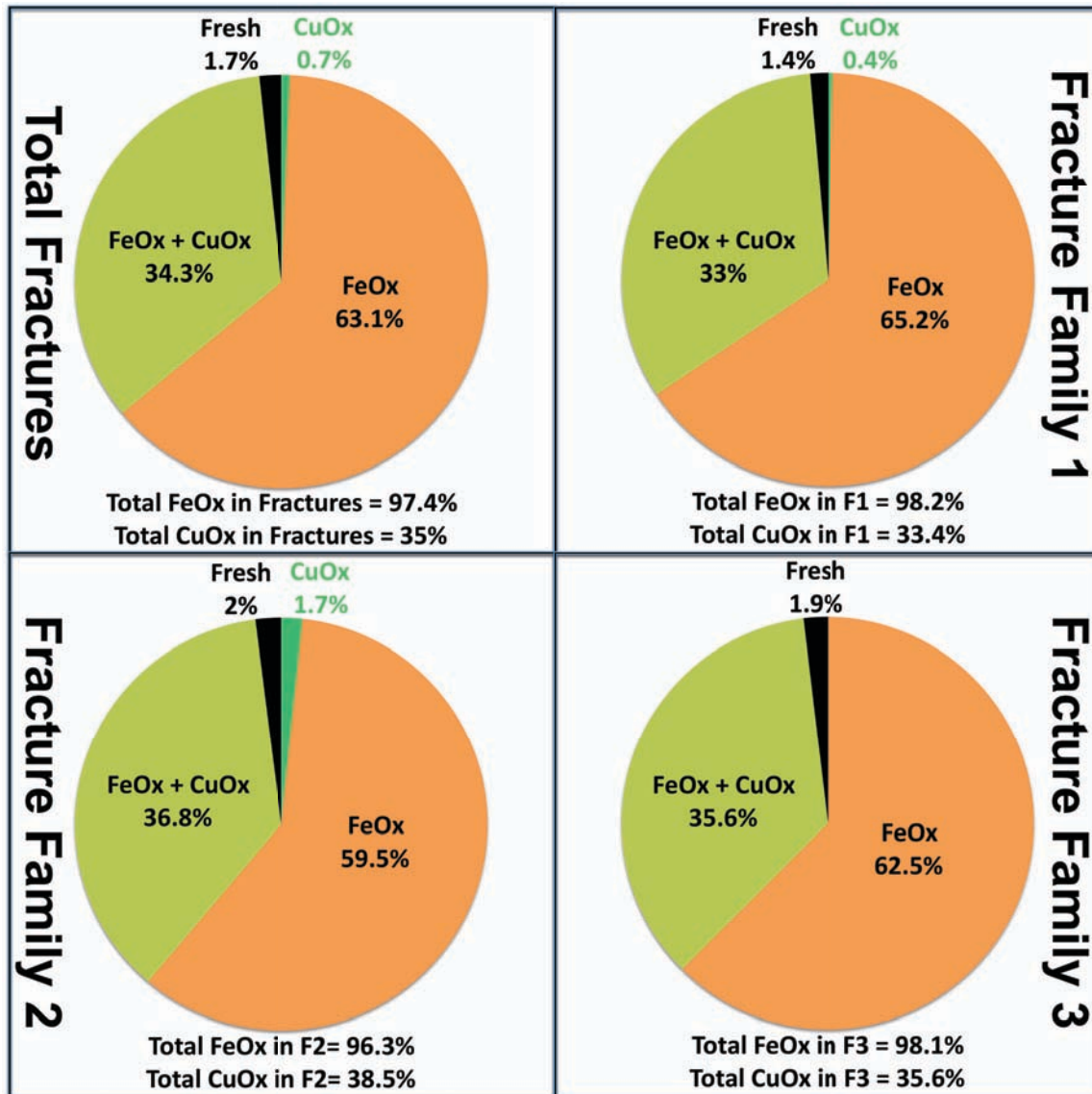


**Figure 10.6.** Pie charts displaying percent oxides (copper and iron) in fracture families. The pie charts demonstrate an overall equal distribution of oxides in fractures.

### 10.6.3. Statistical Analysis

The results of bivariate analysis are presented here. The following discussion will describe variables occurring in groups with correlation scores above 0.9, between 0.9-0.7, and between 0.5-0.7. Bivariate correlations scores above 0.9 show strong relationships with transported FeOx, t-Ox and Density for all fracture families, as well as all T-FeOx and T-Density variables (Table 10.4). This demonstrates that FeOx occurs in almost all fractures increasing or decreasing with density.

**Table 10.4.** Resulting correlation scores from bivariate analysis of fracture density data. A strong relationship between density, iron oxides, and total oxides is seen for all fracture families.

Table 10.4 Correlations With Scores >0.9								
	F1 FeOx	F1 t-Ox	F2 FeOx	F2 t-Ox	F3 FeOx	F3 t-Ox	T-FeOx	T-Ox
F1 t-Ox	0.9990903							
F1 Density	0.9933846	0.9941196						
F2 t-Ox			0.9768446					
F2 Density			0.9648245	0.9868283				
F3 t-Ox					1			
F3 Density					0.9965029	0.9965029		
T-Ox							0.9955529	
T-Density							0.9847589	0.9890363

Correlation scores between 0.7-0.9 can be grouped into three common families each showing different relationships (Table 10.5). The first group shows a correlation between T-CuOx with F1, F2, and F3-CuOx. F2 shows the highest correlation score from this group at 0.88 demonstrating a close relationship with transported CuOx in fractures. The second group shows inter-family relationships for F1, F2, and F3 between FeOx, t-Ox, Density and n. This group demonstrates that iron oxides, density, and number of fractures behave the same in each family. The last group shows a relationship between F1 with T-FeOx, T-Ox, T-Density and T-n. This is due to F1 being the strongest occurring family in the MacArthur pit.

**Table 10.5.** Resulting correlation scores from bivariate analysis of fracture density data. Three groups are defined: copper oxides (shown in black), inter-family oxide and number of fractures (orange), and F1 with Totals (red).

Table 10.5 Correlations With Scores Between 0.7-0.9																
Row	F1 CuOx	F1 FeOx	F1 t-Ox	F1 n	F1 Density	F2 CuOx	F2 FeOx	F2 t-Ox	F2 n	F3 CuOx	F3 FeOx	F3 t-Ox	F3 n	T-FeOx	T-Ox	T-n
F1 n		0.8321	0.8327													
F1 Density				0.8310												
F2 n							0.7534	0.7781								
F2 Density									0.7747							
F3 n											0.8042	0.8042				
F3 Density													0.8081			
T-CuOx	0.8658					0.8760				0.7970						
T-FeOx		0.7221	0.7194													
T-Ox		0.7180	0.7179													
T-n				0.7594										0.7993	0.8067	
T-Density		0.7422	0.7424		0.7334											0.8155

Correlation scores between 0.5-0.7 can be grouped into four common families each showing different relationships (Table 10.6). The first group shows relationships between F1 with Totals for the variables FeOx, Ox, Density and n. This group represents the remaining variables not present in the group with correlations scores between 0.7-0.9. The second group shows a relationship between F3 with T-FeOx, T-Ox, T-Density and T-n. The third group shows a relationship for F1, F2, and F3 - CuOx variable. This suggests that transported CuOx behave similarly in each fracture family. The fourth and final group shows an inter-family relationship in F2 for the variables CuOx, FeOx, t-Ox, and Density. This suggests all oxides in F2 are correlated with fracture density.

**Table 10.6.** Resulting correlation scores from bivariate analysis of fracture density data. Four groups are defined: F1 with Totals (shown in red), F3 with Totals (green), Fracture Families and CuOx (black), and F2 oxides and density (blue).

Table 10.6 Correlation Scores Between 0.5-0.7										
Row	F1 CuOx	F1 FeOx	F1 t-Ox	F1 n	F1 Density	F2 CuOx	F3 FeOx	F3 t-Ox	F3 n	F3 Density
F2 CuOx	0.639423									
F2 FeOx						0.508262				
F2 t-Ox						0.557298				
F2 Density						0.524174				
F3 CuOx	0.502721					0.588475				
T-FeOx				0.581576	0.697587		0.669314	0.669314	0.554914	0.670079
T-Ox				0.584241	0.695811		0.665977	0.665977	0.551193	0.666681
T-n		0.662769	0.664153		0.654586				0.581246	
T-Density				0.612859			0.627512	0.627512	0.531774	0.637912

Multivariate analysis resulted in four factors accounting for 92.33% of the total variance for fracture behavior, two of which are related to family 2 (F2).

*Factor 1* accounts for 42.9% of the total variance and shows high loadings for T-FeOx, T-Ox, T-n, and T-Density (Table 10.7). A sub-factor is also indicated for the same variables in F1. This factor suggests that all three-fracture families have commonalities in those variables with F1 occurring as the dominant fracture system.

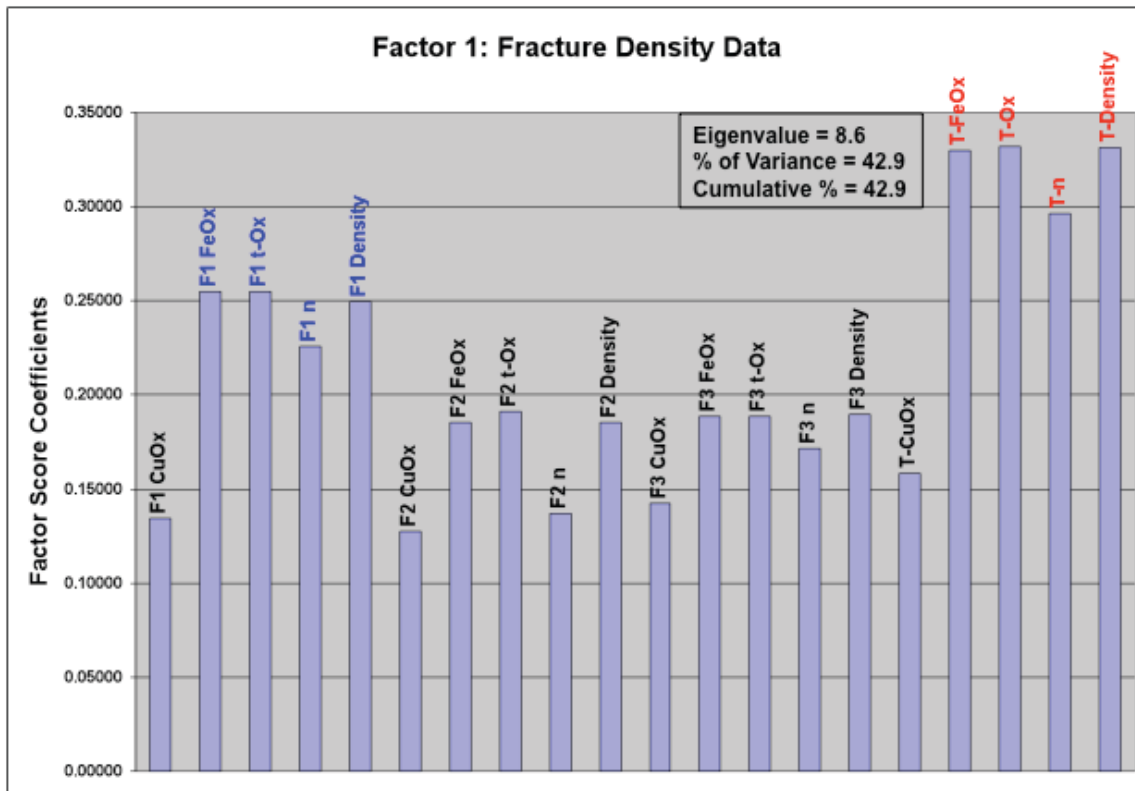


**Figure 10.7.** Fracture density factor 1. This figure shows a relationship between total oxides and fracture density for the MacArthur pit.

Factor 2 accounts for 20.9% of the total variance and includes all variables for F2 (Table 10.8). Factor 2 shows F2 to have a negative relationship for all variables of F3 except CuOx. This factor is interpreted as variables of F3, excluding CuOx, show an opposite behavior to variables of F2 spatially in the MacArthur pit.

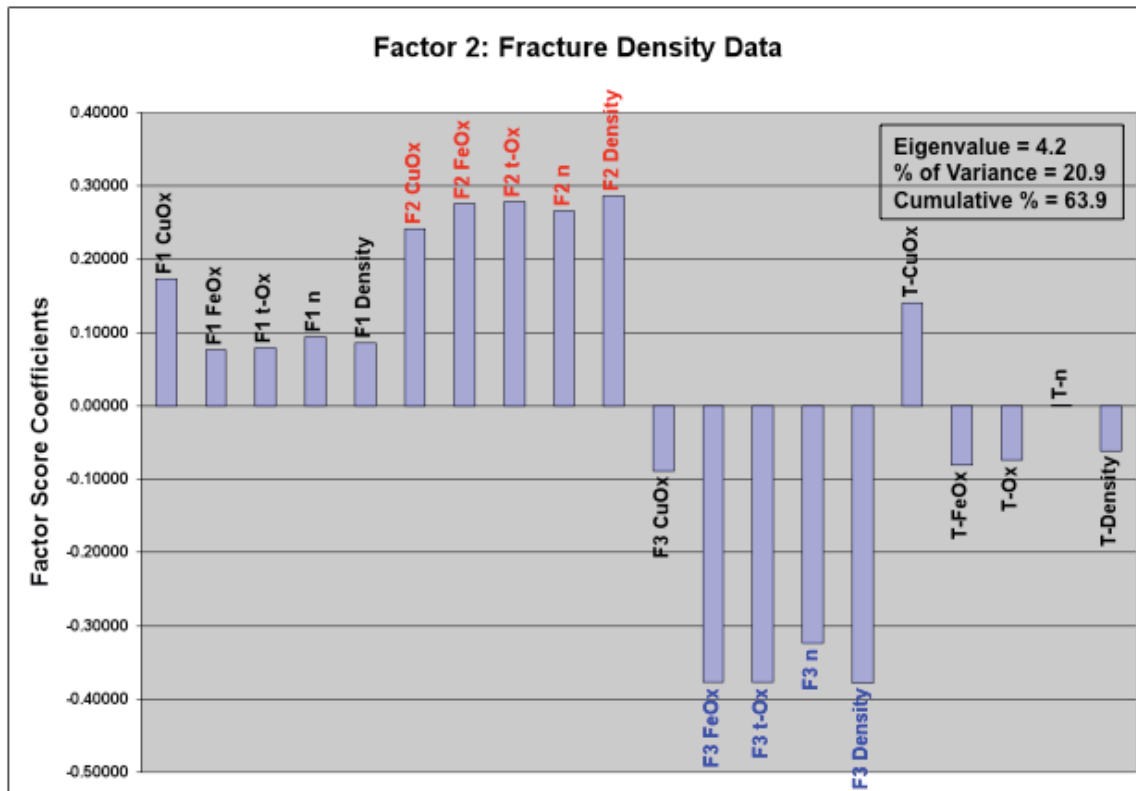


**Figure 10.8.** Fracture density factor 2. This figure shows an inter-family relationship for the variables of F2.

Factor 3 accounts for 15.69% of the total variance and includes all variables for F2 and CuOx from F3 (Table 10.9). Factor 3 shows F2 to have a negative relationship for all variables of F1 except CuOx. Similar to that of factor 2, factor 3 shows a strong family relationship in F2. It is also suggested by both factors that F2 has a closer relationship with CuOx than that of F1 and F3.

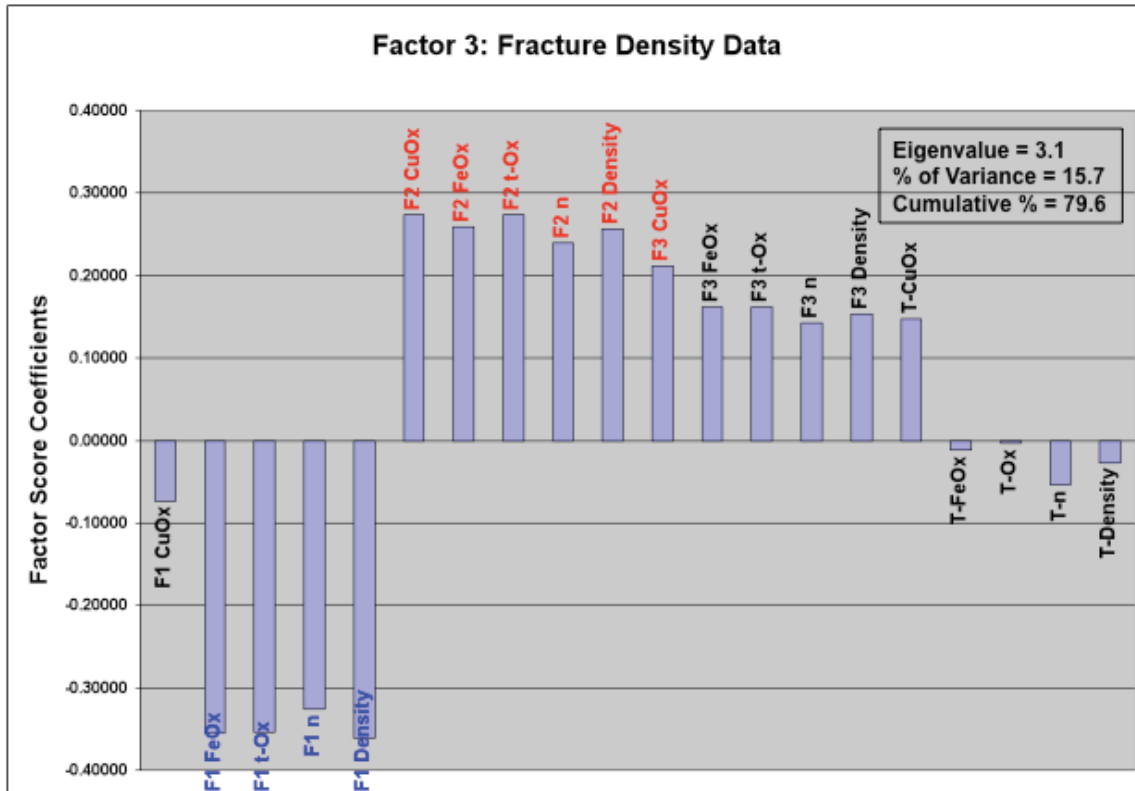


**Figure 10.9.** Fracture density factor 3. This figure shows an inter-family relationship for the variables of F2 including F3 CuOx.

*Factor 4* accounts for 12.77% of the total variance and includes all CuOx variables. This factor suggests that CuOx occurrences in fractures families are similar to each other. It is worthy to note that F2 has the weakest correlation in this factor and the remaining variables of F2 are opposite to the factor. This indicates that CuOx in F2 may deviate in behavior compared to F1 and F3.

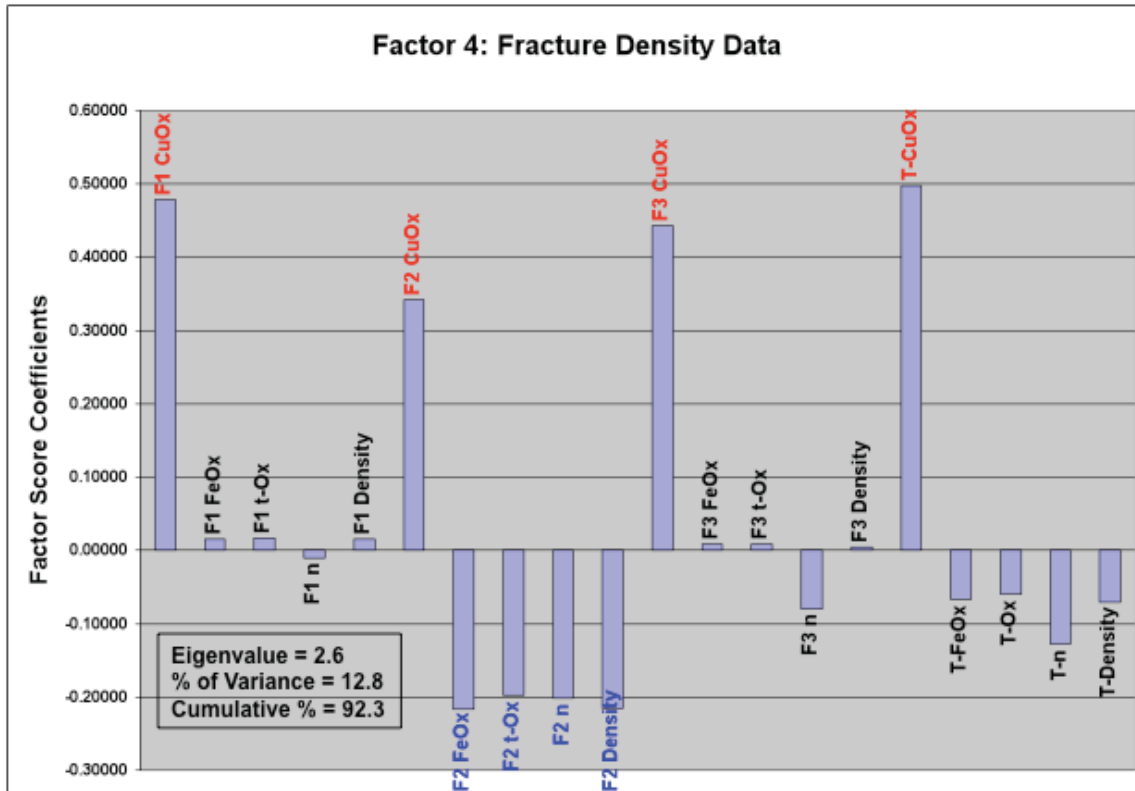


**Figure 10.10.** Fracture density factor 4. This figure shows a relationship for all variables of CuOx. A negative relationship is seen with remaining variables of F2.

#### 10.6.4. Spatial Analysis:

The results of spatial analysis are presented in the form of contour maps (Appendix 5, Fig 5.52 – 5.59). Data is contoured using Golden Software Surfer (<http://www.goldensoftware.com/>) interpreted using natural neighbor method. Low values are purple and color warms to pink for high values.

*Fracture family 1 ( $\rho$ -F1)* shows strong density occurring on the northern sections of benches 4675 and 4700. This density high is associated with the strong fracturing of the rhyolite dike. There is an overall trend of fracture strength decreasing to the south, and the QMPH dike on bench 4600 shows an overall weak density. Weak density in the QMPH dike is likely due to the east-west orientation of the pit wall disguising fractures.

*Fracture family 2 ( $\rho$ -F2)* shows an approximate east-west orientated high along the north sections of the MacArthur pit with a gradual decrease in density to the south. The strong density occurrence on bench 4700 is associated with a rhyolite dike. Low fracture density in F2 is associated with low density in F1 on benches 4750 and 4730 and an inverse relationship is seen on bench 4675.

*Fracture family 3 ( $\rho$ -F3)* shows a low density relationship with F2, and an inverse relationship with F1 on bench 4675. Two density highs on bench 4750 and 4730 show an inverse relationship with F1 and F2. The fracture density high on bench 4700 is due to a vertical andesite dike in which the measurement was recorded. The measurement is also the southern most on the bench, therefore exaggerating the size of the density high.

*Total density ( $\rho$ -T)* shows a strong density high on the central portions of bench 4700 and 4675 associated with a rhyolite and andesite dike. A high area of density also occurs on benches 4630 and 4600 and field observations indicate this area is associated with a moderate fault with transported black and green copper oxides. A common low is seen as well on the southern areas of bench 4750 and 4730 associated with all families except F3.

*CuOx ( $\rho$ -CuOx)* only occurs by itself on bench 4600. This density high represents a QMPH-3 dike in the north-east of the bench and a fault with strong transported black and green copper oxides on the south end of the bench.

*FeOx* ( $\rho$ -*FeOx*) occurs strongest along bench 4700. This is due to only four density intervals on this bench and all but three have strong association with Fe. The low density values on the contour map are not due to lack of Fe, but rather a mixing of Cu and Fe in the same fracture. The lows located in the western areas of the MacArthur pit do show weak correlation with overall low fracture density.

*CuOx and FeOx* ( $\rho$ -*Cu-FeOx*) occur together in an east-west orientation that shows a correlation with F2. This figure also shows the high density values gradually decreasing to the south like F2 fracture density. An overall low in copper and iron mixing occurs along the northern margins of the pit and is weakly associated with total fracture density.

*Fresh Fractures* ( $\rho$ -*Fr*) only occur in 1 interval above bench 4675 located on bench 4800. Fresh fractures on and below bench 4675 tend to cluster along the north margin of the benches showing a correlation with low total fracture density.

### **10.7. Initial Interpretations**

The principal objective for this study is to define controls of oxide enrichment through fracture measurement analyses. Stereonets defined continuity in the three fracture families (Fig 10.4) and field observations of fracture intervals reveal all orientations cut each other therefore showing no relative age relationship. Fractures may be interpreted two ways: development of all families during porphyry emplacement, or two stages of development, through porphyry emplacement and again during Basin and Range extension. Percent total density and density oxides in fractures studies show that 98.3% of all fractures in the MacArthur pit are associated with oxide zone produced copper and iron at an almost even distribution amongst fracture families (Fig 10.6). Although percent density and oxides provide no relative age relationship in

fractures or timing of oxidation events, it demonstrates that strong oxidation and transport occurred after fracture development of all three families.

Bivariate analysis defined a strong relationship in all fracture orientations with FeOx and fracture density as well as F2 having the strongest relationship with copper and F3 to contain no Cu only fractures. Bivariate also shows F2 to be the only fracture orientation to correlate CuOx and Density with a score over 0.5 (Table 10.6). This may suggest that F2 is the strongest control on copper oxide mineralization.

Factor analysis provides powerful statements regarding the behavior and relationships of oxide transport between fracture families and inter-family variables. The four factors each represent a single variable or geologic processes and account for over 92% of the behavioral relationships of oxides in fractures. The first factor shows that T-FeOx and T-Density dominate the system and is also seen in bivariate analysis. This is interpreted as late oxidation of pyrite resulting in FeOx coating all fracture systems. Both factor 2 and 3 show that F2 is the only fracture family to include CuOx as a factor. This again suggests F2 is the strongest control on transported CuOx. The final factor revealed a relationship in all fracture families between the variables of CuOx. This factor shows F2 to have the least influence in the factor and also shows a negative relationship with remaining variables of F2, indicating that CuOx in F2 may deviate in behavior compared to F1 and F3. The special deviation in behavior of F2 is related to the strong control on transported copper oxide mineralization.

Spatial distribution of fracture density helps support this correlation with CuOx and south dipping fractures. Contour maps (FeOx + CuOx) and F2 density (Appendix 5) both show spatial correlation indicated by high-density values through the central pit striking east-west, with density decreasing to the south. Strong transport of CuOx occurred through the south dipping

fracture system of F2. Geochemistry abundance contour for Cu (Fig. 8.9) in the MacArthur shows Cu to be concentrated along the south pit wall supporting F2 as the dominant transport system for CuOx. Contour maps of Fe abundance (Appendix 3) and density of FeOx occurrences in fractures show spatial correlations. The correlations mentioned here represent the overall control of fractures on transported iron and copper in the MacArthur pit.

## **11. DISCUSSION AND INTERPRETATIONS**

### **11.1. Introduction**

The investigations undertaken in this study together provide knowledge and understanding of rocks at the MacArthur pit. Appendix 6 shows two bench face pictures with data from each chapter as layers. The data collected and processed in this study have helped define element associations, alteration, mineralogy, and transport mechanics of oxide mineralization. Using the interpretations of this data, an attempt to define parameters of oxide mineralization in the MacArthur pit is undertaken using interpretations of hydrothermal mineralogy, alteration, oxidation, and oxide transport processes in fracture systems.

### **11.2. Hydrothermal**

Hydrothermal alteration is interpreted in spectral data from oxide derivative mineralogy (Tables 8.10 and 8.11, 9.3 – 9.6 and 9.14). Oxide mineralogy such as jarosite, goethite, malachite, and chrysocolla identified in samples by Spectral Analyst suggest the hydrothermal event at the proto-MacArthur to be rich in Cu and Fe (Section 9.7). Stages of hydrothermal alteration are also identified in geochemical data using statistical analyses. Interpreted from univariate and bivariate methods the hydrothermal event at the MacArthur was rich in metals including Cu, Fe, Co, Mo, Ni, and U (Tables 8.4 – 8.7). Analyses also indicate the elements Al, K, Rb, Ba, Na, and Mn were present in hydrothermal alteration (Section 8.6). Dilles (1987), and Dilles and Proffett (1995), describe the hydrothermal magmatic aqueous fluid associated with the Luhr Hill granite as rich in Cl, Na, K, Fe, S, and Cu. Elements associated with hydrothermal alteration from analyses of data support the observation of Dilles and Proffett.

The hydrothermal signature demonstrates associations with K and Na, occurring as potassic and sodic alteration respectively. Potassic and sodic alteration are described in several

rock samples (Table 6.2), identified in multivariate analysis factor scores (Tables 8.10 and 8.11, Factors 2, 3, 4, and 7), and mapped by Quaterra Resource geologists and others (Figure 2.5). This supports a hydrothermal event rich in Na and K. Figure 2.5 shows sodic, potassic, and phyllic alteration in the east, central, and southwest respectively, in the MacArthur pit. However, as interpreted from average element compositions in granites (Mason, B., and Moore, C.B., 1982), univariate analysis of geochemical data shows that both the surface and subsurface are at least 3x depleted in elements Al, Ca, Ga, K, Li, Na, and Th (Appendix 2.2).

The rock type at the MacArthur is a quartz monzonite and may naturally contain less of these elements. Descriptive statistics (Appendix 2.1) demonstrates the average Na (Sodium) content of the quartz monzonite is 0.138%. When comparing the average value of sodium to rocks described as sodically altered (Table 6.2, samples 66 and 67), an increase in sodium content is seen supporting a “sodically altered” interpretation. It could also be that sodium has been removed from the rocks. Sample 28 (Table 6.2) shows the strongest Na content at 0.487% and is a fault gouge clay sample. The Na in this sample was introduced to the gouge through transport processes.

### **11.3. Alteration**

Although not directly identified by analyses, phyllic alteration is common in the western portions of the MacArthur pit and is identified by the alteration of biotite and hornblende to sericite and feldspars destroyed to clay minerals (Figure 2.5). Propylitic alteration is interpreted from spectrum by the strong presence of chlorite in samples 1 and 7 in RHY-4675 site (Table 9.14). It is also identified in rock descriptions occurring as destruction of biotite and hornblende to chlorite (Table 6.2). Rock descriptions show that the mafic minerals altered to chlorite dominate bench 4630 and 4600. Indicated by rock description table (Table 6.2), Spectral

Analyst did not define propylitic alteration signatures in spectrum from bench 4630 and 4600, perhaps due to strong copper and iron oxide coatings.

Spatially, propylitic alteration occurs in the eastern portions of the MacArthur pit correlating with regions considered as sodic alteration (Figure 2.5). Sodic alteration is defined in this zone by the replacement of primary plagioclase and K-feldspar by secondary oligoclase or albite, perhaps occurring during the primary porphyry stage. Rock descriptions indicate samples on benches 4630 and 4600 are sodically altered but geochemistry of the samples in the sodic alteration zone show an overall leaching of Na, indicated by less than 0.2 percent sodium. This suggests the remobilization of Na during an overprinting by propylitic alteration or oxidation.

#### **11.4. Oxidation**

Oxidation is identified as the dominant alteration type in spectral data and is also recognized in multivariate analysis. Factor score coefficients in multivariate analysis show Mn oxides occurring as neotocite and Fe rich limonites (Tables 8.10 and 8.11). Neotocite is an iron-manganese silicate mineral  $((\text{Fe}, \text{Cu}, \text{Mn})\text{SiO}_2)$  produced in oxidation zones with a questionable chemical formula (Anthony et al., 1995). In factor analysis, neotocite is associated with the elements Cd, Co, As, and Ni interpreted as “absorbed on Mn oxides”. As mentioned in section 8.2 (Geochem Data) a pure neotocite sample was collected and analyzed for 62 elements from the MacArthur pit to define chemical characteristics of neotocite. Table 11.1 shows anomalous values for elements found in pure neotocite vs. the mean value of surface sample geochemistry (Appendix 1).

**Table 11.1.** Pure neotocite vs. mean value of surface sample data for selected elements in the MacArthur pit.

<b>Table 11.1 - Pure Neotocite vs. Mean Value (ppm) of Surface Samples for Selected Elements</b>		
<b>Element</b>	<b>Pure Neotocite</b>	<b>Mean Value</b>
Mn	> 10,000	381
Co	> 5,000	49.5
Ni	165	18.7
Cu	> 10,000	3344
Zn	90	15.5
As	127	2.48
Mo	386	11.3
Ag	2.72	0.16
Cd	3.11	0.07
U	319	6.37

Neotocite is common in the MacArthur pit, often enriched in Cu, and is encountered as coatings and disseminations throughout the oxide zone in drilling programs by Quaterra Resources. Table 11.1 clearly demonstrates that the pure neotocite sample acted like a sponge absorbing anomalous amounts of elements in the oxide zone supporting the interpretations found in tables 8.10 and 8.11.

Spectral Analyst also defined abundant oxidation minerals in the MacArthur pit. Spectral Analyst matches from RHY-4675 and bench 4600 spectrums (Tables 9.6 and 9.14) indicate copper oxide minerals occurring as chrysocolla, malachite, azurite, atacamite, and antlerite. Also defined are strong matches for many iron oxide minerals. An observation at the MacArthur pit shows fracture systems to have strong coatings of iron and copper oxide minerals and is documented in spectral radiometry. An investigation of fracture families and associated oxides revealed a special relationship with F2 and transported copper oxide mineralization.

## 11.5. Fracture Density

Fracture density data analyses defined a direct relationship with southwest fracture family 2 (F2) and copper oxide in every test performed when copper oxide was a variable. Stereonets displaying orientation and oxide occurrences in fractures (Appendix 5) revealed that F2 density decreases and copper oxide occurrences increase in the south of the MacArthur pit, while density and copper in F1 and F3 decrease. Percentages of copper in fractures revealed that F2 contained the most copper by 3 percent and almost 2 percent less iron. Although a close to even distribution of oxides in fractures is evident from figure 10.6, continued analyses using bivariate and multivariate statistical methods confirmed a special relationship with F2 and copper oxides.

Correlation coefficients from bivariate analysis reveal that F2 has highest correlation with total copper, and the lowest correlation with total iron. Table 11.2 shows correlation scores for F1, F2, and F3 CuOx and FeOx variables vs. total iron and copper occurring in fractures. This demonstrates F1 and F3 correlate with copper and iron, and F2 has a less association with iron and shows the strongest correlation with copper. Correlations also show F2 to be the only fracture orientation to correlate CuOx and fracture density with a score over 0.5 (Table 10.6).

**Table 11.2.** Correlation coefficient scores for F1, F2, and F3 CuOx and FeOx vs. total iron and copper in fractures at the MacArthur pit.

<b>Table 11.2 - Correlation Coefficient Scores from Fracture Data</b>			
	<b>CuOx and FeOx in Fracture</b>		
	<b>F1</b>	<b>F2</b>	<b>F3</b>
<b>T-CuOx</b>	0.87	0.88	0.80
<b>T-FeOx</b>	0.72	0.48	0.67

Multivariate factor analysis again defined a relationship with F2 and CuOx. Both factor 2 and 3 (Table 10.8 and 10.9) revealed F2 is the only fracture family to include CuOx as a variable. Factor 4 (Table 10.10) revealed a relationship in all fracture families between the

variables of CuOx. This factor shows F2 to have the least influence in the factor and also shows a negative relationship with remaining variables of F2 indicating that CuOx in F2 may deviate in behavior compared to F1 and F3. The special deviation in behavior of F2 is related to the strong control on transported copper oxide mineralization.

When F2 was investigated spatially, a correlation was observed between F2 density (Appendix 5.5), Cu abundance (Figure 8.9), and stereonet with percent copper in fractures families (Appendix 5.3). The percent copper in F2 is observed to increase to the south of the MacArthur pit and geochemistry abundance contour for Cu (fig 8.9) in the MacArthur shows Cu to be concentrated along the south pit wall. The contour map of F2 density (Appendix 5.5) shows high-density values through the central pit striking east-west, with density decreasing to the south. This indicates that as the density of F2 decreases the occurrence of copper oxides in the ground increase. Further analysis of fractures at the MacArthur prospect may confirm this in either location.

## **12. CONCLUSIONS**

- (1) For both surface and subsurface data the elements Al, Ca, Ga, K, Li, Na, and Th all show at least a 3x depletion factor and elements Co, Cu, Mg, Ni, and S all show at least a 3x enrichment factor compared to average element abundance in granites.
- (2) The high geochemical association of elements Cu, Fe, Co, Mo, Ni, U, and Al, K, Rb, Na, Mn represent the hydrothermal event at the MacArthur.
- (3) Elements U, Mn, Mo, Co, and Ni correlate with Cu in the oxide zone of MacArthur pit and all occur as accessory elements absorbed on neotocite
- (4) Percent total density and density oxides in fractures studies show that 98.3% of all fractures in the MacArthur pit are associated with oxide zone copper and iron at a close to even distribution amongst fracture families.
- (5) Southwest dipping fractures (family 2) display the strongest control on copper oxide mineralization in the MacArthur pit by a small amount.

### **13. RECOMMENDATIONS**

In the processes of data analyzing the tantalizing thought of how to refine controls on the study and what else can this data represent always exists. Presented in this section are recommendations to improve studies by providing more control on methods and analysis and answering questions that have come from the studies.

#### **13.1. Geochemistry**

Statistical and spatial analysis of surface data indicates that U, Mn, Mo, Co, and Ni may serve as pathfinder elements in locating sections of Cu mineralization. These correlations seen in surface data are not seen in the subsurface data. A question is now raised as to why subsurface Cu does not correlate with the same elements it does on the surface. Many outlier data from surface sample univariate analysis are recognized to contain moderate-to high amounts of fault gouge. Most of elements in the raw data set show deviation from normality due to fault gouge.

The MacArthur fault and other smaller unnamed faults with gouge on the MacArthur property often show Cu spikes in drill cutting analytical results. A future analysis of this data with separation of fault gouge samples for surface and subsurface data may provide valuable clues on to the nature of the relationship between rock and fault gouge geochemistry. A further separation of rock samples into individual data for rock type may reveal a geochemical signature for each rock type. If fault gouge samples continue to show anomalous values, a geochemical spatial relationship may be developed between rock samples and gouge samples. The final established geometry of geochemical signatures in fault systems and rock types on the property may prove to be valuable in defining zones where mineralization was derived from and may

provide insight into locating peripheral zones associated with primary porphyry type mineralization.

### **13.2. Spectral Radiometry as Grade Control Method**

Spectral radiometry is used in this study to identify alteration types by mineralogy and tested as a new method of grade control in oxidized sections (Section 9.6.3). Initial results in the study indicate that using percent reflectance data the Spectral Analyst tool has an 80% chance of grouping rocks associated with high copper values from mineralogy (Tables 9.15 and 9.16). To prove reliability of this result, further refinement of this study is needed.

Further studies including detecting line segments of spectrum (wavelength sections) associated with copper grade should be performed. The advantage in analyzing segments is that Spectral Analyst only analyzes the diagnostic line feature segments (Kruse and Lefkoff, 1999). The results of Spectral Analyst demonstrate a strong ability in identification of oxide zone, acid soluble minerals. The best approach to relate spectrum with copper grade would be to identify all oxide zone minerals that contain copper and develop a control spectral library for each type, find the associated line features, and perform peak height analysis for oxide minerals based on high and low copper values. In this method, one may calibrate peak height to grade and reliability of spectrum as a method of grade control may be developed for oxidized sections.

## 14. REFERENCES

<http://www.actlabs.com/>

Actlabs Code 2 Ultra-trace Analytical Method: Retrieved July 15, 2010, from  
<http://www.actlabs.com/page.aspx?page=503&app=226&cat1=549&tp=12&lk=no&menu=64/>

Allmendinger, R.W., 2006, Stereonet 6.3.3X: Retrieved May 19, 2010, from  
<http://www.geo.cornell.edu/geology/faculty/RWA/programs.html>

Anthony, J.W., Bideaux, R.A., Bladh, K.W., and Nichols, M.C., 1995, Handbook of mineralogy: Tucson Arizona, Mineral Data Publishing, v. II, Silica, Silicates, part 1, 446 p.

Anthony, J.W., Bideaux, R.A., Bladh, K.W., and Nichols, M.C., 1995, Handbook of mineralogy: Tucson Arizona, Mineral Data Publishing, v. II, Silica, Silicates, part 2, p. 447-904.

Anthony, J.W., Bideaux, R.A., Bladh, K.W., and Nichols, M.C., 1997, Handbook of mineralogy: Tucson Arizona, Mineral Data Publishing, v. III, Halides, Hydroxides, Oxides, 628 p.

Anthony, J.W., Bideaux, R.A., Bladh, K.W., and Nichols, M.C., 2000, Handbook of mineralogy: Tucson Arizona, Mineral Data Publishing, v. IV, Arsenates, Phosphates, Vanadates, 680 p.

Anthony, J.W., Bideaux, R.A., Bladh, K.W., and Nichols, M.C., 2003, Handbook of mineralogy: Tucson Arizona, Mineral Data Publishing, v. V, Borates, Carbonates, Sulfates, 813 p.

Barton, M.D., 2001, Sodic alteration and Fe-oxide-rich hydrothermal systems [abs.]: The Geological Society of America Abstracts with Programs, v. 33, no. 6, p. 4.

Bonsall, T., 2010, An update of Mineralization and Geology of the MacArthur Prospect, Lyon County, Yerington, Nevada: Unpublished.

Bonsall, T., 2010, Personal Communications from Quaterra Resources Inc.

Chavez, Jr., W.X., 2000, Supergene oxidation of copper deposits: zoning and distribution of copper oxide minerals: Society of Economic Geologists Newsletter, no. 41, 13 p.

- Darlington, R.B., 1997, Factor Analysis: Retrieved April 20, 2009, from <http://comp9.psych.cornell.edu/Darlington/factor.htm>
- Davis, J.C., 2002, Statistics and data analysis in geology: Third edition: Kansas Geological Survey: The University of Kansas: John Wiley & Sons, 638 p.
- Diles, J.H., 1987, Petrology of the Yerington batholith, Nevada: Evidence for evolution of porphyry copper ore fluids: *Economic Geology*, v. 82, p. 1750-1789.
- Diles, J.H., Einaudi, M.T., Proffett, J.M., and Barton, M.D., 2000, Overview of the Yerington porphyry copper district: Magmatic to nonmagmatic sources of hydrothermal fluids: Their flow paths and alteration effects on rocks and Cu-Mo-Fe-Au ores, *in* Thompson, T., ed., *Contrasting styles of intrusion-associated hydrothermal systems*: Society of Economic Geologists, Guidebook Series v. 32, p. 55-66.
- Diles, J.H., and Wright, J.E., 1988, The chronology of early Mesozoic arc magmatism In the Yerington district, Nevada, and its regional implications: *Geological Society of America Bulletin*, v. 100, p. 644-652.
- Eliopulos, G.J., 2008-2010, Current Geologic Map of MacArthur pit: Personal Communications from Quaterra Resources Inc.
- Eliopulos, G.J., 2010, Personal Communications from Quaterra Resources Inc.
- Eliopulos, G.J., and Heatwole, D.A., 2009, Personal Communications from Quaterra Resources Inc.
- <http://www.entreegold.com>
- <http://www.goldensoftware.com/>
- Guilbert, J.M., and Park, Jr., C.F., 1986, *The Geology of Ore Deposits*: Reissued 2007 by Waveland Press, Inc., 985 p.
- Haynes, Frederick M., and Titley, Spencer R., 1980, The Evolution of Fracture-Related Permeability within the Ruby Star Granodiorite, Sierrita Porphyry Copper Deposit, Pima County, Arizona: *Economic Geology*, v. 75, p. 673-683.
- Heatwole, D.A., 1972, Progress Report: Yerington Oxide Project – MacArthur Area: Lyon County, Nevada: The Anaconda Company Geological Department, University of Wyoming Library, 29 p.

Heatwole, D.A., 1978, Controls of oxide copper mineralization, MacArthur property, Lyon County, Nevada: Arizona Geological Society Digest, v. XI, p. 59-66.

Heatwole, D.A., 2010, Personal Communications from Quaterra Resources Inc.

[www.idl-envi.com/ENVIOverview](http://www.idl-envi.com/ENVIOverview)

<http://www.jmp.com/index.shtml>

<http://www.jpl.nasa.gov/>

Kruse, F.A., and Lefkoff, A.B., 1999, Analysis of spectral data of manmade materials, military targets, and background using an Expert System based approach: In Proceedings, ISSSR '99, 31 October – 4 November 1999, Las Vegas, Nevada, published on CD-ROM by ISPRS, p 339-350.

Levinson, A.A., 1974, Introduction to exploration geochemistry: Department of Geology: University of Calgary, Canada: Applied Publishing Ltd., Wilmette, Illinois, U.S.A., 614 p.

Lowell, J.D., and Guilbert, J.M., 1970, Lateral and vertical alteration-mineralization zoning in porphyry ore deposits: Economic Geology, v. 65, p. 373-408.

Mason, B., and Moore, C.B., 1982, Principles of geochemistry: John Wiley and Sons Inc, Second Edition, 352 p.

<http://www.minemarket.com/yerington.htm>, Retrieved 5/5/2010.

<http://www.minemarket.com/Arimetco.htm>, Retrieved 5/5/2010.

<http://www.mineweb.com/>, Retrieved 07/15/2010.

<http://www.nevadacopper.com/> 1.

[http://www.nevadacopper.com/s/PumpkinHollow.asp?ReportID=350712&\\_Type=Pumpkin-Hollow&\\_Title=Project-History](http://www.nevadacopper.com/s/PumpkinHollow.asp?ReportID=350712&_Type=Pumpkin-Hollow&_Title=Project-History), Retrieved 8/17/10.

Palache, C., Berman, H., and Frondel, C., 1961, The system of mineralogy: Harvard University, John Wiley and Sons Inc., v. I, Elements, Sulfides, Sulfosalts, Oxides, Seventh Edition, p. 834.

Proffett, J.M., 1977, Cenozoic geology of the Yerington district, Nevada, and implications for the nature and origin of basin and range faulting: Geological Society of America Bulletin, v. 88, p. 247-266.

Proffett, J.M., 1979, Ore deposits of the western United States: A summary: Nevada Bureau of Mines and Geology, Report 33, p. 13-20.

Proffett, J.M., 2009, High Cu grades in porphyry Cu deposits and their relationship to emplacement depth of magmatic sources: *Geology*, v. 37, p. 675-678.

Proffett, J.M., and Dilles, J.H., 1984, Geologic map of the Yerington district, Nevada: Nevada Bureau of Mines and Geology, scale 1:24,000, 1 sheet.

Proffett, J.M., and Proffett, B.H., 1976, Stratigraphy of the Tertiary ash-flow tuffs in the Yerington district, Nevada: Nevada Bureau of Mines and Geology Open-File Report 27, 28 p.

<http://www.quaterraresources.com>

Rose, A.W., Hawkes, H.E., and Webb, J.S., 1979, Geochemistry in mineral exploration: Second edition: Academic Press Inc., 657 p.

<http://spectravista.com>, Retrieved 7/08/10.

Shuyun, X., *et al.*, 2008, Identification of geochemical anomaly by multifractal analysis: *Journal of China University of Geosciences*, v. 19, i. 4, p. 334-342.

Spiering, E.D., 2010, Quaterra drilling continues to expand acid-soluble copper zone at MacArthur: Mineralization confirmed over 12,00 feet between MacArthur pit and Gallagher zone: September 9<sup>th</sup> News Release, 3 p. Retrieved from, [http://www.quaterraresources.com/\\_resources/news/NR\\_100909\\_Quaterra\\_revised.pdf](http://www.quaterraresources.com/_resources/news/NR_100909_Quaterra_revised.pdf)

Stewart, J. H., and Carlson, J. E., 1978, Geologic Map of Nevada: U.S. Geologic Survey, scale 1:500,000.

Tetra Tech, Inc., 2009, MacArthur Copper Project NI 43-101 Technical Report Lyon County, Nevada, USA, prepared for Quaterra Alaska, Incorporated, 165 p.

<http://tetrattech.com/>

Titley, S. R. *et al.*, 1986, Evolution of Fractures and Alteration in the Sierrita-Esperanza Hydrothermal System, Pima County, Arizona: *Economic Geology*, v. 81, p. 343-370.

<http://www.usgs.gov>

[www.visualstatistics.net](http://www.visualstatistics.net)

[http://en.wikipedia.org/wiki/Principal\\_component\\_analysis](http://en.wikipedia.org/wiki/Principal_component_analysis), Retrieved 6/14/2010.

Yongqing, C., Jingning, H., and Zhen, L., 2008, Geochemical characteristics and zonation of primary halos of Pulang porphyry copper deposit, Northwestern Yunnan Province, Southwest China: Journal of China University of Geosciences, v. 19, i. 4, p. 371-377.

Zumlot, T.Y., 2006, Environmental evaluation of New Mexico stream sediment chemistry using the National Uranium Resource Evaluation (NURE) program data: Dissertation fulfillment for degree of Doctor of Philosophy, University of Texas El Paso Library.

## 15. APPENDIX 1 – GEOCHEMICAL DATA

Appendix 1 displays all geochemical data of surface samples and subsurface samples. 63 Surface samples were collected along bench faces from the MacArthur pit and analyzed using aqua regia ICP/MS ultratrace II method for 62 elements by Actlabs (<http://www.actlabs.com/>). Subsurface data are provided by Quaterra Resources Inc. (<http://www.quaterraresources.com/>). The database includes 1000 samples from thirteen diamond core drill holes, QMT-1 – QMT-13, analyzed by Skyline Assayers (<http://www.skylinelab.com/>). Data is presented in original form as returned from the assayers without processing for analyses performed in this study.

	PAGE
15.1. Appendix 1.1 – Geochemical Data Tables	
Table 1.1 ..... Original multi-element data returned by Actlabs for 63 surface samples.	134
Tables 1.2 – 1.14 ..... Original multi-element data returned by Skyline Assayers for diamond core drill holes QMT-1 – QMT-13.	136

**Table 1.1.** Geochemical analysis results of 63 surface samples using aqua regia extraction ICP/MS ultratrace II method by Actlabs.

?

???

?

???

**Table 1.2.** Geochemical analysis results of QMT-1. Sample analysis commissioned by Quaterra Resources Inc.

[illegible]

**Table 1.3.** Geochemical analysis results of QMT-2. Sample analysis commissioned by Quaterra Resources Inc.

[illegible][illegible]

☐ ☐

[?]
[?][?][?]

**Table 1.5.** Geochemical analysis results of QMT-4. Sample analysis commissioned by Quaterra Resources Inc.

[illegible]

**Table 1.5 cont.** Geochemical analysis results of QMT-4. Sample analysis commissioned by Quaterra Resources Inc.

Year	1990	1991	1992	1993	1994	1995	1996	1997	1998	1999	2000	2001	2002	2003	2004	2005	2006	2007	2008	2009	2010	2011	2012	2013	2014	2015	2016	2017	2018	2019	2020	2021	2022	2023	2024	2025	2026	2027	2028	2029	2030	2031	2032	2033	2034	2035	2036	2037	2038	2039	2040	2041	2042	2043	2044	2045	2046	2047	2048	2049	2050	2051	2052	2053	2054	2055	2056	2057	2058	2059	2060	2061	2062	2063	2064	2065	2066	2067	2068	2069	2070	2071	2072	2073	2074	2075	2076	2077	2078	2079	2080	2081	2082	2083	2084	2085	2086	2087	2088	2089	2090	2091	2092	2093	2094	2095	2096	2097	2098	2099	2100	2101	2102	2103	2104	2105	2106	2107	2108	2109	2110	2111	2112	2113	2114	2115	2116	2117	2118	2119	2120	2121	2122	2123	2124	2125	2126	2127	2128	2129	2130	2131	2132	2133	2134	2135	2136	2137	2138	2139	2140	2141	2142	2143	2144	2145	2146	2147	2148	2149	2150	2151	2152	2153	2154	2155	2156	2157	2158	2159	2160	2161	2162	2163	2164	2165	2166	2167	2168	2169	2170	2171	2172	2173	2174	2175	2176	2177	2178	2179	2180	2181	2182	2183	2184	2185	2186	2187	2188	2189	2190	2191	2192	2193	2194	2195	2196	2197	2198	2199	2200	2201	2202	2203	2204	2205	2206	2207	2208	2209	2210	2211	2212	2213	2214	2215	2216	2217	2218	2219	2220	2221	2222	2223	2224	2225	2226	2227	2228	2229	2230	2231	2232	2233	2234	2235	2236	2237	2238	2239	2240	2241	2242	2243	2244	2245	2246	2247	2248	2249	2250	2251	2252	2253	2254	2255	2256	2257	2258	2259	2260	2261	2262	2263	2264	2265	2266	2267	2268	2269	2270	2271	2272	2273	2274	2275	2276	2277	2278	2279	2280	2281	2282	2283	2284	2285	2286	2287	2288	2289	2290	2291	2292	2293	2294	2295	2296	2297	2298	2299	2300	2301	2302	2303	2304	2305	2306	2307	2308	2309	2310	2311	2312	2313	2314	2315	2316	2317	2318	2319	2320	2321	2322	2323	2324	2325	2326	2327	2328	2329	2330	2331	2332	2333	2334	2335	2336	2337	2338	2339	2340	2341	2342	2343	2344	2345	2346	2347	2348	2349	2350	2351	2352	2353	2354	2355	2356	2357	2358	2359	2360	2361	2362	2363	2364	2365	2366	2367	2368	2369	2370	2371	2372	2373	2374	2375	2376	2377	2378	2379	2380	2381	2382	2383	2384	2385	2386	2387	2388	2389	2390	2391	2392	2393	2394	2395	2396	2397	2398	2399	2400	2401	2402	2403	2404	2405	2406	2407	2408	2409	2410	2411	2412	2413	2414	2415	2416	2417	2418	2419	2420	2421	2422	2423	2424	2425	2426	2427	2428	2429	2430	2431	2432	2433	2434	2435	2436	2437	2438	2439	2440	2441	2442	2443	2444	2445	2446	2447	2448	2449	2450	2451	2452	2453	2454	2455	2456	2457	2458	2459	2460	2461	2462	2463	2464	2465	2466	2467	2468	2469	2470	2471	2472	2473	2474	2475	2476	2477	2478	2479	2480	2481	2482	2483	2484	2485	2486	2487	2488	2489	2490	2491	2492	2493	2494	2495	2496	2497	2498	2499	2500
------	------	------	------	------	------	------	------	------	------	------	------	------	------	------	------	------	------	------	------	------	------	------	------	------	------	------	------	------	------	------	------	------	------	------	------	------	------	------	------	------	------	------	------	------	------	------	------	------	------	------	------	------	------	------	------	------	------	------	------	------	------	------	------	------	------	------	------	------	------	------	------	------	------	------	------	------	------	------	------	------	------	------	------	------	------	------	------	------	------	------	------	------	------	------	------	------	------	------	------	------	------	------	------	------	------	------	------	------	------	------	------	------	------	------	------	------	------	------	------	------	------	------	------	------	------	------	------	------	------	------	------	------	------	------	------	------	------	------	------	------	------	------	------	------	------	------	------	------	------	------	------	------	------	------	------	------	------	------	------	------	------	------	------	------	------	------	------	------	------	------	------	------	------	------	------	------	------	------	------	------	------	------	------	------	------	------	------	------	------	------	------	------	------	------	------	------	------	------	------	------	------	------	------	------	------	------	------	------	------	------	------	------	------	------	------	------	------	------	------	------	------	------	------	------	------	------	------	------	------	------	------	------	------	------	------	------	------	------	------	------	------	------	------	------	------	------	------	------	------	------	------	------	------	------	------	------	------	------	------	------	------	------	------	------	------	------	------	------	------	------	------	------	------	------	------	------	------	------	------	------	------	------	------	------	------	------	------	------	------	------	------	------	------	------	------	------	------	------	------	------	------	------	------	------	------	------	------	------	------	------	------	------	------	------	------	------	------	------	------	------	------	------	------	------	------	------	------	------	------	------	------	------	------	------	------	------	------	------	------	------	------	------	------	------	------	------	------	------	------	------	------	------	------	------	------	------	------	------	------	------	------	------	------	------	------	------	------	------	------	------	------	------	------	------	------	------	------	------	------	------	------	------	------	------	------	------	------	------	------	------	------	------	------	------	------	------	------	------	------	------	------	------	------	------	------	------	------	------	------	------	------	------	------	------	------	------	------	------	------	------	------	------	------	------	------	------	------	------	------	------	------	------	------	------	------	------	------	------	------	------	------	------	------	------	------	------	------	------	------	------	------	------	------	------	------	------	------	------	------	------	------	------	------	------	------	------	------	------	------	------	------	------	------	------	------	------	------	------	------	------	------	------	------	------	------	------	------	------	------	------	------	------	------	------	------	------	------	------	------	------	------	------	------	------	------	------	------	------	------	------	------

**Table 1.6.** Geochemical analysis results of QMT-5. Sample analysis commissioned by Quaterra Resources Inc.

Year	1990	1991	1992	1993	1994	1995	1996	1997	1998	1999	2000	2001	2002	2003	2004	2005	2006	2007	2008	2009	2010	2011	2012	2013	2014	2015	2016	2017	2018	2019	2020	2021	2022	2023	2024	2025	2026	2027	2028	2029	2030	2031	2032	2033	2034	2035	2036	2037	2038	2039	2040	2041	2042	2043	2044	2045	2046	2047	2048	2049	2050	2051	2052	2053	2054	2055	2056	2057	2058	2059	2060	2061	2062	2063	2064	2065	2066	2067	2068	2069	2070	2071	2072	2073	2074	2075	2076	2077	2078	2079	2080	2081	2082	2083	2084	2085	2086	2087	2088	2089	2090	2091	2092	2093	2094	2095	2096	2097	2098	2099	2100	2101	2102	2103	2104	2105	2106	2107	2108	2109	2110	2111	2112	2113	2114	2115	2116	2117	2118	2119	2120	2121	2122	2123	2124	2125	2126	2127	2128	2129	2130	2131	2132	2133	2134	2135	2136	2137	2138	2139	2140	2141	2142	2143	2144	2145	2146	2147	2148	2149	2150	2151	2152	2153	2154	2155	2156	2157	2158	2159	2160	2161	2162	2163	2164	2165	2166	2167	2168	2169	2170	2171	2172	2173	2174	2175	2176	2177	2178	2179	2180	2181	2182	2183	2184	2185	2186	2187	2188	2189	2190	2191	2192	2193	2194	2195	2196	2197	2198	2199	2200	2201	2202	2203	2204	2205	2206	2207	2208	2209	2210	2211	2212	2213	2214	2215	2216	2217	2218	2219	2220	2221	2222	2223	2224	2225	2226	2227	2228	2229	2230	2231	2232	2233	2234	2235	2236	2237	2238	2239	2240	2241	2242	2243	2244	2245	2246	2247	2248	2249	2250	2251	2252	2253	2254	2255	2256	2257	2258	2259	2260	2261	2262	2263	2264	2265	2266	2267	2268	2269	2270	2271	2272	2273	2274	2275	2276	2277	2278	2279	2280	2281	2282	2283	2284	2285	2286	2287	2288	2289	2290	2291	2292	2293	2294	2295	2296	2297	2298	2299	2300	2301	2302	2303	2304	2305	2306	2307	2308	2309	2310	2311	2312	2313	2314	2315	2316	2317	2318	2319	2320	2321	2322	2323	2324	2325	2326	2327	2328	2329	2330	2331	2332	2333	2334	2335	2336	2337	2338	2339	2340	2341	2342	2343	2344	2345	2346	2347	2348	2349	2350	2351	2352	2353	2354	2355	2356	2357	2358	2359	2360	2361	2362	2363	2364	2365	2366	2367	2368	2369	2370	2371	2372	2373	2374	2375	2376	2377	2378	2379	2380	2381	2382	2383	2384	2385	2386	2387	2388	2389	2390	2391	2392	2393	2394	2395	2396	2397	2398	2399	2400	2401	2402	2403	2404	2405	2406	2407	2408	2409	2410	2411	2412	2413	2414	2415	2416	2417	2418	2419	2420	2421	2422	2423	2424	2425	2426	2427	2428	2429	2430	2431	2432	2433	2434	2435	2436	2437	2438	2439	2440	2441	2442	2443	2444	2445	2446	2447	2448	2449	2450	2451	2452	2453	2454	2455	2456	2457	2458	2459	2460	2461	2462	2463	2464	2465	2466	2467	2468	2469	2470	2471	2472	2473	2474	2475	2476	2477	2478	2479	2480	2481	2482	2483	2484	2485	2486	2487	2488	2489	2490	2491	2492	2493	2494	2495	2496	2497	2498	2499	2500
------	------	------	------	------	------	------	------	------	------	------	------	------	------	------	------	------	------	------	------	------	------	------	------	------	------	------	------	------	------	------	------	------	------	------	------	------	------	------	------	------	------	------	------	------	------	------	------	------	------	------	------	------	------	------	------	------	------	------	------	------	------	------	------	------	------	------	------	------	------	------	------	------	------	------	------	------	------	------	------	------	------	------	------	------	------	------	------	------	------	------	------	------	------	------	------	------	------	------	------	------	------	------	------	------	------	------	------	------	------	------	------	------	------	------	------	------	------	------	------	------	------	------	------	------	------	------	------	------	------	------	------	------	------	------	------	------	------	------	------	------	------	------	------	------	------	------	------	------	------	------	------	------	------	------	------	------	------	------	------	------	------	------	------	------	------	------	------	------	------	------	------	------	------	------	------	------	------	------	------	------	------	------	------	------	------	------	------	------	------	------	------	------	------	------	------	------	------	------	------	------	------	------	------	------	------	------	------	------	------	------	------	------	------	------	------	------	------	------	------	------	------	------	------	------	------	------	------	------	------	------	------	------	------	------	------	------	------	------	------	------	------	------	------	------	------	------	------	------	------	------	------	------	------	------	------	------	------	------	------	------	------	------	------	------	------	------	------	------	------	------	------	------	------	------	------	------	------	------	------	------	------	------	------	------	------	------	------	------	------	------	------	------	------	------	------	------	------	------	------	------	------	------	------	------	------	------	------	------	------	------	------	------	------	------	------	------	------	------	------	------	------	------	------	------	------	------	------	------	------	------	------	------	------	------	------	------	------	------	------	------	------	------	------	------	------	------	------	------	------	------	------	------	------	------	------	------	------	------	------	------	------	------	------	------	------	------	------	------	------	------	------	------	------	------	------	------	------	------	------	------	------	------	------	------	------	------	------	------	------	------	------	------	------	------	------	------	------	------	------	------	------	------	------	------	------	------	------	------	------	------	------	------	------	------	------	------	------	------	------	------	------	------	------	------	------	------	------	------	------	------	------	------	------	------	------	------	------	------	------	------	------	------	------	------	------	------	------	------	------	------	------	------	------	------	------	------	------	------	------	------	------	------	------	------	------	------	------	------	------	------	------	------	------	------	------	------	------	------	------	------	------	------	------	------	------	------	------	------	------	------	------	------	------	------	------	------	------	------	------	------	------	------	------	------	------	------	------	------	------	------	------



**Table 1.7. Geochemical analysis results of QMT-6. Sample analysis commissioned by Quaterra Resources Inc.**

1	2	3	4	5	6	7	8	9	10	11	12	13	14	15	16	17	18	19	20	21	22	23	24	25	26	27	28	29	30	31	32	33	34	35	36	37	38	39	40	41	42	43	44	45	46	47	48	49	50	51	52	53	54	55	56	57	58	59	60	61	62	63	64	65	66	67	68	69	70	71	72	73	74	75	76	77	78	79	80	81	82	83	84	85	86	87	88	89	90	91	92	93	94	95	96	97	98	99	100	101	102	103	104	105	106	107	108	109	110	111	112	113	114	115	116	117	118	119	120	121	122	123	124	125	126	127	128	129	130	131	132	133	134	135	136	137	138	139	140	141	142	143	144	145	146	147	148	149	150	151	152	153	154	155	156	157	158	159	160	161	162	163	164	165	166	167	168	169	170	171	172	173	174	175	176	177	178	179	180	181	182	183	184	185	186	187	188	189	190	191	192	193	194	195	196	197	198	199	200	201	202	203	204	205	206	207	208	209	210	211	212	213	214	215	216	217	218	219	220	221	222	223	224	225	226	227	228	229	230	231	232	233	234	235	236	237	238	239	240	241	242	243	244	245	246	247	248	249	250	251	252	253	254	255	256	257	258	259	260	261	262	263	264	265	266	267	268	269	270	271	272	273	274	275	276	277	278	279	280	281	282	283	284	285	286	287	288	289	290	291	292	293	294	295	296	297	298	299	300	301	302	303	304	305	306	307	308	309	310	311	312	313	314	315	316	317	318	319	320	321	322	323	324	325	326	327	328	329	330	331	332	333	334	335	336	337	338	339	340	341	342	343	344	345	346	347	348	349	350	351	352	353	354	355	356	357	358	359	360	361	362	363	364	365	366	367	368	369	370	371	372	373	374	375	376	377	378	379	380	381	382	383	384	385	386	387	388	389	390	391	392	393	394	395	396	397	398	399	400	401	402	403	404	405	406	407	408	409	410	411	412	413	414	415	416	417	418	419	420	421	422	423	424	425	426	427	428	429	430	431	432	433	434	435	436	437	438	439	440	441	442	443	444	445	446	447	448	449	450	451	452	453	454	455	456	457	458	459	460	461	462	463	464	465	466	467	468	469	470	471	472	473	474	475	476	477	478	479	480	481	482	483	484	485	486	487	488	489	490	491	492	493	494	495	496	497	498	499	500	501	502	503	504	505	506	507	508	509	510	511	512	513	514	515	516	517	518	519	520	521	522	523	524	525	526	527	528	529	530	531	532	533	534	535	536	537	538	539	540	541	542	543	544	545	546	547	548	549	550	551	552	553	554	555	556	557	558	559	560	561	562	563	564	565	566	567	568	569	570	571	572	573	574	575	576	577	578	579	580	581	582	583	584	585	586	587	588	589	590	591	592	593	594	595	596	597	598	599	600	601	602	603	604	605	606	607	608	609	610	611	612	613	614	615	616	617	618	619	620	621	622	623	624	625	626	627	628	629	630	631	632	633	634	635	636	637	638	639	640	641	642	643	644	645	646	647	648	649	650	651	652	653	654	655	656	657	658	659	660	661	662	663	664	665	666	667	668	669	670	671	672	673	674	675	676	677	678	679	680	681	682	683	684	685	686	687	688	689	690	691	692	693	694	695	696	697	698	699	700	701	702	703	704	705	706	707	708	709	710	711	712	713	714	715	716	717	718	719	720	721	722	723	724	725	726	727	728	729	730	731	732	733	734	735	736	737	738	739	740	741	742	743	744	745	746	747	748	749	750	751	752	753	754	755	756	757	758	759	760	761	762	763	764	765	766	767	768	769	770	771	772	773	774	775	776	777	778	779	780	781	782	783	784	785	786	787	788	789	790	791	792	793	794	795	796	797	798	799	800	801	802	803	804	805	806	807	808	809	810	811	812	813	814	815	816	817	818	819	820	821	822	823	824	825	826	827	828	829	830	831	832	833	834	835	836	837	838	839	840	841	842	843	844	845	846	847	848	849	850	851	852	853	854	855	856	857	858	859	860	861	862	863	864	865	866	867	868	869	870	871	872	873	874	875	876	877	878	879	880	881	882	883	884	885	886	887	888	889	890	891	892	893	894	895	896	897	898	899	900	901	902	903	904	905	906	907	908	909	910	911	912	913	914	915	916	917	918	919	920	921	922	923	924	925	926	927	928	929	930	931	932	933	934	935	936	937	938	939	940	941	942	943	944	945	946	947	948	949	950	951	952	953	954	955	956	957	958	959	960	961	962	963	964	965	966	967	968	969	970	971	972	973	974	975	976	977	978	979	980	981	982	983	984	985	986	987	988	989	990	991	992	993	994	995	996	997	998	999	1000
---	---	---	---	---	---	---	---	---	----	----	----	----	----	----	----	----	----	----	----	----	----	----	----	----	----	----	----	----	----	----	----	----	----	----	----	----	----	----	----	----	----	----	----	----	----	----	----	----	----	----	----	----	----	----	----	----	----	----	----	----	----	----	----	----	----	----	----	----	----	----	----	----	----	----	----	----	----	----	----	----	----	----	----	----	----	----	----	----	----	----	----	----	----	----	----	----	----	----	-----	-----	-----	-----	-----	-----	-----	-----	-----	-----	-----	-----	-----	-----	-----	-----	-----	-----	-----	-----	-----	-----	-----	-----	-----	-----	-----	-----	-----	-----	-----	-----	-----	-----	-----	-----	-----	-----	-----	-----	-----	-----	-----	-----	-----	-----	-----	-----	-----	-----	-----	-----	-----	-----	-----	-----	-----	-----	-----	-----	-----	-----	-----	-----	-----	-----	-----	-----	-----	-----	-----	-----	-----	-----	-----	-----	-----	-----	-----	-----	-----	-----	-----	-----	-----	-----	-----	-----	-----	-----	-----	-----	-----	-----	-----	-----	-----	-----	-----	-----	-----	-----	-----	-----	-----	-----	-----	-----	-----	-----	-----	-----	-----	-----	-----	-----	-----	-----	-----	-----	-----	-----	-----	-----	-----	-----	-----	-----	-----	-----	-----	-----	-----	-----	-----	-----	-----	-----	-----	-----	-----	-----	-----	-----	-----	-----	-----	-----	-----	-----	-----	-----	-----	-----	-----	-----	-----	-----	-----	-----	-----	-----	-----	-----	-----	-----	-----	-----	-----	-----	-----	-----	-----	-----	-----	-----	-----	-----	-----	-----	-----	-----	-----	-----	-----	-----	-----	-----	-----	-----	-----	-----	-----	-----	-----	-----	-----	-----	-----	-----	-----	-----	-----	-----	-----	-----	-----	-----	-----	-----	-----	-----	-----	-----	-----	-----	-----	-----	-----	-----	-----	-----	-----	-----	-----	-----	-----	-----	-----	-----	-----	-----	-----	-----	-----	-----	-----	-----	-----	-----	-----	-----	-----	-----	-----	-----	-----	-----	-----	-----	-----	-----	-----	-----	-----	-----	-----	-----	-----	-----	-----	-----	-----	-----	-----	-----	-----	-----	-----	-----	-----	-----	-----	-----	-----	-----	-----	-----	-----	-----	-----	-----	-----	-----	-----	-----	-----	-----	-----	-----	-----	-----	-----	-----	-----	-----	-----	-----	-----	-----	-----	-----	-----	-----	-----	-----	-----	-----	-----	-----	-----	-----	-----	-----	-----	-----	-----	-----	-----	-----	-----	-----	-----	-----	-----	-----	-----	-----	-----	-----	-----	-----	-----	-----	-----	-----	-----	-----	-----	-----	-----	-----	-----	-----	-----	-----	-----	-----	-----	-----	-----	-----	-----	-----	-----	-----	-----	-----	-----	-----	-----	-----	-----	-----	-----	-----	-----	-----	-----	-----	-----	-----	-----	-----	-----	-----	-----	-----	-----	-----	-----	-----	-----	-----	-----	-----	-----	-----	-----	-----	-----	-----	-----	-----	-----	-----	-----	-----	-----	-----	-----	-----	-----	-----	-----	-----	-----	-----	-----	-----	-----	-----	-----	-----	-----	-----	-----	-----	-----	-----	-----	-----	-----	-----	-----	-----	-----	-----	-----	-----	-----	-----	-----	-----	-----	-----	-----	-----	-----	-----	-----	-----	-----	-----	-----	-----	-----	-----	-----	-----	-----	-----	-----	-----	-----	-----	-----	-----	-----	-----	-----	-----	-----	-----	-----	-----	-----	-----	-----	-----	-----	-----	-----	-----	-----	-----	-----	-----	-----	-----	-----	-----	-----	-----	-----	-----	-----	-----	-----	-----	-----	-----	-----	-----	-----	-----	-----	-----	-----	-----	-----	-----	-----	-----	-----	-----	-----	-----	-----	-----	-----	-----	-----	-----	-----	-----	-----	-----	-----	-----	-----	-----	-----	-----	-----	-----	-----	-----	-----	-----	-----	-----	-----	-----	-----	-----	-----	-----	-----	-----	-----	-----	-----	-----	-----	-----	-----	-----	-----	-----	-----	-----	-----	-----	-----	-----	-----	-----	-----	-----	-----	-----	-----	-----	-----	-----	-----	-----	-----	-----	-----	-----	-----	-----	-----	-----	-----	-----	-----	-----	-----	-----	-----	-----	-----	-----	-----	-----	-----	-----	-----	-----	-----	-----	-----	-----	-----	-----	-----	-----	-----	-----	-----	-----	-----	-----	-----	-----	-----	-----	-----	-----	-----	-----	-----	-----	-----	-----	-----	-----	-----	-----	-----	-----	-----	-----	-----	-----	-----	-----	-----	-----	-----	-----	-----	-----	-----	-----	-----	-----	-----	-----	-----	-----	-----	-----	-----	-----	-----	-----	-----	-----	-----	-----	-----	-----	-----	-----	-----	-----	-----	-----	-----	-----	-----	-----	-----	-----	-----	-----	-----	-----	-----	-----	-----	-----	-----	-----	-----	-----	-----	-----	-----	-----	-----	-----	-----	-----	-----	-----	-----	-----	-----	-----	-----	-----	-----	-----	-----	-----	-----	-----	-----	-----	-----	-----	-----	-----	-----	-----	-----	-----	-----	-----	-----	-----	-----	-----	-----	-----	-----	-----	-----	-----	-----	-----	-----	-----	-----	-----	-----	-----	-----	-----	-----	-----	-----	-----	-----	-----	-----	-----	-----	-----	-----	-----	-----	-----	-----	-----	-----	-----	-----	-----	-----	-----	-----	-----	-----	-----	-----	-----	-----	-----	-----	-----	-----	-----	-----	-----	-----	-----	-----	-----	-----	-----	-----	-----	-----	-----	-----	-----	-----	-----	-----	-----	-----	-----	-----	-----	-----	-----	-----	-----	-----	-----	-----	-----	-----	-----	-----	-----	-----	-----	-----	-----	-----	-----	-----	-----	-----	-----	-----	-----	-----	-----	-----	-----	-----	-----	-----	-----	-----	-----	-----	-----	-----	-----	-----	-----	-----	-----	-----	-----	-----	-----	-----	-----	-----	-----	-----	-----	-----	-----	-----	-----	-----	-----	-----	-----	-----	-----	-----	-----	-----	-----	-----	-----	-----	-----	-----	-----	-----	-----	-----	-----	-----	-----	-----	-----	-----	-----	-----	-----	-----	-----	-----	-----	-----	-----	-----	-----	-----	-----	-----	-----	-----	-----	-----	-----	-----	-----	-----	-----	-----	-----	-----	-----	-----	-----	------

??

??

?

?

???



?

???

**Table 1.9. Geochemical analysis results of QMT-8. Sample analysis commissioned by Quaterra Resources Inc.**

1	2	3	4	5	6	7	8	9	10	11	12	13	14	15	16	17	18	19	20	21	22	23	24	25	26	27	28	29	30	31	32	33	34	35	36	37	38	39	40	41	42	43	44	45	46	47	48	49	50	51	52	53	54	55	56	57	58	59	60	61	62	63	64	65	66	67	68	69	70	71	72	73	74	75	76	77	78	79	80	81	82	83	84	85	86	87	88	89	90	91	92	93	94	95	96	97	98	99	100										
101	102	103	104	105	106	107	108	109	110	111	112	113	114	115	116	117	118	119	120	121	122	123	124	125	126	127	128	129	130	131	132	133	134	135	136	137	138	139	140	141	142	143	144	145	146	147	148	149	150	151	152	153	154	155	156	157	158	159	160	161	162	163	164	165	166	167	168	169	170	171	172	173	174	175	176	177	178	179	180	181	182	183	184	185	186	187	188	189	190	191	192	193	194	195	196	197	198	199	200										
201	202	203	204	205	206	207	208	209	210	211	212	213	214	215	216	217	218	219	220	221	222	223	224	225	226	227	228	229	230	231	232	233	234	235	236	237	238	239	240	241	242	243	244	245	246	247	248	249	250	251	252	253	254	255	256	257	258	259	260	261	262	263	264	265	266	267	268	269	270	271	272	273	274	275	276	277	278	279	280	281	282	283	284	285	286	287	288	289	290	291	292	293	294	295	296	297	298	299	300										
301	302	303	304	305	306	307	308	309	310	311	312	313	314	315	316	317	318	319	320	321	322	323	324	325	326	327	328	329	330	331	332	333	334	335	336	337	338	339	340	341	342	343	344	345	346	347	348	349	350	351	352	353	354	355	356	357	358	359	360	361	362	363	364	365	366	367	368	369	370	371	372	373	374	375	376	377	378	379	380	381	382	383	384	385	386	387	388	389	390	391	392	393	394	395	396	397	398	399	400										
401	402	403	404	405	406	407	408	409	410	411	412	413	414	415	416	417	418	419	420	421	422	423	424	425	426	427	428	429	430	431	432	433	434	435	436	437	438	439	440	441	442	443	444	445	446	447	448	449	450	451	452	453	454	455	456	457	458	459	460	461	462	463	464	465	466	467	468	469	470	471	472	473	474	475	476	477	478	479	480	481	482	483	484	485	486	487	488	489	490	491	492	493	494	495	496	497	498	499	500										
501	502	503	504	505	506	507	508	509	510	511	512	513	514	515	516	517	518	519	520	521	522	523	524	525	526	527	528	529	530	531	532	533	534	535	536	537	538	539	540	541	542	543	544	545	546	547	548	549	550	551	552	553	554	555	556	557	558	559	560	561	562	563	564	565	566	567	568	569	570	571	572	573	574	575	576	577	578	579	580	581	582	583	584	585	586	587	588	589	590	591	592	593	594	595	596	597	598	599	600										
601	602	603	604	605	606	607	608	609	610	611	612	613	614	615	616	617	618	619	620	621	622	623	624	625	626	627	628	629	630	631	632	633	634	635	636	637	638	639	640	641	642	643	644	645	646	647	648	649	650	651	652	653	654	655	656	657	658	659	660	661	662	663	664	665	666	667	668	669	670	671	672	673	674	675	676	677	678	679	680	681	682	683	684	685	686	687	688	689	690	691	692	693	694	695	696	697	698	699	700										
701	702	703	704	705	706	707	708	709	710	711	712	713	714	715	716	717	718	719	720	721	722	723	724	725	726	727	728	729	730	731	732	733	734	735	736	737	738	739	740	741	742	743	744	745	746	747	748	749	750	751	752	753	754	755	756	757	758	759	760	761	762	763	764	765	766	767	768	769	770	771	772	773	774	775	776	777	778	779	780	781	782	783	784	785	786	787	788	789	790	791	792	793	794	795	796	797	798	799	800										
801	802	803	804	805	806	807	808	809	810	811	812	813	814	815	816	817	818	819	820	821	822	823	824	825	826	827	828	829	830	831	832	833	834	835	836	837	838	839	840	841	842	843	844	845	846	847	848	849	850	851	852	853	854	855	856	857	858	859	860	861	862	863	864	865	866	867	868	869	870	871	872	873	874	875	876	877	878	879	880	881	882	883	884	885	886	887	888	889	890	891	892	893	894	895	896	897	898	899	900										
901	902	903	904	905	906	907	908	909	910	911	912	913	914	915	916	917	918	919	920	921	922	923	924	925	926	927	928	929	930	931	932	933	934	935	936	937	938	939	940	941	942	943	944	945	946	947	948	949	950	951	952	953	954	955	956	957	958	959	960	961	962	963	964	965	966	967	968	969	970	971	972	973	974	975	976	977	978	979	980	981	982	983	984	985	986	987	988	989	990																				
991	992	993	994	995	996	997	998	999	1000	1001	1002	1003	1004	1005	1006	1007	1008	1009	1010	1011	1012	1013	1014	1015	1016	1017	1018	1019	1020	1021	1022	1023	1024	1025	1026	1027	1028	1029	1030	1031	1032	1033	1034	1035	1036	1037	1038	1039	1040	1041	1042	1043	1044	1045	1046	1047	1048	1049	1050	1051	1052	1053	1054	1055	1056	1057	1058	1059	1060	1061	1062	1063	1064	1065	1066	1067	1068	1069	1070	1071	1072	1073	1074	1075	1076	1077	1078	1079	1080	1081	1082	1083	1084	1085	1086	1087	1088	1089	1090	1091	1092	1093	1094	1095	1096	1097	1098	1099	1100

?

??

??

?

???

**Table 1.10.** Geochemical analysis results of QMT-9. Sample analysis commissioned by Quaterra Resources Inc.

	1	2	3	4	5	6	7	8	9	10	11	12	13	14	15	16	17	18	19	20	21	22	23	24	25	26	27	28	29	30	31	32	33	34	35	36	37	38	39	40	41	42	43	44	45	46	47	48	49	50	51	52	53	54	55	56	57	58	59	60	61	62	63	64	65	66	67	68	69	70	71	72	73	74	75	76	77	78	79	80	81	82	83	84	85	86	87	88	89	90	91	92	93	94	95	96	97	98	99	100
1	1	2	3	4	5	6	7	8	9	10	11	12	13	14	15	16	17	18	19	20	21	22	23	24	25	26	27	28	29	30	31	32	33	34	35	36	37	38	39	40	41	42	43	44	45	46	47	48	49	50	51	52	53	54	55	56	57	58	59	60	61	62	63	64	65	66	67	68	69	70	71	72	73	74	75	76	77	78	79	80	81	82	83	84	85	86	87	88	89	90	91	92	93	94	95	96	97	98	99	100
2	1	2	3	4	5	6	7	8	9	10	11	12	13	14	15	16	17	18	19	20	21	22	23	24	25	26	27	28	29	30	31	32	33	34	35	36	37	38	39	40	41	42	43	44	45	46	47	48	49	50	51	52	53	54	55	56	57	58	59	60	61	62	63	64	65	66	67	68	69	70	71	72	73	74	75	76	77	78	79	80	81	82	83	84	85	86	87	88	89	90	91	92	93	94	95	96	97	98	99	100
3	1	2	3	4	5	6	7	8	9	10	11	12	13	14	15	16	17	18	19	20	21	22	23	24	25	26	27	28	29	30	31	32	33	34	35	36	37	38	39	40	41	42	43	44	45	46	47	48	49	50	51	52	53	54	55	56	57	58	59	60	61	62	63	64	65	66	67	68	69	70	71	72	73	74	75	76	77	78	79	80	81	82	83	84	85	86	87	88	89	90	91	92	93	94	95	96	97	98	99	100
4	1	2	3	4	5	6	7	8	9	10	11	12	13	14	15	16	17	18	19	20	21	22	23	24	25	26	27	28	29	30	31	32	33	34	35	36	37	38	39	40	41	42	43	44	45	46	47	48	49	50	51	52	53	54	55	56	57	58	59	60	61	62	63	64	65	66	67	68	69	70	71	72	73	74	75	76	77	78	79	80	81	82	83	84	85	86	87	88	89	90	91	92	93	94	95	96	97	98	99	100
5	1	2	3	4	5	6	7	8	9	10	11	12	13	14	15	16	17	18	19	20	21	22	23	24	25	26	27	28	29	30	31	32	33	34	35	36	37	38	39	40	41	42	43	44	45	46	47	48	49	50	51	52	53	54	55	56	57	58	59	60	61	62	63	64	65	66	67	68	69	70	71	72	73	74	75	76	77	78	79	80	81	82	83	84																

Region	North America										Europe										Asia										Africa										Oceania										Global																																																																																																																																																																																																																																																																																																																																																																																											
	NA1	NA2	NA3	NA4	NA5	NA6	NA7	NA8	NA9	NA10	EU1	EU2	EU3	EU4	EU5	EU6	EU7	EU8	EU9	EU10	AS1	AS2	AS3	AS4	AS5	AS6	AS7	AS8	AS9	AS10	AF1	AF2	AF3	AF4	AF5	AF6	AF7	AF8	AF9	AF10	OC1	OC2	OC3	OC4	OC5	OC6	OC7	OC8	OC9	OC10																																																																																																																																																																																																																																																																																																																																																																																												
Region A	10	15	20	25	30	35	40	45	50	55	60	65	70	75	80	85	90	95	100	105	110	115	120	125	130	135	140	145	150	155	160	165	170	175	180	185	190	195	200	205	210	215	220	225	230	235	240	245	250	255	260	265	270	275	280	285	290	295	300	305	310	315	320	325	330	335	340	345	350	355	360	365	370	375	380	385	390	395	400	405	410	415	420	425	430	435	440	445	450	455	460	465	470	475	480	485	490	495	500	505	510	515	520	525	530	535	540	545	550	555	560	565	570	575	580	585	590	595	600	605	610	615	620	625	630	635	640	645	650	655	660	665	670	675	680	685	690	695	700	705	710	715	720	725	730	735	740	745	750	755	760	765	770	775	780	785	790	795	800	805	810	815	820	825	830	835	840	845	850	855	860	865	870	875	880	885	890	895	900	905	910	915	920	925	930	935	940	945	950	955	960	965	970	975	980	985	990	995	1000	1005	1010	1015	1020	1025	1030	1035	1040	1045	1050	1055	1060	1065	1070	1075	1080	1085	1090	1095	1100	1105	1110	1115	1120	1125	1130	1135	1140	1145	1150	1155	1160	1165	1170	1175	1180	1185	1190	1195	1200	1205	1210	1215	1220	1225	1230	1235	1240	1245	1250	1255	1260	1265	1270	1275	1280	1285	1290	1295	1300	1305	1310	1315	1320	1325	1330	1335	1340	1345	1350	1355	1360	1365	1370	1375	1380	1385	1390	1395	1400	1405	1410	1415	1420	1425	1430	1435	1440	1445	1450	1455	1460	1465	1470	1475	1480	1485	1490	1495	1500	1505	1510	1515	1520	1525	1530	1535	1540	1545	1550	1555	1560	1565	1570	1575	1580	1585	1590	1595	1600	1605	1610	1615	1620	1625	1630	1635	1640	1645	1650	1655	1660	1665	1670	1675	1680	1685	1690	1695	1700	1705	1710	1715	1720	1725	1730	1735	1740	1745	1750	1755	1760	1765	1770	1775	1780	1785	1790	1795	1800	1805	1810	1815	1820	1825	1830	1835	1840	1845	1850	1855	1860	1865	1870	1875	1880	1885	1890	1895	1900	1905	1910	1915	1920	1925	1930	1935	1940	1945	1950	1955	1960	1965	1970	1975	1980	1985	1990	1995	2000	2005	2010	2015	2020	2025	2030	2035	2040	2045	2050	2055	2060	2065	2070	2075	2080	2085	2090	2095	2100	2105	2110	2115	2120	2125	2130	2135	2140	2145	2150	2155

[illegible]

**Table 1.11.** Geochemical analysis results of QMT-10. Sample analysis commissioned by Quaterra Resources Inc.

Year	2010	2011	2012	2013	2014	2015	2016	2017	2018	2019	2020	2021	2022	2023	2024	2025	2026	2027	2028	2029	2030	2031	2032	2033	2034	2035	2036	2037	2038	2039	2040	2041	2042	2043	2044	2045	2046	2047	2048	2049	2050	2051	2052	2053	2054	2055	2056	2057	2058	2059	2060	2061	2062	2063	2064	2065	2066	2067	2068	2069	2070	2071	2072	2073	2074	2075	2076	2077	2078	2079	2080	2081	2082	2083	2084	2085	2086	2087	2088	2089	2090	2091	2092	2093	2094	2095	2096	2097	2098	2099	2100																																																																						
Population	7.9	8.0	8.1	8.2	8.3	8.4	8.5	8.6	8.7	8.8	8.9	9.0	9.1	9.2	9.3	9.4	9.5	9.6	9.7	9.8	9.9	10.0	10.1	10.2	10.3	10.4	10.5	10.6	10.7	10.8	10.9	11.0	11.1	11.2	11.3	11.4	11.5	11.6	11.7	11.8	11.9	12.0	12.1	12.2	12.3	12.4	12.5	12.6	12.7	12.8	12.9	13.0	13.1	13.2	13.3	13.4	13.5	13.6	13.7	13.8	13.9	14.0	14.1	14.2	14.3	14.4	14.5	14.6	14.7	14.8	14.9	15.0	15.1	15.2	15.3	15.4	15.5	15.6	15.7	15.8	15.9	16.0	16.1	16.2	16.3	16.4	16.5	16.6	16.7	16.8	16.9	17.0	17.1	17.2	17.3	17.4	17.5	17.6	17.7	17.8	17.9	18.0	18.1	18.2	18.3	18.4	18.5	18.6	18.7	18.8	18.9	19.0	19.1	19.2	19.3	19.4	19.5	19.6	19.7	19.8	19.9	20.0																																							
GDP	50.0	55.0	60.0	65.0	70.0	75.0	80.0	85.0	90.0	95.0	100.0	105.0	110.0	115.0	120.0	125.0	130.0	135.0	140.0	145.0	150.0	155.0	160.0	165.0	170.0	175.0	180.0	185.0	190.0	195.0	200.0	205.0	210.0	215.0	220.0	225.0	230.0	235.0	240.0	245.0	250.0	255.0	260.0	265.0	270.0	275.0	280.0	285.0	290.0	295.0	300.0	305.0	310.0	315.0	320.0	325.0	330.0	335.0	340.0	345.0	350.0	355.0	360.0	365.0	370.0	375.0	380.0	385.0	390.0	395.0	400.0	405.0	410.0	415.0	420.0	425.0	430.0	435.0	440.0	445.0	450.0	455.0	460.0	465.0	470.0	475.0	480.0	485.0	490.0	495.0	500.0																																																																						
Urbanization	55	57	59	61	63	65	67	69	71	73	75	77	79	81	83	85	87	89	91	93	95	97	99	101	103	105	107	109	111	113	115	117	119	121	123	125	127	129	131	133	135	137	139	141	143	145	147	149	151	153	155	157	159	161	163	165	167	169	171	173	175	177	179	181	183	185	187	189	191	193	195	197	199	201	203	205	207	209	211	213	215	217	219	221	223	225	227	229	231	233	235	237	239	241	243	245	247	249	251	253	255	257	259	261	263	265	267	269	271	273	275	277	279	281	283	285	287	289	291	293	295	297	299	301	303	305	307	309	311	313	315	317	319	321	323	325	327	329	331	333	335	337	339	341	343	345	347	349	351	353	355	357	359	361	363	365	367	369	371	373	

**Table 1.11 cont.** Geochemical analysis results of QMT-10. Sample analysis commissioned by Quaterra Resources Inc.

[illegible]

?

???

???

?

???

???

?

???

1

## 16. APPENDIX 2 – STATISTICAL ANALYSES

Appendix 2 displays all figures and tables for statistical analyses and is split into several sections. These sections include:

	PAGE
16.1. Appendix 2.1. Descriptive Statistics	
Tables 2.1 – 2.6 .....	154
Descriptive statistics results for surface and subsurface multi-element samples for raw data, outlier removed data, and log-transformed data.	
16.2. Appendix 2.2. Univariate Analysis	
Figures 2.1 – 2.33 .....	160
Univariate analysis for surface and subsurface multi-element samples from left to right for: raw data, outlier removed data, and log-transformed data histograms, outlier boxes, and normal quantile plots. A vertical blue line is seen on raw or outlier removed histograms and represents the average elemental abundance in granitic rocks.	
16.3. Appendix 2.3. Bivariate Analysis	
Tables 2.7 – 2.8 and Figures 2.34 – 2.36.....	193
Bivariate analysis figures for surface and subsurface samples displayed as correlation coefficient matrix, correlation scatter plots, and pairwise correlations. Due to computer error the scatter plot matrix is not displayed for subsurface data. Bivariate analysis is performed using log-transformed data.	
16.4. Appendix 2.4. Multivariate Analysis	
Figures 2.37 – 2.52 .....	202
Multivariate analysis figures showing geochemical families for surface and subsurface data indicated by factor score coefficients. Multivariate analysis is performed using log-transformed data.	
16.5. Appendix 2.5. Spatial Distribution of Factor Scores	
Figures 2.52 – 2.60 .....	210
Spatial distribution of factor scores coefficients derived from principal component analysis. Spatial distributions of factor score figures are in the form of contour diagrams.	

**Table 2.1.** Descriptive statistics for raw surface data showing number of samples (N), minimum, 1<sup>st</sup> quartile, median, 3<sup>rd</sup> quartile, maximum, mean, standard deviation, skewness and kurtosis.

Table 2.1 - Descriptive Statistics for Raw Surface Data										
Element	N	Min	0.25	Median	0.75	Max	Mean	S.D.	Skewness	Kurtosis
Ag	63	0.006	0.0885	0.12	0.18	0.745	0.16	0.14	2.63	7.90
Al	63	0.18	1.105	1.26	1.81	4.45	1.51	0.71	1.62	4.24
As	63	0.05	0.075	1.2	3	22.3	2.48	4.05	3.29	12.10
B	63	1	3	4	7	66	7.00	8.86	5.11	32.17
Ba	63	24.5	71.9	110	142.5	273	110.41	49.95	0.50	0.55
Be	63	0.05	0.4	0.5	0.8	2	0.62	0.37	1.31	2.21
Ca	63	0.11	0.36	0.55	0.7	18.4	1.17	2.96	5.28	27.80
Cd	63	0.005	0.01	0.02	0.04	1.53	0.07	0.20	6.41	44.67
Ce	63	2.3	25.55	32.3	44.5	205	38.17	26.46	4.19	25.33
Co	63	1.2	3.2	6.7	18.8	801	49.05	147.15	4.09	16.44
Cr	63	0.9	6.35	7.6	8.9	201	12.56	25.76	6.65	47.93
Cs	63	0.2	0.95	1.6	2.2	37.2	2.58	4.84	6.22	43.51
Cu	63	21.6	1295	2090	4365	9900	3344.95	3065.09	1.29	0.35
Dy	63	0.1	1.15	1.4	1.9	16.5	2.09	2.58	4.26	20.22
Er	63	0.1	0.6	0.7	0.95	10	1.14	1.67	4.41	20.59
Eu	63	0.05	0.5	0.6	0.9	4.9	0.86	0.78	3.33	13.28
Fe	63	0.23	0.975	1.35	1.71	4.37	1.45	0.67	1.70	5.34
Ga	63	0.58	4.815	5.94	8.075	15.4	6.65	2.88	1.01	1.47
Gd	63	0.2	1.7	2.3	2.9	20.9	3.02	3.09	3.95	19.04
Ho	63	0.001	0.2	0.3	0.4	3.5	0.42	0.58	4.30	20.06
K	63	0.05	0.2	0.31	0.5	0.92	0.36	0.21	0.83	0.23
La	63	1.1	12.75	16.1	22.5	105	19.43	14.22	3.90	21.23
Li	63	1.9	4.95	7.5	11.4	45.8	9.07	6.75	3.02	13.58
Mg	63	0.21	0.615	0.8	1.085	2.77	0.91	0.49	1.52	2.94
Mn	63	19	71	93	171.5	6290	381.71	1030.02	4.59	21.96
Mo	63	0.95	3.475	6.11	12.6	126	11.38	17.95	4.77	27.59
Na	63	0.079	0.1195	0.138	0.217	0.487	0.17	0.08	1.61	3.57
Nd	63	1.02	11.75	15.2	20.2	95.7	18.33	13.69	3.54	17.07
Ni	63	1	8.8	12.1	18.45	199	18.69	25.78	5.80	39.58
P	63	0.015	0.0685	0.089	0.107	1.45	0.13	0.20	5.46	32.82
Pr	63	0.3	3.1	3.9	5.25	25.2	4.57	3.28	4.23	25.17
Rb	63	3	11	21.5	31.35	111	24.16	18.11	2.16	7.78
S	63	0.003	0.011	0.014	0.023	0.249	0.03	0.05	3.32	11.18
Sb	63	0.03	0.09	0.14	0.195	0.69	0.16	0.12	1.96	5.15
Sc	63	0.3	3.15	3.6	4.15	10.3	3.74	1.60	1.44	5.18
Se	63	0.05	0.35	0.8	1.6	21.8	1.48	2.84	6.18	43.79
Sm	63	0.2	2.2	2.9	3.65	17.3	3.57	2.97	3.19	11.83
Sn	63	0.025	0.34	0.49	0.655	1.64	0.52	0.25	1.51	5.51
Sr	63	28	72.5	109	133.5	755	126.57	105.43	3.85	20.29
Tb	63	0.05	0.2	0.3	0.4	2.9	0.40	0.44	4.05	19.36
Th	63	0.9	4.3	6.7	8.45	10.6	6.37	2.58	-0.17	-1.05
Ti	63	0.005	0.03	0.1	0.13	0.21	0.09	0.06	0.13	-1.13
U	63	0.5	2.55	3.3	4.75	61	6.73	10.75	3.66	13.96
V	63	8	39	47	56.5	138	50.65	21.12	1.49	4.69
Y	63	0.74	5.755	7.15	9.555	123	12.47	19.94	4.38	20.55
Yb	63	0.05	0.5	0.6	0.8	8.8	0.93	1.49	4.59	21.94
Zn	63	3.3	7.05	11.7	19.05	80.4	15.58	12.78	2.63	9.97
Zr	63	0.05	0.3	0.6	1.05	3.8	0.84	0.76	1.63	3.15

2

2

2

222

**Table 2.2.** Descriptive statistics for outlier-removed surface data showing number of samples (N), minimum, 1<sup>st</sup> quartile, median, 3<sup>rd</sup> quartile, maximum, mean, standard deviation, skewness and kurtosis.

<b>Table 2.2 - Descriptive Statistics for Outlier-Removed Surface Data</b>										
<b>Element</b>	<b>N</b>	<b>Min</b>	<b>0.25</b>	<b>Median</b>	<b>0.75</b>	<b>Max</b>	<b>Mean</b>	<b>S.D.</b>	<b>Skewness</b>	<b>Kurtosis</b>
Ag	59	0.006	0.088	0.106	0.1655	0.318	0.13	0.07	0.79	0.51
Al	60	0.18	1.095	1.25	1.675	2.57	1.41	0.52	0.47	0.04
As	60	0.05	0.05	1.05	2.725	7.2	1.69	1.84	1.31	1.27
B	57	1	3	4	6	13	4.91	2.65	1.57	2.45
Ba	62	24.5	71.2	109	141.5	208	107.79	45.78	0.08	-0.69
Be	62	0.05	0.4	0.5	0.8	1.4	0.60	0.32	0.84	0.09
Ca	59	0.11	0.345	0.54	0.68	1.97	0.57	0.33	1.92	5.54
Cd	56	0.005	0.01	0.02	0.03	0.07	0.02	0.02	0.97	0.45
Ce	62	2.3	25.375	31.8	43.4	74.4	35.48	15.74	0.60	0.20
Co	57	1.2	3	4.9	13.1	44.9	10.14	10.39	1.63	2.18
Cr	58	0.9	6.3	7.6	8.475	12.5	7.35	1.94	-0.66	2.15
Cs	57	0.2	0.9	1.5	2.1	3.8	1.53	0.85	0.70	0.43
Cu	63	21.6	1295	2090	4365	9900	3344.95	3065.09	1.29	0.35
Dy	54	0.1	1	1.3	1.6	2.3	1.33	0.48	-0.13	-0.10
Er	56	0.1	0.575	0.7	0.825	1.5	0.70	0.28	0.40	0.88
Eu	58	0.05	0.5	0.6	0.8	1.4	0.67	0.28	0.47	0.30
Fe	61	0.23	0.97	1.31	1.69	2.62	1.37	0.50	0.37	-0.14
Ga	60	0.58	4.8	5.855	7.445	13.2	6.25	2.31	0.43	0.63
Gd	55	0.2	1.6	2	2.65	4.2	2.13	0.83	0.37	0.44
Ho	57	0.001	0.2	0.3	0.3	0.7	0.27	0.14	1.05	2.10
K	60	0.05	0.19	0.315	0.4725	0.89	0.34	0.19	0.69	0.28
La	60	1.1	12.375	15.7	21.6	32	16.97	6.99	0.28	-0.20
Li	60	1.9	4.85	7.35	9.65	19.8	7.99	4.11	0.91	0.48
Mg	59	0.21	0.605	0.75	1.02	1.78	0.82	0.35	0.75	0.48
Mn	58	19	66.5	87	128.75	463	125.48	99.95	1.98	3.32
Mo	58	0.95	3.27	5.57	10.75	24	7.26	5.25	1.14	0.76
Na	59	0.079	0.1185	0.125	0.1495	0.22	0.14	0.03	1.02	0.77
Nd	57	1.02	11.6	14.8	19.3	30.1	15.03	5.98	0.24	0.20
Ni	58	1	8.7	11.1	17.375	33.6	13.43	7.22	0.99	0.52
P	57	0.015	0.066	0.087	0.1	0.147	0.08	0.03	-0.06	0.57
Pr	61	0.3	3.1	3.8	5	8.7	4.12	1.76	0.46	0.09
Rb	61	3	10	21.3	30.8	61.3	22.04	13.37	0.79	0.71
S	62	0.003	0.011	0.014	0.022	0.249	0.03	0.05	3.64	13.52
Sb	57	0.03	0.08	0.13	0.17	0.35	0.13	0.07	0.90	0.69
Sc	53	2	3.2	3.6	4.1	4.9	3.62	0.68	-0.22	-0.28
Se	59	0.05	0.3	0.8	1.55	3.4	0.98	0.83	1.13	0.90
Sm	58	0.2	2.2	2.85	3.575	5.8	2.83	1.14	0.41	0.48
Sn	62	0.025	0.34	0.485	0.64	1.08	0.50	0.21	0.27	-0.01
Sr	59	28	68.6	107	129	229	105.42	48.73	0.61	0.17
Tb	57	0.05	0.2	0.3	0.3	0.7	0.28	0.13	0.95	1.57
Th	63	0.9	4.3	6.7	8.45	10.6	6.37	2.58	-0.17	-1.05
Ti	63	0.005	0.03	0.1	0.13	0.21	0.09	0.06	0.13	-1.13
U	54	0.5	2.5	3.05	4.075	8	3.42	1.56	1.12	1.58
V	59	8	39	47	55	76	46.63	14.09	-0.41	0.72
Y	55	0.74	5.12	6.84	8.46	16.2	7.00	3.01	0.80	1.78
Yb	57	0.05	0.4	0.5	0.7	1.2	0.56	0.24	0.44	0.63
Zn	60	3.3	6.775	11.4	18.475	36.3	13.59	8.42	1.16	0.72
Zr	61	0.05	0.3	0.6	1	2.3	0.75	0.61	1.00	0.29

?

?

?

?

???

**Table 2.3.** Descriptive statistics for log-transformed surface data showing number of samples (N), minimum, 1<sup>st</sup> quartile, median, 3<sup>rd</sup> quartile, maximum, mean, standard deviation, skewness and kurtosis.

<b>Table 2.3 - Descriptive Statistics for Log-Transformed Surface Data</b>										
<b>Element</b>	<b>N</b>	<b>Min</b>	<b>0.25</b>	<b>Median</b>	<b>0.75</b>	<b>Max</b>	<b>Mean</b>	<b>S.D.</b>	<b>Skewness</b>	<b>Kurtosis</b>
Ag	63	-1.22	-0.05	0.08	0.26	0.50	0.05	0.32	-1.30	2.99
Al	63	0.26	1.04	1.10	1.26	1.54	1.13	0.21	-1.05	4.61
As	63	-0.30	-0.15	1.08	1.48	1.86	0.83	0.76	-0.51	-1.29
B	63	1.00	1.48	1.60	1.85	2.11	1.68	0.24	0.09	-0.09
Ba	63	2.39	2.86	3.04	3.15	3.32	2.99	0.22	-0.88	0.25
Be	63	-0.30	0.60	0.70	0.90	1.15	0.72	0.27	-0.83	2.10
Ca	63	0.04	0.54	0.74	0.84	1.29	0.70	0.24	-0.32	0.62
Cd	63	-1.30	-1.00	-0.70	-0.40	-0.15	-0.69	0.34	-0.28	-0.97
Ce	63	1.36	2.41	2.51	2.65	2.87	2.50	0.24	-1.82	6.92
Co	63	1.08	1.51	1.83	2.27	2.65	1.88	0.47	0.10	-1.14
Cr	63	0.95	1.80	1.88	1.95	2.10	1.86	0.17	-2.79	12.51
Cs	63	0.30	0.98	1.20	1.34	1.58	1.15	0.30	-0.74	0.06
Cu	63	2.33	4.11	4.32	4.64	5.00	4.34	0.46	-1.16	4.51
Dy	63	0.00	1.06	1.15	1.28	1.36	1.12	0.22	-2.45	9.64
Er	63	0.00	0.78	0.85	0.98	1.18	0.83	0.23	-1.51	3.75
Eu	63	-0.30	0.70	0.78	0.95	1.15	0.80	0.24	-1.75	5.87
Fe	63	0.36	0.99	1.13	1.23	1.42	1.11	0.19	-1.03	2.90
Ga	63	0.76	1.68	1.77	1.91	2.12	1.77	0.20	-2.04	8.60
Gd	63	0.30	1.23	1.36	1.46	1.62	1.32	0.23	-1.68	5.70
Ho	63	-2.00	0.30	0.48	0.60	0.85	0.39	0.39	-3.91	23.11
K	63	-0.30	0.30	0.54	0.70	0.96	0.48	0.29	-0.54	-0.29
La	63	1.04	2.11	2.21	2.35	2.51	2.19	0.24	-2.05	7.83
Li	63	1.28	1.69	1.88	2.06	2.30	1.87	0.24	-0.20	-0.39
Mg	63	0.32	0.79	0.90	1.04	1.25	0.89	0.20	-0.55	0.36
Mn	63	2.28	2.85	2.97	3.23	3.67	3.05	0.31	0.45	-0.30
Mo	63	0.98	1.54	1.79	2.10	2.38	1.79	0.34	-0.17	-0.80
Na	63	-0.10	0.08	0.10	0.20	0.34	0.13	0.11	0.30	-0.36
Nd	63	1.01	2.07	2.18	2.31	2.48	2.16	0.24	-2.06	7.83
Ni	63	1.00	1.94	2.08	2.27	2.53	2.09	0.26	-1.11	3.36
P	63	-0.82	-0.16	-0.04	0.00	0.17	-0.09	0.17	-2.07	6.31
Pr	63	0.48	1.49	1.59	1.72	1.94	1.58	0.24	-1.75	6.25
Rb	63	1.48	2.04	2.33	2.50	2.79	2.26	0.32	-0.74	-0.10
S	63	-1.52	-0.96	-0.85	-0.64	0.40	-0.76	0.41	1.11	1.51
Sb	63	-0.52	-0.05	0.15	0.29	0.54	0.10	0.26	-0.31	-0.72
Sc	63	1.30	1.51	1.59	1.65	1.69	1.57	0.09	-0.91	0.59
Se	63	-0.30	0.54	0.90	1.20	1.53	0.83	0.51	-0.74	-0.09
Sm	63	0.30	1.34	1.46	1.56	1.76	1.43	0.24	-1.88	7.32
Sn	63	-0.60	0.53	0.69	0.82	1.03	0.66	0.24	-2.31	10.23
Sr	63	2.45	2.86	3.04	3.13	3.36	2.99	0.22	-0.59	-0.29
Tb	63	-0.30	0.30	0.48	0.60	0.85	0.44	0.23	-0.62	0.83
Th	63	0.95	1.63	1.83	1.93	2.03	1.76	0.22	-1.22	1.68
Ti	63	-1.30	-0.52	0.00	0.11	0.32	-0.25	0.49	-0.90	-0.52
U	63	0.70	1.41	1.52	1.68	1.90	1.54	0.24	-0.61	1.38
V	63	1.90	2.59	2.67	2.75	2.88	2.65	0.18	-2.18	6.87
Y	63	0.87	1.76	1.85	1.98	2.21	1.85	0.25	-1.21	3.33
Yb	63	-0.30	0.70	0.78	0.90	1.08	0.72	0.25	-1.74	4.71
Zn	63	1.52	1.85	2.07	2.28	2.56	2.07	0.26	-0.02	-0.77
Zr	63	-0.30	0.48	0.78	1.02	1.36	0.72	0.44	-0.51	-0.74

?

?

?

???

**Table 2.4.** Descriptive statistics for raw subsurface data showing number of samples (N), minimum, 1<sup>st</sup> quartile, median, 3<sup>rd</sup> quartile, maximum, mean, standard deviation, skewness and kurtosis.

Table 2.4 - Descriptive Statistics for Raw Subsurface Data										
Element	N	Min	0.25	Median	0.75	Max	Mean	S.D.	Skewness	Kurtosis
Ag	1000	0.01	0.047	0.115	0.1973	28.554	0.21	0.96	25.82	748.77
Al	1000	124	7067.5	8825	11200	59800	10210.57	5860.87	3.23	16.15
As	1000	0.1	1.1375	1.605	2.36	209	2.64	9.01	17.75	360.94
Au	1000	0.045	0.045	0.045	0.045	2.85	0.07	0.16	10.77	138.92
Ba	1000	1.06	58.25	73.75	104	784	93.57	73.19	3.68	20.69
Be	1000	0.003	0.17275	0.25	0.3633	1.81	0.29	0.19	2.50	10.52
Ca	1000	66.4	3447.5	4400	5555	50800	5065.32	3602.84	6.19	62.57
Ce	1000	0.617	11.4	15.5	20.625	74.5	17.04	8.61	1.75	5.46
Co	1000	0.035	5.72	8.17	12.125	116	11.34	10.94	4.26	25.82
Cr	1000	0.827	14.075	23.5	34.425	604	41.44	66.62	4.22	20.24
Cu	1000	0.025	728.25	1303.26	2206.3	25500	1841.14	2157.65	5.31	42.04
CuOX	1000	0.5	284.5	699.185	1365.4	20755	1188.66	1778.50	5.14	40.02
Dy	1000	0.04	0.47775	0.745	1.02	8.37	0.87	0.75	4.22	28.32
Er	1000	0.035	0.35175	0.537	0.8273	5.484	0.67	0.53	2.93	14.71
Eu	1000	0.01	0.321	0.418	0.5353	2.38	0.47	0.27	2.53	10.85
Fe	1000	203	12775	15600	20700	68400	18115.81	8505.39	2.22	6.71
Ga	1000	0.01	4.623	5.4985	6.7255	25.018	6.07	2.67	2.27	8.06
Gd	1000	0.045	3.27	4.115	5.6025	15.7	4.69	2.05	1.73	4.06
K	1000	58.1	1947.5	3020	4132.5	21700	3377.34	2407.26	2.38	9.19
La	1000	0.566	8.09	10.4	13.7	40.9	11.06	4.80	0.98	2.50
Li	1000	0.025	0.2335	1.13	2.5225	53.9	2.23	4.36	6.37	55.17
Lu	1000	0.01	0.41675	0.5505	1.11	15.1	0.92	0.99	4.89	48.01
Mg	1000	34.1	5490	7150	8792.5	48900	8227.70	5497.32	3.23	14.40
Mn	1000	0.05	80	101	136	1920	137.36	137.91	5.58	46.90
Mo	1000	0.045	3.25	5.345	9.48	102	8.05	8.62	3.87	24.27
Na	1000	35.2	556.75	760.5	1080	4250	922.27	569.89	2.25	6.55
Nd	1000	0.125	6.265	8.32	11.125	35.3	9.13	5.00	1.36	3.70
Ni	1000	0.643	18.5	25	36.8	162	30.36	19.22	2.47	9.25
P	1000	5.44	733	873.5	986.25	3000	876.88	300.21	1.38	6.61
Pb	1000	0.045	7.785	14.8	25.525	70.3	17.85	12.12	1.00	0.76
Pr	1000	0.025	0.025	0.9205	1.5625	6.71	1.04	1.06	1.47	3.18
Rb	1000	0.25	2.375	6.65	11.505	50.2	7.99	7.38	1.68	4.40
S	1000	5	93.3	176	708.25	49200	1545.75	4174.87	5.81	45.78
Sc	1000	0.05	1.53	1.965	2.57	19.3	2.36	1.79	4.80	32.76
Se	1000	0.15	0.15	0.6625	1.5425	20.6	1.23	1.83	4.54	32.05
Si	1000	25	1577.5	2385	4230	67600	3311.28	3076.84	9.84	191.14
Sm	1000	0.015	1.1475	1.58	2.2925	12.6	1.86	1.19	1.96	8.61
Sn	1000	0.04	0.699	1.05	1.43	10.2	1.21	1.13	3.78	21.90
Sr	1000	3.76	44.075	65.55	92.05	502	79.42	59.41	2.92	12.21
Tb	1000	0.025	0.5395	0.909	1.33	7.47	1.10	0.90	1.97	6.51
Te	1000	0.45	1.247	2.174	3.1903	14.898	2.42	1.66	1.66	5.75
Th	1000	0.45	1.62	5.235	7.97	39.9	5.88	5.83	2.45	8.24
Ti	1000	4.68	695	1010	1300	6030	1078.55	627.57	2.29	9.93
Tl	1000	0.011	0.011	0.011	0.5403	10.7	0.60	1.33	3.96	18.78
Tm	1000	0.004	0.189	0.3395	0.654	25	0.49	0.89	20.86	565.05
U	1000	0.45	0.45	0.675	2.2673	54.041	2.02	3.68	6.93	73.47
V	1000	0.46	32.2	39.1	47.8	189	43.64	22.53	2.53	9.41
W	1000	0.04	0.54975	0.7955	1.29	269	1.48	8.83	28.24	848.15
Y	1000	0.055	3.43	4.52	5.865	62.6	5.59	4.90	5.71	47.36
Yb	1000	0.025	0.279	0.386	0.511	5.013	0.47	0.41	5.06	38.42
Zn	1000	3.18	13.2	17.8	26.8	424	25.84	30.41	6.23	57.98
Zr	1000	0.248	1.8475	2.64	3.7325	21.8	3.26	2.36	2.95	12.51

2

2

222

**Table 2.5.** Descriptive statistics for outlier-removed subsurface data showing number of samples (N), minimum, 1<sup>st</sup> quartile, median, 3<sup>rd</sup> quartile, maximum, mean, standard deviation, skewness and kurtosis.

<b>Table 2.5 - Descriptive Statistics for Outlier-Removed Subsurface Data</b>										
<b>Element</b>	<b>N</b>	<b>Min</b>	<b>0.25</b>	<b>Median</b>	<b>75%</b>	<b>Max</b>	<b>Mean</b>	<b>S.D.</b>	<b>Skewness</b>	<b>Kurtosis</b>
Ag	932	0.01	0.04	0.107	0.176	0.432	0.12	0.10	0.884	0.382
Al	916	124	6897.50	8470	10400	17400	8812.46	2786.40	0.550	0.467
As	926	0.1	1.09	1.52	2.14	4.34	1.65	0.90	0.598	0.258
Au	916	0.045	0.05	0.045	0.045	0.1	0.05	0.01	8.322	67.927
Ba	907	1.06	56.00	69.8	92.2	175	75.38	31.54	0.646	0.552
Be	964	0.003	0.17	0.245	0.3445	0.695	0.27	0.13	0.868	0.262
Ca	935	66.4	3350.00	4330	5260	9000	4402.76	1572.63	0.506	0.300
Ce	962	0.617	11.30	15.2	19.975	35.2	15.92	6.41	0.484	-0.133
Co	917	0.035	5.59	7.71	11	22.9	8.78	4.22	1.095	0.742
Cr	892	0.827	12.78	21.3	30.125	64.2	22.99	11.65	0.761	0.257
Cu	938	0.025	713.07	1221.1	2005.5	4481.4	1441.98	957.39	0.953	0.380
CuOx	914	0.5	263.15	627.95	1151.45	2997.1	777.06	649.64	1.033	0.580
Dy	939	0.04	0.46	0.7	0.957	1.9	0.73	0.38	0.562	0.342
Er	952	0.035	0.35	0.516	0.76775	1.6	0.59	0.33	0.867	0.229
Eu	924	0.01	0.31	0.4045	0.49925	0.838	0.41	0.16	0.209	0.092
Fe	944	203	12600.00	15200	19700	32800	16579.24	5430.70	0.863	0.405
Ga	924	1.7	4.57	5.4225	6.40975	9.991	5.54	1.54	0.436	0.384
Gd	954	0.045	3.23	4.02	5.28	9.01	4.39	1.51	0.866	0.274
K	947	58.1	1875.00	2910	3875	7500	2952.41	1504.07	0.417	0.063
La	973	0.566	8.01	10.3	13.2	21.9	10.66	4.16	0.333	-0.149
Li	928	0.025	0.20	0.9045	2.145	5.9	1.38	1.41	1.156	0.643
Lu	911	0.01	0.41	0.515	0.8795	2.14	0.68	0.44	1.279	1.041
Mg	916	836	5347.50	6875	8350	13900	6954.19	2454.44	0.310	0.234
Mn	905	0.05	78.00	96.4	124	219	103.61	37.08	0.868	0.732
Mo	930	0.045	3.13	4.985	8.43	19.8	6.25	4.22	1.123	0.716
Na	940	35.2	546.00	736	1010	1900	811.70	347.34	0.841	0.274
Nd	953	0.125	6.14	8.11	10.5	19	8.40	3.79	0.240	0.248
Ni	949	0.643	18.00	24.3	34.3	64.3	27.14	12.36	0.877	0.187
P	917	358	741.00	865	971	1350	849.23	187.48	-0.165	0.104
Pb	989	0.045	7.76	14.7	25.2	52.4	17.39	11.38	0.798	-0.023
Pr	972	0.025	0.03	0.894	1.48	3.88	0.93	0.86	0.686	-0.216
Rb	967	0.25	2.18	6.5	11.1	25.2	7.14	5.76	0.747	0.224
S	821	5	83.90	133	281	1540	250.24	287.25	2.190	4.757
Sc	910	0.05	1.48	1.9	2.3675	4.1	1.95	0.68	0.400	0.332
Se	933	0.15	0.15	0.576	1.29	3.74	0.86	0.84	1.242	0.875
Si	960	25	1560.00	2275	3950	8180	2956.16	1791.34	0.976	0.195
Sm	943	0.015	1.12	1.52	2.15	4	1.66	0.84	0.564	0.075
Sn	939	0.04	0.66	1.01	1.36	2.51	1.00	0.57	0.102	-0.255
Sr	926	3.76	42.63	61.15	83.175	163	66.15	30.51	0.775	0.288
Tb	919	0.025	0.49	0.849	1.21	2.51	0.90	0.57	0.564	0.112
Te	960	0.45	1.22	2.113	3.093	6.176	2.21	1.27	0.492	-0.184
Th	961	0.45	1.43	5	7.6	17.2	4.97	3.60	0.429	-0.373
Ti	951	4.68	680.00	978	1240	2180	975.17	407.60	0.129	-0.146
Tl	872	0.011	0.01	0.011	0.30075	1.33	0.20	0.32	1.822	2.549
Tm	958	0.004	0.18	0.3155	0.6095	1.35	0.41	0.32	0.741	-0.158
U	937	0.45	0.45	0.45	1.984	5.001	1.28	1.11	1.224	0.563
V	915	9.01	31.65	38.2	46	70.8	38.78	11.41	0.165	0.283
W	936	0.04	0.54	0.765	1.16	2.4	0.89	0.52	0.903	0.398
Y	905	0.055	3.32	4.35	5.4	9.49	4.46	1.61	0.605	0.400
Yb	917	0.025	0.27	0.366	0.473	0.866	0.38	0.16	0.590	0.195
Zn	908	3.18	12.80	16.7	23.2	46.9	18.86	8.79	1.002	0.657
Zr	927	0.248	1.80	2.51	3.42	6.58	2.73	1.22	0.844	0.369

2

2

222

**Table 2.6.** Descriptive statistics for log-transformed subsurface data showing number of samples (N), minimum, 1<sup>st</sup> quartile, median, 3<sup>rd</sup> quartile, maximum, mean, standard deviation, skewness and kurtosis.

<b>Table 2.6 - Descriptive Statistics for Log-Transformed Subsurface Data</b>										
<b>Element</b>	<b>N</b>	<b>Min</b>	<b>0.25</b>	<b>Median</b>	<b>0.75</b>	<b>Max</b>	<b>Mean</b>	<b>S.D.</b>	<b>Skewness</b>	<b>Kurtosis</b>
Ag	1000	-1.00	-0.33	0.06	0.30	0.64	-0.07	0.52	-0.71	-0.63
Al	1000	3.09	4.85	4.95	5.05	5.24	4.95	0.17	-1.40	13.23
As	1000	0.00	1.06	1.21	1.37	1.64	1.16	0.36	-1.52	2.85
Au	1000	-0.35	-0.35	-0.35	-0.35	0.00	-0.31	0.10	2.73	5.48
Ba	1000	1.03	2.77	2.87	3.02	3.24	2.87	0.24	-1.19	5.22
Be	1000	-1.52	0.24	0.40	0.56	0.84	0.39	0.23	-0.63	4.13
Ca	1000	2.82	4.54	4.64	4.74	4.95	4.63	0.19	-1.22	8.20
Ce	1000	0.79	2.06	2.19	2.31	2.55	2.18	0.20	-0.75	2.06
Co	1000	-0.46	1.76	1.91	2.08	2.36	1.93	0.24	-0.82	9.23
Cr	1000	0.92	2.15	2.37	2.54	2.81	2.35	0.27	-0.21	-0.14
Cu	1000	-0.60	3.86	4.12	4.34	4.65	4.08	0.39	-2.31	21.54
CuOx	1000	0.70	3.45	3.84	4.14	4.48	3.73	0.58	-1.20	1.67
Dy	1000	-0.40	0.68	0.87	1.01	1.28	0.81	0.34	-1.62	3.77
Er	1000	-0.46	0.55	0.73	0.92	1.20	0.72	0.30	-0.92	2.12
Eu	1000	-1.00	0.51	0.62	0.73	0.92	0.59	0.24	-2.18	10.59
Fe	1000	3.31	5.11	5.19	5.32	5.52	5.21	0.16	-1.38	18.04
Ga	1000	1.23	1.67	1.74	1.83	2.00	1.75	0.14	-0.30	0.55
Gd	1000	-0.35	1.51	1.61	1.75	1.95	1.63	0.17	-1.35	18.17
K	1000	2.76	4.29	4.48	4.62	4.88	4.42	0.32	-1.40	2.89
La	1000	0.75	1.91	2.02	2.14	2.34	2.00	0.21	-1.10	2.69
Li	1000	-0.60	0.37	1.05	1.40	1.77	0.84	0.73	-0.71	-0.59
Lu	1000	-1.00	0.62	0.74	1.05	1.33	0.78	0.40	-2.03	7.95
Mg	1000	3.92	4.74	4.86	4.95	5.14	4.84	0.19	-0.88	1.80
Mn	1000	-0.30	2.90	3.00	3.13	3.34	3.02	0.21	-4.10	65.00
Mo	1000	-0.35	1.51	1.73	1.98	2.30	1.73	0.38	-1.51	6.81
Na	1000	2.55	3.75	3.88	4.03	4.28	3.89	0.21	-0.21	1.05
Nd	1000	0.10	1.80	1.92	2.05	2.28	1.85	0.39	-3.12	11.31
Ni	1000	0.81	2.27	2.40	2.57	2.81	2.41	0.22	-0.34	2.18
P	1000	3.55	3.88	3.95	4.00	4.13	3.93	0.12	-0.56	0.45
Pb	1000	-0.35	1.89	2.17	2.41	2.72	2.12	0.41	-2.22	9.64
Pr	1000	-0.60	-0.60	0.96	1.19	1.59	0.55	0.82	-0.55	-1.45
Rb	1000	0.40	1.38	1.82	2.06	2.40	1.60	0.64	-0.96	-0.42
S	1000	1.70	2.97	3.25	3.85	4.19	3.35	0.55	0.05	-0.81
Sc	1000	-0.30	1.18	1.29	1.41	2.60	1.38	0.42	1.95	4.03
Se	1000	0.18	0.18	0.82	1.19	1.57	0.76	0.50	0.05	-1.44
Si	1000	2.40	4.20	4.38	4.63	4.91	4.41	0.30	-1.07	5.56
Sm	1000	-0.82	1.06	1.20	1.36	1.60	1.15	0.40	-3.09	12.75
Sn	1000	-0.40	0.84	1.02	1.16	1.40	0.87	0.51	-1.69	1.77
Sr	1000	1.58	2.64	2.82	2.96	3.21	2.80	0.23	-0.31	0.32
Tb	1000	-0.60	0.73	0.96	1.12	1.40	0.84	0.51	-1.70	2.50
Te	1000	0.65	1.10	1.34	1.50	1.79	1.27	0.32	-0.65	-0.43
Th	1000	0.65	1.21	1.72	1.90	2.24	1.52	0.51	-0.76	-0.84
Ti	1000	1.67	3.84	4.00	4.11	4.34	3.95	0.26	-2.03	9.16
Tl	1000	-0.96	-0.96	-0.96	0.73	1.12	-0.18	0.88	0.37	-1.68
Tm	1000	-1.40	0.28	0.53	0.82	1.13	0.33	0.76	-1.46	0.95
U	1000	0.65	0.65	0.80	1.36	1.70	1.00	0.38	0.45	-1.38
V	1000	1.95	2.51	2.59	2.68	2.85	2.59	0.16	-0.74	1.40
W	1000	-0.40	0.74	0.90	1.11	1.38	0.89	0.34	-1.39	3.55
Y	1000	-0.26	1.54	1.66	1.77	1.98	1.65	0.20	-1.10	8.67
Yb	1000	-0.60	0.45	0.59	0.71	0.94	0.57	0.22	-0.69	1.50
Zn	1000	1.50	2.12	2.25	2.43	2.67	2.27	0.23	-0.05	-0.23
Zr	1000	0.39	1.27	1.42	1.57	1.82	1.42	0.22	-0.11	-0.08

?

?

?

???

## 16.2. Appendix 2.2. Univariate Analysis

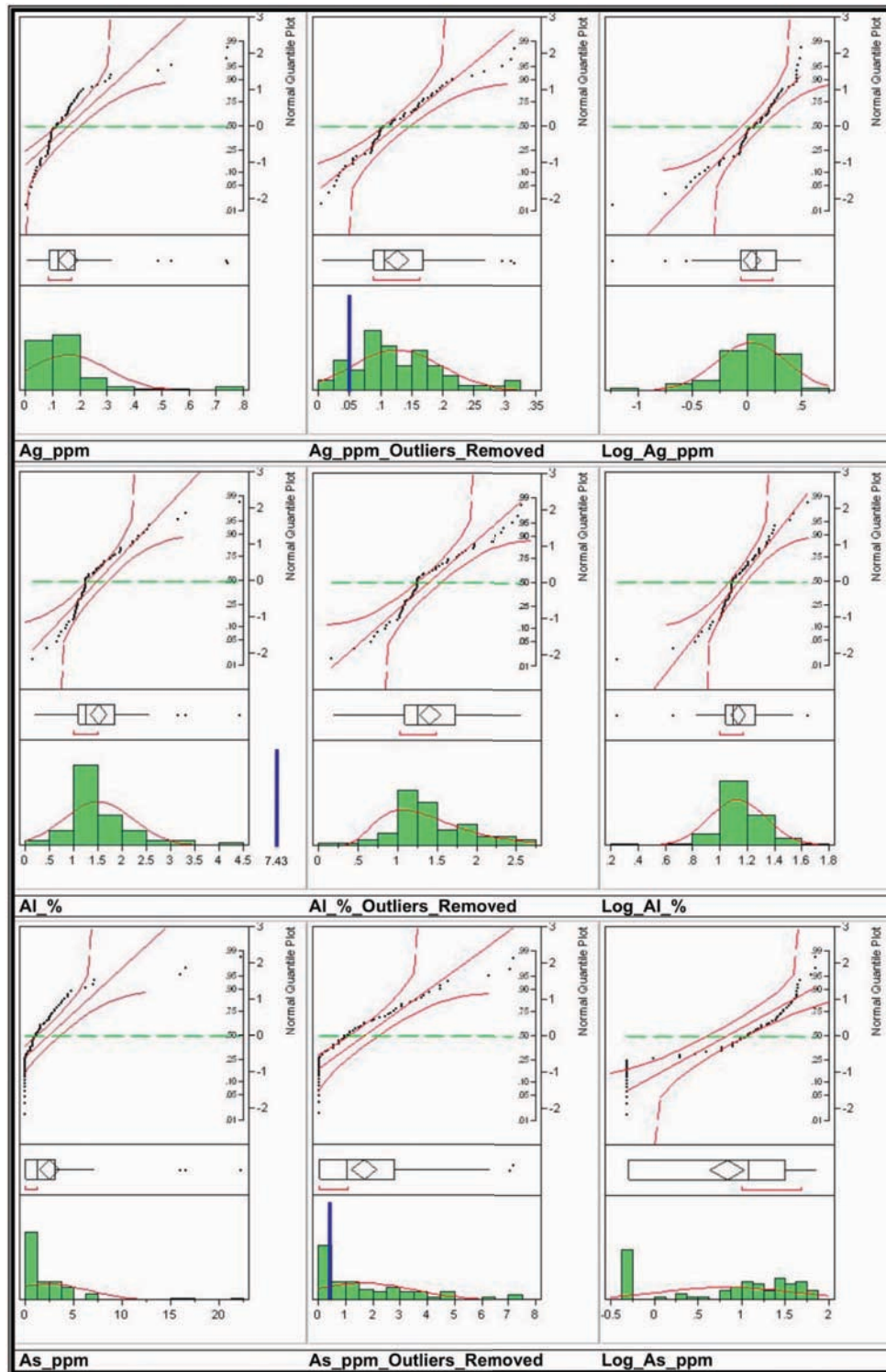


**Figure 2.1.** Surface data univariate analysis histograms, outlier-box plots, and normal quantile plots for elements Ag, Al, and As.

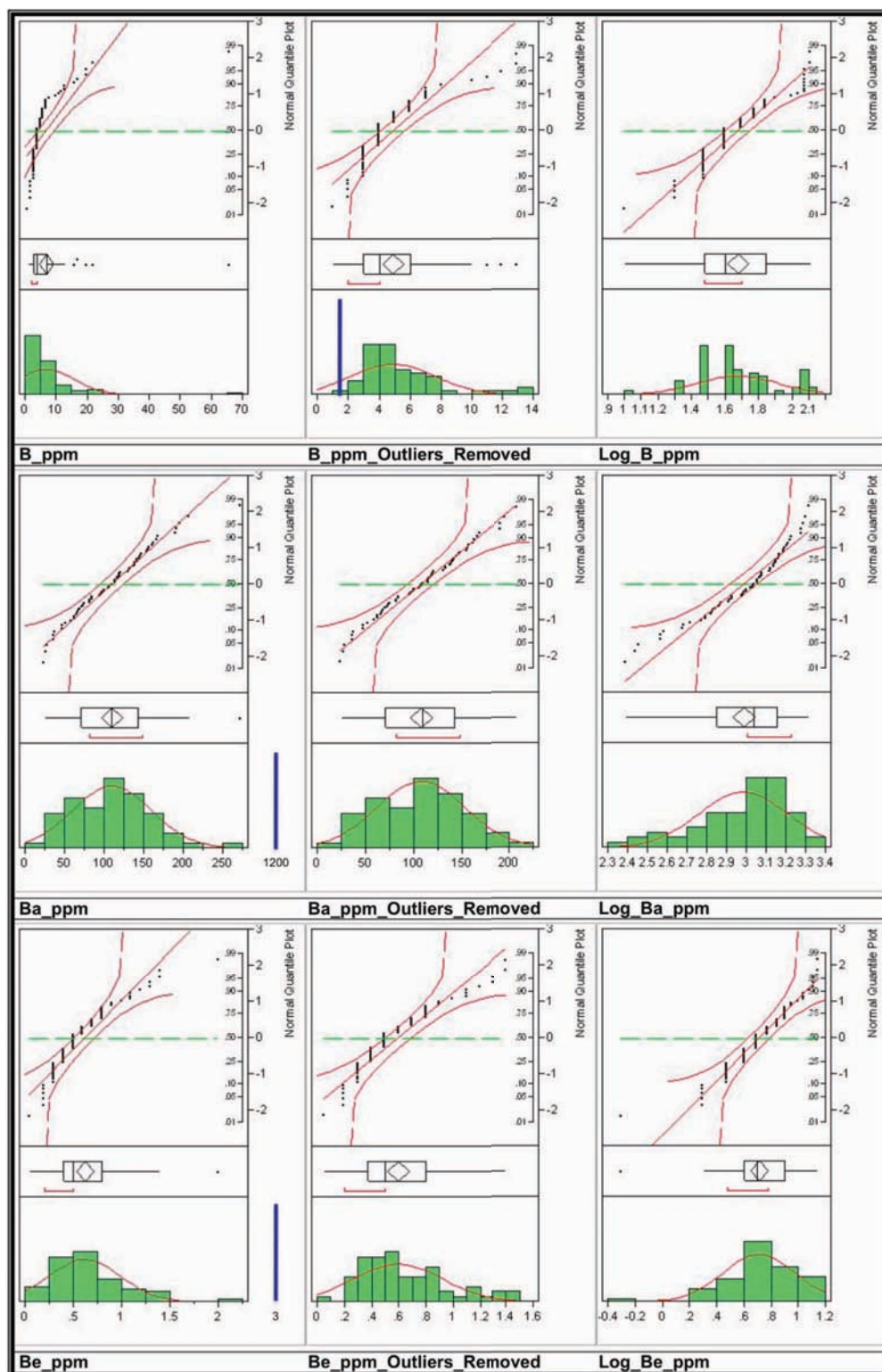


**Figure 2.2.** Surface data univariate analysis histograms, outlier-box plots, and normal quantile plots for elements B, Ba, and Be.

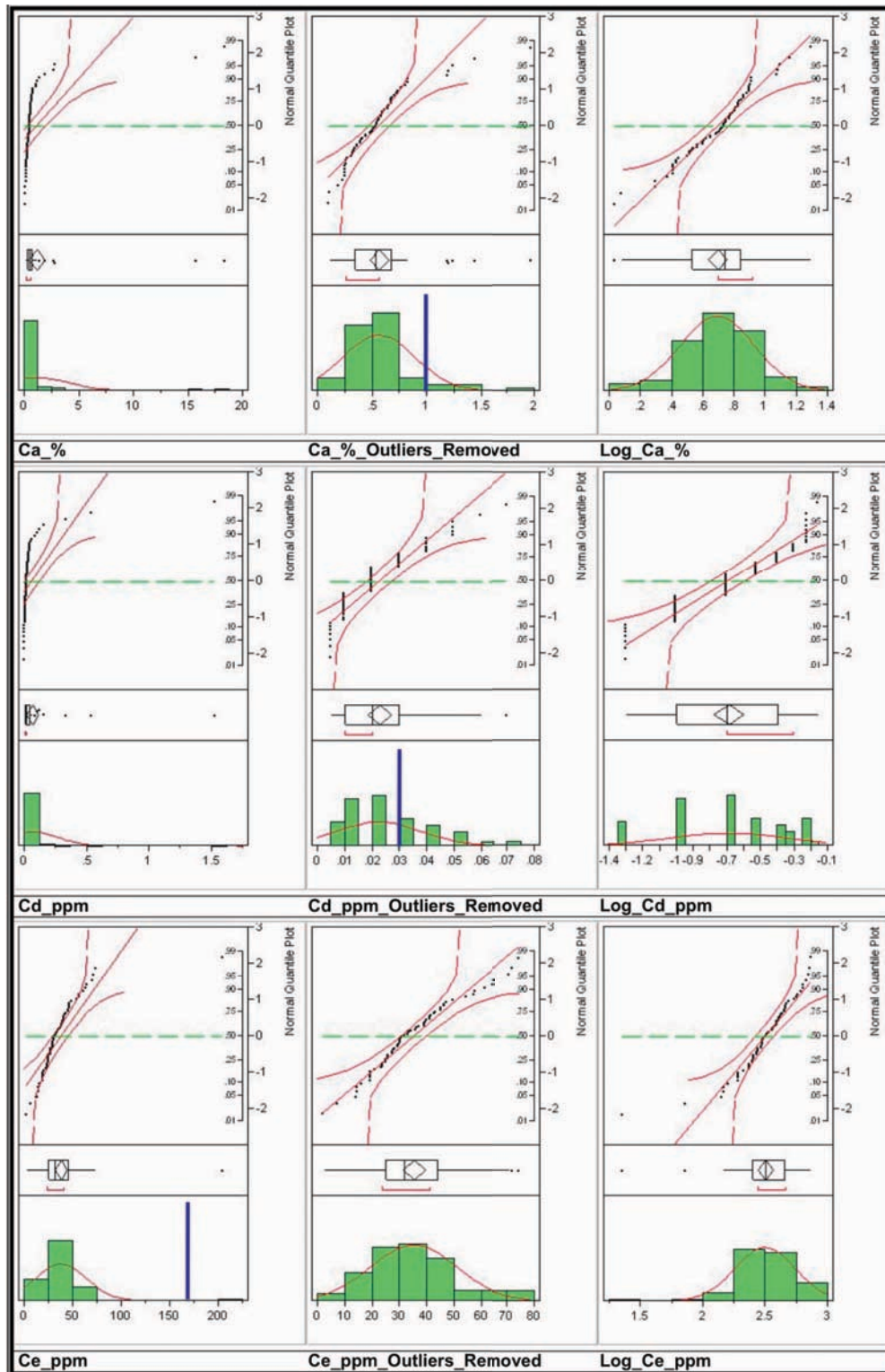


**Figure 2.3.** Surface data univariate analysis histograms, outlier-box plots, and normal quantile plots for elements Ca, Cd, and Ce.

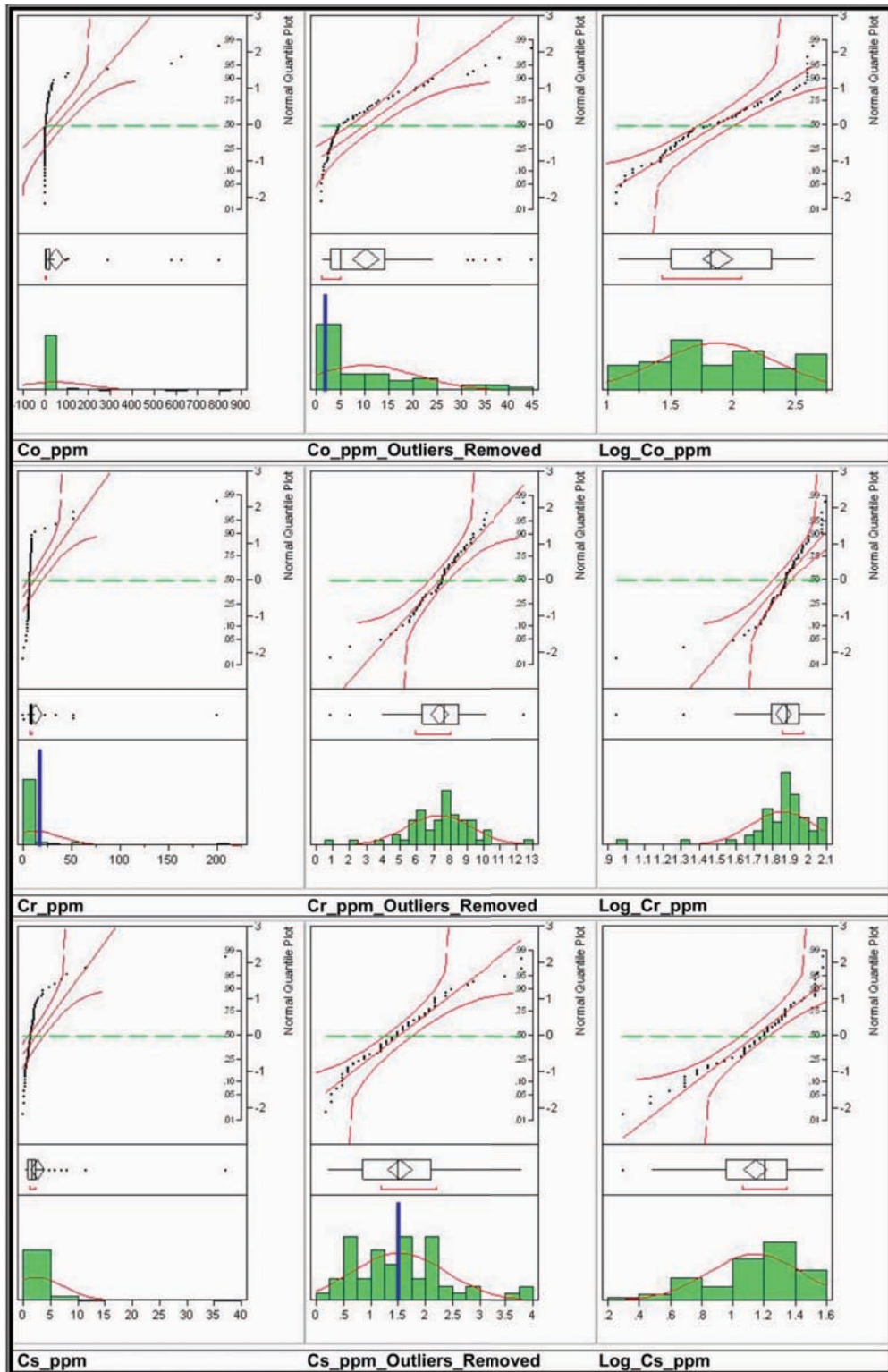


**Figure 2.4.** Surface data univariate analysis histograms, outlier-box plots, and normal quantile plots for elements Co, Cr, and Cs.

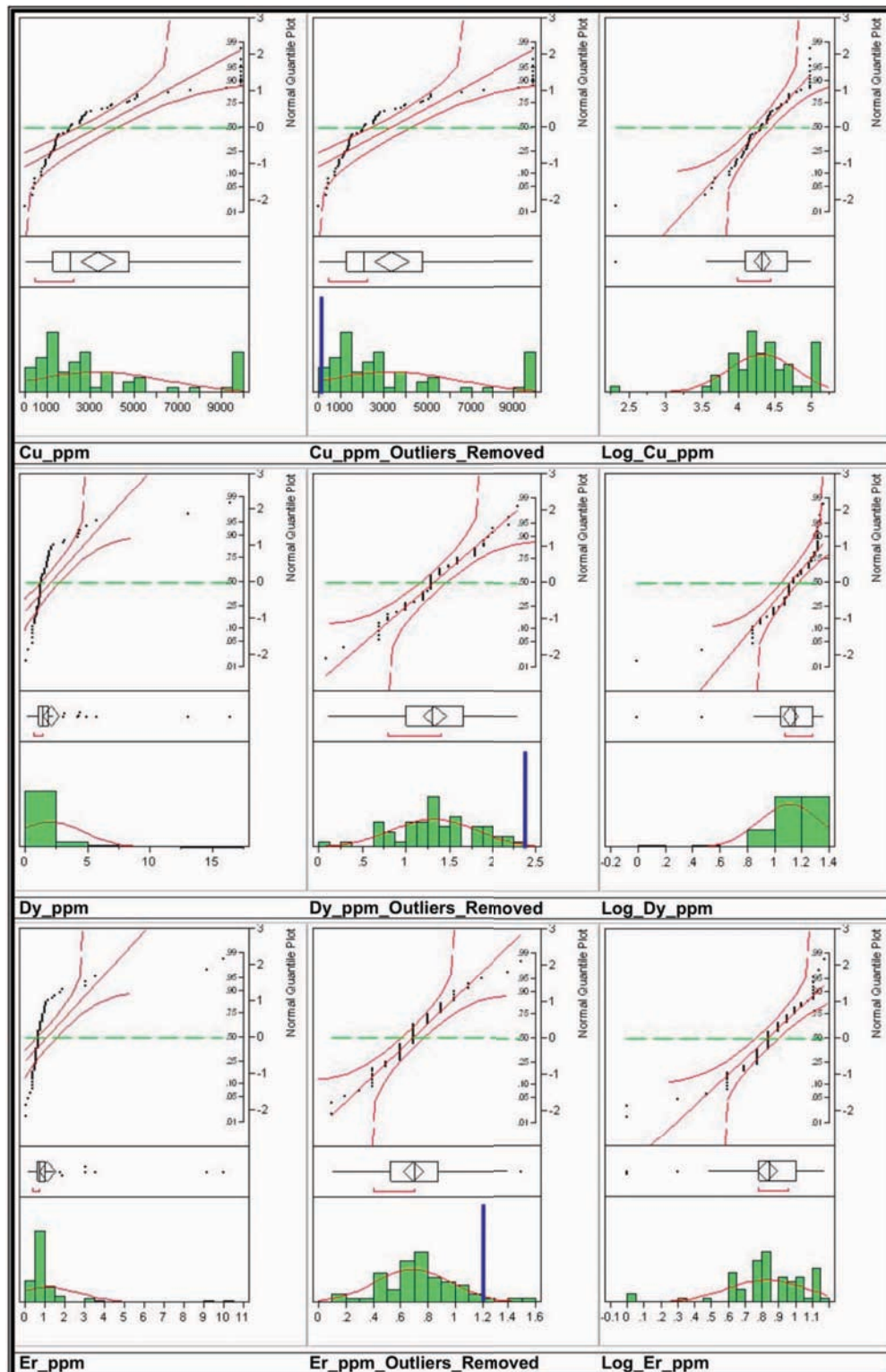


**Figure 2.5.** Surface data univariate analysis histograms, outlier-box plots, and normal quantile plots for elements Cu, Dy, and Er.

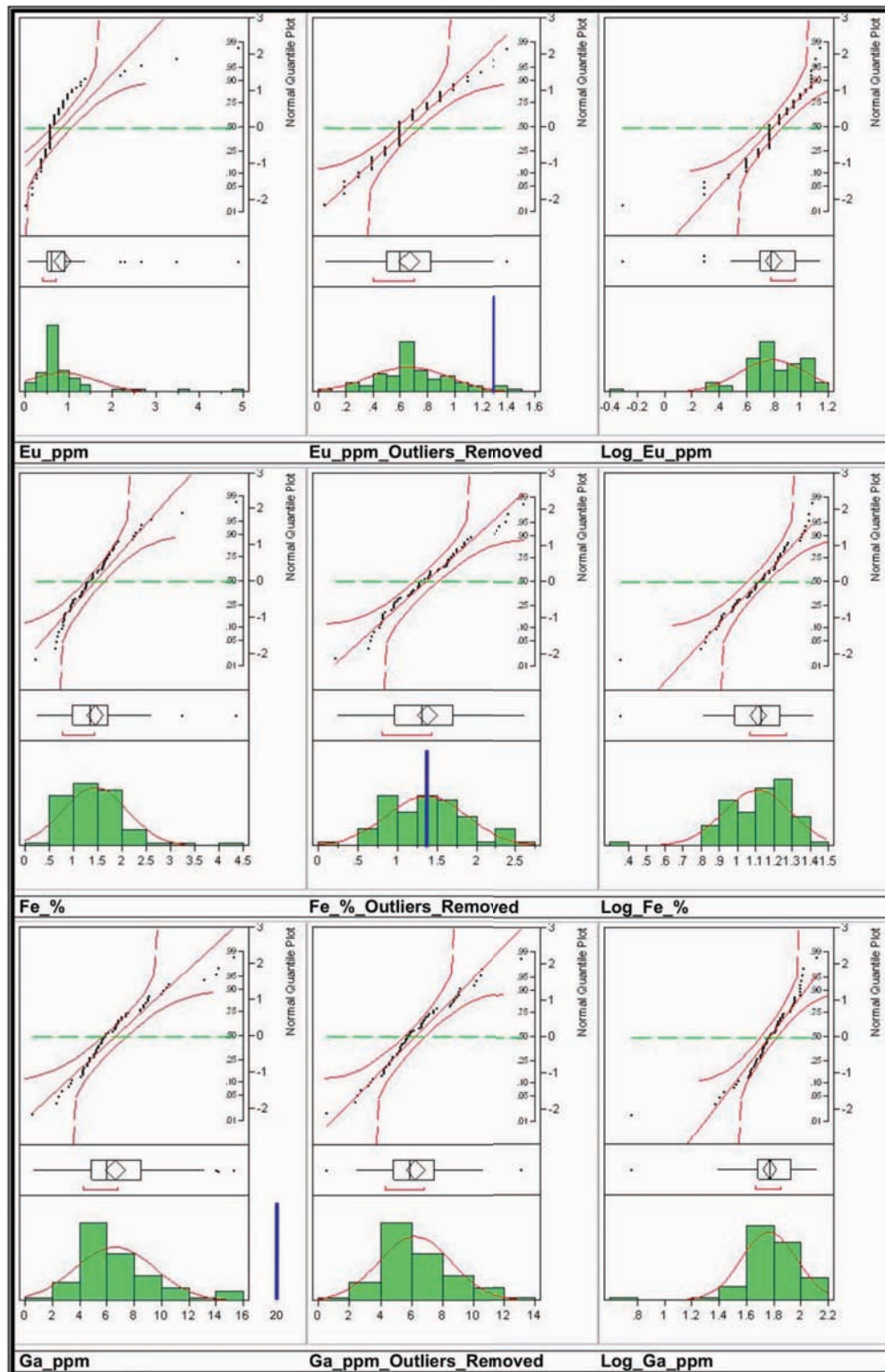


**Figure 2.6.** Surface data univariate analysis histograms, outlier-box plots, and normal quantile plots for elements Eu, Fe, and Ga.

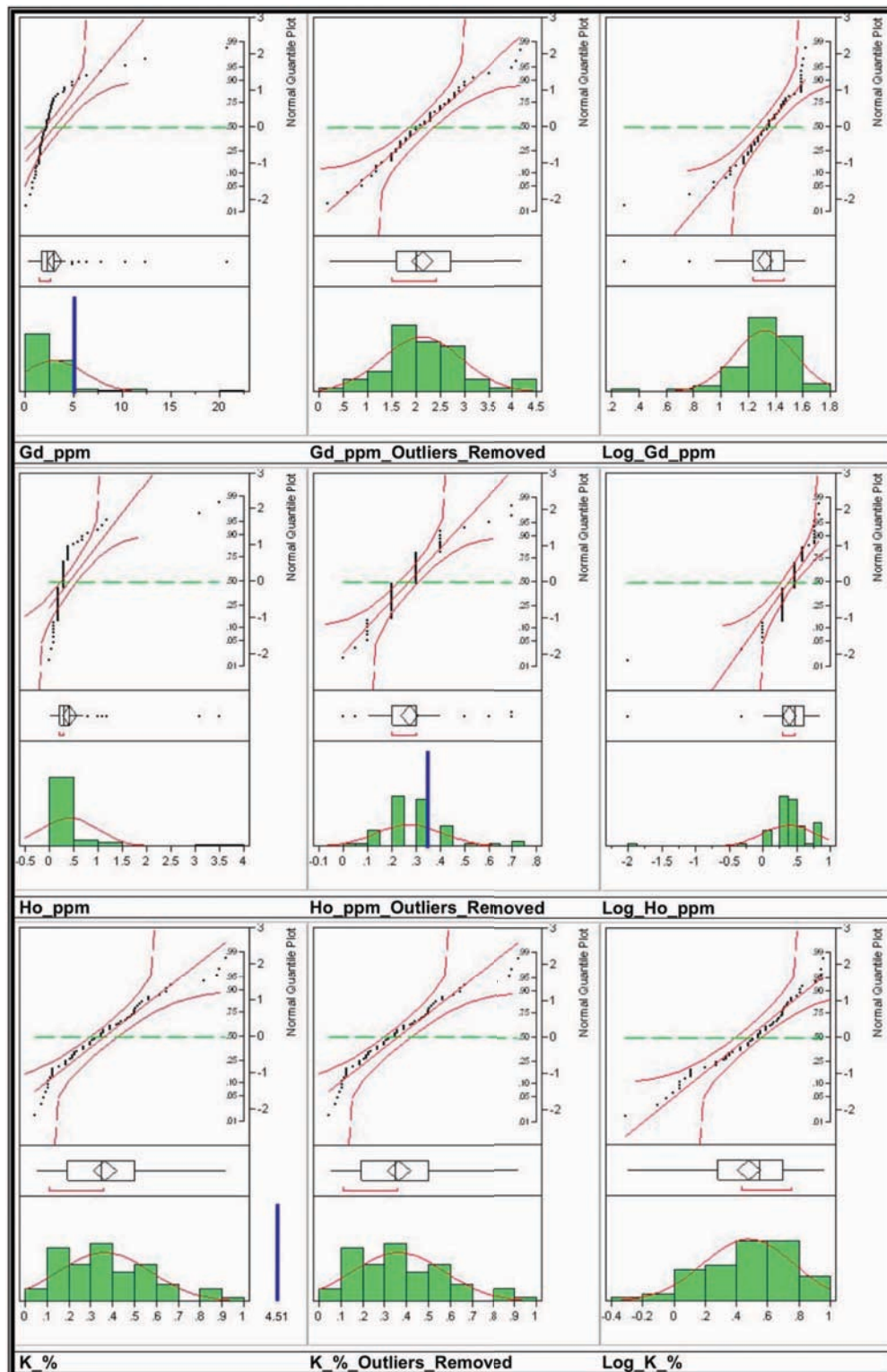


**Figure 2.7.** Surface data univariate analysis histograms, outlier-box plots, and normal quantile plots for elements Gd, Ho, and K.

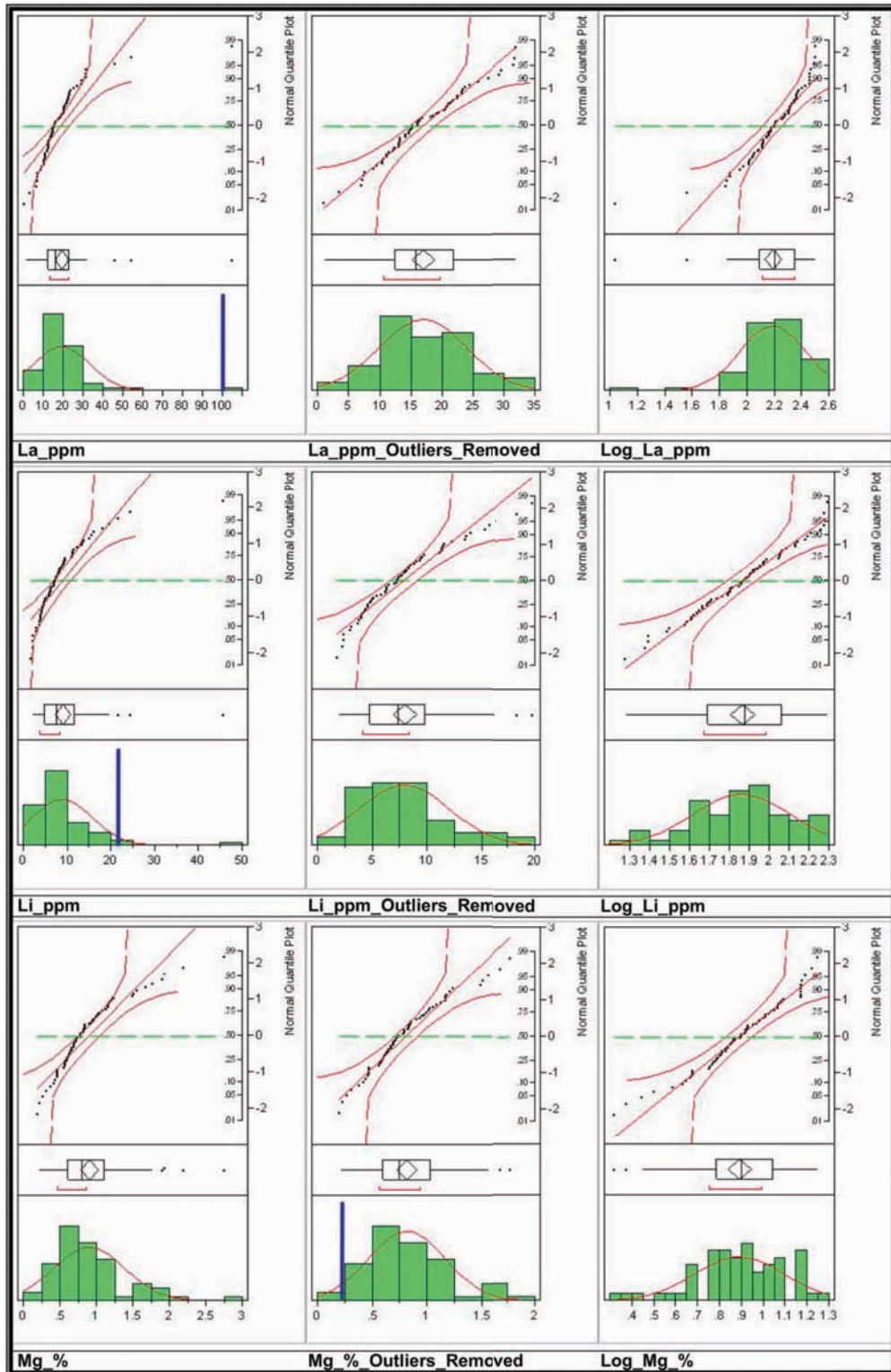


**Figure 2.8.** Surface data univariate analysis histograms, outlier-box plots, and normal quantile plots for elements La, Li, and Mg.

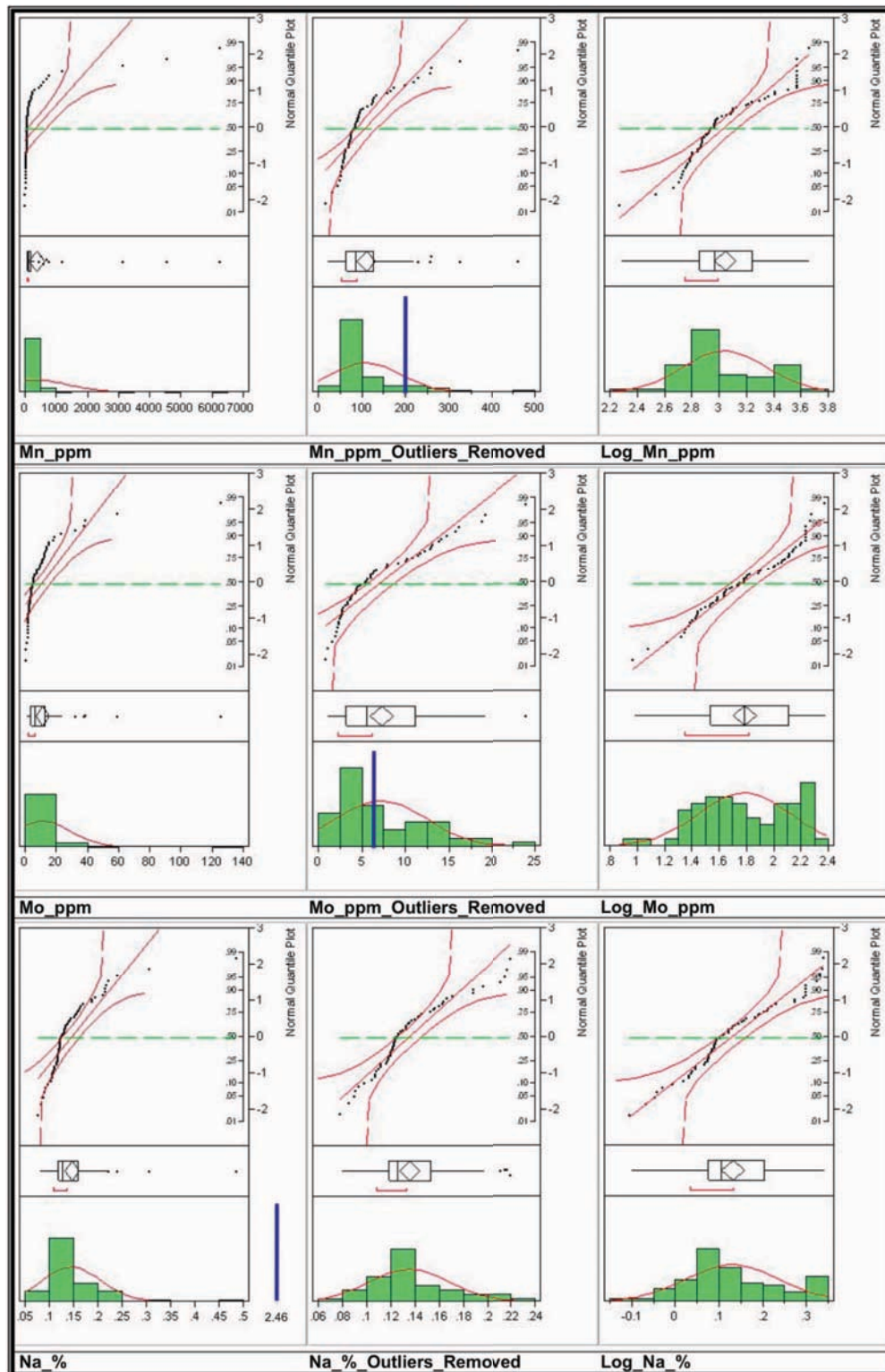


**Figure 2.9.** Surface data univariate analysis histograms, outlier-box plots, and normal quantile plots for elements Mn, Mo, and Na.

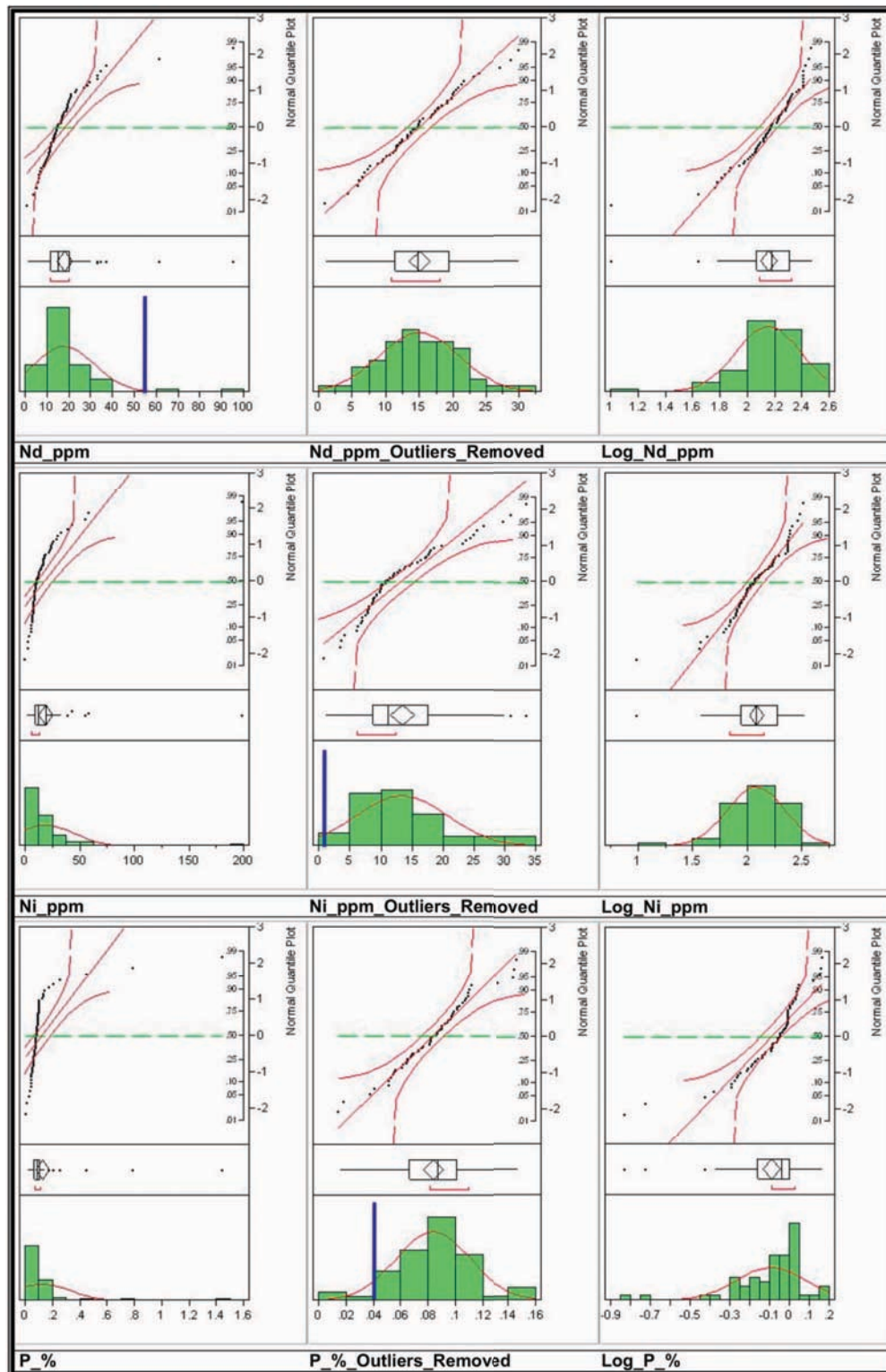


**Figure 2.10.** Surface data univariate analysis histograms, outlier-box plots, and normal quantile plots for elements Nd, Ni, and P.

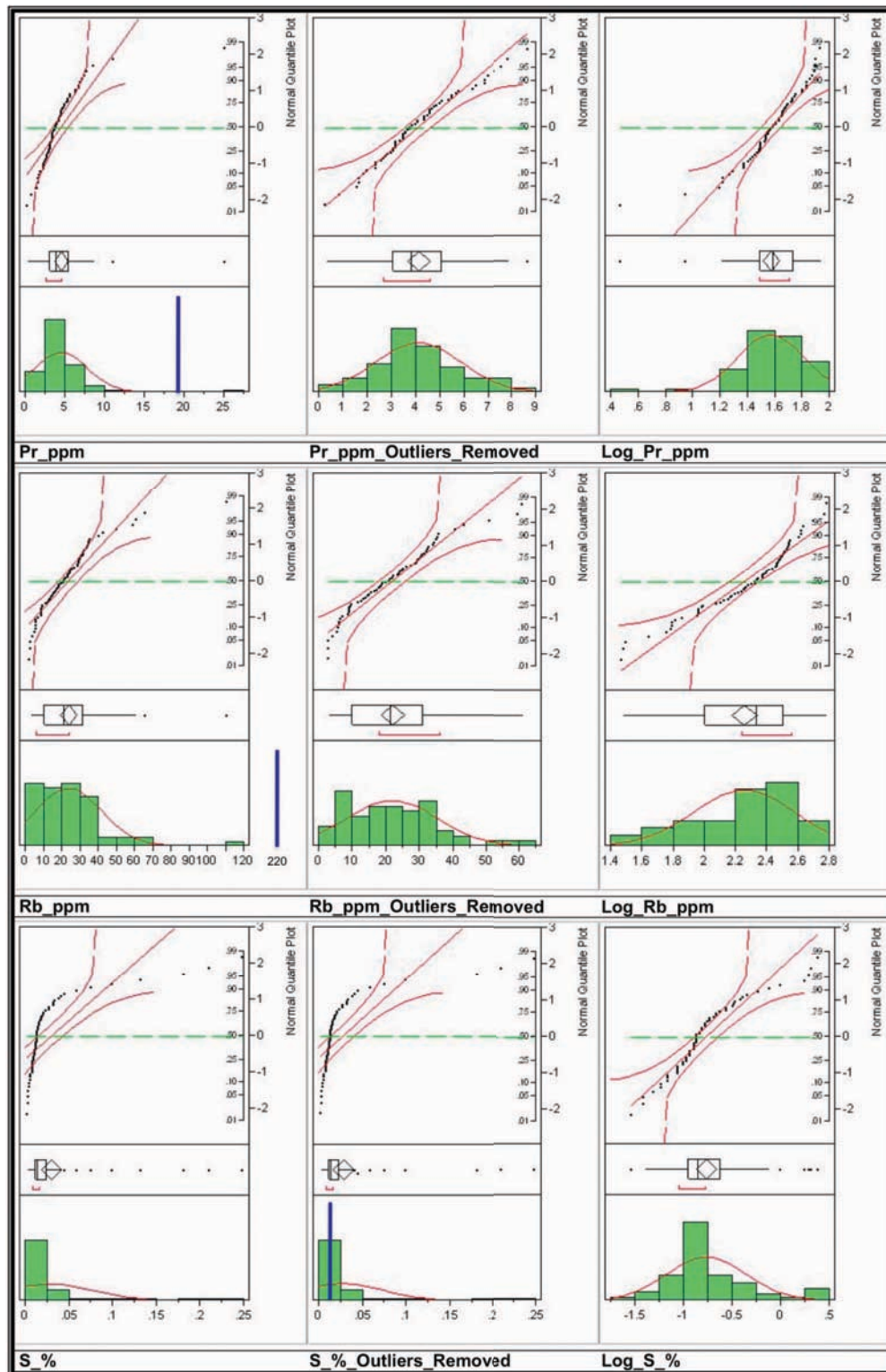


**Figure 2.11.** Surface data univariate analysis histograms, outlier-box plots, and normal quantile plots for elements Pr, Rb, and S.

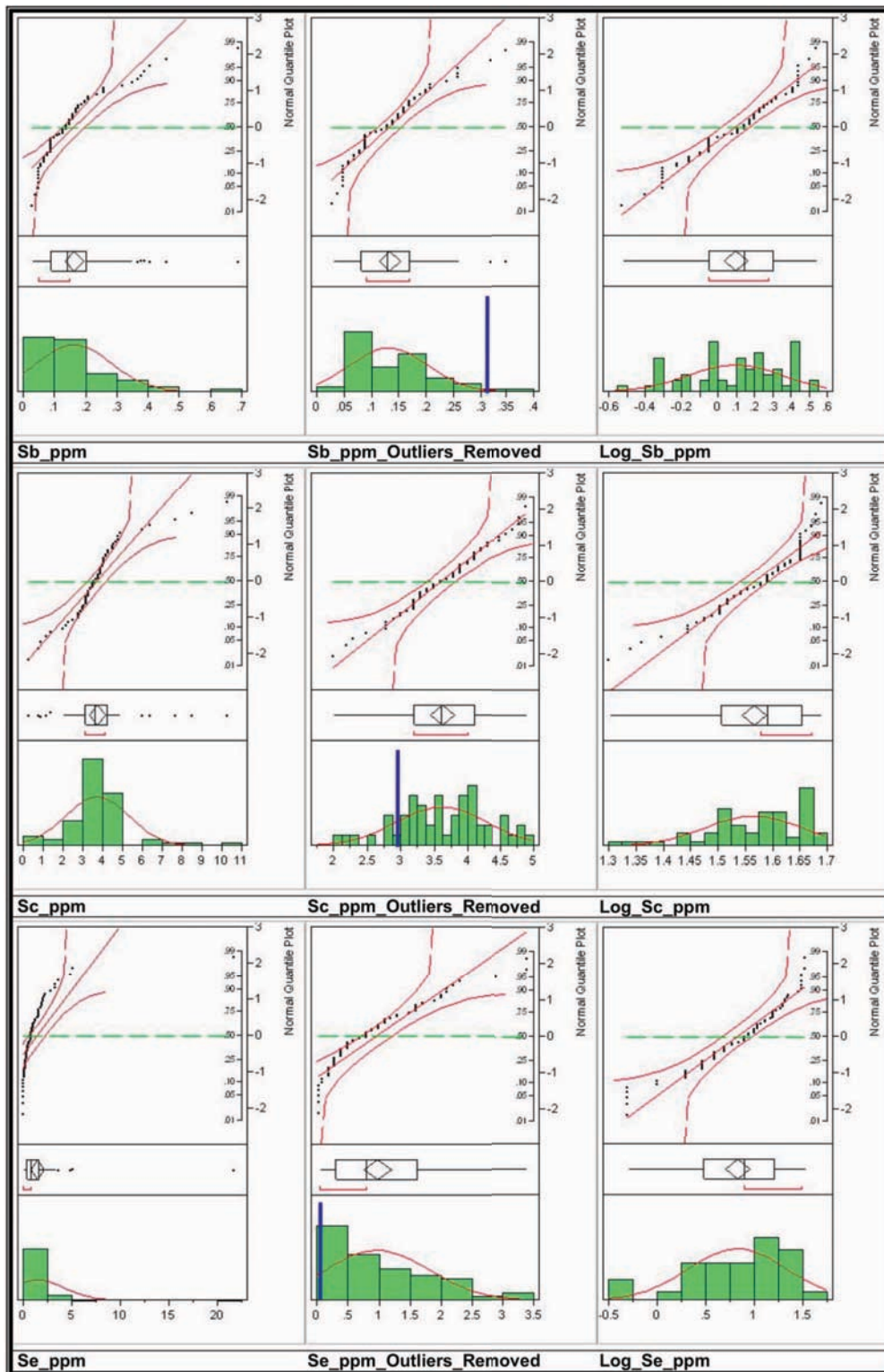


**Figure 2.12.** Surface data univariate analysis histograms, outlier-box plots, and normal quantile plots for elements Sb, Sc, and Se.

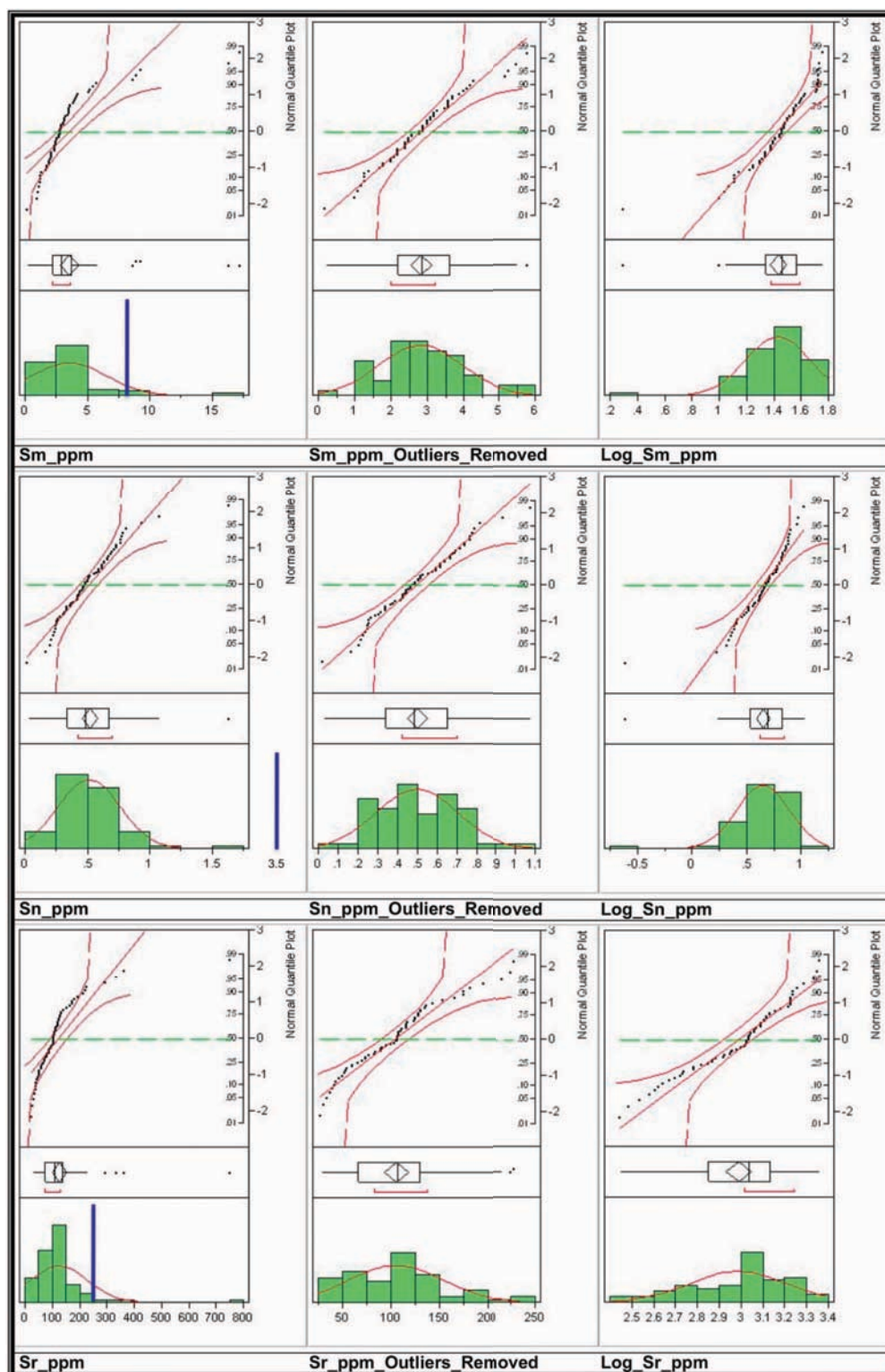


**Figure 2.13.** Surface data univariate analysis histograms, outlier-box plots, and normal quantile plots for elements Sm, Sn, and Sr.

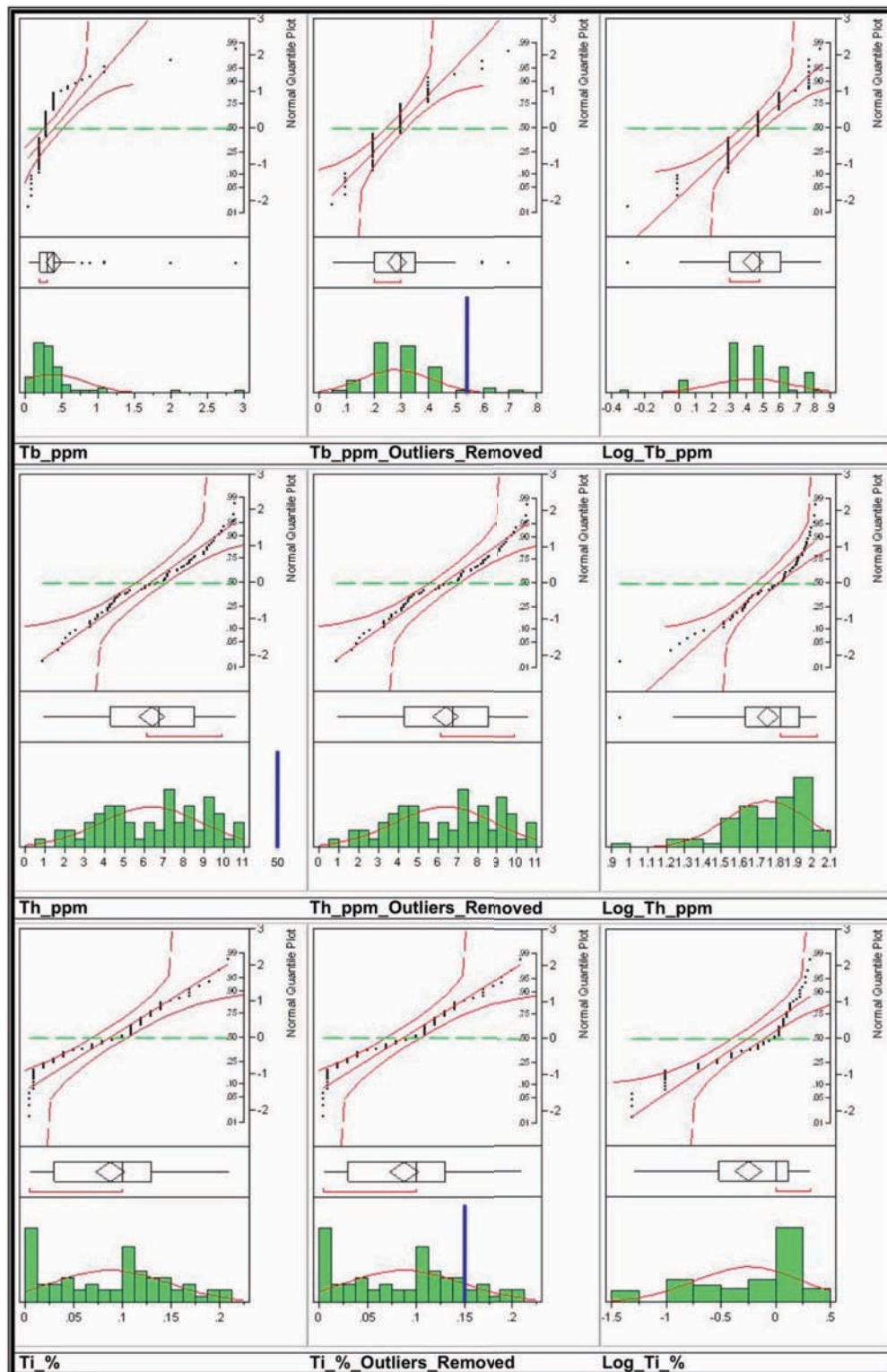


**Figure 2.14.** Surface data univariate analysis histograms, outlier-box plots, and normal quantile plots for elements Tb, Th, and Ti.

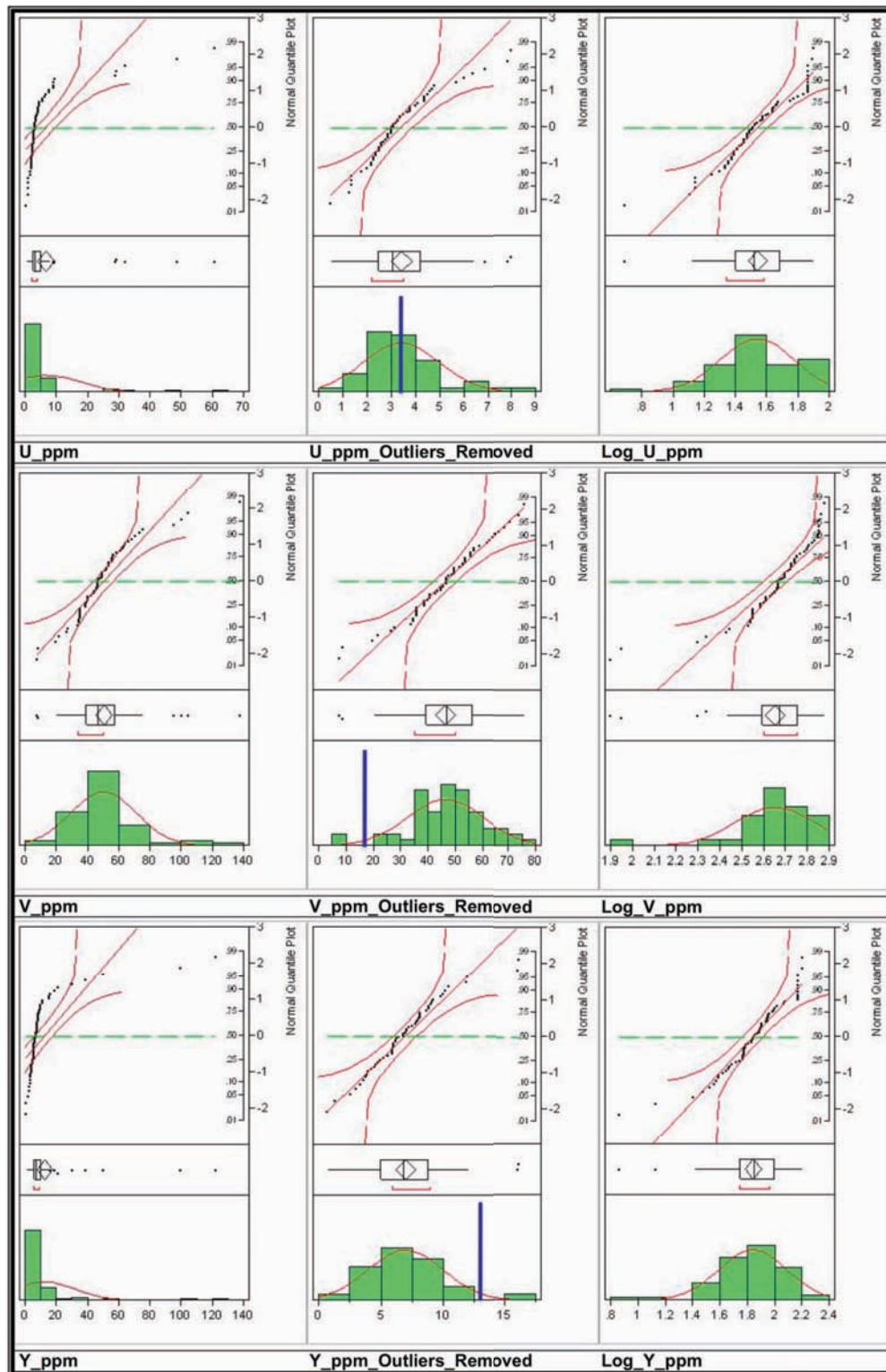


**Figure 2.15.** Surface data univariate analysis histograms, outlier-box plots, and normal quantile plots for elements U, V, and Y.

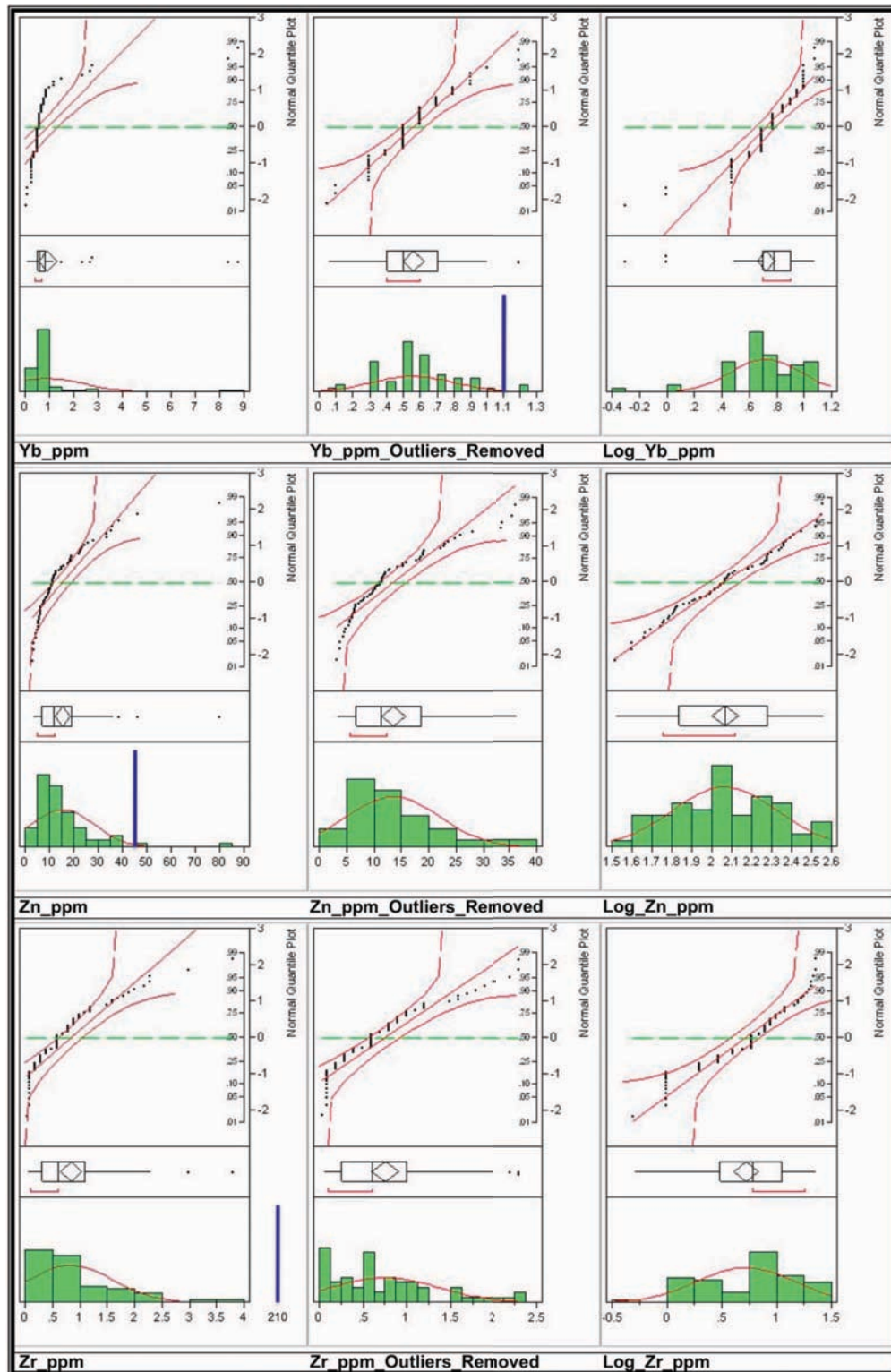


**Figure 2.16.** Surface data univariate analysis histograms, outlier-box plots, and normal quantile plots for elements Yb, Zn, and Zr.

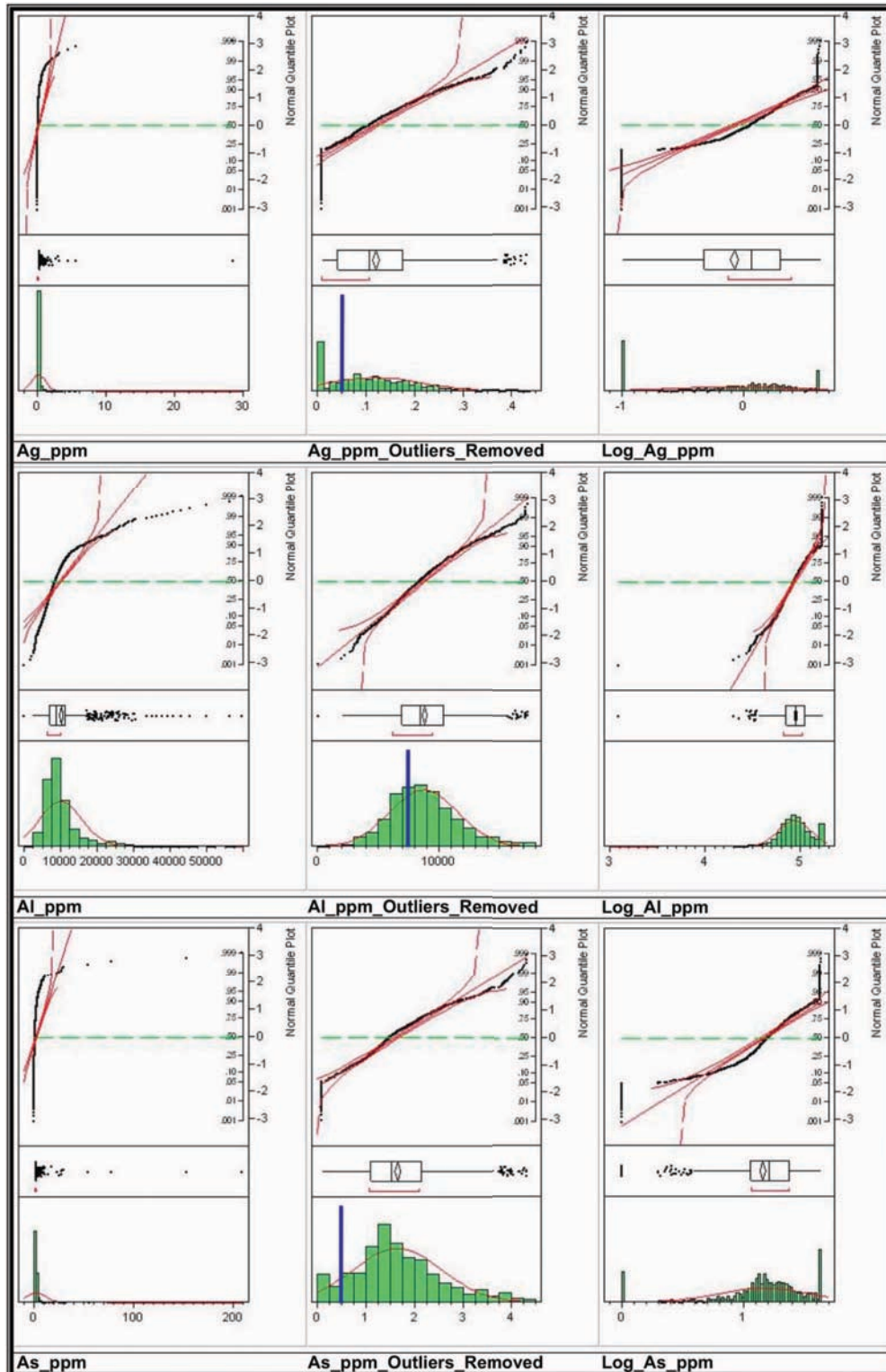


**Figure 2.17.** Subsurface data univariate analysis histograms, outlier-box plots, and normal quantile plots for elements Ag, Al, and As.

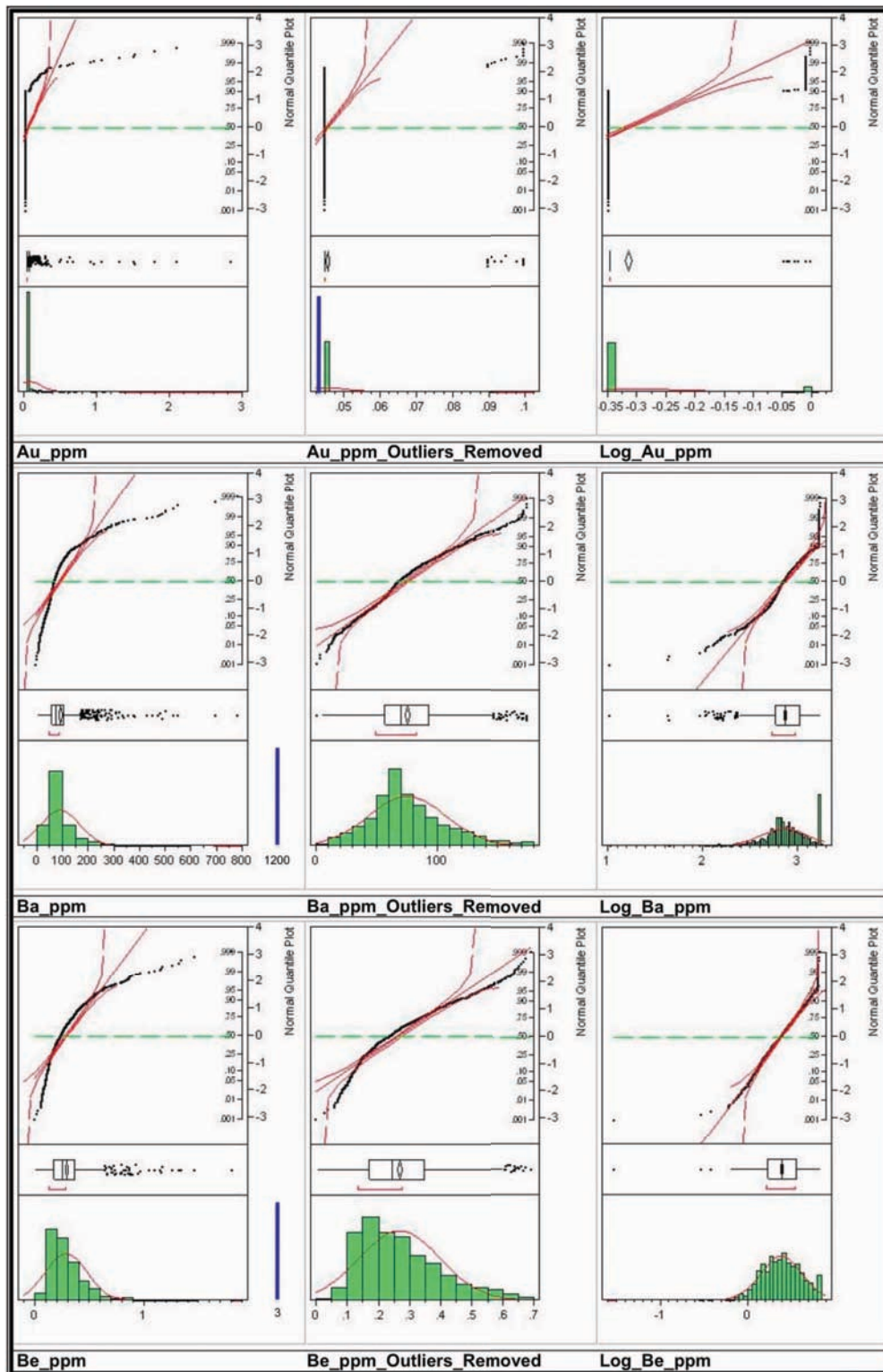


**Figure 2.18.** Subsurface data univariate analysis histograms, outlier-box plots, and normal quantile plots for elements Au, Ba, and Be.

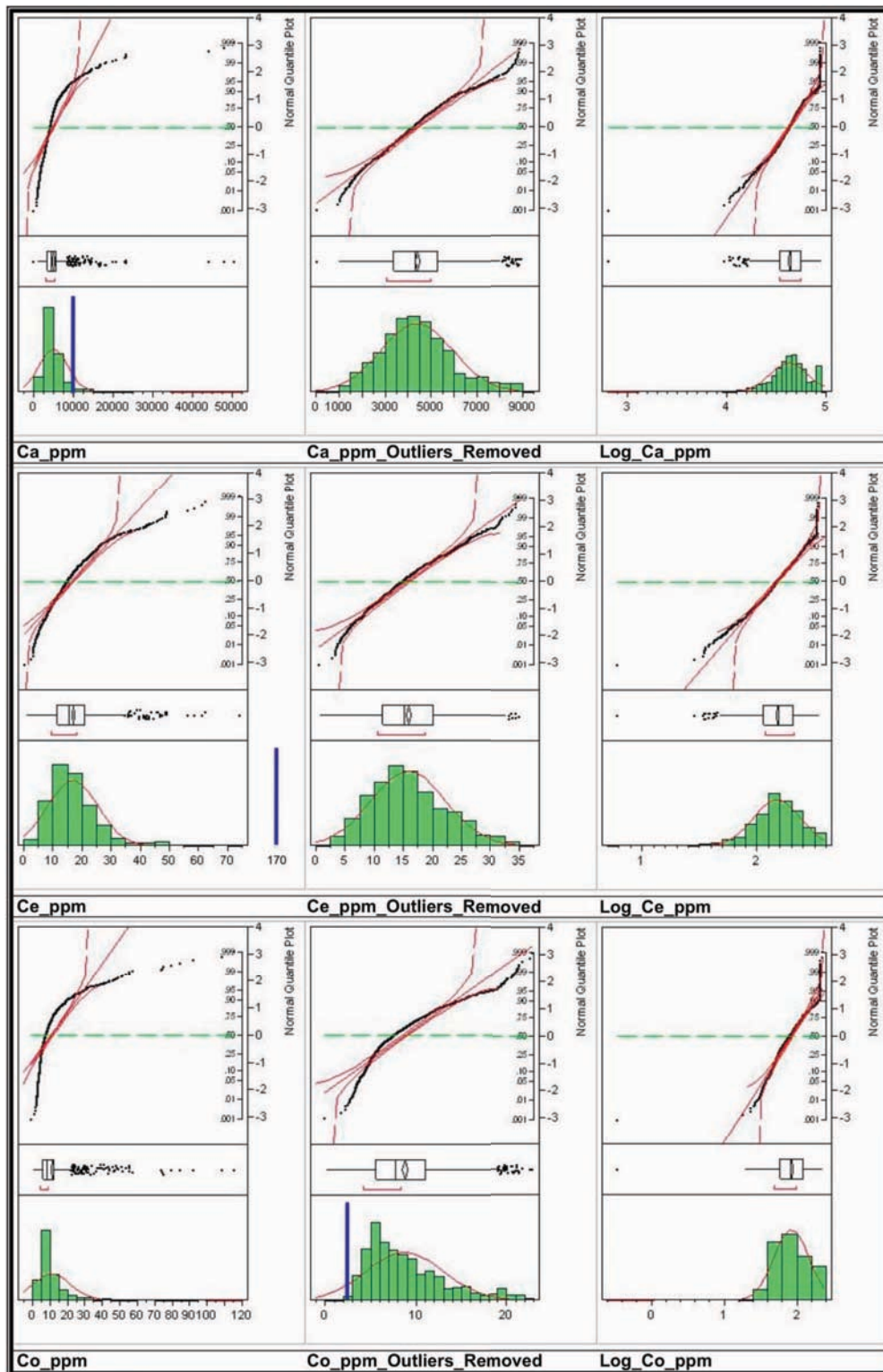


**Figure 2.19.** Subsurface data univariate analysis histograms, outlier-box plots, and normal quantile plots for elements Ca, Ce, and Co.

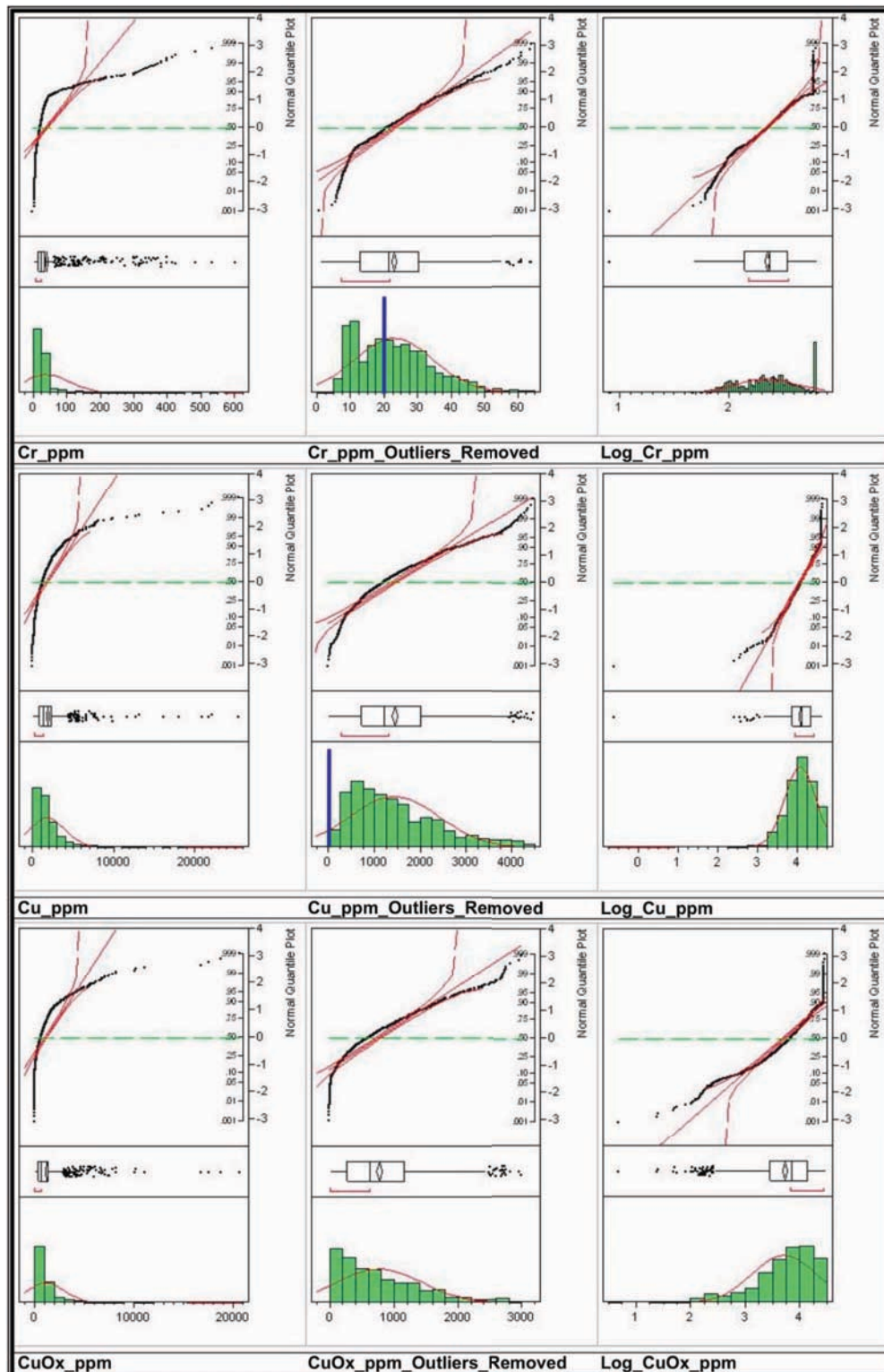


**Figure 2.20.** Subsurface data univariate analysis histograms, outlier-box plots, and normal quantile plots for elements Cr, Cu, and CuOx.

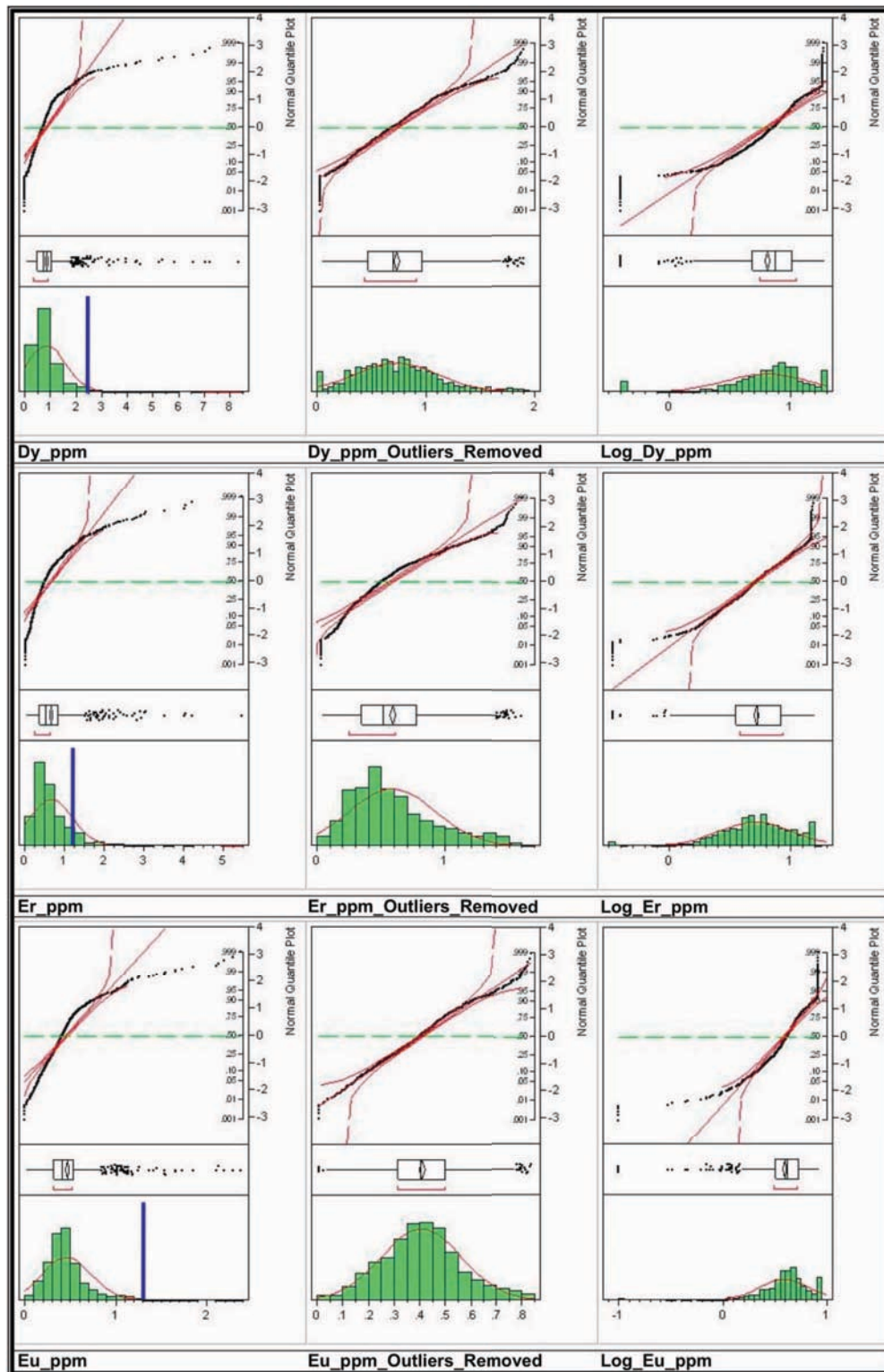


**Figure 2.21.** Subsurface data univariate analysis histograms, outlier-box plots, and normal quantile plots for elements Dy, Er, and Eu.

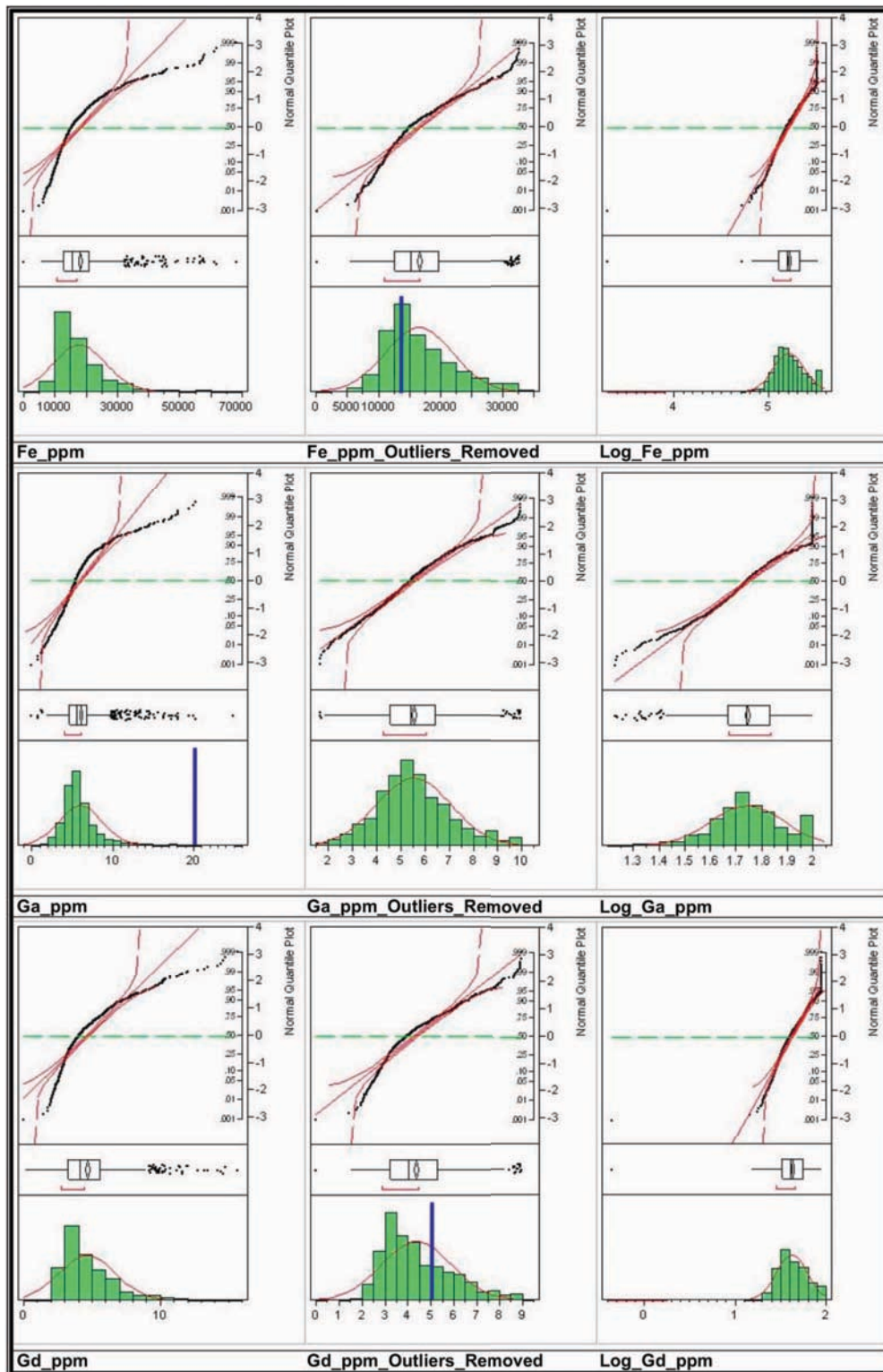


**Figure 2.22.** Subsurface data univariate analysis histograms, outlier-box plots, and normal quantile plots for elements Fe, Ga, and Gd.

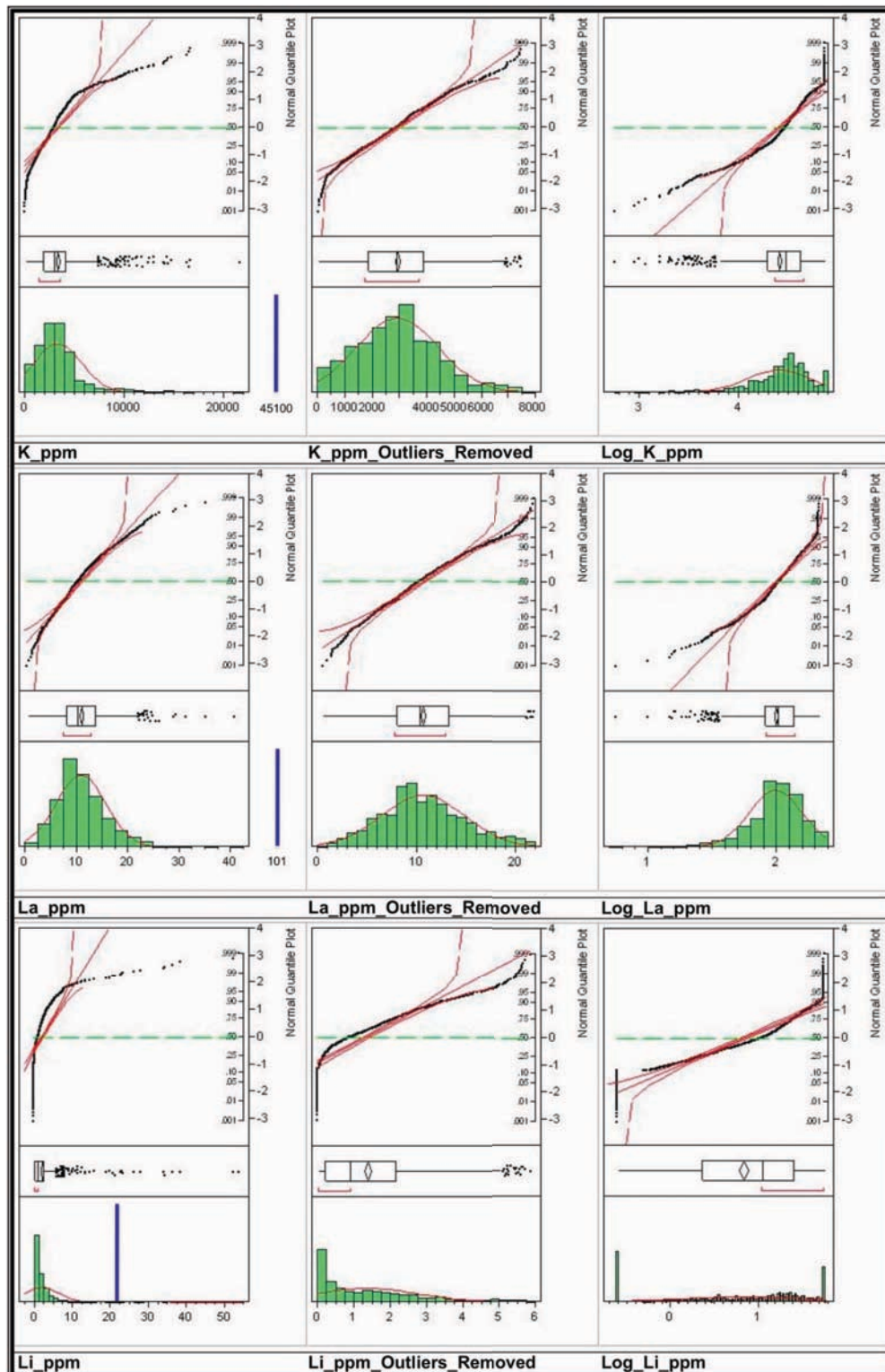


**Figure 2.23.** Subsurface data univariate analysis histograms, outlier-box plots, and normal quantile plots for elements K, La, and Li.

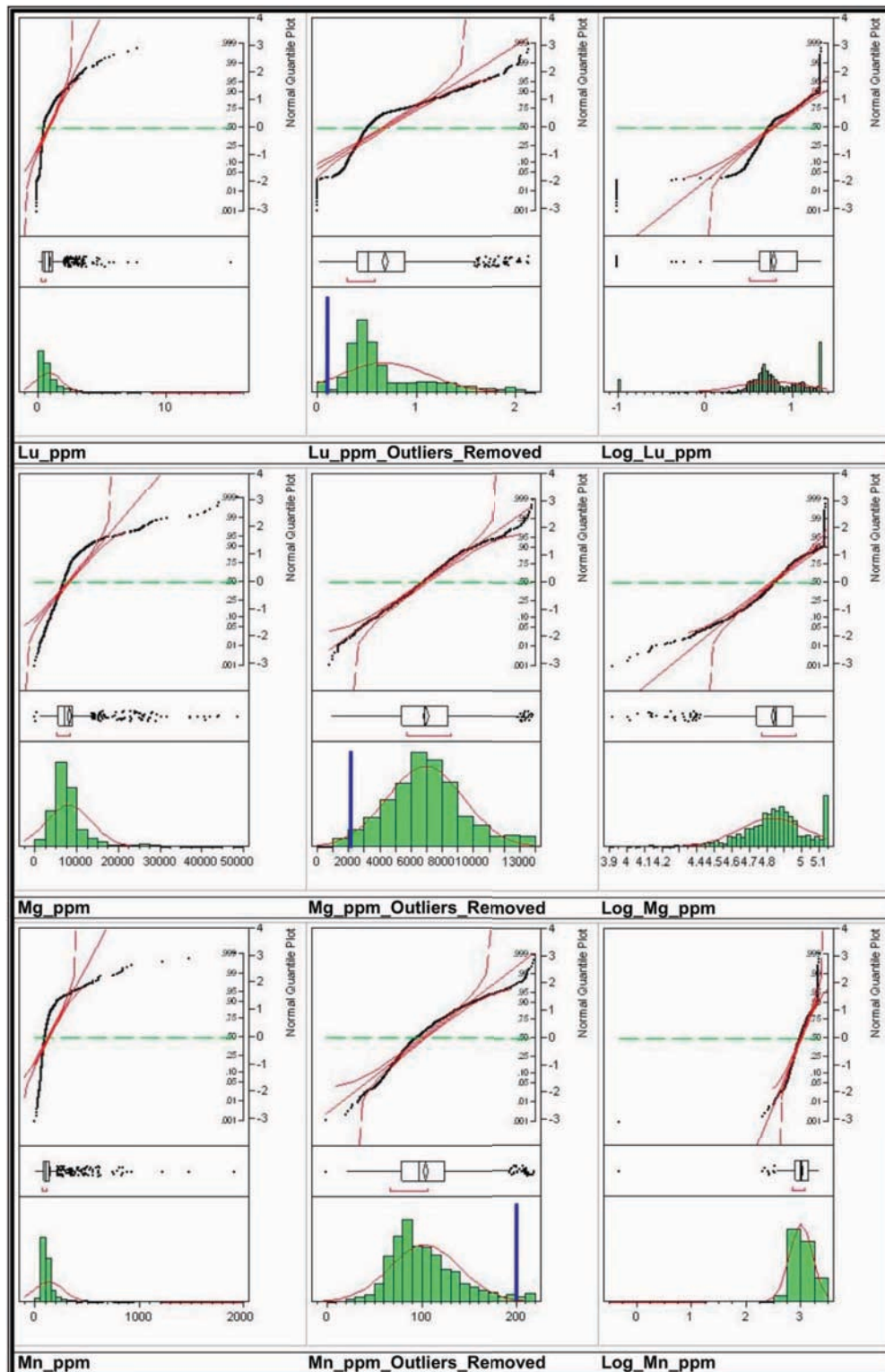


**Figure 2.24.** Subsurface data univariate analysis histograms, outlier-box plots, and normal quantile plots for elements Lu, Mg, and Mn.

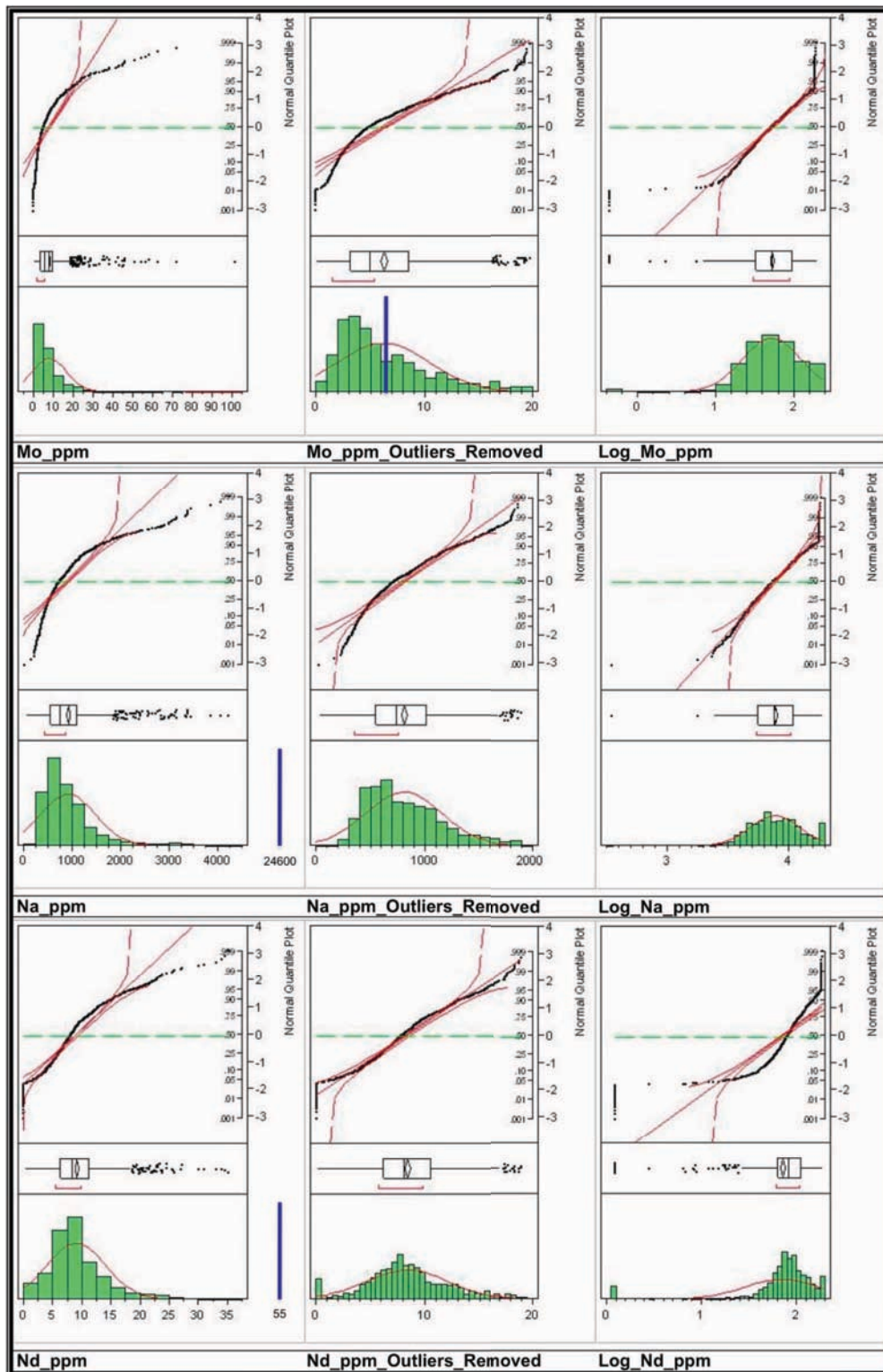


**Figure 2.25.** Subsurface data univariate analysis histograms, outlier-box plots, and normal quantile plots for elements Mo, Na, and Nd.

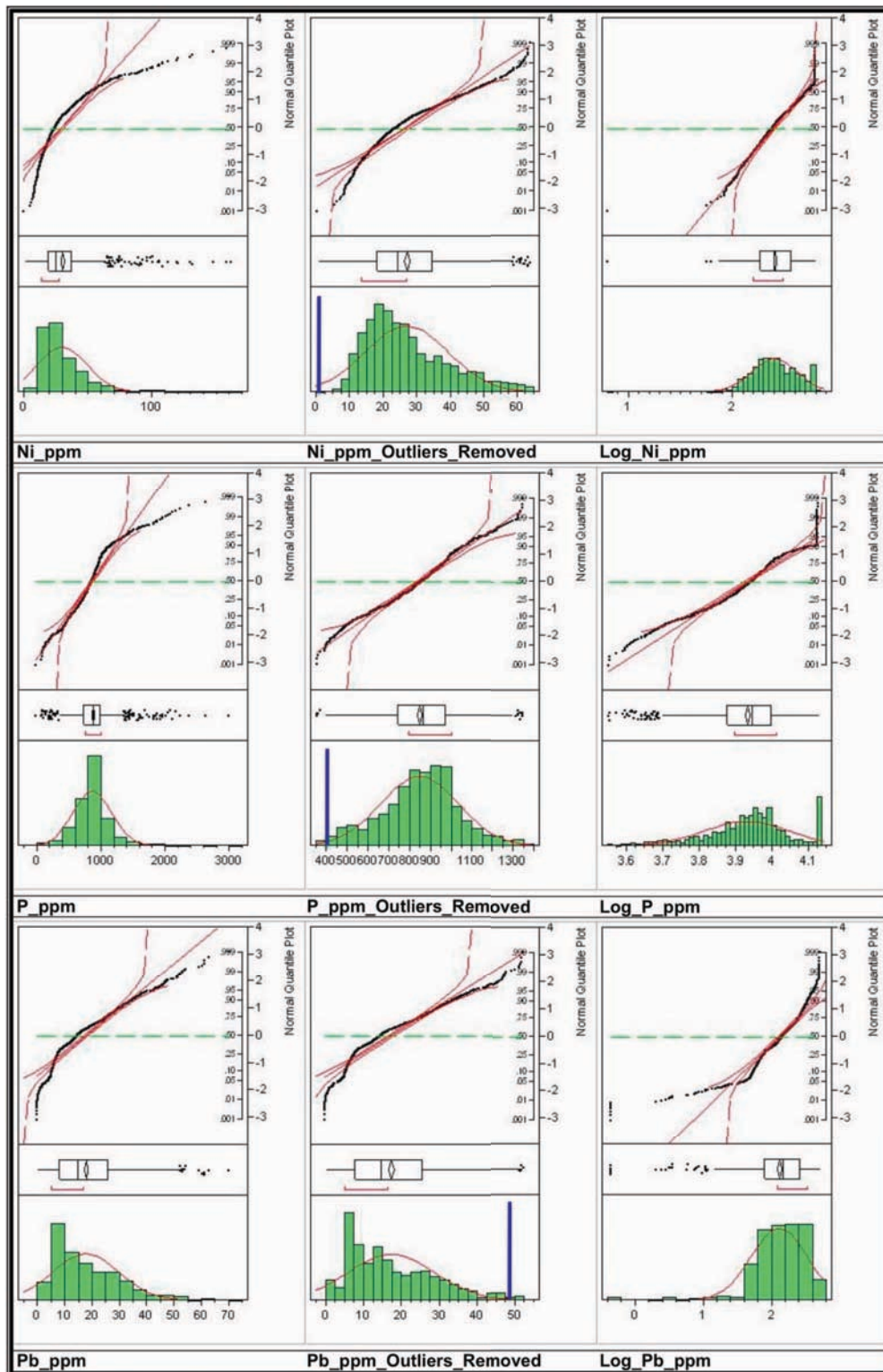


**Figure 2.26.** Subsurface data univariate analysis histograms, outlier-box plots, and normal quantile plots for elements N, P, and Pb.

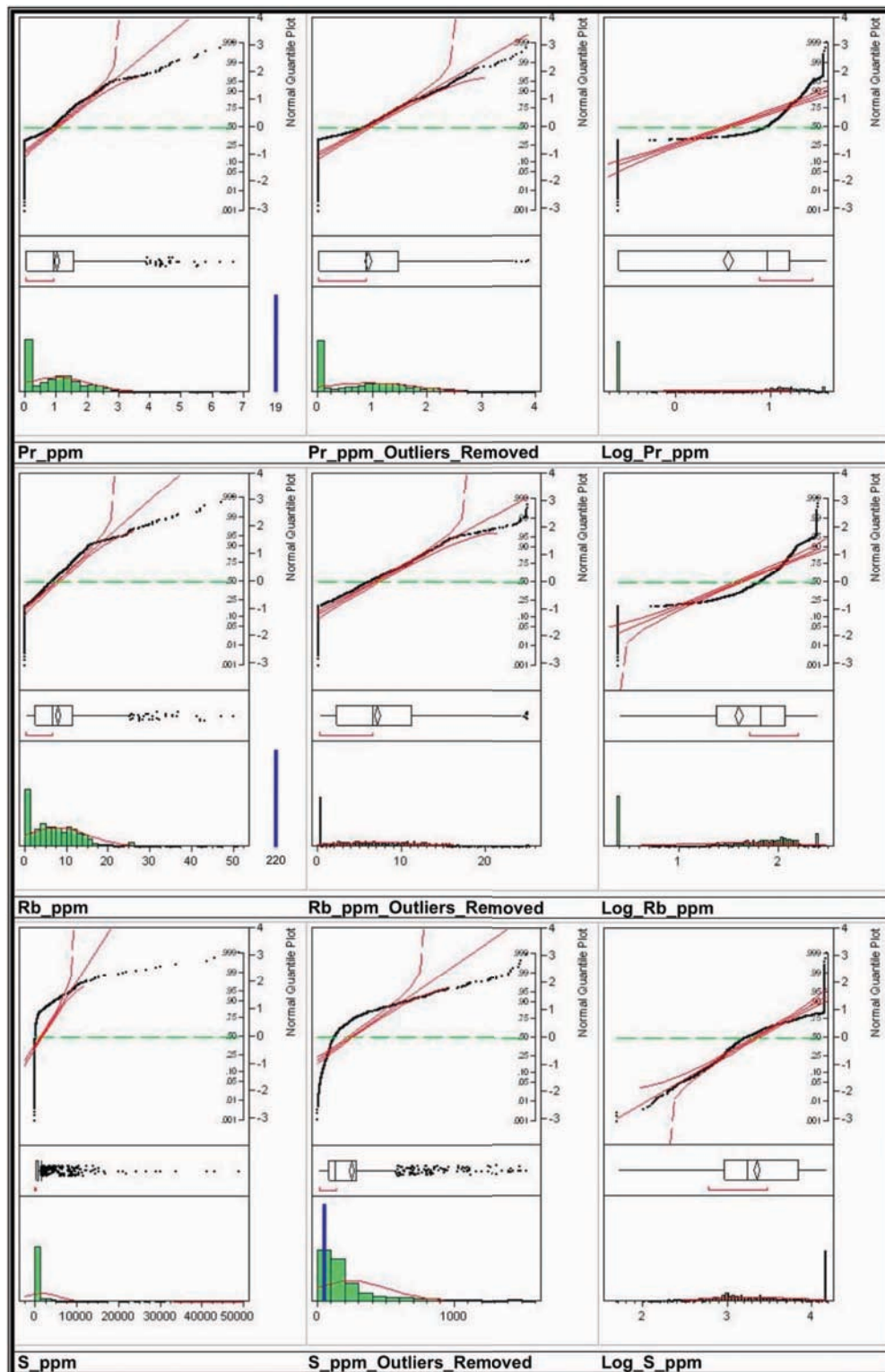


**Figure 2.27.** Subsurface data univariate analysis histograms, outlier-box plots, and normal quantile plots for elements Pr, Rb, and S.

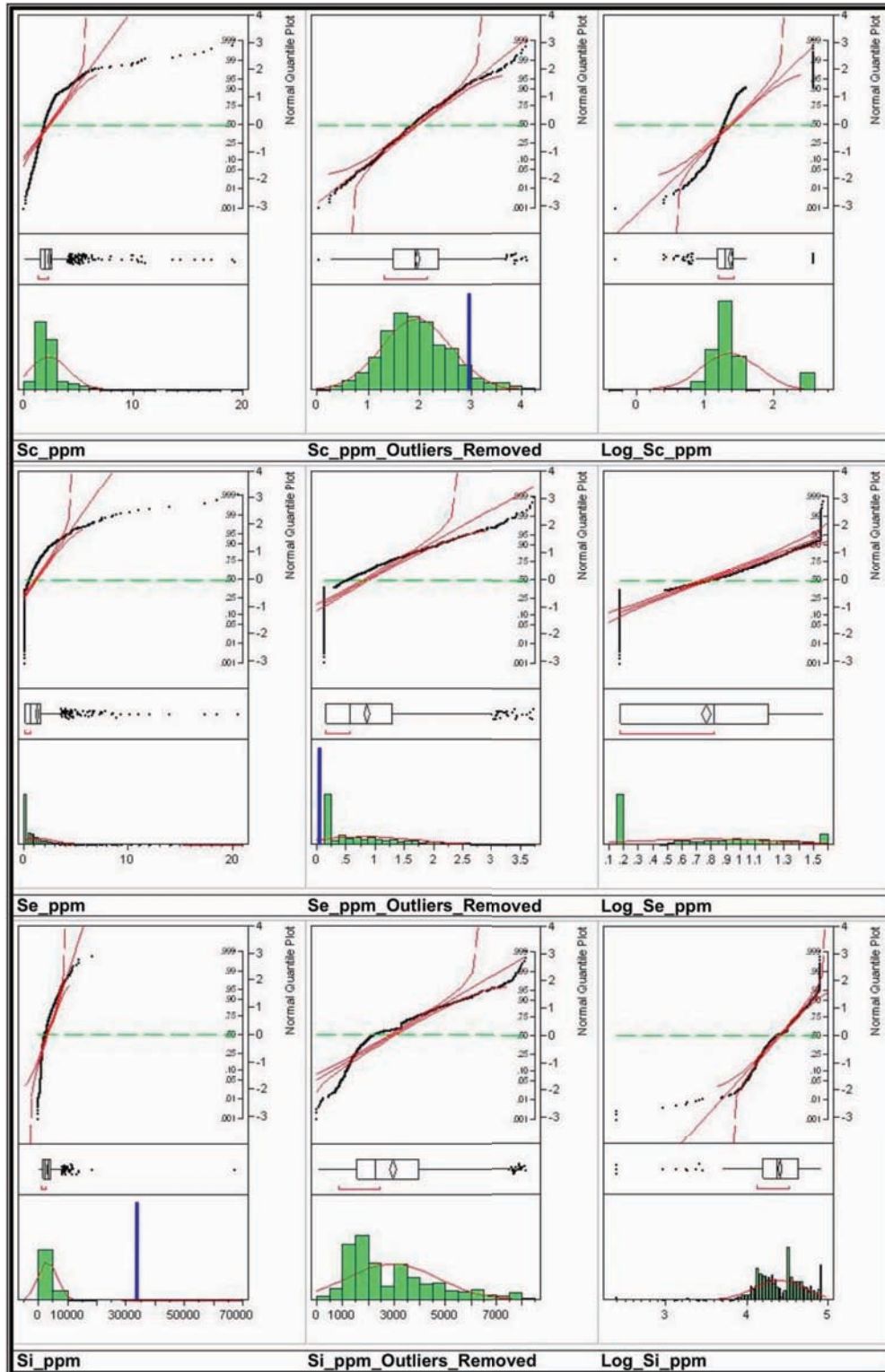


**Figure 2.28.** Subsurface data univariate analysis histograms, outlier-box plots, and normal quantile plots for elements Sc, Se, and Si.

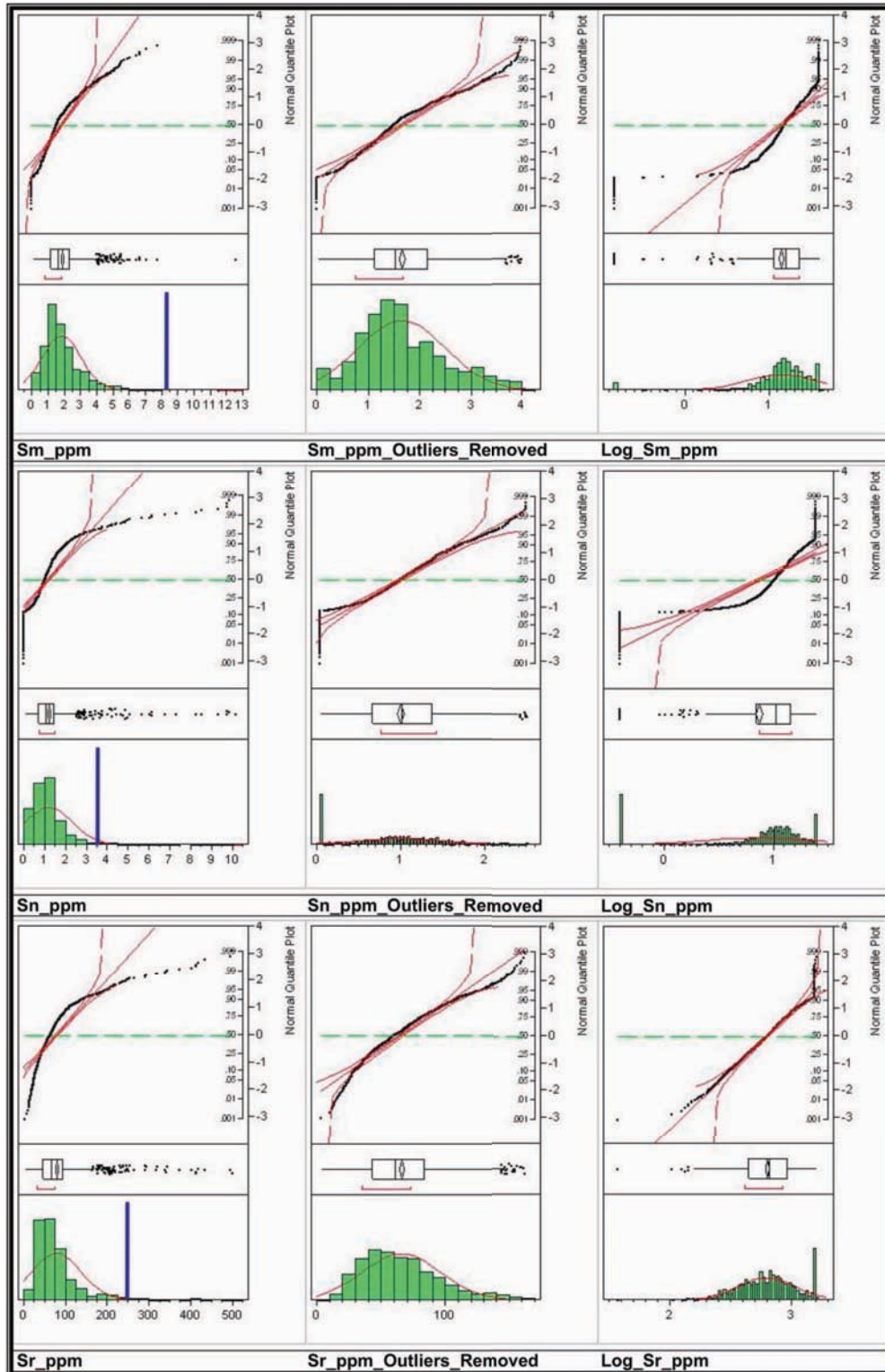


**Figure 2.29.** Subsurface data univariate analysis histograms, outlier-box plots, and normal quantile plots for elements Sm, Sn, and Sr.

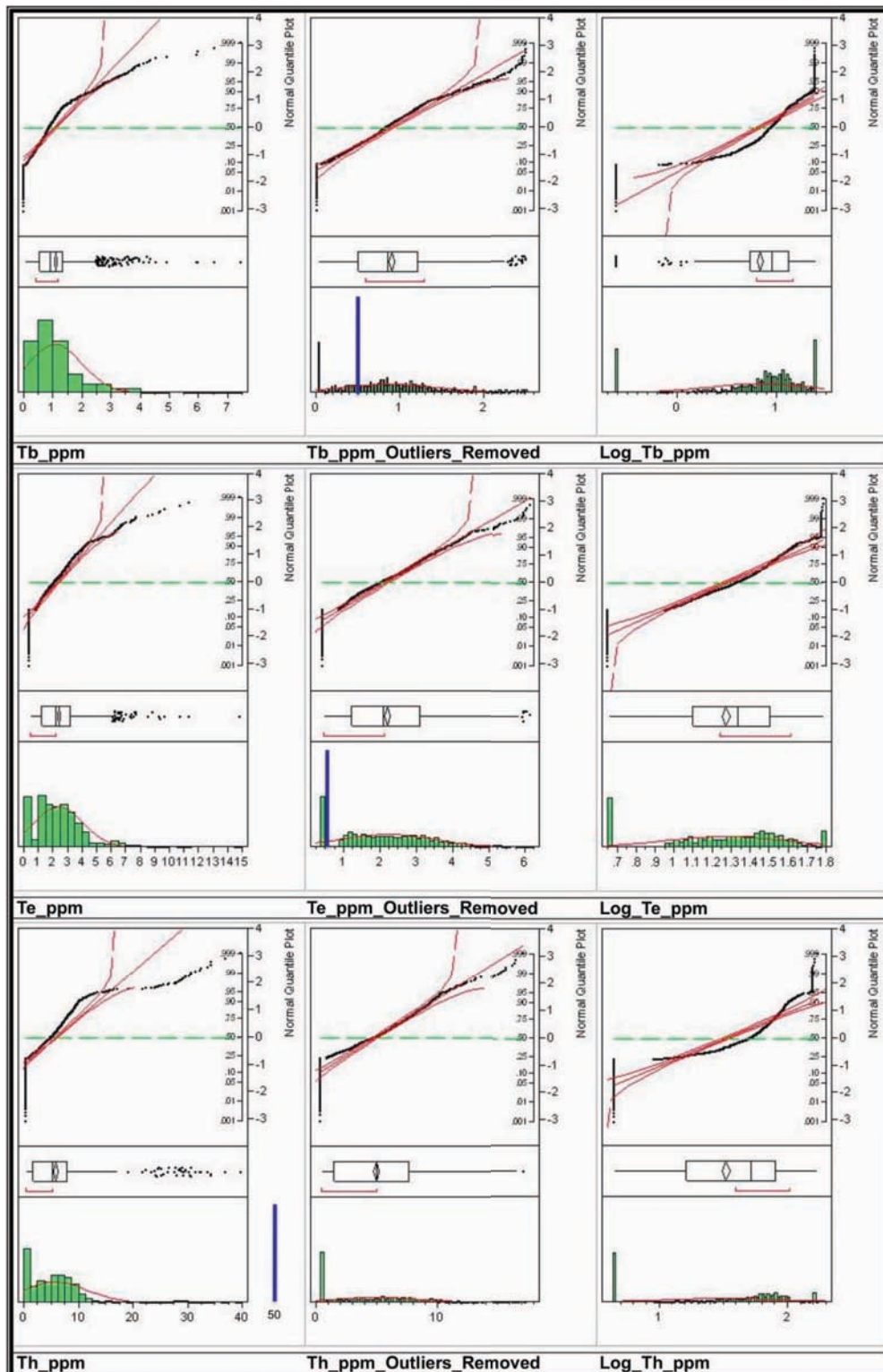


**Figure 2.30.** Subsurface data univariate analysis histograms, outlier-box plots, and normal quantile plots for elements Tb, Te, and Th.

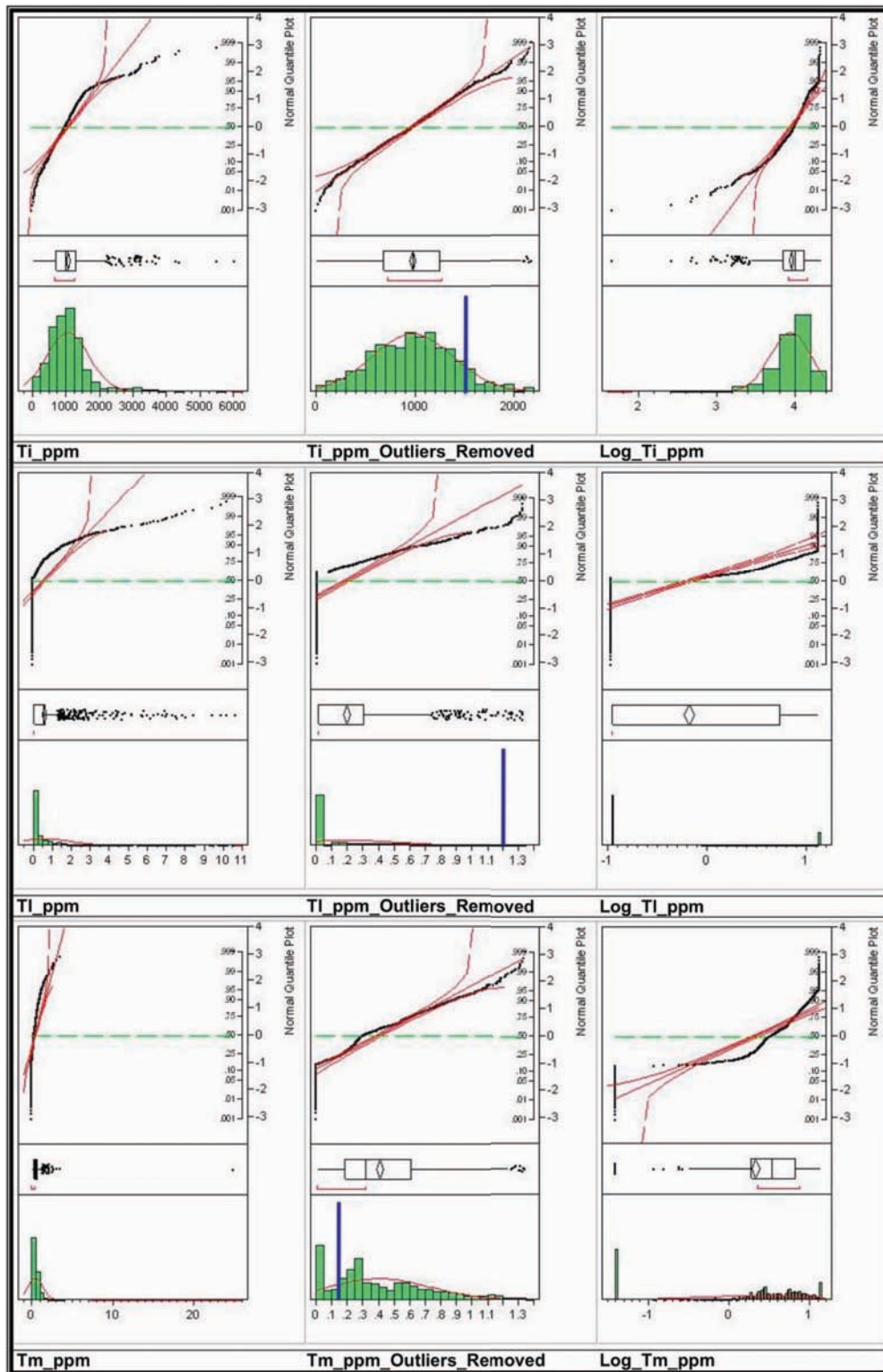


**Figure 2.31.** Subsurface data univariate analysis histograms, outlier-box plots, and normal quantile plots for elements Ti, Tl, and Tm.

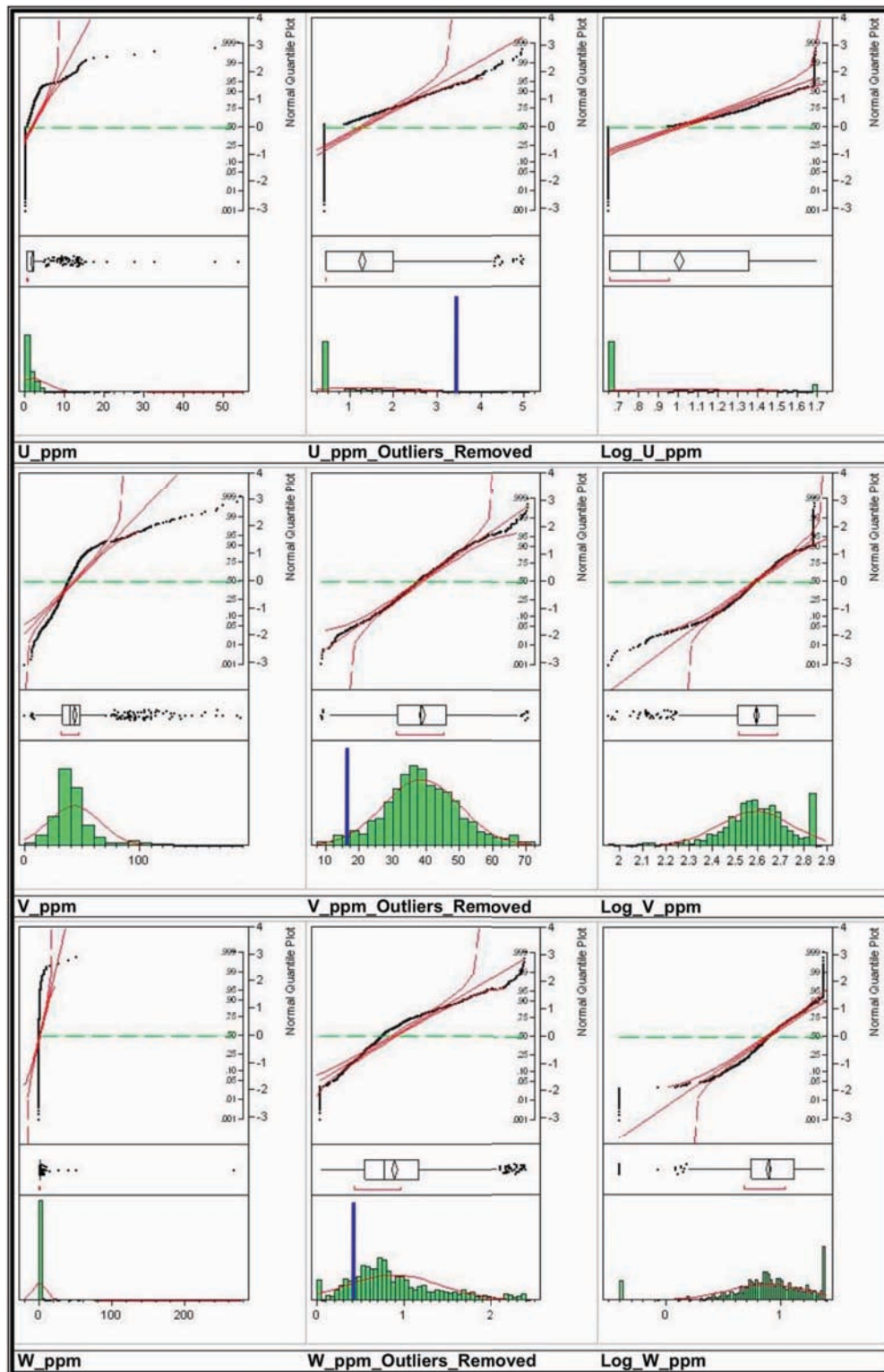


**Figure 2.32.** Subsurface data univariate analysis histograms, outlier-box plots, and normal quantile plots for elements U, V, and W.

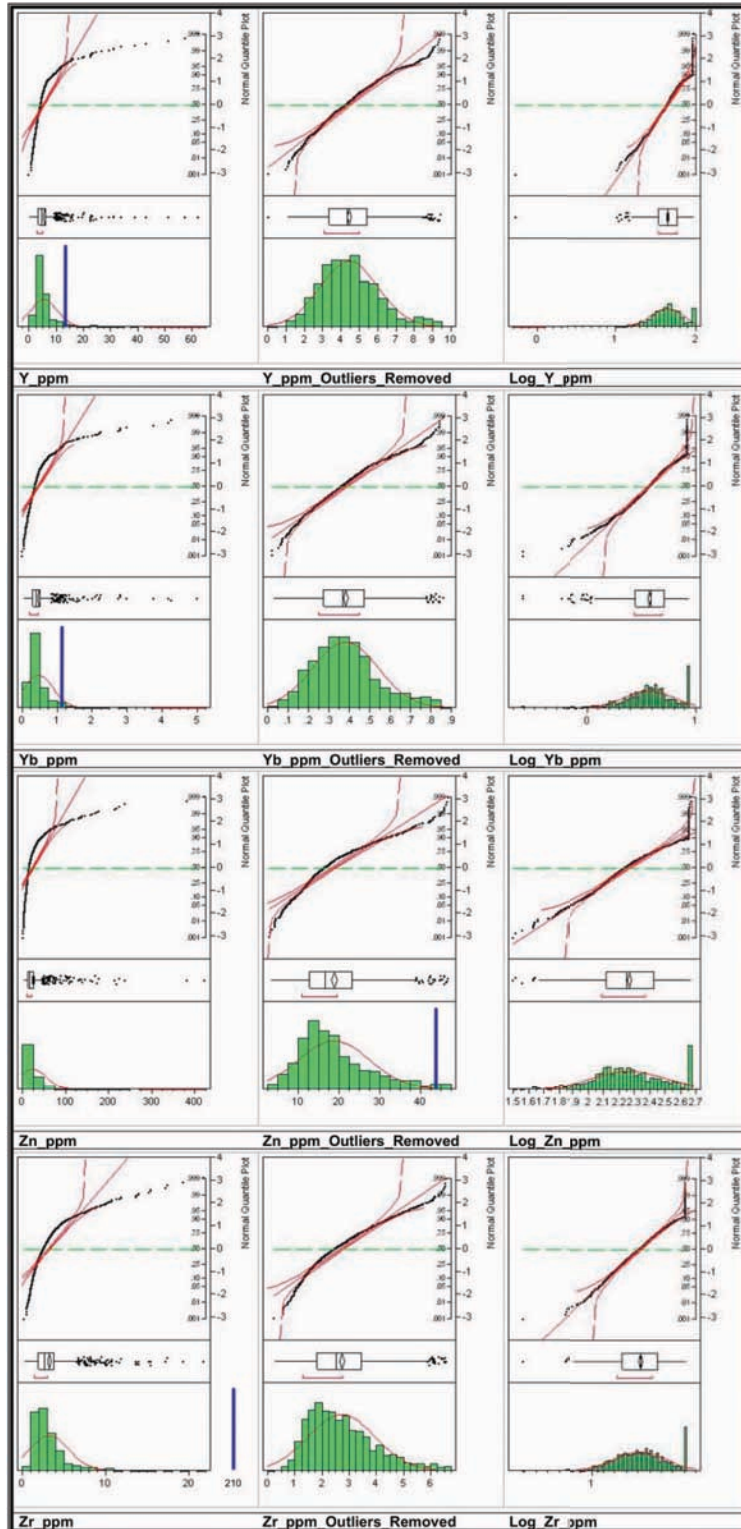


**Figure 2.33.** Subsurface data univariate analysis histograms, outlier-box plots, and normal quantile plots for elements Y, Yb, Zn, and Zr.

## 16.3. Appendix 2.3 – Bivariate Analysis

**Table 2.7.** Surface data correlation coefficient matrix for bivariate analysis.

Row	Ag	Al	As	B	Ba	Be	Ca	Cd	Ce	Co	Cr	Cs	Cu	Dy	Er	Eu
Ag	1															
Al	-0.1009749	1														
As	0.1219615	-0.2820304	1													
B	-0.0811405	0.4319069	-0.0903131	1												
Ba	0.25822466	-0.0293465	0.27041809	-0.1396734	1											
Be	-0.1734176	0.61860755	-0.1816301	0.25365762	0.11327751	1										
Ca	-0.1469752	0.27572549	-0.1402367	0.3734684	-0.0251563	0.39608585	1									
Cd	-0.1306478	-0.0362958	-0.0220259	0.36004806	0.11265186	0.34962532	0.41556621	1								
Ce	-0.1459496	0.50352588	-0.1661382	0.03284642	-0.2215775	0.29282274	0.18568737	-0.1938077	1							
Co	-0.2447072	0.47165256	-0.5515002	0.36675127	-0.2682394	0.44838595	0.23460159	0.28393876	0.25385477	1						
Cr	0.40220182	0.27802127	-0.0092492	-0.1111618	0.02188925	0.2404661	-0.0783508	-0.1315388	0.18859704	-0.0040595	1					
Cs	-0.0210127	0.68713762	-0.1304076	0.50525965	0.37559352	0.31009727	-0.0159846	0.32161588	0.44245809	0.37742467	0.4610753	1				
Cu	0.21053201	0.38980483	-0.4909661	0.28776285	-0.1758278	0.20491452	0.11966813	0.19246346	0.22472542	0.62193086	0.35039508	0.22811554	1			
Dy	-0.0335499	0.70733806	-0.3007517	0.2157997	-0.2516884	0.30964257	-0.0544258	0.77975718	0.44245809	0.37742467	0.4610753	0.59228292	0.94204639	1		
Er	0.03728182	0.63371351	-0.31573	0.29017565	-0.2249648	0.41781937	0.36380527	0.05345559	0.66206236	0.51224077	0.39481243	0.41550538	0.59228292	0.94204639	1	
Eu	-0.0670087	0.70170067	-0.2595244	0.25240848	-0.2572523	0.36317922	0.3192921	-0.1483462	0.6524072	0.35637833	0.26465319	0.51129963	0.3383613	0.92733846	0.82455479	1
Fe	0.09449659	0.67646717	-0.0062749	0.11363713	0.28250185	0.5282801	0.05305373	-0.1439741	0.39777416	0.21527351	0.28426803	0.56880143	0.13631442	0.13631442	0.26822913	0.43666389
Ga	-0.1265519	0.88808825	-0.1781264	0.22423624	-0.028589	0.4471258	0.19246859	-0.1927254	0.58304703	0.29325771	0.26786077	0.66952966	0.27424107	0.69534156	0.56744837	0.69321913
Gd	-0.0541371	0.67280383	-0.2907343	0.23842596	-0.284759	0.40258444	0.32084554	-0.1026704	0.84442148	0.42057381	0.26683212	0.46484204	0.41873028	0.96566983	0.89714595	0.97381277
Ho	-0.0205622	0.50631092	-0.2470031	0.3452995	-0.2847933	0.29771568	0.47557323	0.15823821	0.52109357	0.40386001	0.19483264	0.35485263	0.44634672	0.78737498	0.87346003	0.69325919
K	0.13795475	0.36357524	0.26128466	-0.0733847	0.56238629	0.35222378	0.00625048	-0.2080669	0.17792862	-0.2955046	0.28907866	0.56350516	-0.1572748	0.14631559	0.05202058	0.17762274
La	-0.1859884	0.49866079	-0.1994467	0.00820699	-0.230201	0.32318322	0.18539287	-0.1715098	0.98810487	0.26095722	0.1758594	0.32817981	0.22269708	0.7729402	0.64367891	0.83375241
Li	-0.1639384	0.75108903	-0.1062664	0.47163198	-0.1470868	0.3521991	0.21471216	-0.0187023	0.29471392	0.34695966	0.05826787	0.72314152	0.27298631	0.46020642	0.40340032	0.46506034
Mg	0.08327628	0.7824437	-0.0723898	0.34911101	-0.0064061	0.35183837	0.15852853	-0.0866826	0.31381321	0.34839397	0.34651409	0.68815935	0.42650328	0.58971367	0.56197043	0.53330674
Mn	-0.282157	0.50600282	-0.4600836	0.26422453	0.04305843	0.49028692	0.2666932	0.24920506	0.27917239	0.70859704	-0.0696787	0.34345355	0.3601373	0.36219914	0.34838696	0.29634524
Mo	0.2048106	0.29684856	0.07876743	0.25055126	0.17680008	0.28115908	-0.1158951	-0.0125957	0.00512954	0.12470666	0.18488793	0.36188889	0.23156212	0.13567974	0.13115142	0.12751665
Na	-0.0305684	0.39213564	-0.1726707	0.36464003	0.10389353	0.14928394	-0.0427438	-0.1170034	0.12425102	0.27010031	0.16214456	0.25018746	0.18733608	0.27010593	0.247902	0.25756372
Nd	-0.1305691	0.58025528	-0.2061566	0.07521431	-0.2325814	0.34057752	0.25016323	0.22805067	0.97186256	0.28644396	0.22044514	0.41179852	0.25415131	0.85780014	0.73765288	0.92808743
NI	0.06026785	0.51986195	-0.286312	0.21639427	0.38770535	0.2080059	0.11304856	0.23850568	0.58711169	0.08791169	0.50561085	0.3056503	0.73469508	0.56355144	0.65652445	0.41101666
P	-0.012128	0.38028799	-0.1597268	0.45225391	-0.1155651	0.28606828	0.49853598	0.14920469	0.36149746	0.37217879	0.18654327	0.44125846	0.2969208	0.50870384	0.5438035	0.56631156
Pr	-0.1217452	0.53260218	-0.1568536	0.06189474	-0.2125933	0.32238819	0.22805067	-0.1672814	0.98854821	0.25223837	0.20190313	0.35934387	0.23827034	0.80639591	0.69321261	0.88636943
Rb	0.15974364	0.41193891	0.20478019	0.032894	0.35630454	0.33305571	0.06304346	-0.1555511	0.19155515	0.13791411	0.08791169	0.50561085	0.26519797	0.70181556	-0.0693407	0.23866009
S	0.08095921	-0.0325151	0.18579468	0.44122721	0.39940088	0.03146776	0.01289484	0.06037607	-0.1801922	0.02098182	-0.0849454	0.31808159	-0.0875377	-0.2313367	-0.1770488	-0.0994421
Sb	0.16097317	0.28477	-0.0182448	0.41371207	0.19646041	0.0095193	0.19762768	-0.0032493	0.1414041	0.3126448	0.08330254	0.31860802	0.33289973	0.33560908	0.4414781	0.2732489
Sc	0.00237658	0.20345025	0.05072678	0.13594547	0.14440043	-0.050355	0.03711484	-0.0482158	0.13791411	-0.1018317	0.08791169	0.50561085	0.26519797	0.70181556	-0.0693407	0.23866009
Se	0.21667215	0.01448516	0.38655249	0.09720396	0.27046062	0.18492469	-0.0546489	0.14953121	0.03965204	-0.1104659	0.21976121	0.41573574	0.01613955	-0.0045714	0.06781461	0.01707674
Sm	-0.0801423	0.63325474	-0.2135647	0.13825967	0.35050171	0.25684922	-0.1938661	0.92669846	0.30234189	0.26474948	0.44534678	0.29934467	0.91100831	0.80501588	0.9709904	0.84831956
Sn	0.09880174	0.23352278	0.04753567	0.2282548	0.00796165	0.35130713	-0.0198567	-0.1204482	0.41905771	0.0072376	0.55288566	0.02935091	-0.0216408	0.35623913	0.24728368	0.3715183
Sr	0.26888285	0.0032475	0.225729	0.2570054	0.56842792	0.16850442	0.25521963	0.3034953	0.03515655	-0.1165196	0.24332886	0.17450058	-0.0974728	-0.0330732	0.02120932	0.02298269
Tb	-0.0143133	0.6177152	-0.3022897	0.31382439	-0.1942702	0.31382439	0.3673628	-0.0578463	0.7627563	0.48238881	0.20022907	0.44252471	0.48881416	0.89245637	0.87774422	0.9057576
Th	0.11895942	0.17230808	-0.0838667	-0.303808	-0.0654994	0.08325665	-0.1361707	-0.1361854	0.48611577	0.05882728	0.26155036	0.14380516	0.28617496	0.47902387	0.47040492	0.35740613
Ti	0.21672345	-0.1442038	0.18131343	-0.3275467	0.23528094	0.08049766	0.1642846	-0.0660439	0.18170048	-0.2935703	0.30780163	-0.1248176	-0.3065477	0.06129939	-0.0251825	0.11045532
U	0.31840129	0.13884916	-0.1590388	0.39904751	0.20260751	0.13053638	0.26162423	0.36831257	0.19351402	0.31018479	0.18873437	0.16805515	0.62800748	0.26613767	0.21826667	0.21826667
V	0.14680674	0.66898346	-0.0174917	0.2324568	0.07674362	0.53552124	0.27487963	-0.0099101	0.43916266	0.27311149	0.55638169	0.53819636	0.34296348	0.6363872	0.5798195	0.6363872
Y	-0.0303474	0.68924824	-0.3721956	0.32808165	-0.241993	0.45124986	0.33051283	0.03376621	0.688610674	0.57959829	0.33511535	0.43422614	0.80383236	0.94847341	0.97802044	0.84831956
Yb	0.07695373	0.62430225	-0.2862527	0.21578191	-0.2332784	0.45060531	0.31417856	0.03093847	0.64846056	0.49589899	0.48081564	0.37319096	0.58024691	0.931444	0.97579873	0.78687998
Zn	-0.224617	0.516876	-0.3573299	0.39921202	-0.123922	0.31080125	0.37179074	0.19656876	0.32510518	0.61635428	-0.1823767	0.3549497	0.40863077	0.42566312	0.47734304	0.38454719
Zr	0.15499263	-0.0680432	0.12449528	0.0155403	0.04883121	0.27924617	0.3082223	0.26904428	-0.0187186	0.04354646	0.09865166	-0.1081711	-0.1841303	-0.0033988	-0.0169735	-0.0087711

**Table 2.7 cont.** Surface data correlation coefficient matrix for bivariate analysis.

	Fe	Ga	Gd	Ho	K	La	Lu	Mg	Mn	Mo	Na	Nd	Ni	P	Pr	Rb
Fe	1															
Ga	0.71663028	1														
Gd	0.38629658	0.66220045	1													
Ho	0.11766943	0.37715192	0.75331461	1												
K	0.59355746	0.4372751	0.10542705	-0.050462	1											
La	0.39314567	0.58843519	0.82674667	0.49764163	0.18253867	1										
Lu	0.45917746	0.73125454	0.43809218	0.34120476	0.22170186	0.30674764	1									
Mg	0.55638686	0.79481902	0.51946641	0.43842135	0.35149617	0.29678343	0.8084396	1								
Mn	0.43794956	0.4751268	0.33056012	0.26108693	0.04631344	0.29759496	0.36316632	0.39227932	1							
Mo	0.3766544	0.25352719	0.10493534	-0.0436556	0.35633995	0.00662031	0.10704329	0.3043372	0.12874557	1						
Na	0.28046251	0.36398521	0.24744804	0.2362217	-0.0169141	0.09671891	0.26307935	0.3395436	0.2571222	0.1270723	1					
Nd	0.4356338	0.65763689	0.91912097	0.58967776	0.21382968	0.9617937	0.37213758	0.42638674	0.2999034	0.03347074	0.17468437	1				
Ni	0.24465212	0.4465006	0.46924525	0.52652757	-0.0320879	0.23721942	0.49507407	0.67613864	0.31794396	0.1798954	0.18738418	0.31368291	1			
P	0.17354681	0.29874609	0.5504352	0.50486306	0.01756389	0.33330445	0.34222191	0.44030403	0.09842648	0.12011066	0.18864326	0.47454129	0.45362793	1		
Pr	0.4056359	0.60156269	0.87726379	0.55861286	0.1960082	0.97632315	0.32281023	0.36470167	0.26247684	0.01406229	0.13370138	0.98695459	0.26856308	0.42051604	1	
Rb	0.57771816	0.48886306	0.20113674	0.03963118	0.95286526	0.19897564	0.30397209	0.45819104	0.05735236	0.4790757	0.01633623	0.25591577	0.05652256	0.17596112	0.22100294	1
S	0.11157934	-0.1073111	-0.1516946	-0.2431639	0.17088165	-0.1925328	0.0815534	0.01483613	-0.1581464	0.28643412	0.13065006	-0.1549749	-0.1161541	0.31635201	-0.1531329	0.28931789
Sb	0.24107633	0.26277811	0.30836315	0.36424965	0.00659529	0.10978753	0.19393667	0.27766912	0.25836727	0.22052347	0.2510338	0.17438545	0.30412433	0.2545344	0.13377581	0.09535575
Sc	0.27683831	0.26244457	-0.0349733	0.00426662	0.30362901	0.13714541	0.30184647	0.29233746	0.08428833	0.07329191	0.01365744	0.08306054	0.03864581	-0.0705619	0.11504023	0.29806683
Se	0.32190163	0.01381485	0.00945364	-0.0175257	0.38509633	0.00870567	-0.0961275	0.11775094	-0.0154714	0.47426499	-0.1506366	0.0243871	0.02226979	0.01529127	0.0622273	0.38787418
Sm	0.42148636	0.67815983	0.96655986	0.65034013	0.20487681	0.90851845	0.40084037	0.48632864	0.2687851	0.07295997	0.19749217	0.97966687	0.36296636	0.51037714	0.95464908	0.27034761
Sn	0.36710747	0.29570114	0.32575238	0.0430417	0.41922254	0.40595244	-0.0897204	0.12936389	0.01735746	0.30695593	0.01742835	0.42173662	0.12223494	0.16292397	0.41550727	0.37412035
Sr	0.23040026	-0.0526687	0.0259555	0.01136022	0.31900174	0.01898514	-0.1683214	-0.0672808	-0.1601302	0.1318239	0.02475825	0.01621737	-0.13696524	0.21784916	0.04497776	0.34387718
Tb	0.35017766	0.57684149	0.93741782	0.7325434	0.04678003	0.37335254	0.37286699	0.48550636	0.36399986	0.14565733	0.23220552	0.83078455	0.44622446	0.56285864	0.79198514	0.15968241
Th	0.20977056	0.36640727	0.42530699	0.29571713	0.21970696	0.51282669	0.10396138	0.31166504	0.10608636	0.0765644	-0.1815988	0.49848925	0.40465908	0.1310254	0.49103715	0.25808876
Ti	0.15702228	-0.0117784	0.05487962	-0.0561263	0.27750957	0.1696306	-0.3342671	-0.0879271	-0.1195142	-0.0932226	-0.087541	0.2044065	-0.1460531	0.1279702	0.19854308	0.21696895
U	-0.0031406	-0.000044	0.27580536	0.38554551	-0.1811839	0.19344248	0.03064187	0.17561706	0.051602	0.18949229	0.00203181	0.18190761	0.4020514	0.38447062	0.22091973	-0.0520195
V	0.69308281	0.69304651	0.61389149	0.39468605	0.46822543	0.42841581	0.45908073	0.72566688	0.29026896	0.39798067	0.2344822	0.54799798	0.56123629	0.52730876	0.48894094	0.53765168
Y	0.31205173	0.62918946	0.91579241	0.82574006	0.02494471	0.67035988	0.45622553	0.57952171	0.42061446	0.13820019	0.32740144	0.75944616	0.64298823	0.51621314	0.71386224	0.13016604
Yb	0.29130402	0.57820184	0.87420294	0.63077666	0.08402094	0.63807788	0.39441834	0.55617832	0.31530597	0.14468465	0.22456712	0.72453681	0.67917337	0.52349922	0.67692681	0.18506683
Zn	0.33689033	0.45630954	0.42710684	0.49847236	-0.1891182	0.31001638	0.50965592	0.44489197	0.65156334	-0.1027967	0.2565575	0.34394603	0.48124258	0.3067918	0.31741885	-0.1394028
Zr	0.07963542	-0.1593018	-0.0259286	-0.0229143	-0.0368026	-0.0367463	-0.1602536	-0.1284537	-0.0397418	-0.0942772	0.02741931	-0.0131568	-0.11153291	0.0677965	0.01091296	-0.0526301

**Table 2.7 cont.** Surface data correlation coefficient matrix for bivariate analysis.

	S	Sb	Sc	Se	Sm	Sn	Sr	Tb	Th	Ti	U	V	Y	Yb	Zn	Zr
S	1															
Sb	0.3069981	1														
Sc	0.00131151	0.00373051	1													
Se	0.31717563	0.12232653	0.23953594	1												
Sm	-0.1434982	0.21266115	0.03931121	0.03190842	1											
Sn	-0.1352697	-0.1468979	0.05138877	0.39880873	0.40484149	1										
Sr	0.56852464	0.26545429	0.11335454	0.35628129	0.007949	0.2369927	1									
Tb	-0.0442865	0.41555975	0.00800612	0.04586292	0.88685093	0.21737359	0.05802303	1								
Th	-0.301003	0.13266163	0.10739431	0.15524172	0.464181	0.33428904	-0.1172988	0.36725336	1							
Ti	-0.083918	-0.1405872	0.01397954	0.21324567	0.15059047	0.56723586	0.45565319	0.01008163	0.14338675	1						
U	0.20827702	0.33994173	0.1764905	0.29407173	0.20279384	0.0009051	0.31232585	0.37382353	0.23448303	-0.0956608	1					
V	0.06403262	0.21783929	0.14222677	0.362305	0.58686415	0.5789119	0.25145572	0.58224807	0.34108661	0.2948545	0.22213105	1				
Y	-0.1335875	0.46032771	-0.0362791	0.00804314	0.82453142	0.21842912	-0.0172428	0.89596894	0.42737734	-0.0914528	0.40492062	0.57188927	1			
Yb	-0.1572735	0.4278349	-0.0533264	0.074827	0.79188696	0.31388293	0.03020823	0.83686428	0.51775216	0.00970523	0.43479803	0.61765142	0.95808386	1		
Zn	-0.1372609	0.43799901	0.10120977	-0.2260698	0.33727526	-0.2948507	-0.2320622	0.47145219	0.15844866	-0.3229262	0.21546489	0.23019088	0.5358444	0.43682377	1	
Zr	0.23742382	0.001596	-0.0687281	0.25540787	-0.0220919	0.25174706	0.50293937	-0.0549647	-0.2331371	0.51118966	0.11636257	0.07213843	-0.0193167	-0.0008173	-0.1714316	1

**Table 2.8.** Subsurface data correlation coefficient matrix for bivariate analysis.

Row	Ag	Ag	Al	As	Au	Ba	Be	Ca	Ce	Co	Cr	Cu	CuOx	Dy	Er	Eu	Fe
1	0.10370155	0.24637522	0.00390984	1	0.00117789	0.020456	0.23175397	0.33096803	0.39822844	1	0.22171282	1	0.70652063	1	0.12981527	0.41199465	1
As	0.32147395	0.00390984	1														
Au	0.01302866	0.00808853	0.01000016	1													
Ba	0.0149478	0.60068149	0.01000016		1												
Be	0.21568705	0.47120348	0.47933354	0.000456	0.23175397	1											
Ca	0.22715069	0.55541804	0.31694778	0.0430659	0.30100234	0.33096803	1										
Ce	0.12477456	0.48513406	0.33964812	0.03487176	0.23598552	0.33133635	0.39822844	1									
Co	0.06613491	0.4510682	0.2762406	-0.004161	0.23600797	0.40928084	0.40381171	0.20970982	1								
Cr	0.10372028	0.34749494	0.0353387	-0.0474871	0.27712135	0.00460507	0.22017745	0.00404127	0.22171282	1							
Cu	0.01812596	0.0553945	0.02573787	-0.0768472	0.06186811	0.20005294	0.11545401	0.17389146	0.25474451	-0.0859946	1						
CuOx	0.08832065	0.08039911	0.06170664	-0.02822387	0.10366337	0.05634101	0.11482536	0.00427167	-0.0503012	-0.0503012	0.2204751	1					
Dy	0.1226837	0.53640882	0.42080438	0.06133751	0.22735521	0.38847572	0.43556327	0.63087879	0.32865959	0.32865959	0.12981527	0.41199465	1				
Er	0.20218268	0.64709375	0.43267146	0.03812832	0.35470422	0.46296539	0.44858216	0.72705428	0.38509217	0.02760192	0.20594408	0.08269769	0.79787928	1			
Eu	0.03242447	0.41297093	0.29639474	0.04968433	0.3755537	0.31635861	0.30822658	0.13771625	0.53116111	0.32885652	0.0298989	-0.0740361	0.20657774	0.12119302	1		
Fe	0.07083349	0.21860929	0.24814352	0.08581846	0.49368646	0.33323887	0.30842313	0.41627333	0.37424677	0.23675916	0.13063979	0.04414685	0.42909508	0.32077214	0.53237874	1	
Gd	-0.2114974	0.55111212	0.1341295	-0.0277917	0.35832208	0.3338911	0.25275315	0.42860708	0.52376341	0.30645891	0.16487928	0.10230406	0.25494484	0.47797478	0.40623084	0.60308858	0.54575559
K	0.13739309	0.49078819	0.000431	0.03749847	0.17339586	0.28522872	0.19133656	0.16323962	0.15057449	0.088119287	-0.0579739	0.23113635	0.08658002	0.3316131	0.21945553	0.46797142	
La	0.23629297	0.58706724	0.4792348	0.03148601	0.20980844	0.37329387	0.38451066	0.75941821	0.92262072	0.12406704	0.00302468	-0.0470211	0.55197395	0.22687963	0.64832581	0.21735067	0.31171702
Li	0.38853116	0.20765802	0.34862788	0.0891029	0.28787889	0.31515222	0.21788879	0.17472287	0.07771884	0.07771884	0.02524441	0.1067381	-0.1385104	0.37996868	0.12231792	0.33182713	
Lu	-0.0855171	0.40275611	-0.0117011	-0.0332607	0.08812088	0.08695526	0.26386699	0.22881051	0.23564628	-0.029758	0.21235033	0.16329506	0.3332121	0.47484488	0.2748291	0.11263287	0.21260857
Mg	0.16213047	0.7166235	0.17762224	0.01442548	0.5211274	0.4105894	0.36409577	0.19239677	0.29457317	0.21685076	0.1536746	0.0623124	0.38639461	0.1685876	0.44316207	0.24426093	0.65686203
Mn	0.01309633	0.38493319	0.13187094	-0.0093654	0.23050867	0.01065397	0.41139046	0.08617459	0.51158814	0.29232812	0.1355373	0.15564704	0.06779654	0.06426006	0.11465016	0.42709384	0.22787173
Mo	0.09801812	0.1268046	0.00748204	0.00348204	0.202688	0.1793611	-0.0412606	0.21971027	0.02286455	0.00231701	0.13432648	0.04643356	0.03967484	0.17231076	0.18427681	0.21343504	0.03846644
Nb	0.32946441	0.38073465	0.1612302	0.08716524	0.25667719	0.06898813	0.32041971	0.22522783	0.0011254	0.46877539	-0.0282407	-0.0052192	0.23983832	0.1946308	0.21671702	0.11043127	0.25640444
Ni	0.23463388	0.33403465	0.3286385	0.0267948	0.20390944	0.342063	0.28725473	0.54464503	0.23240462	-0.0110784	0.11935222	0.03986308	0.621395	0.31603485	0.60897225	0.2373865	0.15163103
Nd	-0.005274	0.28732354	0.0381802	0.028228	0.19078799	0.10596218	0.22744982	-0.057685	0.22464932	0.65175315	0.08860955	-0.026385	0.03762313	0.04087021	0.2830515	0.15433146	
Pb	0.1888871	0.35350506	0.27000089	0.05276181	0.20598576	0.25333119	0.3664629	0.31406537	0.28015329	0.18472807	0.25542807	0.15433268	0.07434368	0.17231076	0.29371959	0.21156088	0.41641361
Pr	0.46141271	0.1382261	0.44419769	0.08071769	0.14179984	0.25510962	0.12070589	0.38535993	0.08894709	-0.031525	-0.0222278	-0.0884563	0.51285054	-0.1376152	0.4676761	0.18989294	0.20415974
Rb	0.0278462	0.33974303	0.15505891	0.07923247	0.25573276	0.16212129	0.200971	0.20215919	0.08571048	0.07446735	0.05872845	-0.0741246	0.38058173	0.0299791	0.3840452	0.18875203	0.34107281
Rh	0.19015813	0.05614088	0.0684889	0.0684889	0.27567923	0.15312787	0.03464929	0.13512787	0.0201478	0.02203088	0.02299134	-0.1078868	-0.4827642	0.05765631	0.1645958	0.286723704	0.19305604
Sn	0.15577848	-0.008329	0.10700841	0.2181812	0.11391137	0.0943637	0.02990451	-0.0007525	-0.0715157	0.29167753	-0.0019814	0.04562796	-0.096201	0.47964705	0.13291447	0.02257404	
Sm	-0.0037245	0.4658804	0.13824666	0.10241735	0.45374341	0.05433053	0.38195686	0.44070703	0.1773624	0.24691638	0.00667253	-0.1020153	0.26210143	0.32050227	0.37917776	0.25915295	0.45684614
Tb	0.1798787	0.20254669	0.04151268	0.02966717	0.22006922	0.20395804	0.35151294	0.05511785	0.11493853	0.2287687	0.04537613	0.10760333	0.07517264	0.16760033	0.18732065	0.21856666	0.77201268
Ti	0.3607884	0.21216659	0.30454659	0.01078322	0.22001892	-0.20399697	0.19379697	0.17864737	0.17272888	0.1643434	-0.0568877	-0.1119333	-0.10862571	0.1019133	0.06796988	0.26739688	0.18873937
Th	0.34077653	0.20250793	0.29891172	0.12293884	0.19366877	0.09817946	0.24922233	0.40003944	-0.00203944	-0.0129433	0.33132001	0.08626279	-0.0313059	0.50707816	-0.0116082	0.40804781	0.0739336
Tl	0.00417462	0.0114877	-0.1240514	0.02575429	0.06208914	-0.0099514	0.10179739	0.02046859	-0.0391543	0.00339446	0.00025472	0.04798784	0.09762891	0.1019373	0.04719458	0.07466132	0.171784576
Tm	0.00969582	0.08180888	0.04086035	0.07225892	0.00700314	0.00684876	0.05506465	-0.02208113	0.00300384	0.00343385	-0.00235839	-0.1247109	0.24119458	0.087149629	0.087149629	0.025413728	0.10525125
V	0.19466286	0.28426658	0.08793059	0.08793059	0.03930240	0.14749254	0.00634874	0.03933884	0.03648614	0.03933884	-0.0176452	-0.140629	0.1874242	0.024313728	0.024313728	0.05434989	0.4246159
W	0.04000075	0.66792383	0.22401538	0.0808087	0.5288368	0.30612745	0.30268246	0.3810944	0.30865653	0.22515634	0.16777031	0.08649352	0.42008717	0.32703165	0.56434989	0.4246159	0.73297191
X	0.12867559	0.14863918	0.14186761	-0.0293146	0.08814671	0.08855167	0.08855167	0.26292303	0.12290627	0.044539101	0.10741412	0.08737988	0.15309412	0.11020579	0.74717539	0.57754493	0.08797941
Y	0.0256876	0.6588287	0.32881765	0.24633753	0.43533539	0.5326133	0.66201221	0.44539101	0.10741412	0.27477814	0.27477814	0.12102579	0.74717539	0.57754493	0.71285608	0.20680866	0.43964922
Zn	0.02545688	0.28781135	-0.0126329	0.0813684	0.36377382	0.50067101	0.80075907	0.304143709	0.05895841	0.28523224	0.19622248	0.16100331	0.28523224	0.19622248	0.16100331	0.59853383	0.30289842
Zr	0.06817975	0.18935629	0.13199201	0.00531669	0.08281553	0.27371654	0.15786631	-0.0090474	0.3861671	0.0868227	0.06719632	0.05838443	0.12988872	0.05519533	0.14505861	0.2028802	0.21929367
Zr	0.01393701	0.28030104	0.10455898	0.11154846	0.1632918	-0.0621686	0.43352425	0.20393389	0.16924102	0.45793204	0.00003548	0.09138131	0.11237746	0.2531672	0.1280984	0.22768793	0.28675672

**Table 2.8 cont.** Subsurface data correlation coefficient matrix for bivariate analysis.

	Gd	K	La	Li	Lu	Mg	Mn	Mo	Na	Nd	Ni	P	Pb	Pr	Rb	S	Sc	Se	Si	Sn	Sr	Tb	Ti	Tl	Tm	U	V	W	Y	Yb	Zn	Zr	
Gd	1																																
K	0.18212539	1																															
La	0.22460933	0.15602208	1																														
Li	-0.1232779	0.32763444	0.29720995	1																													
Lu	0.35794243	0.01325112	0.10369355	-0.2775868	1																												
Mg	0.20004682	0.67548649	0.22488411	0.51244613	0.04367179	1																											
Mn	0.4690966	0.09469085	0.06919203	0.15437788	0.10919404	0.23685534	1																										
Mo	0.1157206	0.22704797	0.21805082	0.03862596	0.07889588	0.09580886	-0.0560301	1																									
Na	-0.0203917	0.17720679	0.32293835	0.29687082	-0.0845475	0.21650399	0.10902946	0.05841491	1																								
Nd	0.19494325	0.1559081	0.51900741	0.17655668	0.39004108	0.1913548	0.05538336	0.13614406	0.19901624	1																							
Ni	0.21334173	0.16299461	0.15212489	0.08787182	-0.0152403	0.26547199	0.43238343	0.06146714	0.26710955	-0.0359301	1																						
P	0.20181441	0.21956609	0.34265683	0.3167099	0.14239104	0.39339879	0.21182544	0.04242737	0.19901509	0.23218614	0.18630726	1																					
Pb	0.03451332	0.03834337	0.31904431	0.13853795	-0.2490518	0.06880199	-0.0425881	-0.0845463	0.12526071	-0.0506442	0.04763523	-0.051671	1																				
Pr	-0.2364593	0.16727351	0.50227532	0.708204	-0.2649291	0.27462632	-0.0487547	0.0715859	0.32053909	0.41173837	-0.0343622	0.28621611	0.19896308	1																			
Rb	-0.0742771	0.71333788	0.35757058	0.43799547	-0.0362565	0.54702466	-0.061314	0.2104373	0.23286374	0.35281799	0.13265633	0.31955541	0.04200228	0.1507647	1																		
S	0.1127029	0.35686877	0.19747258	0.08452302	-0.0379779	0.15205963	-0.1048559	0.22012231	-0.0312207	0.14248844	-0.0691807	0.07153931	0.15107647	0.15471316	0.3066448	1																	
Sc	0.53879558	0.31284004	0.38281635	0.26841721	0.1814211	0.52973875	0.21346648	0.1101496	0.23298122	0.3355832	0.1808257	0.30653922	0.10800506	0.23701435	0.23095312	0.14652371	1																
Se	0.14812385	0.19245444	0.28824675	-0.0130309	0.1605569	0.12101195	-0.0836449	0.27808338	0.05165226	0.22550669	-0.0529786	0.13289569	0.18378164	0.08309934	0.26854796	0.46701619	0.16799384	0.18378164	0.03093934	0.20349795	0.28618583	-0.056007	0.16477199	0.11044827	-0.0318994	0.48736351	0.38368705						
Si	-0.025225	0.19039031	0.35190736	0.09789628	0.01005969	0.16610063	0.11247505	0.09284169	0.54963918	0.20540449	0.42164454	0.14244269	0.06863369	0.17939863	0.08704518	0.0849585	0.02960797	0.14521703	0.2247293														
Sn	0.22850234	0.06122124	0.45003476	0.10417067	0.22830445	0.145658	0.02336305	0.02126718	0.12574439	0.27479227	0.03451238	0.15195156	0.18803502	0.10401753	0.13168293	0.11848565	0.02960797	0.14521703	0.2247293														
Sr	0.01447013	0.07798884	0.11431136	0.01316796	-0.1068181	0.10975583	0.22958955	0.07416593	0.14655689	0.03109699	0.33292745	0.0950723	0.10401753	0.13168293	0.11848565	0.02960797	0.14521703	0.2247293															
Tb	0.02314017	0.26624726	0.17173815	0.14894276	0.11030734	0.21112077	0.08716887	0.00940749	0.21951702	0.18436626	0.21429767	0.18097884	-0.0685791	0.18811997	0.40526437	0.06834333	0.19262223																
Ti	-0.0721412	0.1350386	0.38948809	0.32157119	0.10326528	0.16705244	0.08786829	0.02180522	0.1631277	0.31403829	0.14644968	0.27728611	0.16150563	0.48052	0.39761887	0.15105854	0.23490706																
Tl	-0.2674804	0.25852671	0.43073519	0.4901255	-0.0949258	0.17433769	-0.1110427	0.02863196	0.28992817	0.37835241	-0.0984257	0.30987934	0.04543183	0.65775651	0.48435912	0.1079241	0.04746543																
Tm	0.1118281	0.13975811	0.07460817	0.03688882	0.20304716	0.07771211	-0.1079988	0.04363443	0.14710089	0.16540759	0.025147	0.1164085	0.06536582	0.35518734	0.16793318	0.16879476	0.01740626																
U	-0.0908409	0.11166378	0.2137246	0.21679806	-0.1325983	0.07771211	-0.1079988	0.04363443	0.14710089	0.16540759	0.025147	0.1164085	0.06536582	0.35518734	0.16793318	0.16879476	0.01740626																
V	0.47552158	0.56937005	0.30133687	0.2893816	0.21563625	0.65285109	0.14682659	0.16025553	0.1744622	0.2754147	0.19179643	0.35770569	0.02731724	0.17502799	0.43263178	0.21280067	0.65542062																
W	0.10593616	-0.0093927	0.15884075	-0.0819949	0.34040717	0.04801596	0.10105567	-0.0027825	0.23530693	0.24720519	0.1937993	0.19064328	0.02107517	-0.0496857	0.06720068	-0.2004557	0.13363432																
Y	0.55658668	0.20175711	0.51359943	0.23405125	0.25122975	0.28537183	0.05889194	0.2333485	0.38123407	0.10163102	0.33645114	0.07375421	0.2147569	0.11044827	-0.0318994	0.48736351	0.38368705																
Yb	0.50039606	0.14615177	0.4872842	0.03059413	0.32498568	0.26122986	0.16026308	0.04747436	0.14871363	0.34102264	0.02864753	0.28830698	0.09651548	0.02774628	0.04988001	-0.0344123	0.38368705																
Zn	0.25990522	0.00505553	0.06606014	0.07504493	0.08465092	0.18744311	0.32843861	-0.056201	-0.1858633	0.08741894	0.23491281	0.19640274	0.09403222	0.0668465	-0.0183073	0.0554024	0.23290581																
Zr	0.3557345	-0.0492045	0.14162037	-0.0399095	0.27492038	-0.0034535	0.32891933	-0.1222792	0.4554177	0.16441617	0.27361643	0.17237398	-0.0693437	-0.0629401	-0.0777774	-0.1497902	0.33295367																

**Table 2.8 cont.** Subsurface data correlation coefficient matrix for bivariate analysis.

	Se	Si	Sm	Sn	Sr	Tb	Te	Th	Ti	Tl	Tm	U	V	W	X	Y	Yb	Zn	Zr
Se	1																		
Si	0.1270276	1																	
Sm	0.1400196	0.13917819	1																
Sn	-0.0056198	0.40612441	-0.0308431	1															
Sr	0.1480592	0.1967236	0.2213261	0.0294105	1														
Tb	0.0809038	0.2481668	-0.0497273	0.16315273	0.26129057	1													
Te	0.2006806	0.22575922	0.0858037	0.23244871	0.11247094	0.38115362	1												
Th	0.08942441	0.26517926	0.21580555	0.01619834	0.07901857	0.15344235	0.31504509	1											
Ti	0.00981684	0.23341887	0.1098433	0.1328147	0.57937963	0.49523021	0.21276566	0.10694073	1										
Tl	-0.0045168	0.09587005	-0.0501759	-0.0984297	0.19802727	0.15644512	-0.0009603	0.04693933	0.18132722	1									
Tm	0.2246162	0.20131825	0.09036346	-0.0203055	0.06493464	0.15261726	0.21578408	0.192953	0.0493997	0.05564037	1								
U	0.1125423	0.22838032	0.08500837	0.24908867	0.16446386	0.11458309	0.09822567	0.38775346	0.10386944	-0.0500042	0.177663	1							
V	0.14730257	0.17149195	0.28623692	0.10142474	0.42837892	0.19708672	0.21609241	0.11297462	0.42001728	0.08152351	0.08090361	0.08242502	1						
W	0.08653992	0.22443807	0.12902404	0.12026207	0.05313025	0.19797235	0.1664127	0.06123568	0.17552178	0.10220553	0.03932914	0.04416072	0.07543338	1					
X	0.03432057	0.15888605	0.41750336	-0.0926251	0.33977285	0.0880867	0.07577865	0.26945204	0.31300116	0.0273921	-0.0156294	0.15047773	0.42260404	0.20977582	1				
Y	0.11091702	0.17251153	0.40344976	-0.0785477	0.29891338	0.0376033	-0.0501242	0.22530689	0.2615848	-0.0028268	-0.0399097	0.17936896	0.33161061	0.27315061	0.89442393	1			
Yb	0.04177741	-0.0133154	0.05100454	0.16803332	-0.0072214	0.006838	0.24489297	-0.0456649	-0.0223504	-0.0980649	0.09794324	0.07688699	0.17488295	0.16041831	0.19215038	0.12327857	1		
Zn	-0.0543345	0.30687083	0.07824191	0.19849742	-0.49273235	0.33106826	0.22559787	-0.0542582	0.65484812	0.1614797	0.00394481	0.02261874	0.22165962	0.29147	0.21846955	0.18217555	0.0289269	1	
Zr																			1

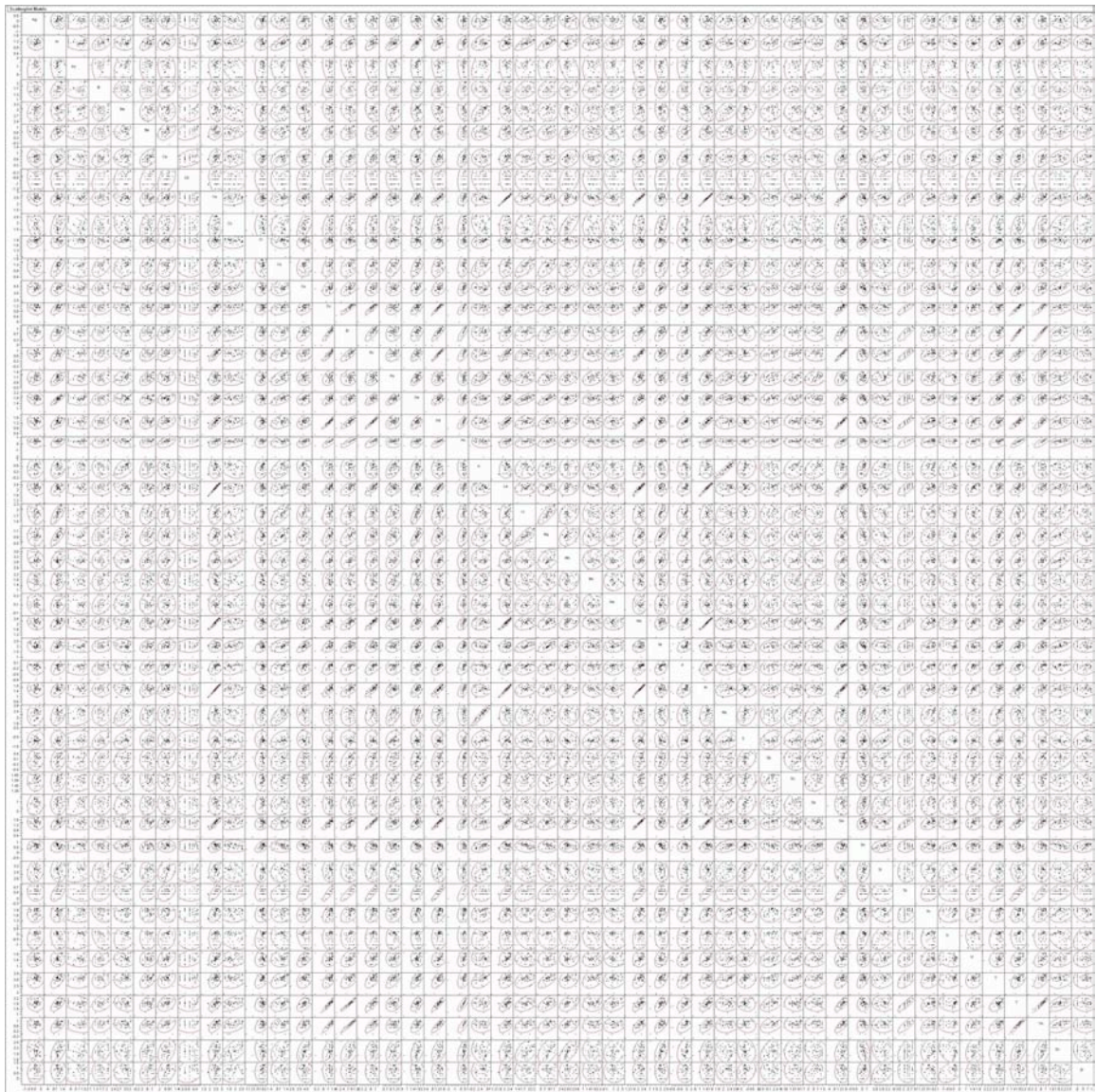


**Figure 2.34.** surface data scatter plot matrix for bivariate analysis.

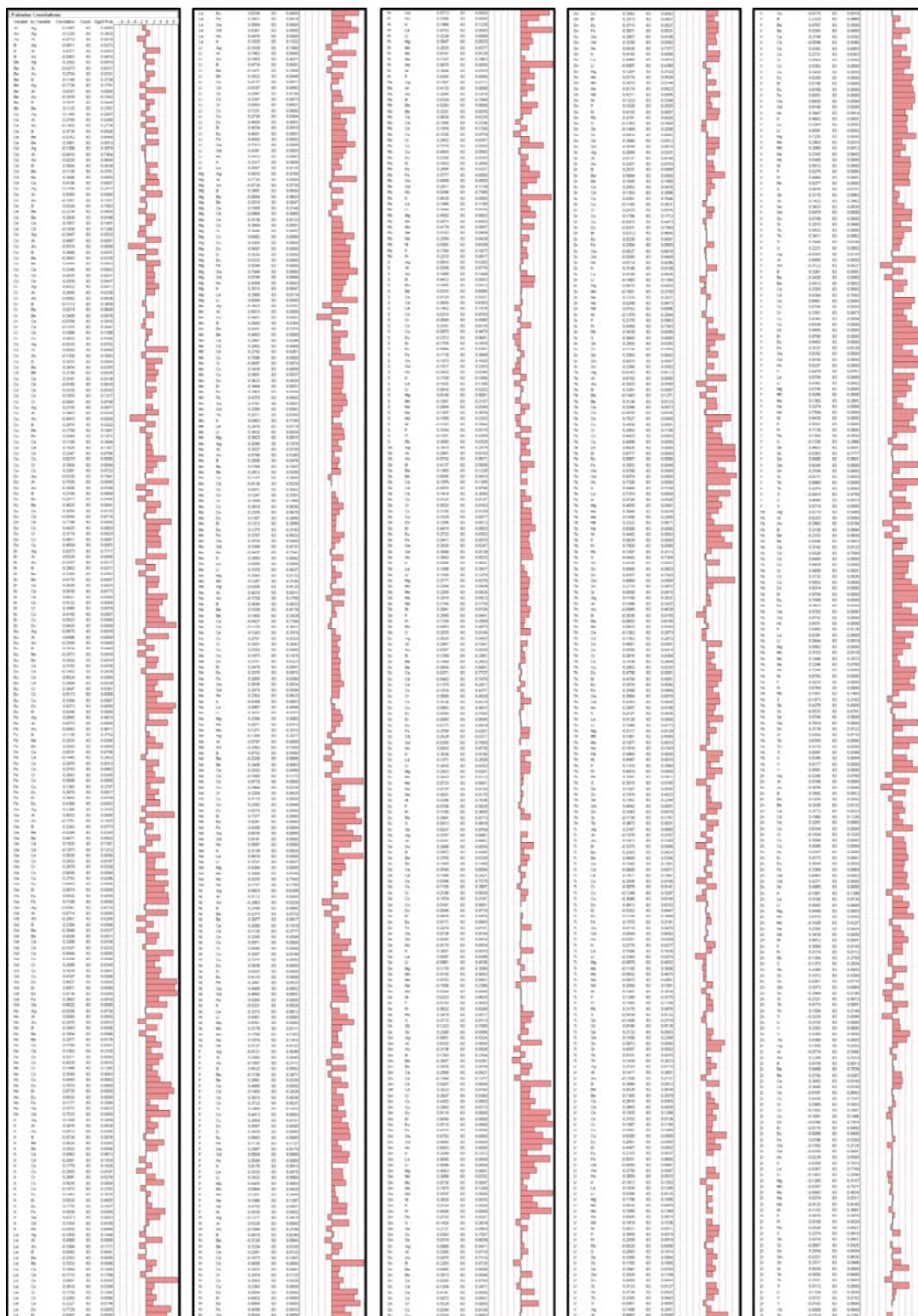


**Figure 2.35.** Surface data pairwise correlations for bivariate analysis.

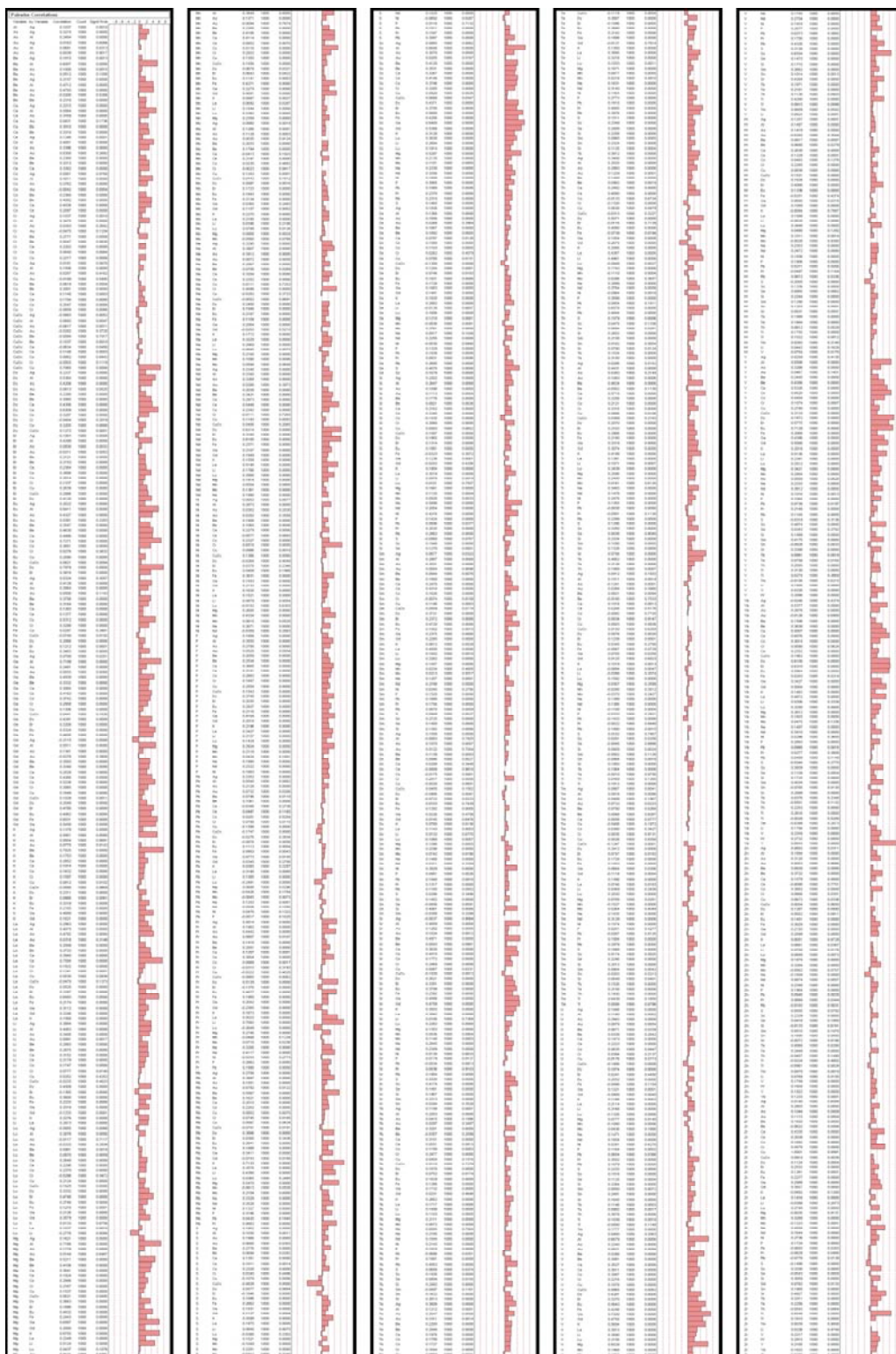


**Figure 2.36.** Subsurface data pairwise correlations for bivariate

## 16.4. Appendix 2.4. Multivariate Factor Analysis

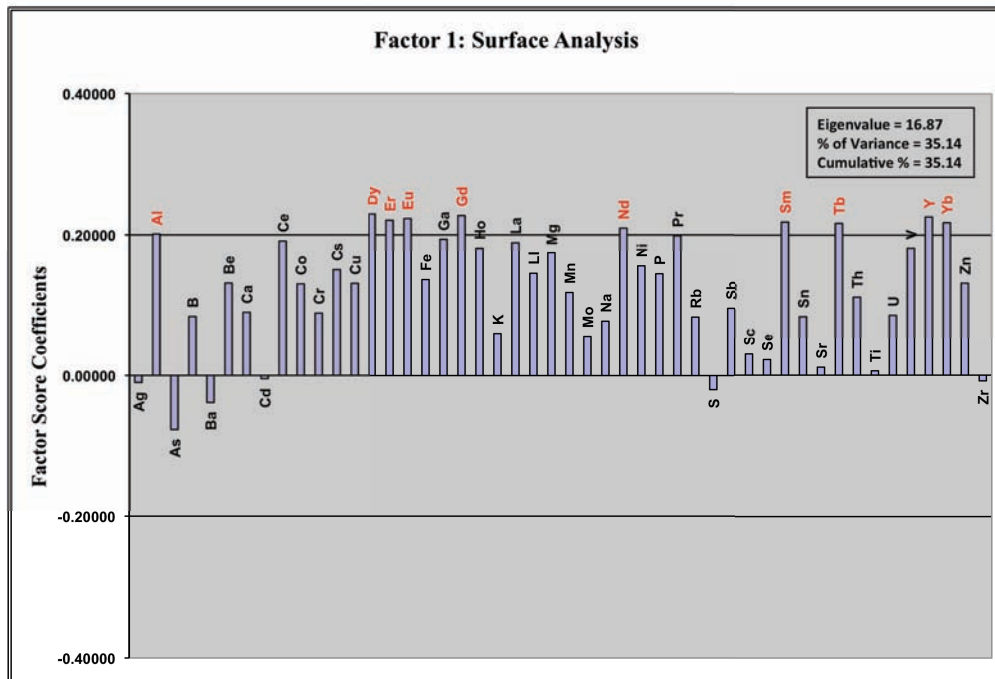


**Figure 2.37.** Factor 1 surface geochemical families (Red) indicated by factor score coefficients.

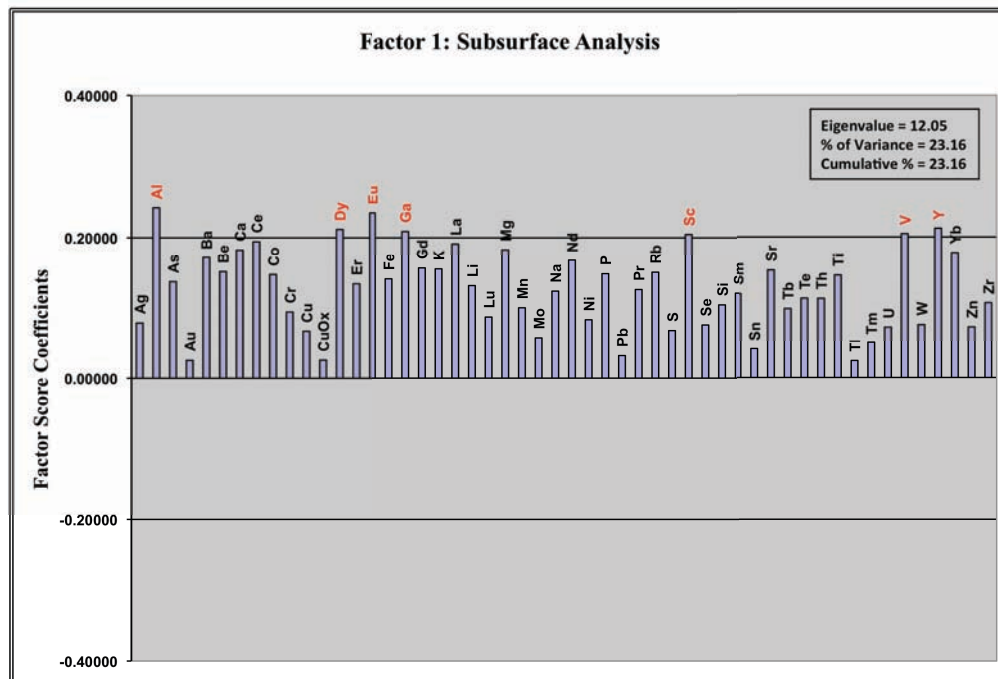


**Figure 2.38.** Factor 1 subsurface geochemical families (Red) indicated by factor score coefficients.

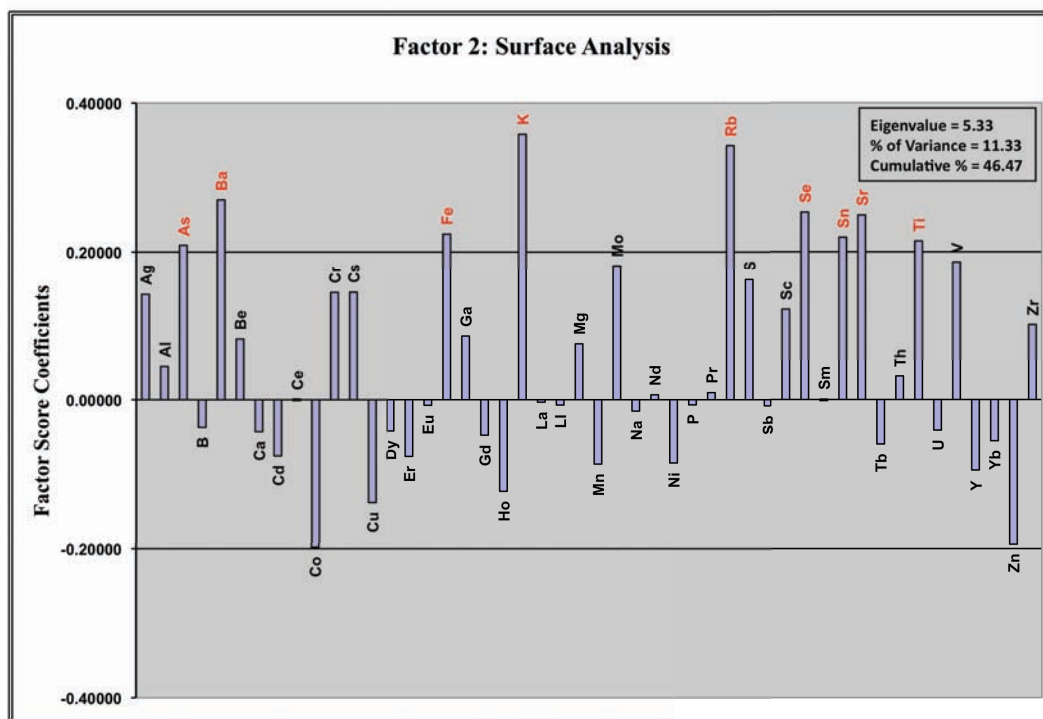


**Figure 2.39.** Factor 2 surface geochemical families (Red) indicated by factor score coefficients.

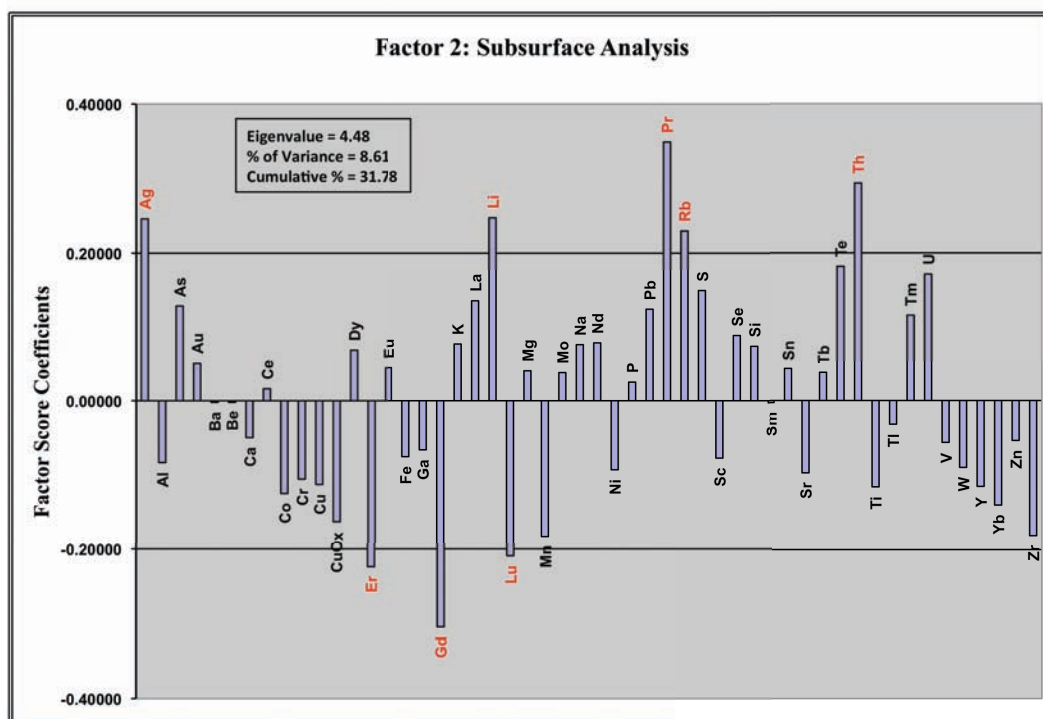


**Figure 2.40.** Factor 2 subsurface geochemical families (Red) indicated by factor score coefficients.

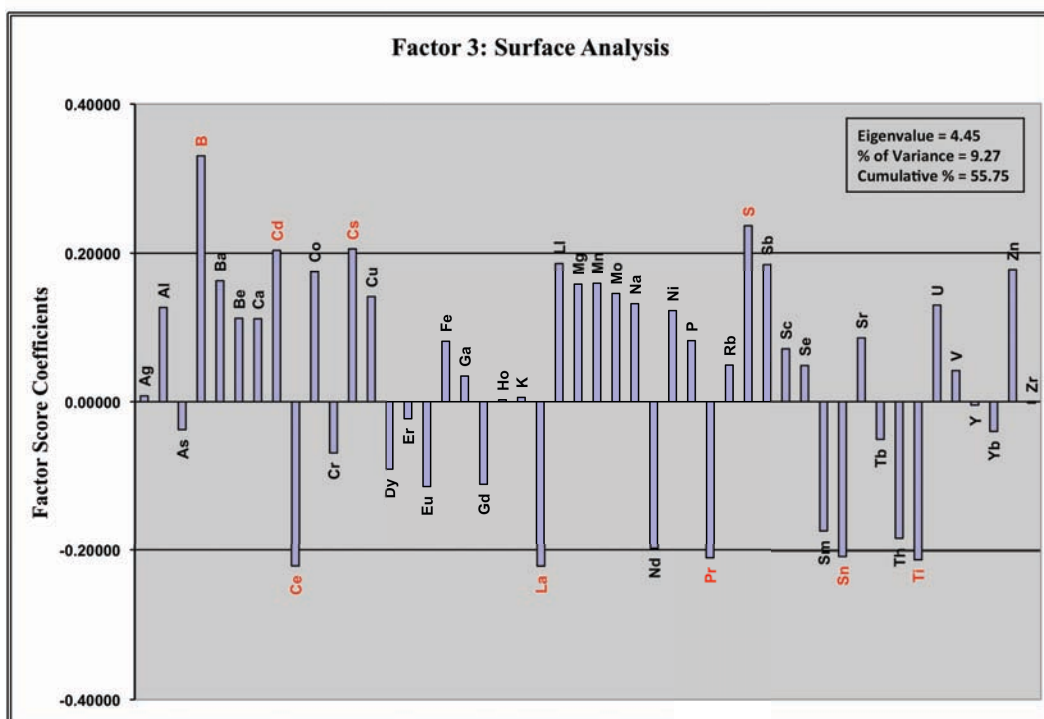


**Figure 2.41.** Factor 3 surface geochemical families (Red) indicated by factor score coefficients.

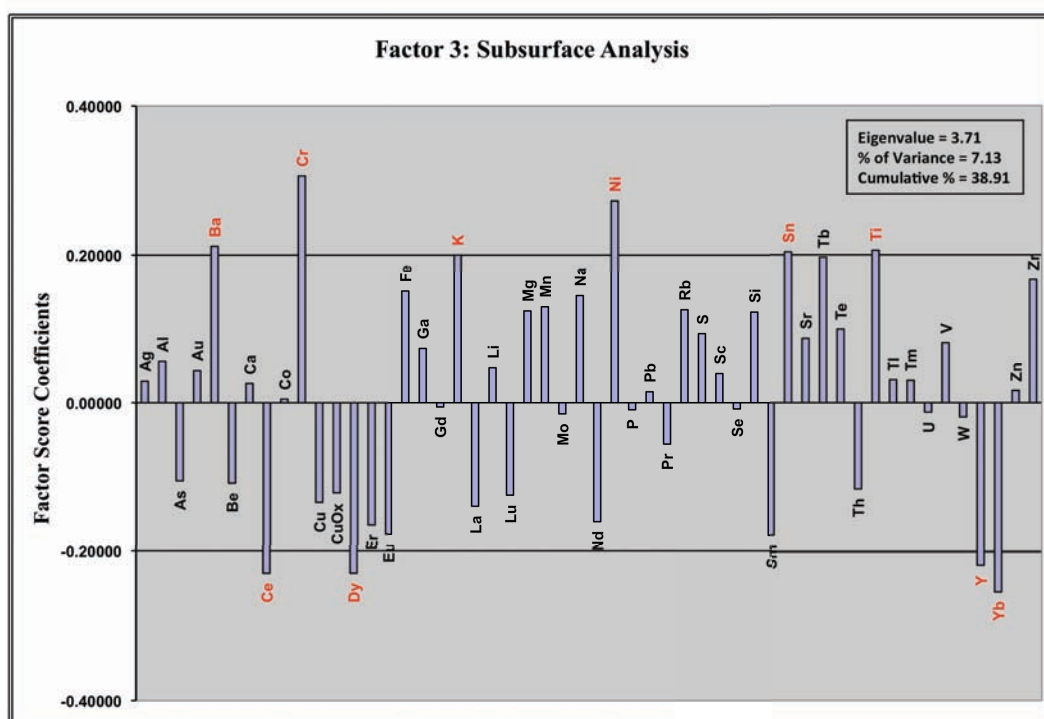


**Figure 2.42.** Factor 3 subsurface geochemical families (Red) indicated by factor score coefficients.

?

?

?

???

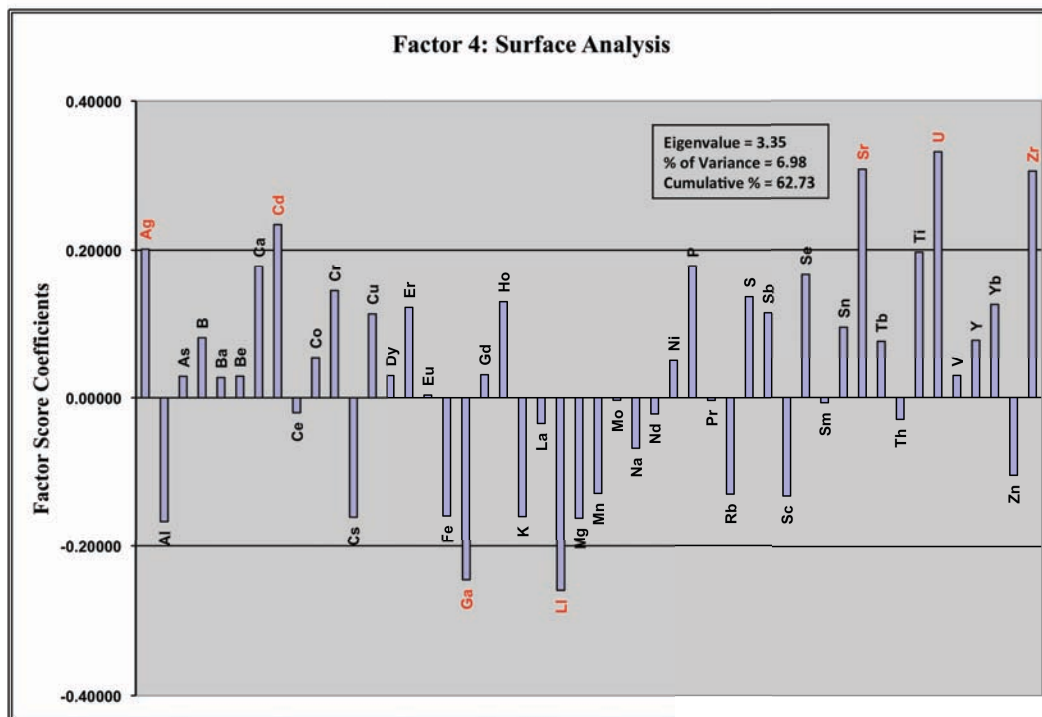


**Figure 2.43.** Factor 4 surface geochemical families (Red) indicated by factor score coefficients.

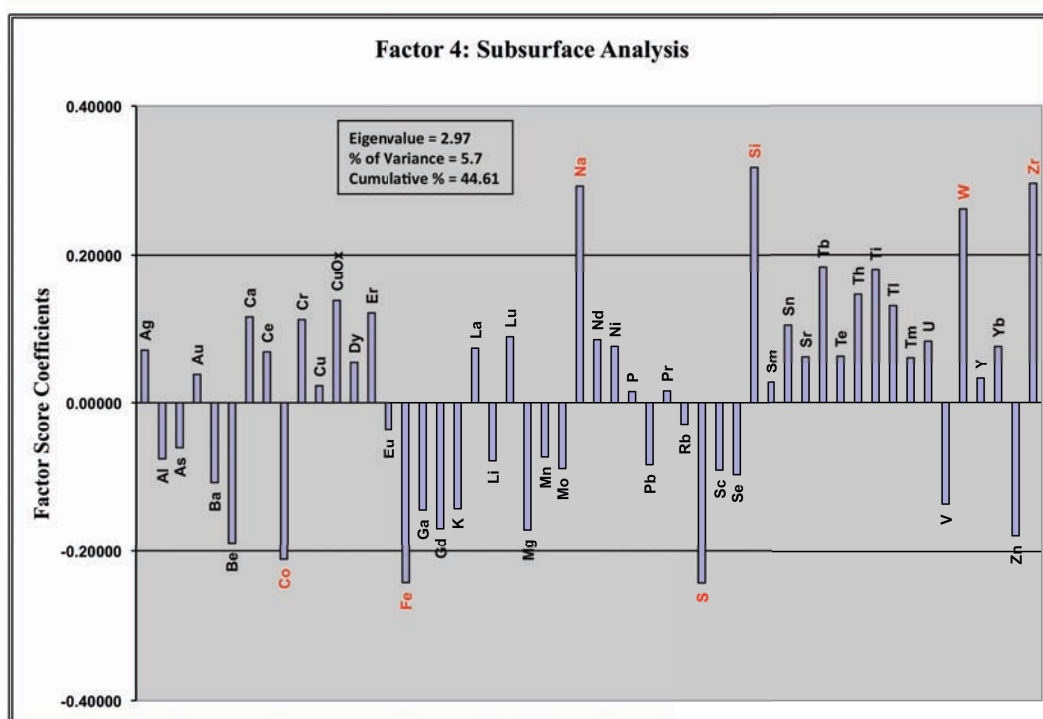


**Figure 2.44.** Factor 4 subsurface geochemical families (Red) indicated by factor score coefficients.

?

?

?

???

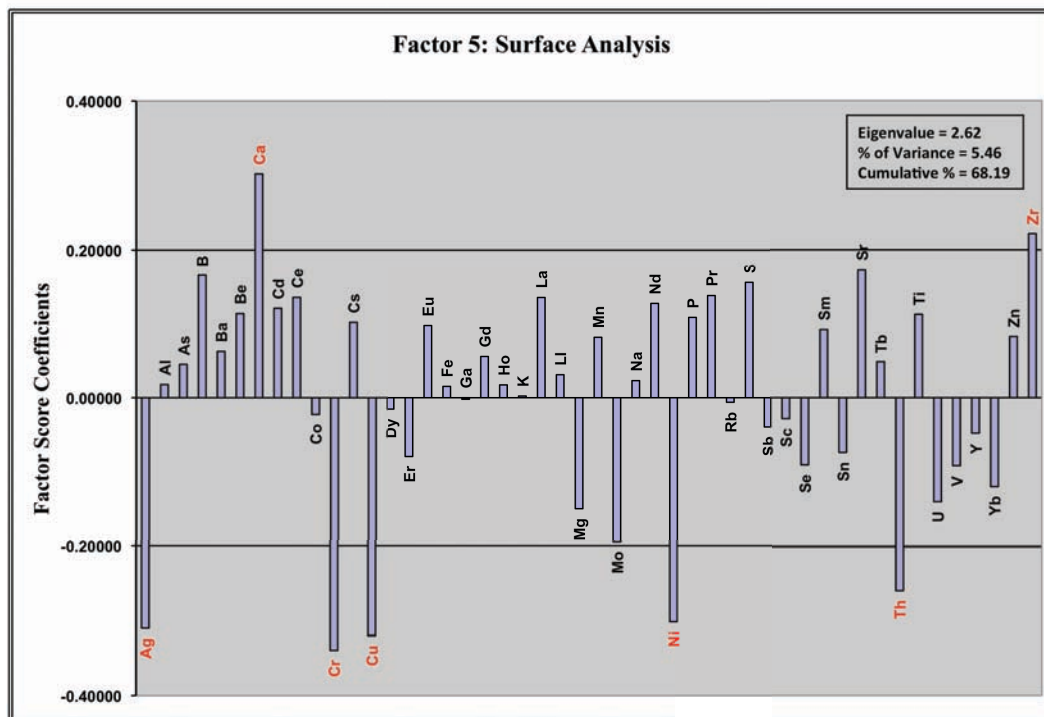


**Figure 2.45.** Factor 5 surface geochemical families (Red) indicated by factor score coefficients.

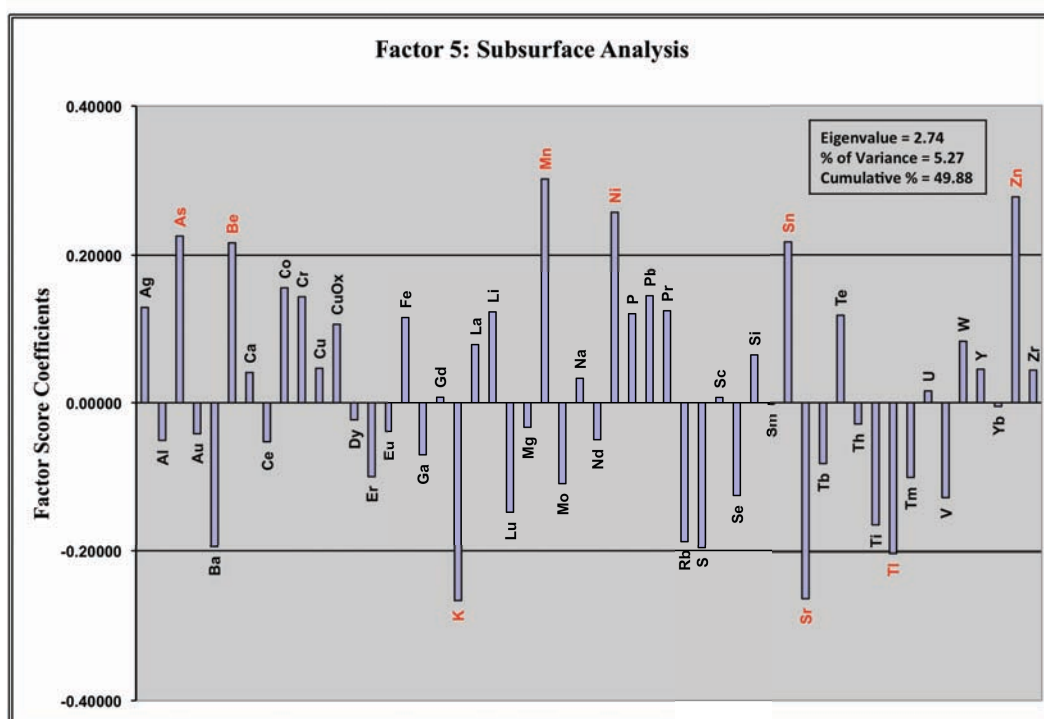


**Figure 2.46.** Factor 5 subsurface geochemical families (Red) indicated by factor score coefficients.

?

?

?

???

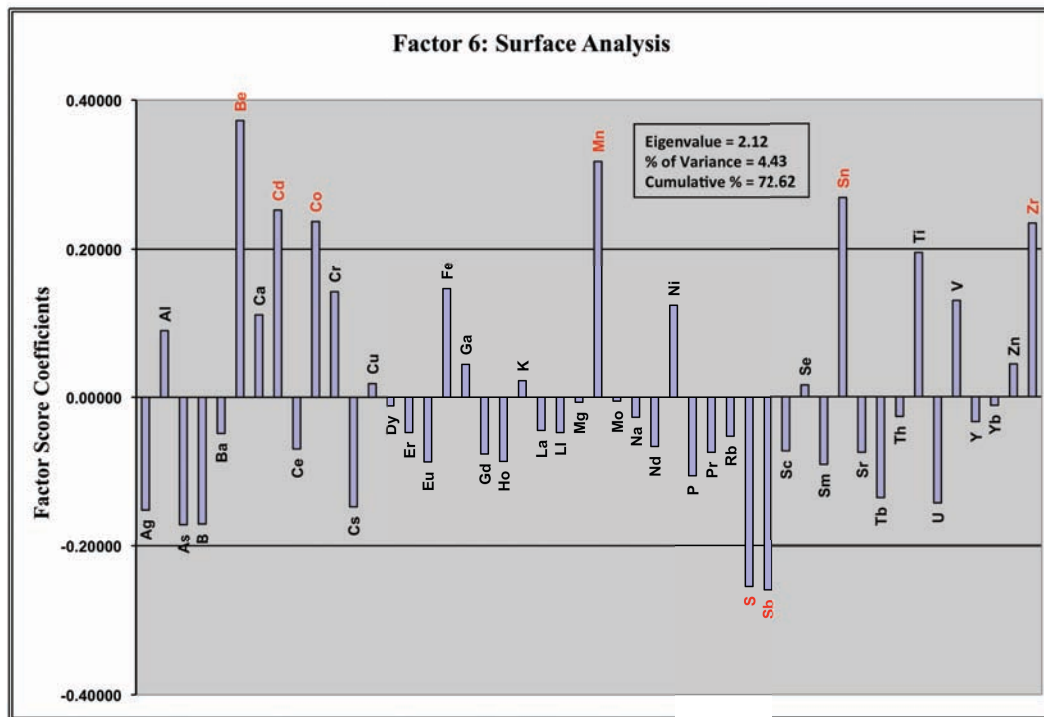


**Figure 2.47.** Factor 6 surface geochemical families (Red) indicated by factor score coefficients.

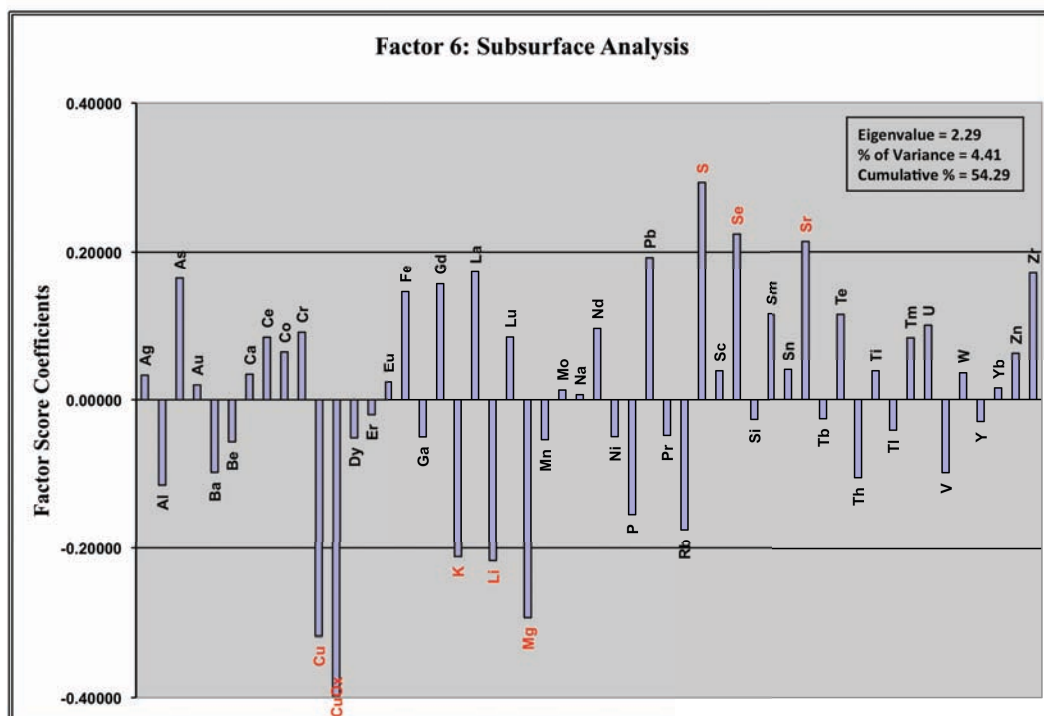


**Figure 2.48.** Factor 6 subsurface geochemical families (Red) indicated by factor score coefficients.

?

?

?

???

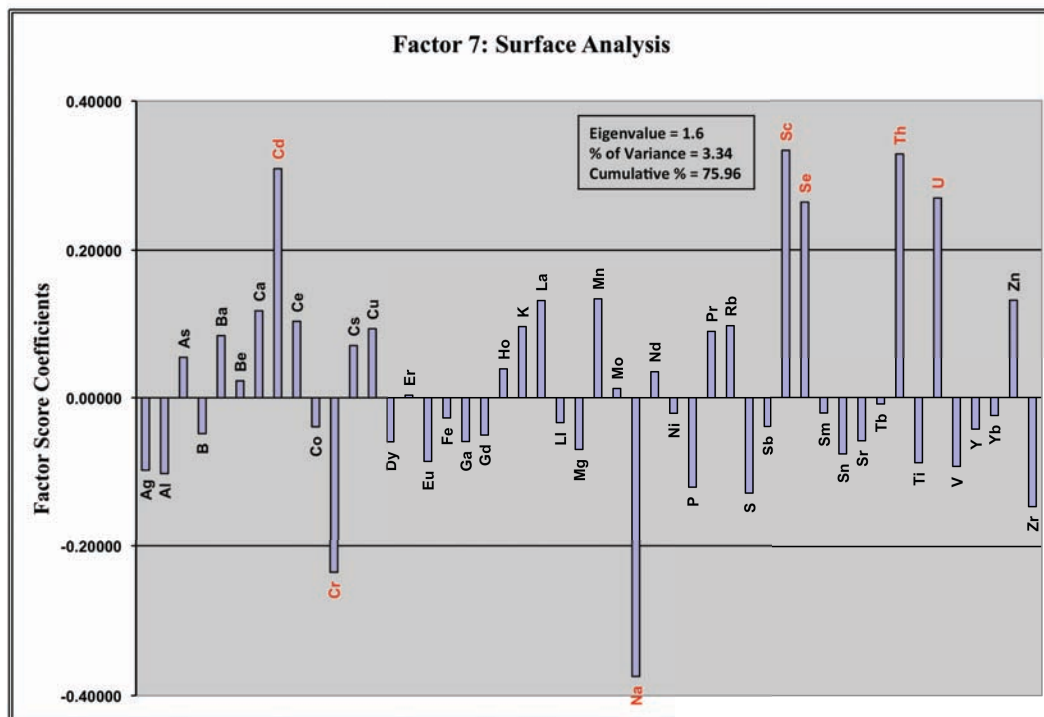


**Figure 2.49.** Factor 7 surface geochemical families (Red) indicated by factor score coefficients.

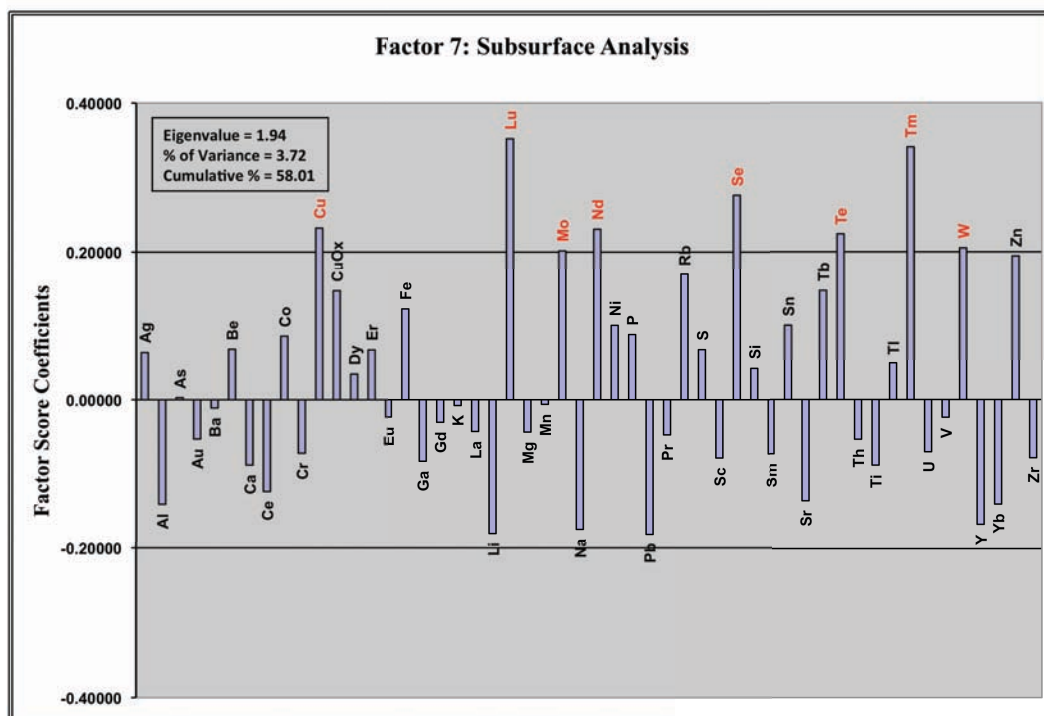


**Figure 2.50.** Factor 7 subsurface geochemical families (Red) indicated by factor score coefficients.

?

?

?

???

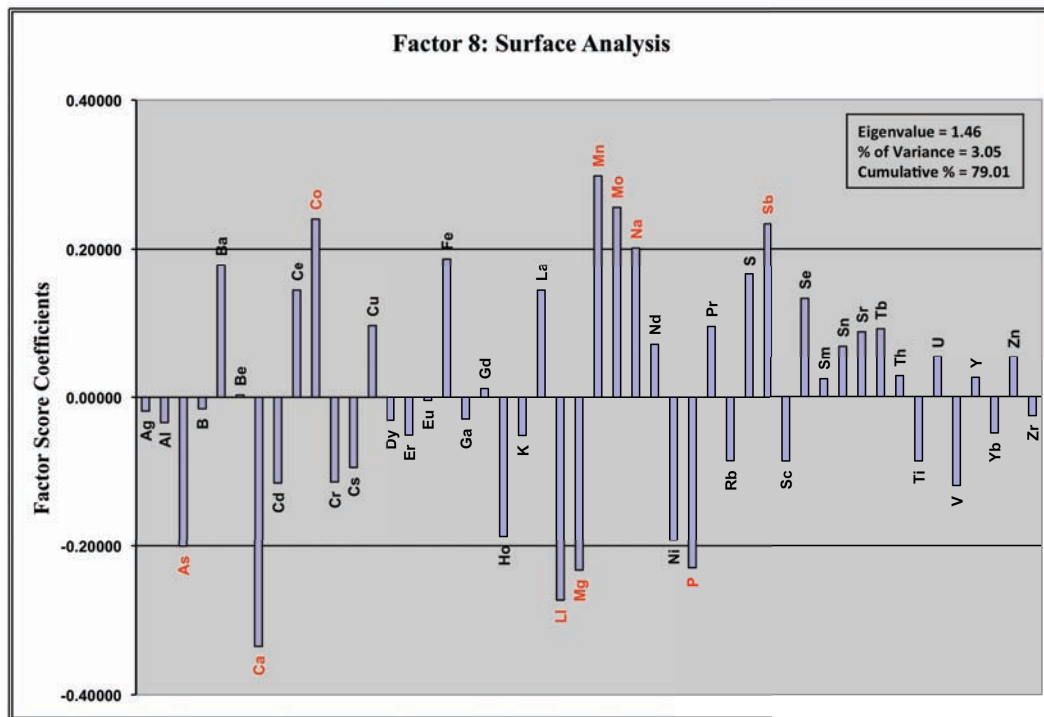


**Figure 2.51.** Factor 8 surface geochemical families (Red) indicated by factor score coefficients.

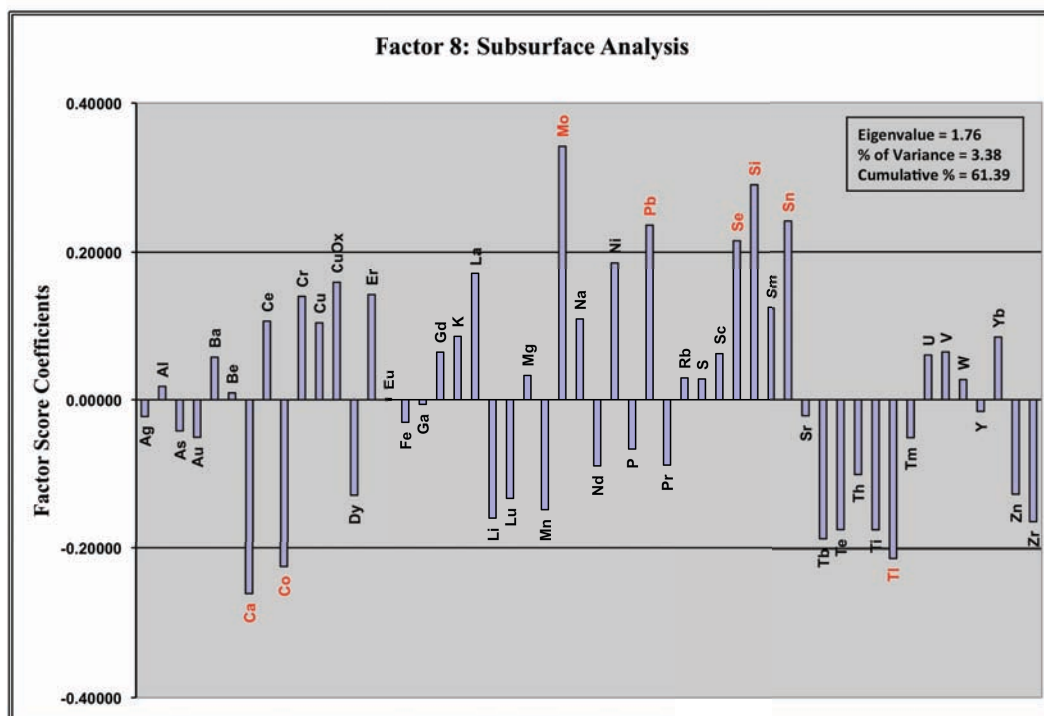


**Figure 2.52.** Factor 8 subsurface geochemical families (Red) indicated by factor score coefficients.

?

?

???

## 16.5. Appendix 2.5. Spatial Distribution of Factor Score Coefficients

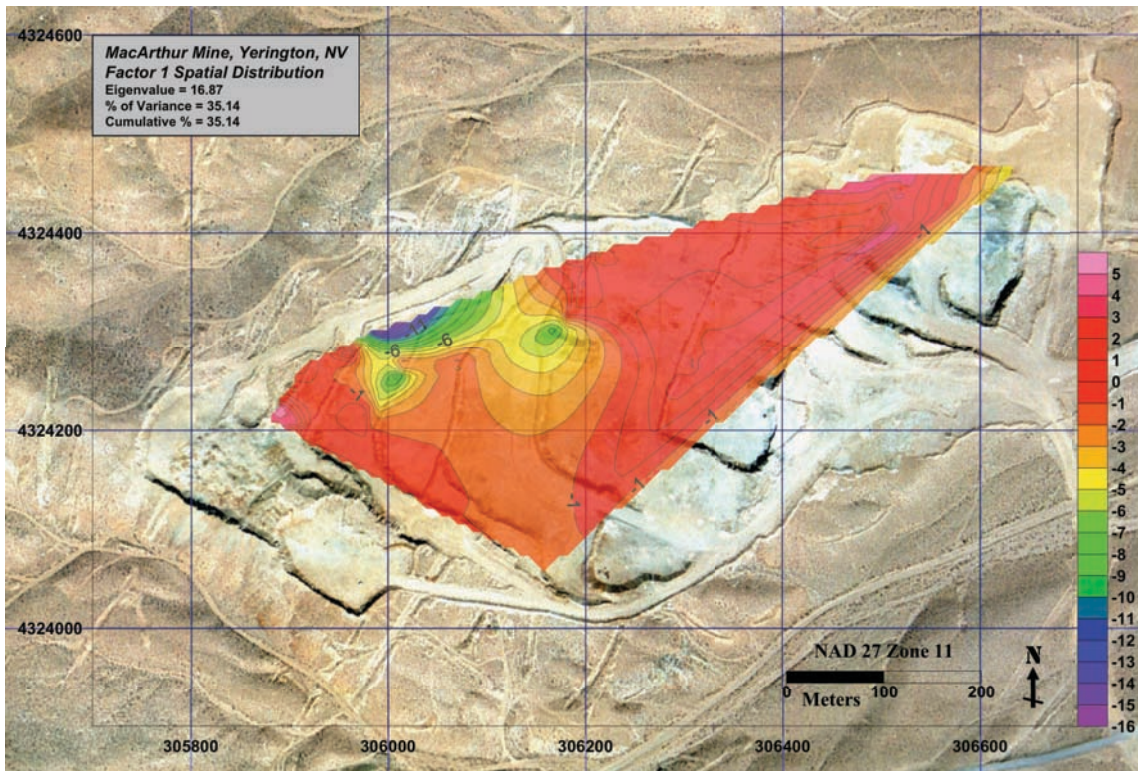


Figure 3.53. Factor 1 spatial distribution.

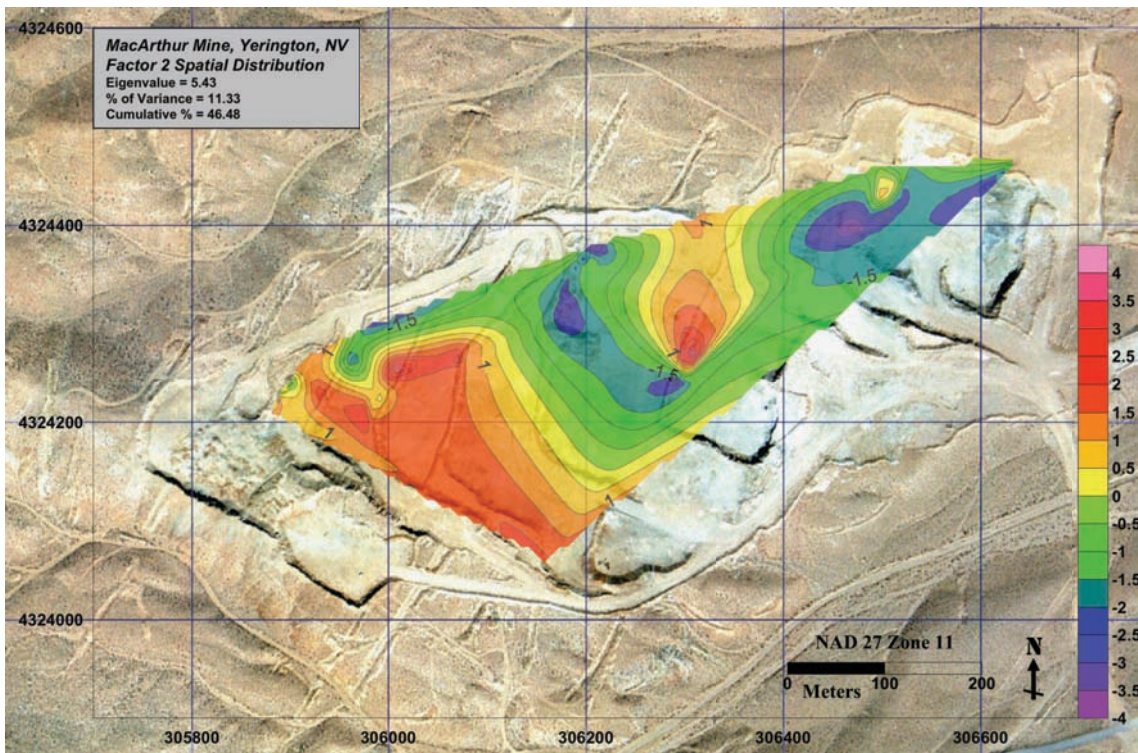


Figure 3.54. Factor 2 spatial distribution.

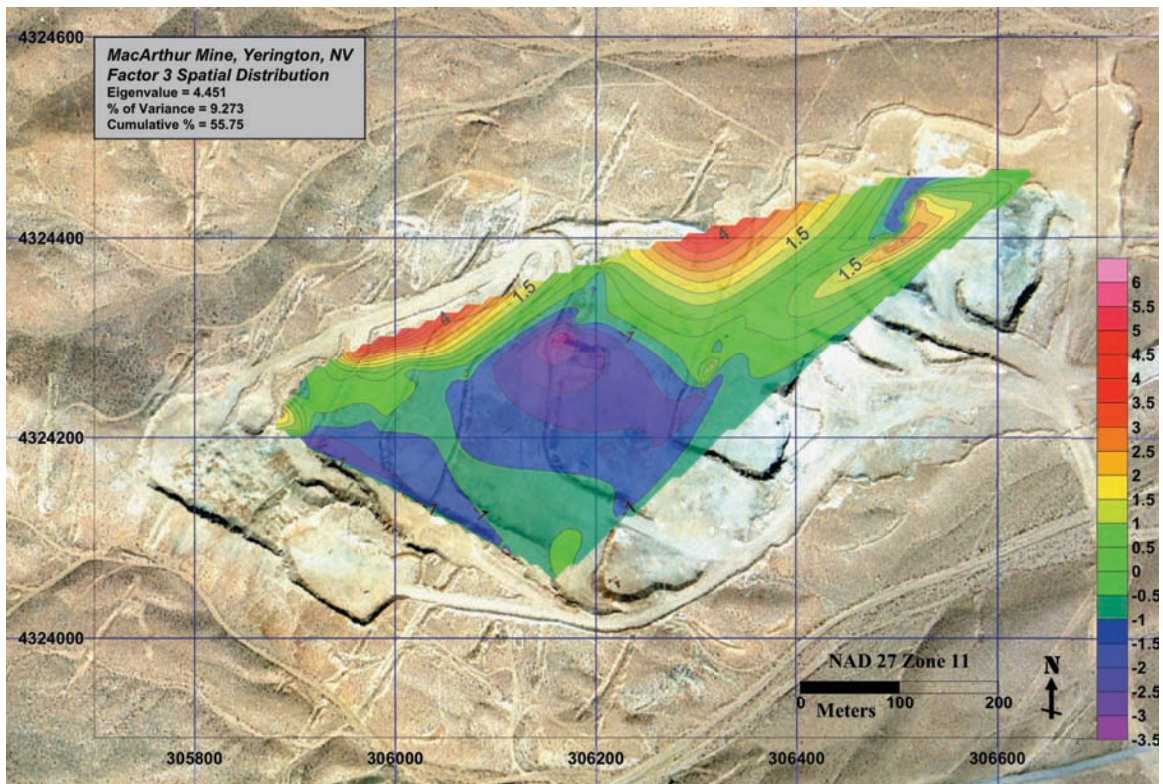


Figure 3.55 Factor 3 spatial distribution.

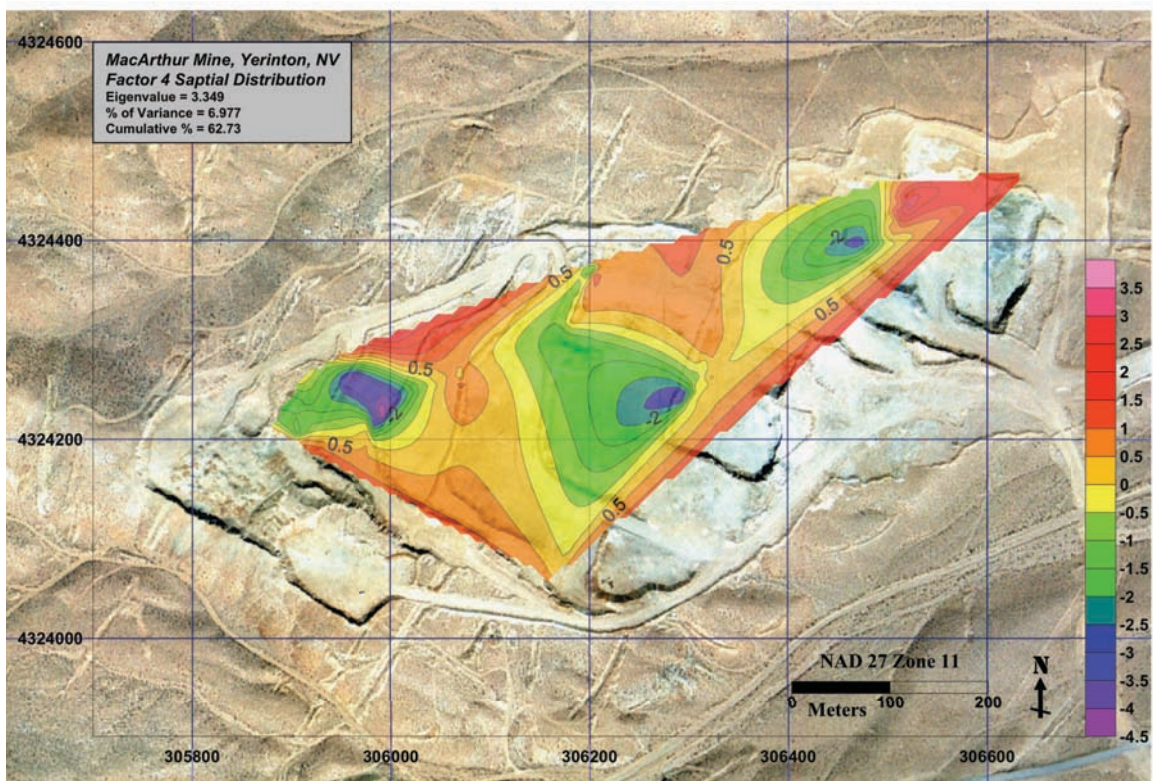


Figure 3.56. Factor 4 spatial distribution.

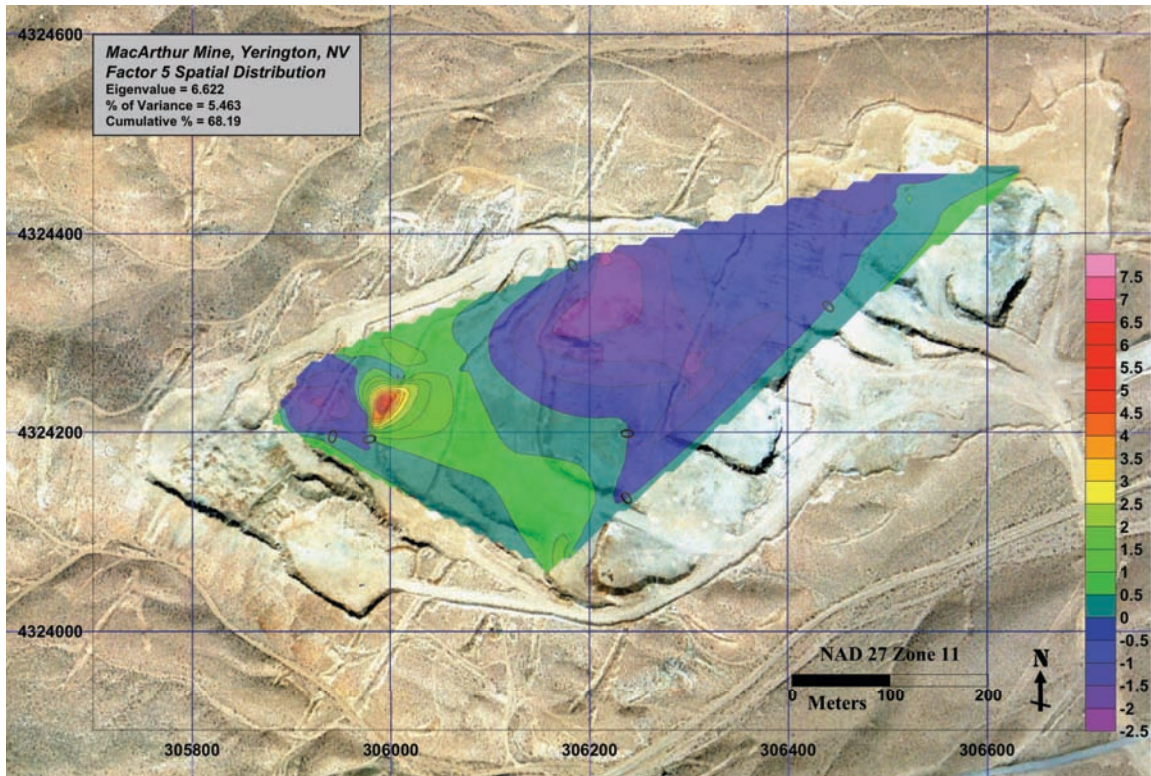


Figure 3.57. Factor 5 spatial distribution.

?

?

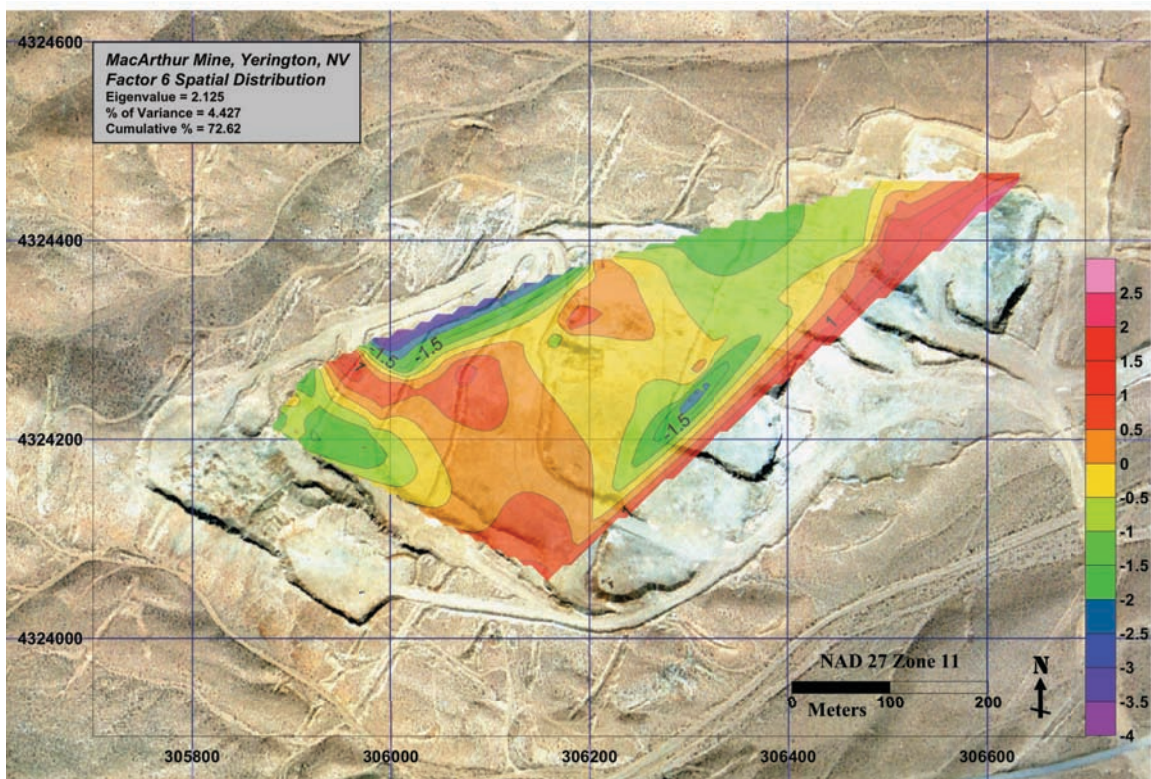


Figure 3.58. Factor 6 spatial distribution.

?

???

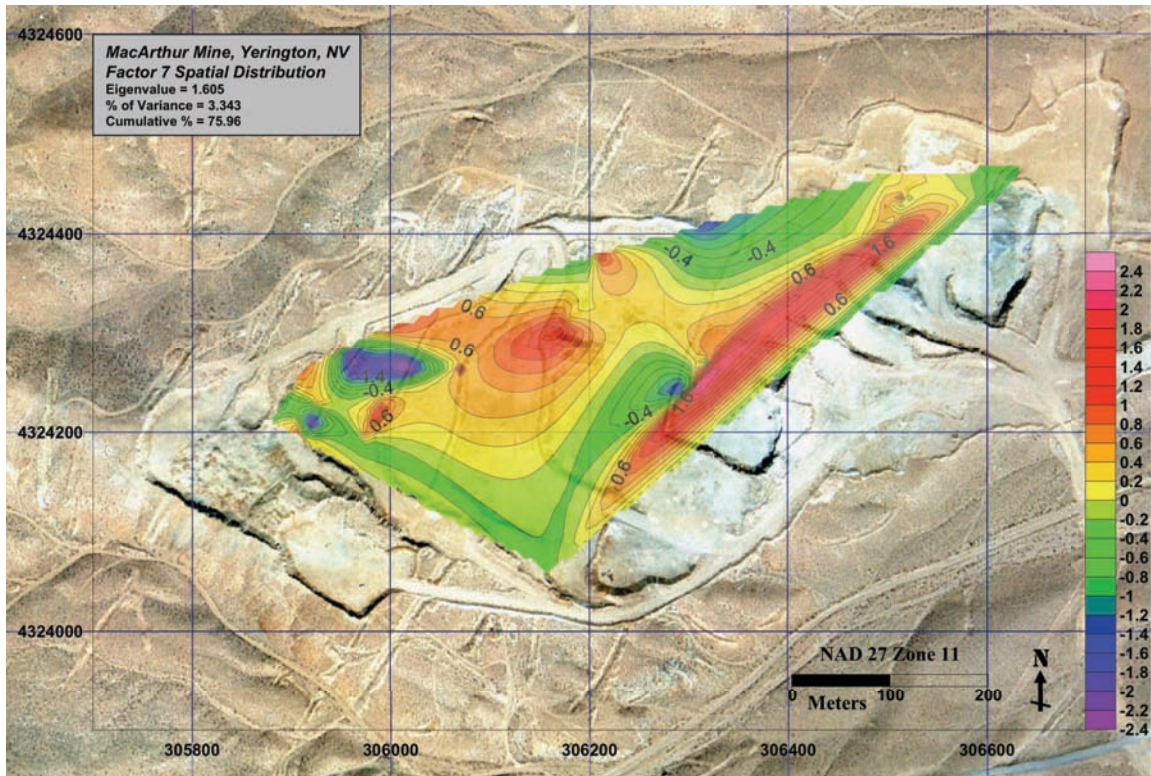


Figure 3.59. Factor 7 spatial distribution.

?

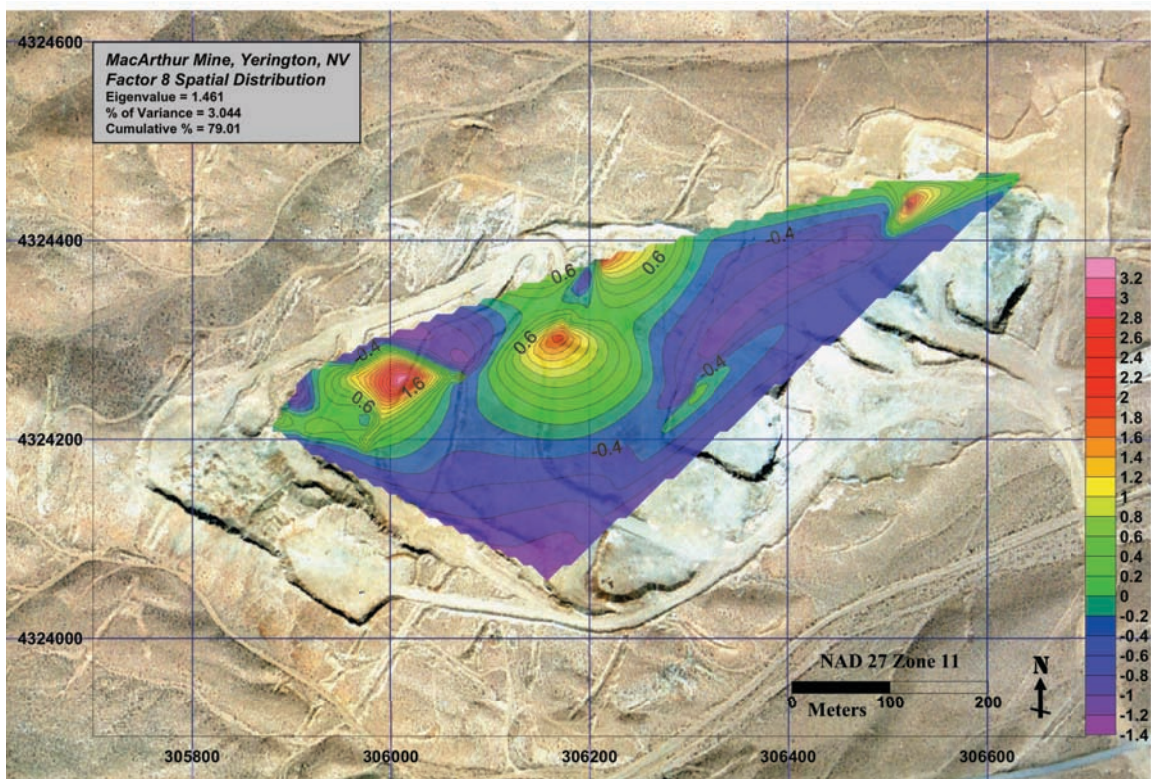


Figure 3.60. Factor 8 spatial distribution.

?

???

## 17. APPENDIX 3 – ELEMENT ABUNDANCE

Appendix 3 displays all contour maps of element distribution of surface sample data set. Contour maps showing element abundance for the surface data are created using Surfer by Golden Software (<http://www.goldensoftware.com/>).

	PAGE
17.1. Appendix 1.1 – Element Abundance Contour Maps	
Figures 3.1 – 3.6.....	215

## 17.1. Appendix 3.1. Element Abundance Contour Maps

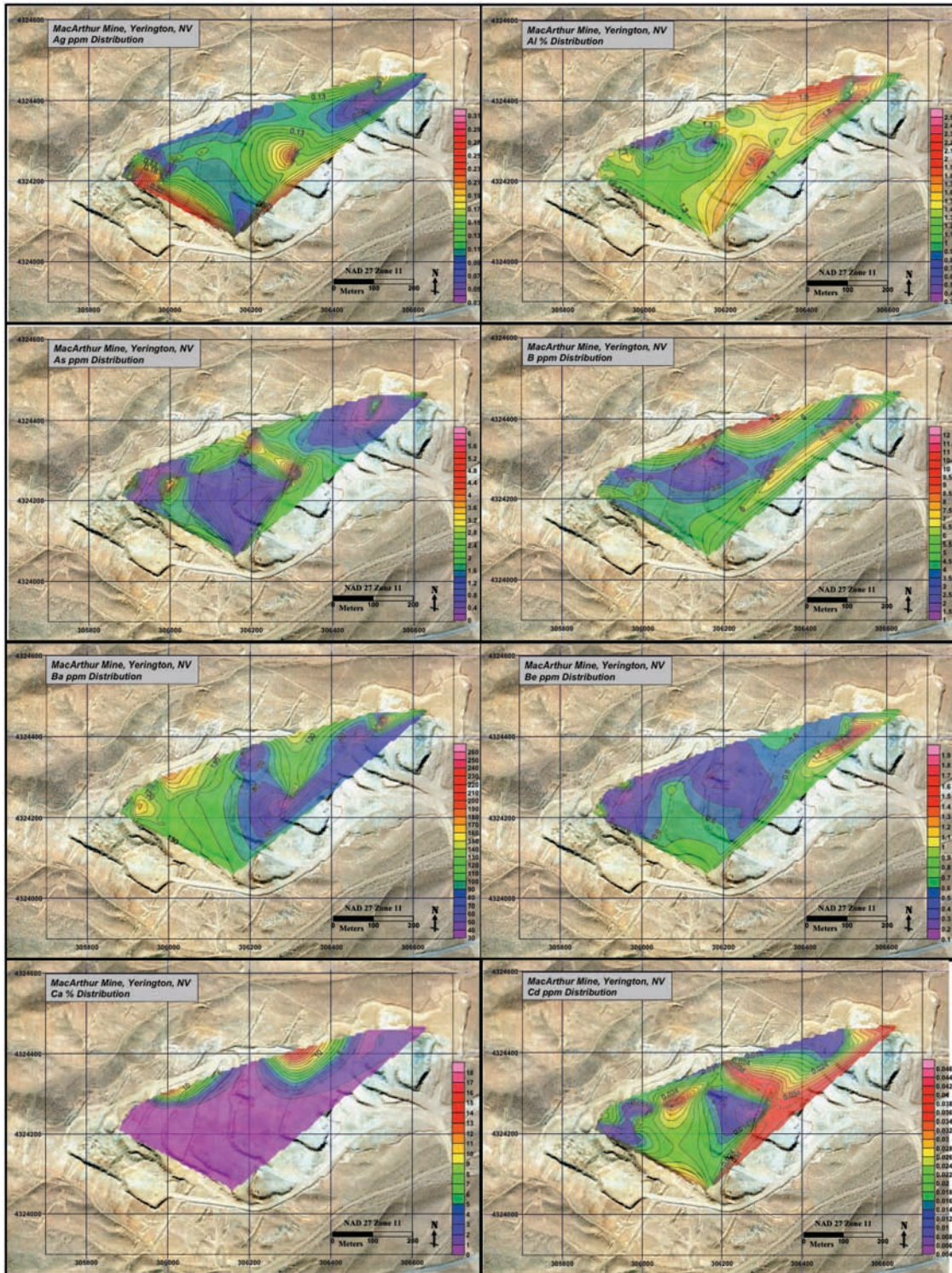


**Figure 3.1.** Contour maps of Ag, Al, As, B, Ba, Be, Ca, and Cd, MacArthur mine, Yerington Nevada.

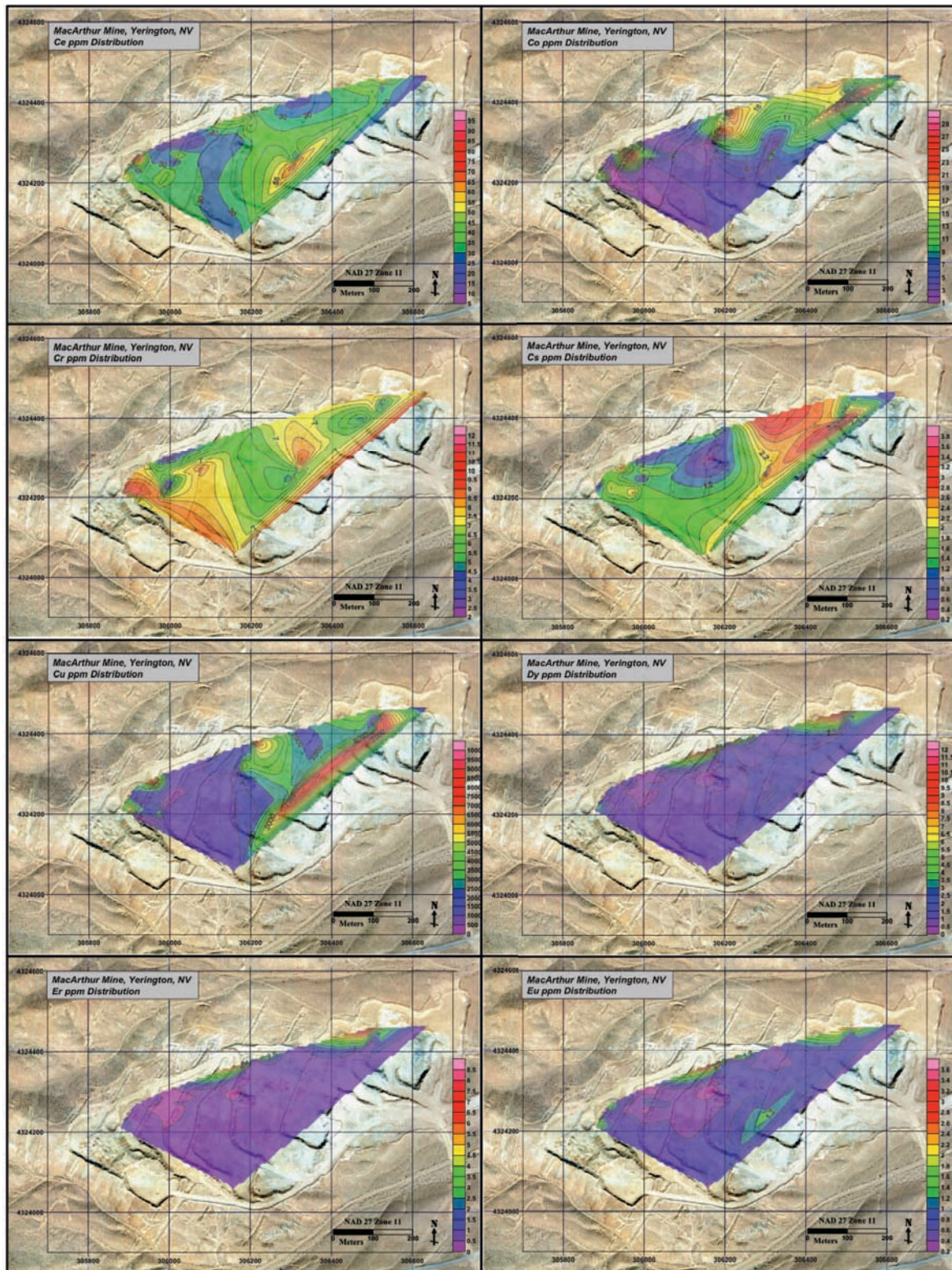


**Figure 3.2.** Contour maps of Ce, Co, Cr, Cs, Cu, Dy, Er, and Eu, MacArthur mine, Yerington Nevada.

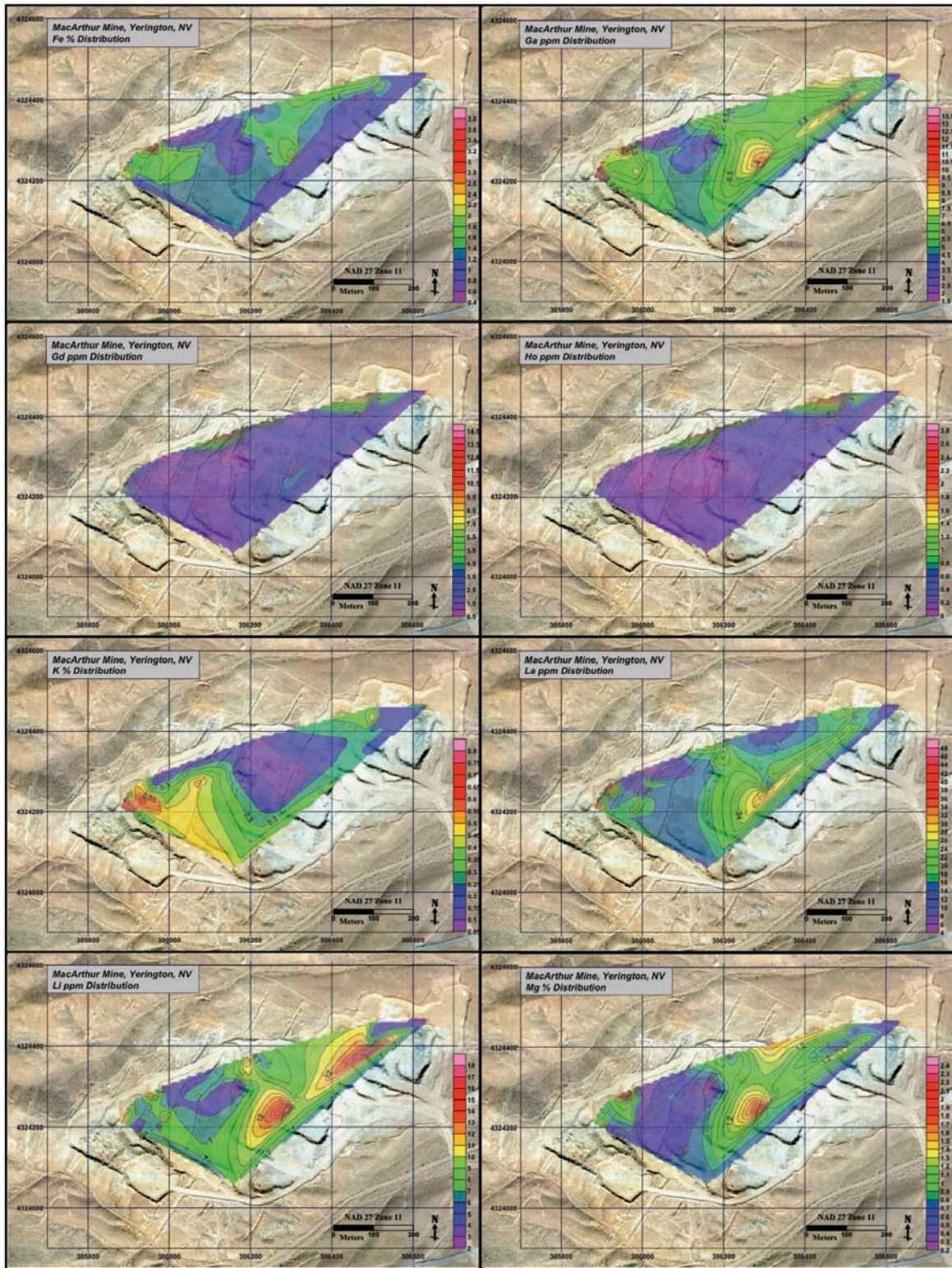


**Figure 3.3.** Contour maps of Fe, Ga, Gd, Ho, K, La, Li, and Mg, MacArthur mine, Yerington Nevada.

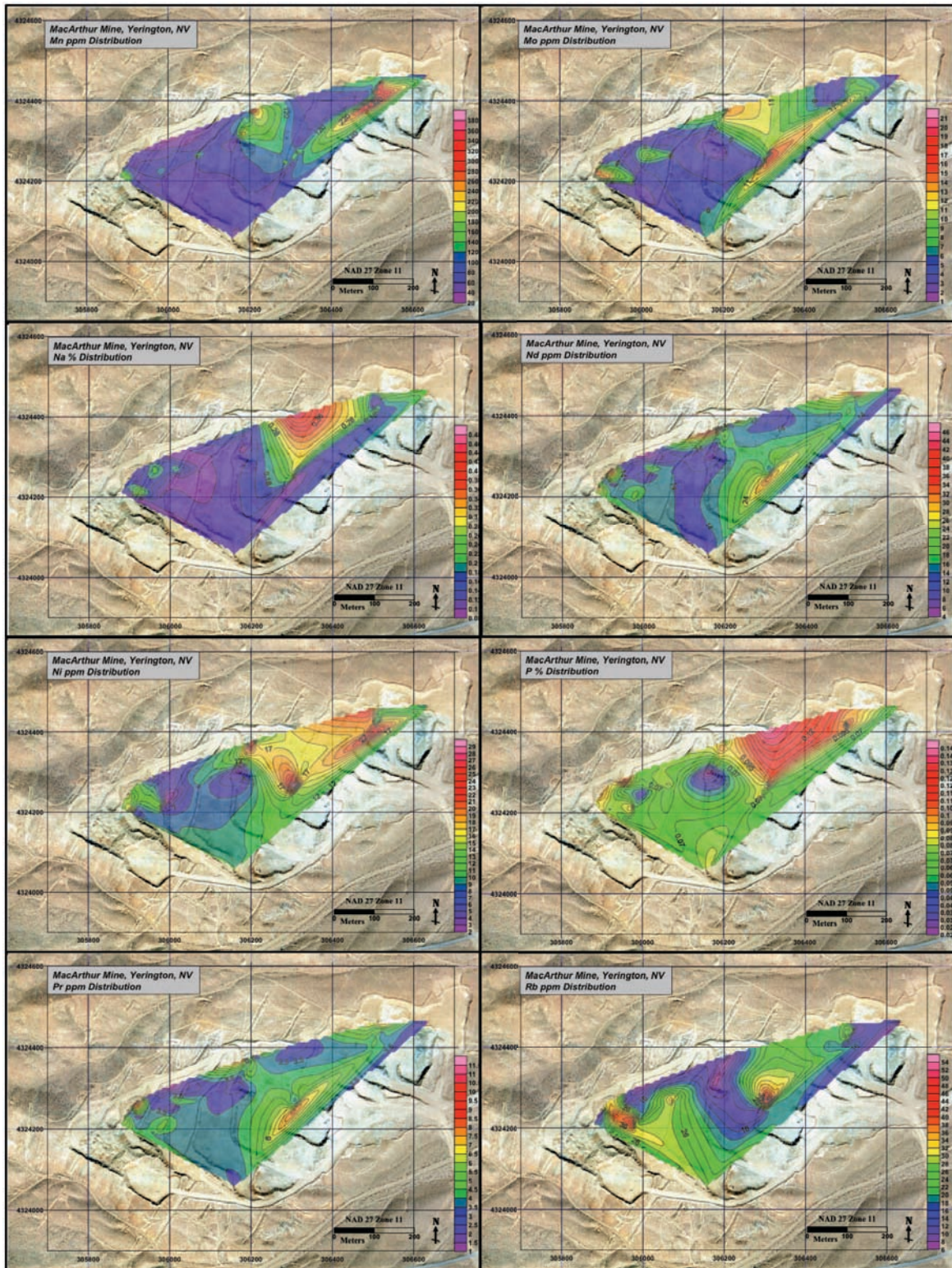


**Figure 3.4.** Contour maps of Mn, Mo, Na, Nd, Ni, P, Pr, and Rb, MacArthur mine, Yerington Nevada.

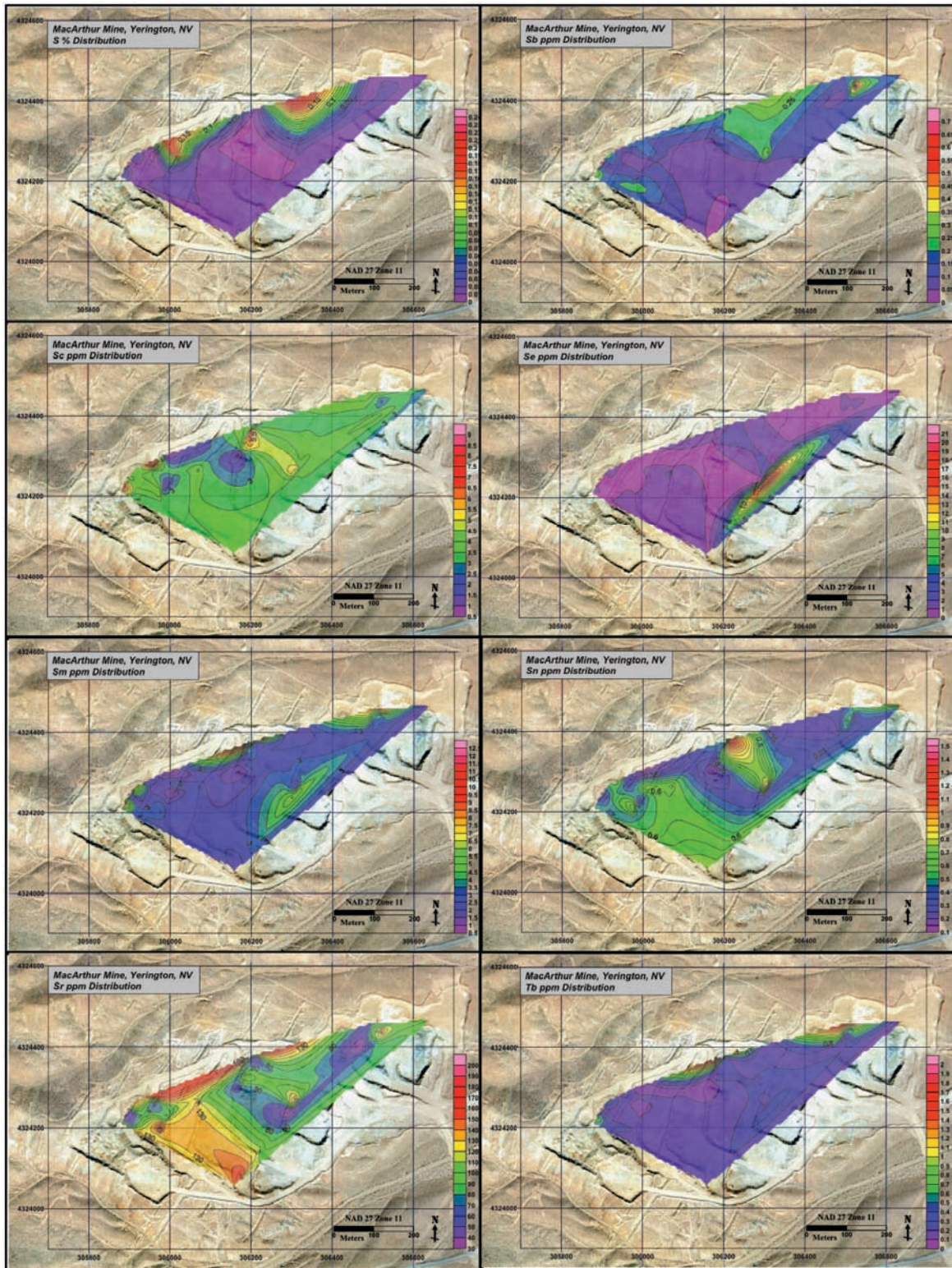


**Figure 3.5.** Contour maps of S, Sb, Sc, Se, Sm, Sn, Sr, and Tb, MacArthur mine, Yerington Nevada.

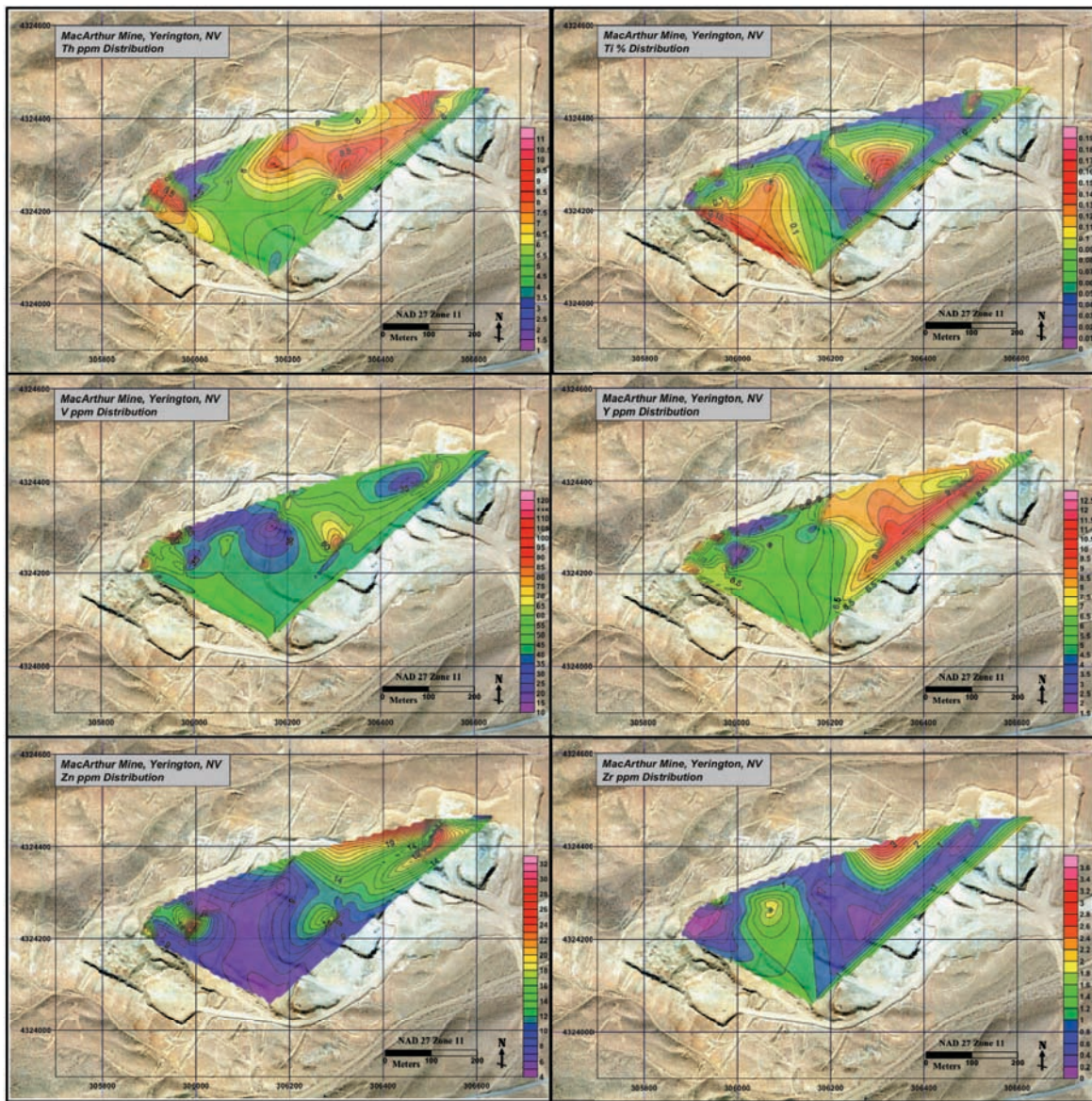


**Figure 3.6.** Contour maps of Th, Ti, V, Y, Zn, and Zr, MacArthur mine, Yerington Nevada.

## 18. APPENDIX 4 – SPECTRAL PROFILES

Appendix 4 displays all spectral profiles from homogeneity tests and 52 geochemical spectrum from surface samples collected in the MacArthur pit (figure 7.1). Spectral data is collected using the GER 3700 spectral radiometer. Appendix 4 also displays spectral profiles for minerals from USGS (<http://www.usgs.gov/>) and JPL (<http://www.jpl.nasa.gov/>) spectral libraries that Spectral Analyst identified in MacArthur spectrum. Appendix 3 is split into several sections:

	PAGE
18.1. Appendix 4.1. Spectral Profiles of 52 Geochemical Samples	
Figures 4.1 – 4.52 .....	223
Spectral profiles of 52 geochemical spectrum from samples collected in the MacArthur pit. Wavelength is the x-axis and percent reflectance is the y-axis.	
18.2. Appendix 4.2. Spectral Profiles of QMP-4780	
Figures 4.53 – 4.55 .....	249
Spectral profiles of QMP-4780 homogeneity test. Wavelength is the x-axis and percent reflectance is the y-axis.	
18.3. Appendix 4.3. Spectral Profiles of QMP-4750	
Figures 4.56 – 4.60 .....	251
Spectral profiles of QMP-4750 homogeneity test. Wavelength is the x-axis and percent reflectance is the y-axis.	
18.4. Appendix 4.4. Spectral Profiles of QMP-4600	
Figures 4.61 – 4.69 .....	254
Spectral profiles of QMP-4600 homogeneity test. Wavelength is the x-axis and percent reflectance is the y-axis.	
18.5. Appendix 3.5. Spectral Profiles of RHY-4700	
Figures 4.70 – 4.78 .....	259
Spectral profiles of RHY-4700 homogeneity test. Wavelength is the x-axis and percent reflectance is the y-axis.	
18.6. Appendix 4.6. Spectral Profiles of RHY-4675	
Figures 4.79 – 4.87 .....	264
Spectral profiles of RHY-4675 homogeneity test. Wavelength is the x-axis and percent reflectance is the y-axis.	
18.7. Appendix 4.7. Spectral Profiles from USGS Spectral Library	
Figures 4.88 – 4.106 .....	269
Spectral profiles of 19 minerals from the USGS spectral library indentified to have common absorption features with MacArthur pit samples using ENVI Spectral Analyst tool. Wavelength is the x-axis and percent reflectance is the y-axis.	

	PAGE
18.8. Appendix 4.8. Spectral Profiles from JPL Spectral Library	
Figures 4.107 – 4.126 .....	279
Spectral profiles of 20 minerals from the JPL spectral library indentified to have common absorption features with MacArthur pit samples using ENVI Spectral Analyst tool. Wavelength is the x-axis and percent reflectance is the y-axis.	

### 18.1. Appendix 4.1. Spectral Profiles of 52 Geochemical Samples

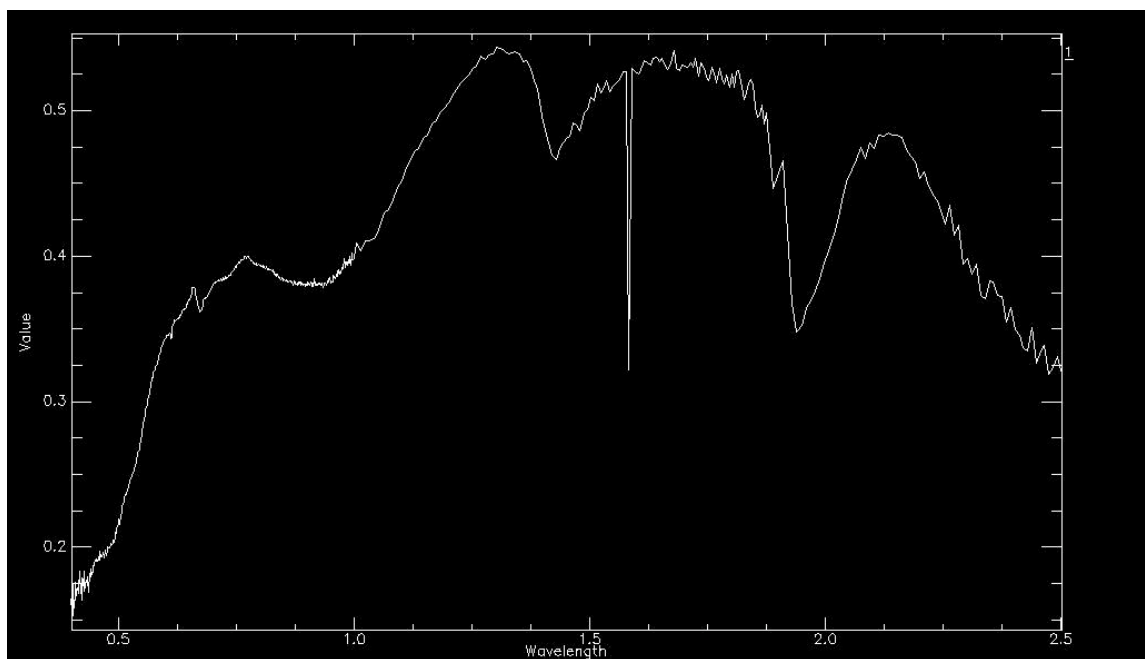


**Figure 4.1.** Spectral profile of sample 1.

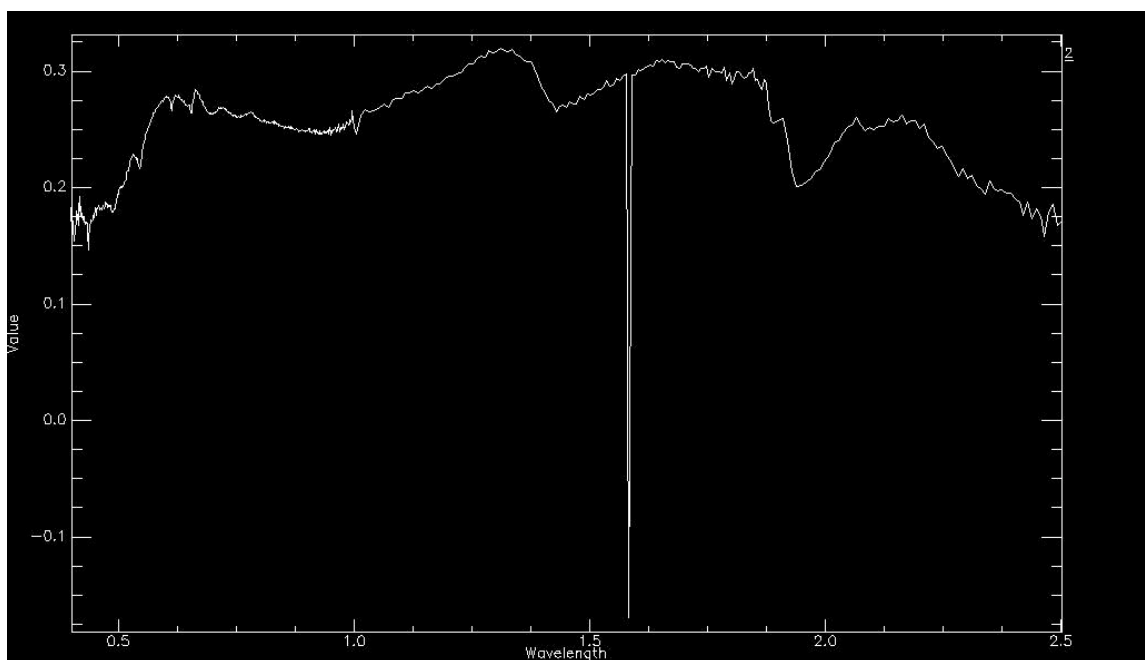


**Figure 4.2.** Spectral profile of sample 2.

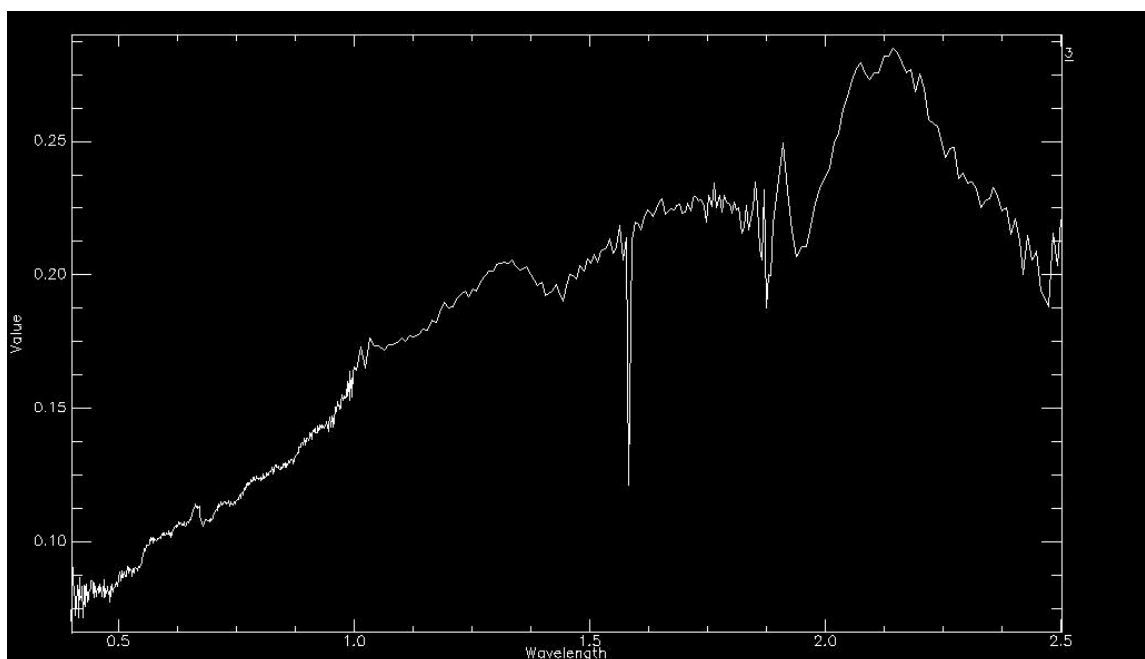


**Figure 4.3.** Spectral profile of sample 3.

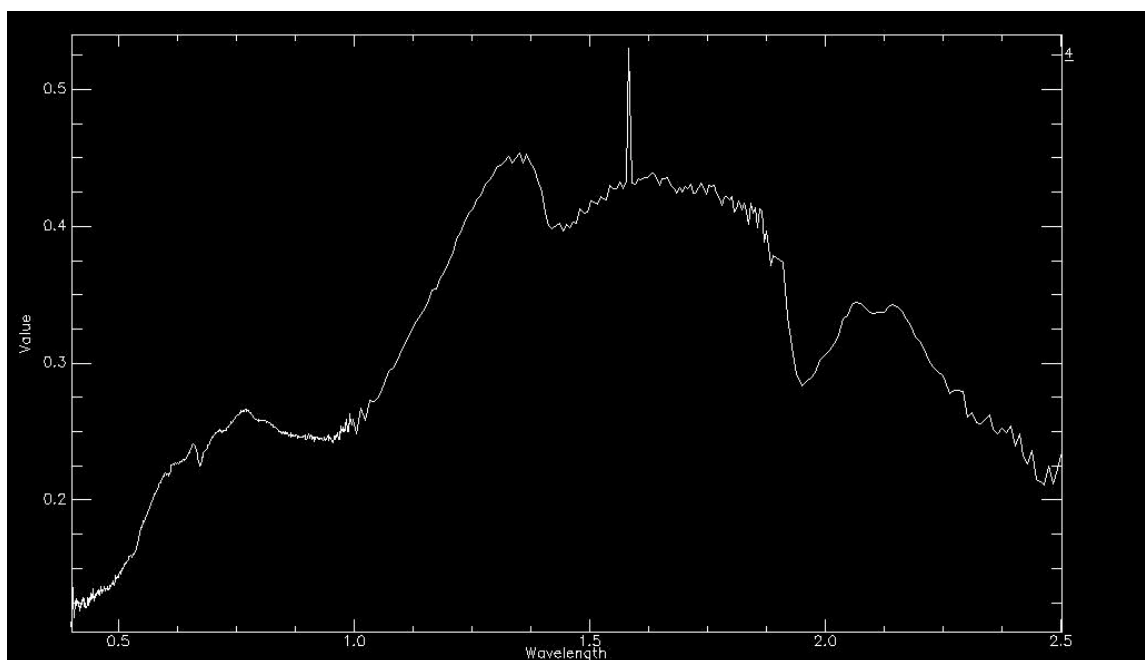


**Figure 4.4.** Spectral profile of sample 4.

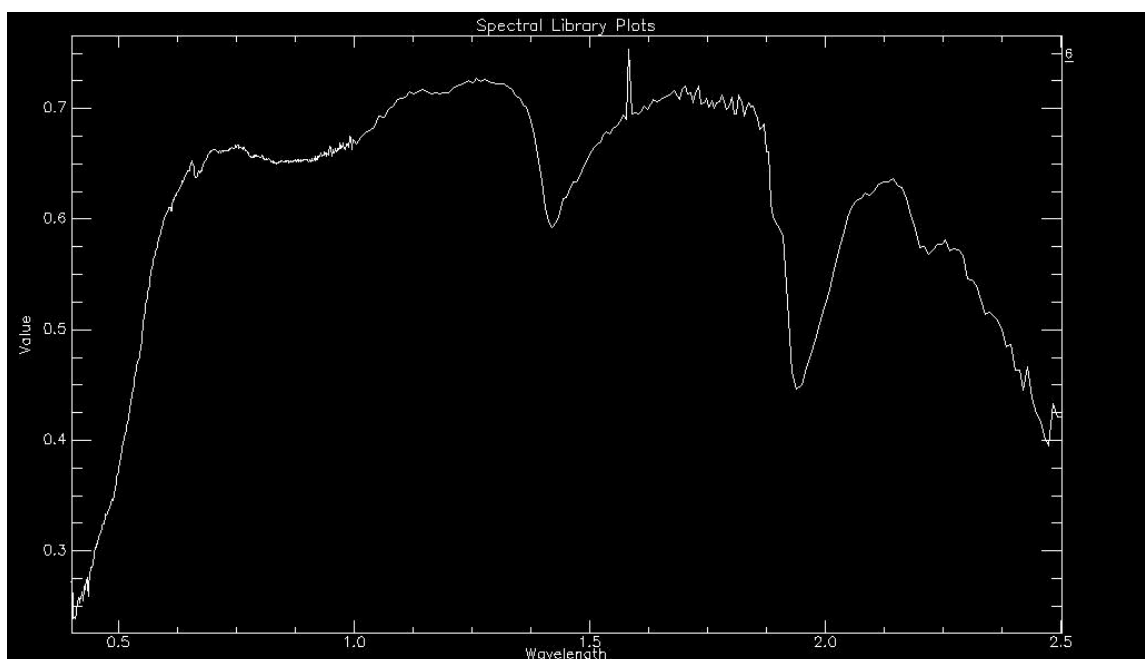


**Figure 4.5.** Spectral profile of sample 6.

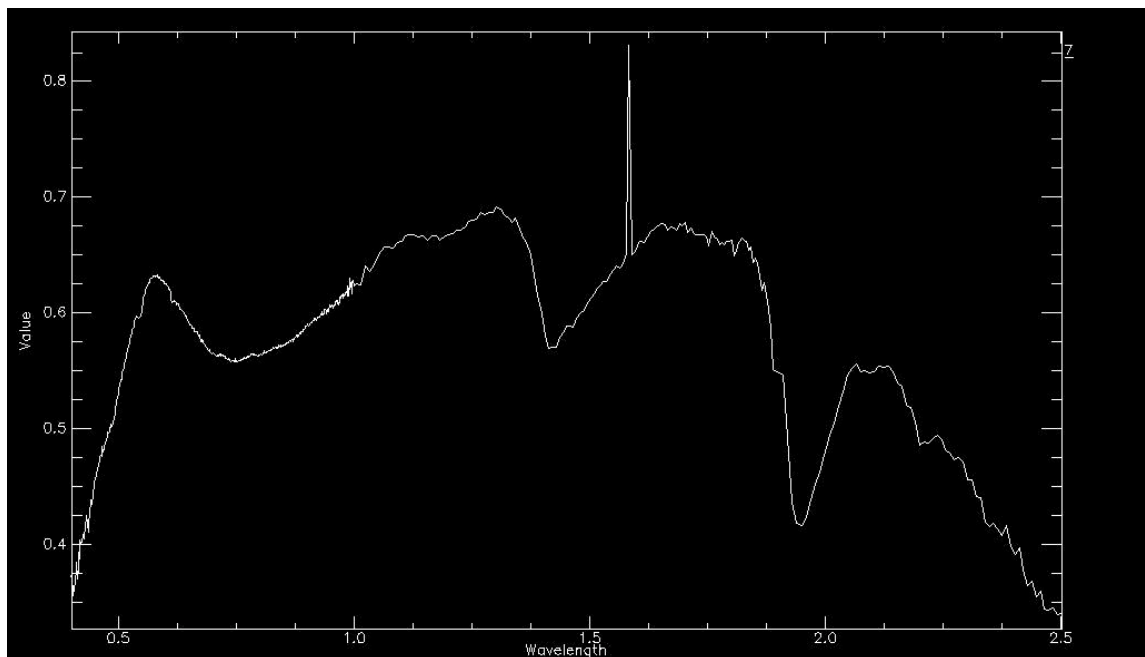


**Figure 4.6.** Spectral profile of sample 7.

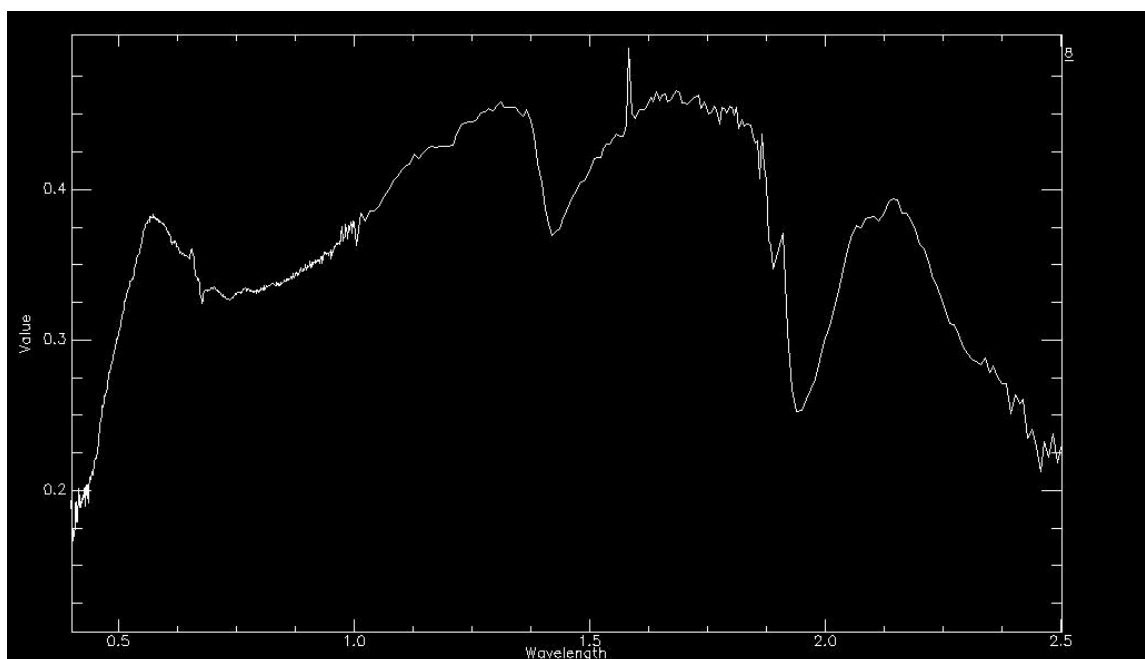


**Figure 4.7.** Spectral profile of sample 8.

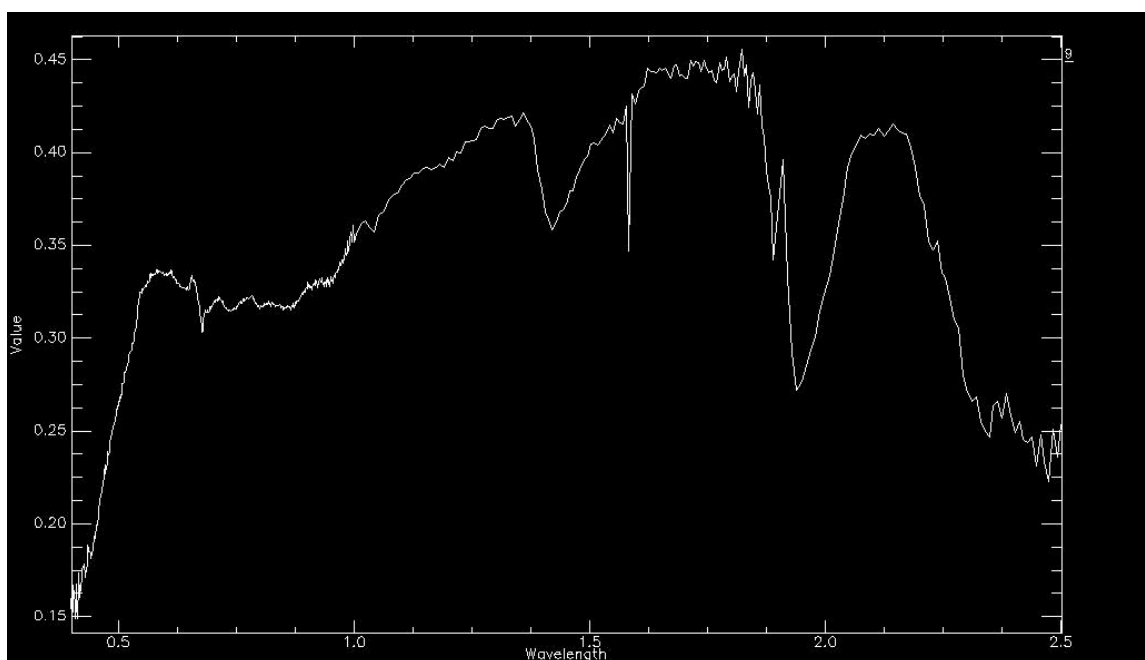


**Figure 4.8.** Spectral profile of sample 9.

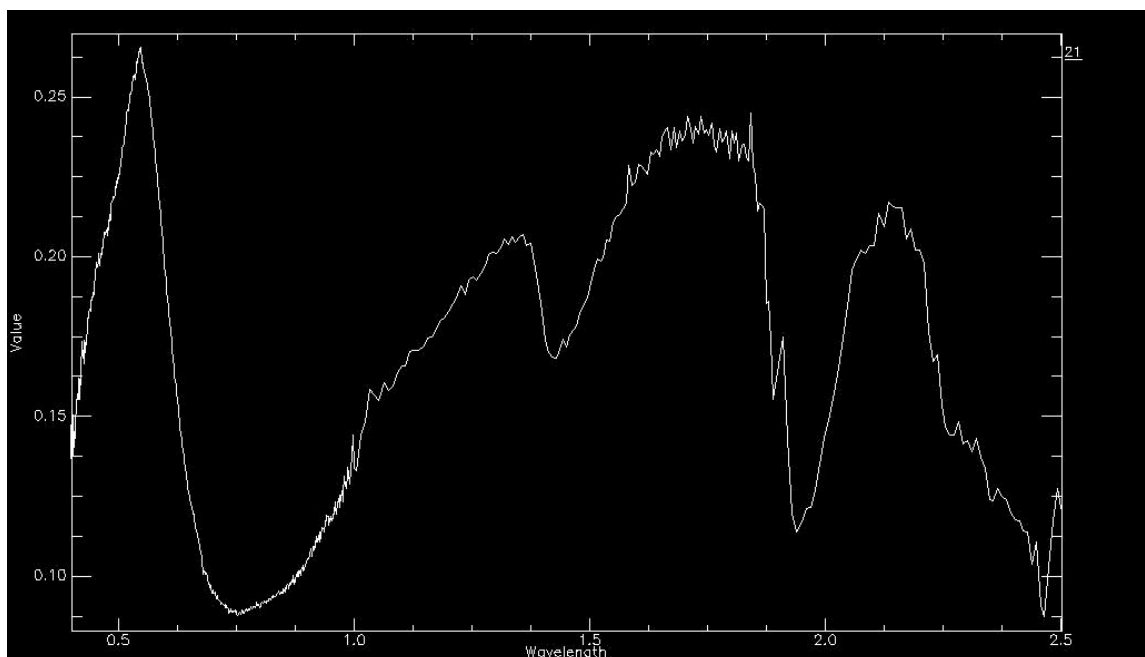


**Figure 4.9.** Spectral profile of sample 21.

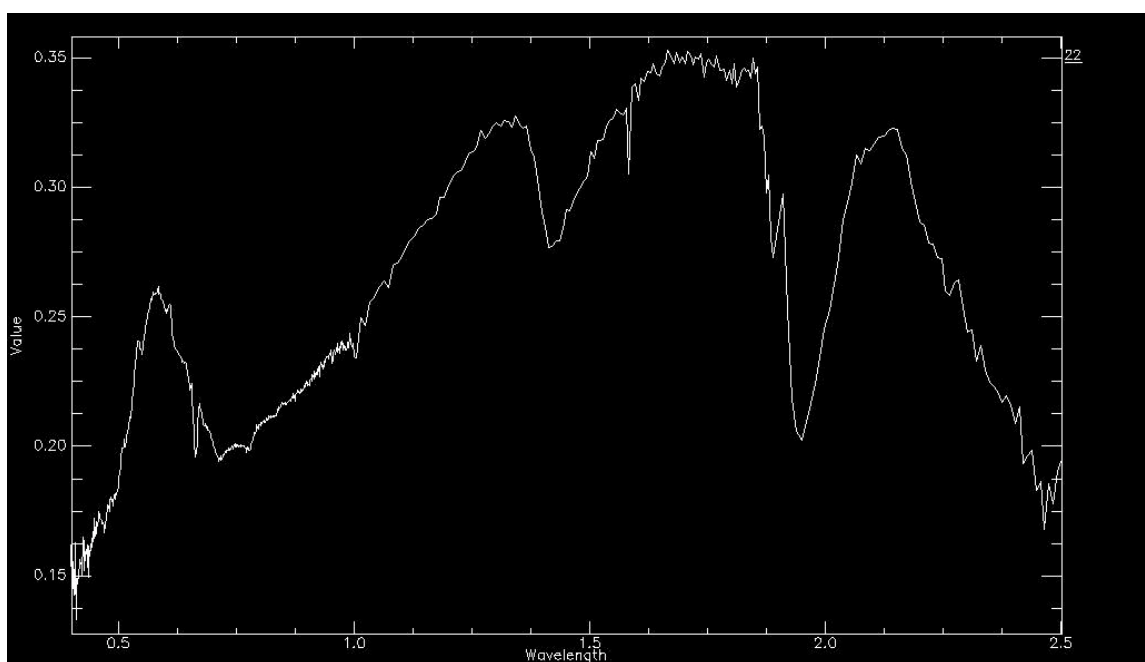


**Figure 4.10.** Spectral profile of sample 22.

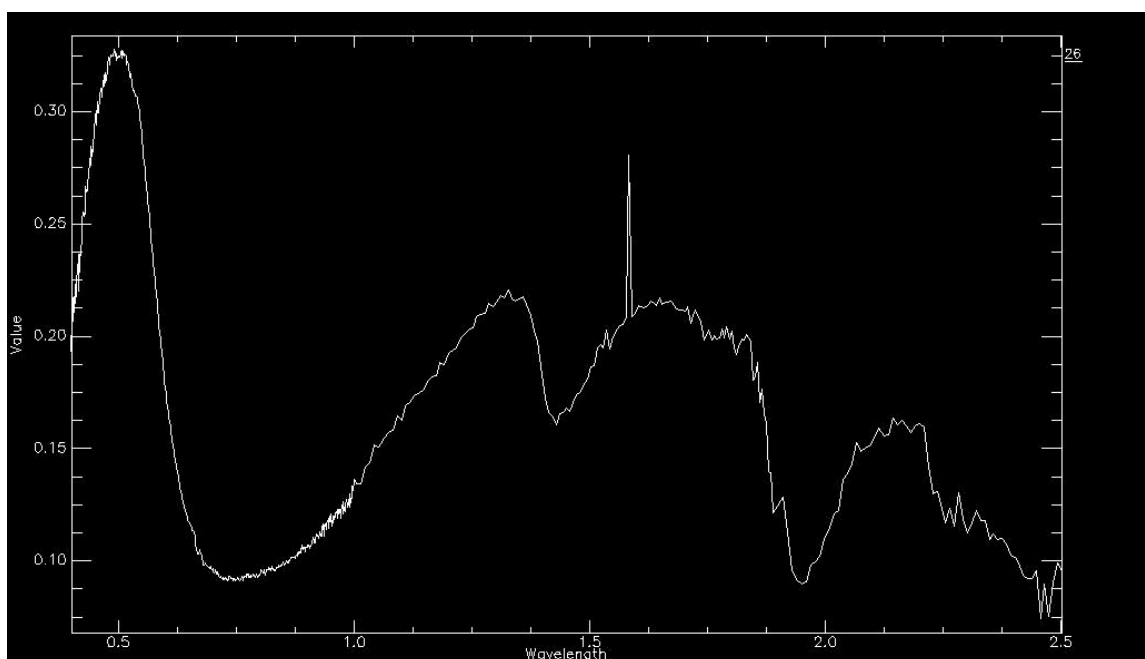


**Figure 4.11.** Spectral profile of sample 26.

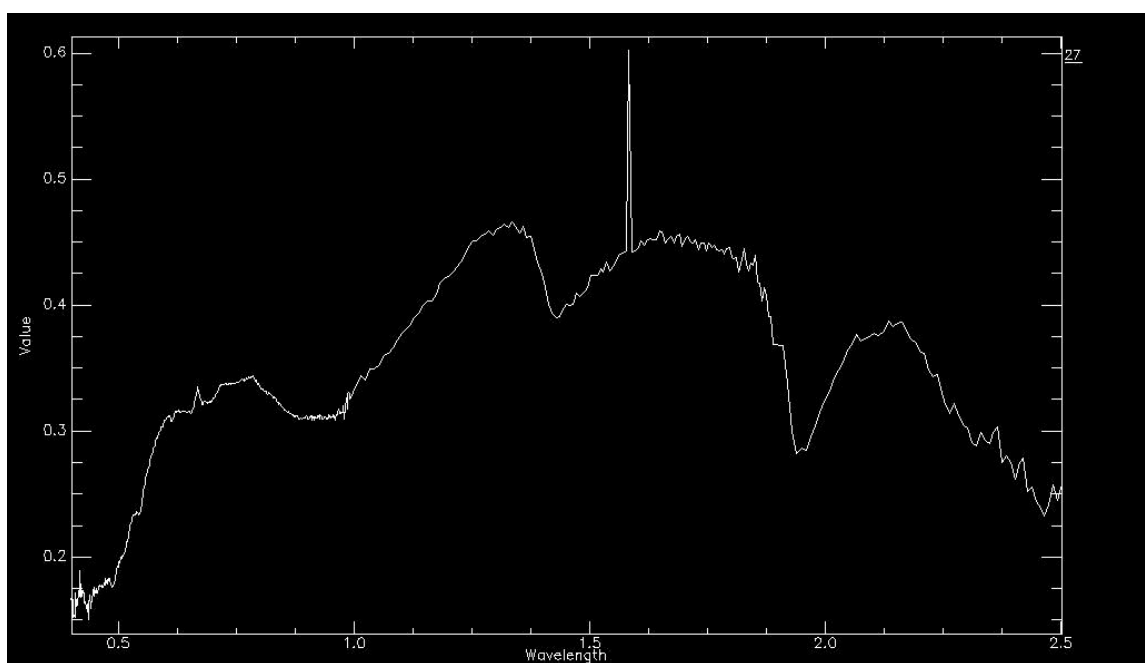


**Figure 4.12.** Spectral profile of sample 27.

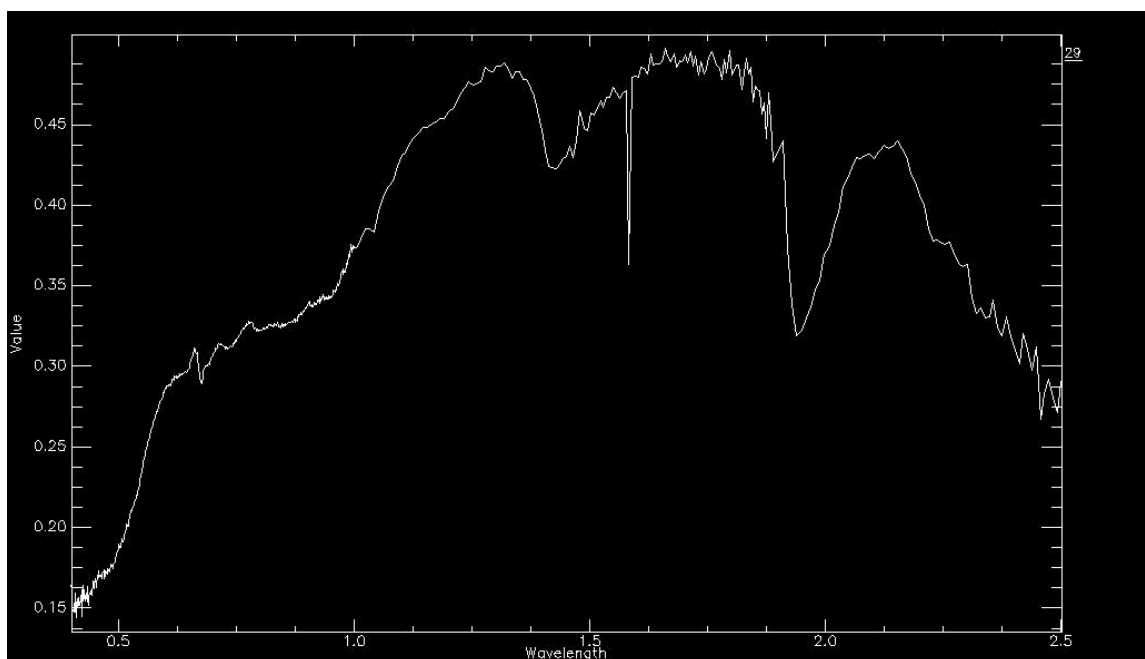


**Figure 4.13.** Spectral profile of sample 29.

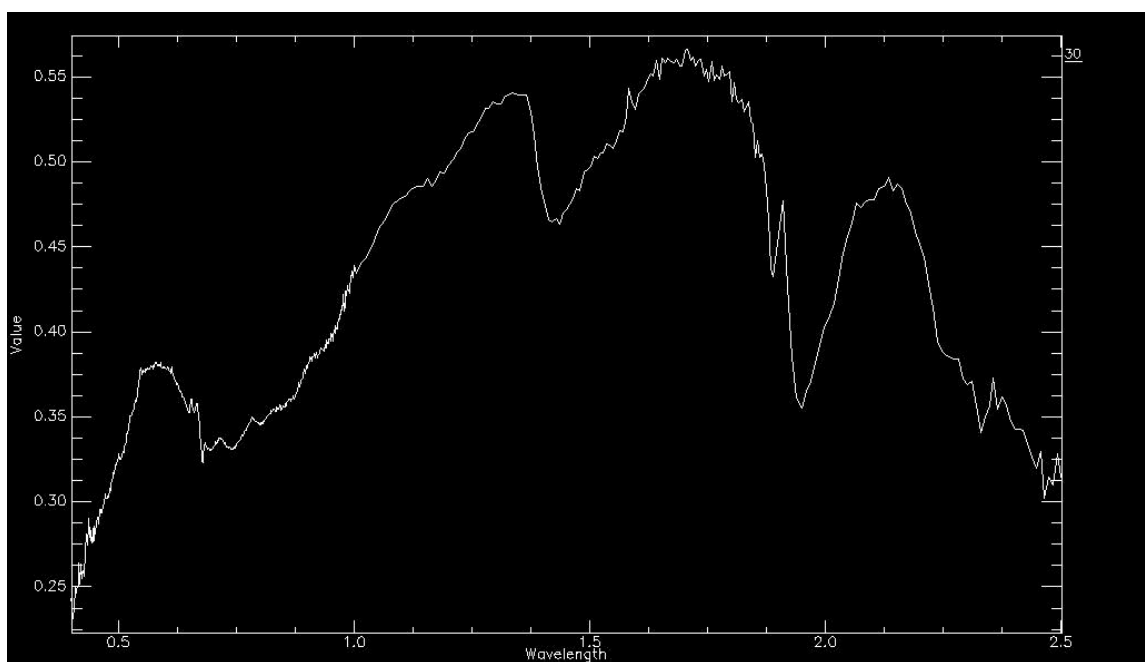


**Figure 4.14.** Spectral profile of sample 30.

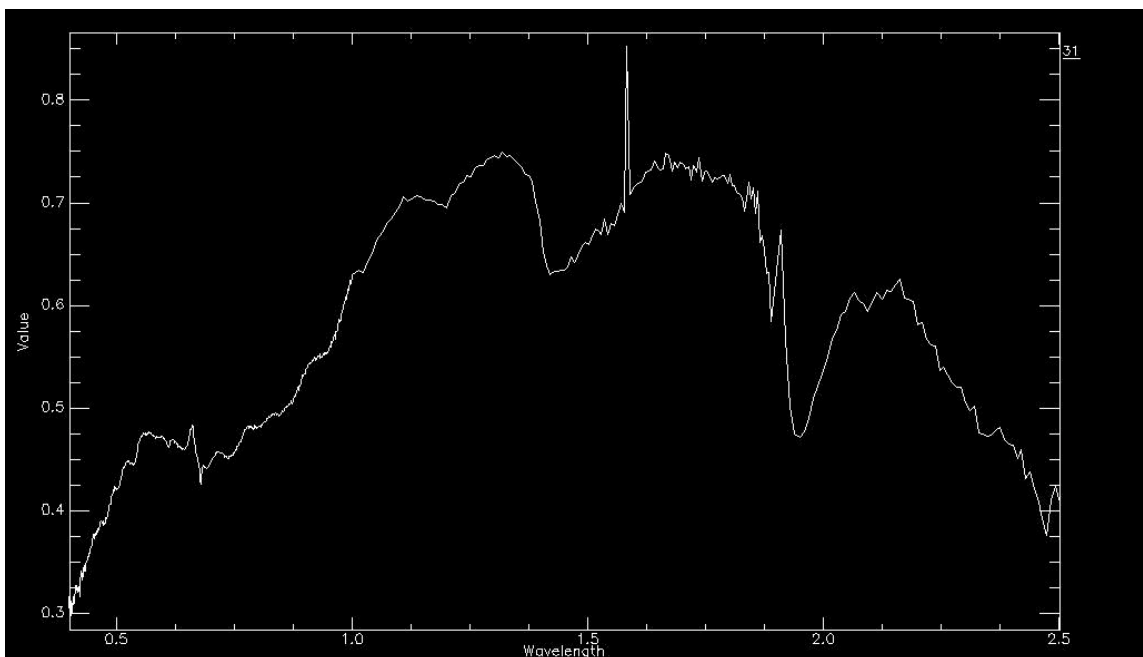


**Figure 4.15.** Spectral profile of sample 31.

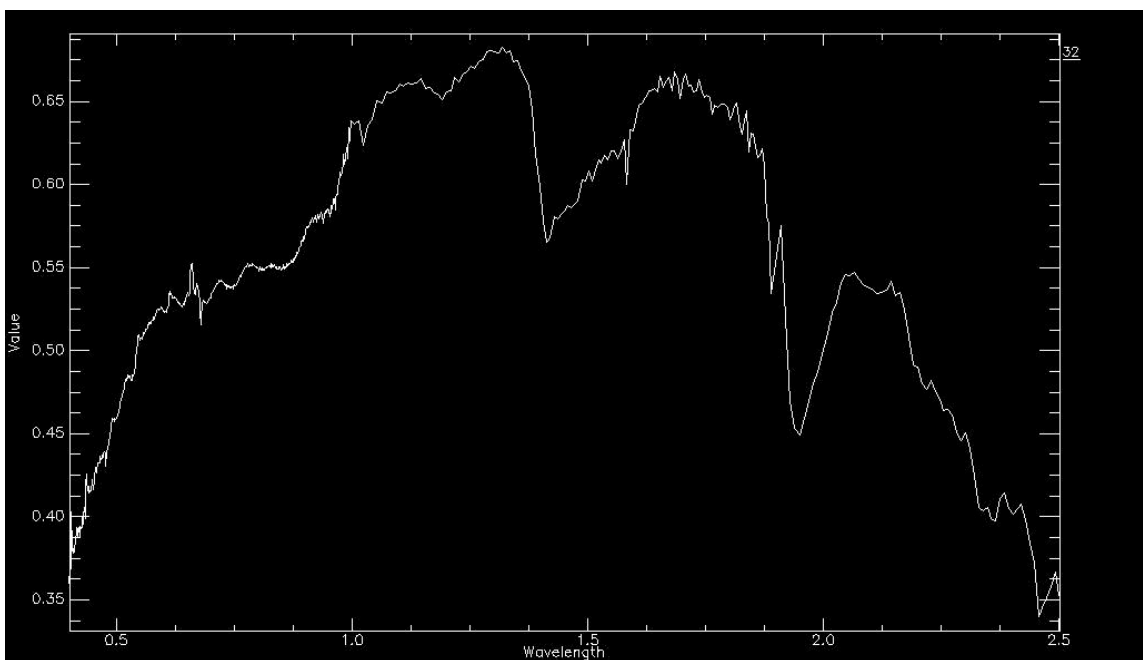


**Figure 4.16.** Spectral profile of sample 32.

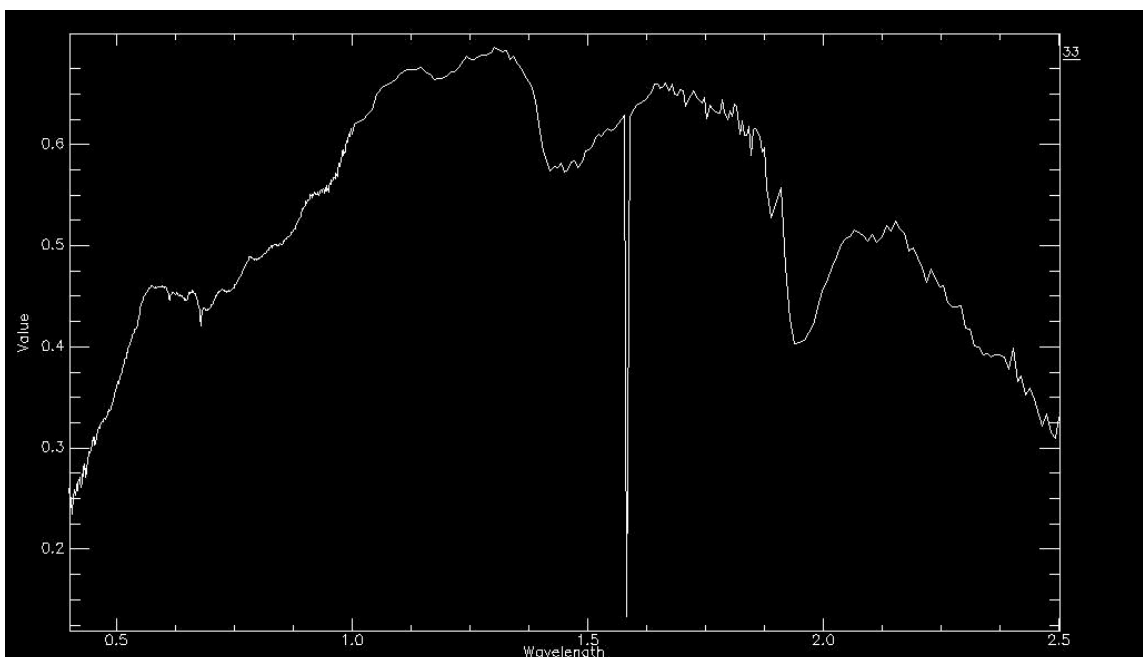


**Figure 4.17.** Spectral profile of sample 33.

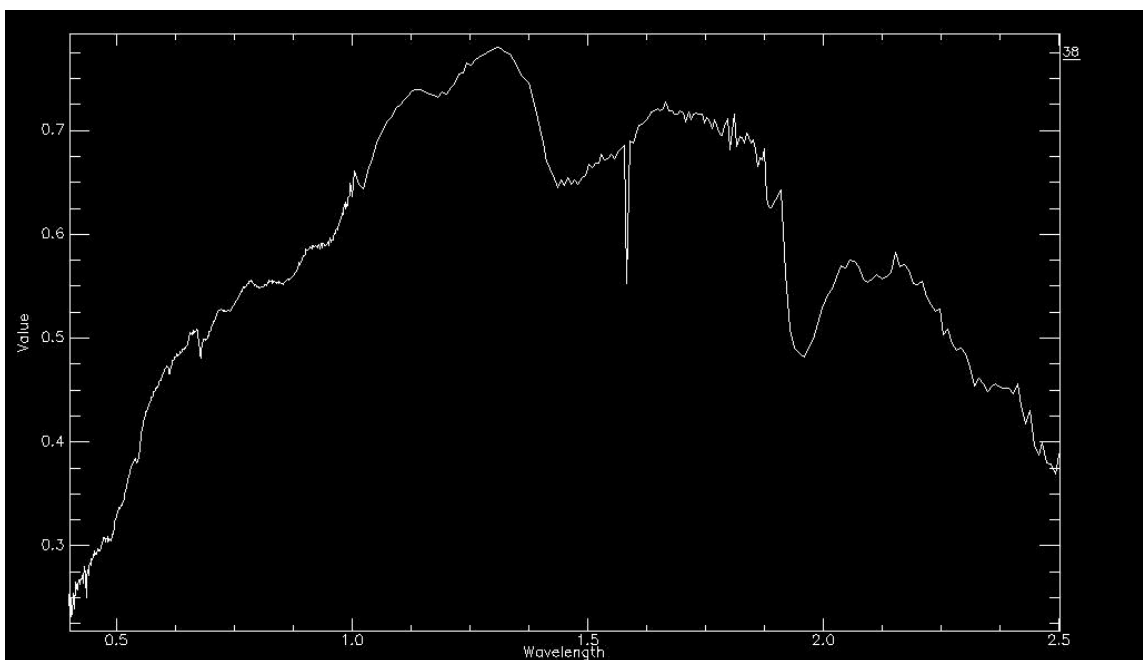


**Figure 4.18.** Spectral profile of sample 38.

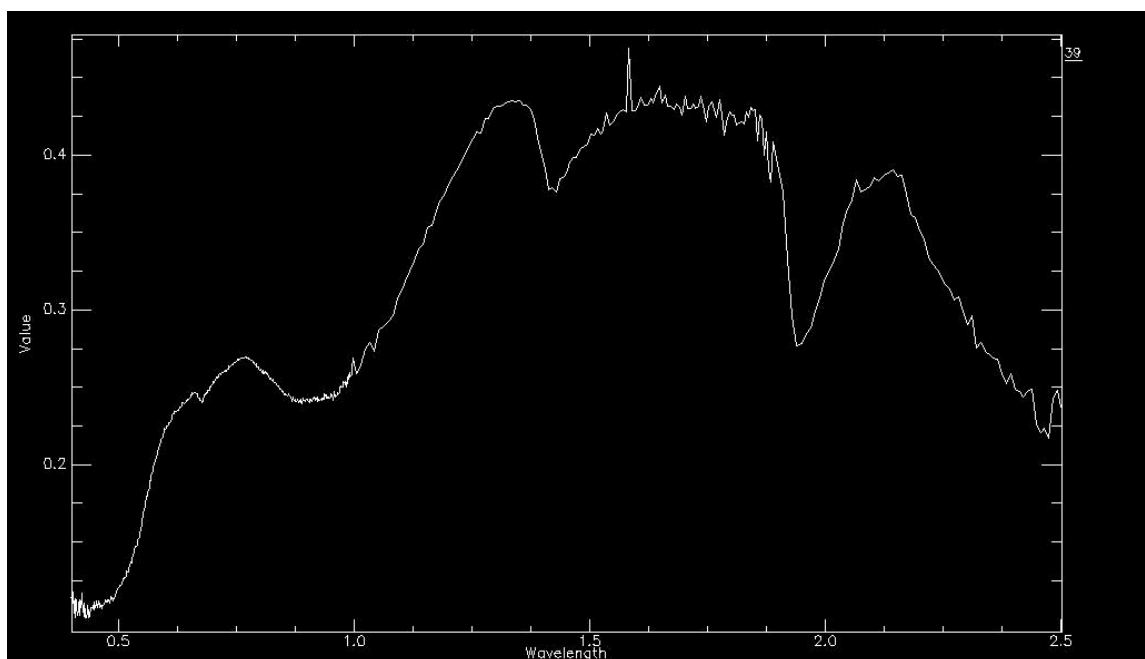


**Figure 4.19.** Spectral profile of sample 39.

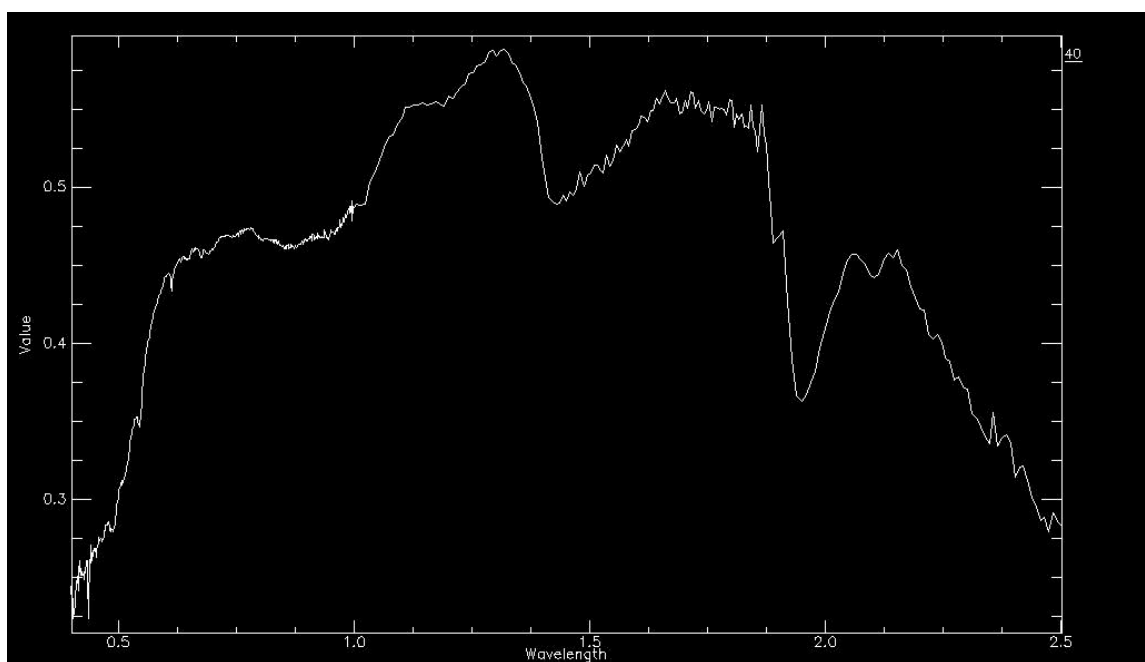


**Figure 4.20.** Spectral profile of sample 40.

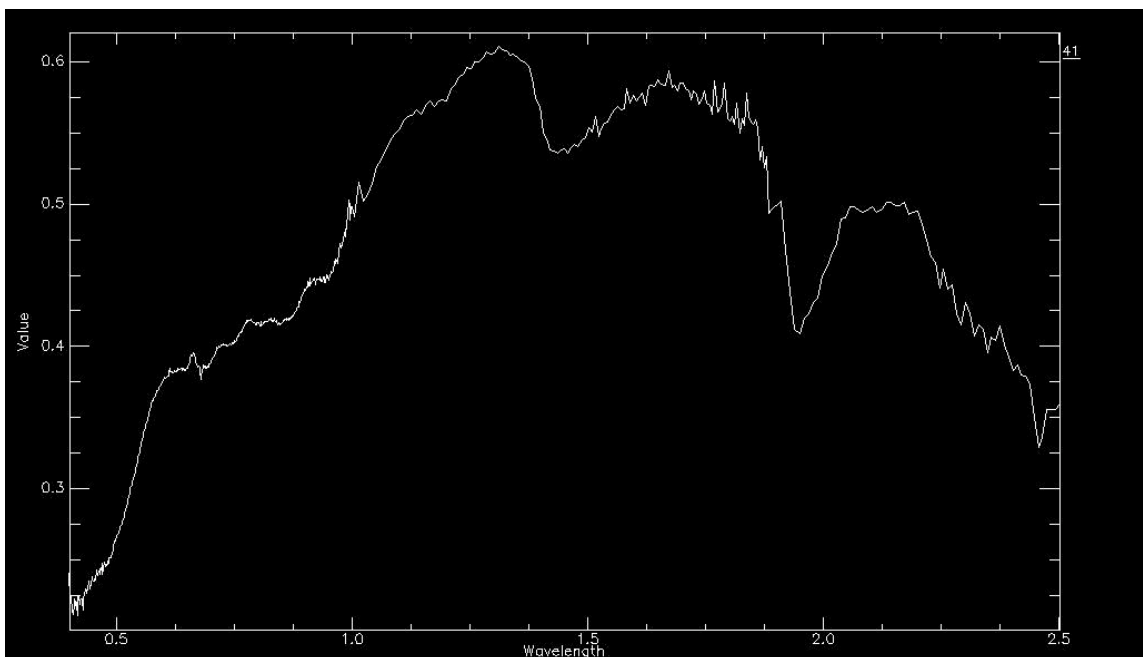


**Figure 4.21.** Spectral profile of sample 41.

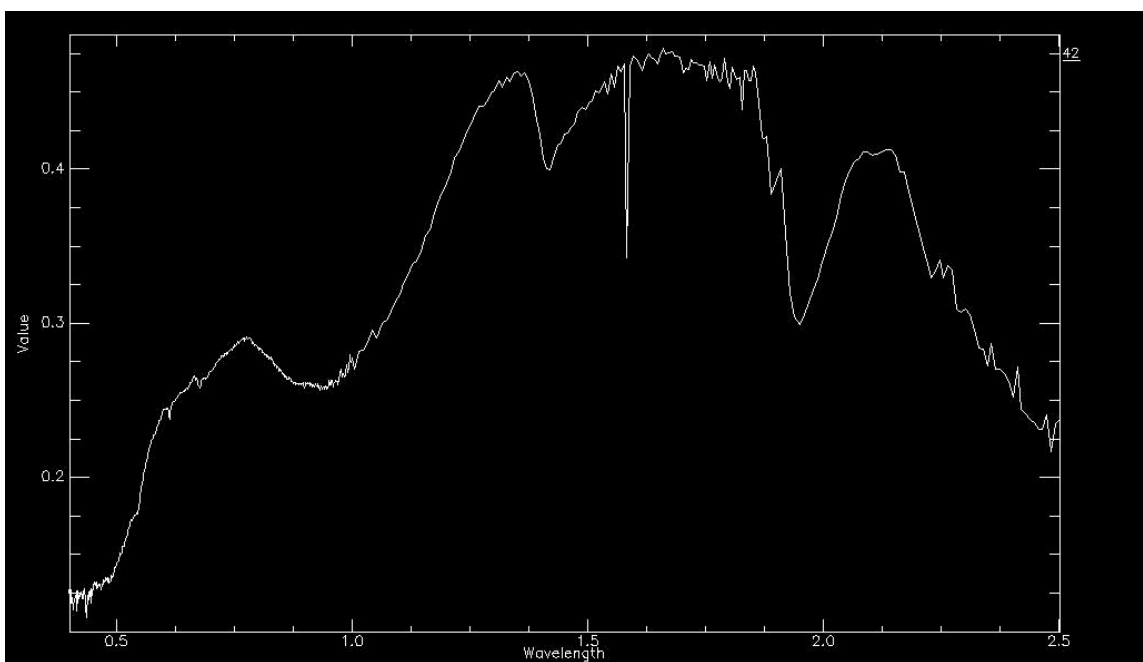


**Figure 4.22.** Spectral profile of sample 42.

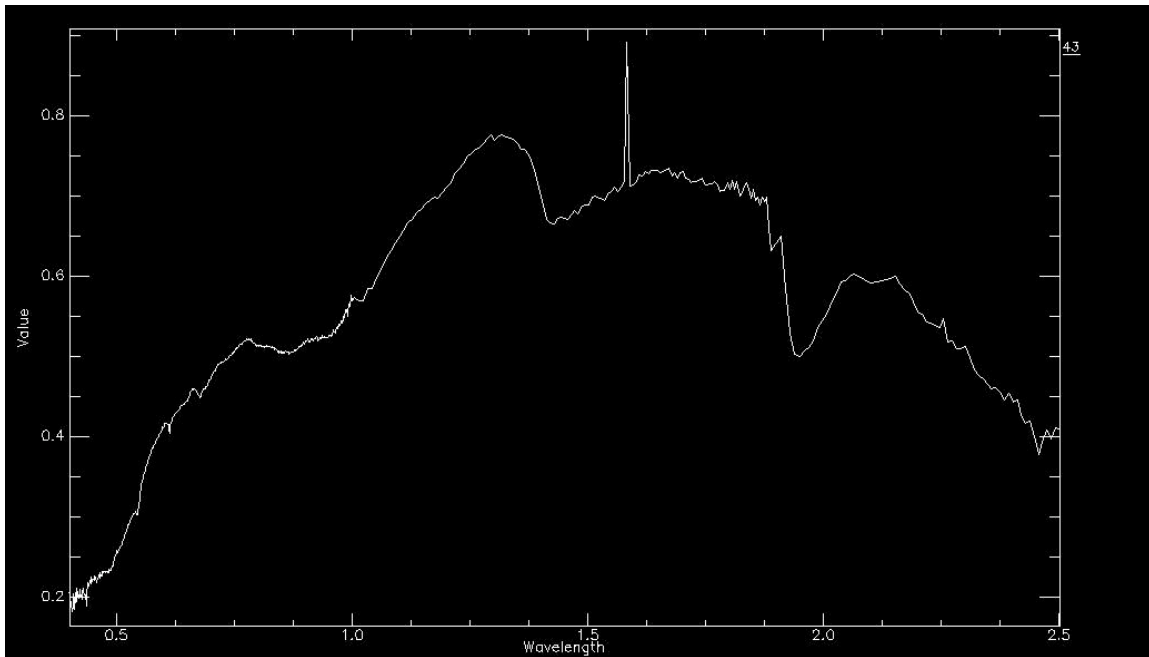


**Figure 4.23.** Spectral profile of sample 43.

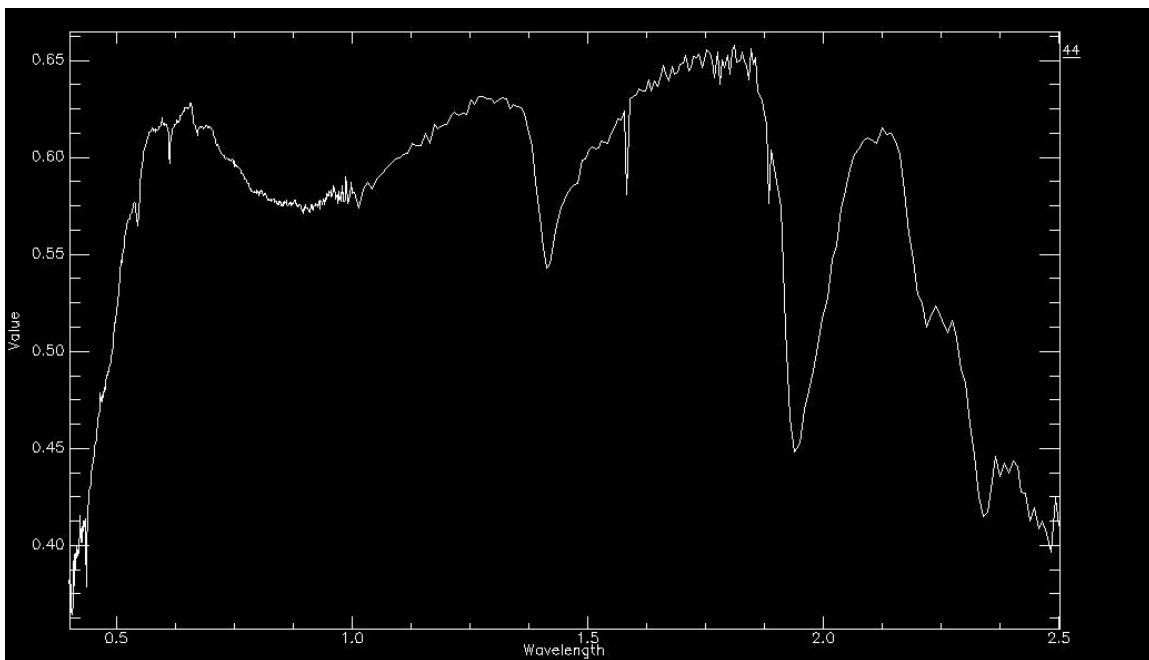


**Figure 4.24** Spectral profile of sample 44.

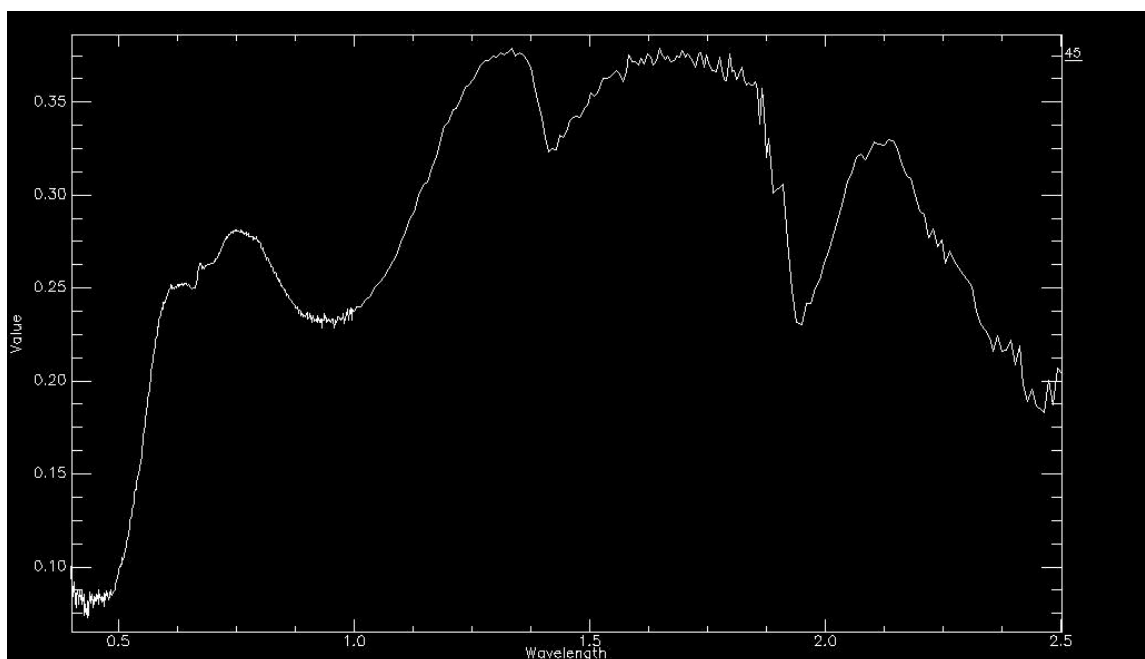


**Figure 4.25.** Spectral profile of sample 45.

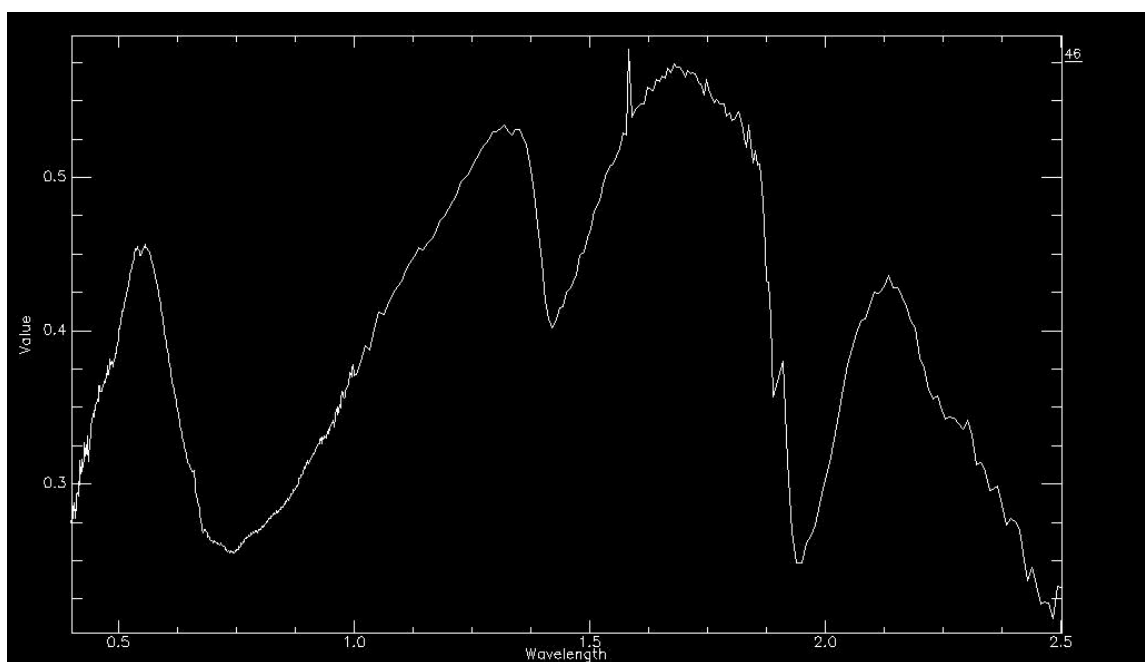


**Figure 4.26.** Spectral profile of sample 46.

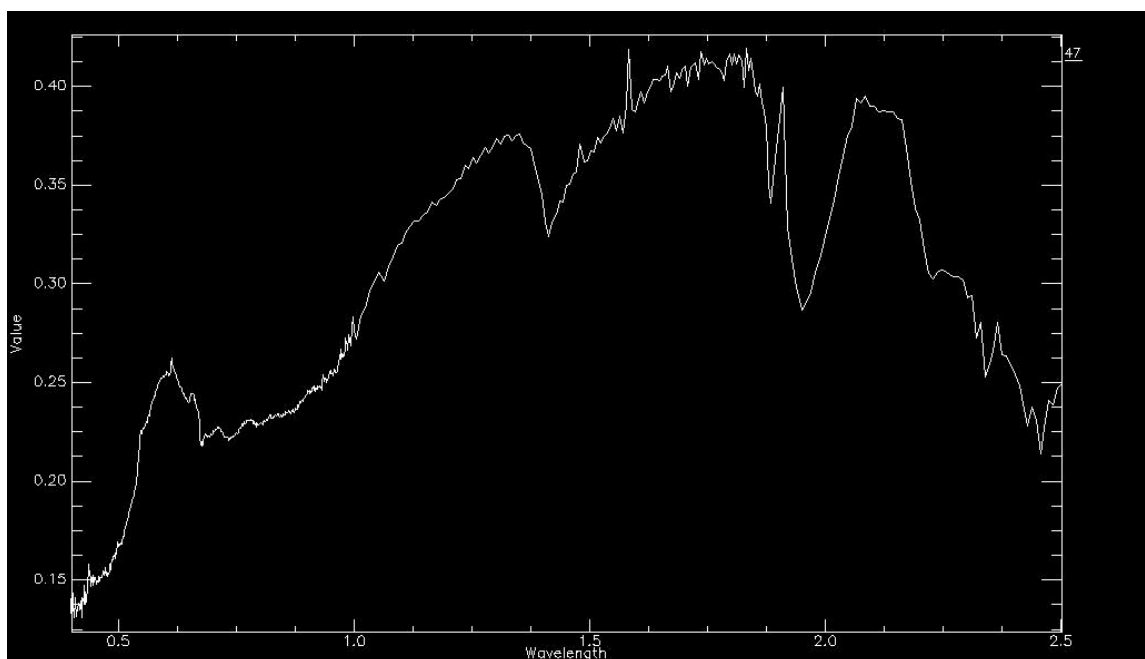


**Figure 4.27.** Spectral profile of sample 47.

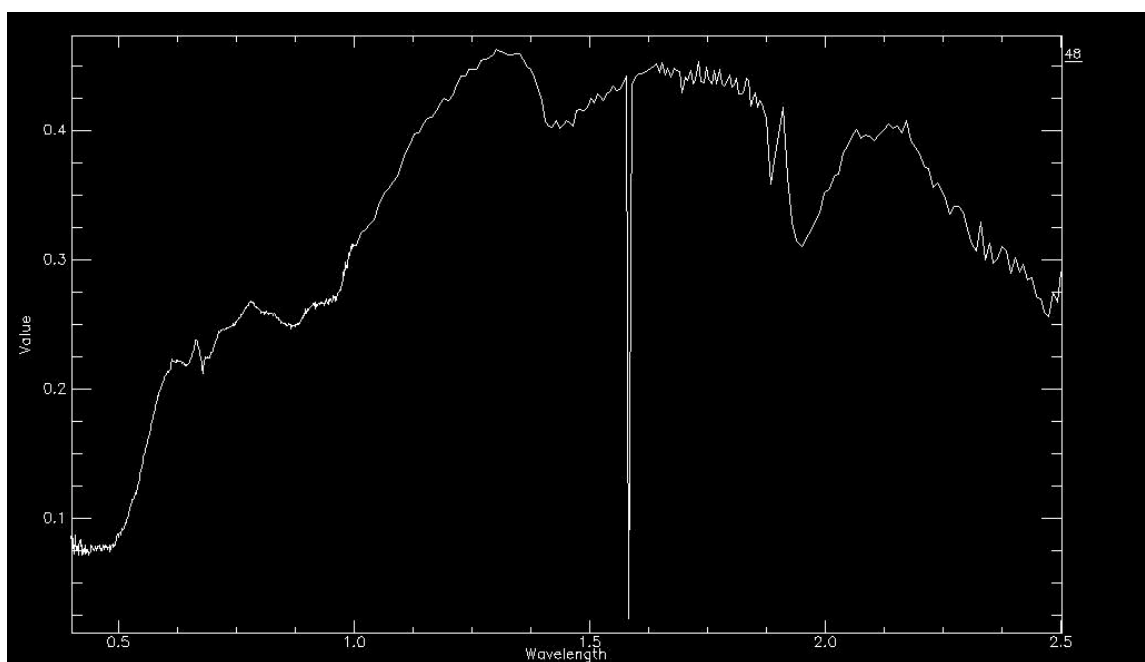


**Figure 4.28.** Spectral profile of sample 48.

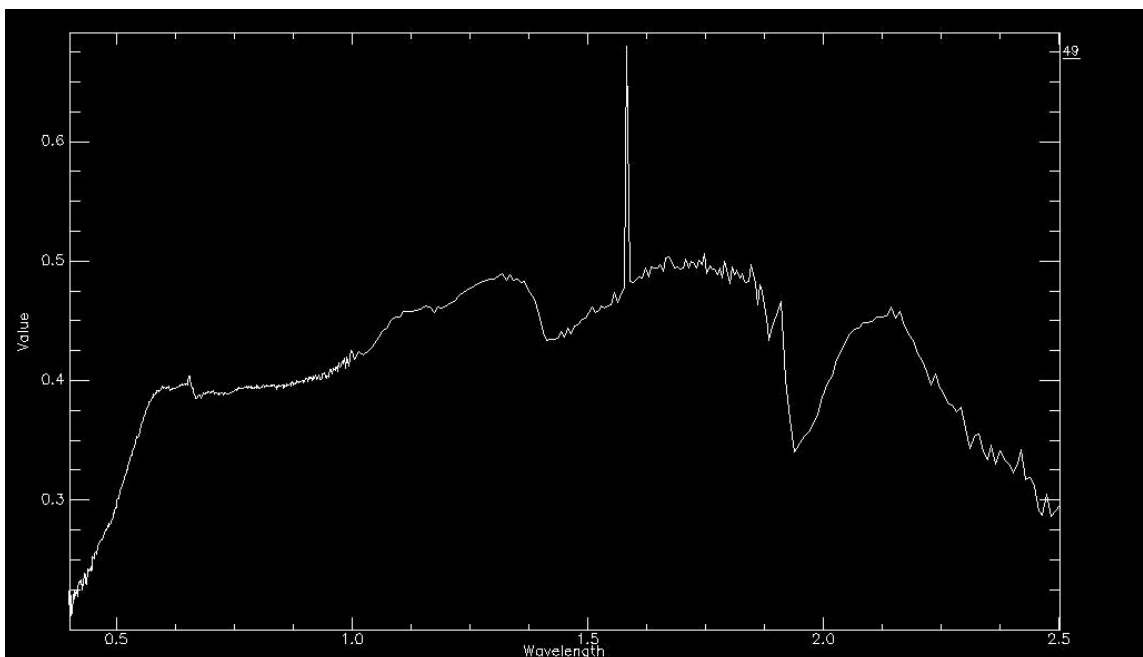


**Figure 4.29.** Spectral profile of sample 49.

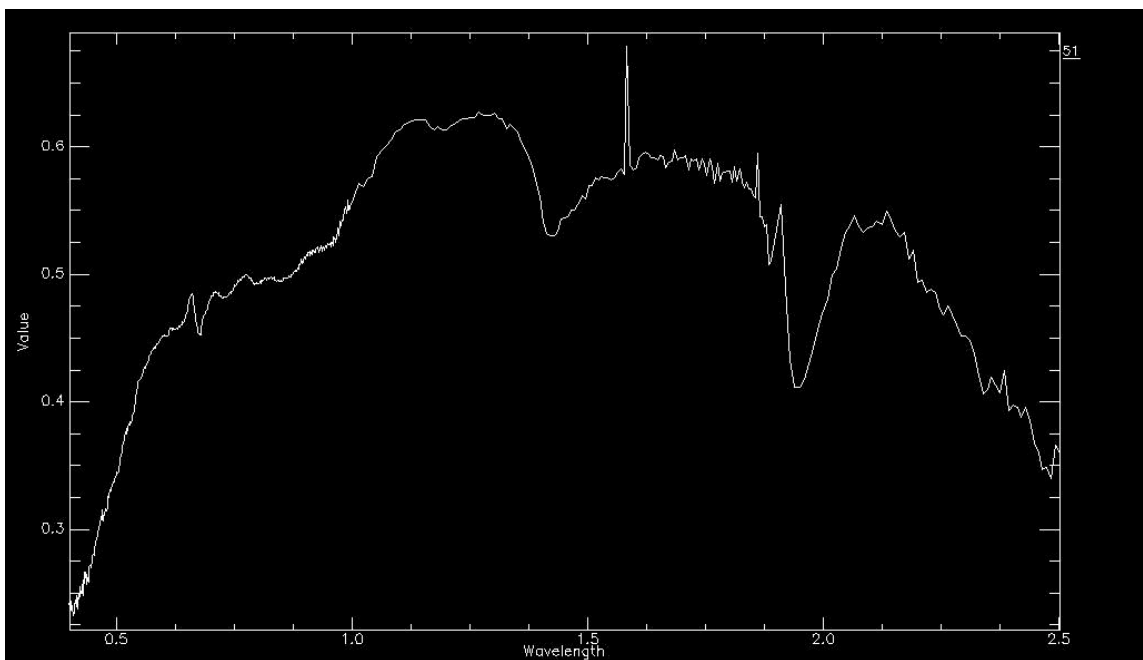


**Figure 4.30.** Spectral profile of sample 51.

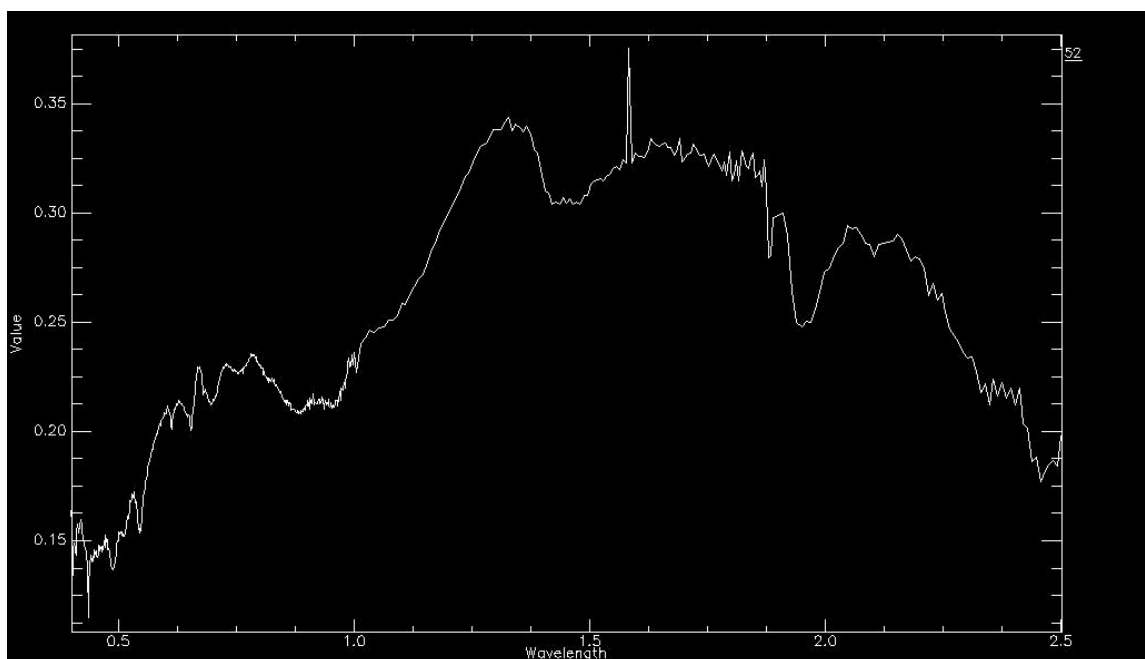


**Figure 4.31.** Spectral profile of sample 52.

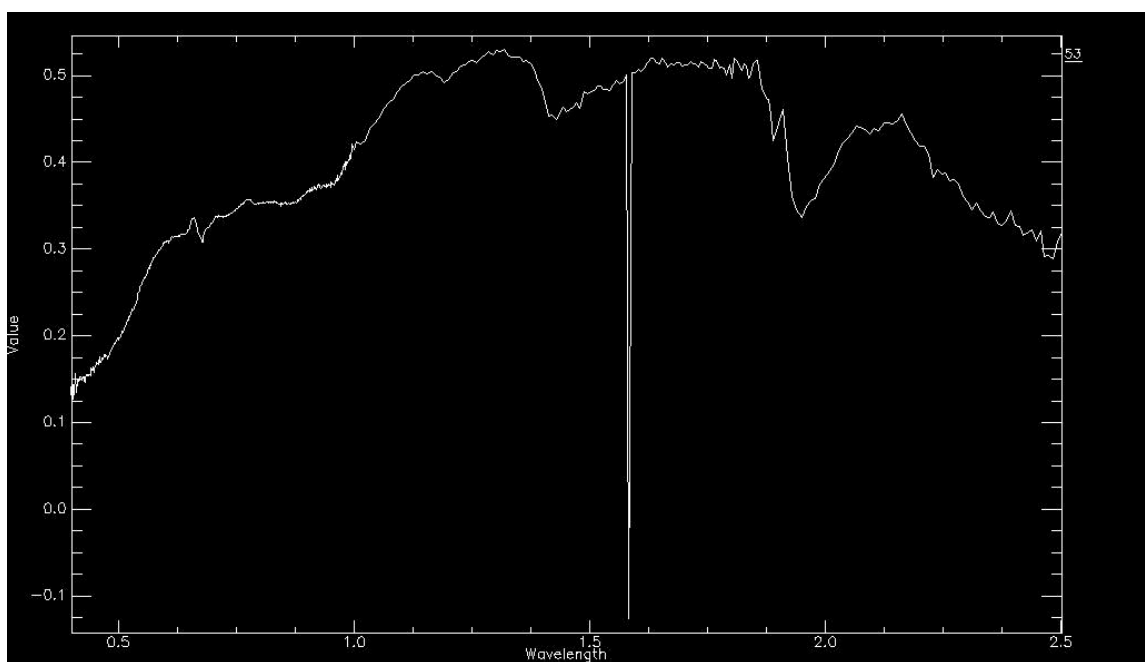


**Figure 4.32.** Spectral profile of sample 53.

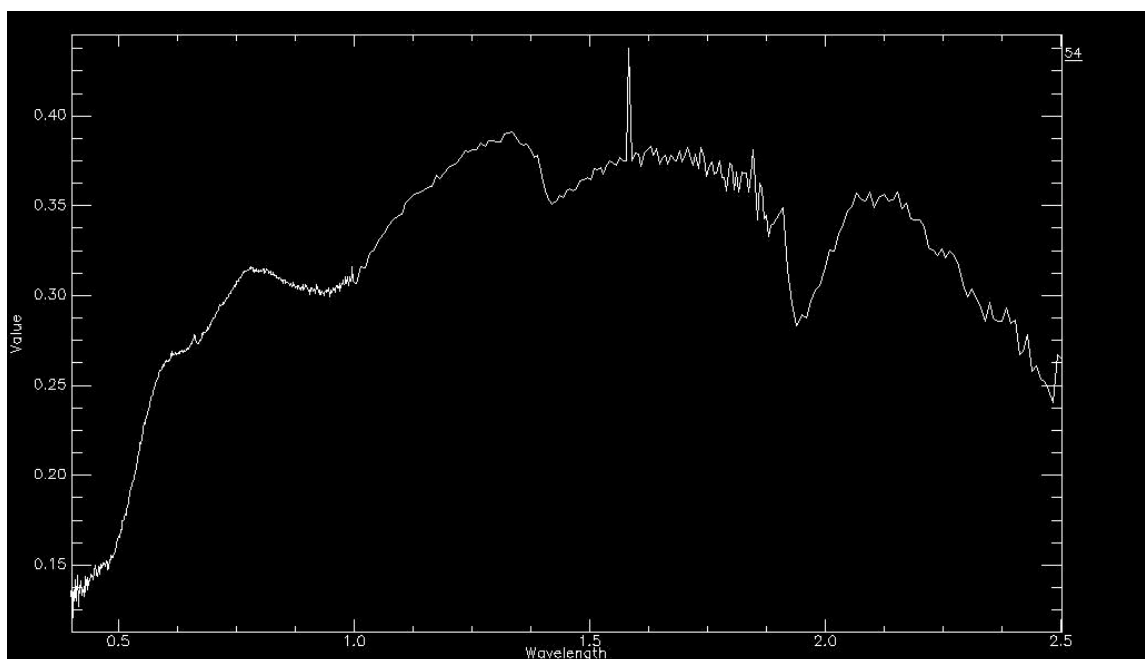


**Figure 4.33.** Spectral profile of sample 54.

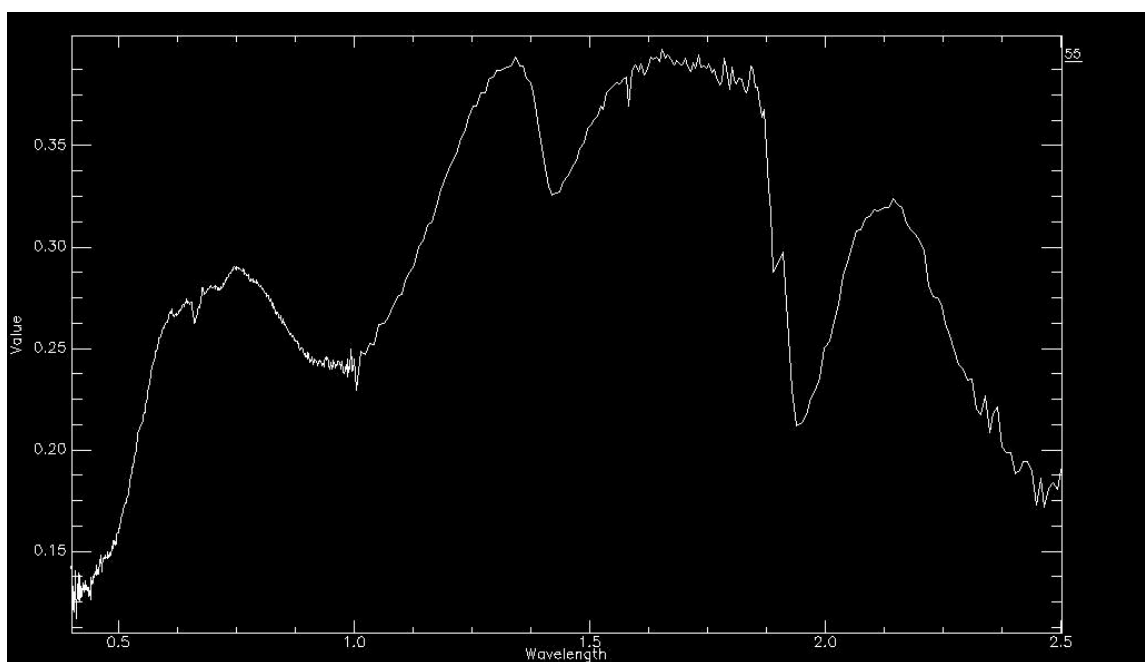


**Figure 4.34.** Spectral profile of sample 55.

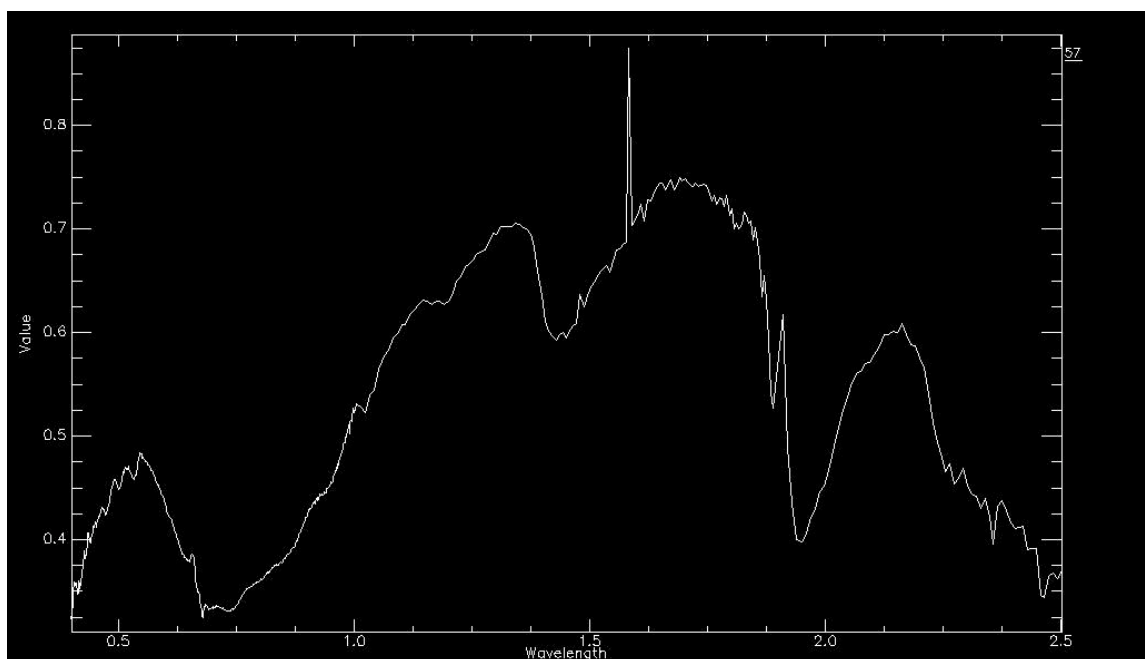


**Figure 4.35.** Spectral profile of sample 57.

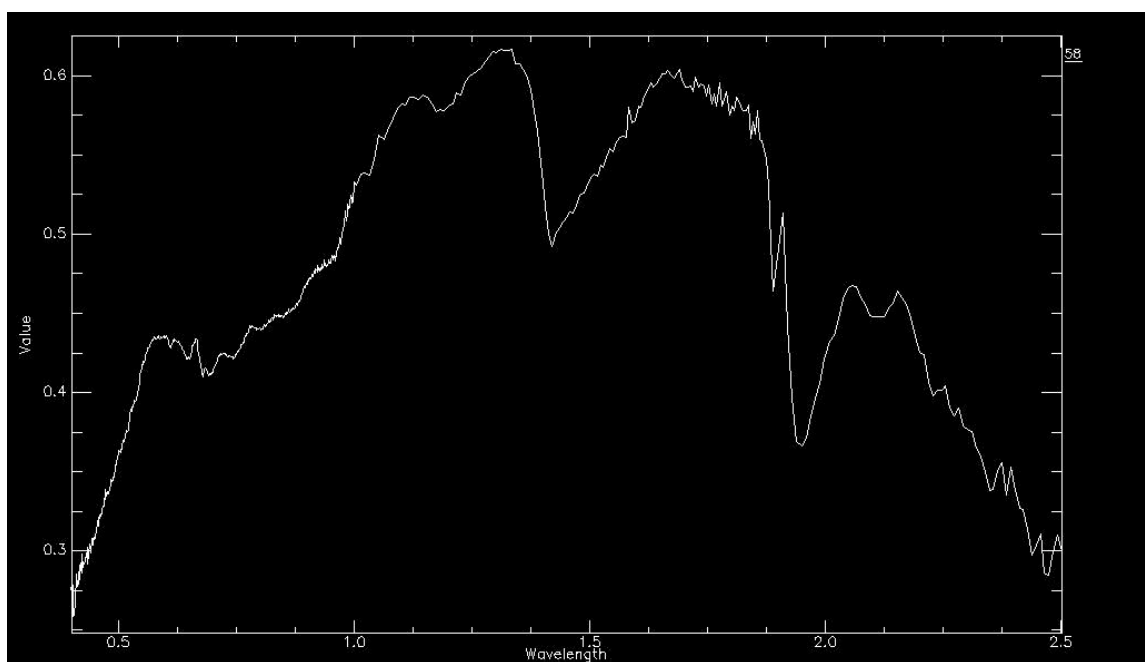


**Figure 4.36.** Spectral profile of sample 58.

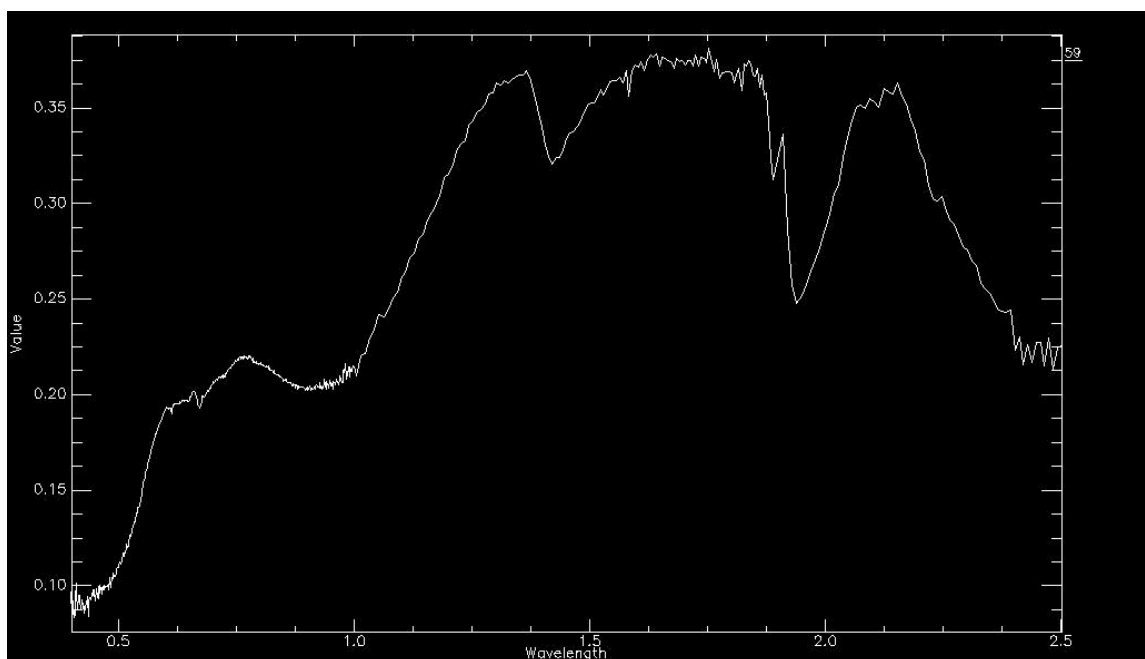


**Figure 4.37.** Spectral profile of sample 59.

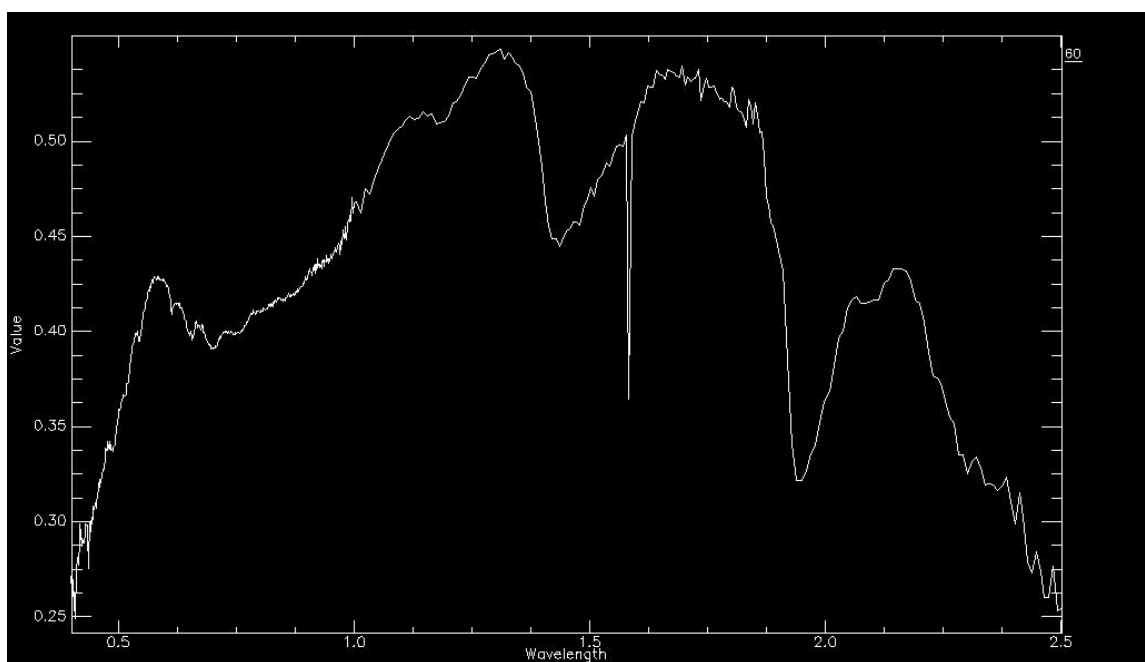


**Figure 4.38.** Spectral profile of sample 60.

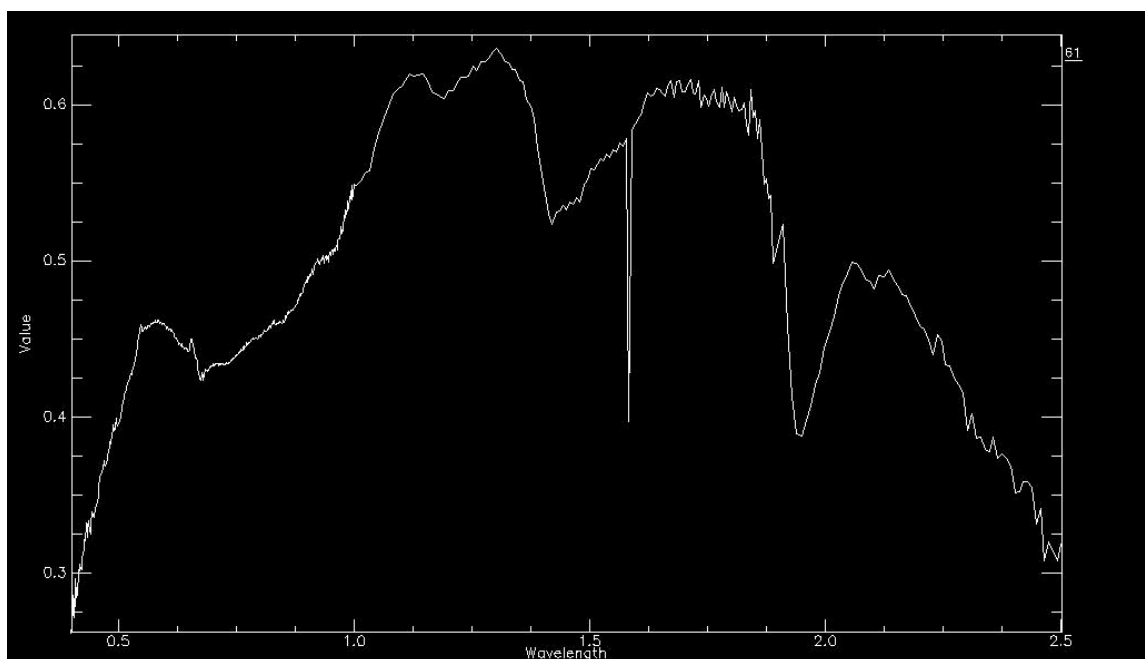


**Figure 4.39.** Spectral profile of sample 61.

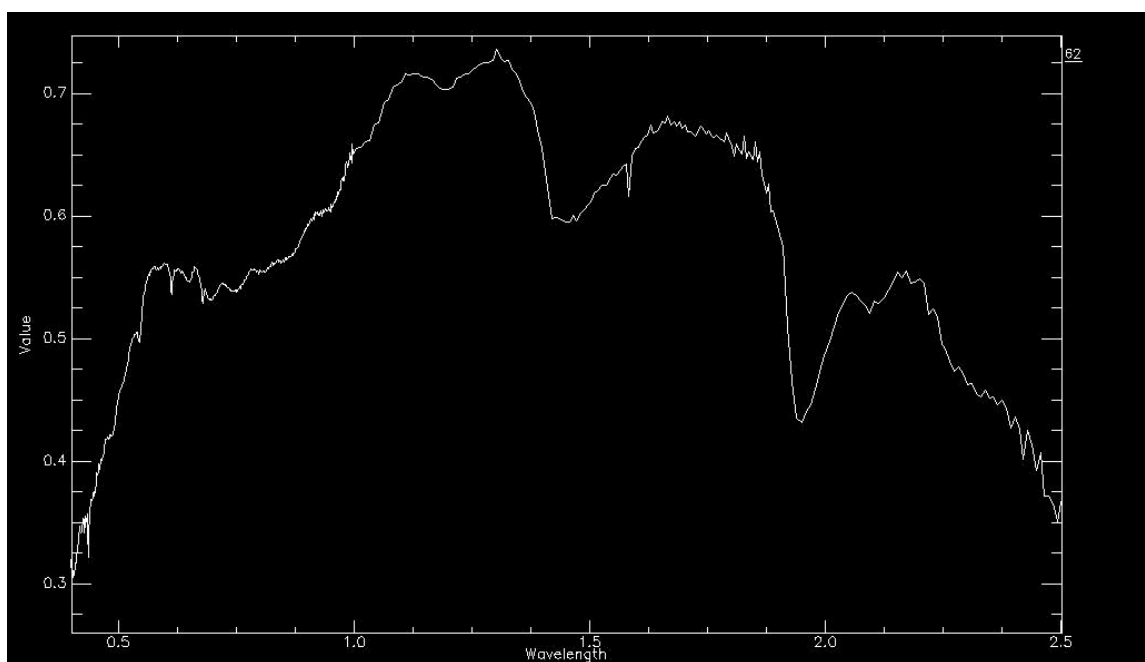


**Figure 4.40.** Spectral profile of sample 62.

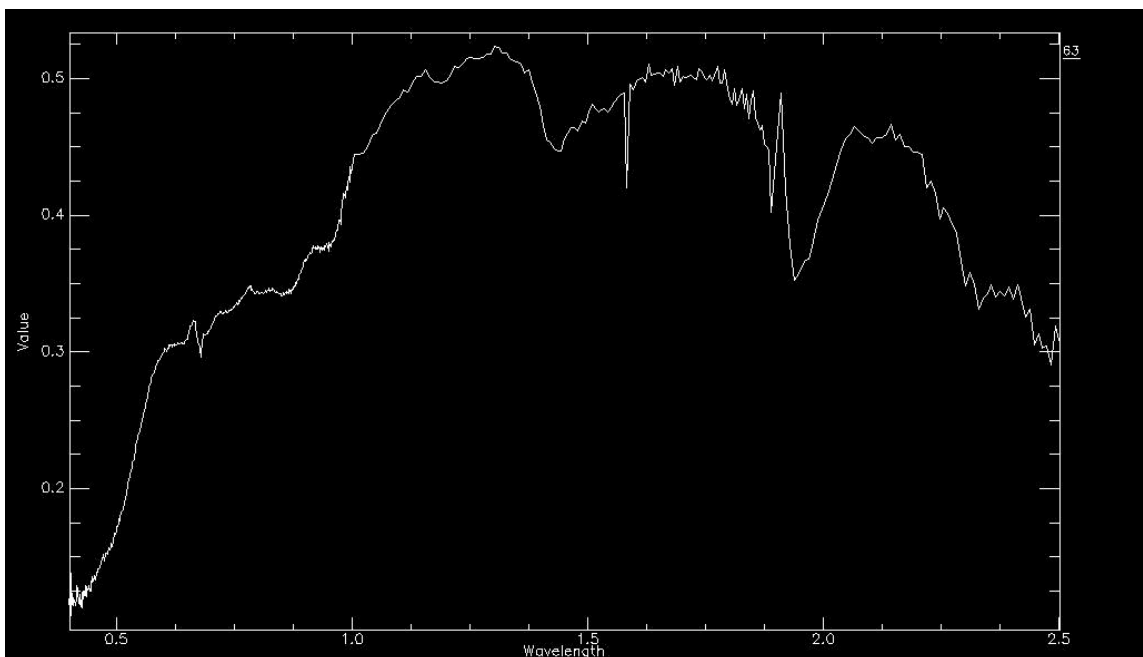


**Figure 4.41.** Spectral profile of sample 63.

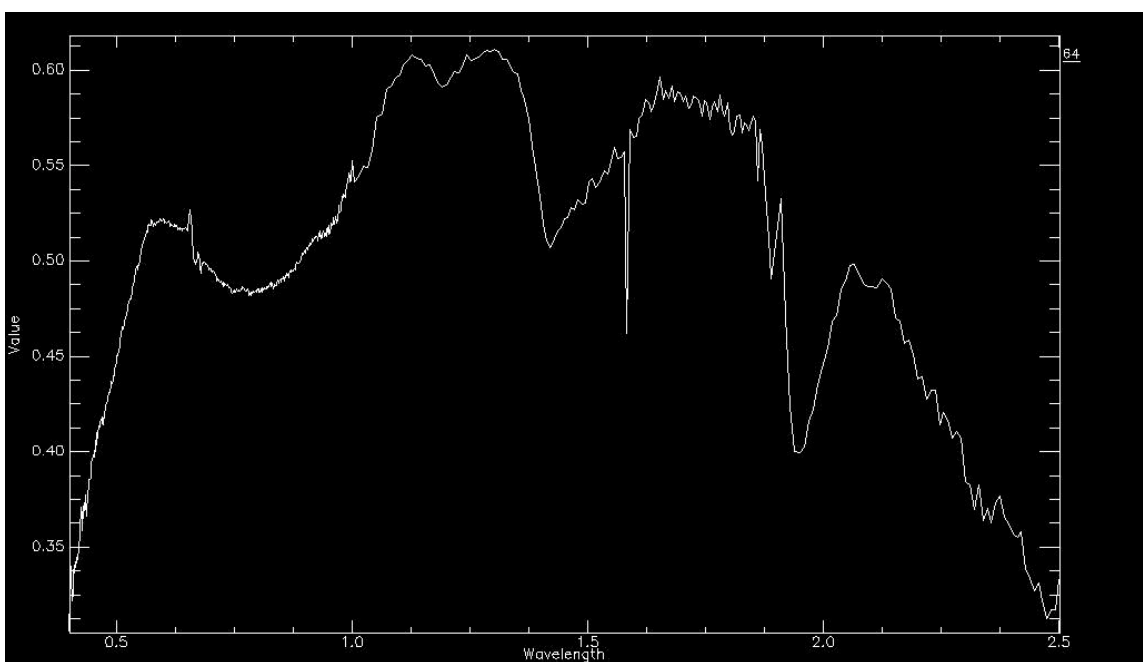


**Figure 4.42.** Spectral profile of sample 64.

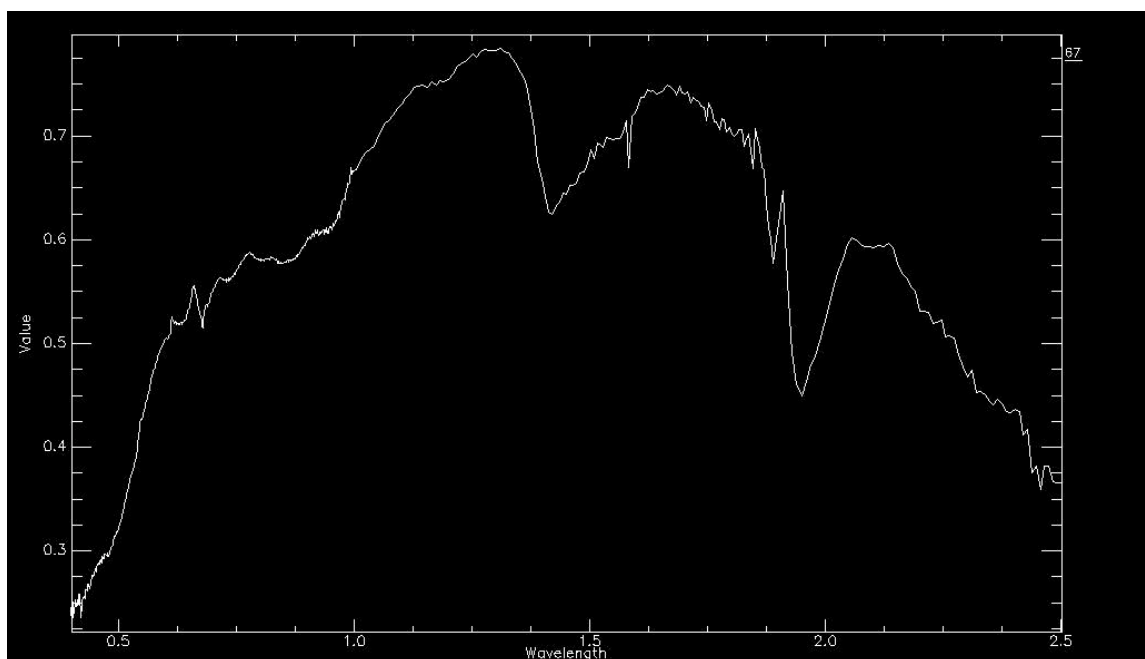


**Figure 4.43.** Spectral profile of sample 67.

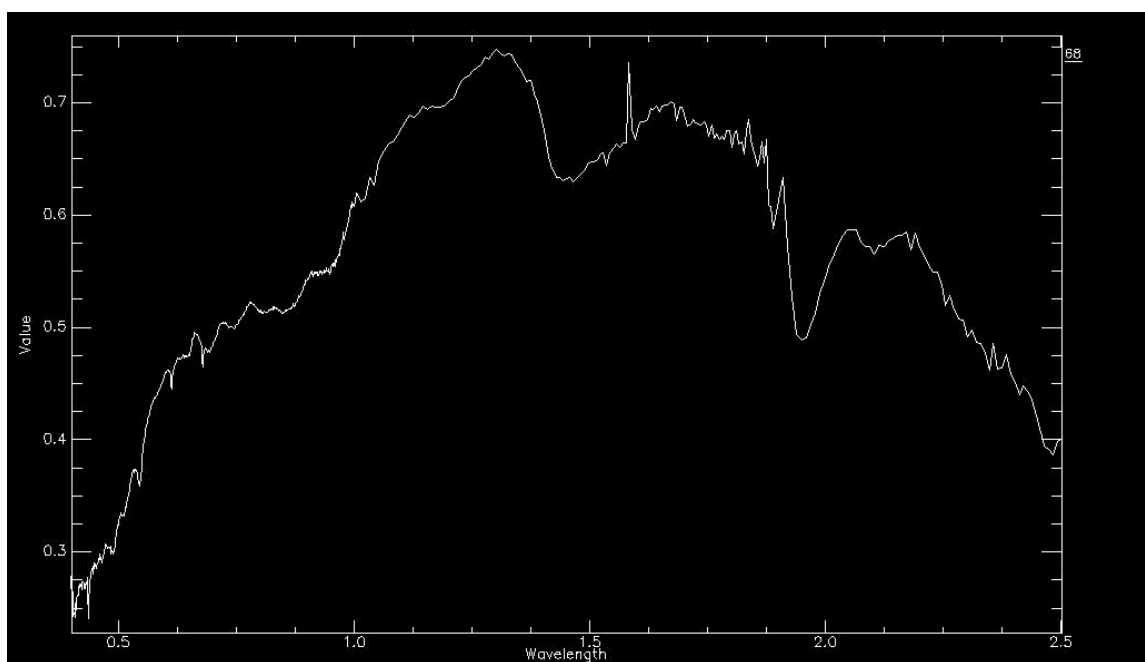


**Figure 4.44.** Spectral profile of sample 68.

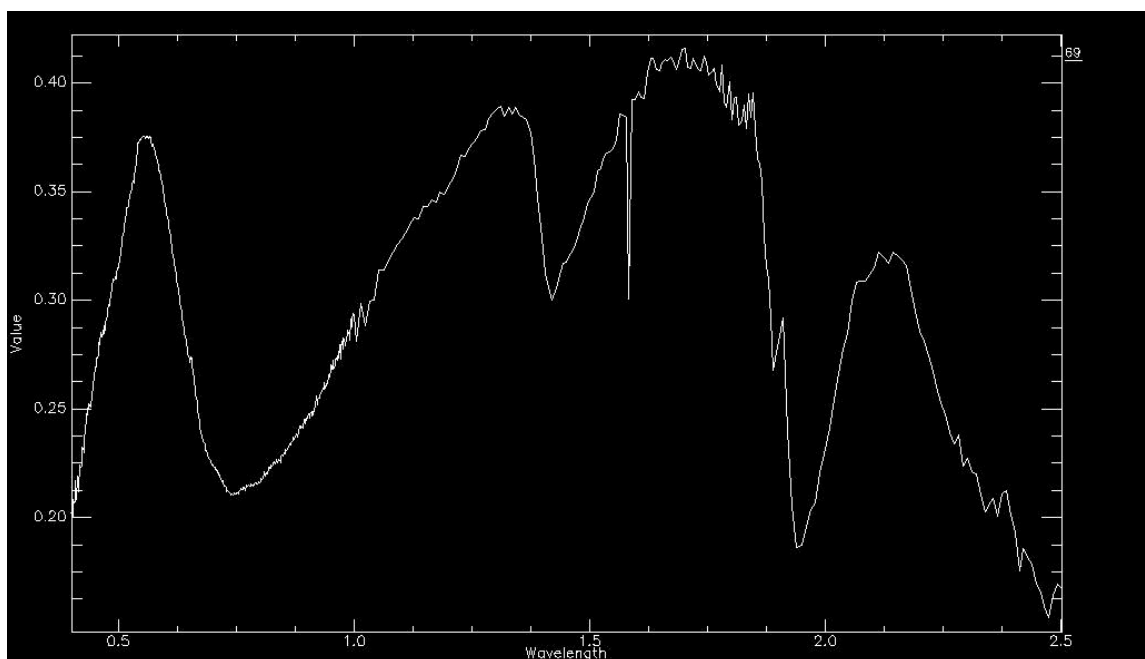


**Figure 4.45.** Spectral profile of sample 69.

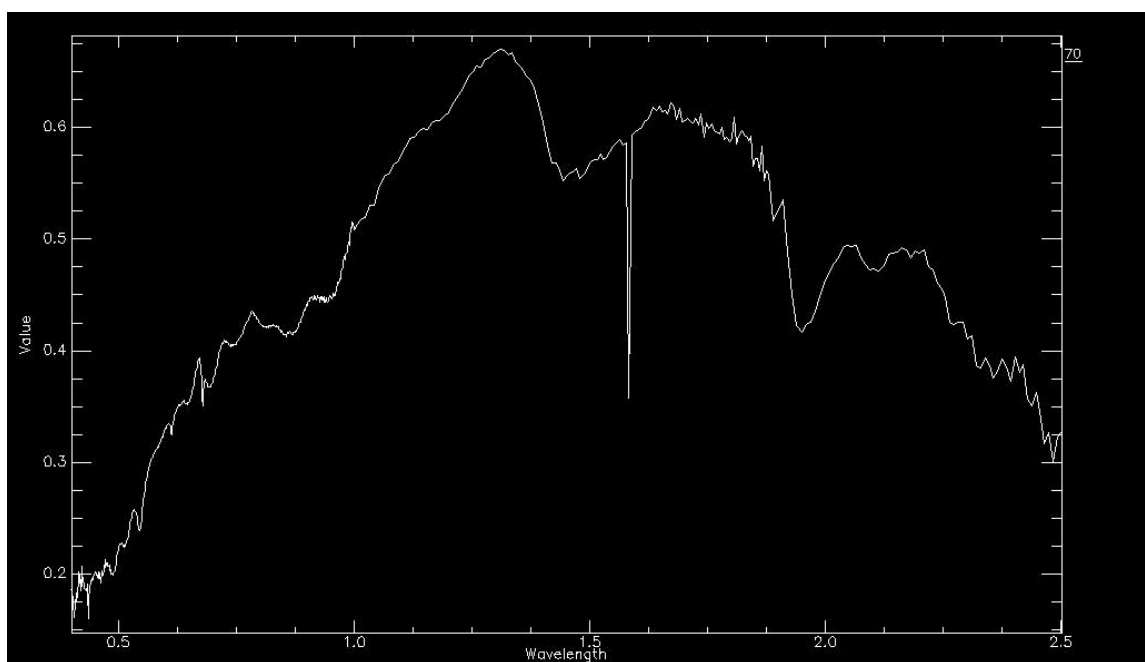


**Figure 4.46.** Spectral profile of sample 70.

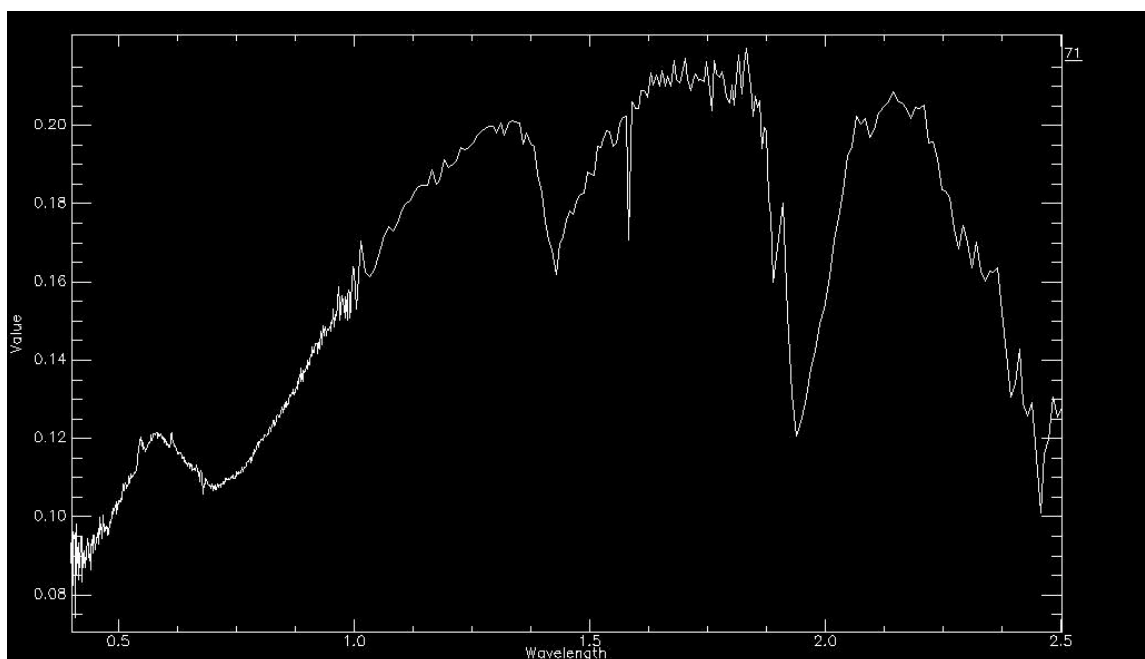


**Figure 4.47.** Spectral profile of sample 71.

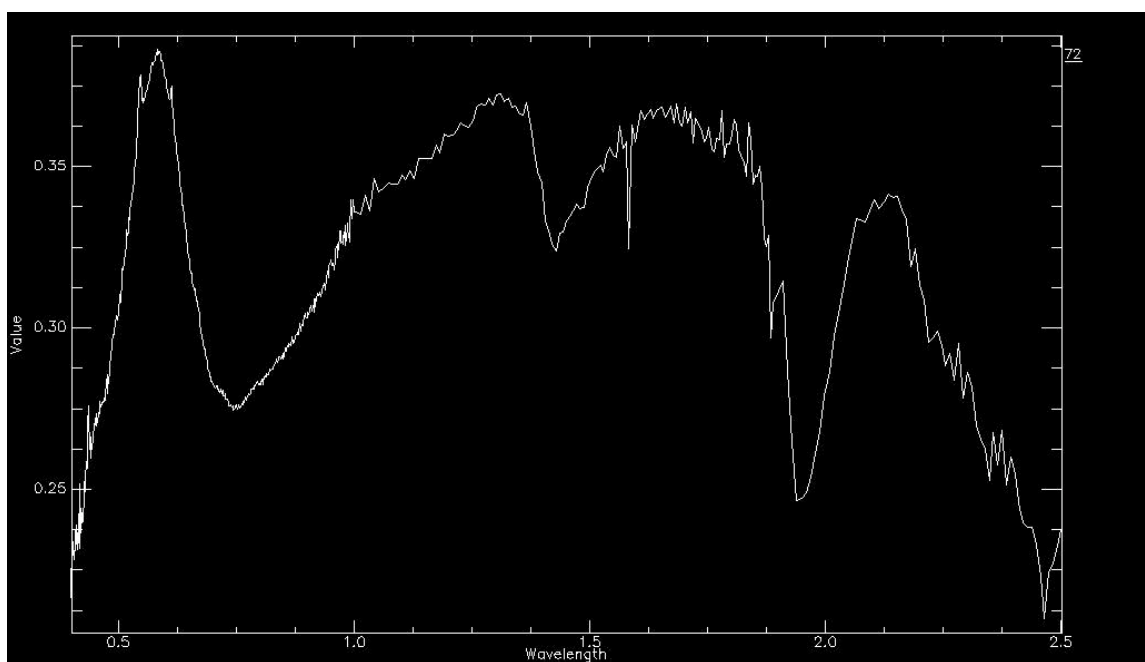


**Figure 4.48.** Spectral profile of sample 72.

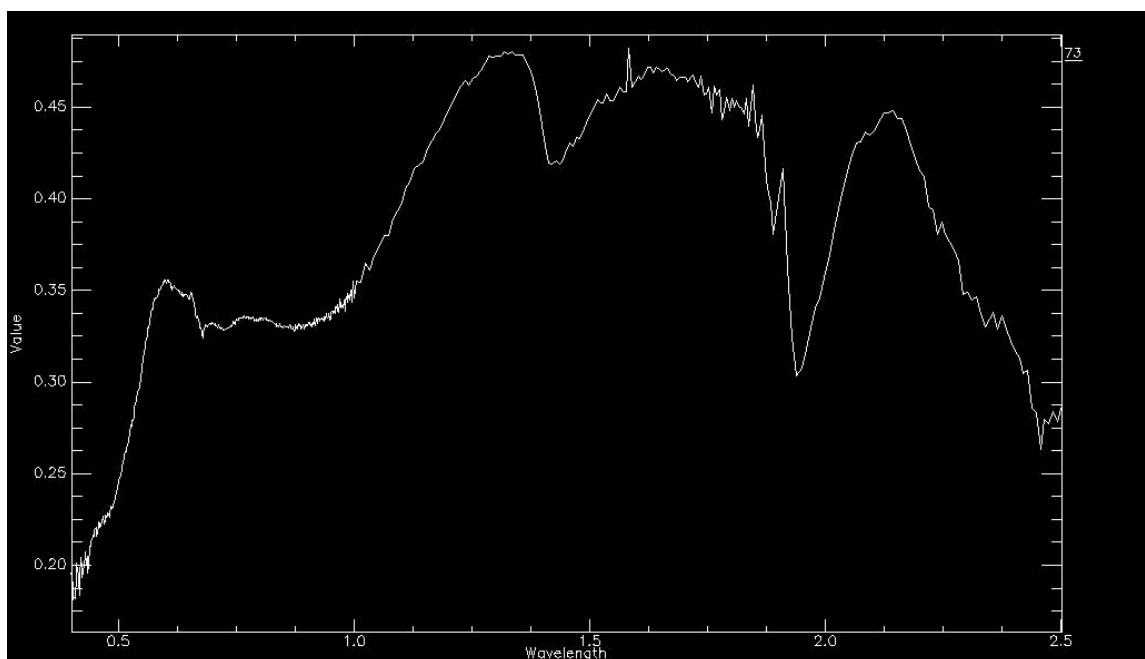


**Figure 4.49.** Spectral profile of sample 73.

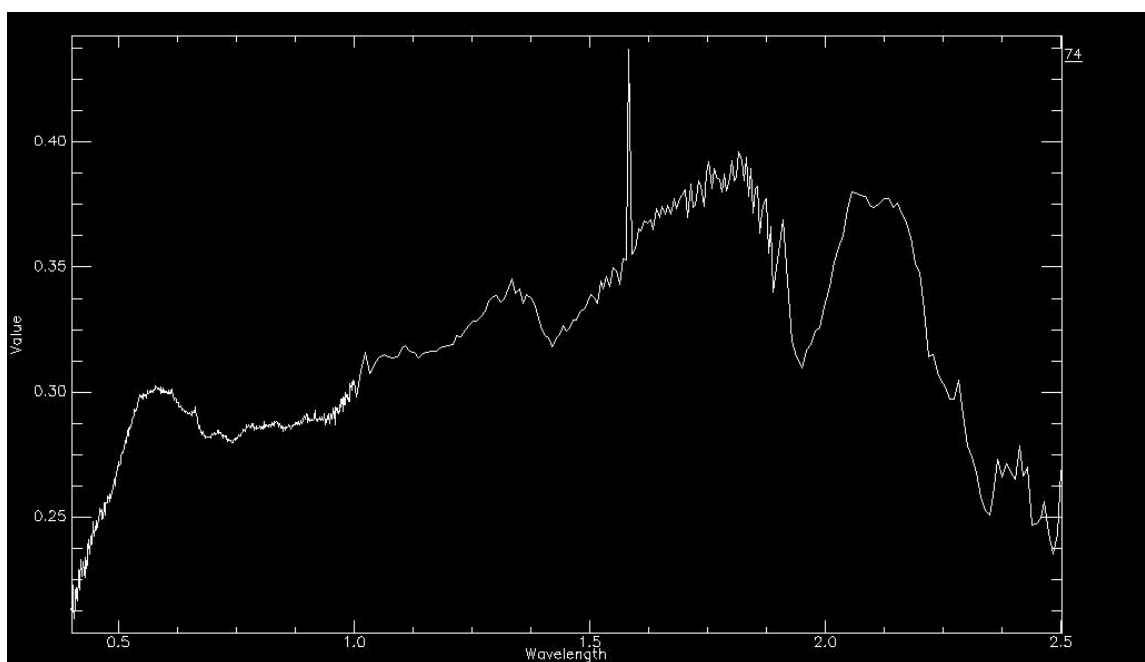


**Figure 4.51.** Spectral profile of sample 74.

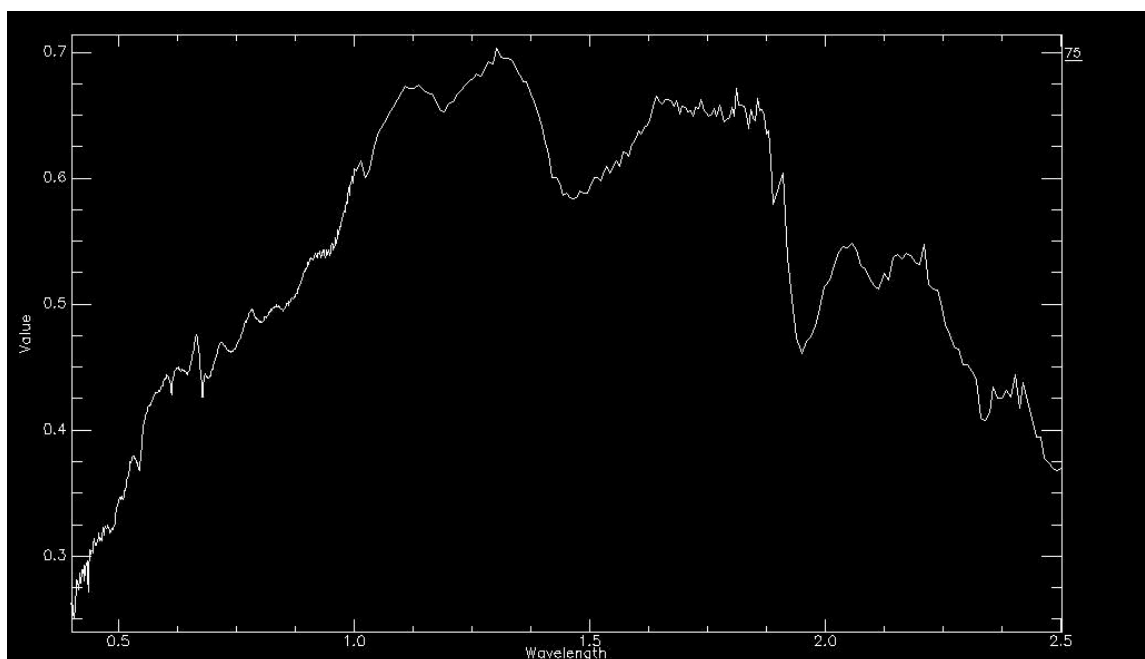


**Figure 4.52.** Spectral profile of sample 75.

## 18.2. Appendix 4.2. Spectral Profiles of QMP-4780

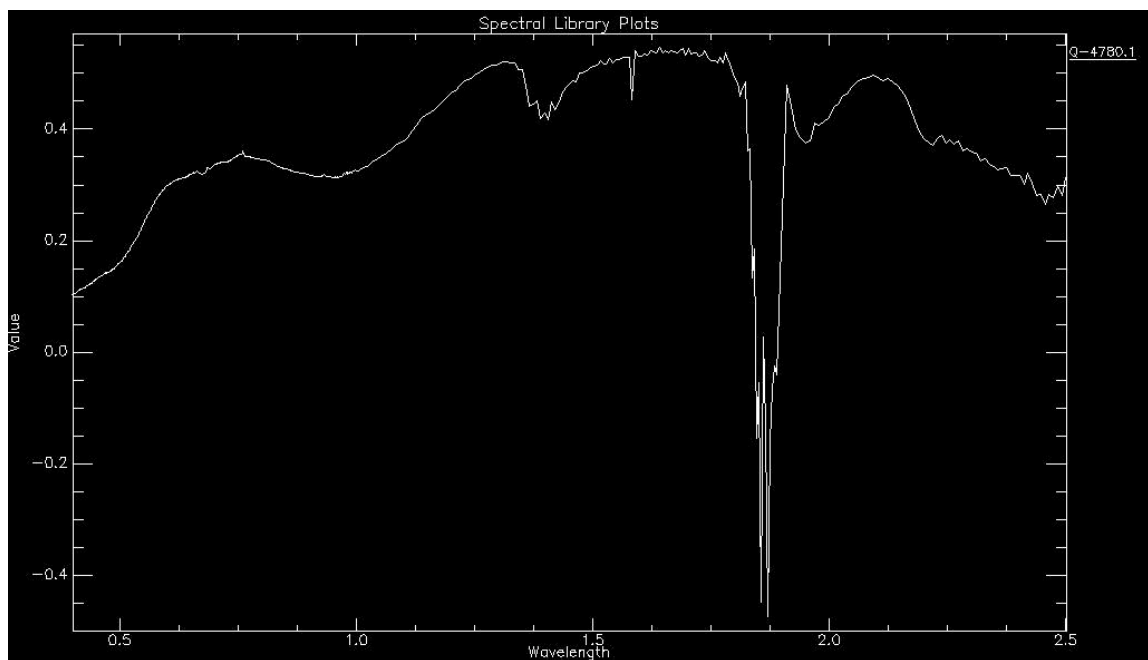


Figure 4.53. Spectral profile of Q-4780.1.

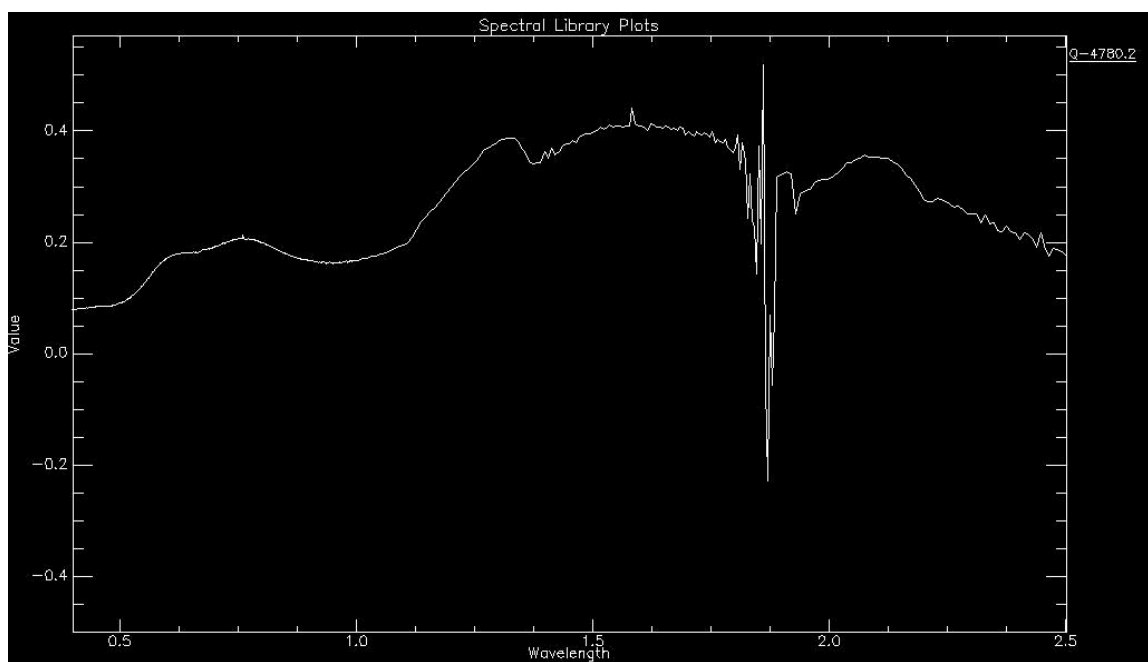
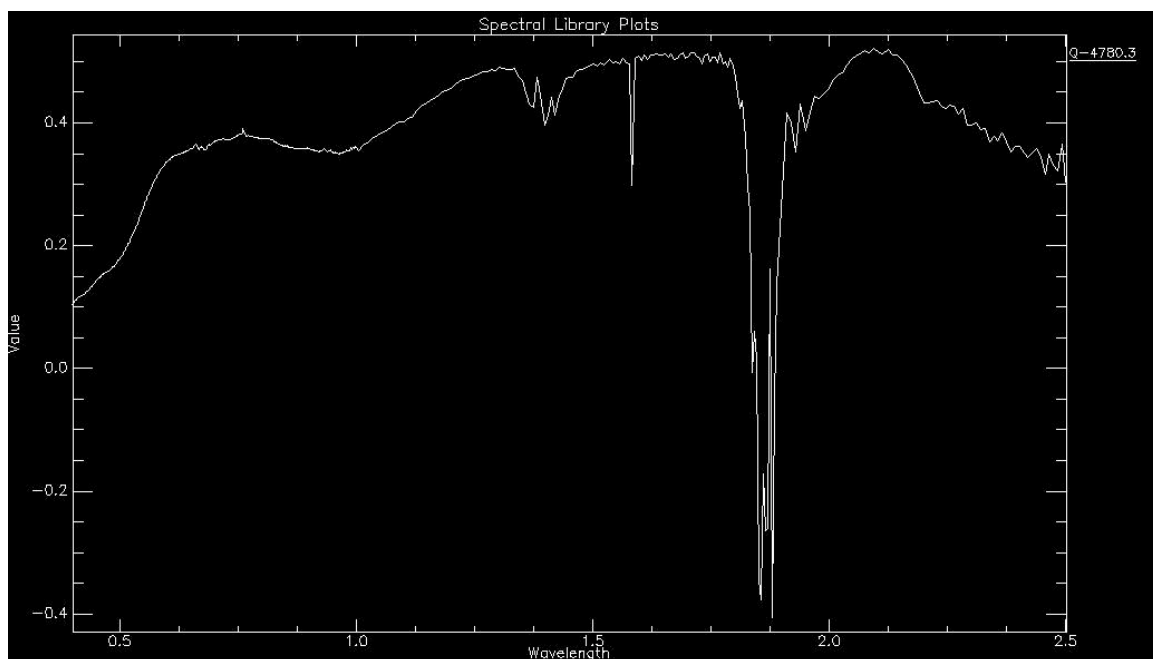
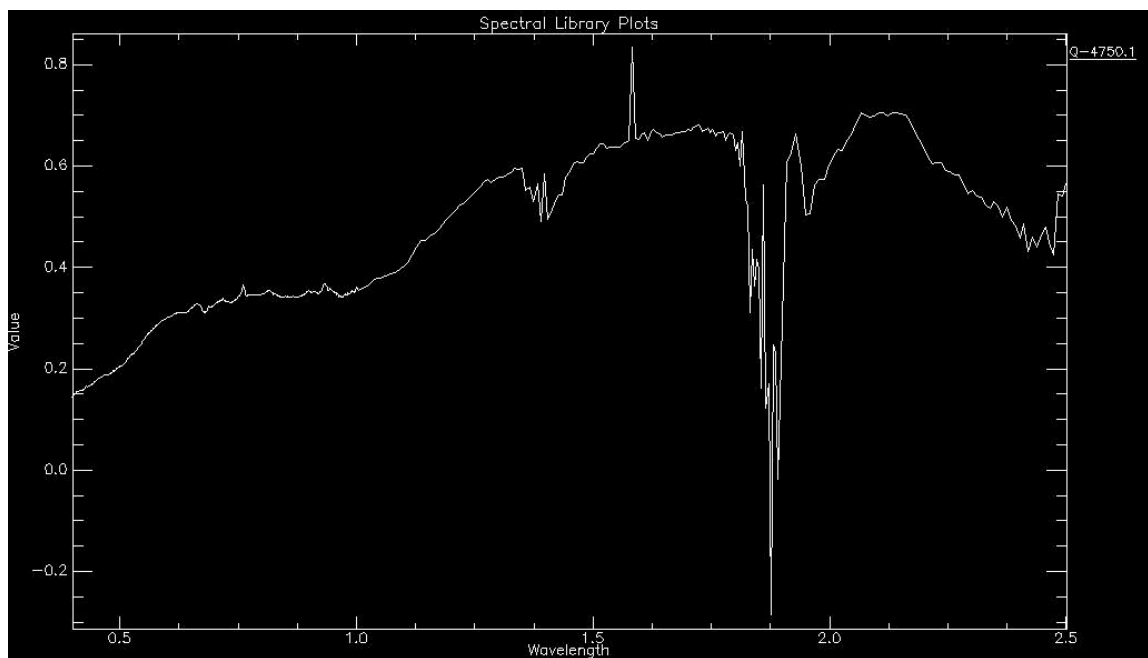


Figure 4.54. Spectral profile of Q-4780.2.



**Figure 4.55.** Spectral profile of Q-4780.3.

### 18.3. Appendix 4.3. Spectral Profiles of QMP-4750



**Figure 4.56.** Spectral profile of sample Q-4750.1.

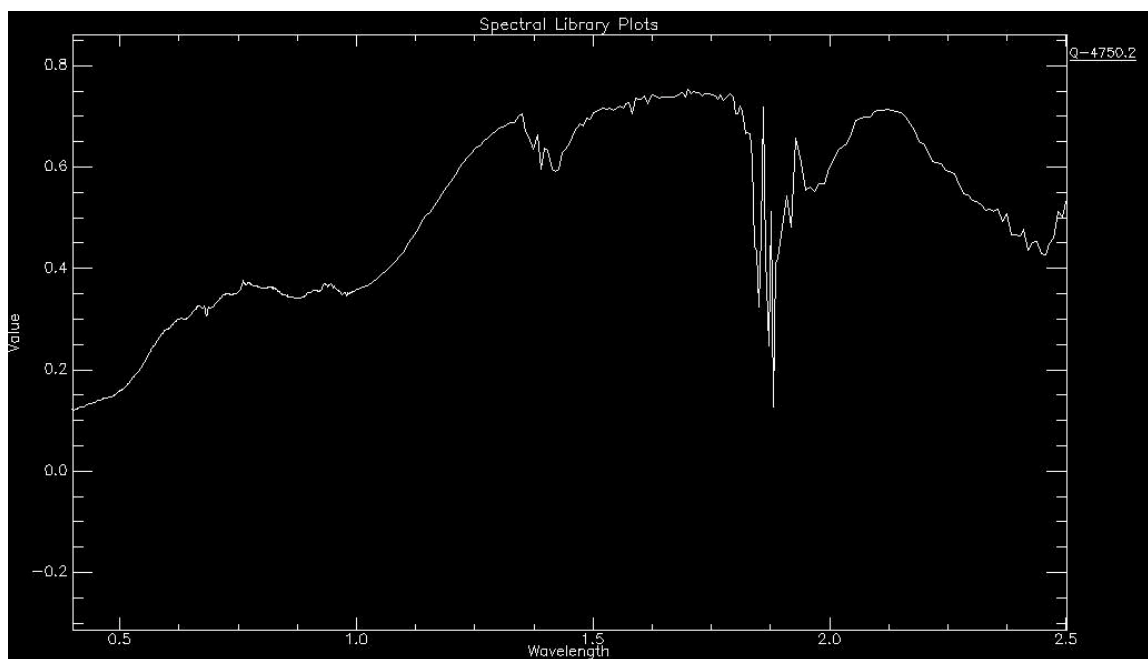


**Figure 4.57.** Spectral profile of sample Q-4750.2.

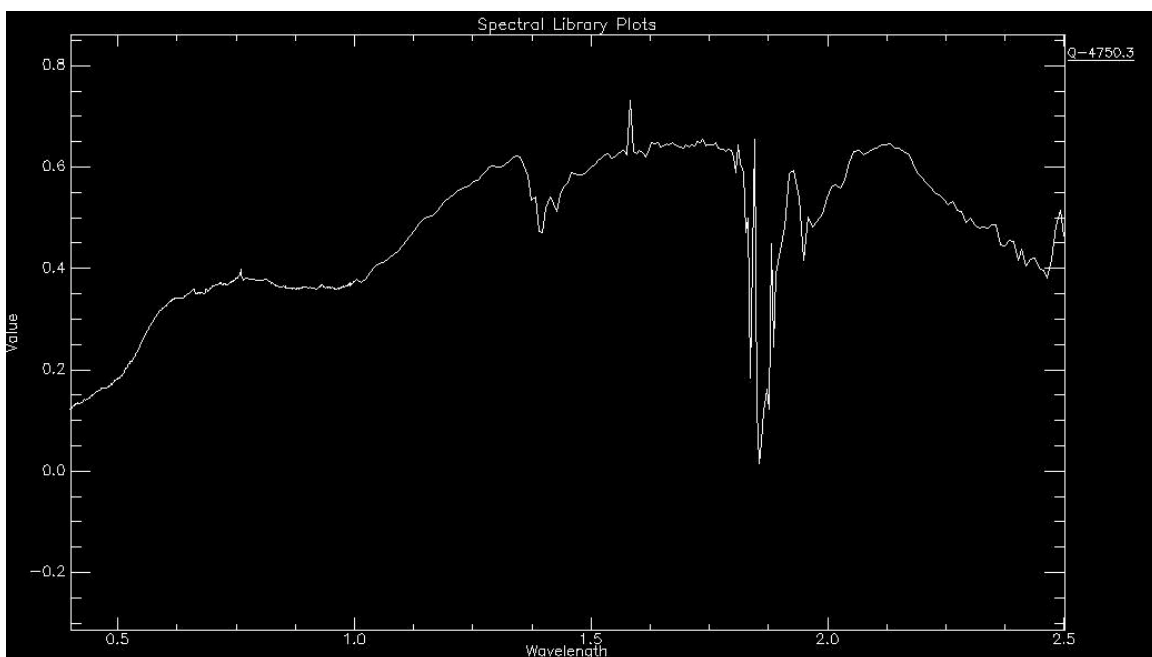


**Figure 4.58.** Spectral profile of sample Q-4750.3.

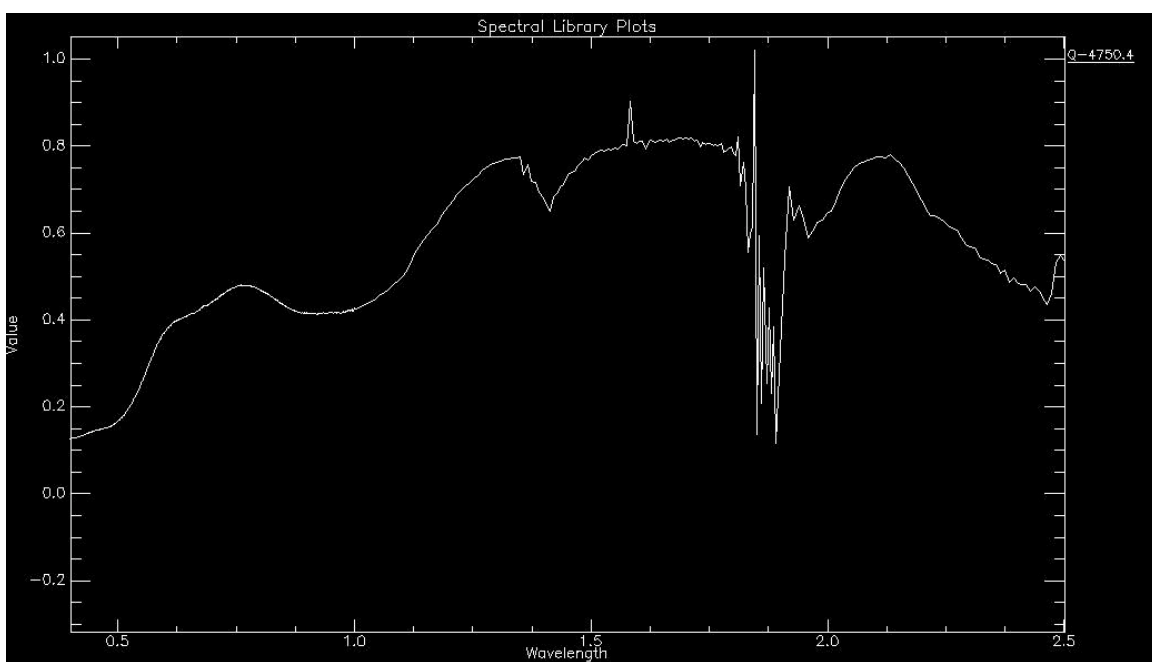


**Figure 4.59.** Spectral profile of sample Q-4750.4.

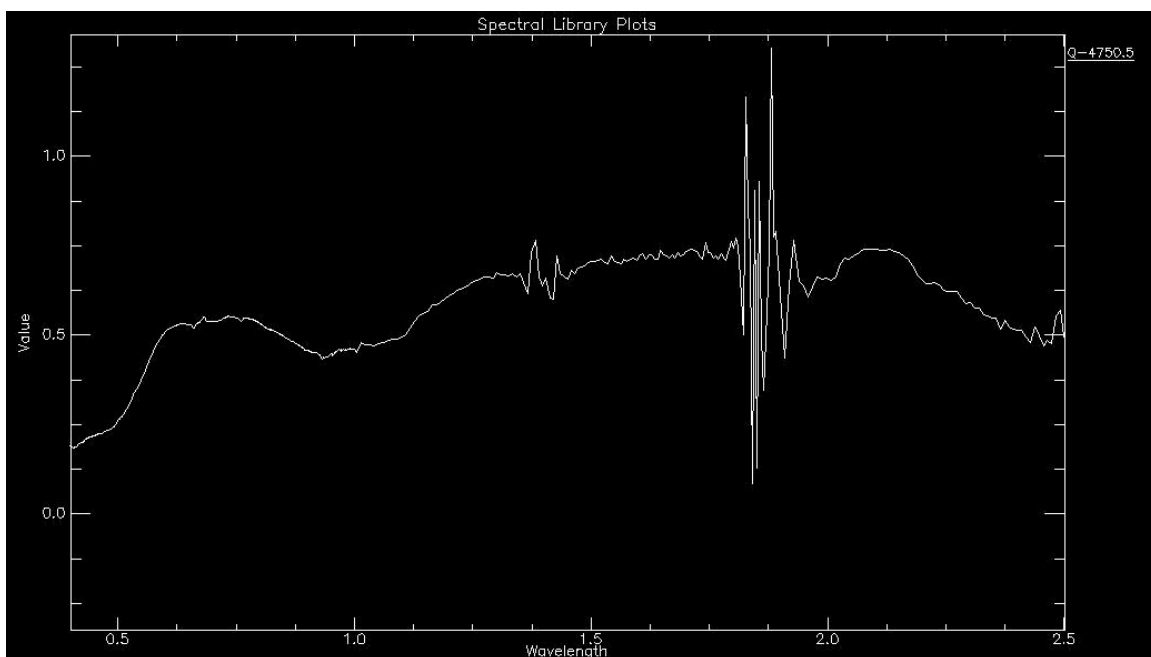


**Figure 4.60.** Spectral profile of sample Q-4750.5.

#### 18.4. Appendix 4.4. Spectral Profiles of QMP-4600

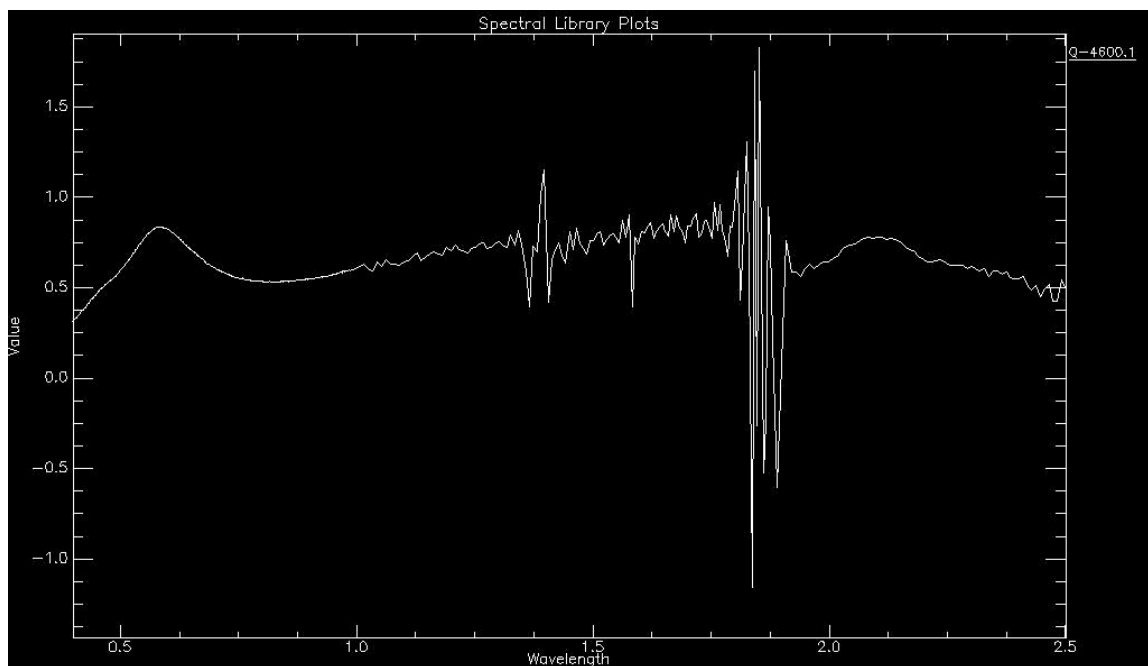


**Figure 4.61.** Spectral profile of sample Q-4600.1.

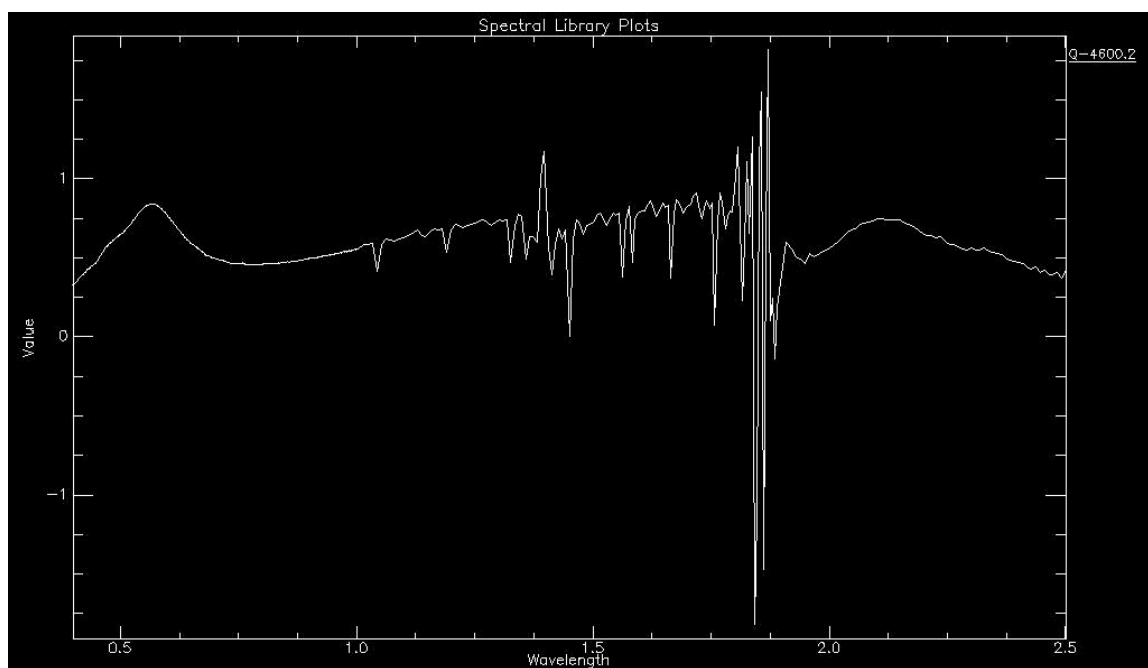


**Figure 4.62.** Spectral profile of sample Q-4600.2.

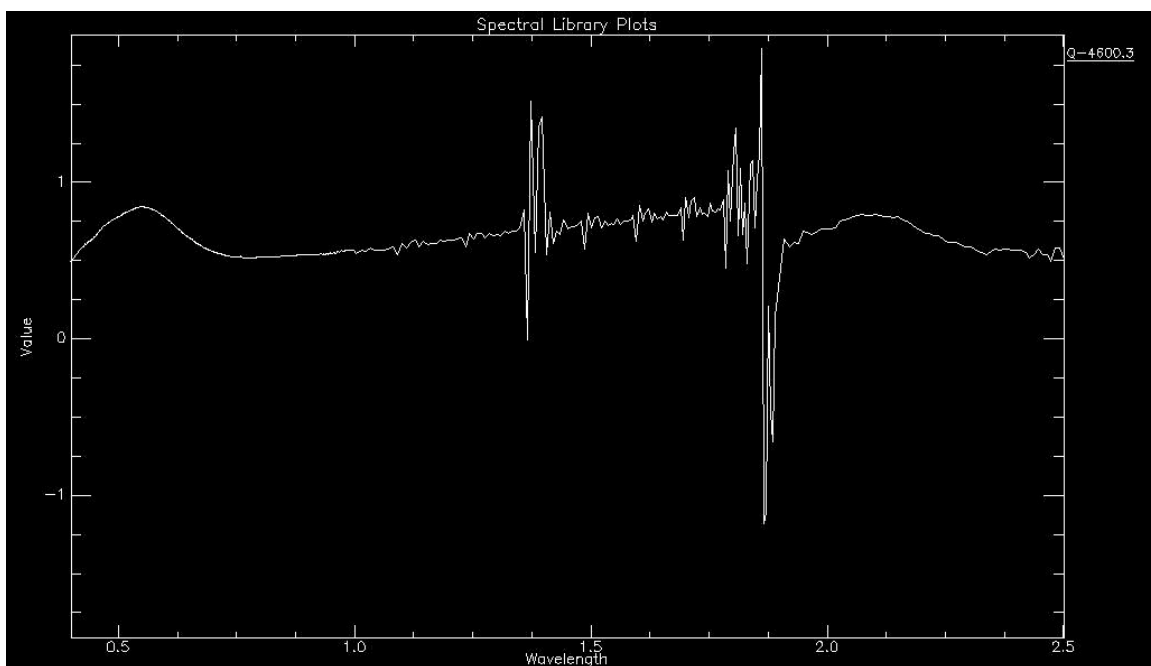


**Figure 4.63.** Spectral profile of sample Q-4600.3.

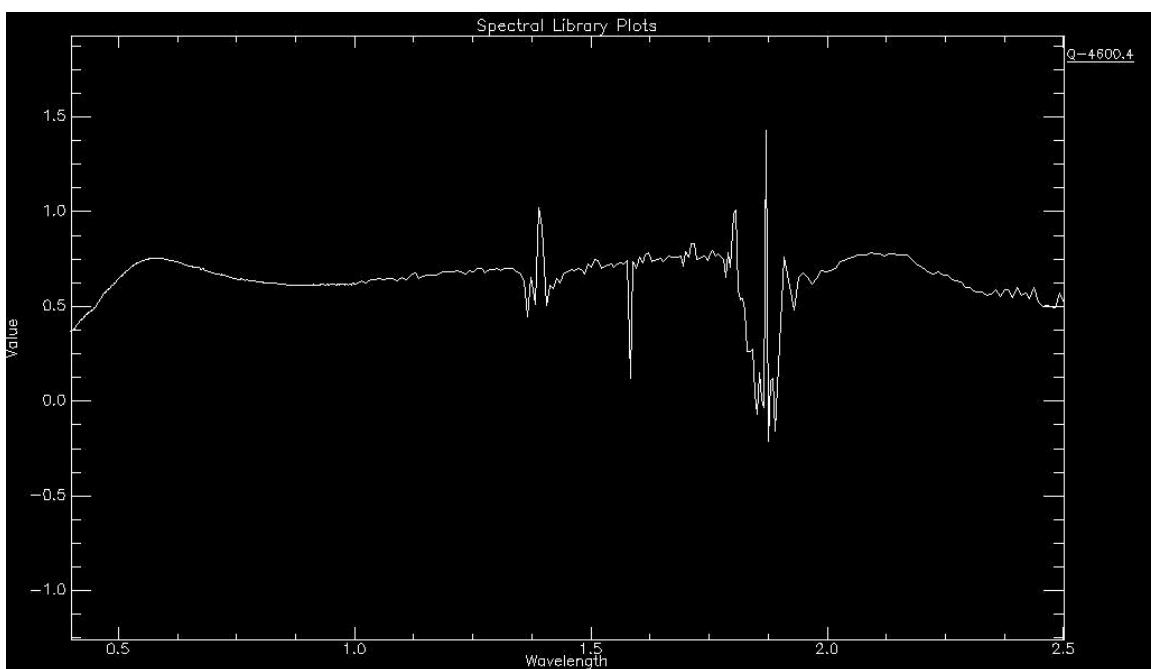


**Figure 4.64.** Spectral profile of sample Q-4600.4.

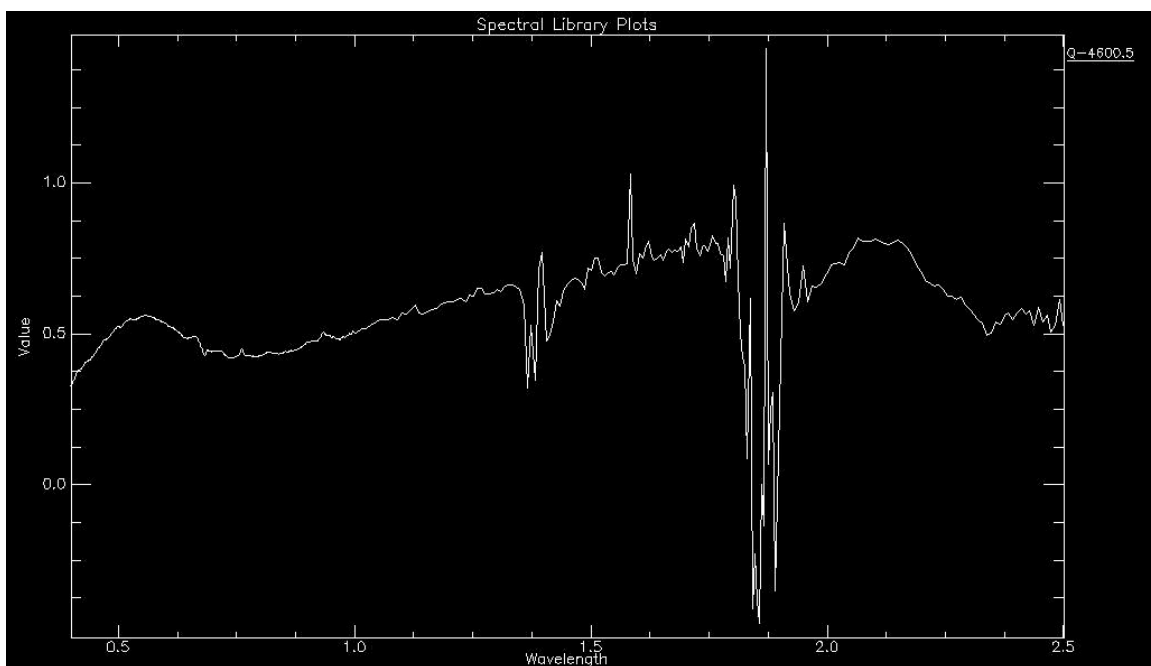


**Figure 4.65.** Spectral profile of sample Q-4600.5.

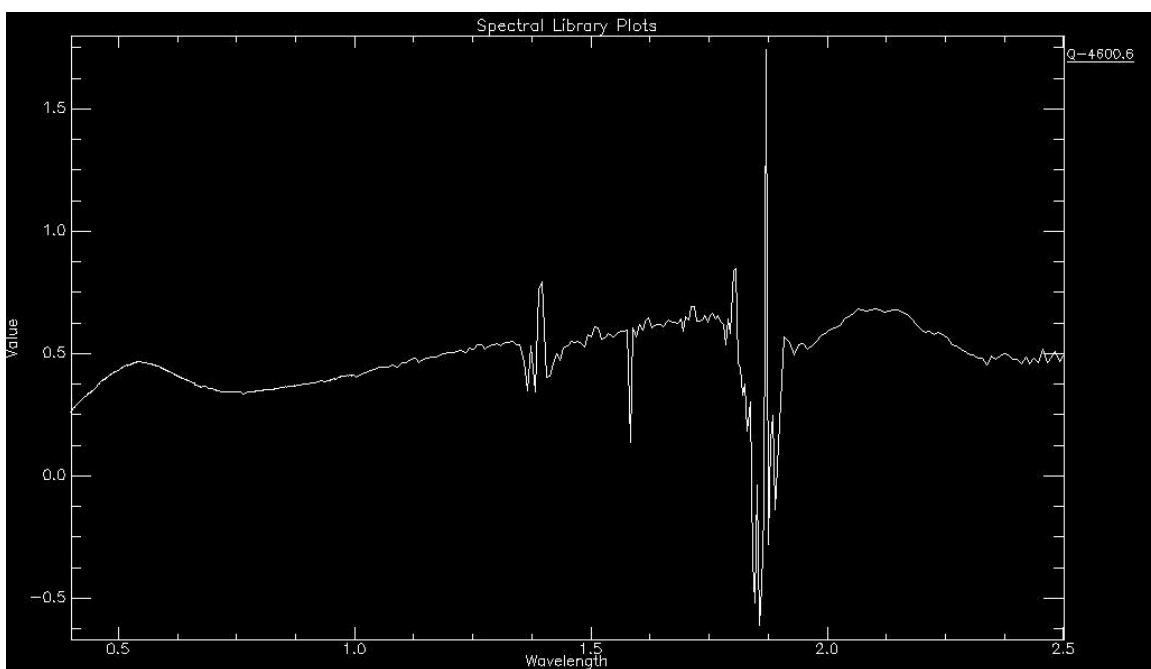


**Figure 4.66.** Spectral profile of sample Q-4600.6.

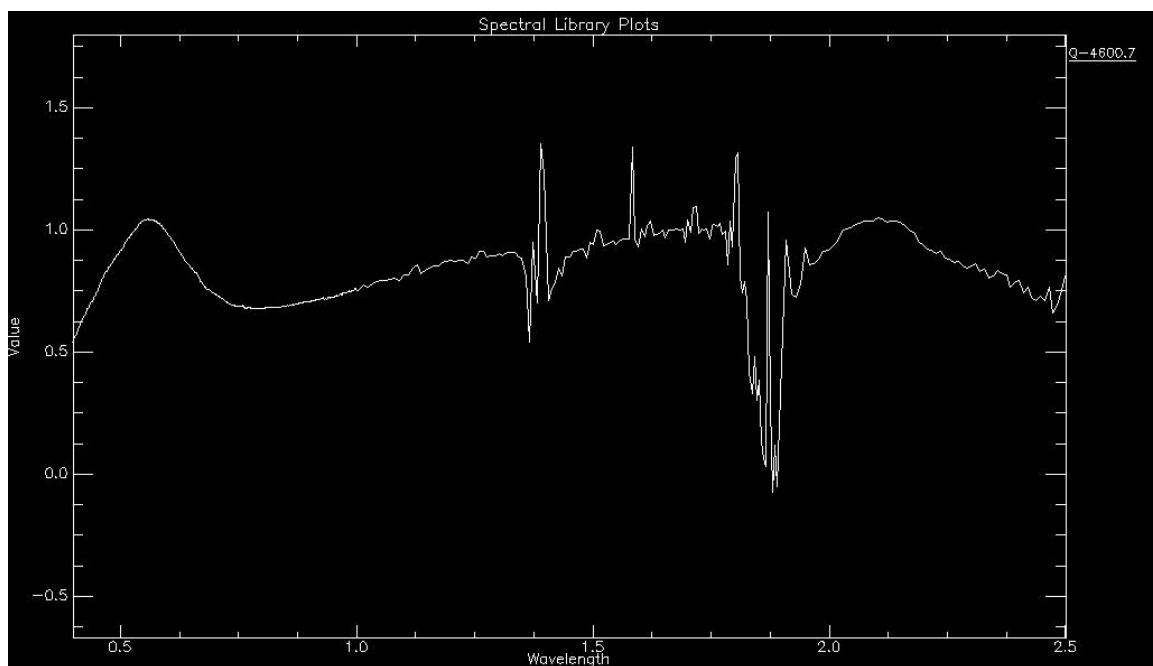


**Figure 4.67.** Spectral profile of sample Q-4600.7.

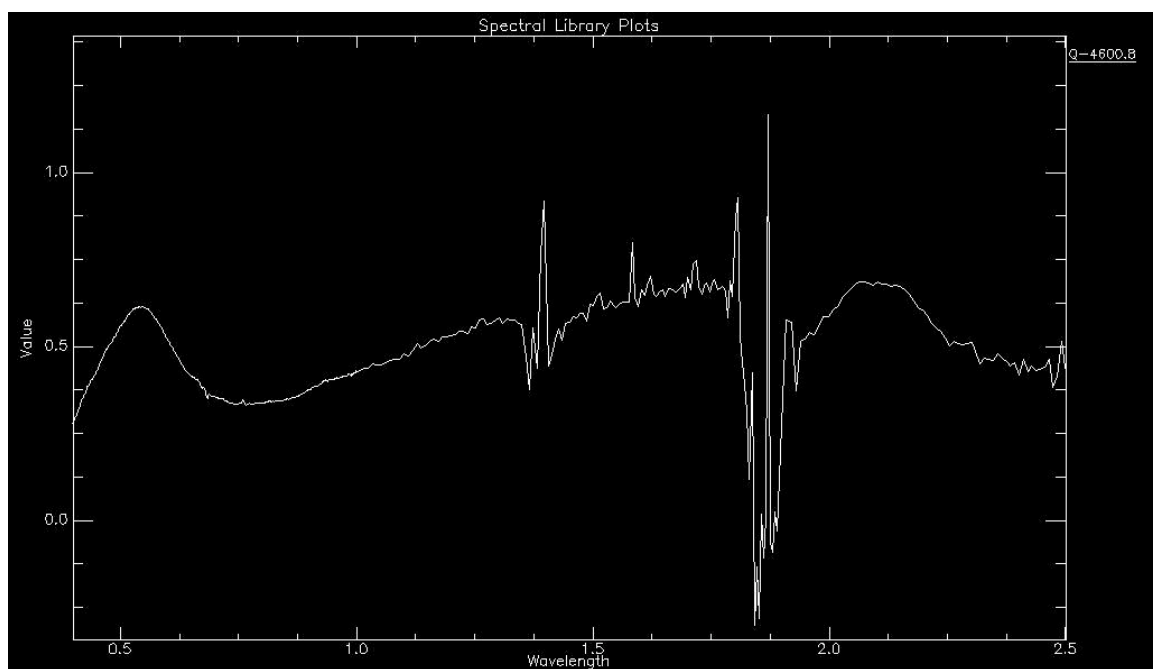


**Figure 4.68.** Spectral profile of sample Q-4600.8.

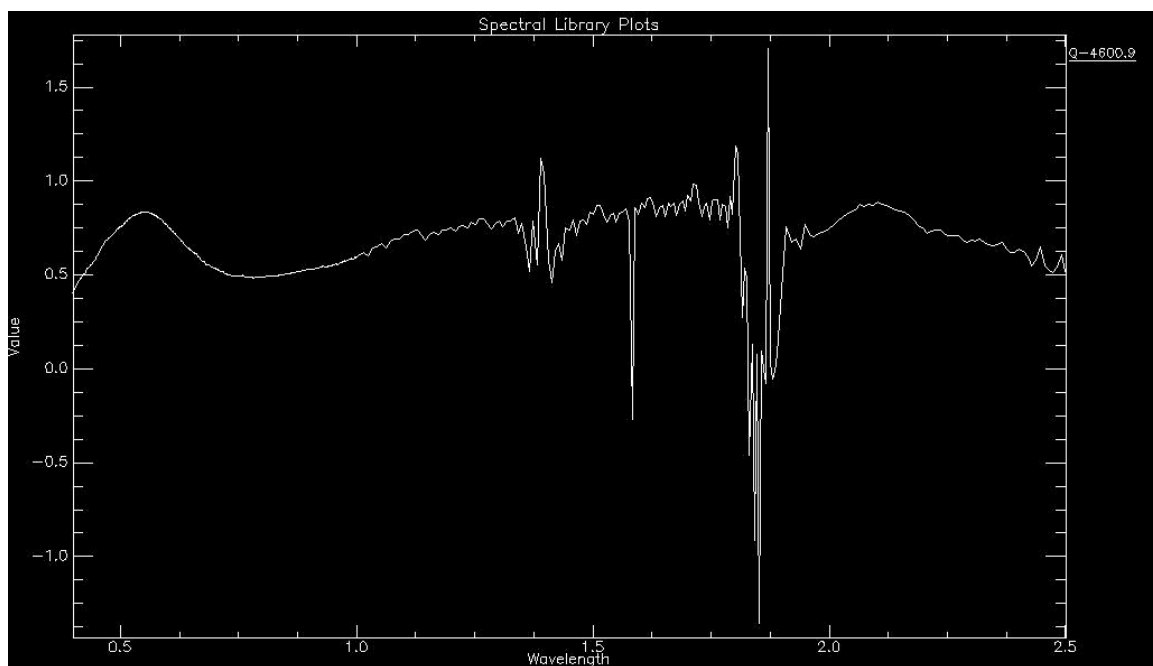


**Figure 4.69.** Spectral profile of sample Q-4600.9.

### 18.5. Appendix 4.5. Spectral Profiles of RHY-4700

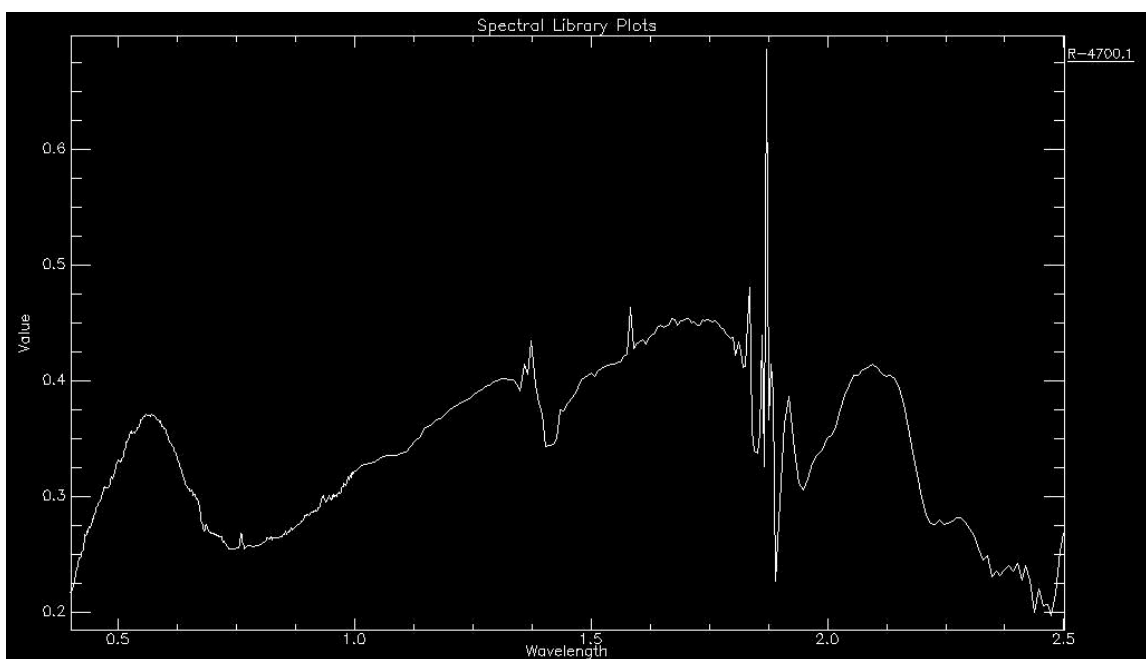


Figure 4.70. Spectral profile of sample R-4700.1.

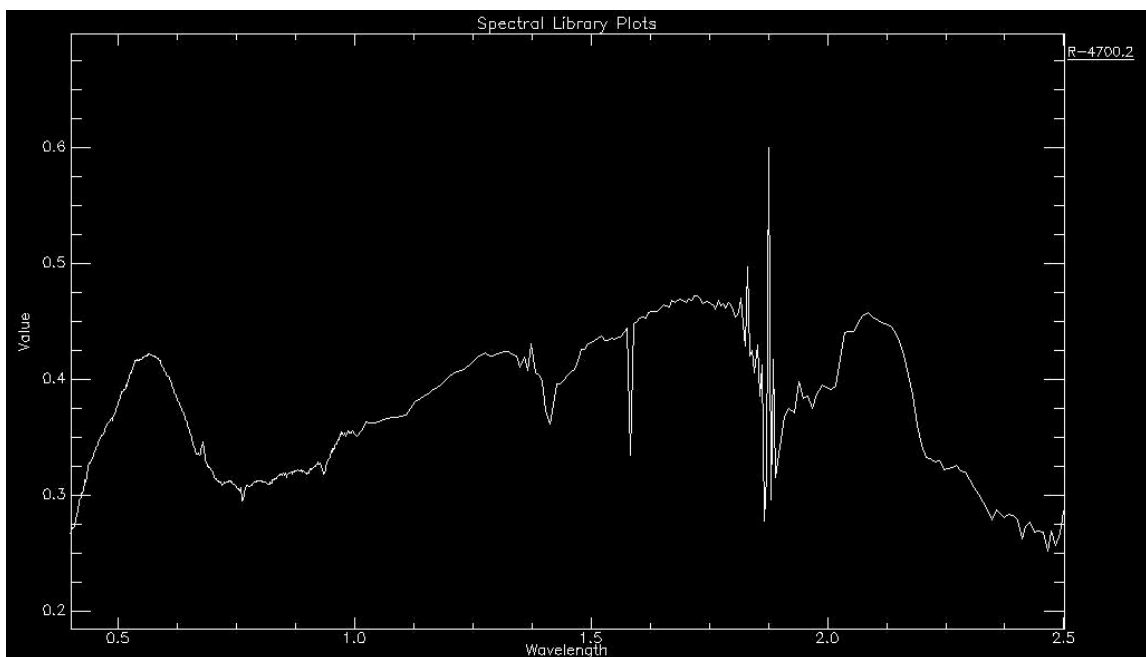
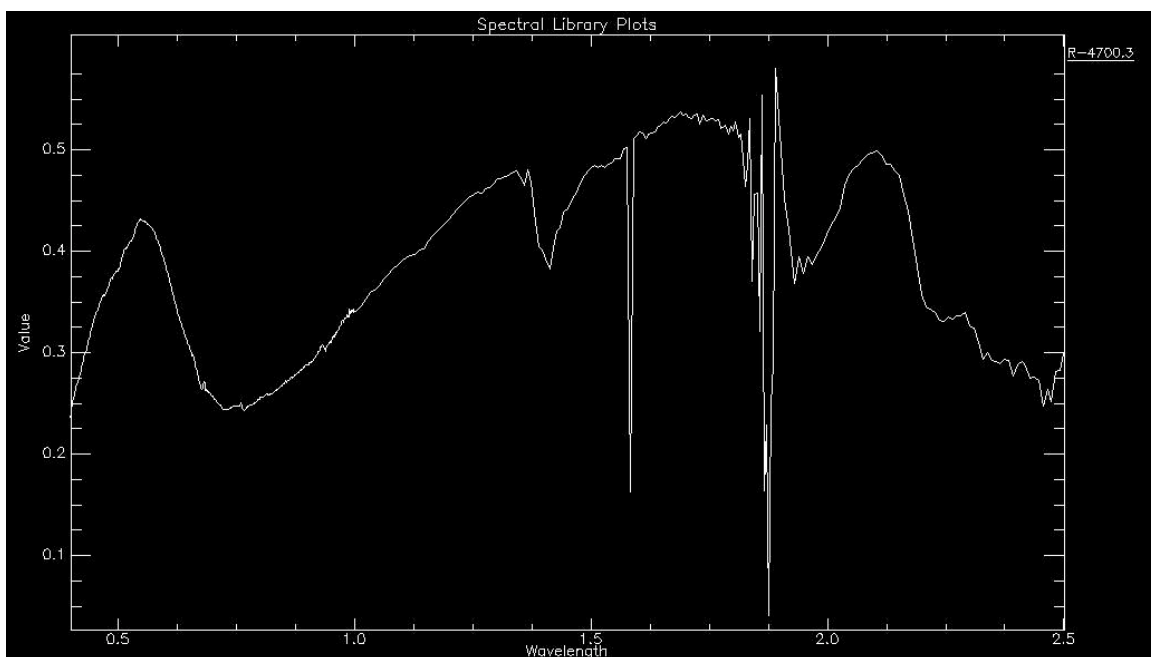
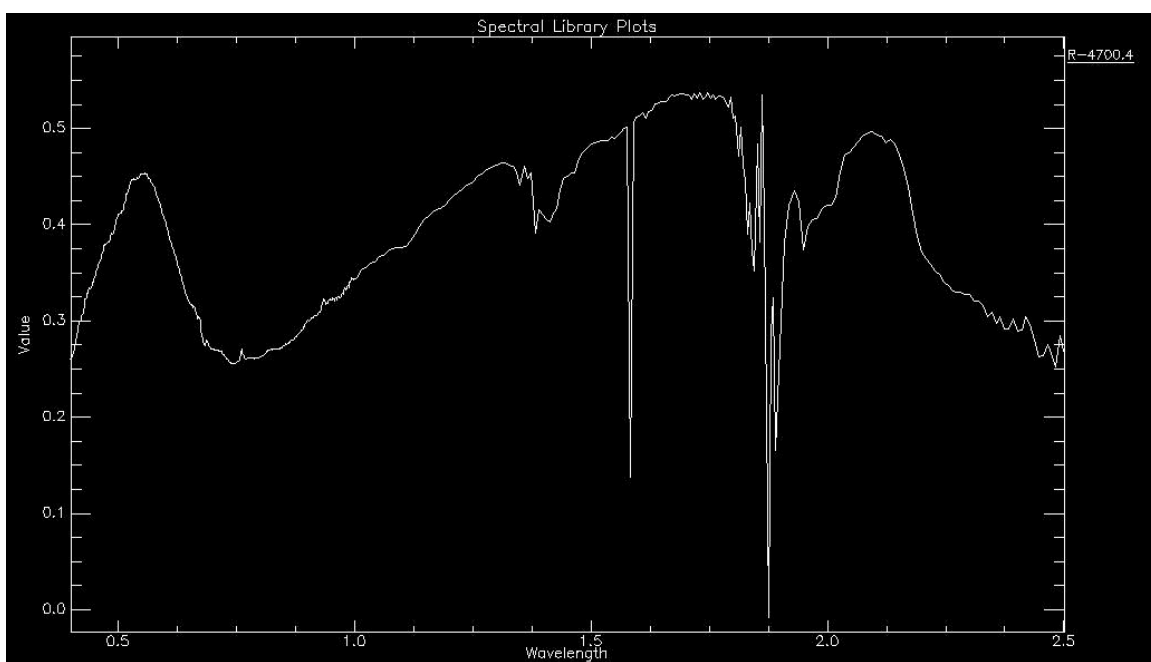


Figure 4.71. Spectral profile of sample R-4700.2.



**Figure 4.72.** Spectral profile of sample R-4700.3.



**Figure 4.73.** Spectral profile of sample R-4700.4.

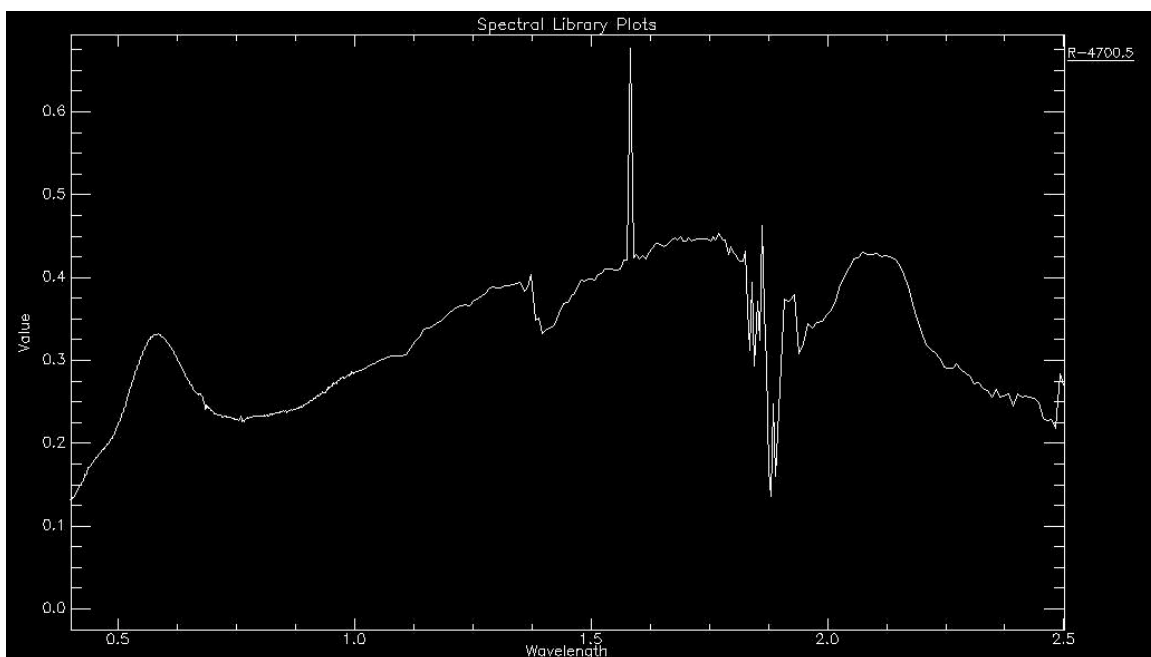


**Figure 4.74.** Spectral profile of sample R-4700.5.

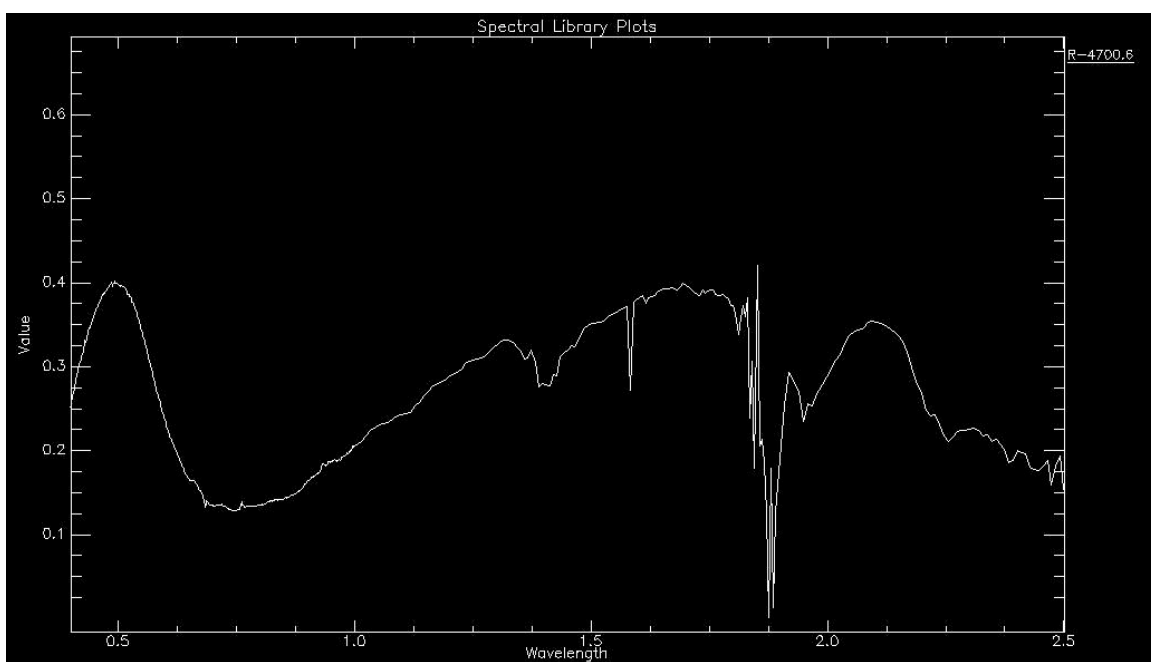


**Figure 4.75.** Spectral profile of sample R-4700.6.

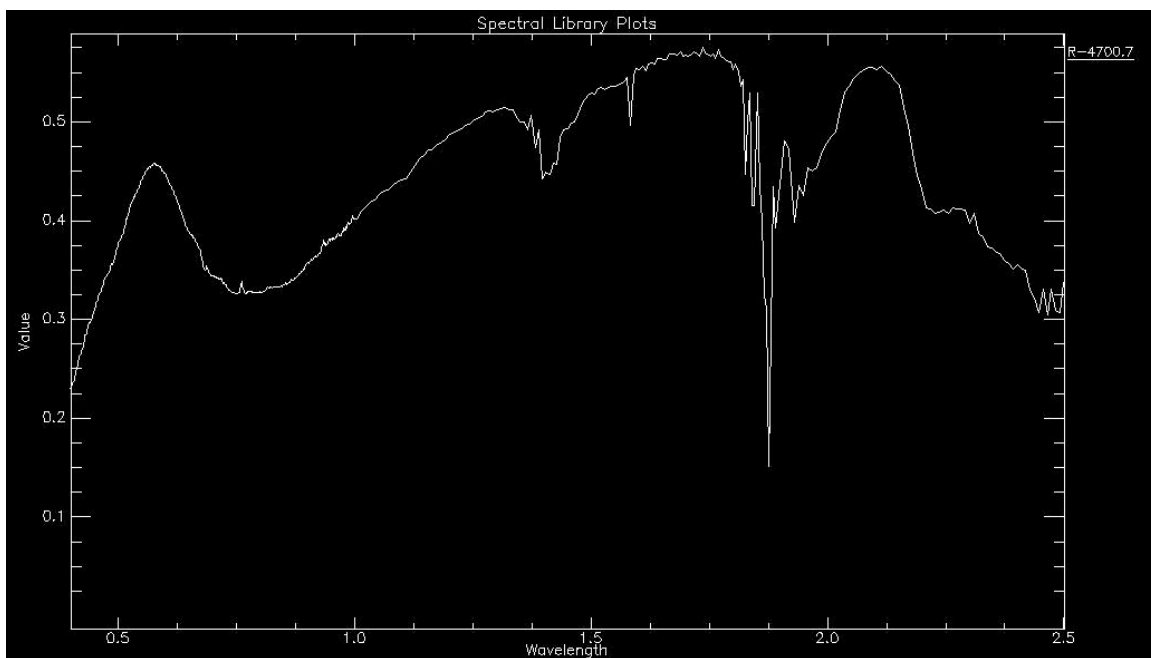


**Figure 4.76.** Spectral profile of sample R-4700.7.

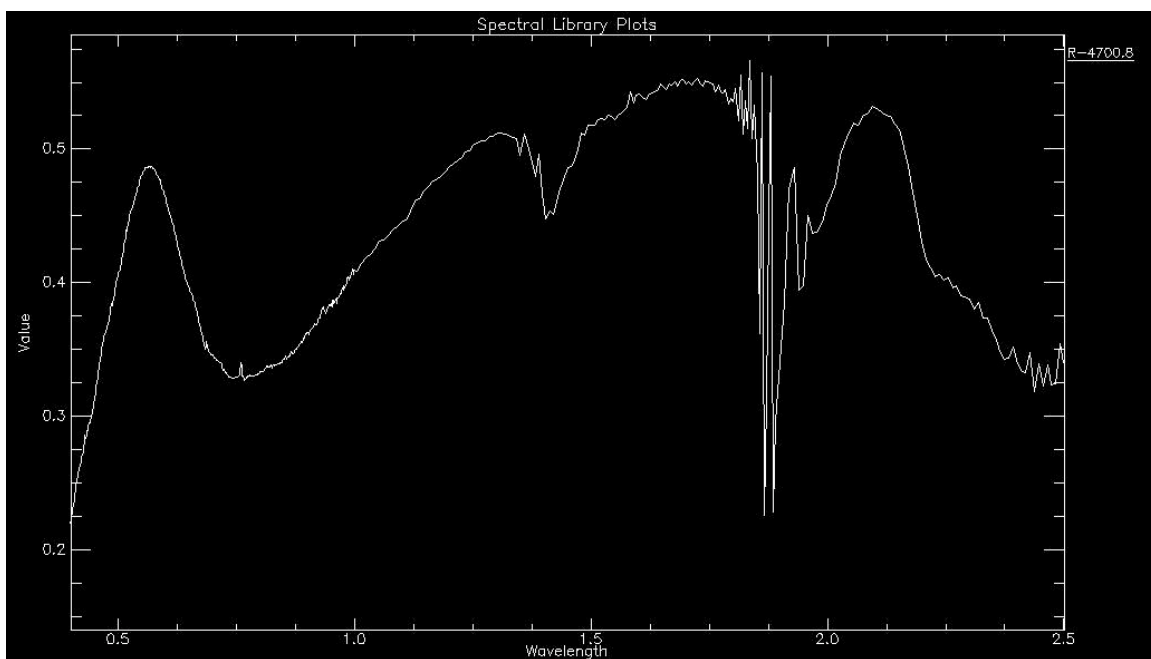


**Figure 4.77.** Spectral profile of sample R-4700.8.

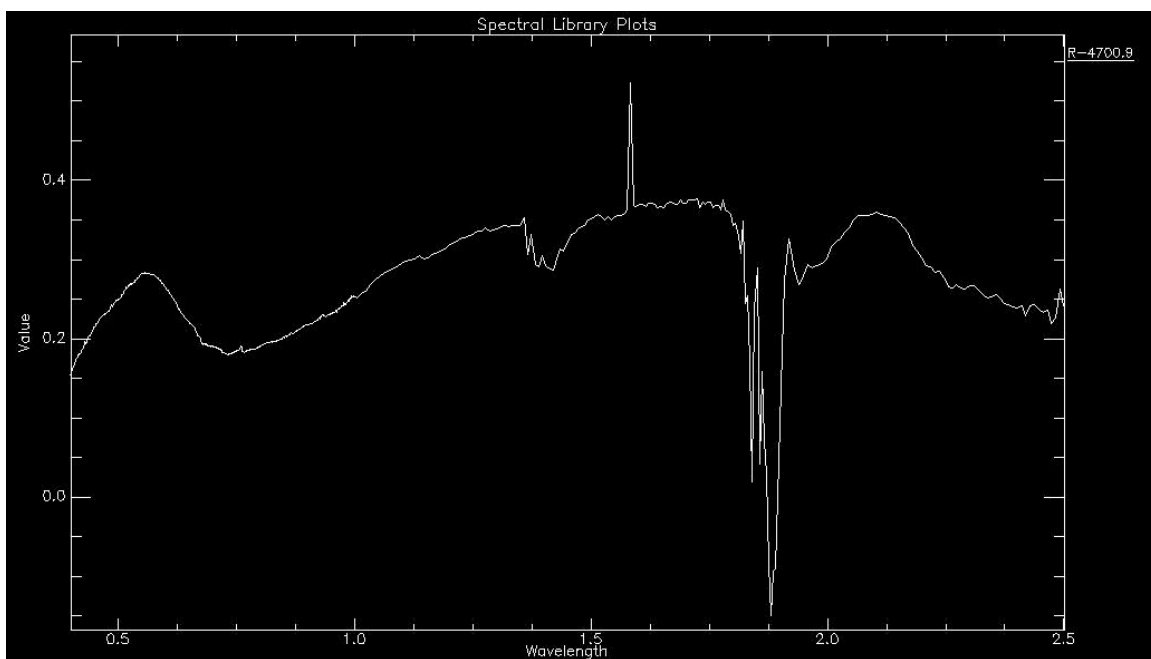


**Figure 4.78.** Spectral profile of sample R-4700.9.

## 18.6. Appendix 4.6. Spectral Profiles of RHY-4675

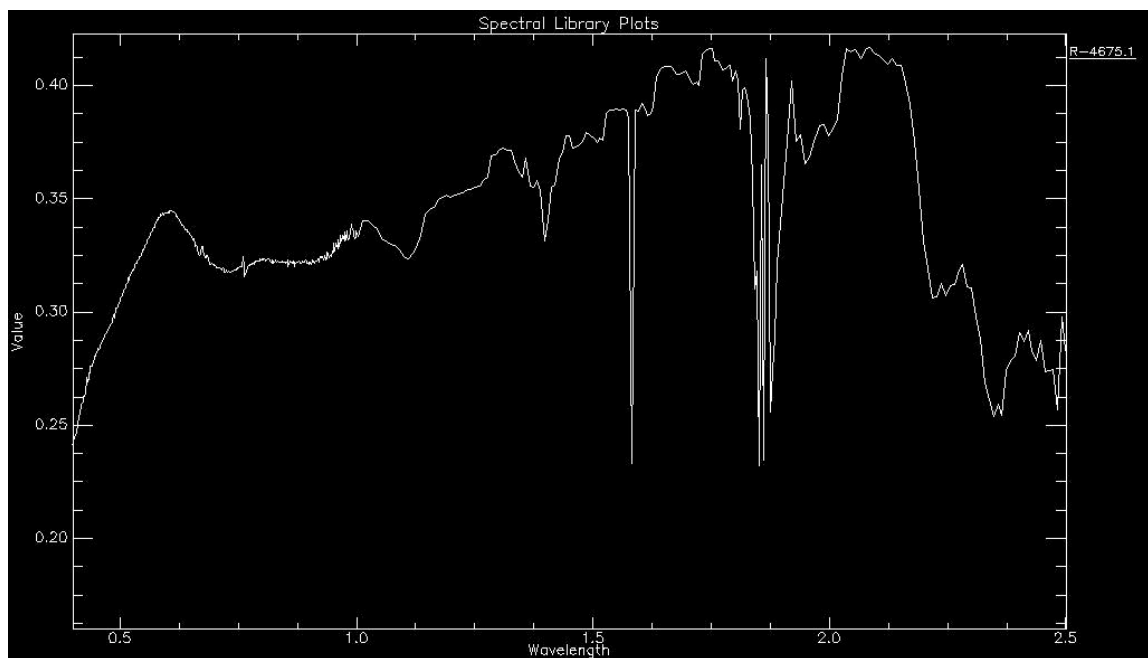


**Figure 4.79.** Spectral profile of sample R-4675.1.

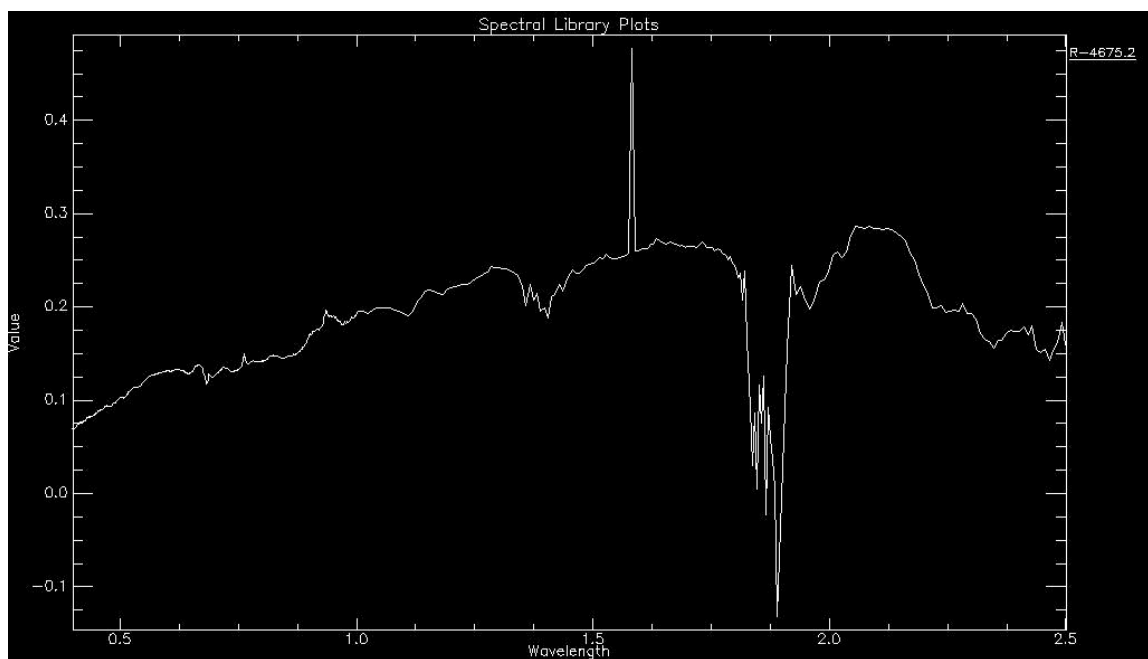


**Figure 4.80.** Spectral profile of sample R-4675.2.

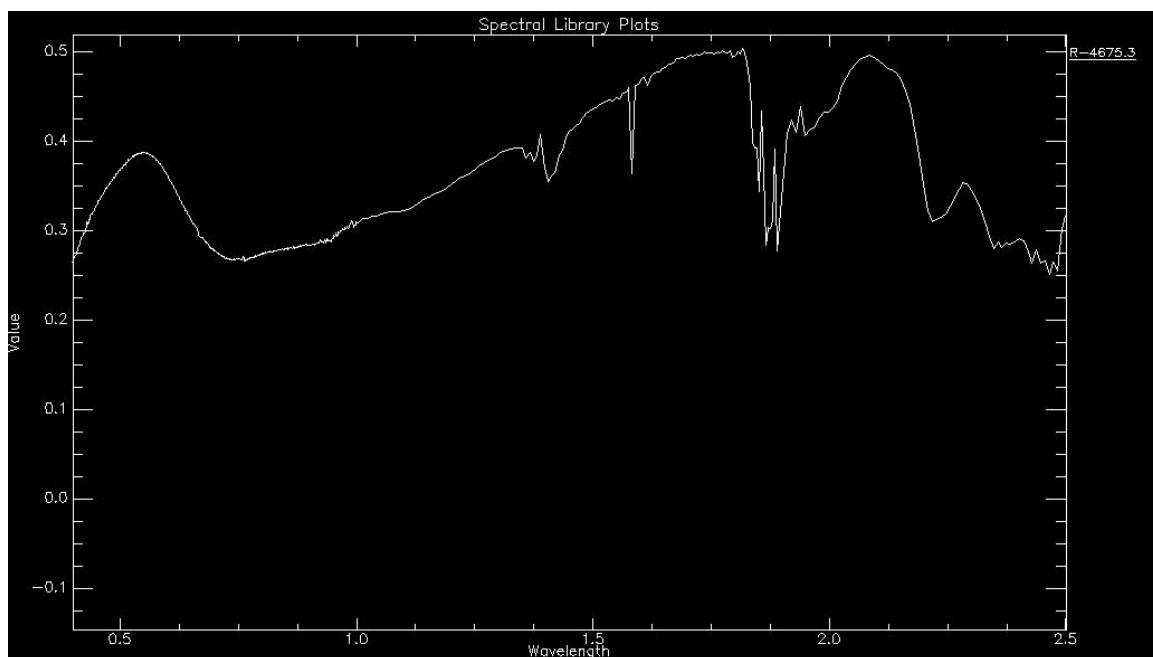


**Figure 4.81.** Spectral profile of sample R-4675.3.

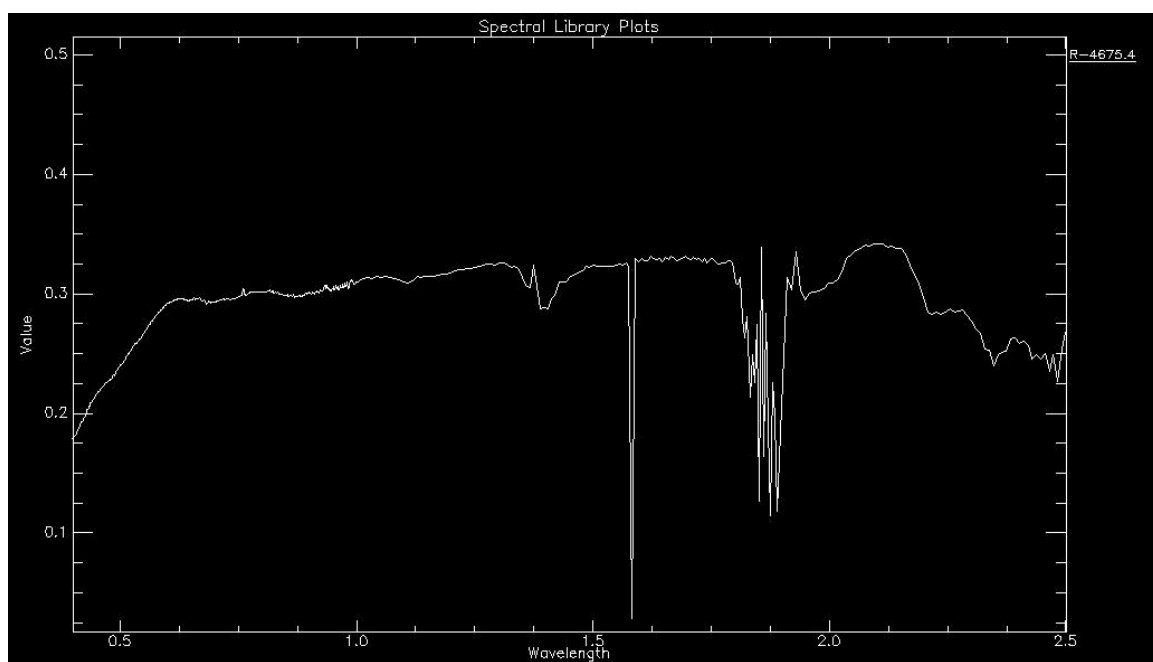


**Figure 4.82.** Spectral profile of sample R-4675.4.

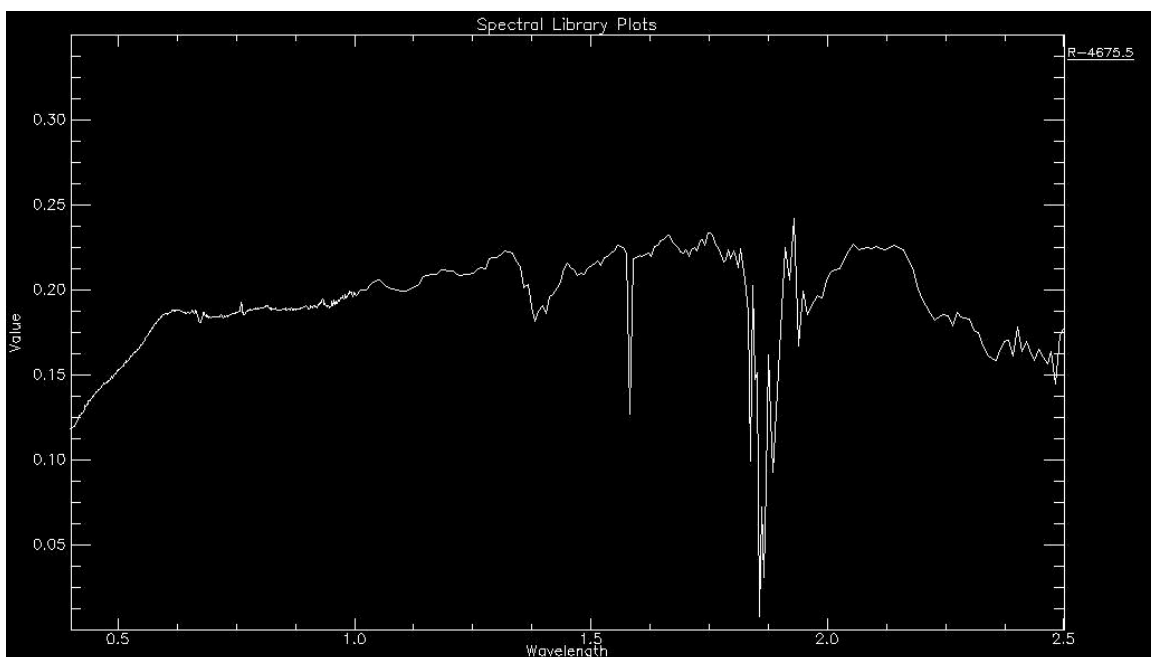


**Figure 4.83.** Spectral profile of sample R-4675.5.

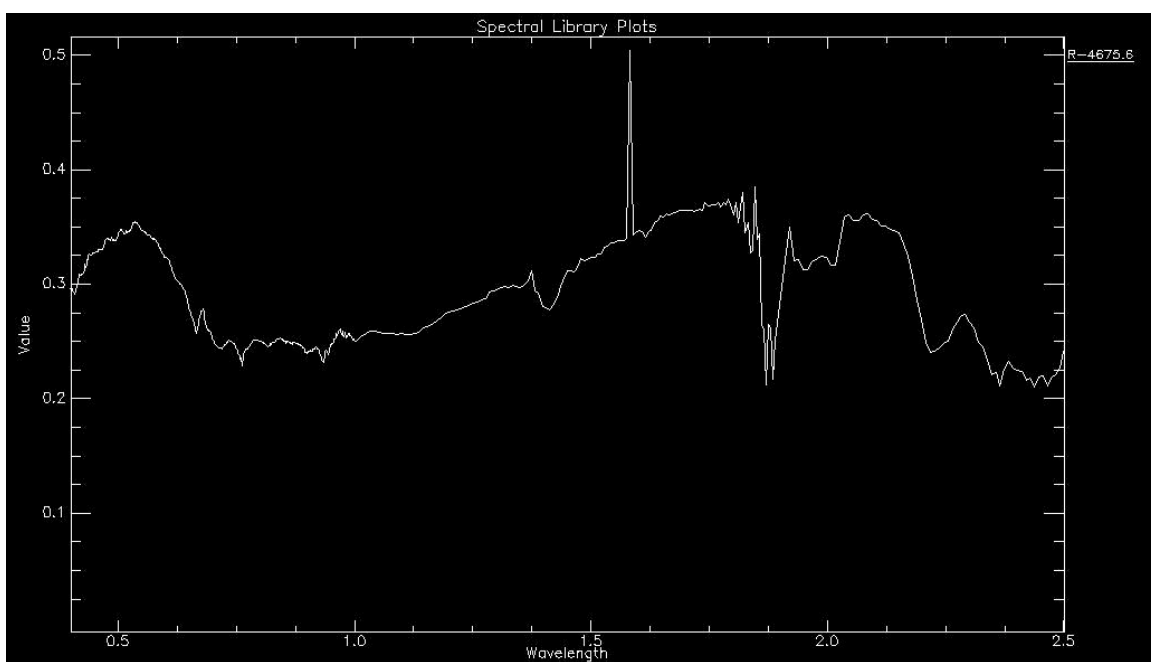


**Figure 4.84.** Spectral profile of sample R-4675.6.

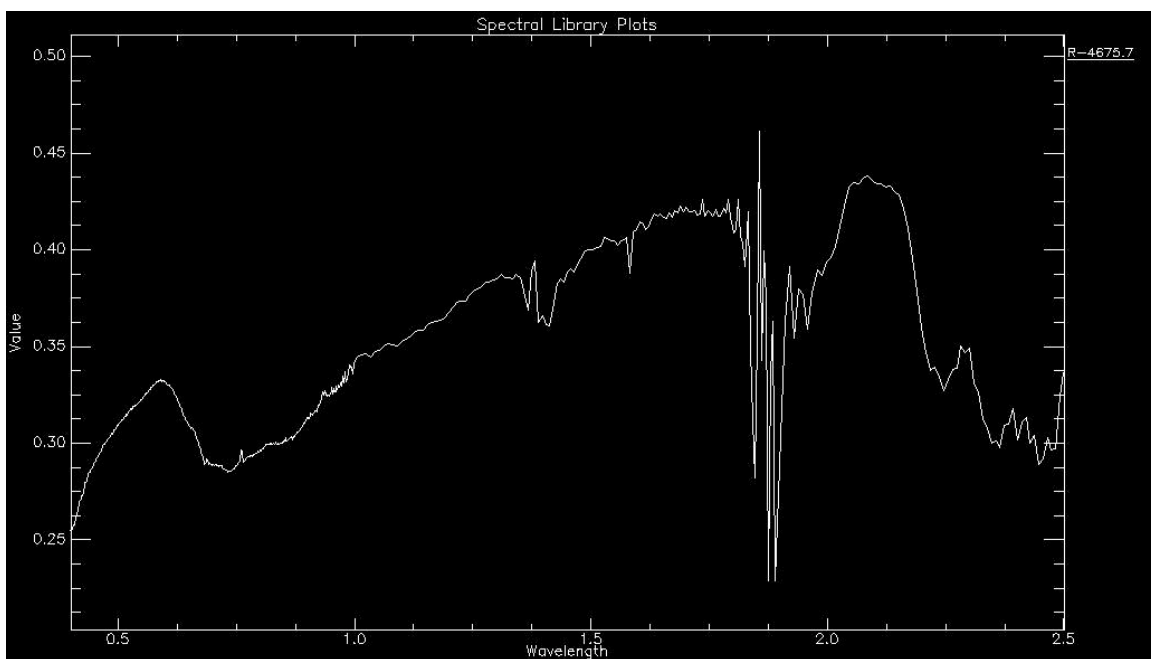


**Figure 4.85.** Spectral profile of sample R-4675.7.

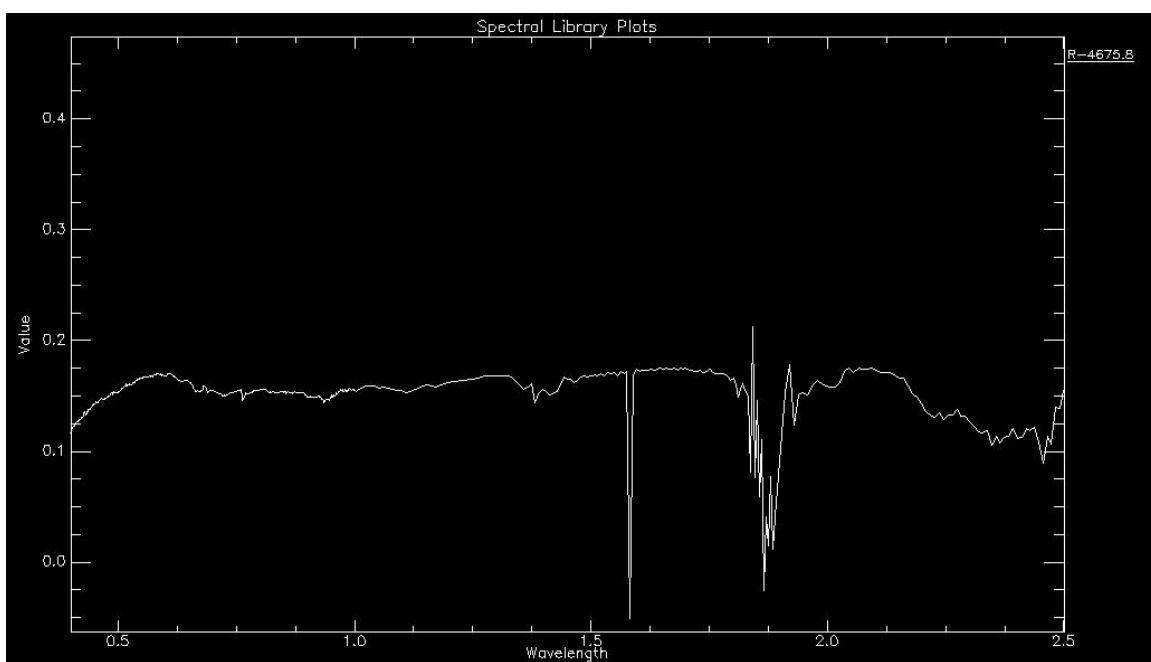


**Figure 4.86.** Spectral profile of sample R-4675.8.

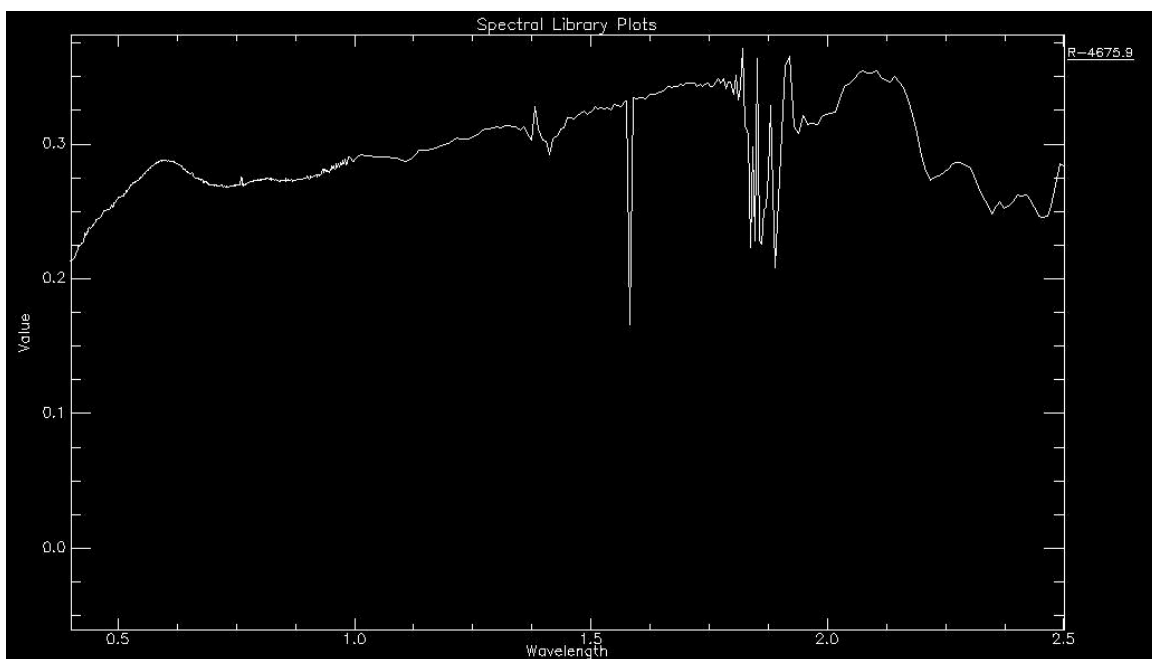


**Figure 4.87.** Spectral profile of sample R-4675.9.

## 18.7. Appendix 4.7. Spectral Profiles from USGS Spectral Library

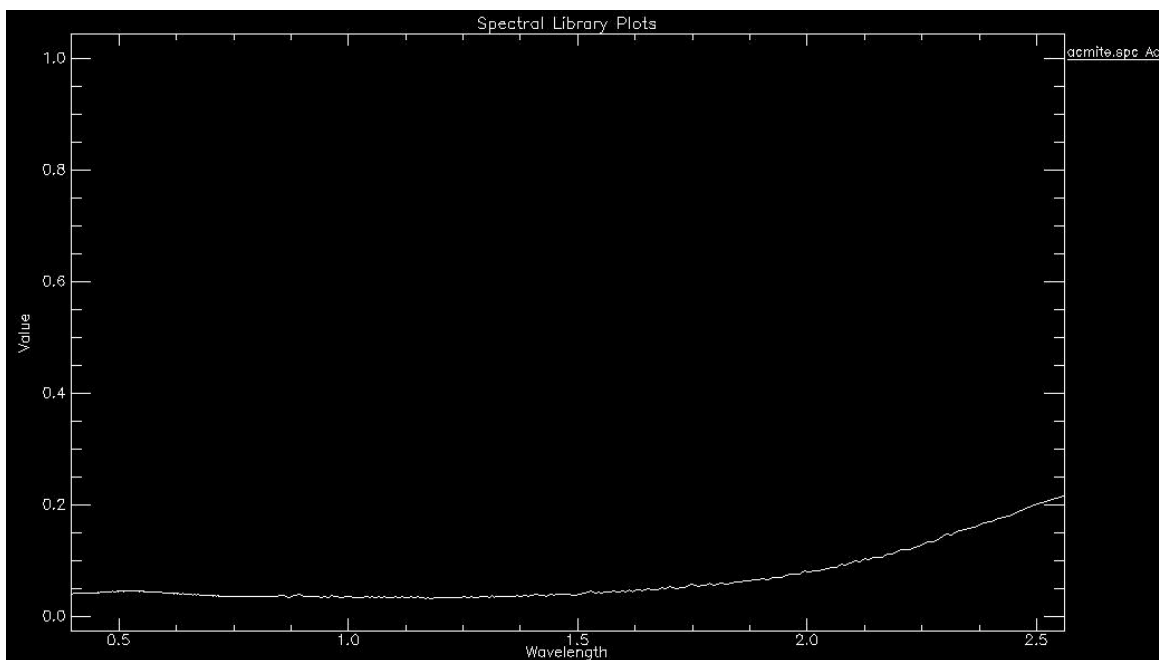


**Figure 4.88.** Spectral profile of atacamite from the USGS spectral library.

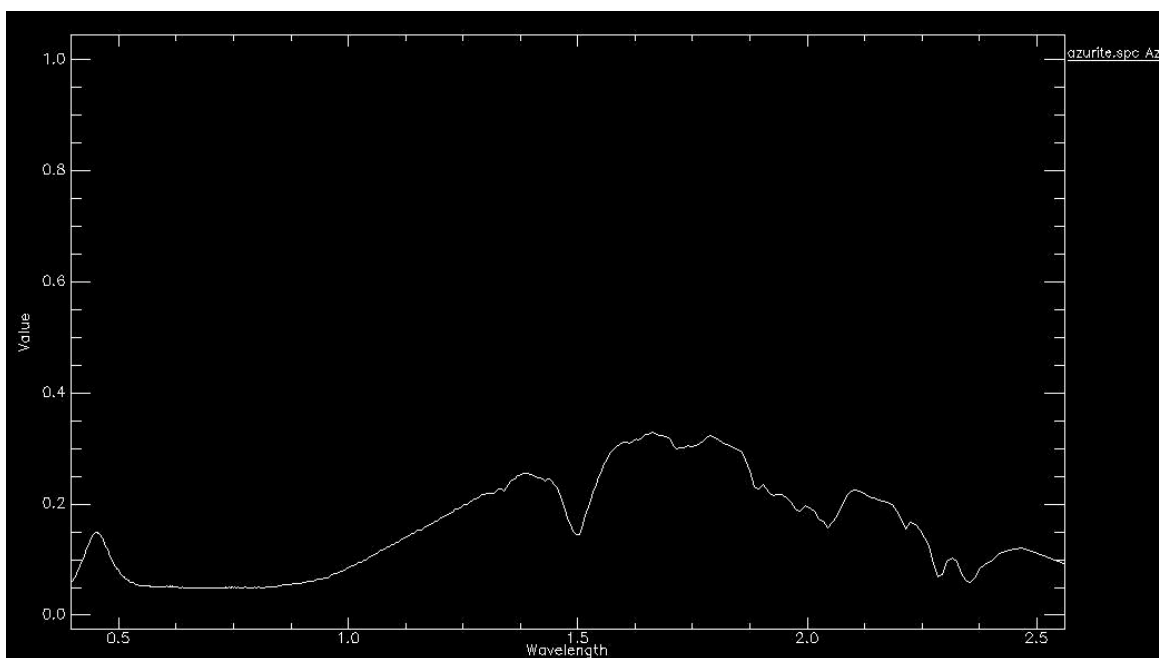


**Figure 4.89.** Spectral profile of azurite from the USGS spectral library.

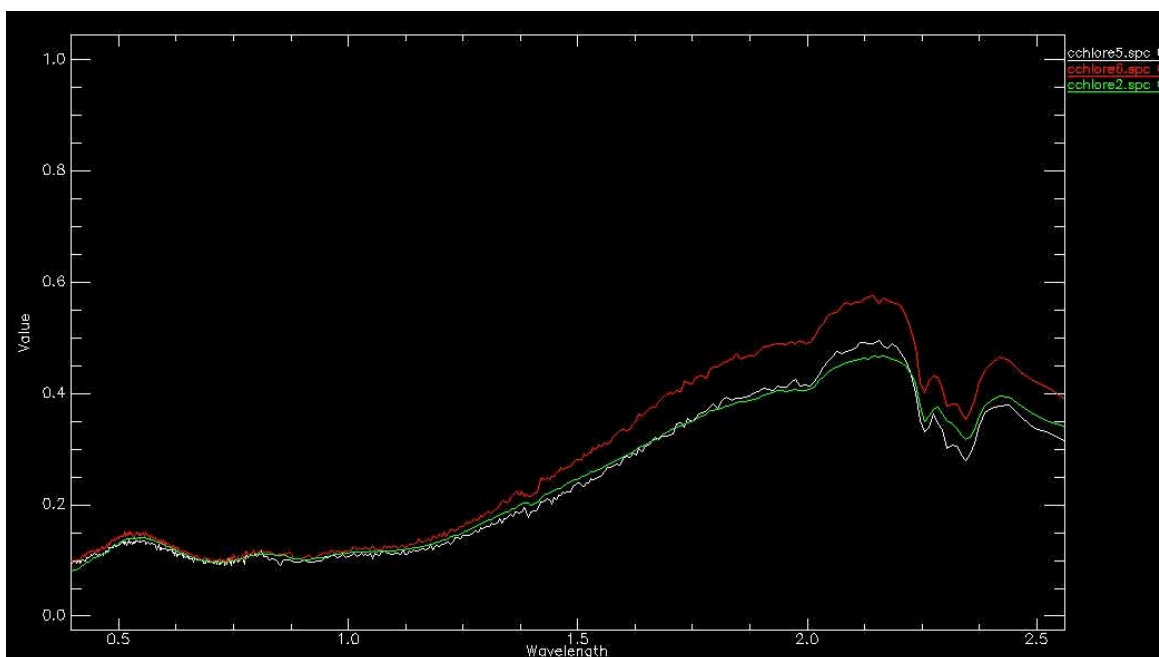


**Figure 4.90.** Spectral profiles of chlorite from the USGS spectral library.

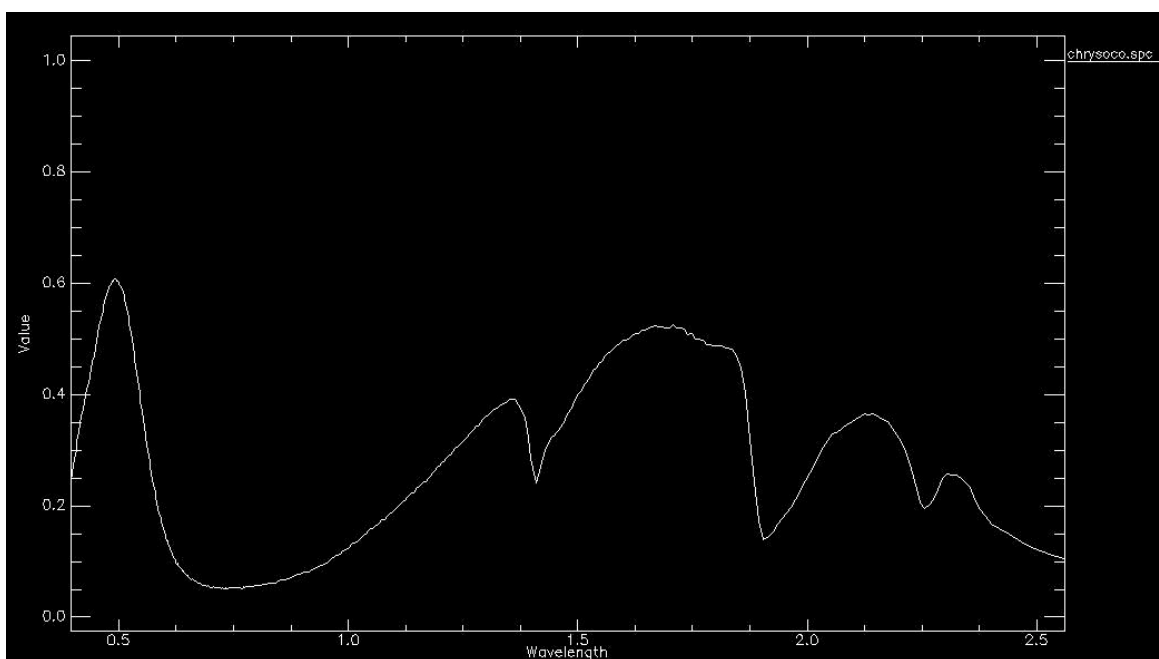


**Figure 4.91.** Spectral profile of chrysocolla from the USGS spectral library.

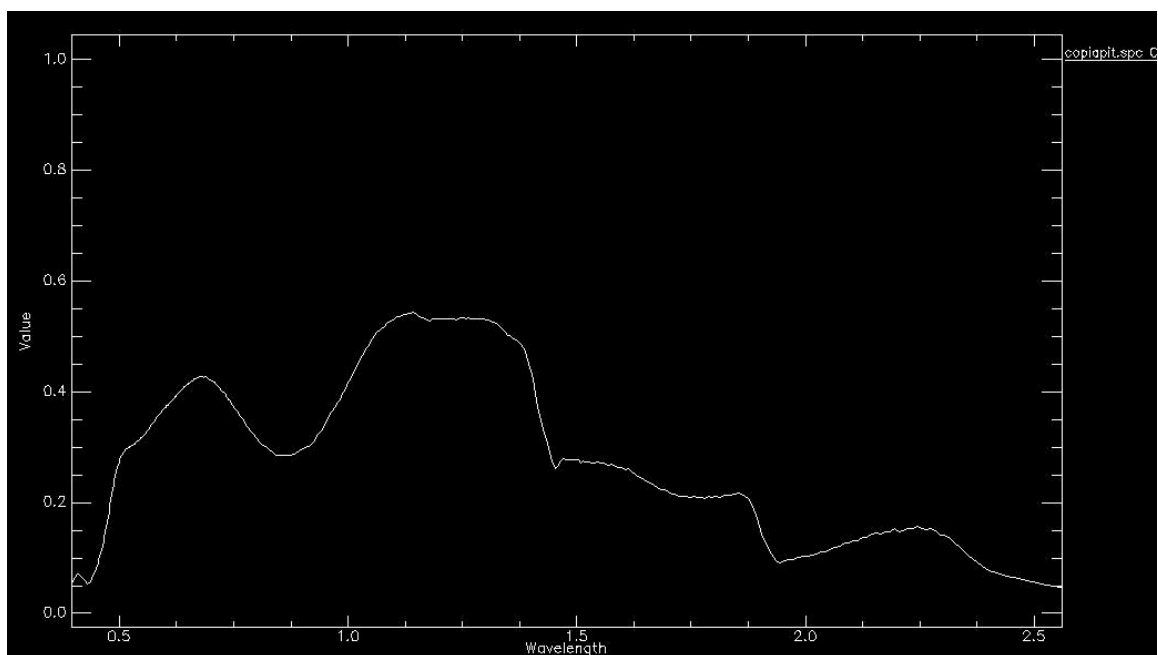


**Figure 4.92.** Spectral profile of copiapite from the USGS spectral library.

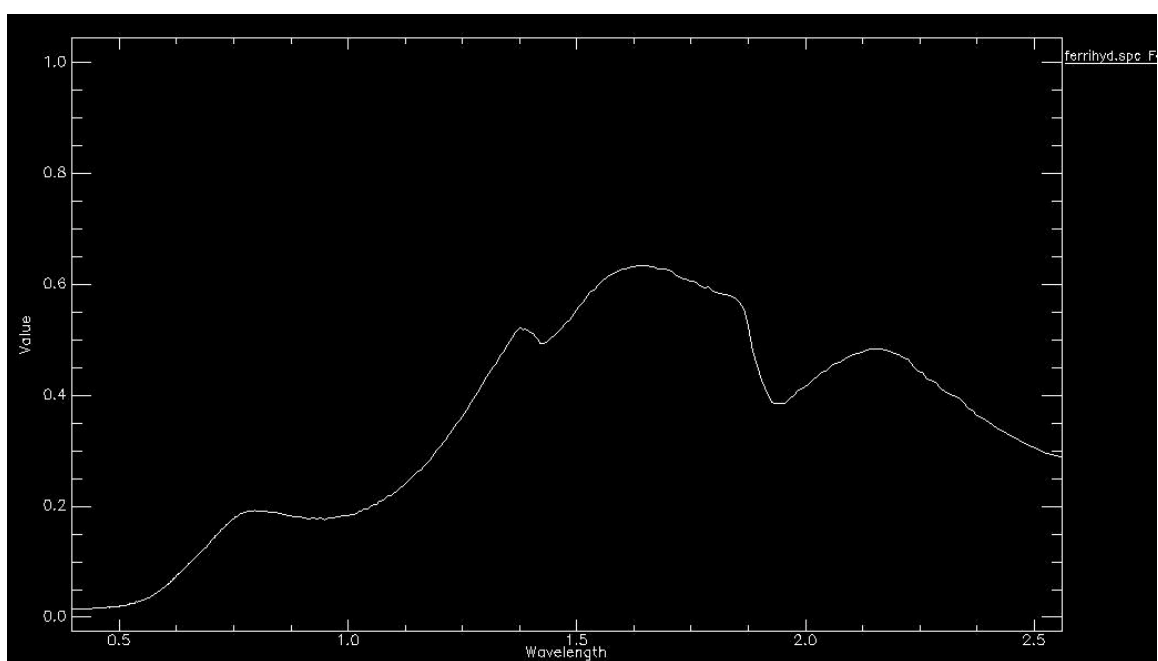


**Figure 4.93.** Spectral profile of ferrihydrite from the USGS spectral library.

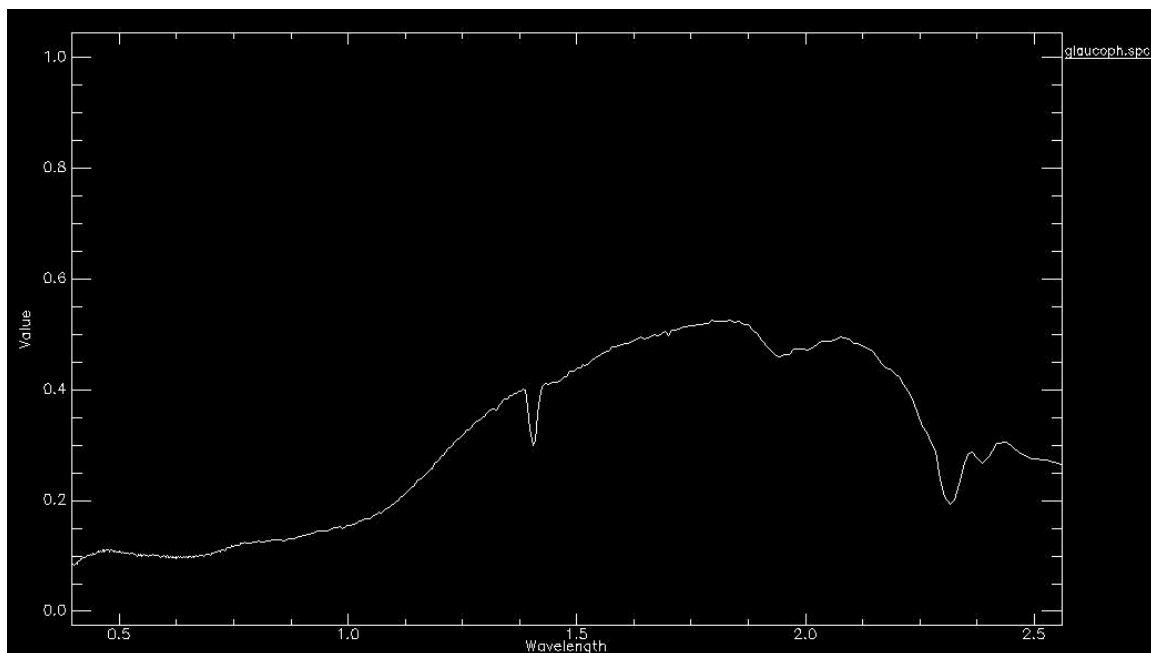


**Figure 4.94.** Spectral profile of glaucophane from the USGS spectral library.

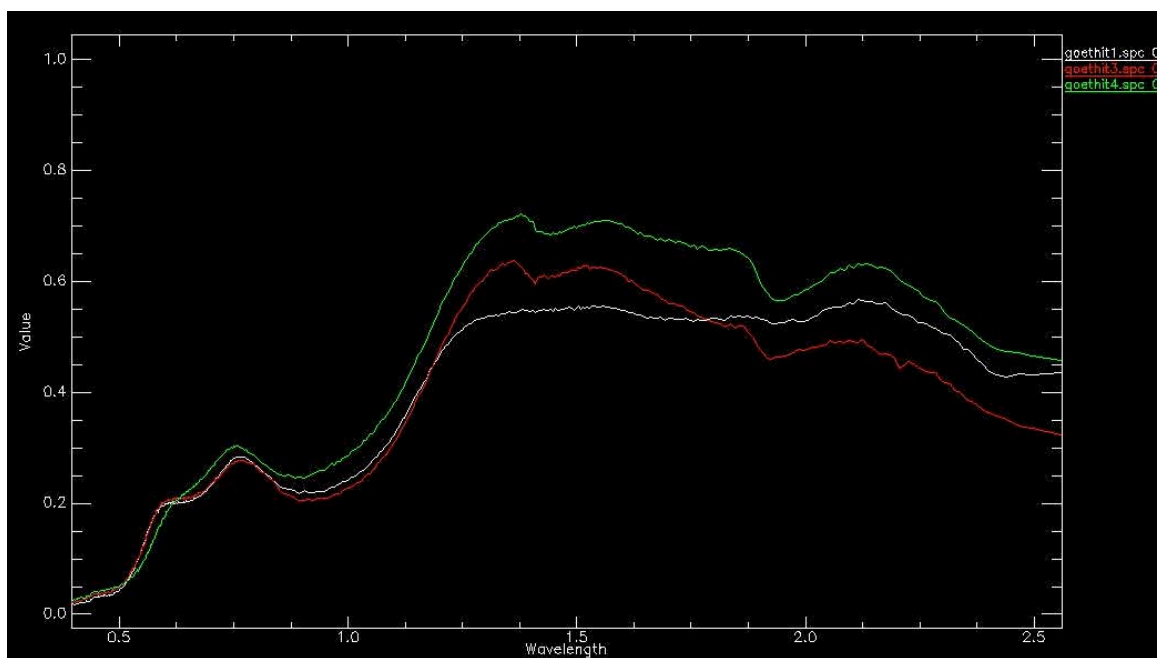


**Figure 4.95.** Spectral profiles of goethite from the USGS spectral library.

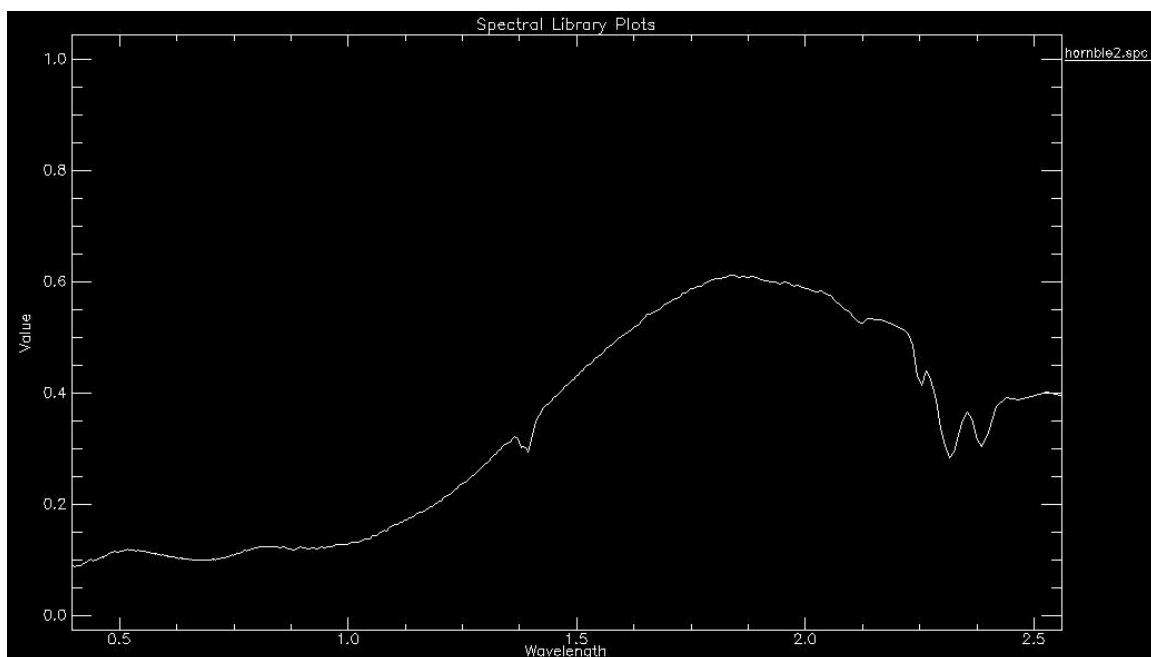


**Figure 4.96.** Spectral profile of hornblende from the USGS spectral library.

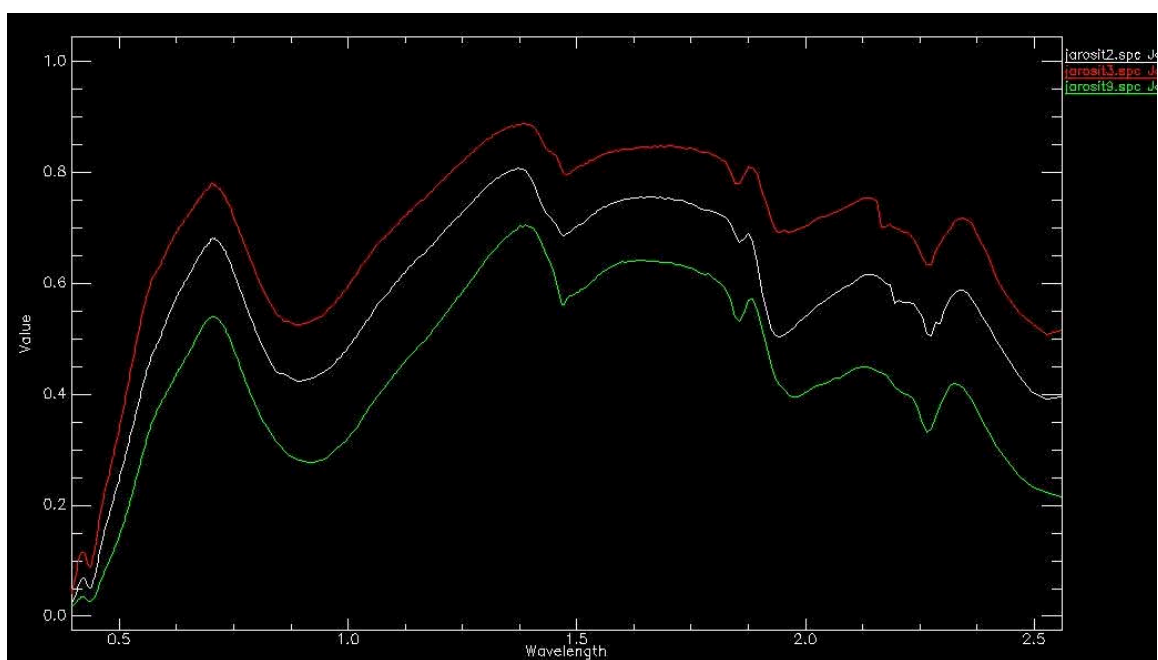


**Figure 4.97.** Spectral profiles of jarosite from the USGS spectral library.

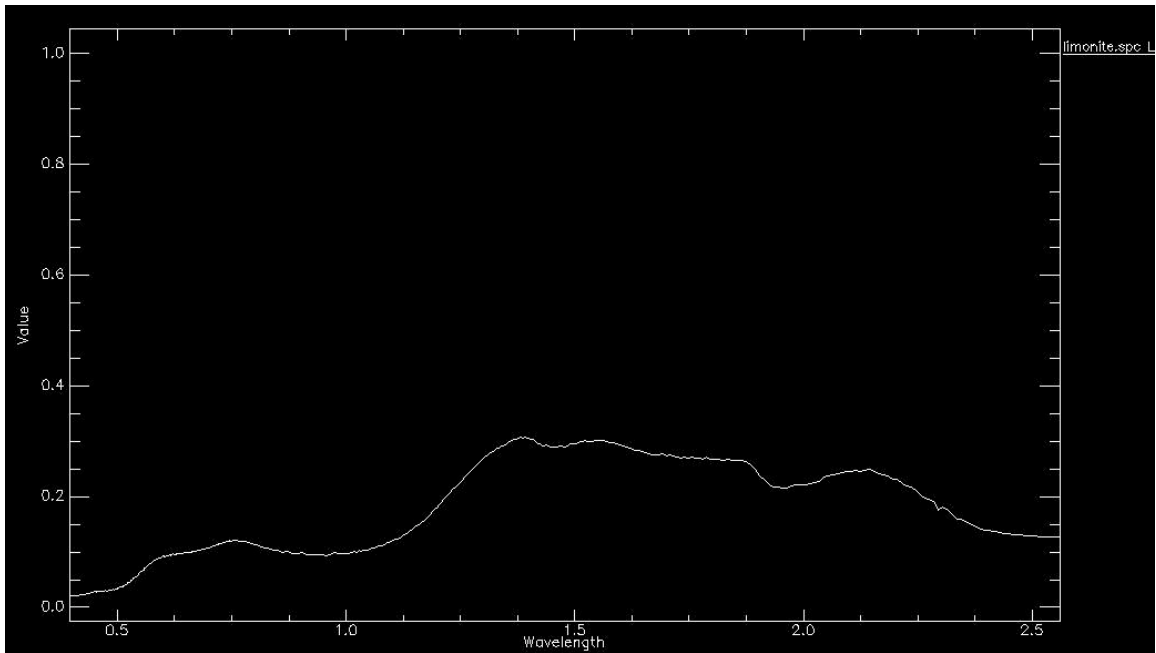


**Figure 4.98.** Spectral profile of limonite from the USGS spectral library.

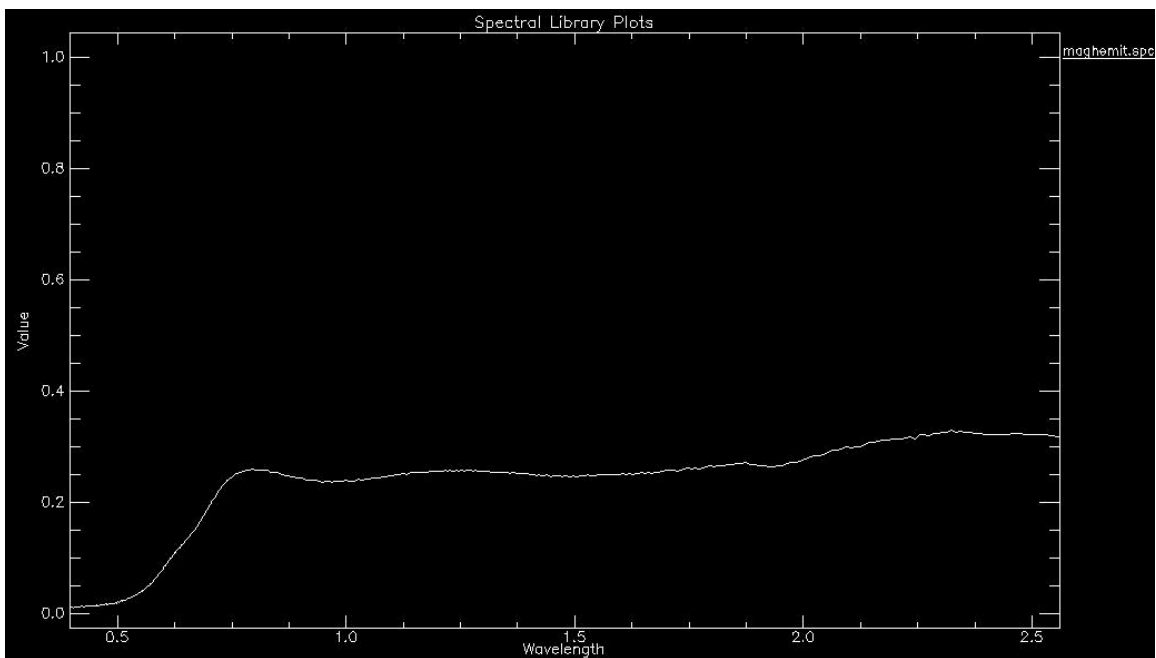


**Figure 4.99.** Spectral profile of maghemite from the USGS spectral library.

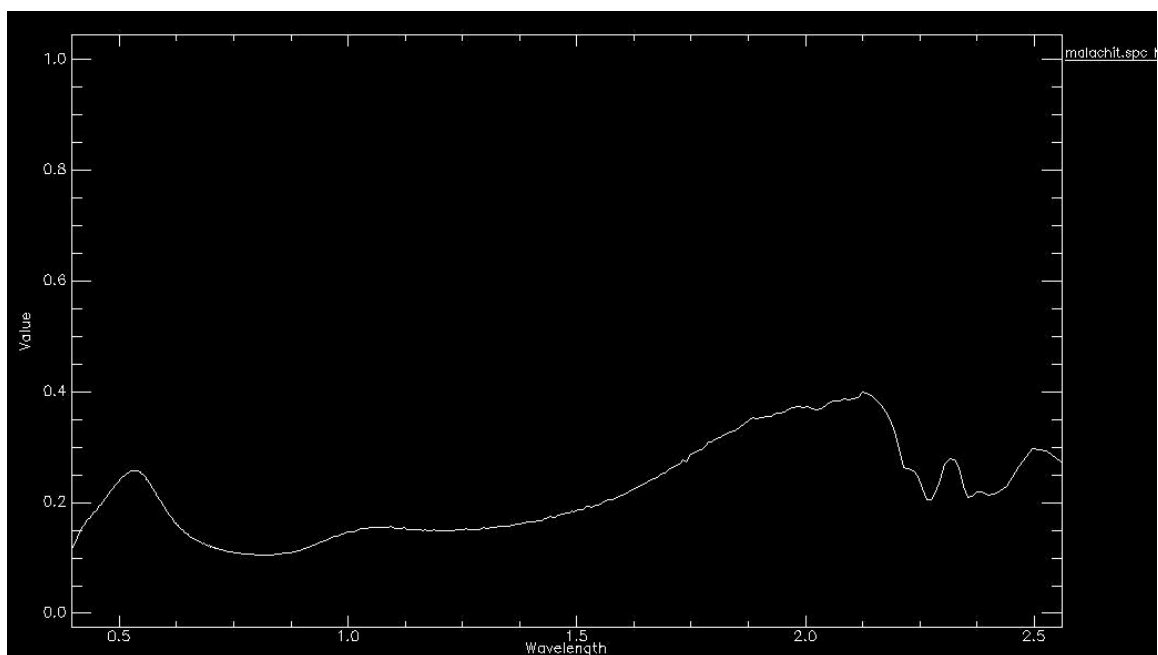


**Figure 4.100.** Spectral profile of malachite from the USGS spectral library.

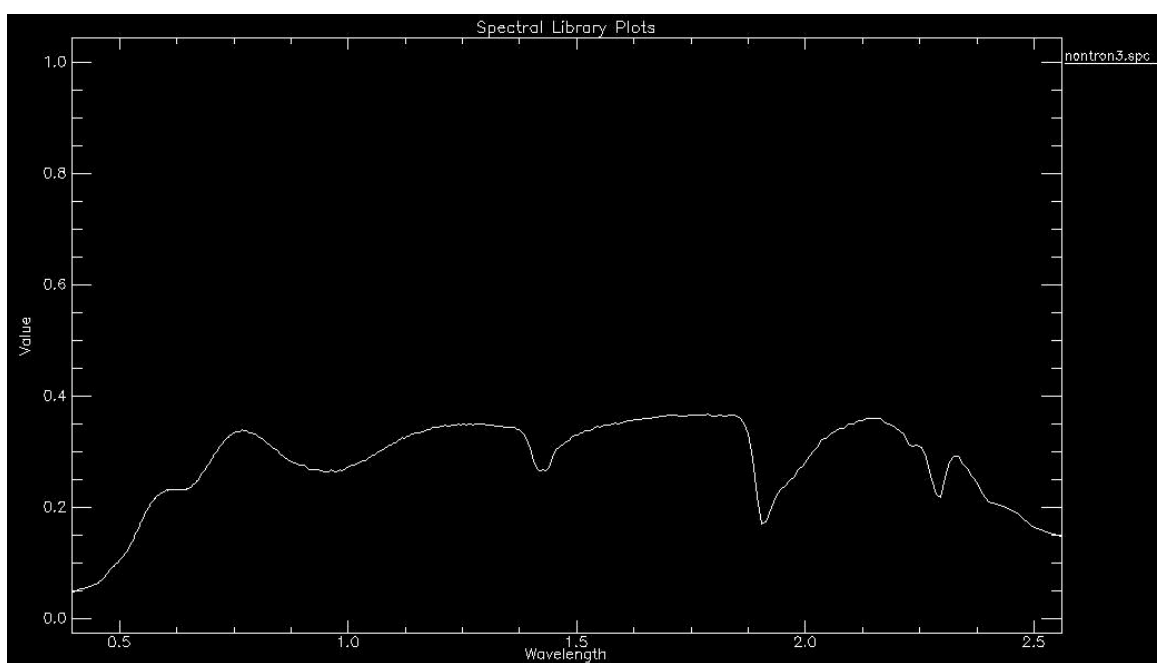


**Figure 4.101.** Spectral profile of nontronite from the USGS spectral library.

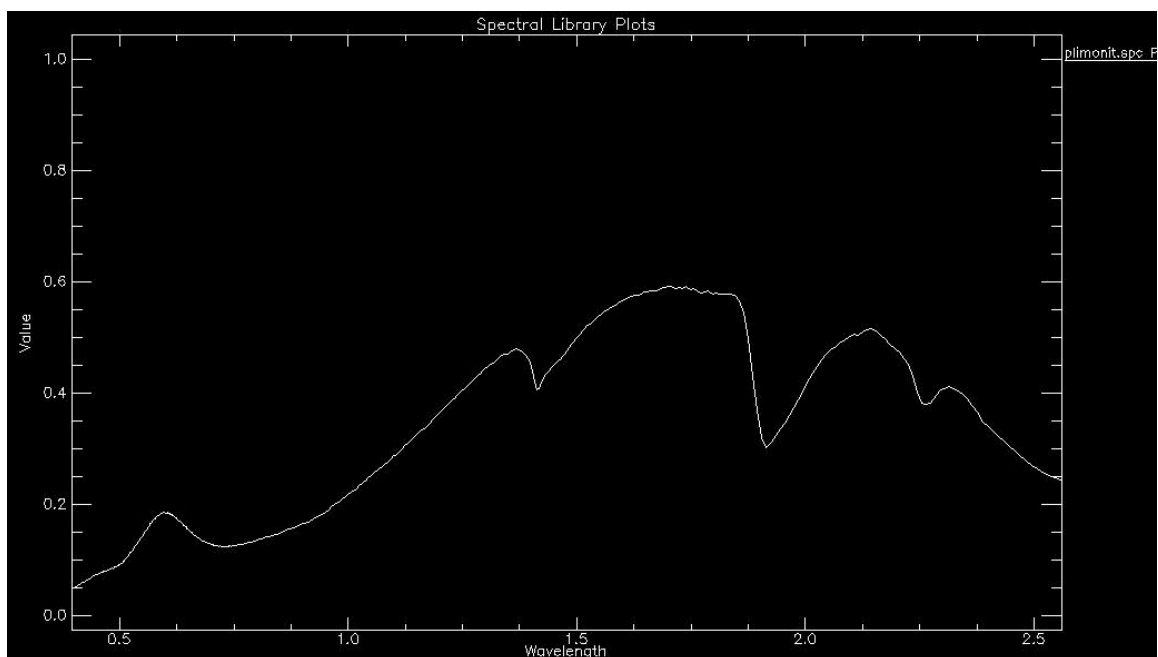


**Figure 4.102.** Spectral profile of pitch limonite from the USGS spectral library.

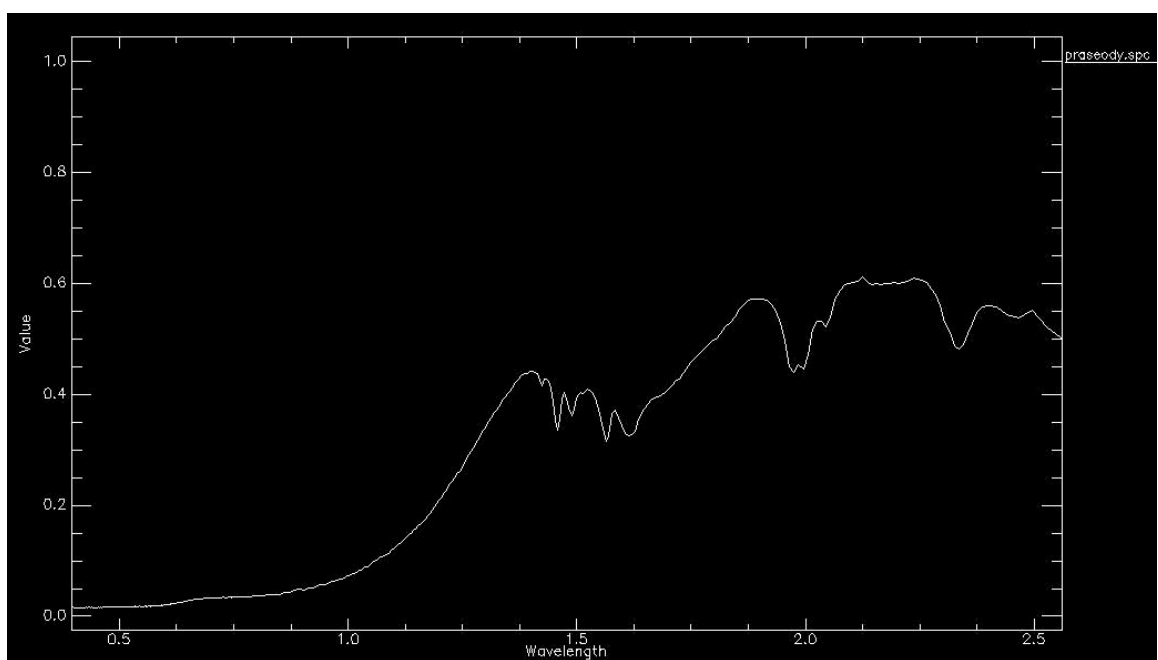


**Figure 4.103.** Spectral profile of praseodymium from the USGS spectral library.

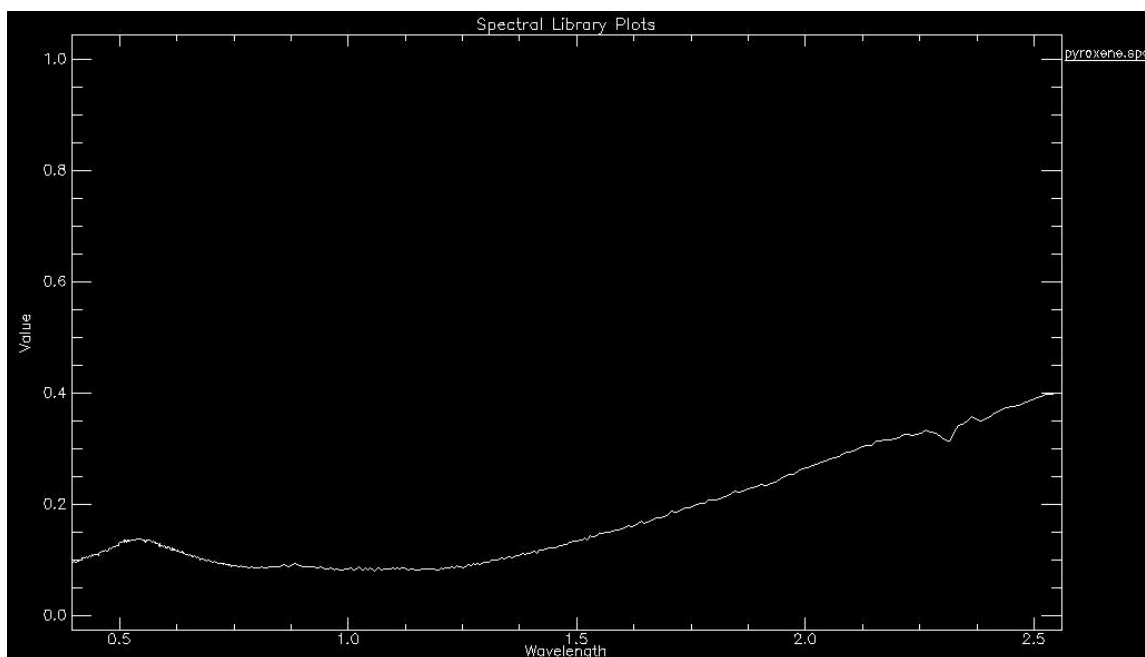


**Figure 4.104.** Spectral profile of pyroxene from the USGS spectral library.

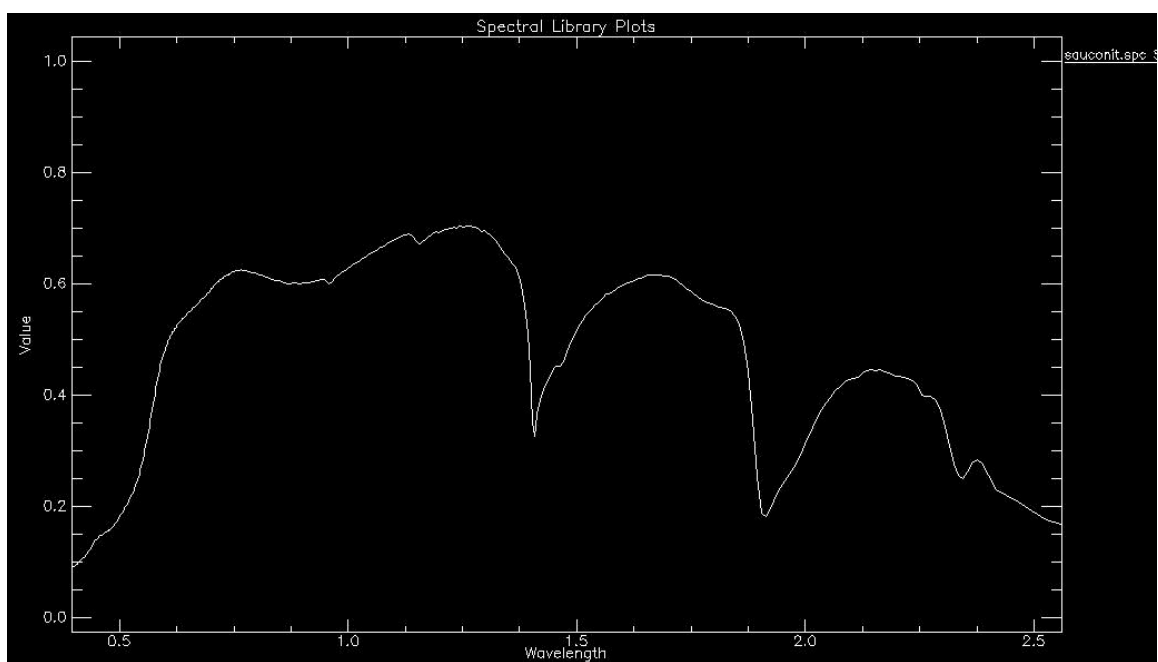


**Figure 4.105.** Spectral profile of sauconite from the USGS spectral library.

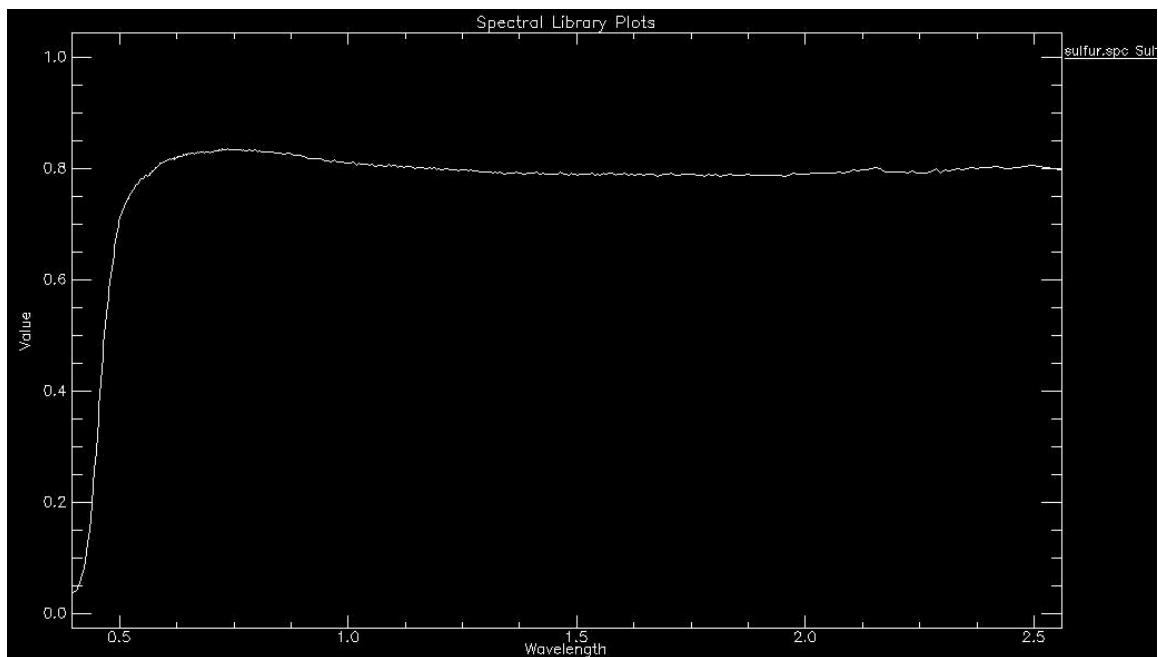


**Figure 4.106.** Spectral profile of sulfur from the USGS spectral library.

## 18.8. Appendix 4.8. Spectral Profiles from the JPL Spectral Library

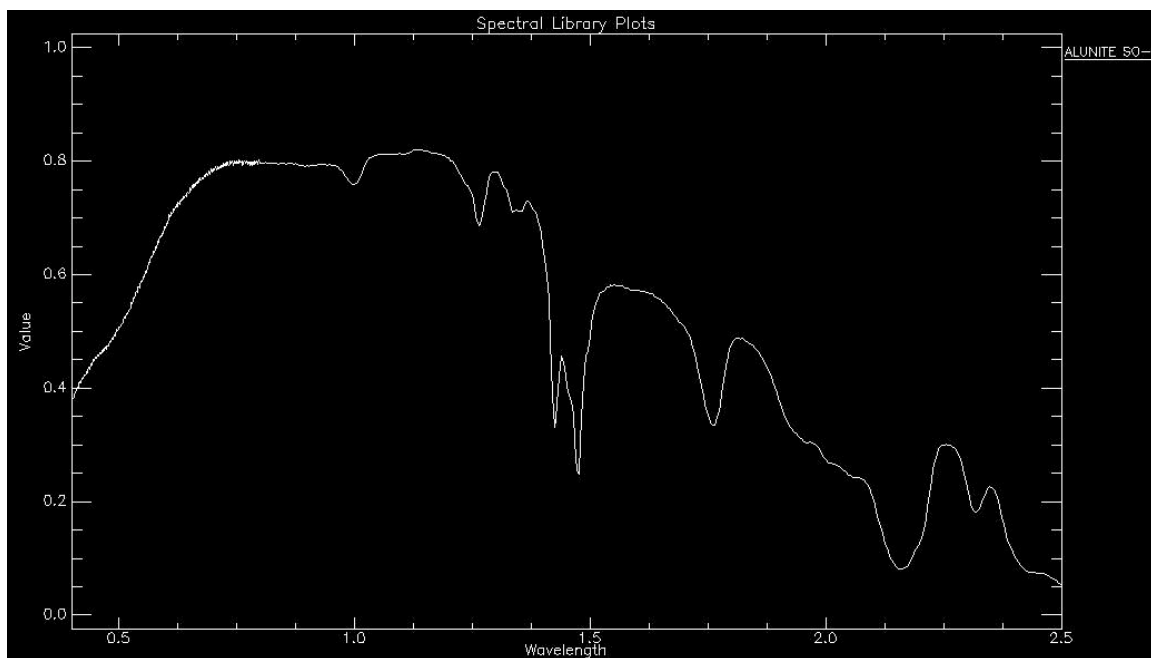


**Figure 4.107.** Spectral profile of alunite from the JPL spectral library.

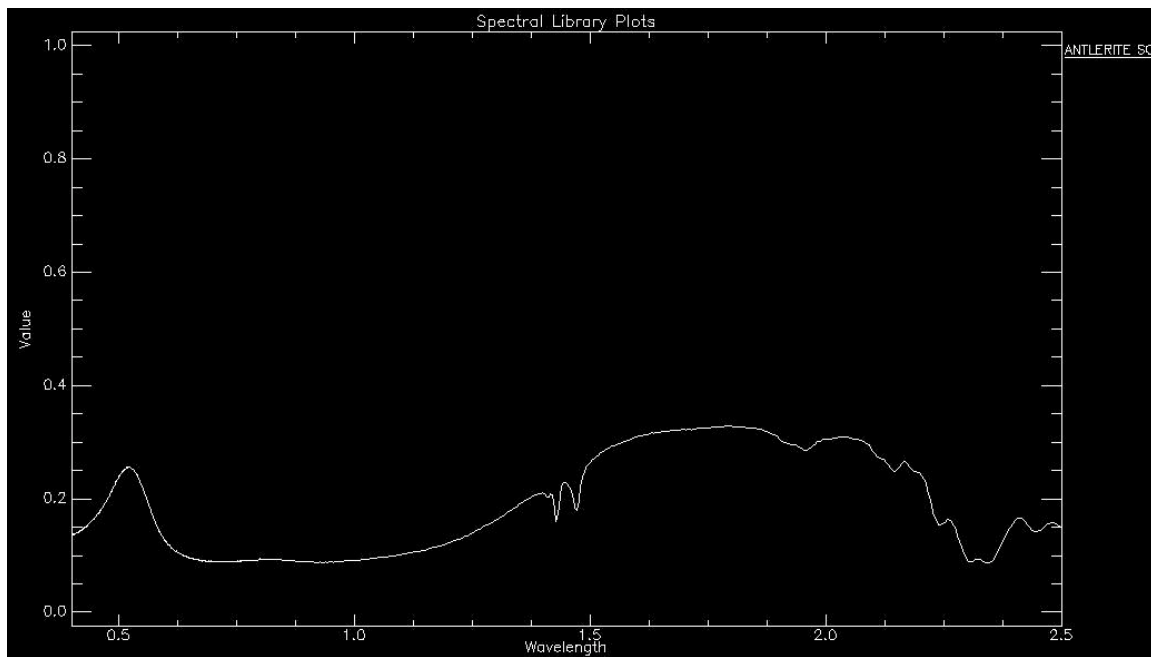


**Figure 4.108.** Spectral profile of antlerite from the JPL spectral library.

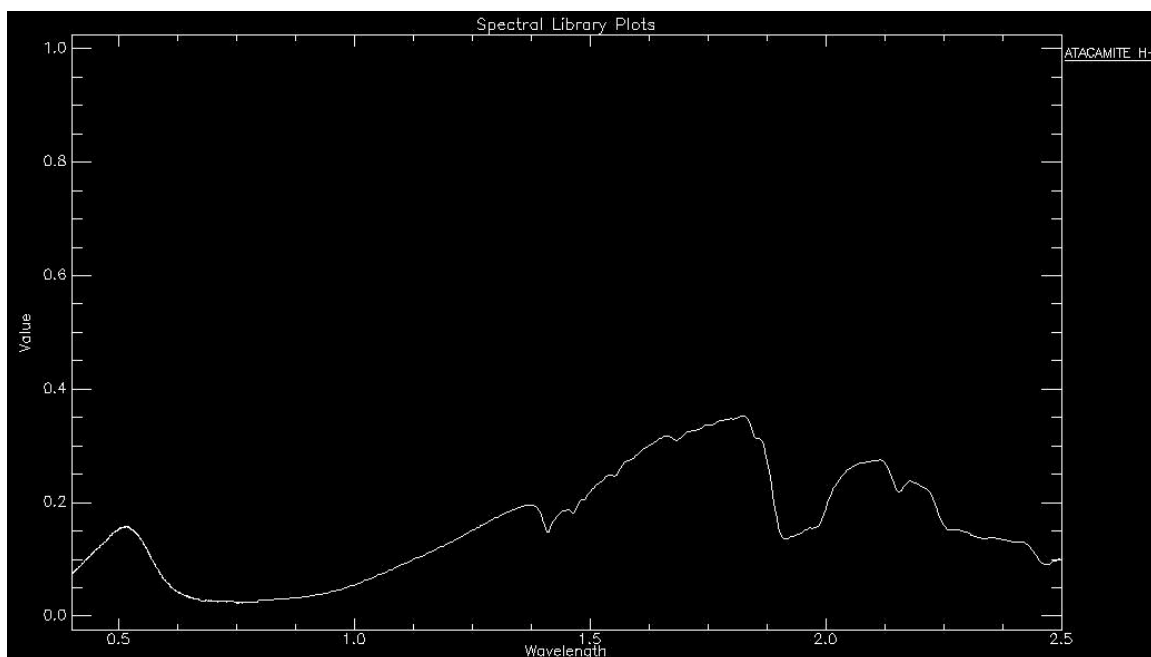


**Figure 4.109.** Spectral profile of atacamite from the JPL spectral library.

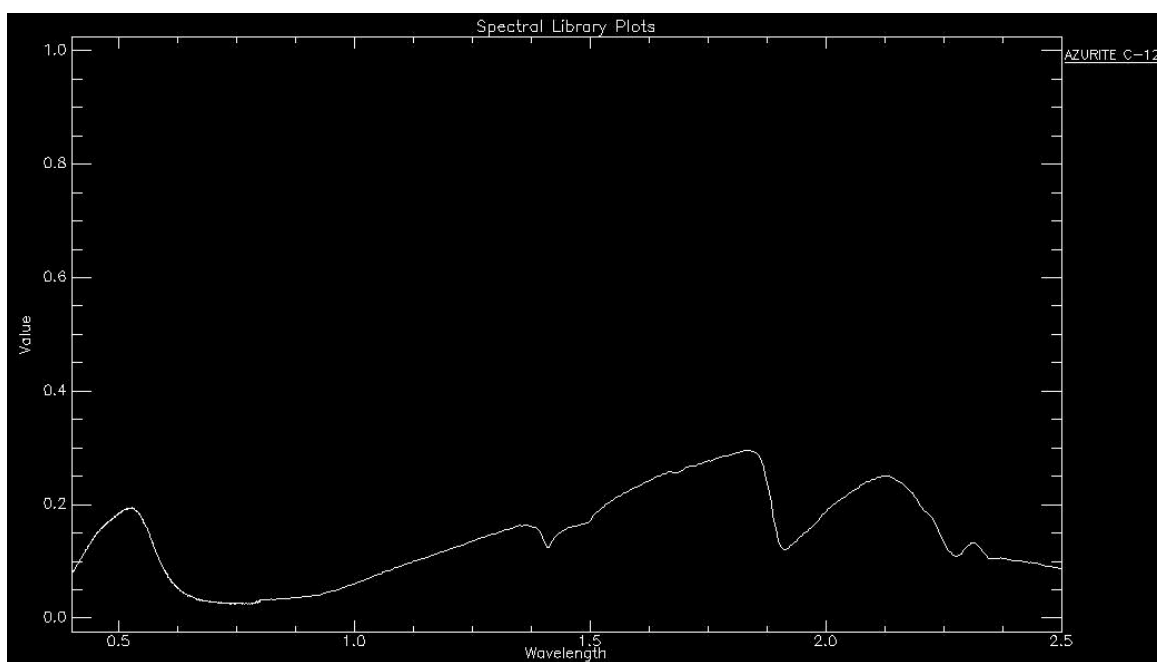


**Figure 4.110.** Spectral profile of azurite from the JPL spectral library.

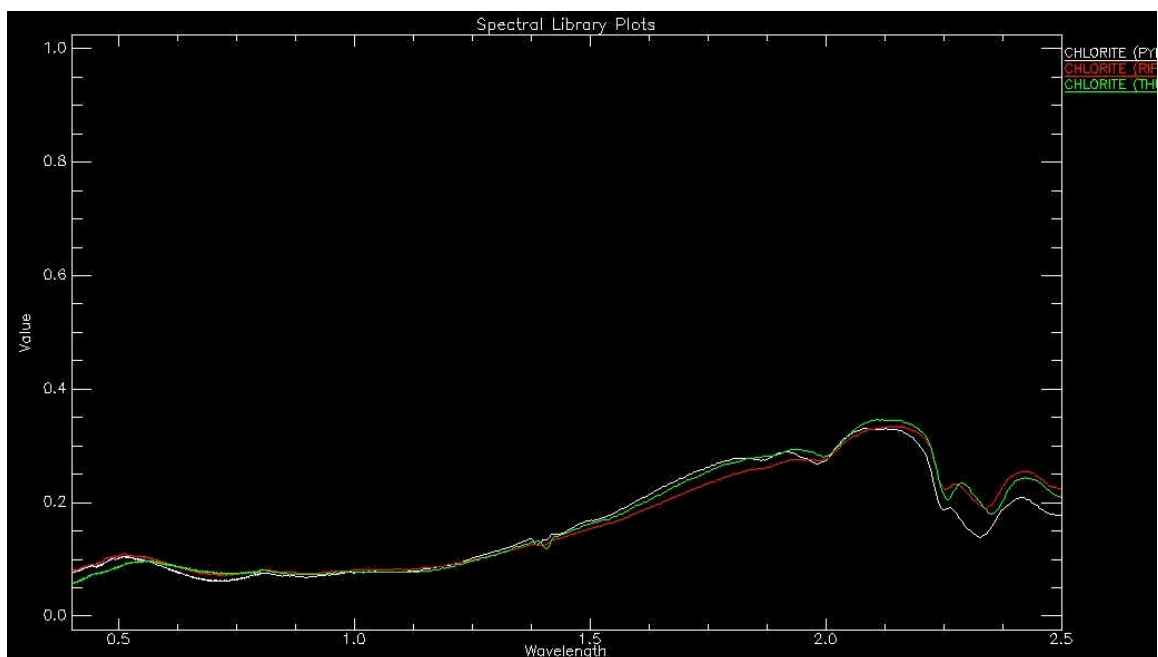


**Figure 4.111.** Spectral profile of P, R, and T chlorite from the JPL spectral library.

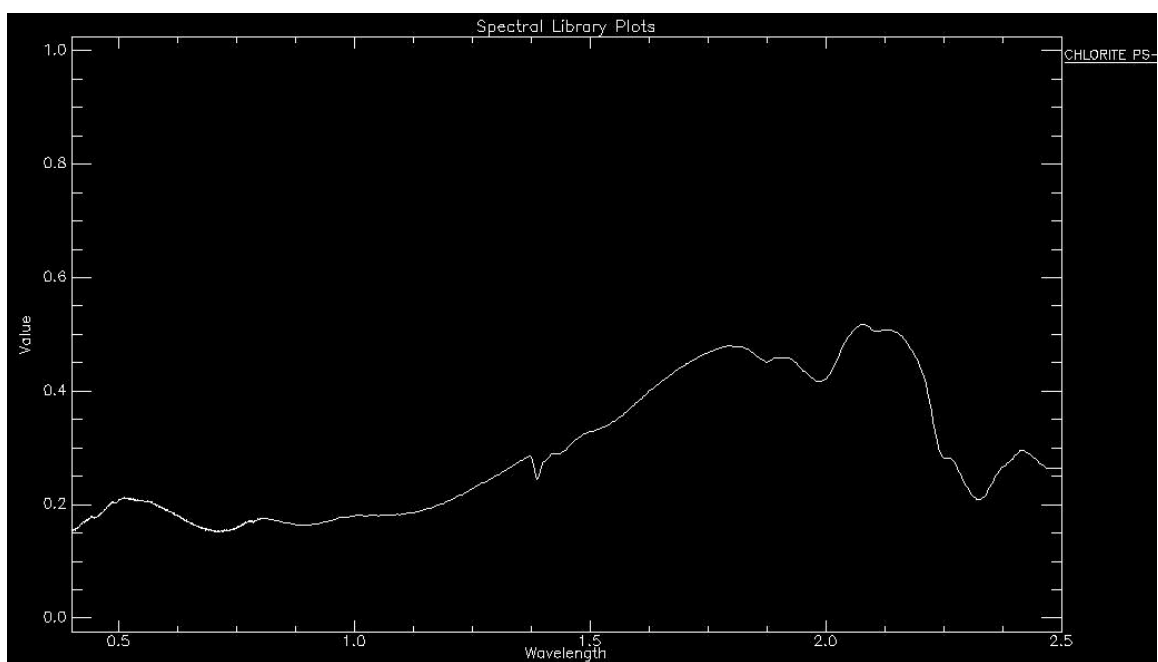


**Figure 4.112.** Spectral profile of PS-12 chlorite from the JPL spectral library.

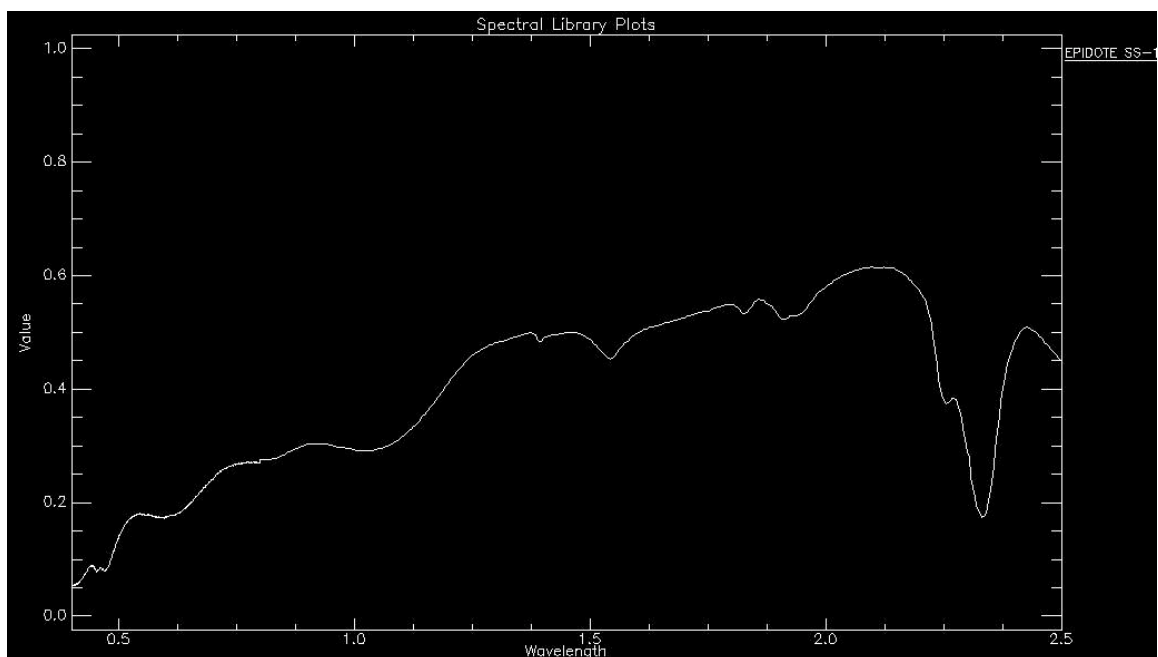


**Figure 4.113.** Spectral profile of epidote from the JPL spectral library.

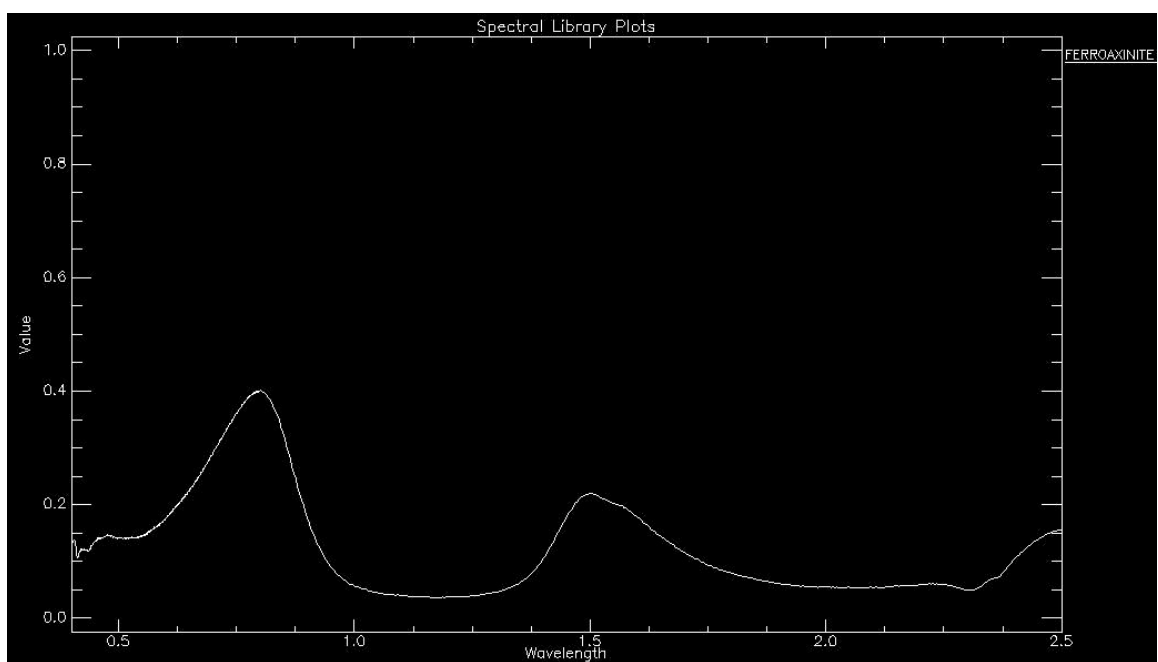


**Figure 4.114.** Spectral profile of ferroaxinite from the JPL spectral library.

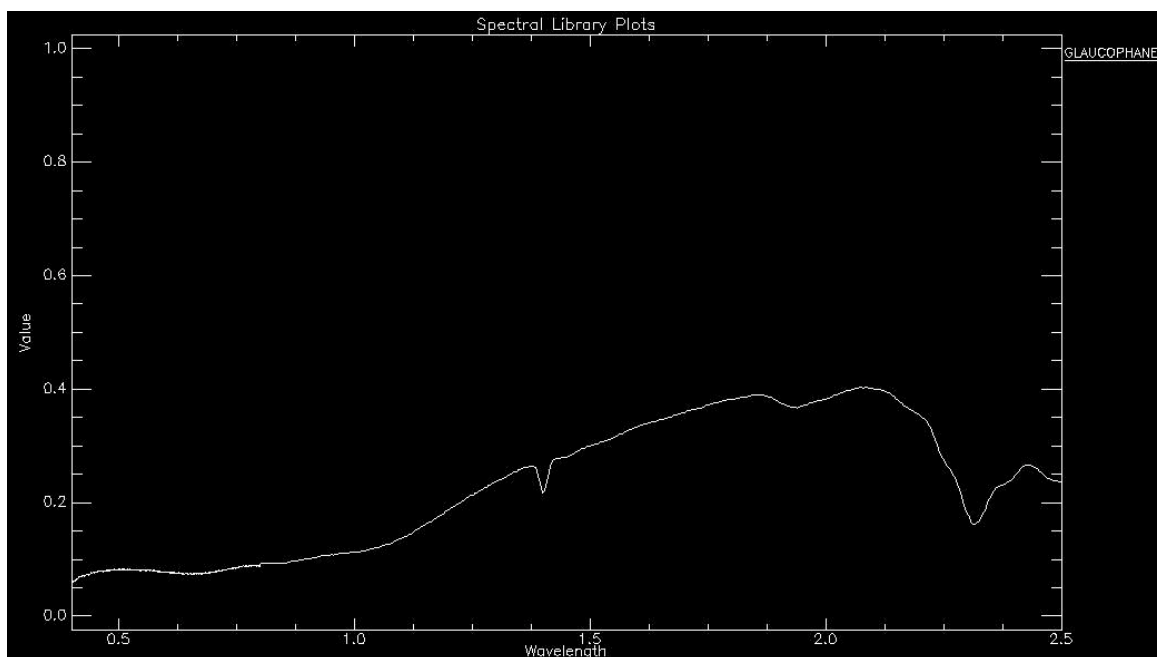


**Figure 4.115.** Spectral profile of glaucophane from the JPL spectral library.

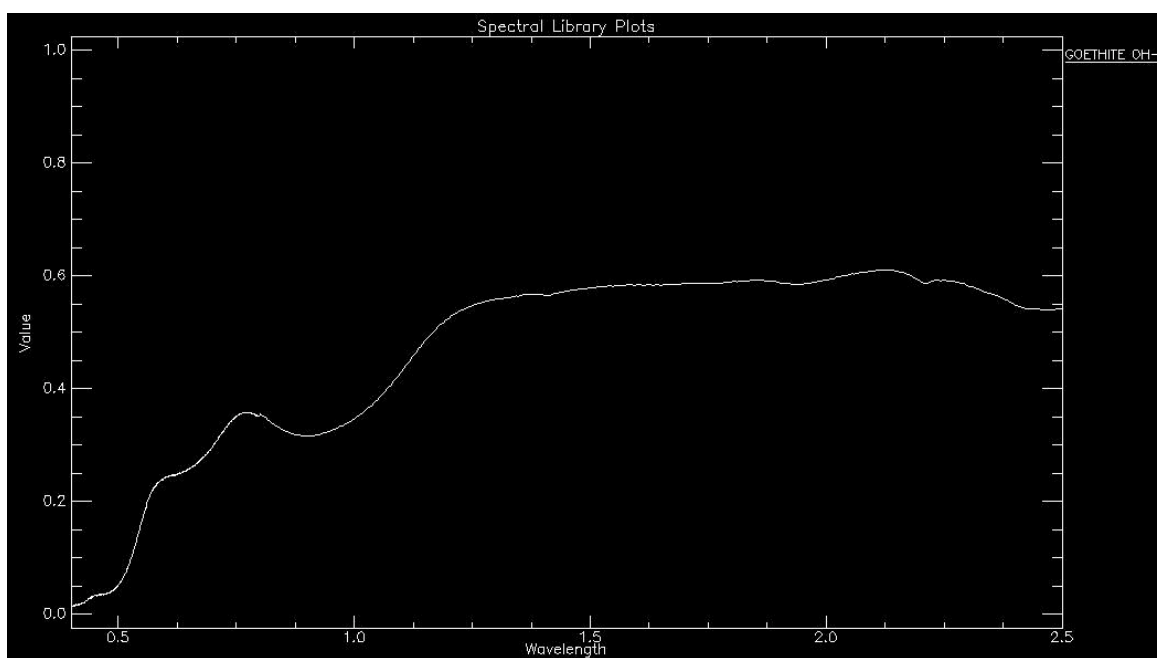


**Figure 4.116.** Spectral profile of goethite from the JPL spectral library.

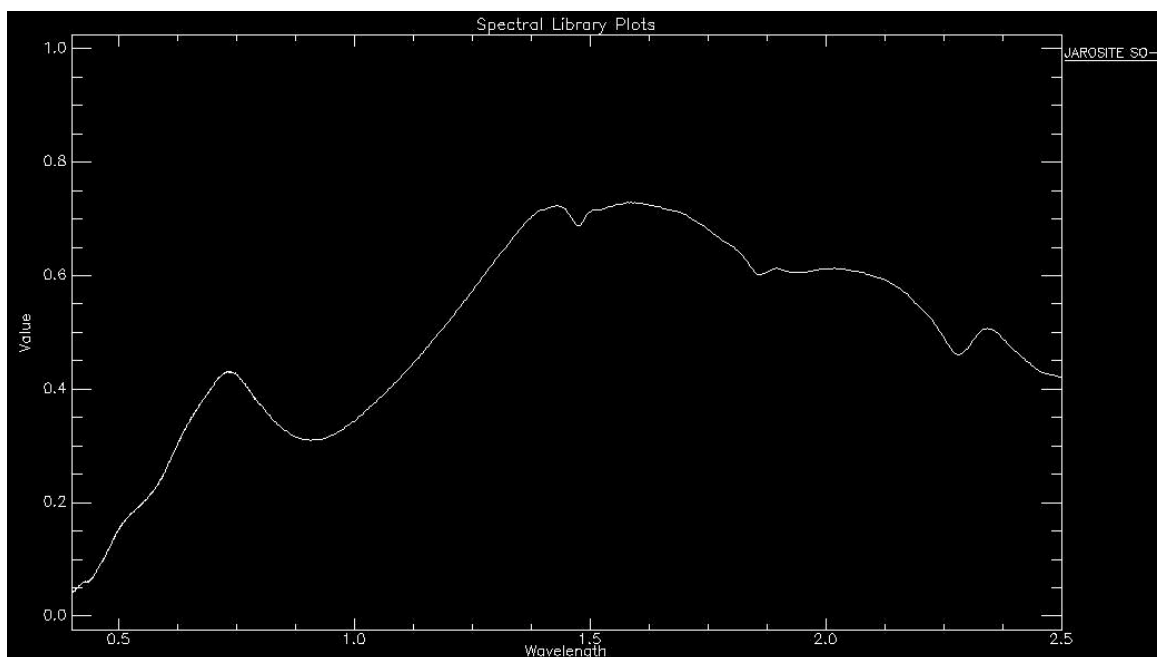


**Figure 4.117.** Spectral profile of jarosite from the JPL spectral library.

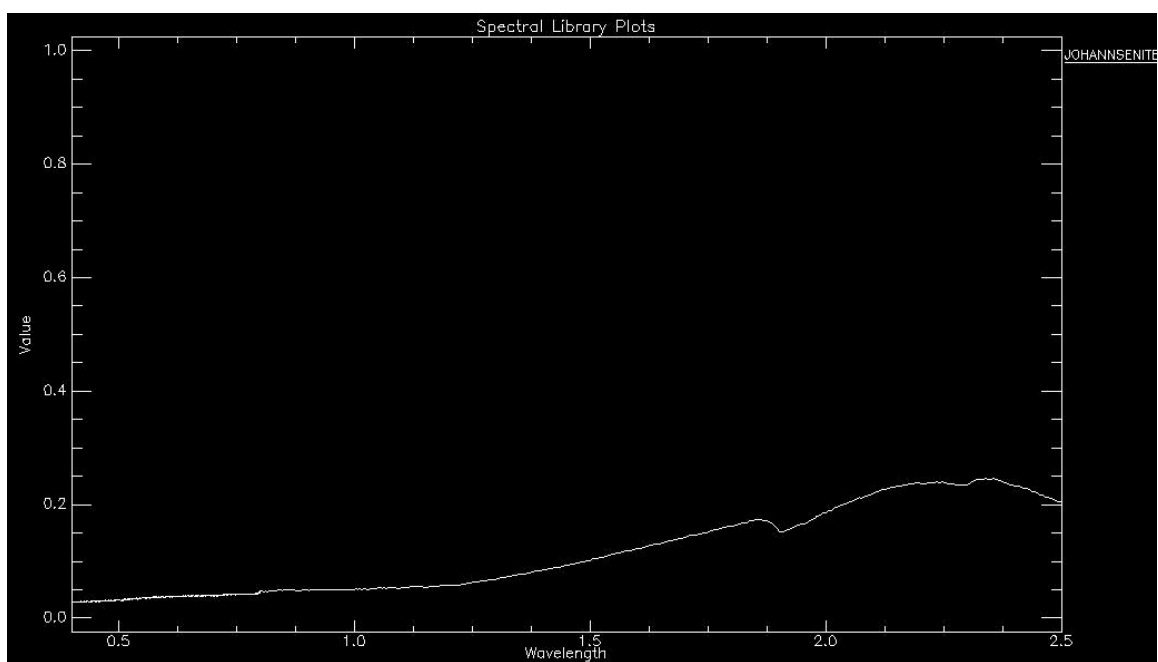


**Figure 4.118.** Spectral profile of johannsenite from the JPL spectral library.

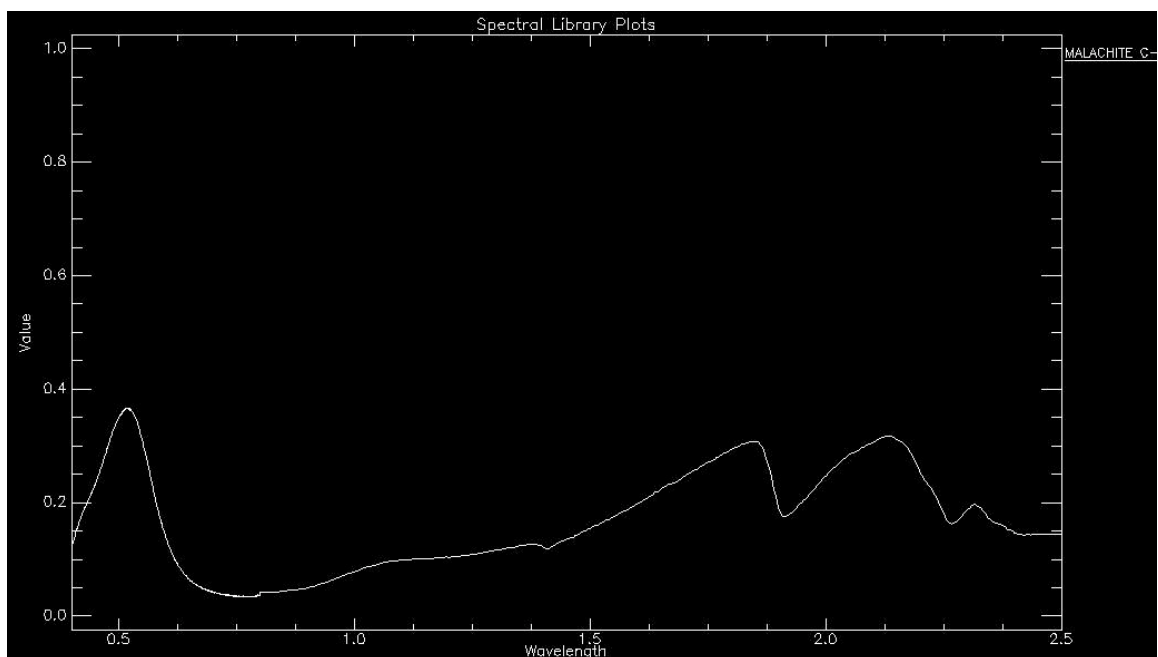


**Figure 4.119.** Spectral profile of malachite from the JPL spectral library.

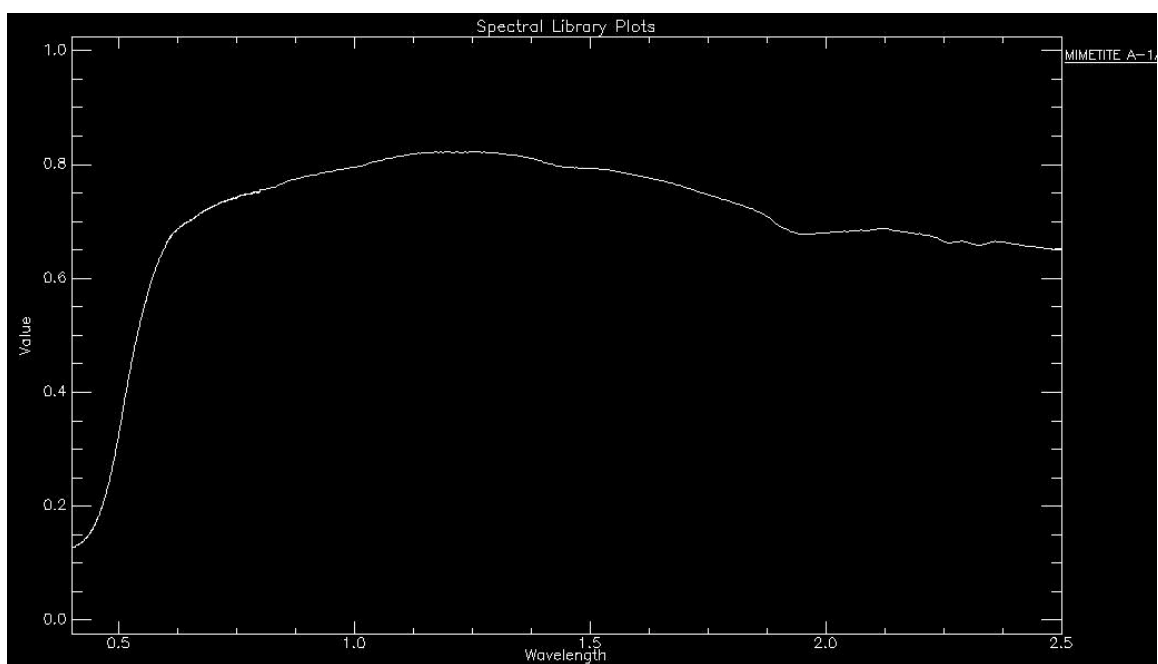


**Figure 4.120.** Spectral profile of mimetite from the JPL spectral library.

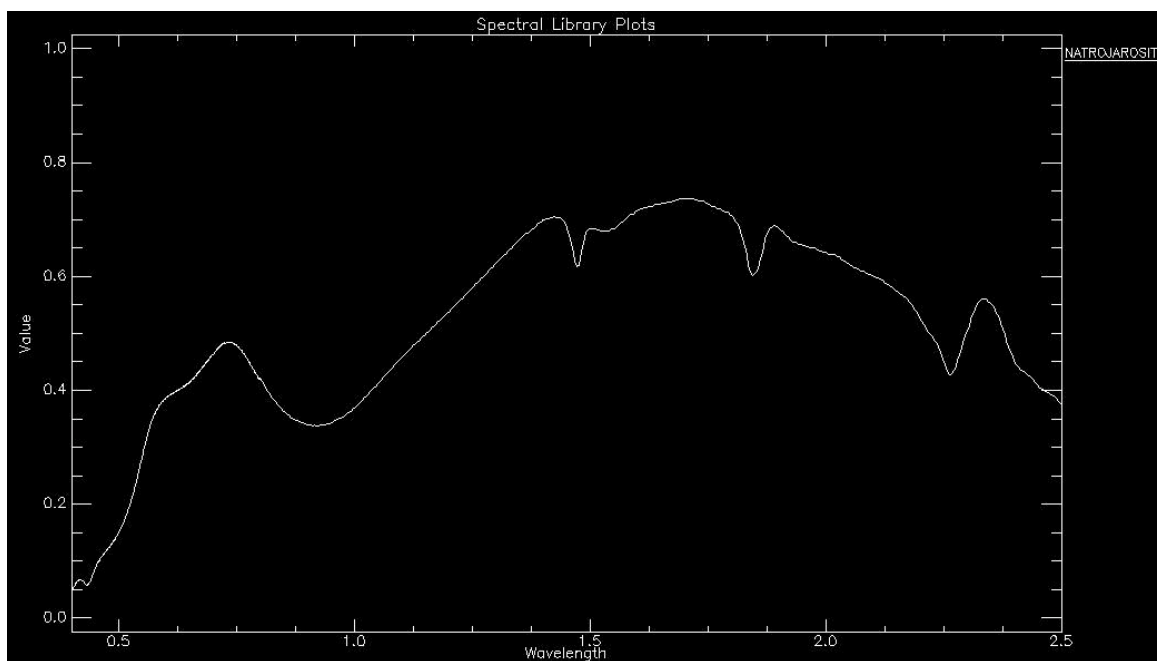


**Figure 4.121.** Spectral profile of natrojarosite from the JPL spectral library.

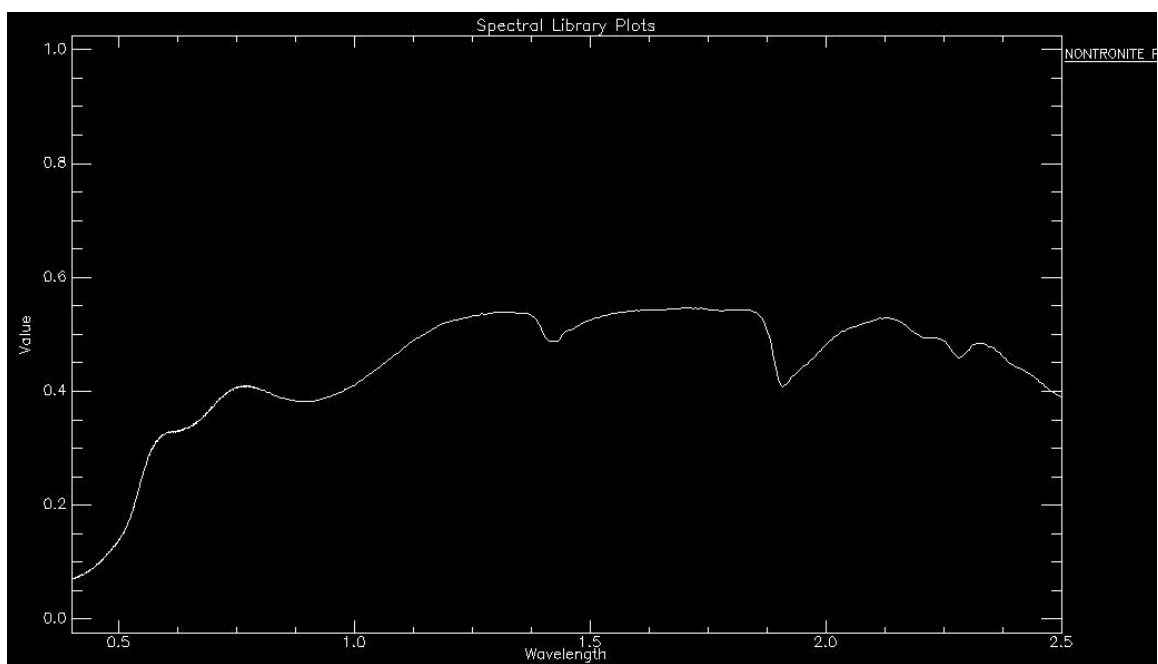


**Figure 4.122.** Spectral profile of nontronite from the JPL spectral library.

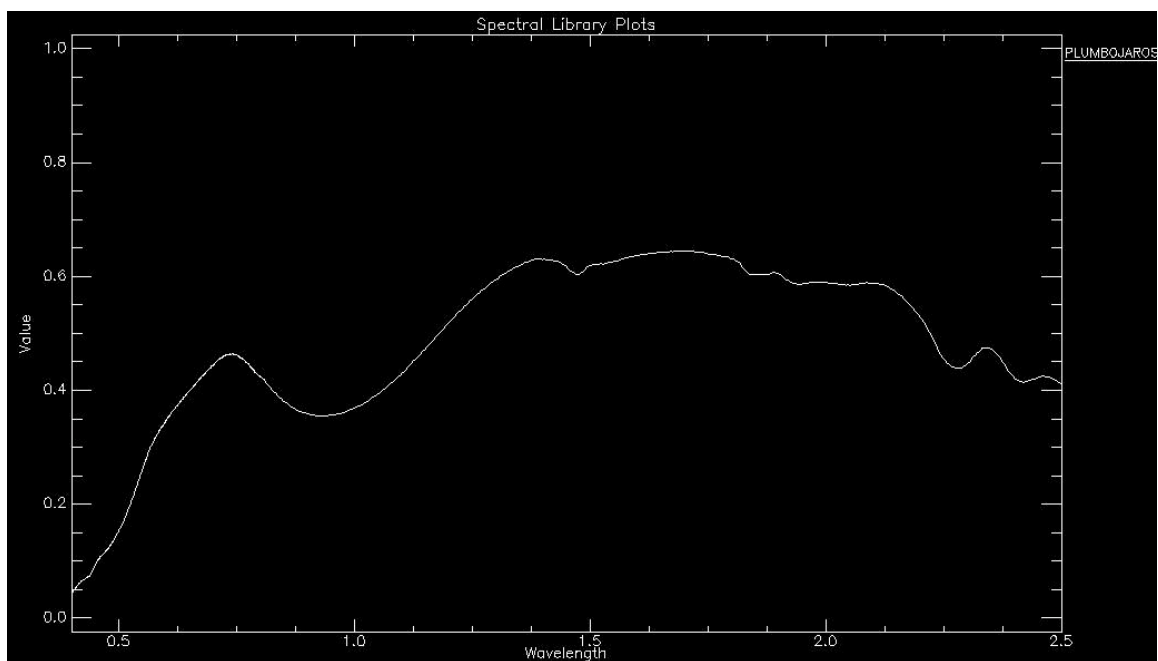


**Figure 4.123.** Spectral profile of plumbojarosite from the JPL spectral library.

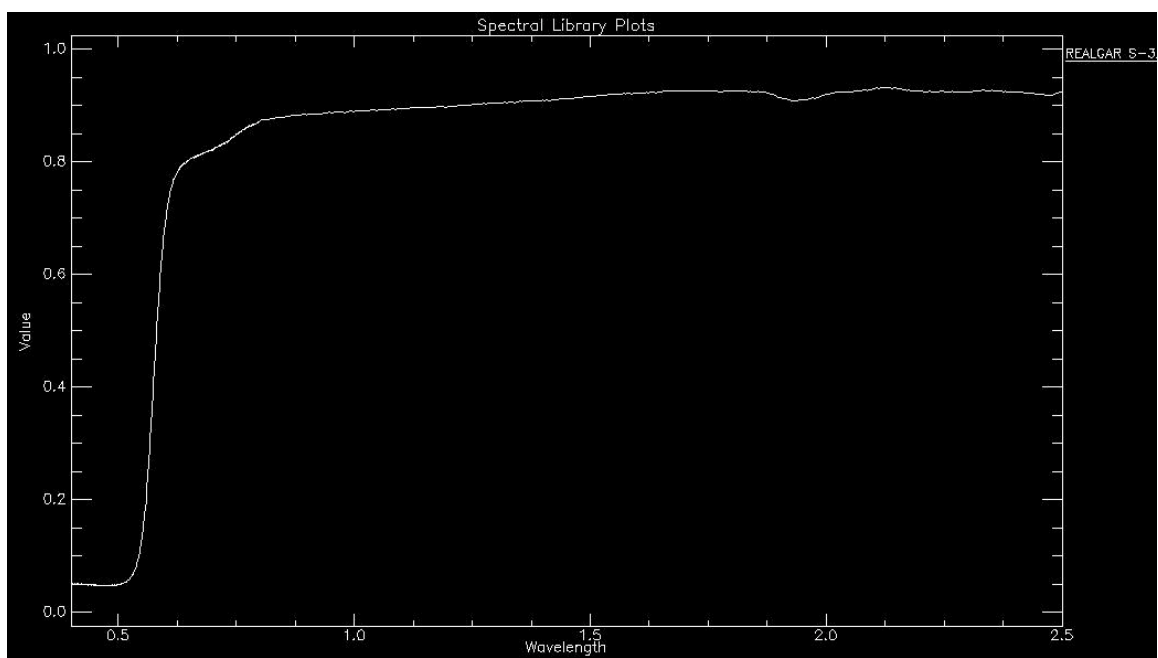


**Figure 4.124.** Spectral profile of realgar from the JPL spectral library.

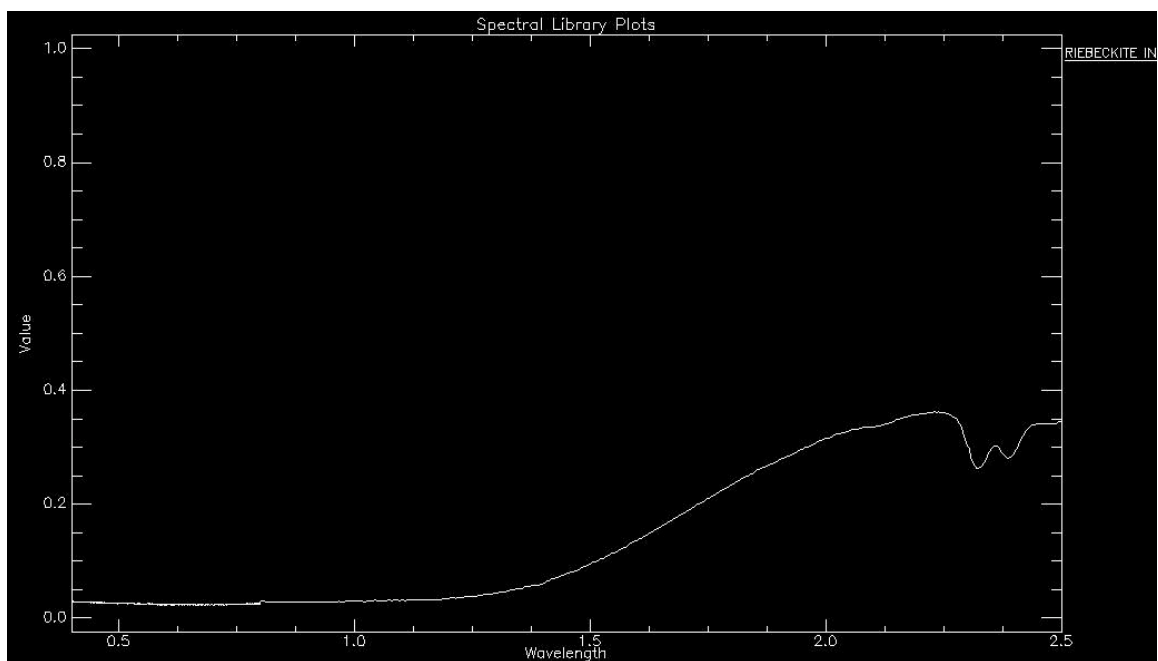


**Figure 4.125.** Spectral profile of riebeckite from the JPL spectral library.

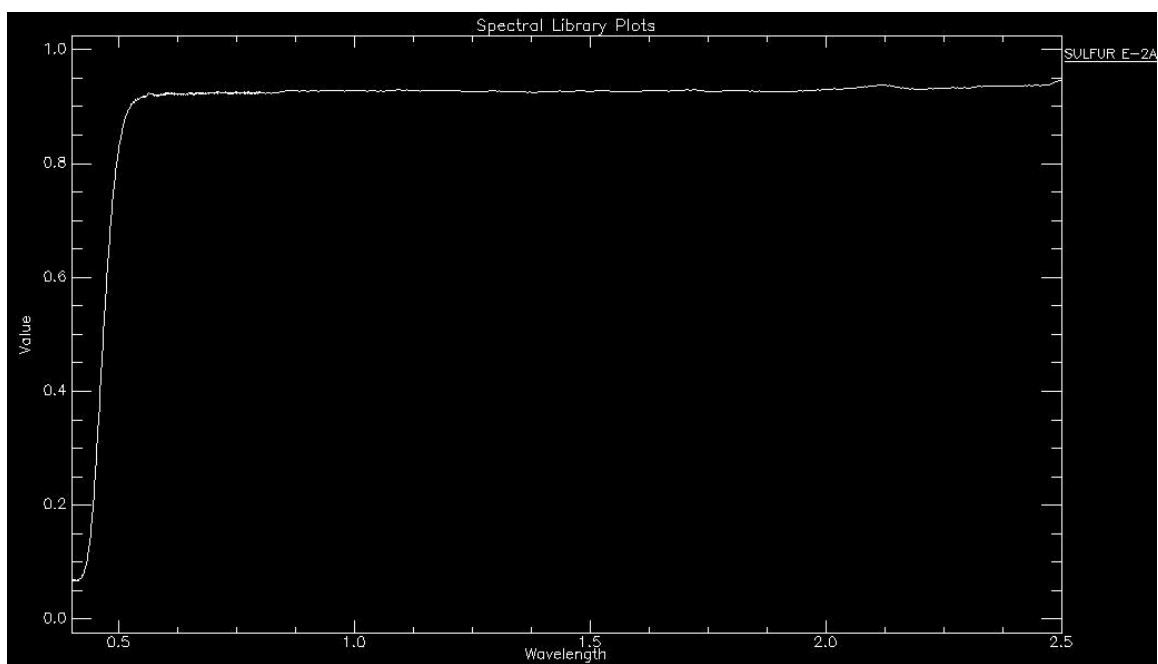


**Figure 4.126.** Spectral profile of sulfur from the JPL spectral library.

## 19. APPENDIX 5 – FRACTURE DENSITY

Appendix 5 displays tables of all the fracture density data variables, stereonet with percent copper and iron in fracture families, and bivariate analysis correlation coefficients and scatter plot matrix. Data found in tables was collected using a 2x2 foot frame and recording pre-determined variables in each fracture orientation (Section 10.3). Appendix 5 is split into several sections:

	PAGE
19.1. Appendix 5.1 – Bench Interval UTM Locations and Total Density	
Table 5.1 ..... Bench interval sample number, UTM locations, and total fracture density.	290
19.2. Appendix 5.2 – Bench Interval Fracture Density Variables	
Tables 5.2 – 5.9 ..... Data used in fracture density analyses. Variables include for F1, F2, and F3: copper only fractures (Cu), iron only fractures (Fe), mix of iron and copper (Fe+Cu), Fresh Fractures, and density per bench interval. Variables excluding density are given in inches.	292
19.3. Appendix 5.3 – Steronets with % Cu and % Fe in Fractures	
Figures 5.1 – 5.50 ..... Stereonets of bench interval fracture density measurements. Stereonets show orientation, number of fractures, and fracture density per fracture family. Bar charts are color coordinated and show percent copper and iron occurring in each fracture family.	299
19.4. Appendix 5.4 – Fracture Density Bivariate Analyses	
Table 5.10 and Figure 5.51 ..... Fracture density data correlation coefficient matrix and scatter plot matrix.	324
19.5. Appendix 5.5 – Spatial Distribution of Fracture Density Data	
Figures 5.52 – 5.59 ..... Contour figures of spatial distribution for fracture density data including variables: CuOx + FeOx, CuOx only, FeOx only, Fresh Fractures, F1 Density, F2 Density, F3 Density, and Total Density.	327

## 19.1. Appendix 5.1. Bench Interval UTM Locations and Total Density.

**Table 4.1.** Bench interval sample number, UTM locations, and total fracture density.

<b>Table 5.1 - Fracture Density Sample Locations and Total Density</b>			
<b>Sample #</b>	<b>Northing</b>	<b>Easting</b>	<b>Total <math>\rho</math> in<sup>-1</sup></b>
4800-25	305940	4324280	0.439236111
4800-50	305935	4324276	0.378472222
4800-75	305930	4324270	0.692708333
4800-125	305920	4324260	0.319444444
4800-150	305916	4324254	0.267361111
4800-175	305911	4324248	0.666666667
4800-200	305907	4324242	0.467013889
4800-225	305903	4324235	0.444444444
4800-275	305894	4324225	0.595486111
4800-300	305888	4324220	0.432291667
4800-325	305884	4324214	0.486111111
4800-350	305880	4324208	0.428819444
4780-00	306010	4324320	0.539930556
4780-25	306002	4324317	0.444444444
4780-50	305994	4324314	0.529513889
4780-75	305986	4324311	0.394097222
4780-100	305978	4324308	0.342013889
4780-150	305969	4324294	0.559027778
4780-175	305967	4324288	0.942708333
4780-200	305964	4324283	0.534722222
4780-225	305959	4324274	0.368055556
4780-250	305954	4324266	0.163194444
4780-275	305949	4324259	0.395833333
4780-325	305941	4324245	0.532986111
4780-350	305939	4324238	0.628472222
4780-375	305935	4324230	0.583333333
4780-400	305932	4324222	0.40625
4780-425	305928	4324215	0.303819444
4780-450	305925	4324208	0.817708333
4750-00	306033	4324290	0.512152778
4750-25	306029	4324283	0.434027778
4750-50	306025	4324275	0.536458333
4750-75	306021	4324268	0.418402778
4750-100	306018	4324260	0.461805556
4750-125	306015	4324253	0.475694444
4750-150	306013	4324245	0.302083333
4750-175	306008	4324239	0.595486111
4750-200	306003	4324233	0.625
4750-225	305999	4324226	0.326388889
4750-250	305995	4324220	0.545138889
4750-275	305992	4324211	0.756944444
4750-300	305989	4324202	0.65625
4750-325	305991	4324193	0.270833333
4730-00	306135	4324323	0.756944444
4730-25	306130	4324319	0.510416667
4730-50	306126	4324314	0.171875
4730-75	306121	4324308	0.397569444
4730-100	306116	4324302	0.291666667
4730-150	306104	4324295	0.572916667

**Table 4.1 cont.** Bench interval sample number, UTM locations, and total fracture density.

<b>Table 5.1 - Fracture Density Sample Locations and Total Density</b>			
<b>Sample #</b>	<b>Northing</b>	<b>Easting</b>	<b>Total <math>\rho</math> in<sup>-1</sup></b>
4730-175	306098	4324289	0.605902778
4730-200	306093	4324283	0.741319444
4730-275	306079	4324268	0.515625
4730-300	306076	4324260	0.763888889
4730-325	306075	4324252	0.638888889
4730-350	306074	4324244	0.456597222
4370-375	306073	4324236	0.111111111
4730-400	306073	4324228	0.385416667
4730-450	306070	4324217	0.418402778
4730-475	306069	4324209	0.362847222
4730-525	306064	4324194	0.338541667
4730-550	306062	4324186	0.861111111
4730-575	306059	4324179	0.534722222
4730-600	306055	4324171	0.493055556
4700-00	306208	4324392	0.506944444
4700-25	306199	4324379	0.559027778
4700-200	306193	4324331	0.675347222
4700-300	306172	4324311	1.276041667
4675-00	306337	4324351	0.65625
4675-25	306335	4324342	0.392361111
4675-50	306333	4324336	0.460069444
4675-75	306330	4324329	0.583333333
4675-125	306325	4324315	0.743055556
4675-150	306322	4324309	0.333333333
4675-175	306319	4324302	0.524305556
4675-200	306316	4324295	0.385416667
4675-225	306312	4324286	0.414930556
4675-250	306309	4324278	0.765625
4675-275	306306	4324271	0.371527778
4675-300	306304	4324264	0.786458333
4675-325	306301	4324259	0.324652778
4675-350	306299	4324253	0.550347222
4675-375	306295	4324246	0.491319444
4675-400	306291	4324240	0.411458333
4630-00	306477	4324447	0.357638889
4630-25	306473	4324440	0.552083333
4630-125	306461	4324412	0.697916667
4630-200	306457	4324389	0.71875
4600-00	306511	4324444	0.303819444
4600-25	306509	4324438	0.447916667
4600-50	306507	4324433	0.564236111
4600-100	306495	4324419	0.491319444
4600-125	306491	4324412	0.552083333
4600-150	306487	4324405	0.335069444
4600-175	306485	4324397	0.522569444
4600-00B	306616	4324450	0.616319444
4600-25B	306611	4324455	0.706597222
4600-50B	306607	4324460	0.59375
4600-75B	306600	4324463	0.571180556
4600-100B	306593	4324466	0.34375

## 19.2. Appendix 5.2. Bench Interval Fracture Density Variables

**Table 5.2.** Bench 4600 copper only fractures (Cu), iron only fractures (Fe), mix of iron and copper (Fe+Cu), Fresh Fractures, and density per bench interval.

<b>Table 5.2 - Bench 4600 Fracture Data</b>						
<b>Sample #</b>	<b>Cu</b>	<b>Fe</b>	<b>Fe + Cu</b>	<b>Fresh</b>	<b>n</b>	<b><math>\rho = \text{in}^2</math></b>
4600-00	0	52	12	0	6	0.111
4600-25	0	97	22	5	7	0.215
4600-50	0	97	33	9	12	0.241
4600-100	8	90	39	7	12	0.250
4600-125	12	97	55	0	11	0.285
4600-150	0	51	14	3	4	0.118
4600-175	14	62	42	0	10	0.205
4600-00B	15	37	81	0	14	0.231
4600-25B	0	92	18	0	12	0.191
4600-50B	0	87	62	11	10	0.278
4600-75B	0	132	14	0	9	0.253
4600-100B	0	55	16	0	10	0.123
4600-00	0	83	14	0	7	0.168
4600-25	0	32	42	18	5	0.160
4600-50	10	89	21	12	10	0.229
4600-100	0	79	21	9	8	0.189
4600-125	0	88	24	9	9	0.210
4600-150	0	99	4	10	8	0.196
4600-175	22	45	31	0	13	0.170
4600-00B	42	23	62	0	8	0.220
4600-25B	66	28	79	0	14	0.300
4600-50B	10	32	89	0	11	0.227
4600-75B	0	82	26	0	11	0.188
4600-100B	0	75	12	0	9	0.151
4600-00	0	0	0	14	2	0.024
4600-25	0	39	0	3	2	0.073
4600-50	0	16	38	0	4	0.094
4600-100	0	6	22	2	4	0.052
4600-125	0	8	4	21	3	0.057
4600-150	0	0	0	12	1	0.021
4600-175	0	32	53	0	8	0.148
4600-00B	0	8	87	0	9	0.165
4600-25B	0	16	108	0	8	0.215
4600-50B	0	12	39	0	5	0.089
4600-75B	0	43	32	0	5	0.130
4600-100B	0	22	18	0	5	0.069

**Family 1**

**Family 2**

**Family 3**

**Table 5.3.** Bench 4630 copper only fractures (Cu), iron only fractures (Fe), mix of iron and copper (Fe+Cu), Fresh Fractures, and density per bench interval.

<b>Table 5.3 - Bench 4630 Fracture Data</b>							
<b>Sample #</b>	<b>Cu</b>	<b>Fe</b>	<b>Fe + Cu</b>	<b>Fresh</b>	<b>n</b>	<b><math>\rho = \text{in}^2</math></b>	
4630-00	0	41	0	15	11	0.097	<b>Family 1</b>
4630-25	0	127	0	15	18	0.247	
4630-125	0	164	0	0	13	0.285	
4630-200	0	47	42	0	11	0.155	
4630-00	0	75	0	27	5	0.177	<b>Family 2</b>
4630-25	0	111	0	36	9	0.255	
4630-125	0	130	0	0	7	0.226	
4630-200	0	108	98	0	16	0.358	
4630-00	0	32	0	16	11	0.083	<b>Family 3</b>
4630-25	0	15	0	14	4	0.050	
4630-125	0	108	0	0	10	0.188	
4630-200	0	52	67	0	14	0.207	

**Table 5.4.** Bench 4700 copper only fractures (Cu), iron only fractures (Fe), mix of iron and copper (Fe+Cu), Fresh Fractures, and density per bench interval.

<b>Table 5.4 - Bench 4700 Fracture Data</b>							
<b>Sample #</b>	<b>Cu</b>	<b>Fe</b>	<b>Fe + Cu</b>	<b>Fresh</b>	<b>n</b>	<b><math>\rho = \text{in}^2</math></b>	
4700-00	0	143	0	0	12	0.248	<b>Family 1</b>
4700-25	0	0	73	0	8	0.127	
4700-200	0	162	0	0	13	0.281	
4700-300	0	194	80	0	24	0.476	
4700-00	0	73	0	0	4	0.127	<b>Family 2</b>
4700-25	0	15	167	0	17	0.316	
4700-200	0	155	0	0	19	0.269	
4700-300	0	34	72	0	6	0.184	
4700-00	0	76	0	0	5	0.132	<b>Family 3</b>
4700-25	0	15	52	0	7	0.116	
4700-200	0	72	0	0	9	0.125	
4700-300	0	192	163	0	24	0.616	

**Table 5.5.** Bench 4675 copper only fractures (Cu), iron only fractures (Fe), mix of iron and copper (Fe+Cu), Fresh Fractures, and density per bench interval.

<b>Table 5.5 - Bench 4680 Fracture Data</b>						
<b>Sample #</b>	<b>Cu</b>	<b>Fe</b>	<b>Fe + Cu</b>	<b>Fresh</b>	<b>n</b>	<b><math>\rho = \text{in}^{-1}</math></b>
4675-00	0	26	189	43	19	0.448
4675-25	0	46	38	0	12	0.146
4675-50	0	22	70	0	11	0.160
4675-75	0	141	0	0	12	0.245
4675-125	0	206	17	44	18	0.464
4675-150	0	63	0	0	6	0.109
4675-175	0	124	0	0	8	0.215
4675-200	0	58	13	2	7	0.127
4675-225	0	102	0	0	14	0.177
4675-250	0	173	0	0	12	0.300
4675-275	0	0	78	0	5	0.135
4675-300	0	144	40	0	11	0.319
4675-325	0	94	0	0	9	0.163
4675-350	0	111	0	0	10	0.193
4675-375	0	0	92	0	7	0.160
4675-400	0	41	0	0	6	0.071
<b>Family 1</b>						
4675-00	0	0	69	0	3	0.120
4675-25	0	8	44	0	3	0.090
4675-50	0	14	63	0	5	0.134
4675-75	0	58	0	25	7	0.144
4675-125	0	82	6	26	12	0.198
4675-150	0	77	0	0	8	0.134
4675-175	0	107	0	0	11	0.186
4675-200	0	58	24	0	7	0.142
4675-225	0	72	0	0	8	0.125
4675-250	0	138	10	0	11	0.257
4675-275	0	0	75	0	10	0.130
4675-300	0	64	56	0	11	0.208
4675-325	0	62	0	0	9	0.108
4675-350	0	84	0	0	5	0.146
4675-375	0	0	112	0	14	0.194
4675-400	0	0	119	0	9	0.207
<b>Family 2</b>						
4675-00	0	0	28	23	7	0.089
4675-25	0	29	61	0	6	0.156
4675-50	0	6	90	0	8	0.167
4675-75	0	100	0	12	8	0.194
4675-125	0	24	9	14	5	0.082
4675-150	0	52	0	0	9	0.090
4675-175	0	71	0	0	6	0.123
4675-200	0	53	11	3	12	0.116
4675-225	0	65	0	0	9	0.113
4675-250	0	120	0	0	14	0.208
4675-275	0	7	54	0	11	0.106
4675-300	0	67	82	0	14	0.259
4675-325	0	31	0	0	2	0.054
4675-350	0	122	0	0	12	0.212
4675-375	0	0	79	0	8	0.137
4675-400	0	0	77	0	7	0.134
<b>Family 3</b>						

**Table 5.6.** Bench 4730 copper only fractures (Cu), iron only fractures (Fe), mix of iron and copper (Fe+Cu), Fresh Fractures, and density per bench interval.

Table 5.6 - Bench 4730 Fracture Data						
Sample #	Cu	Fe	Fe + Cu	Fresh	n	$\rho = \text{in}^2$
4730-00	0	254	75	0	37	0.571
4730-25	0	87	0	0	14	0.151
4730-50	0	34	0	0	3	0.059
4730-75	0	26	50	0	5	0.132
4730-100	0	0	42	0	4	0.073
4730-150	0	60	74	0	11	0.233
4730-175	0	0	56	0	5	0.097
4730-200	0	0	250	0	16	0.434
4730-275	0	59	83	0	14	0.247
4730-300	0	109	0	0	6	0.189
4730-325	0	52	30	0	4	0.142
4730-350	0	14	0	0	2	0.024
4370-375	0	31	0	0	2	0.054
4730-400	0	10	50	0	4	0.104
4730-450	0	5	88	0	5	0.161
4730-475	0	62	0	0	5	0.108
4730-525	0	24	18	0	3	0.073
4730-550	0	82	18	0	6	0.174
4730-575	0	120	0	0	9	0.208
4730-600	0	57	0	0	4	0.099
4730-00	0	79	3	0	5	0.137
4730-25	0	117	0	0	8	0.203
4730-50	0	64	0	0	4	0.111
4730-75	0	26	12	9	3	0.082
4730-100	0	9	70	0	6	0.137
4730-150	0	51	45	0	6	0.167
4730-175	0	56	144	0	11	0.347
4730-200	0	0	116	0	10	0.201
4730-275	0	39	115	0	8	0.267
4730-300	0	90	0	0	6	0.156
4730-325	0	23	34	0	4	0.099
4730-350	0	20	33	0	3	0.092
4370-375	0	32	0	0	4	0.056
4730-400	0	20	38	0	3	0.101
4730-450	0	0	49	0	5	0.085
4730-475	0	44	0	0	3	0.076
4730-525	0	19	29	0	3	0.083
4730-550	0	63	18	0	5	0.141
4730-575	0	92	0	0	6	0.160
4730-600	0	71	0	0	5	0.123
4730-00	0	28	0	0	7	0.049
4730-25	0	90	0	0	6	0.156
4730-50	0	1	0	0	1	0.002
4730-75	0	34	72	0	5	0.184
4730-100	0	10	37	0	6	0.082
4730-150	0	43	57	0	7	0.174
4730-175	0	17	76	0	5	0.161
4730-200	0	0	61	0	4	0.106
4730-275	0	1	0	0	1	0.002
4730-300	0	241	0	0	12	0.418
4730-325	0	149	80	0	11	0.398
4730-350	0	107	89	0	13	0.340
4370-375	0	1	0	0	1	0.002
4730-400	0	24	80	0	6	0.181
4730-450	0	17	82	0	4	0.172
4730-475	0	103	0	0	6	0.179
4730-525	0	72	33	0	16	0.182
4730-550	0	228	87	0	30	0.547
4730-575	0	96	0	0	4	0.167
4730-600	0	156	0	0	8	0.271

Family 1

Family 2

Family 3

**Table 5.7.** Bench 4750 copper only fractures (Cu), iron only fractures (Fe), mix of iron and copper (Fe+Cu), Fresh Fractures, and density per bench interval.

<b>Table 5.7 - Bench 4750 Fracture Data</b>						
<b>Sample #</b>	<b>Cu</b>	<b>Fe</b>	<b>Fe + Cu</b>	<b>Fresh</b>	<b>n</b>	<b><math>\rho = \text{in}^2</math></b>
4750-00	0	8	121	0	10	0.224
4750-25	0	82	6	0	11	0.153
4750-50	0	168	0	0	9	0.292
4750-75	0	17	87	0	8	0.181
4750-100	0	104	0	0	10	0.181
4750-125	0	99	0	0	12	0.172
4750-150	0	76	0	0	11	0.132
4750-175	0	94	0	0	9	0.163
4750-200	0	83	0	0	8	0.144
4750-225	0	0	103	0	8	0.179
4750-250	0	103	0	0	7	0.179
4750-275	0	144	0	0	12	0.250
4750-300	0	125	0	0	12	0.217
4750-325	0	33	0	0	5	0.057
<b>Family 1</b>						
4750-00	0	0	85	0	9	0.148
4750-25	0	51	0	0	4	0.089
4750-50	0	93	0	0	7	0.161
4750-75	0	17	21	0	6	0.066
4750-100	0	97	0	0	8	0.168
4750-125	0	45	0	0	4	0.078
4750-150	0	64	0	0	6	0.111
4750-175	0	132	0	0	11	0.229
4750-200	0	145	0	0	13	0.252
4750-225	0	0	24	0	4	0.042
4750-250	0	103	0	0	9	0.179
4750-275	0	108	34	0	8	0.247
4750-300	0	110	0	0	10	0.191
4750-325	0	72	0	0	9	0.125
<b>Family 2</b>						
4750-00	0	7	74	0	6	0.141
4750-25	0	111	0	0	8	0.193
4750-50	0	48	0	0	6	0.083
4750-75	0	74	25	0	10	0.172
4750-100	0	65	0	0	8	0.113
4750-125	0	130	0	0	8	0.226
4750-150	0	34	0	0	5	0.059
4750-175	0	117	0	0	9	0.203
4750-200	0	132	0	0	11	0.229
4750-225	0	0	61	0	3	0.106
4750-250	0	108	0	0	6	0.188
4750-275	0	144	6	0	7	0.260
4750-300	0	143	0	0	12	0.248
4750-325	0	51	0	0	6	0.089
<b>Family 3</b>						

**Table 5.8.** Bench 4780 copper only fractures (Cu), iron only fractures (Fe), mix of iron and copper (Fe+Cu), Fresh Fractures, and density per bench interval.

<b>Table 5.8 - Bench 4780 Fracture Data</b>						
<b>Sample #</b>	<b>Cu</b>	<b>Fe</b>	<b>Fe + Cu</b>	<b>Fresh</b>	<b>n</b>	<b><math>\rho = \text{in}^2</math></b>
4780-00	0	158	0	0	13	0.274
4780-25	0	89	0	0	11	0.155
4780-50	0	92	87	0	25	0.311
4780-75	0	0	13	0	2	0.023
4780-100	0	12	52	0	5	0.111
4780-150	0	0	73	0	8	0.127
4780-175	0	112	168	0	37	0.486
4780-200	0	0	98	0	10	0.170
4780-225	0	0	84	0	7	0.146
4780-250	0	0	36	0	3	0.063
4780-275	0	0	83	0	5	0.144
4780-325	0	88	0	0	8	0.153
4780-350	0	91	57	0	12	0.257
4780-375	0	148	0	0	6	0.257
4780-400	0	83	0	0	7	0.144
4780-425	0	0	56	0	6	0.097
4780-450	0	0	235	0	16	0.408
4780-00	0	92	0	0	6	0.160
4780-25	0	53	0	0	5	0.092
4780-50	0	23	87	0	8	0.191
4780-75	0	0	40	0	7	0.069
4780-100	0	21	76	0	9	0.168
4780-150	0	15	167	0	15	0.316
4780-175	0	26	57	0	6	0.144
4780-200	0	0	109	0	7	0.189
4780-225	0	0	83	0	6	0.144
4780-250	0	0	57	0	5	0.099
4780-275	0	0	67	0	4	0.116
4780-325	0	76	0	0	6	0.132
4780-350	0	65	87	0	12	0.264
4780-375	0	53	0	0	3	0.092
4780-400	0	54	0	0	6	0.094
4780-425	0	66	0	0	8	0.115
4780-450	0	0	158	0	12	0.274
4780-00	0	61	0	0	6	0.106
4780-25	0	114	0	0	11	0.198
4780-50	0	4	12	0	3	0.028
4780-75	0	0	174	0	12	0.302
4780-100	0	12	24	0	3	0.063
4780-150	0	15	52	0	4	0.116
4780-175	0	68	112	0	10	0.313
4780-200	0	0	101	0	9	0.175
4780-225	0	0	45	0	5	0.078
4780-250	0	0	1	0	1	0.002
4780-275	0	0	78	0	3	0.135
4780-325	0	143	0	0	13	0.248
4780-350	0	28	34	0	8	0.108
4780-375	0	135	0	0	9	0.234
4780-400	0	70	0	27	6	0.168
4780-425	0	0	53	0	7	0.092
4780-450	0	0	78	0	4	0.135

**Family 1**

**Family 2**

**Family 3**

**Table 5.9.** Bench 4800 copper only fractures (Cu), iron only fractures (Fe), mix of iron and copper (Fe+Cu), Fresh Fractures, and density per bench interval.

<b>Table 5.9 - Bench 4800 Fracture Data</b>						
<b>Sample #</b>	<b>Cu</b>	<b>Fe</b>	<b>Fe + Cu</b>	<b>Fresh</b>	<b>n</b>	<b><math>\rho = \text{in}^2</math></b>
4800-25	0	115	0	0	8	0.200
4800-50	0	45	94	0	9	0.241
4800-75	0	164	64	0	17	0.396
4800-125	0	117	0	0	11	0.203
4800-150	0	30	53	0	7	0.144
4800-175	0	177	6	17	14	0.347
4800-200	0	56	53	0	11	0.189
4800-225	0	119	0	0	9	0.207
4800-275	0	145	0	0	11	0.252
4800-300	0	9	124	0	8	0.231
4800-325	0	91	62	0	6	0.266
4800-350	0	55	0	0	5	0.095
<b>Family 1</b>						
4800-25	0	87	0	0	6	0.151
4800-50	0	4	33	0	4	0.064
4800-75	0	36	39	0	7	0.130
4800-125	0	48	0	0	7	0.083
4800-150	0	22	48	0	3	0.122
4800-175	0	91	0	0	6	0.158
4800-200	0	33	39	0	6	0.125
4800-225	0	53	10	0	7	0.109
4800-275	0	70	0	0	8	0.122
4800-300	0	27	50	0	6	0.134
4800-325	0	22	13	0	10	0.061
4800-350	0	70	55	0	12	0.217
<b>Family 2</b>						
4800-25	0	51	0	0	5	0.089
4800-50	0	0	42	0	4	0.073
4800-75	0	22	74	0	8	0.167
4800-125	0	19	0	0	6	0.033
4800-150	0	1	0	0	1	0.002
4800-175	0	93	0	0	5	0.161
4800-200	0	20	68	0	4	0.153
4800-225	0	74	0	0	7	0.128
4800-275	0	128	0	0	13	0.222
4800-300	0	8	31	0	8	0.068
4800-325	0	46	46	0	6	0.160
4800-350	0	67	0	0	7	0.116
<b>Family 3</b>						

### 19.3. Appendix 5.3. Stereonets with % Cu and % Fe in Fractures

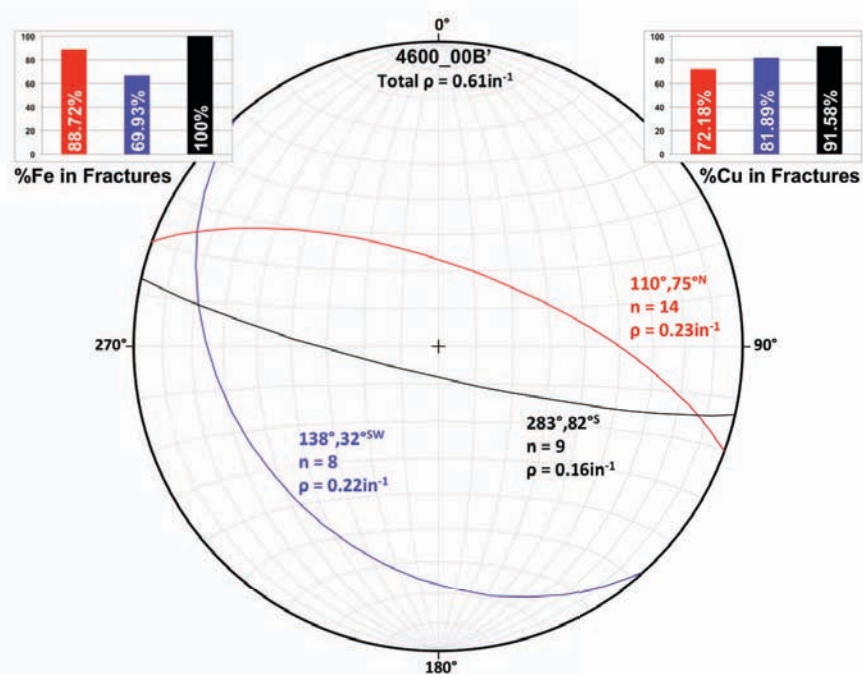


**Figure 5.1.** Stereonet of interval 4600\_00B showing orientation, number of fractures, and fracture density per fracture family. Bar charts are color coordinated and show percent copper and iron occurring in each fracture family.

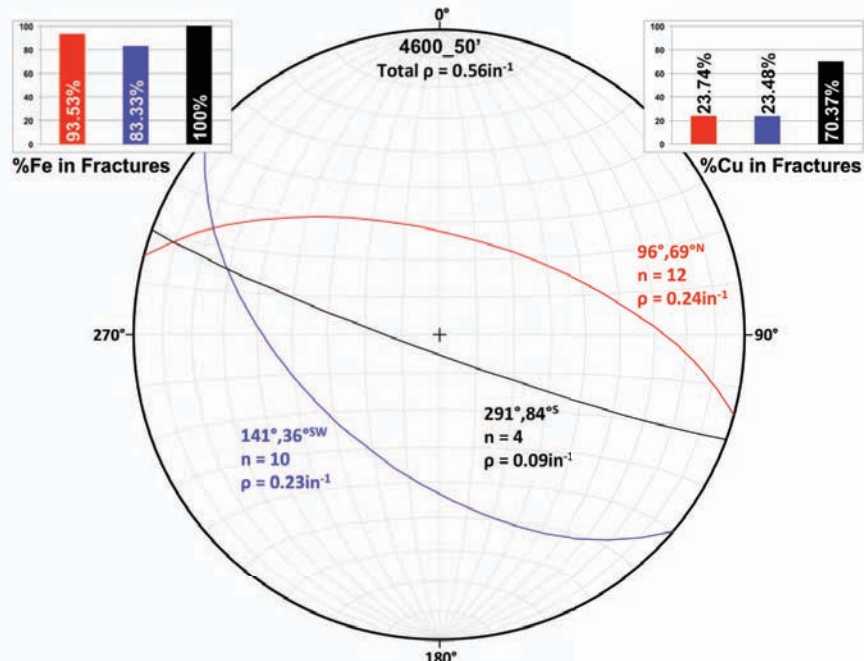


**Figure 5.2.** Stereonet of interval 4600\_50 showing orientation, number of fractures, and fracture density per fracture family. Bar charts are color coordinated and show percent copper and iron occurring in each fracture family.

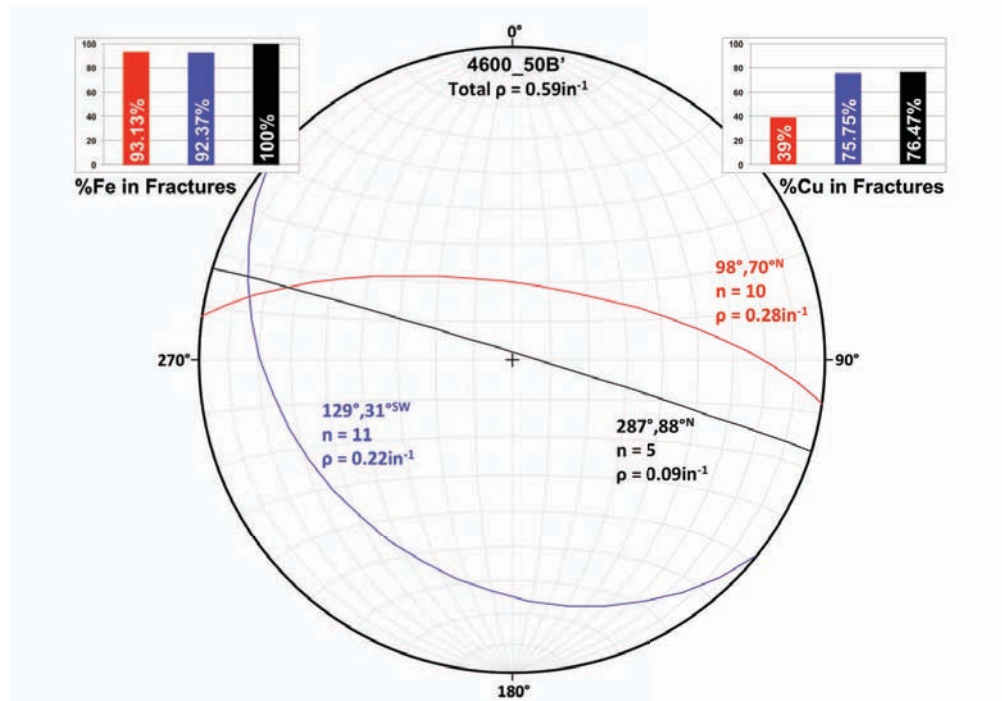


**Figure 5.3.** Stereonet of interval 4600\_50B showing orientation, number of fractures, and fracture density per fracture family. Bar charts are color coordinated and show percent copper and iron occurring in each fracture family.

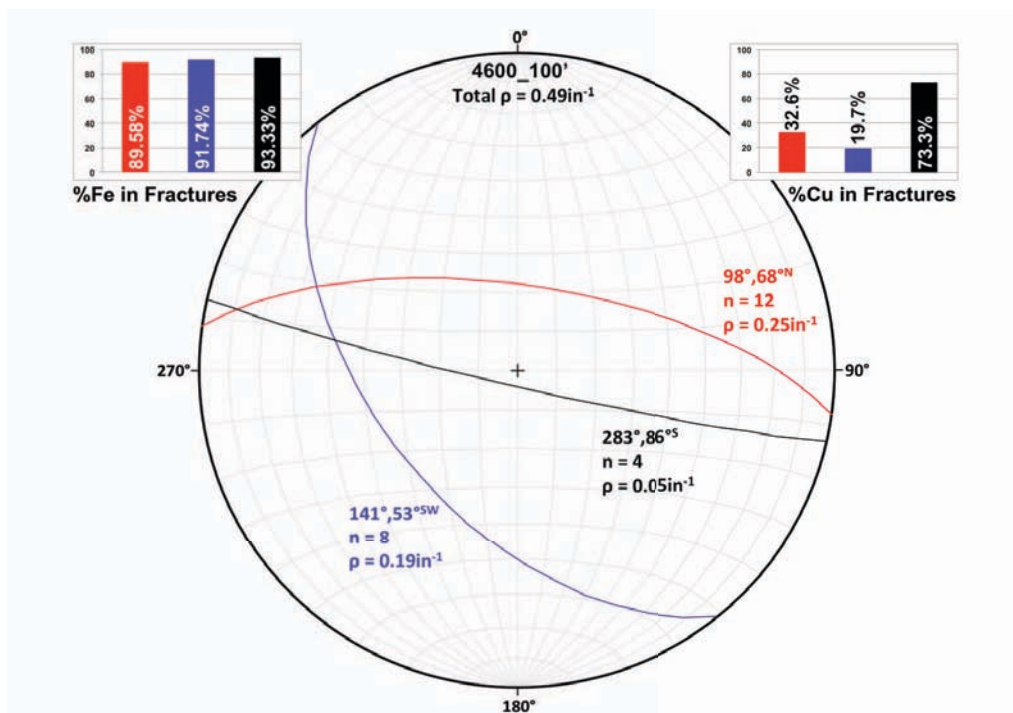


**Figure 5.4.** Stereonet of interval 4600\_100 showing orientation, number of fractures, and fracture density per fracture family. Bar charts are color coordinated and show percent copper and iron occurring in each fracture family.

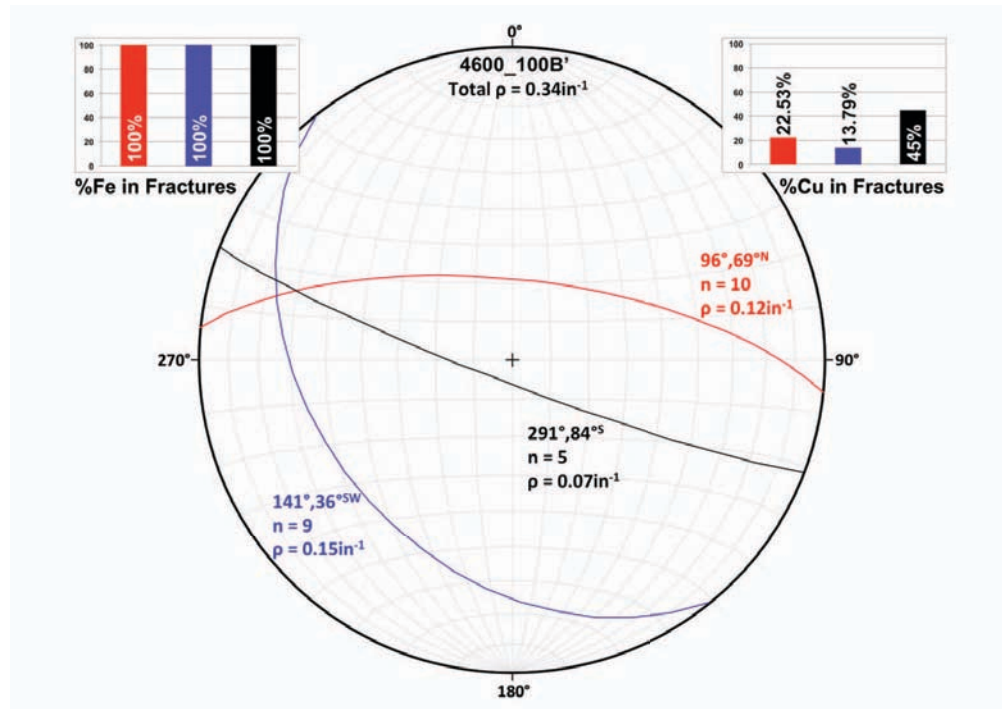


**Figure 5.5.** Stereonet of interval 4600\_100B showing orientation, number of fractures, and fracture density per fracture family. Bar charts are color coordinated and show percent copper and iron occurring in each fracture family.

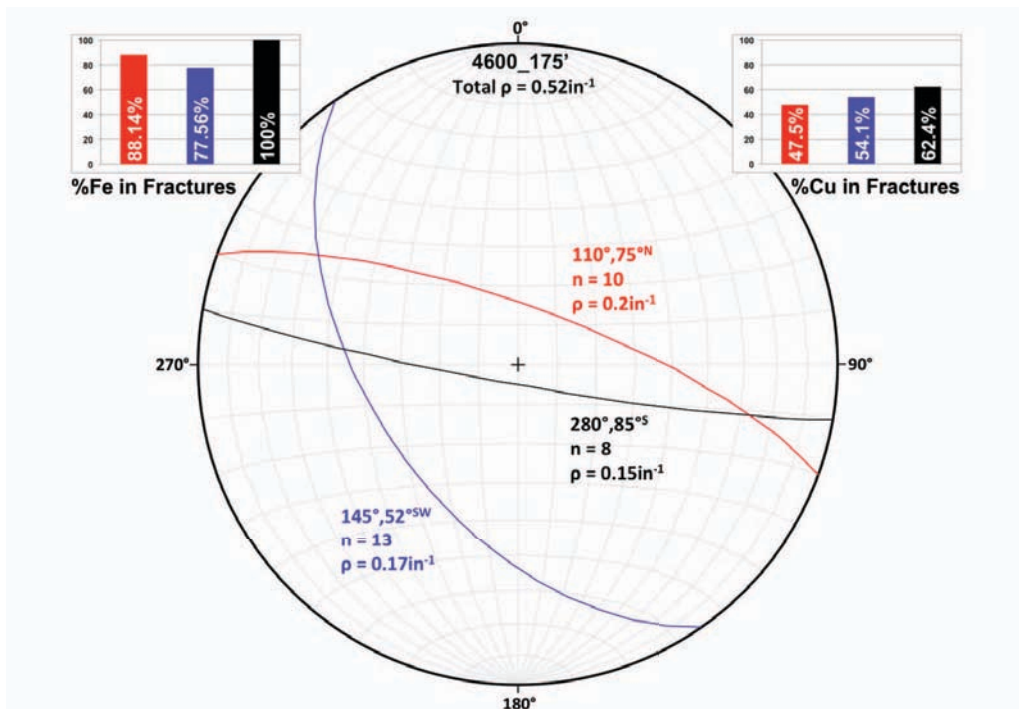


**Figure 5.6.** Stereonet of interval 4600\_175 showing orientation, number of fractures, and fracture density per fracture family. Bar charts are color coordinated and show percent copper and iron occurring in each fracture family.

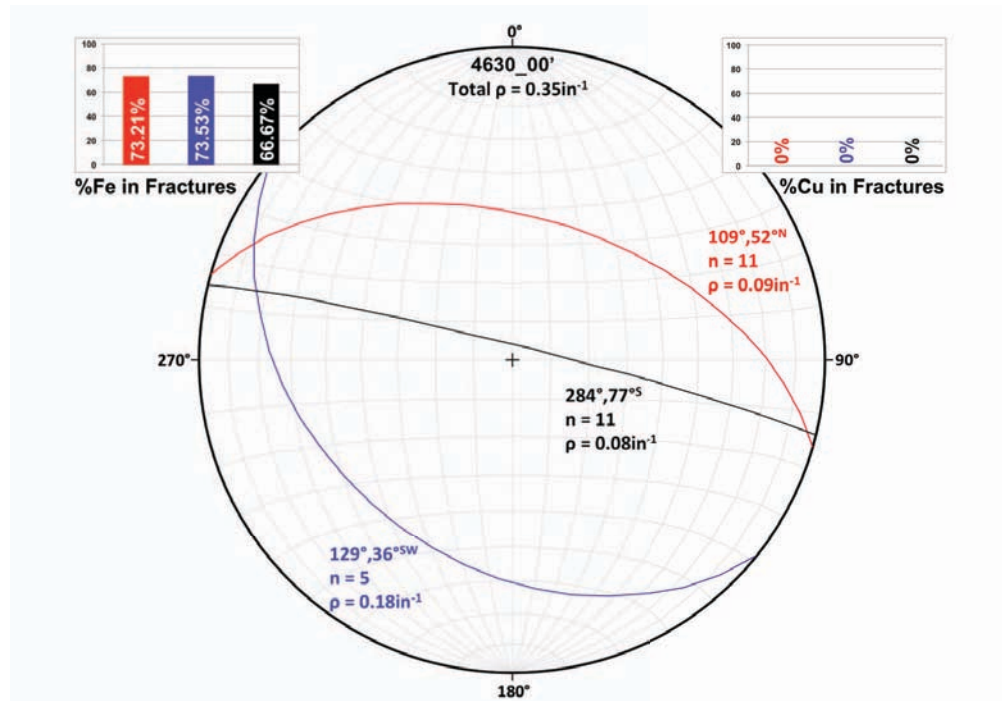


**Figure 5.7.** Stereonet of interval 4630\_00 showing orientation, number of fractures, and fracture density per fracture family. Bar charts are color coordinated and show percent copper and iron occurring in each fracture family.

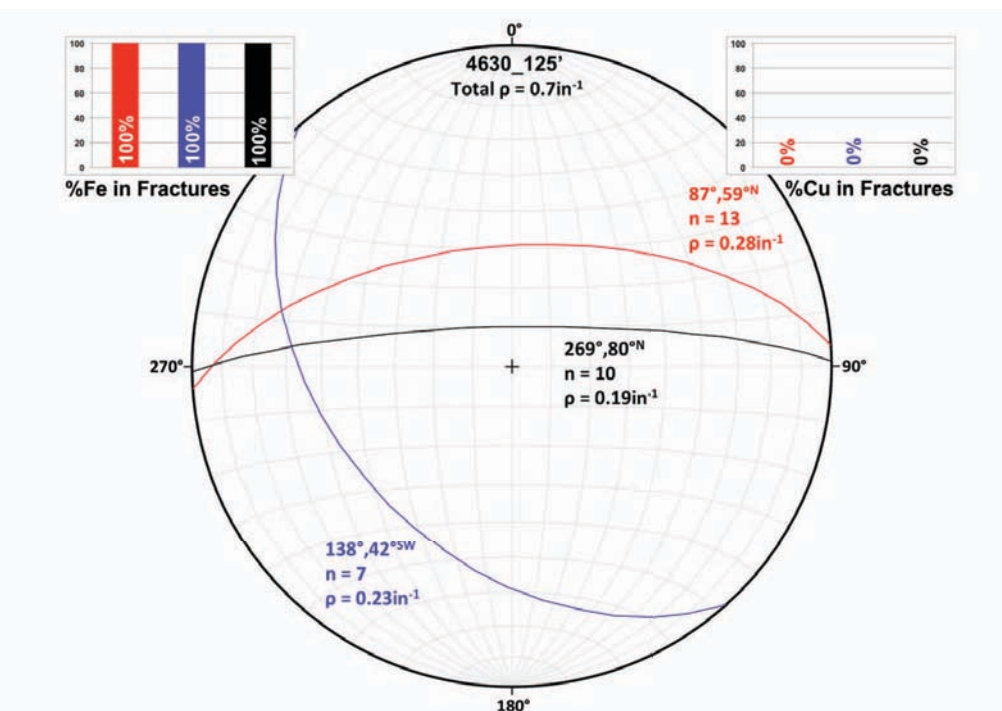


**Figure 5.8.** Stereonet of interval 4630\_125 showing orientation, number of fractures, and fracture density per fracture family. Bar charts are color coordinated and show percent copper and iron occurring in each fracture family.

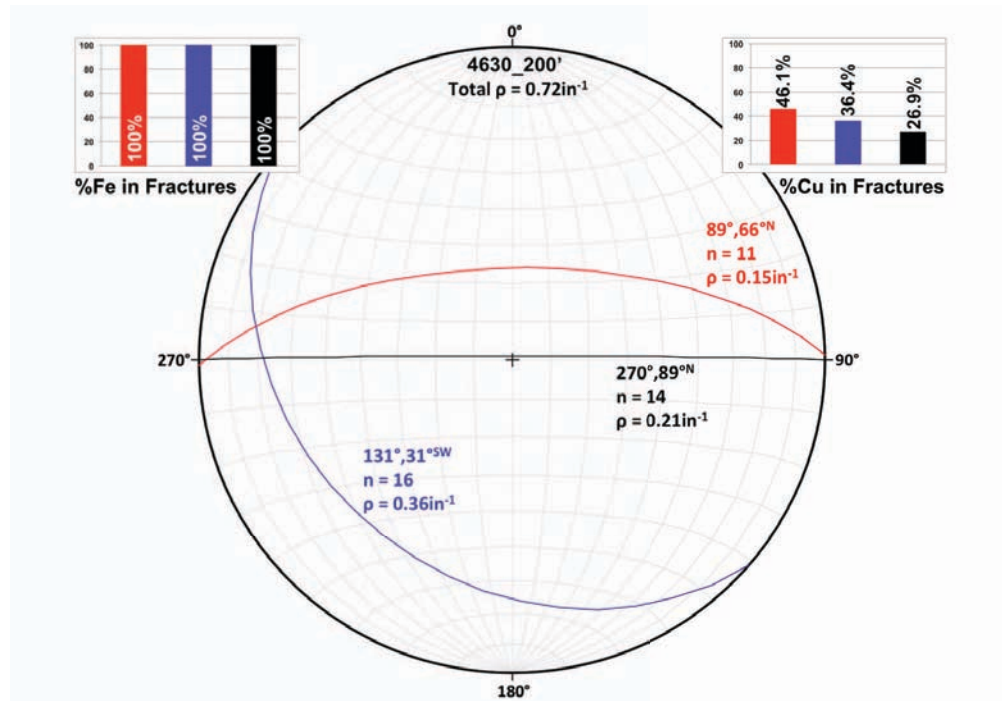


**Figure 5.9.** Stereonet of interval 4630\_200 showing orientation, number of fractures, and fracture density per fracture family. Bar charts are color coordinated and show percent copper and iron occurring in each fracture family..

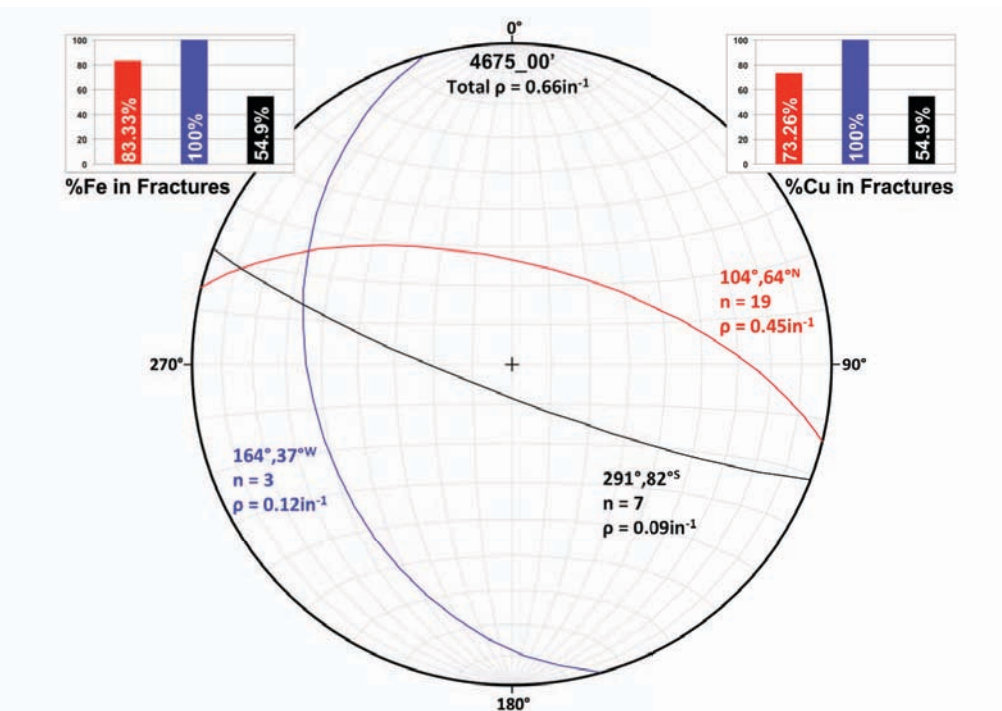


**Figure 5.10.** Stereonet of interval 4675\_00 showing orientation, number of fractures, and fracture density per fracture family. Bar charts are color coordinated and show percent copper and iron occurring in each fracture family.

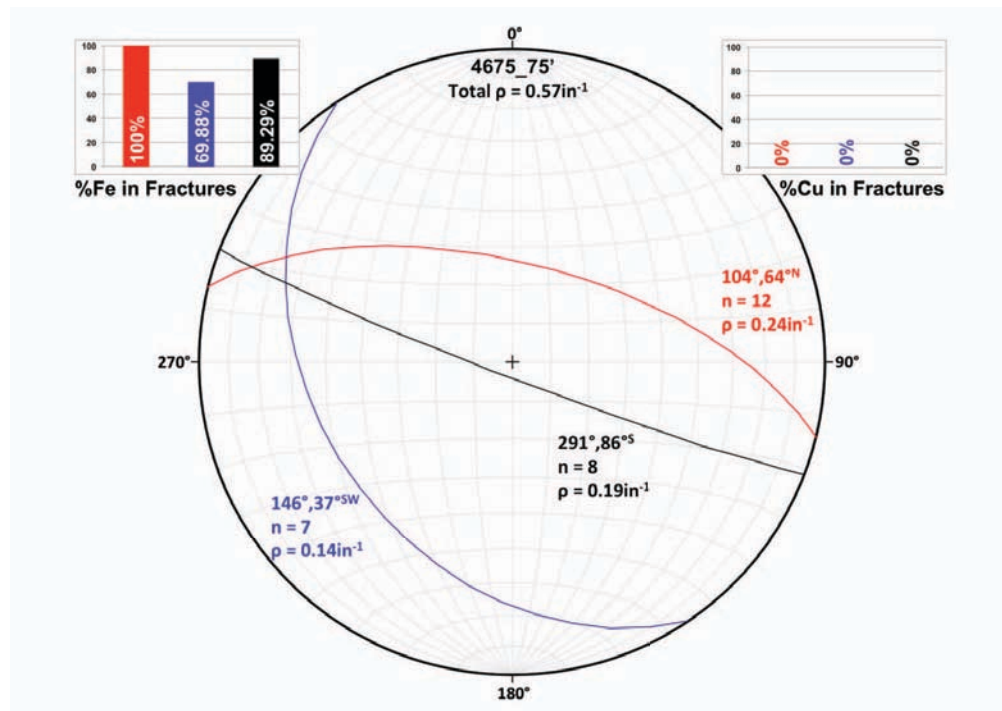


**Figure 5.11.** Stereonet of interval 4675\_75 showing orientation, number of fractures, and fracture density per fracture family. Bar charts are color coordinated and show percent copper and iron occurring in each fracture family.

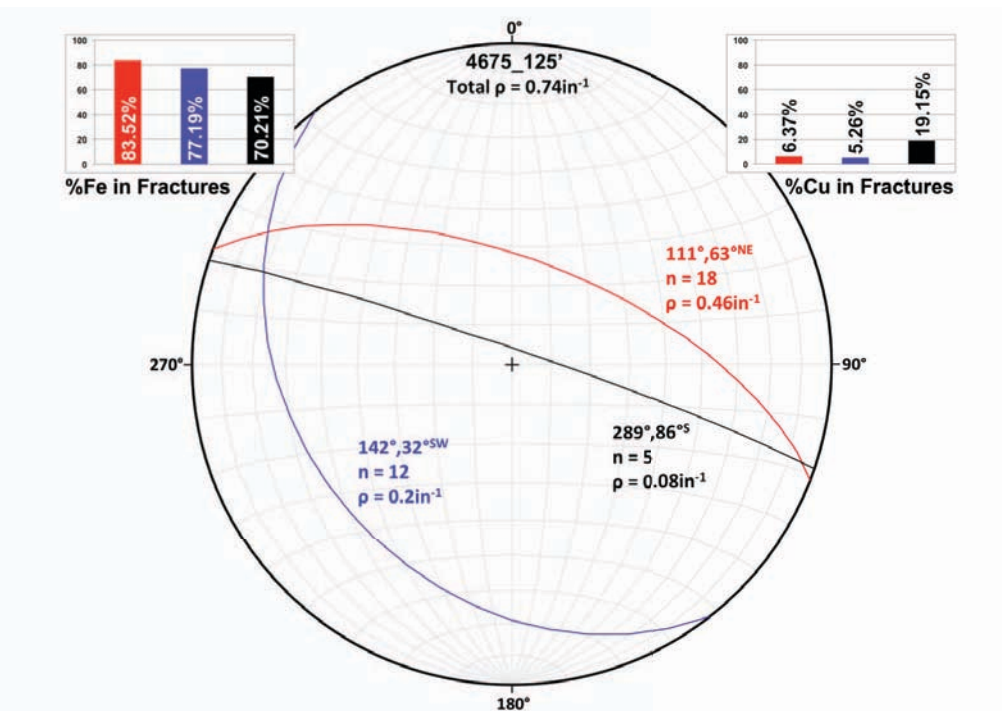


**Figure 5.12.** Stereonet of interval 4675\_125 showing orientation, number of fractures, and fracture density per fracture family. Bar charts are color coordinated and show percent copper and iron occurring in each fracture family.

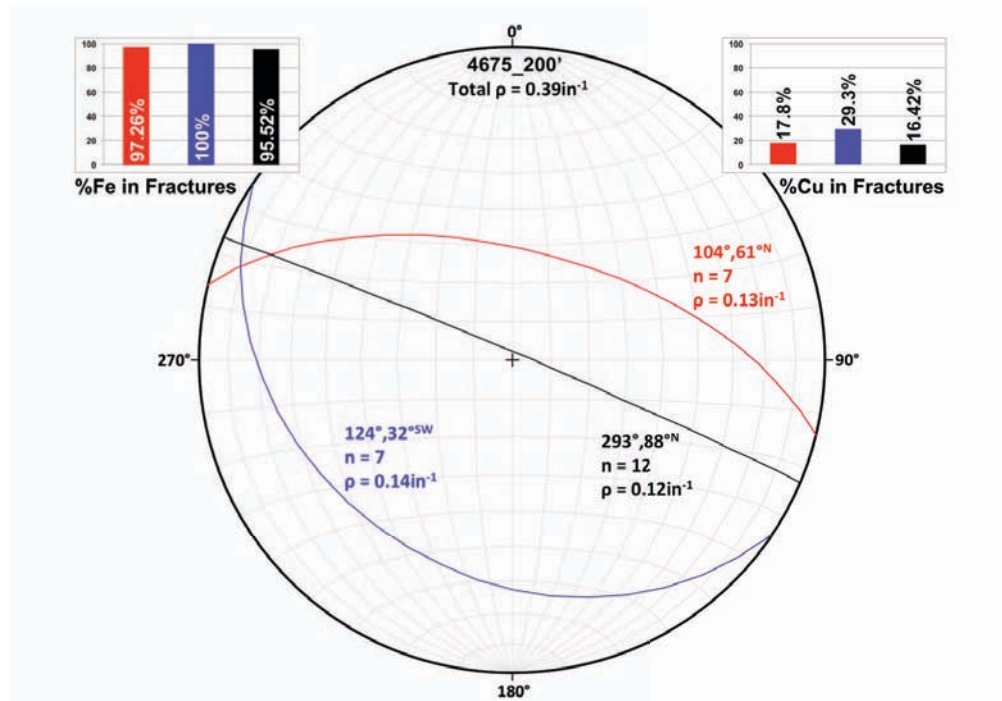


**Figure 5.13** Stereonet of interval 4675\_200 showing orientation, number of fractures, and fracture density per fracture family. Bar charts are color coordinated and show percent copper and iron occurring in each fracture family.

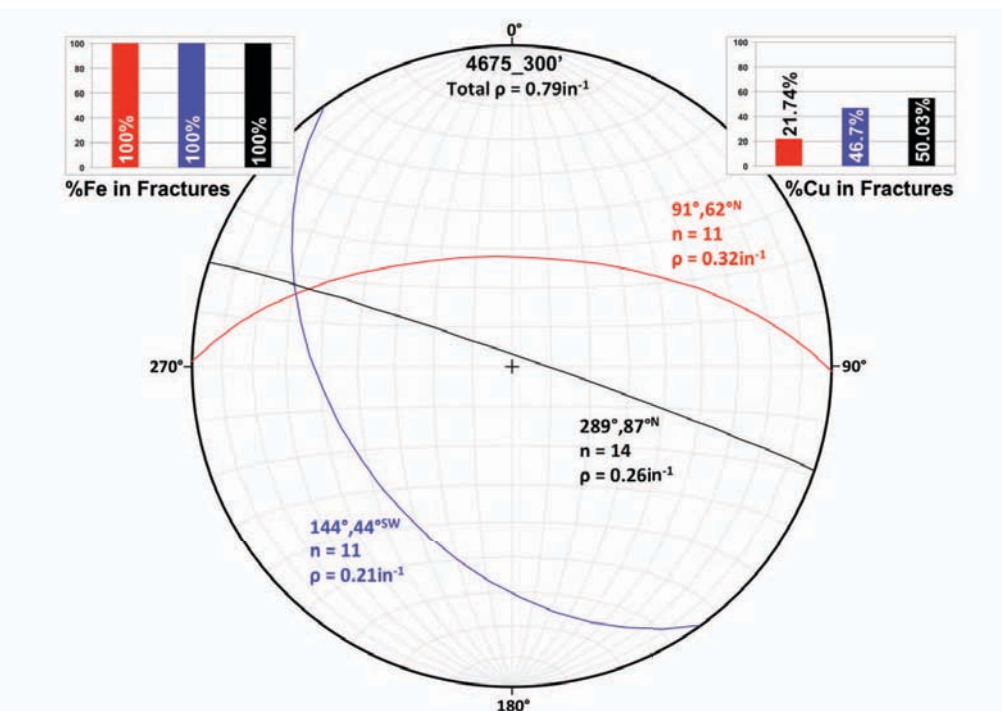


**Figure 5.14.** Stereonet of interval 4675\_300 showing orientation, number of fractures, and fracture density per fracture family. Bar charts are color coordinated and show percent copper and iron occurring in each fracture family.

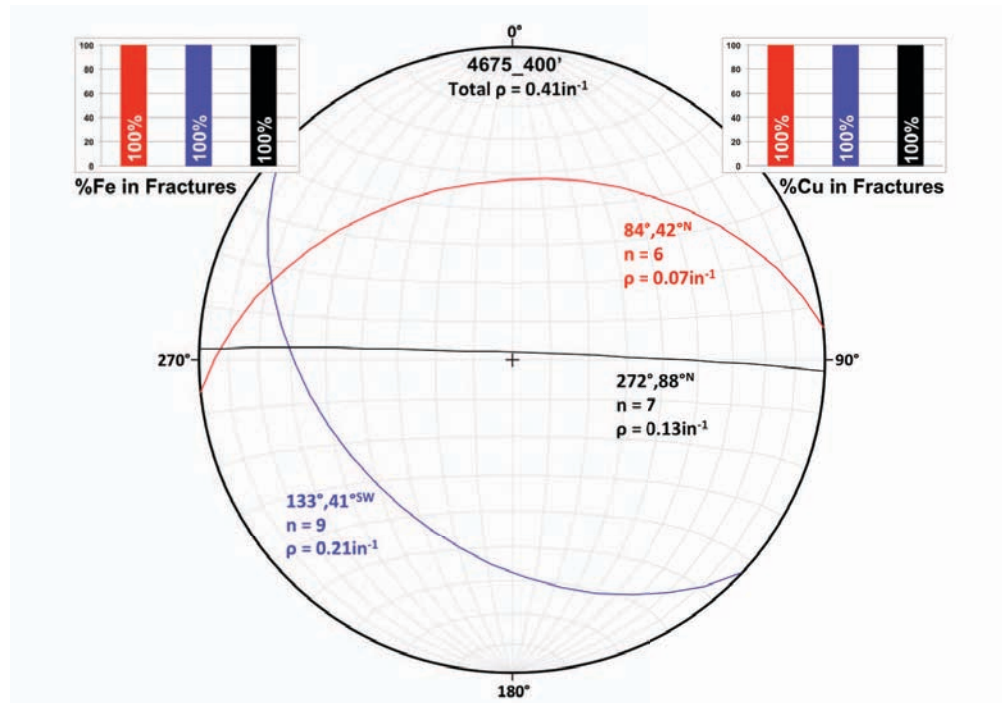


**Figure 5.15.** Stereonet of interval 4675\_400 showing orientation, number of fractures, and fracture density per fracture family. Bar charts are color coordinated and show percent copper and iron occurring in each fracture family.

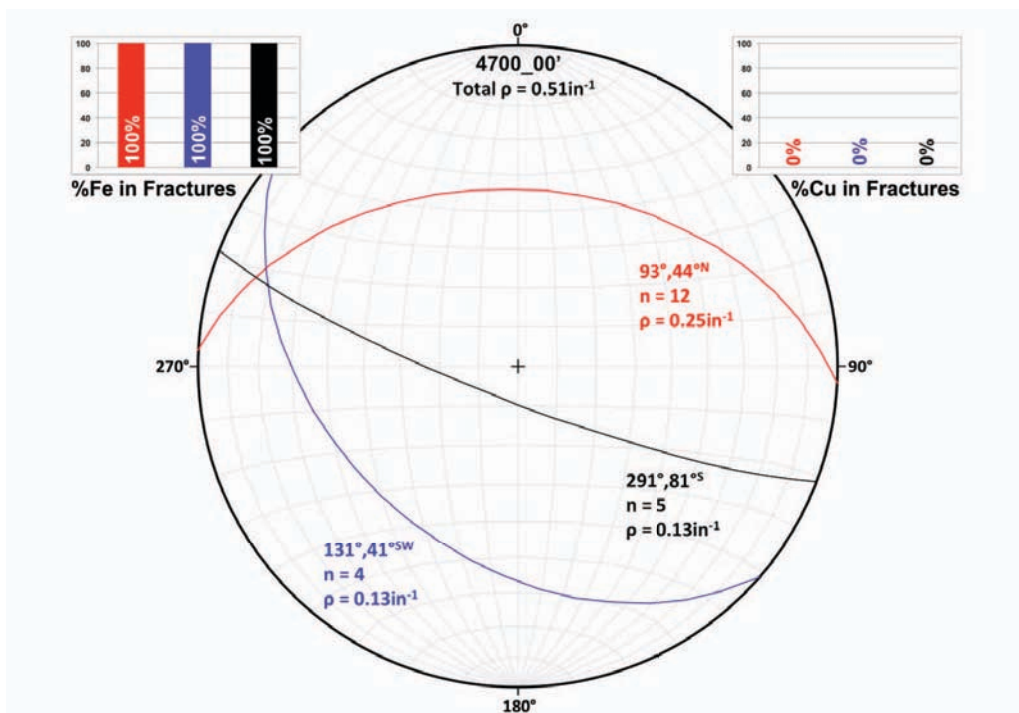


**Figure 5.16.** Stereonet of interval 4700\_00 showing orientation, number of fractures, and fracture density per fracture family. Bar charts are color coordinated and show percent copper and iron occurring in each fracture family.

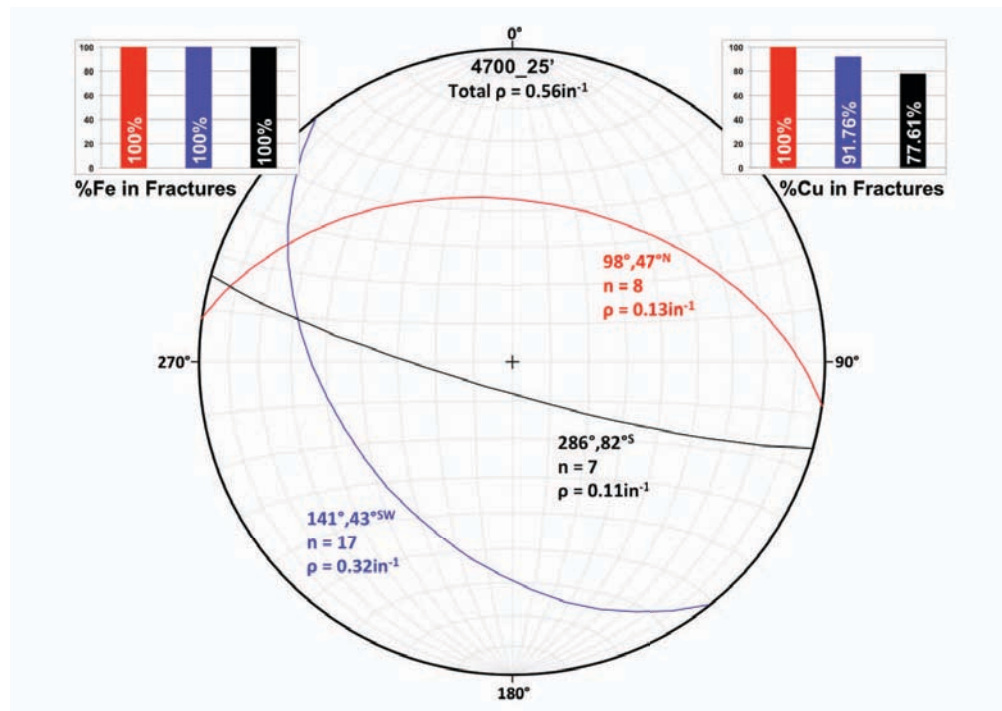


**Figure 5.17.** Stereonet of interval 4700\_25 showing orientation, number of fractures, and fracture density per fracture family. Bar charts are color coordinated and show percent copper and iron occurring in each fracture family.

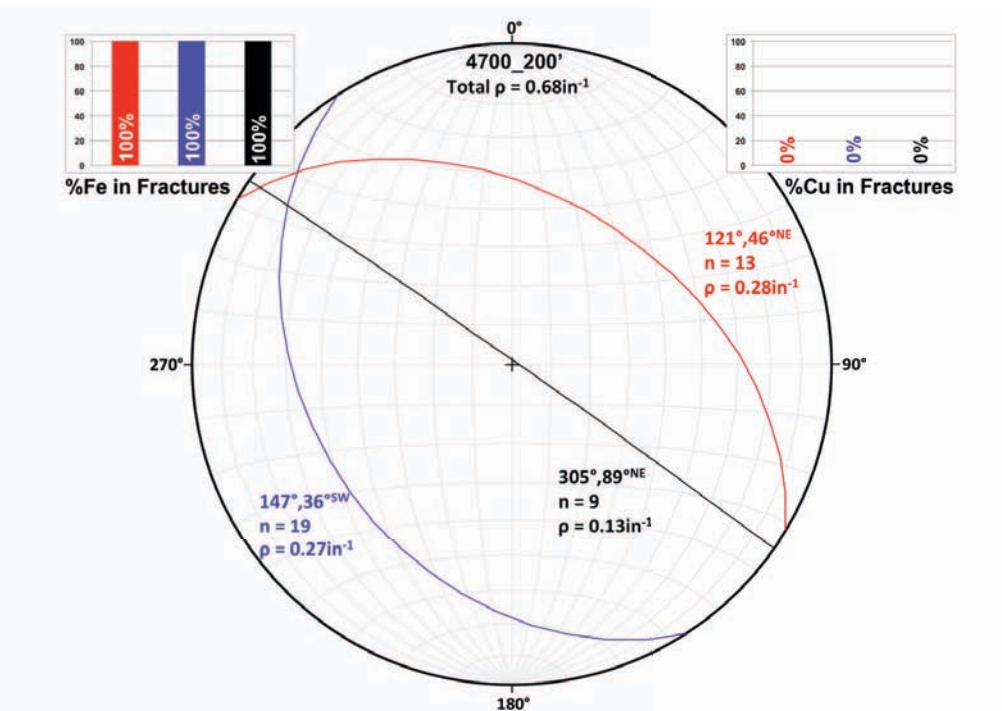


**Figure 5.18.** Stereonet of interval 4700\_200 showing orientation, number of fractures, and fracture density per fracture family. Bar charts are color coordinated and show percent copper and iron occurring in each fracture family.

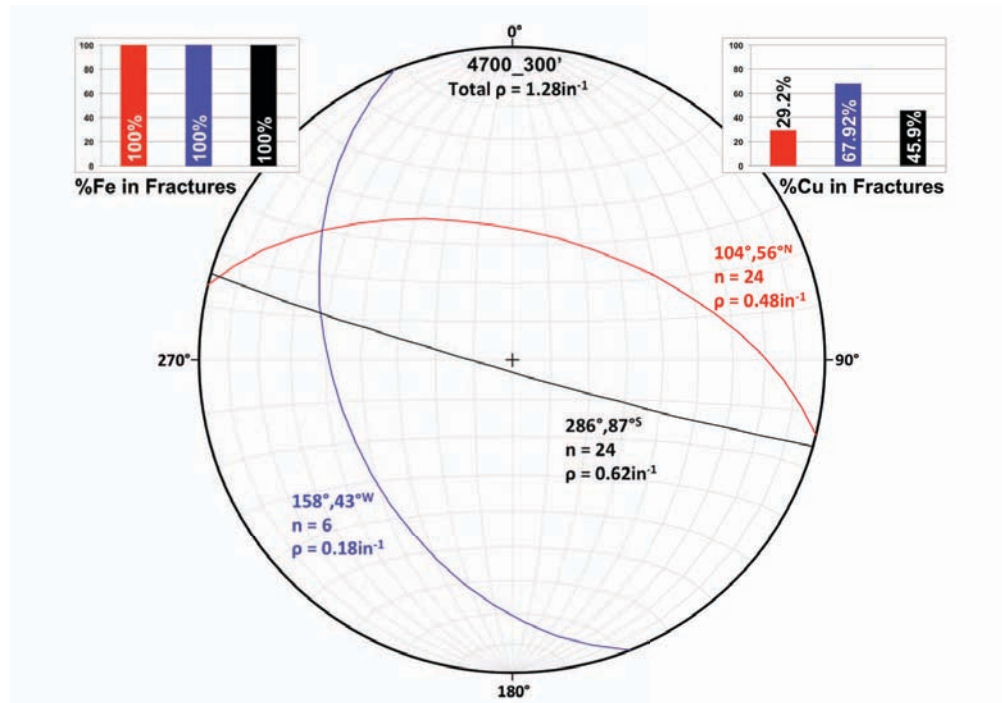


**Figure 5.19.** Stereonet of interval 4700\_300 showing orientation, number of fractures, and fracture density per fracture family. Bar charts are color coordinated and show percent copper and iron occurring in each fracture family.

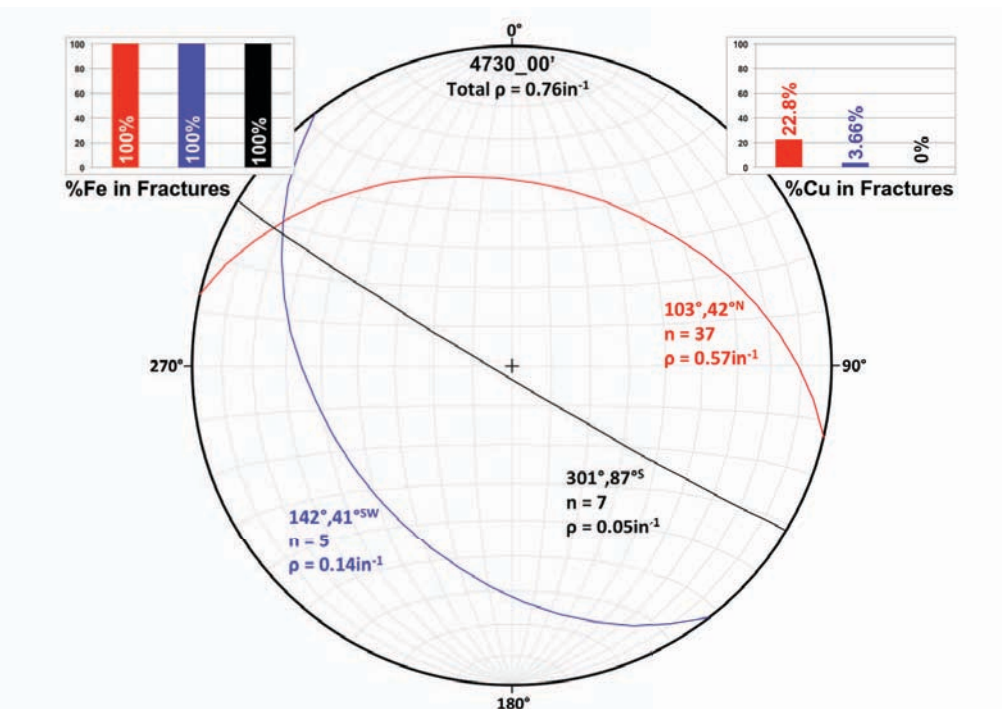


**Figure 5.20.** Stereonet of interval 4730\_00 showing orientation, number of fractures, and fracture density per fracture family. Bar charts are color coordinated and show percent copper and iron occurring in each fracture family.

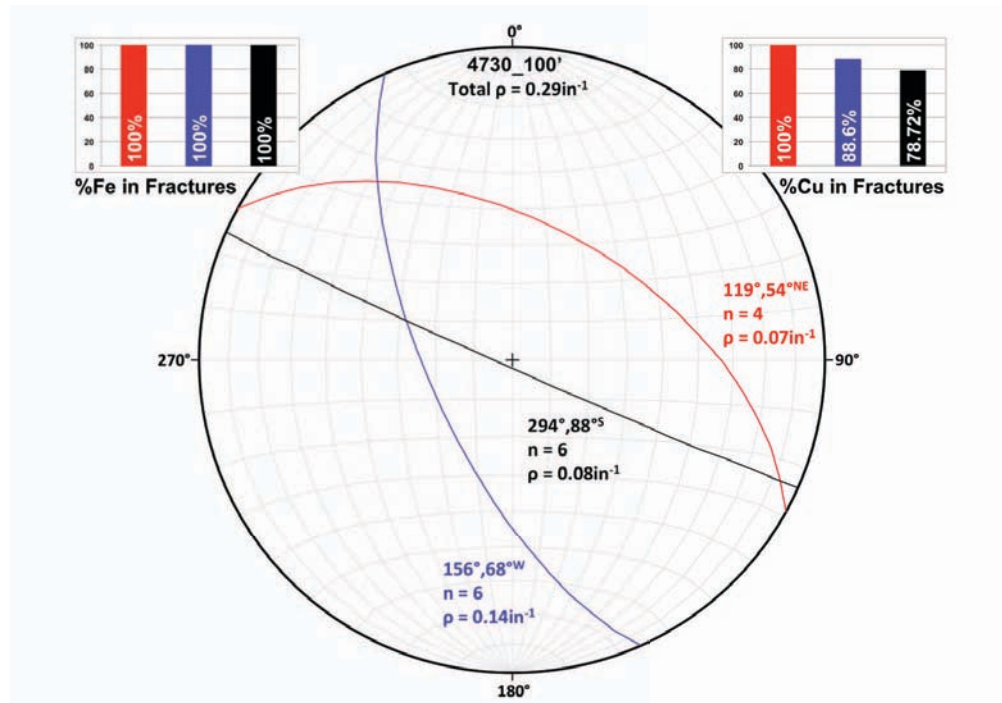


**Figure 5.21.** Stereonet of interval 4730\_100 showing orientation, number of fractures, and fracture density per fracture family. Bar charts are color coordinated and show percent copper and iron occurring in each fracture family.

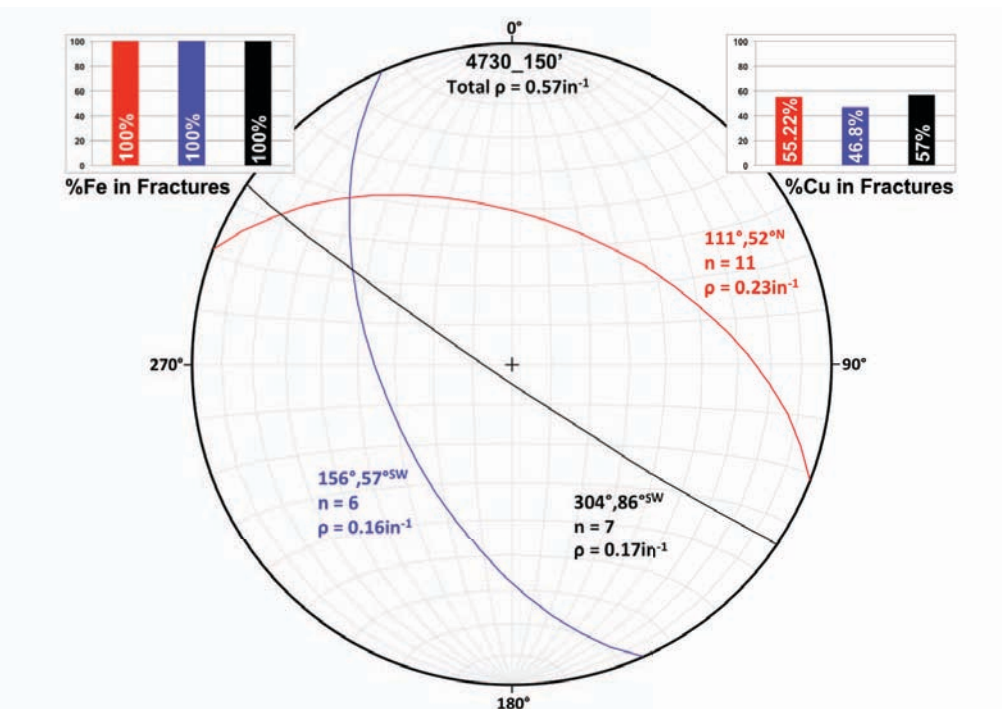


**Figure 5.22.** Stereonet of interval 4730\_150 showing orientation, number of fractures, and fracture density per fracture family. Bar charts are color coordinated and show percent copper and iron occurring in each fracture family.

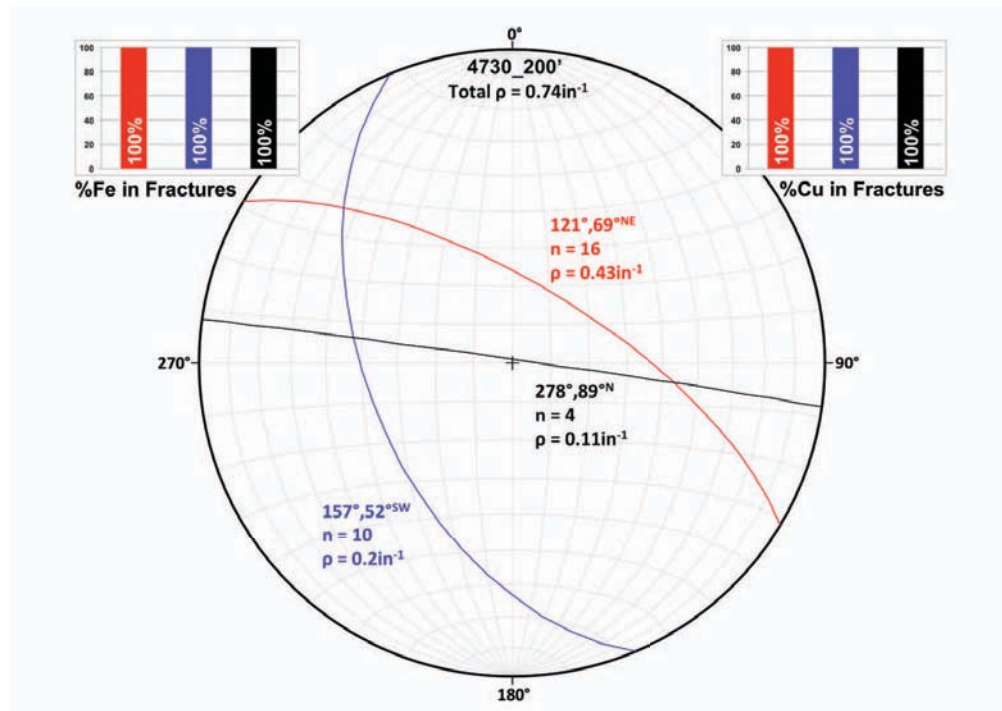


**Figure 5.23.** Stereonet of interval 4730\_200 showing orientation, number of fractures, and fracture density per fracture family. Bar charts are color coordinated and show percent copper and iron occurring in each fracture family.

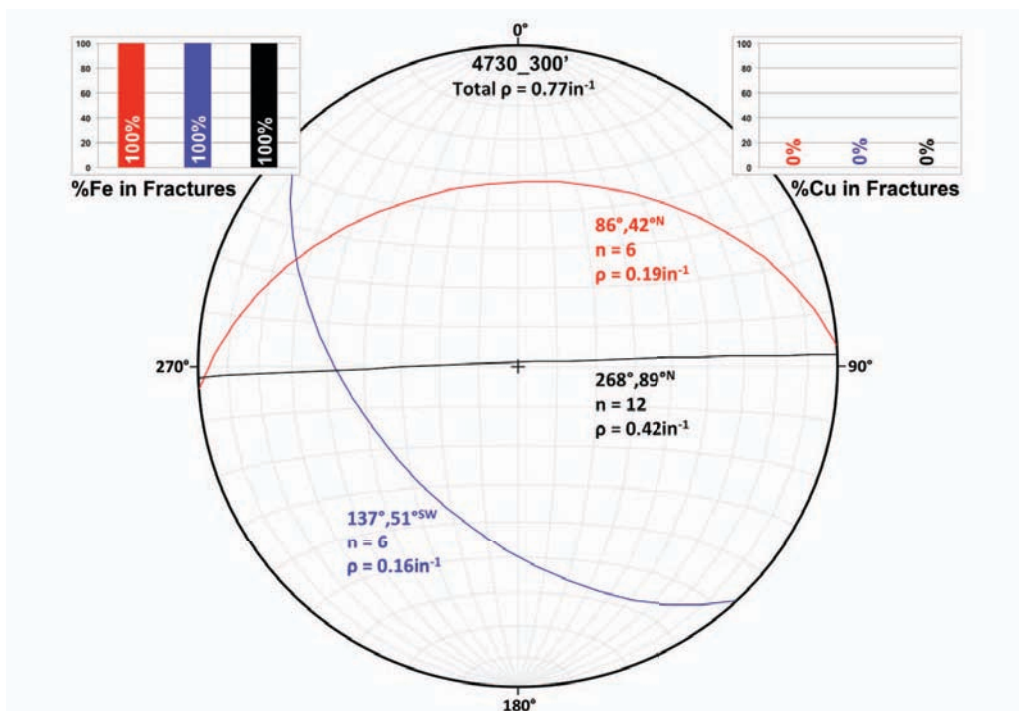


**Figure 5.24.** Stereonet of interval 4730\_300 showing orientation, number of fractures, and fracture density per fracture family. Bar charts are color coordinated and show percent copper and iron occurring in each fracture family.

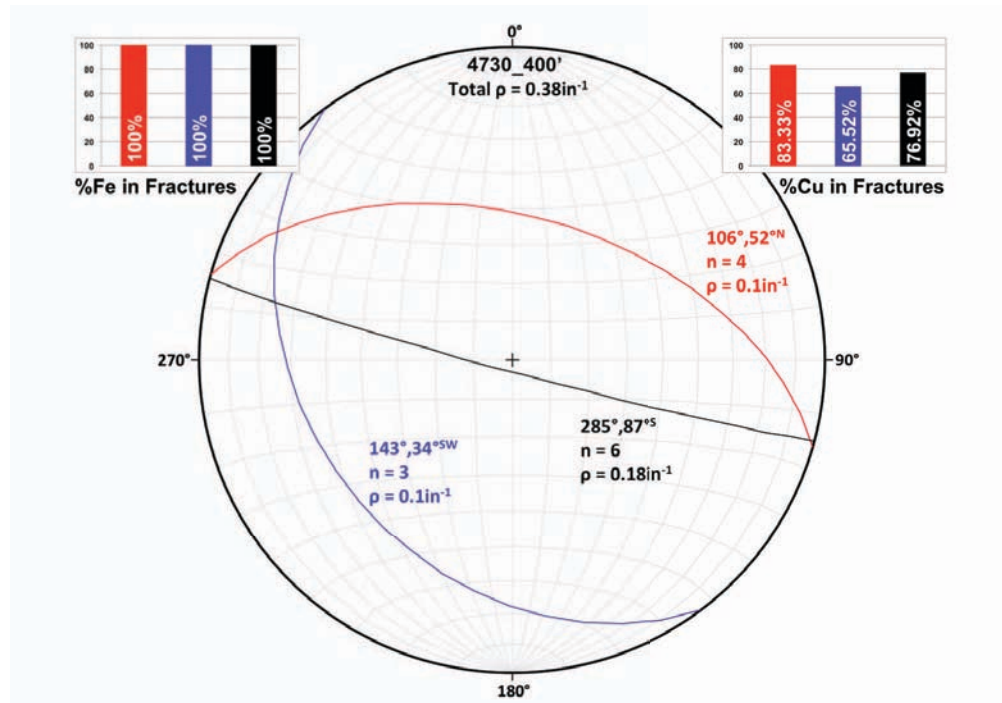


**Figure 5.25.** Stereonet of interval 4730\_400 showing orientation, number of fractures, and fracture density per fracture family. Bar charts are color coordinated and show percent copper and iron occurring in each fracture family.

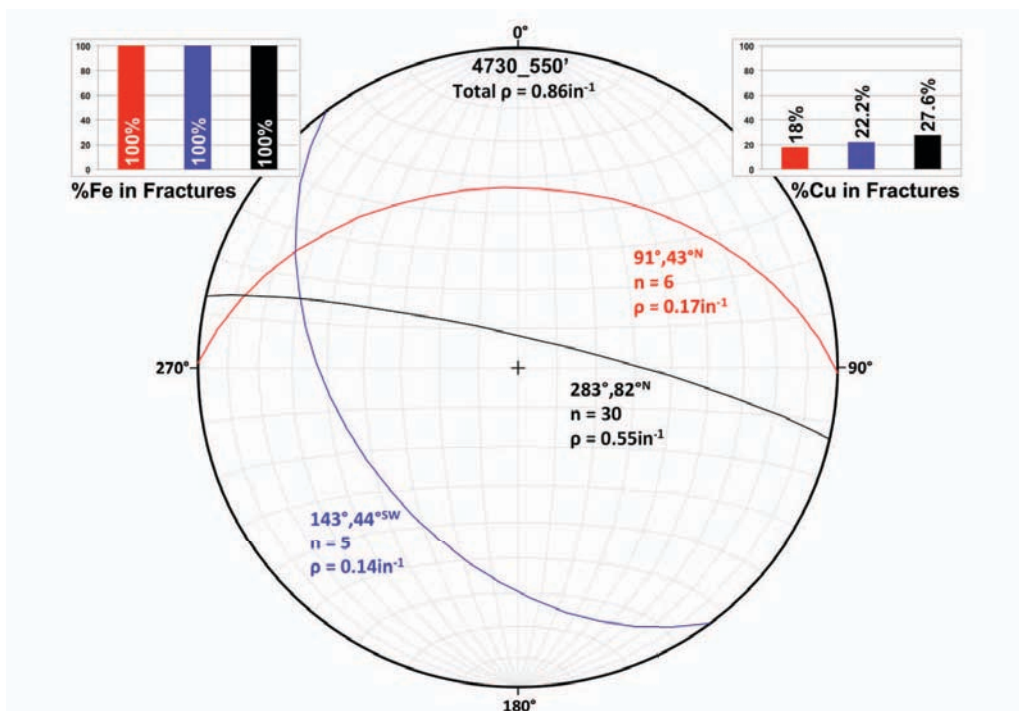


**Figure 5.26.** Stereonet of interval 4730\_550 showing orientation, number of fractures, and fracture density per fracture family. Bar charts are color coordinated and show percent copper and iron occurring in each fracture family.

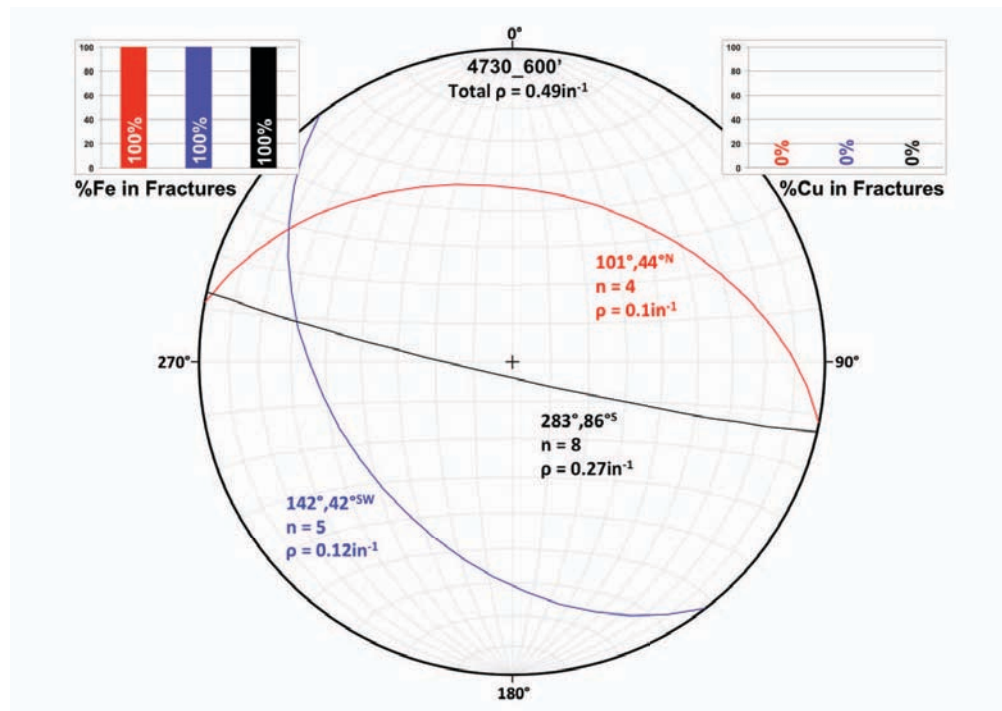


**Figure 5.27.** Stereonet of interval 4730\_600 showing orientation, number of fractures, and fracture density per fracture family. Bar charts are color coordinated and show percent copper and iron occurring in each fracture family.

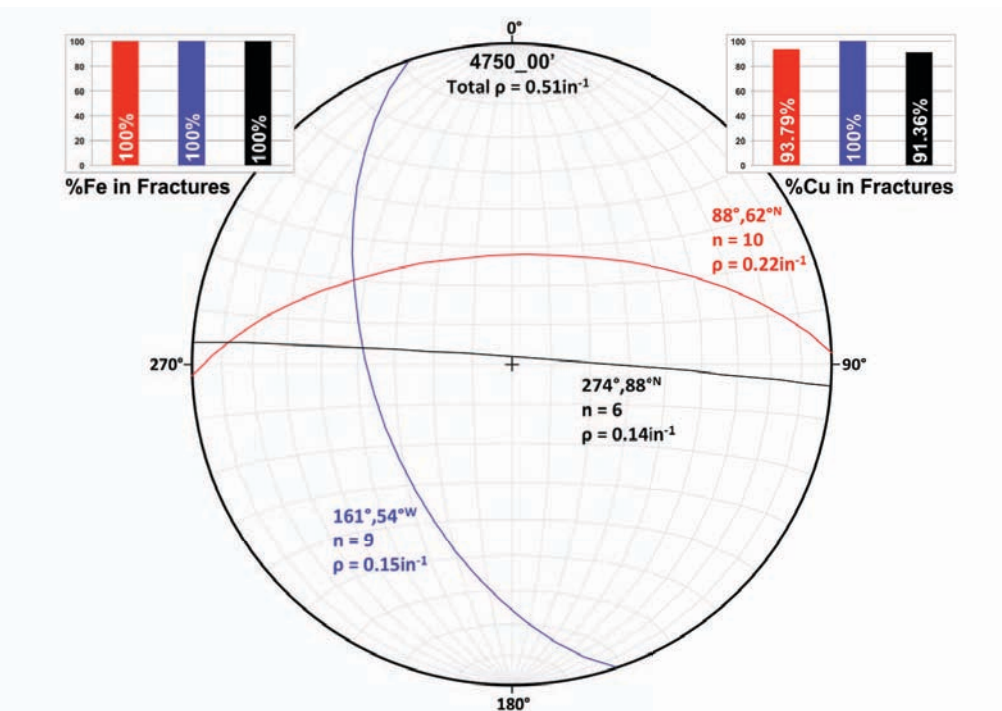


**Figure 5.28.** Stereonet of interval 4750\_00 showing orientation, number of fractures, and fracture density per fracture family. Bar charts are color coordinated and show percent copper and iron occurring in each fracture family.

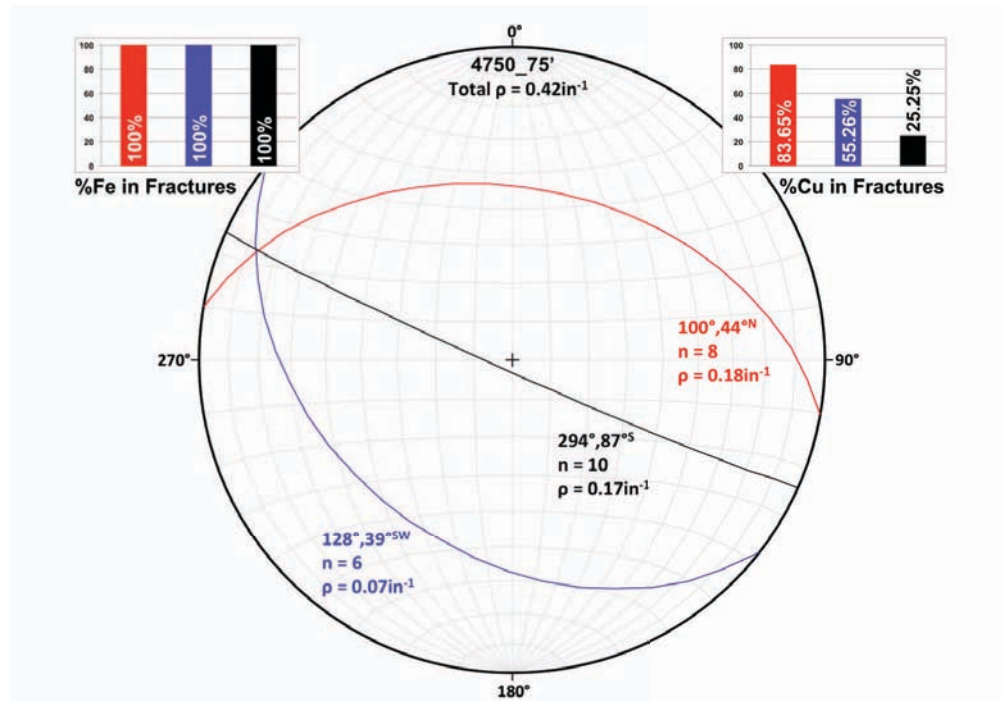


**Figure 5.29.** Stereonet of interval 4750\_75 showing orientation, number of fractures, and fracture density per fracture family. Bar charts are color coordinated and show percent copper and iron occurring in each fracture family.

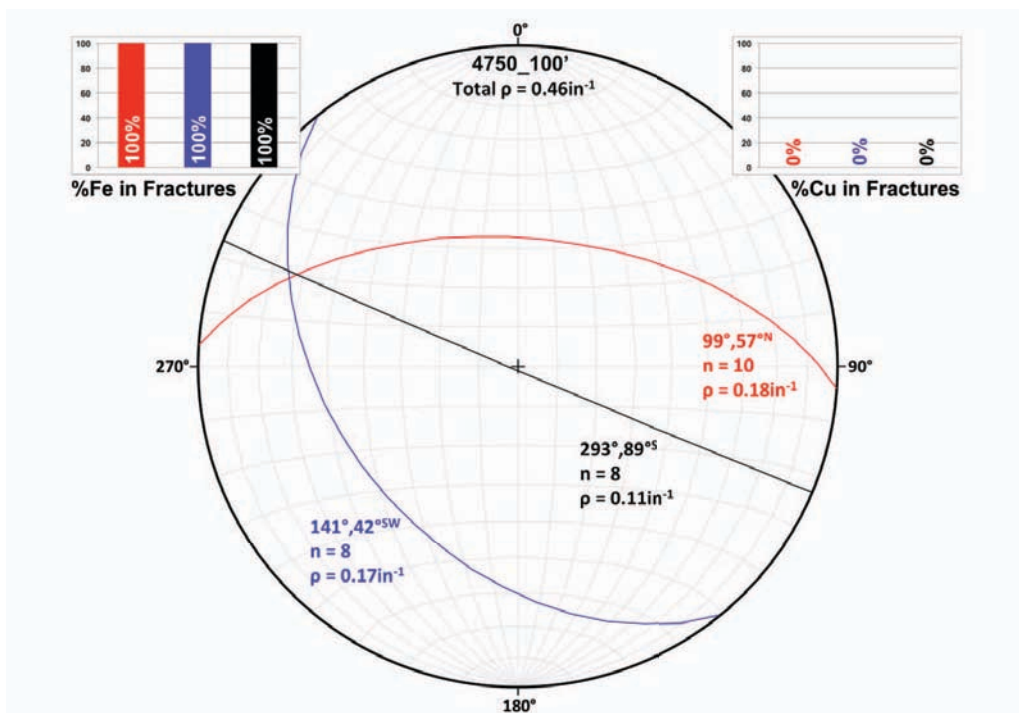


**Figure 5.30.** Stereonet of interval 4750\_100 showing orientation, number of fractures, and fracture density per fracture family. Bar charts are color coordinated and show percent copper and iron occurring in each fracture family.

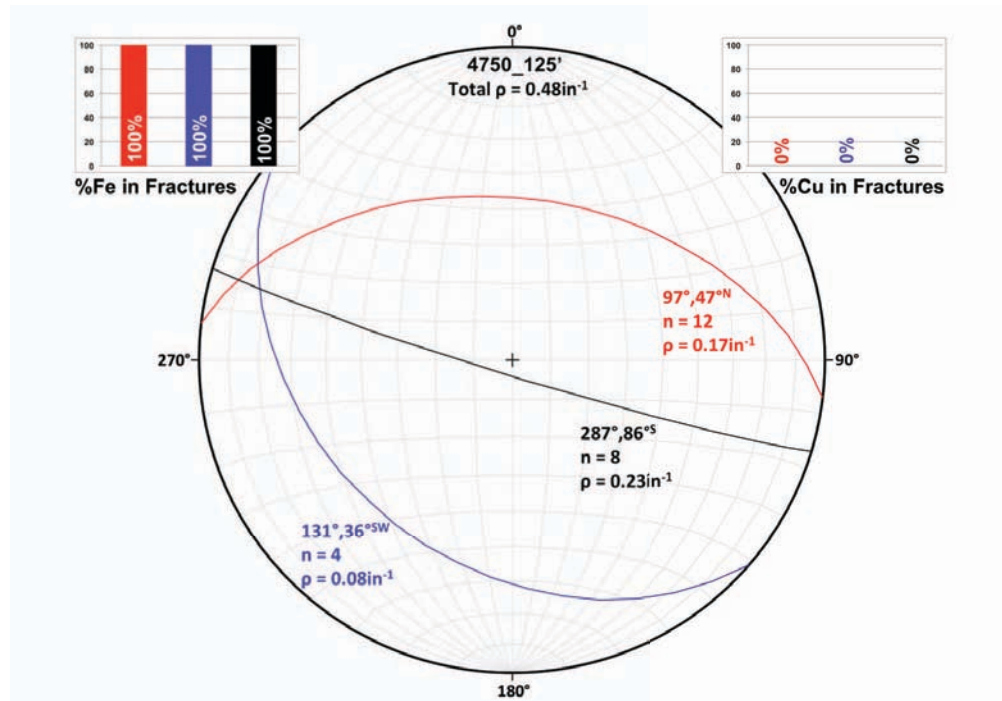


**Figure 5.31** Stereonet of interval 4750\_125 showing orientation, number of fractures, and fracture density per fracture family. Bar charts are color coordinated and show percent copper and iron occurring in each fracture family.

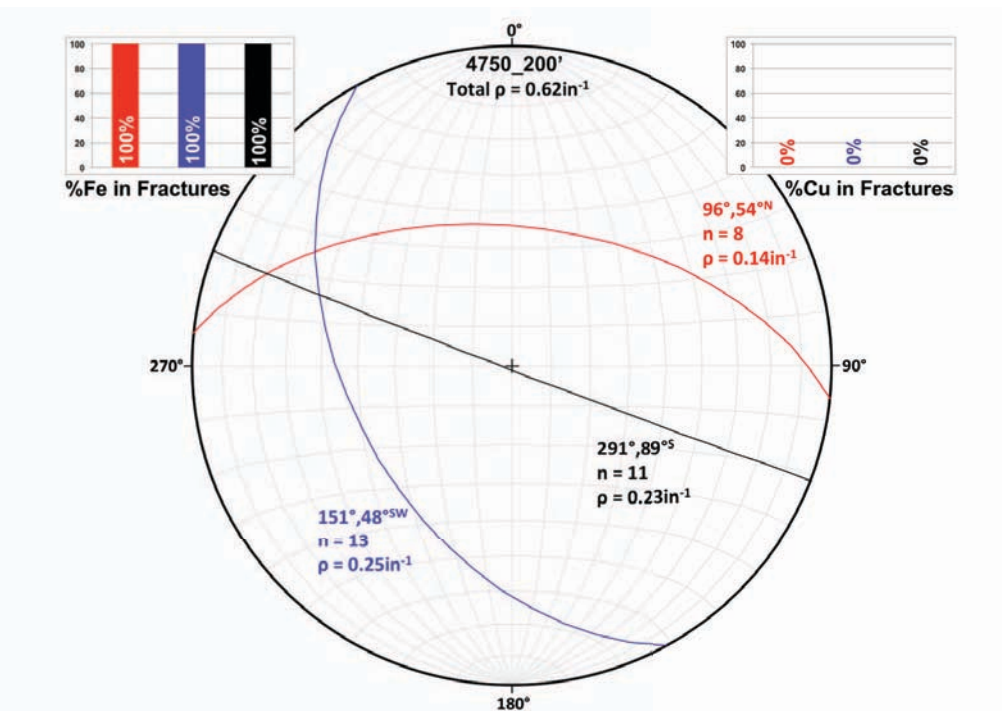


**Figure 5.32.** Stereonet of interval 4750\_200 showing orientation, number of fractures, and fracture density per fracture family. Bar charts are color coordinated and show percent copper and iron occurring in each fracture family.

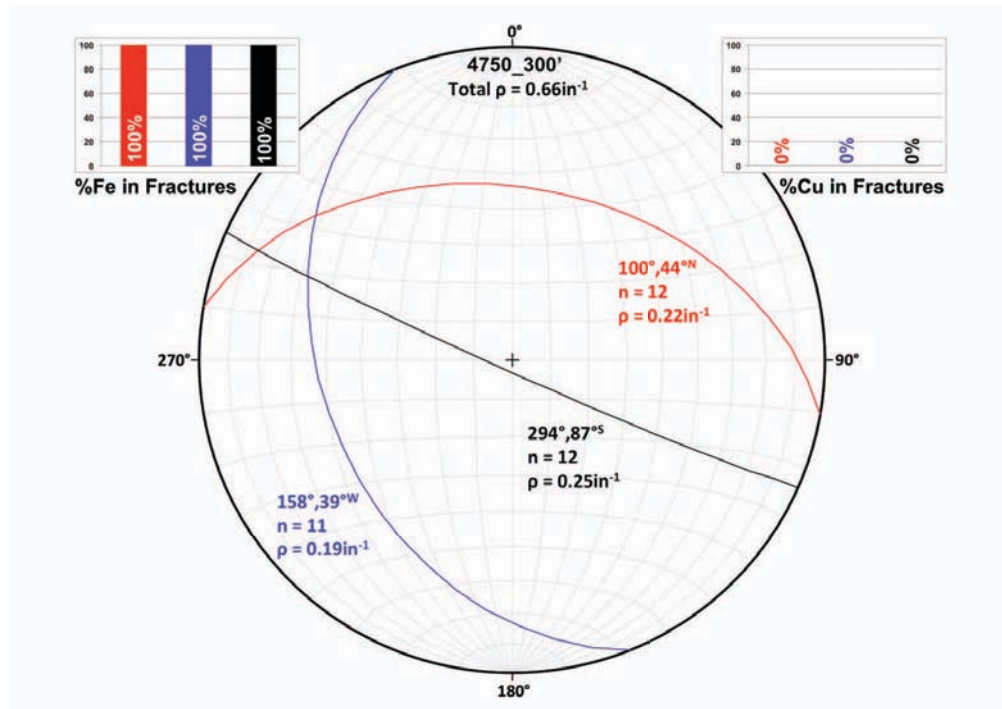


**Figure 5.33.** Stereonet of interval 4750\_300 showing orientation, number of fractures, and fracture density per fracture family. Bar charts are color coordinated and show percent copper and iron occurring in each fracture family.

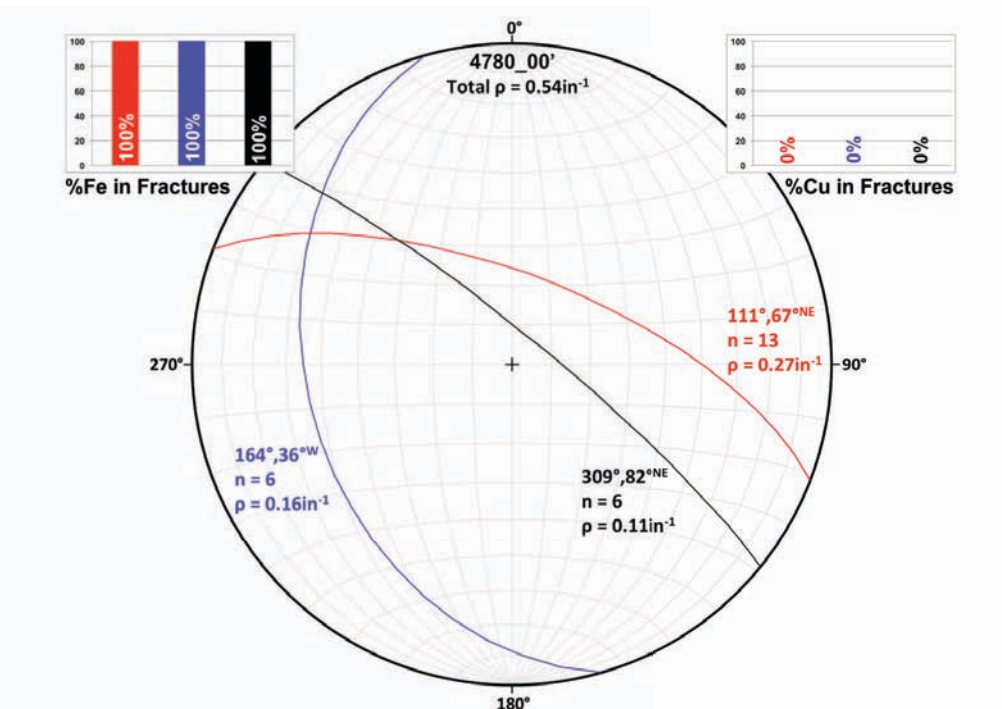


**Figure 5.34.** Stereonet of interval 4780\_00 showing orientation, number of fractures, and fracture density per fracture family. Bar charts are color coordinated and show percent copper and iron occurring in each fracture family.

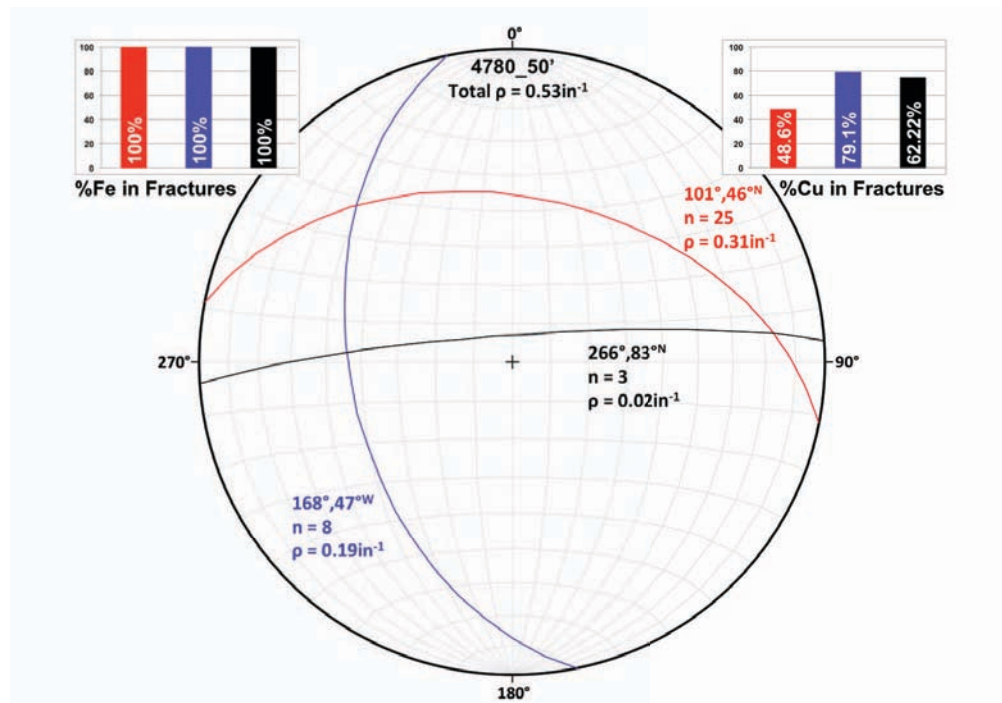


**Figure 5.35.** Stereonet of interval 4780\_50 showing orientation, number of fractures, and fracture density per fracture family. Bar charts are color coordinated and show percent copper and iron occurring in each fracture family.

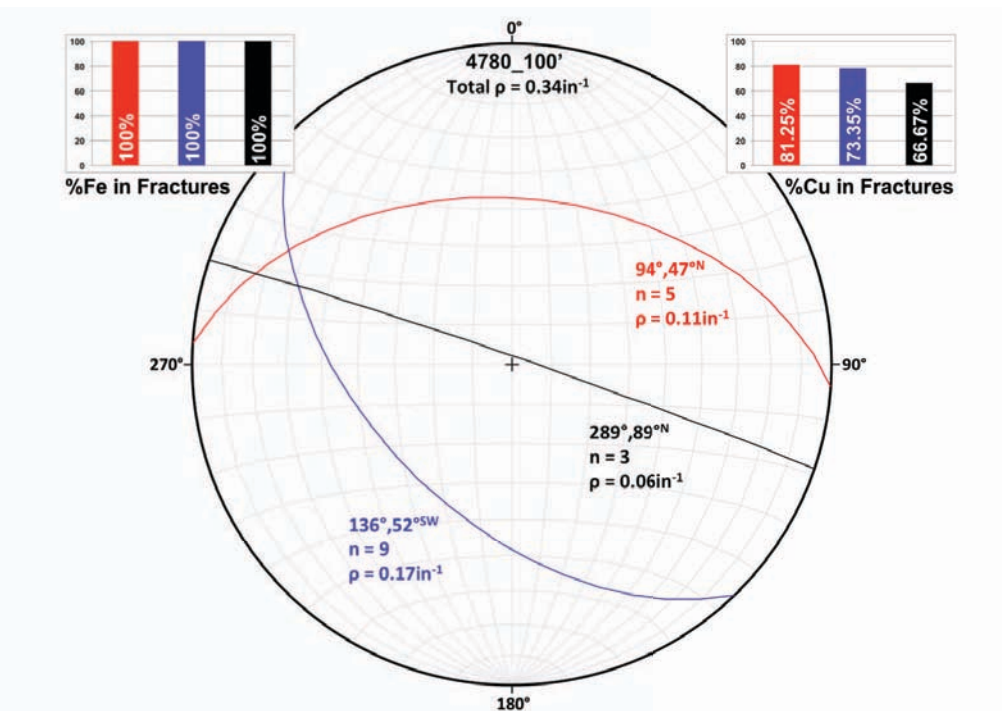


**Figure 5.36.** Stereonet of interval 4780\_100 showing orientation, number of fractures, and fracture density per fracture family. Bar charts are color coordinated and show percent copper and iron occurring in each fracture family.

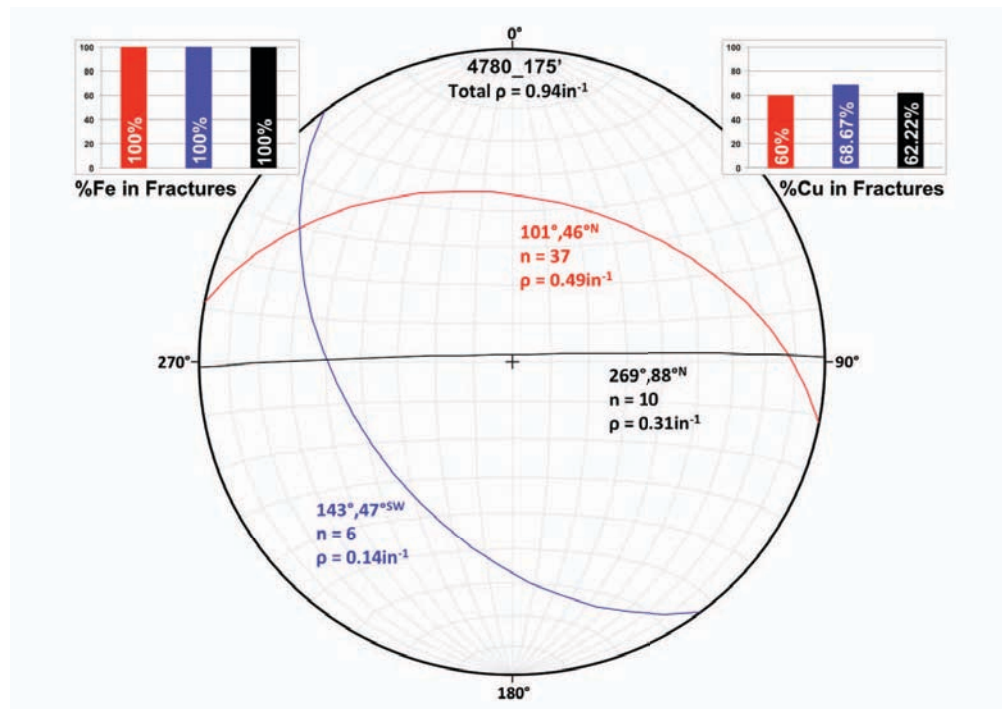


**Figure 5.37.** Stereonet of interval 4780\_175 showing orientation, number of fractures, and fracture density per fracture family. Bar charts are color coordinated and show percent copper and iron occurring in each fracture family.

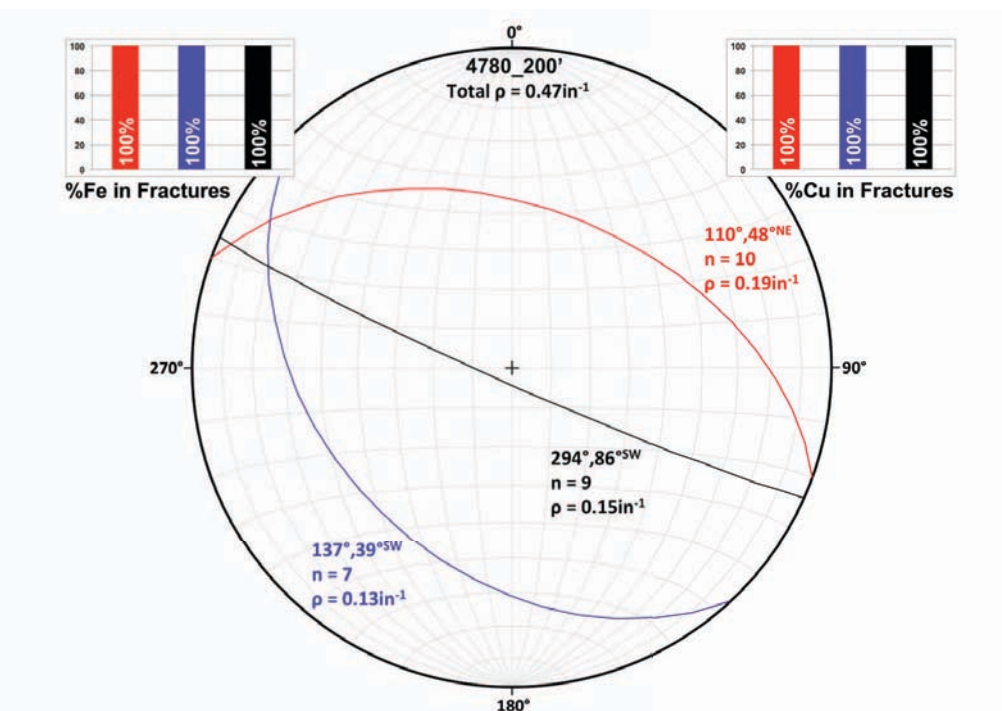


**Figure 5.38.** Stereonet of interval 4780\_200 showing orientation, number of fractures, and fracture density per fracture family. Bar charts are color coordinated and show percent copper and iron occurring in each fracture family.

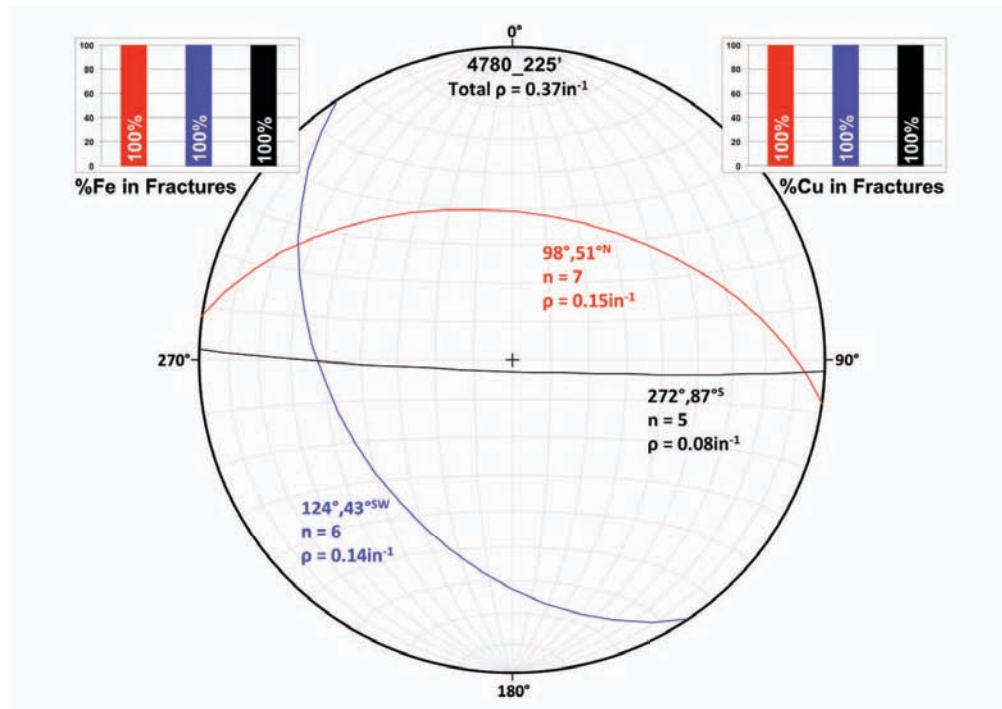


**Figure 5.39.** Stereonet of interval 4780\_225 showing orientation, number of fractures, and fracture density per fracture family. Bar charts are color coordinated and show percent copper and iron occurring in each fracture family.

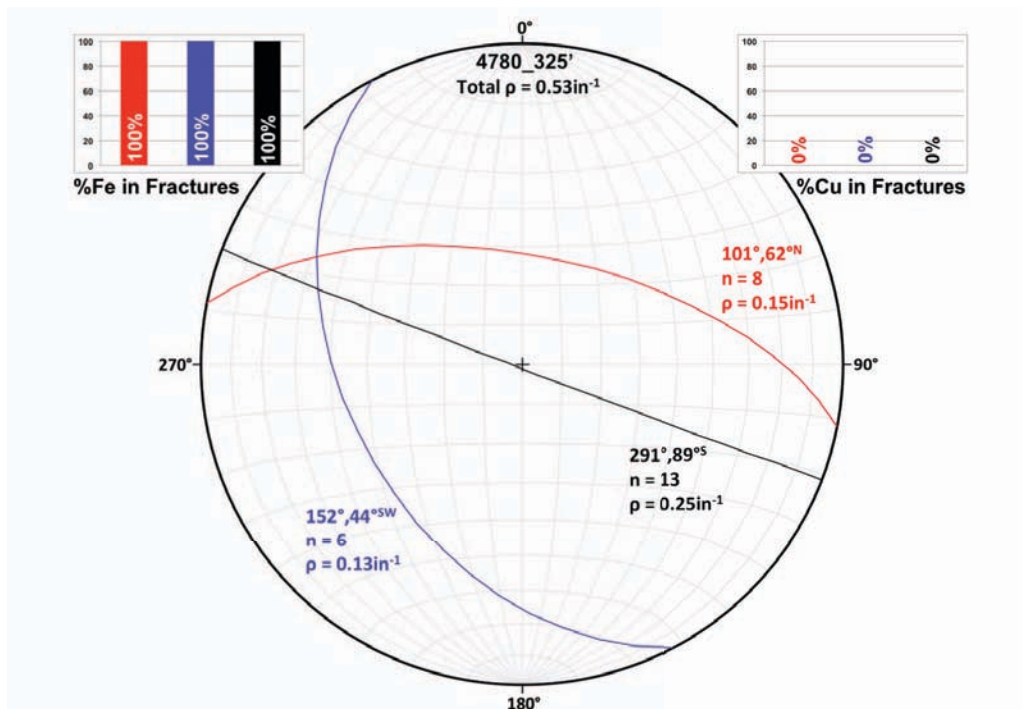


**Figure 5.40.** Stereonet of interval 4780\_325 showing orientation, number of fractures, and fracture density per fracture family. Bar charts are color coordinated and show percent copper and iron occurring in each fracture family.

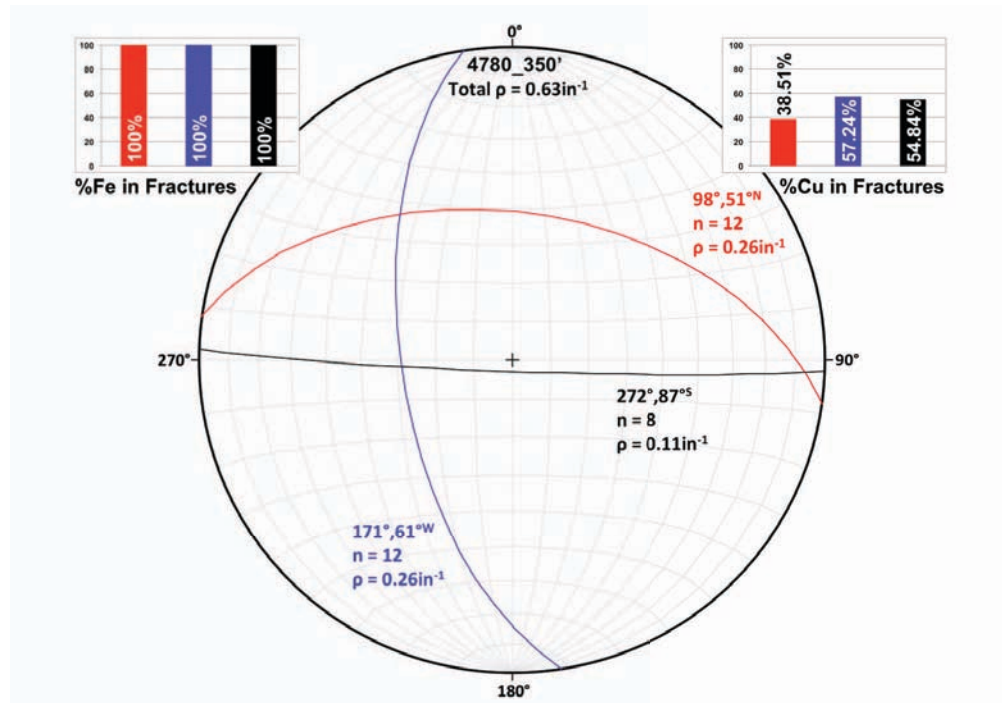


**Figure 5.41.** Stereonet of interval 4780\_350 showing orientation, number of fractures, and fracture density per fracture family. Bar charts are color coordinated and show percent copper and iron occurring in each fracture family.

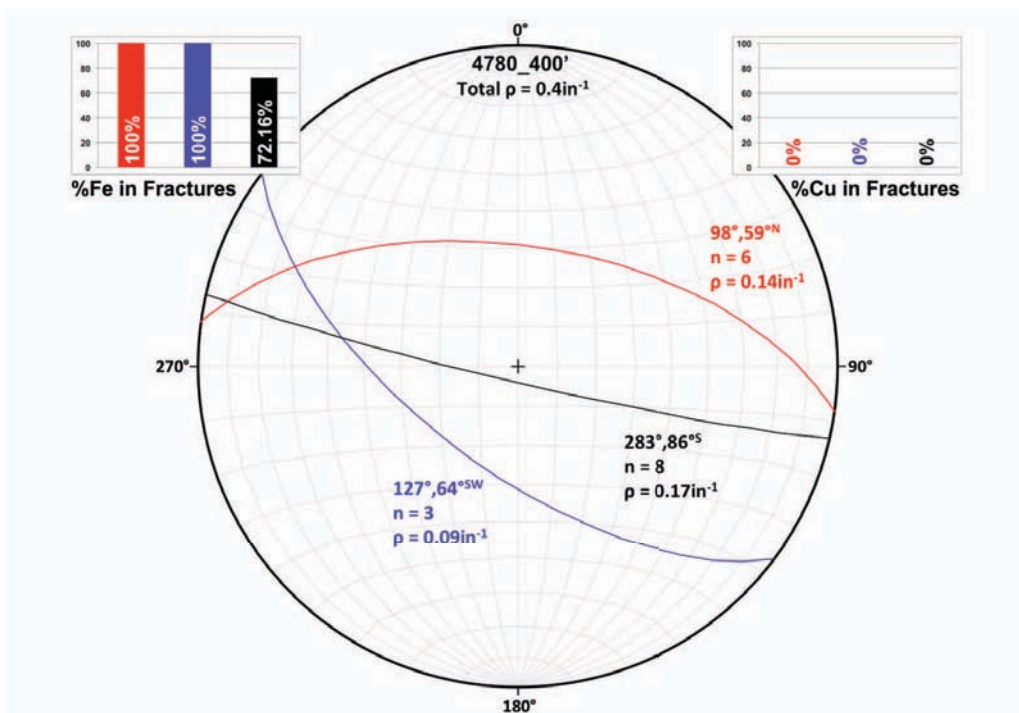


**Figure 5.42.** Stereonet of interval 4780\_400 showing orientation, number of fractures, and fracture density per fracture family. Bar charts are color coordinated and show percent copper and iron occurring in each fracture family.

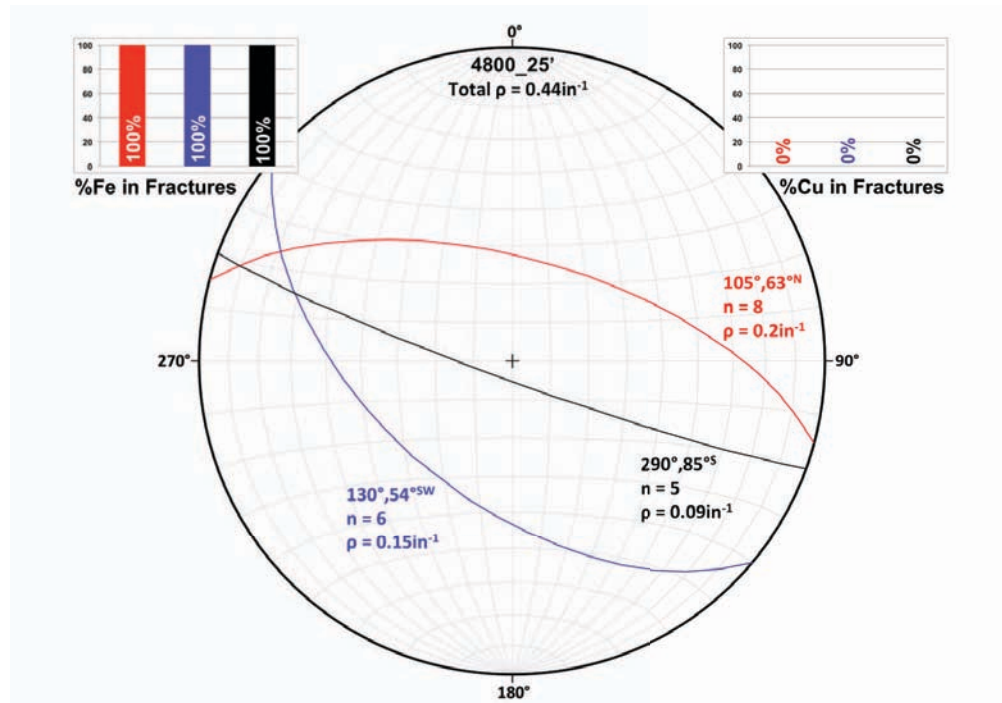


**Figure 5.43.** Stereonet of interval 4800\_25 showing orientation, number of fractures, and fracture density per fracture family. Bar charts are color coordinated and show percent copper and iron occurring in each fracture family.

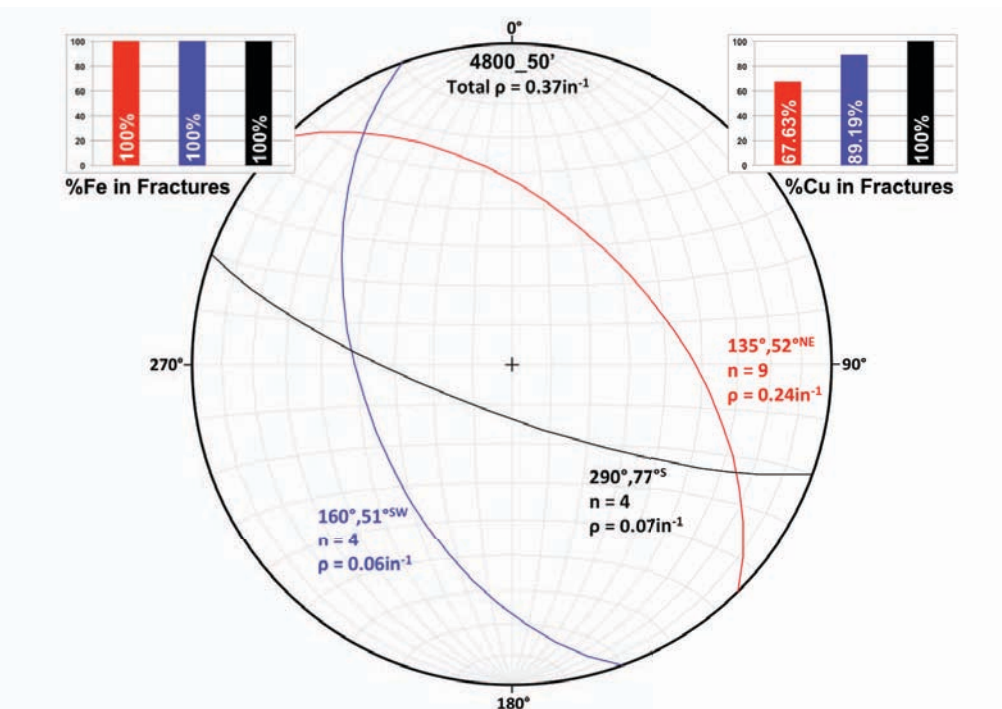


**Figure 5.44.** Stereonet of interval 4800\_50 showing orientation, number of fractures, and fracture density per fracture family. Bar charts are color coordinated and show percent copper and iron occurring in each fracture family.

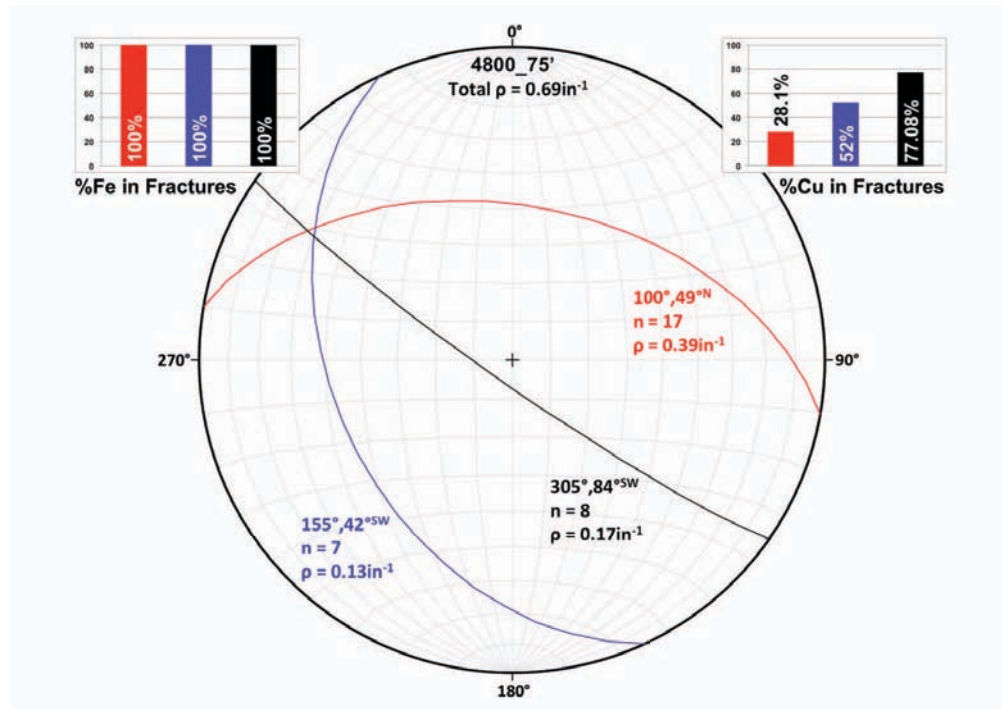


**Figure 5.45.** Stereonet of interval 4800\_75 showing orientation, number of fractures, and fracture density per fracture family. Bar charts are color coordinated and show percent copper and iron occurring in each fracture family.

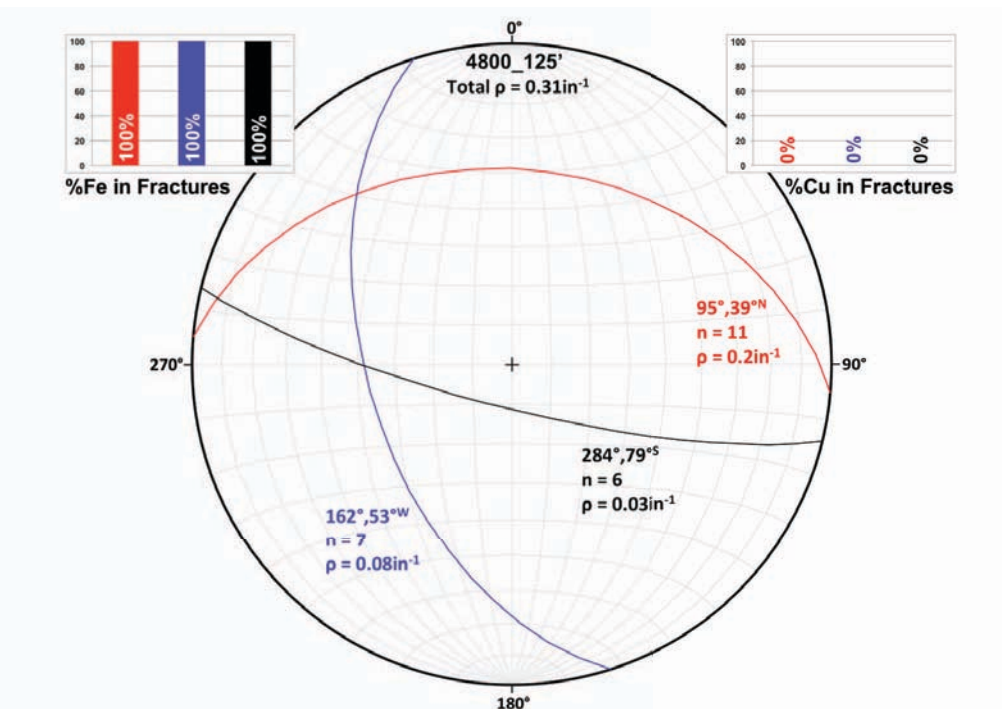


**Figure 5.46.** Stereonet of interval 4800\_125 showing orientation, number of fractures, and fracture density per fracture family. Bar charts are color coordinated and show percent copper and iron occurring in each fracture family.

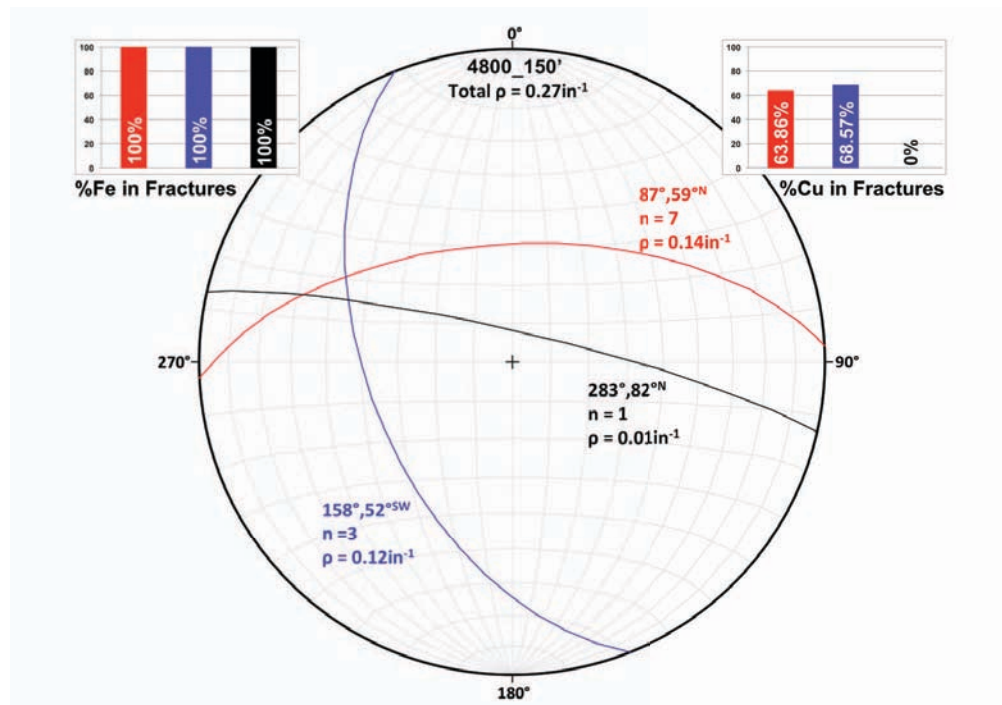


**Figure 5.47.** Stereonet of interval 4800\_150 showing orientation, number of fractures, and fracture density per fracture family. Bar charts are color coordinated and show percent copper and iron occurring in each fracture family.

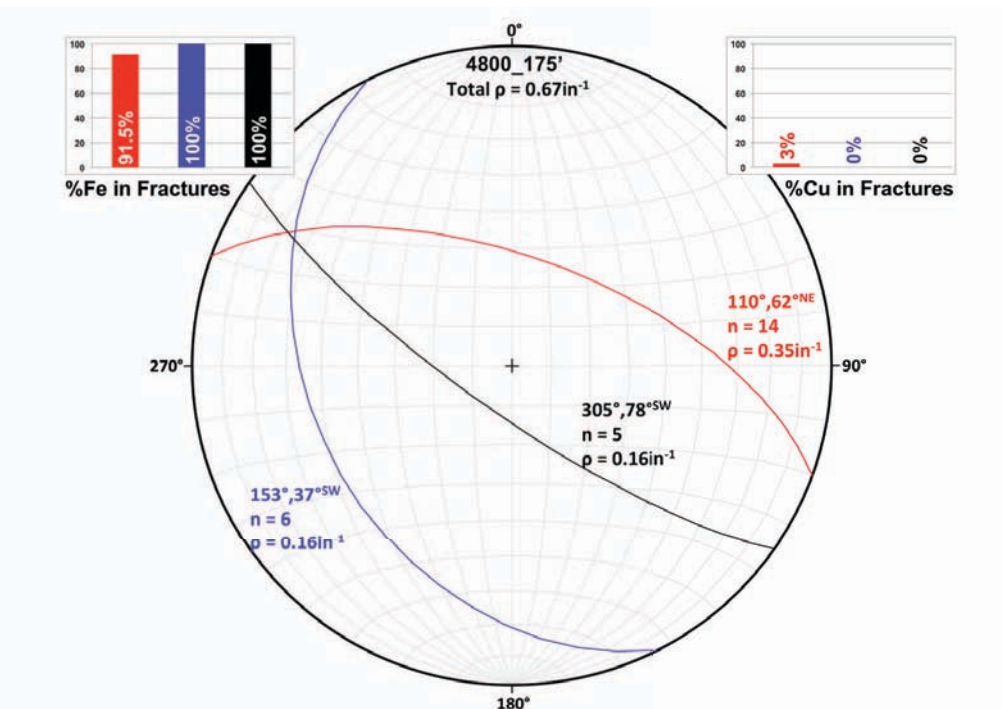


**Figure 5.48.** Stereonet of interval 4800\_175 showing orientation, number of fractures, and fracture density per fracture family. Bar charts are color coordinated and show percent copper and iron occurring in each fracture family.

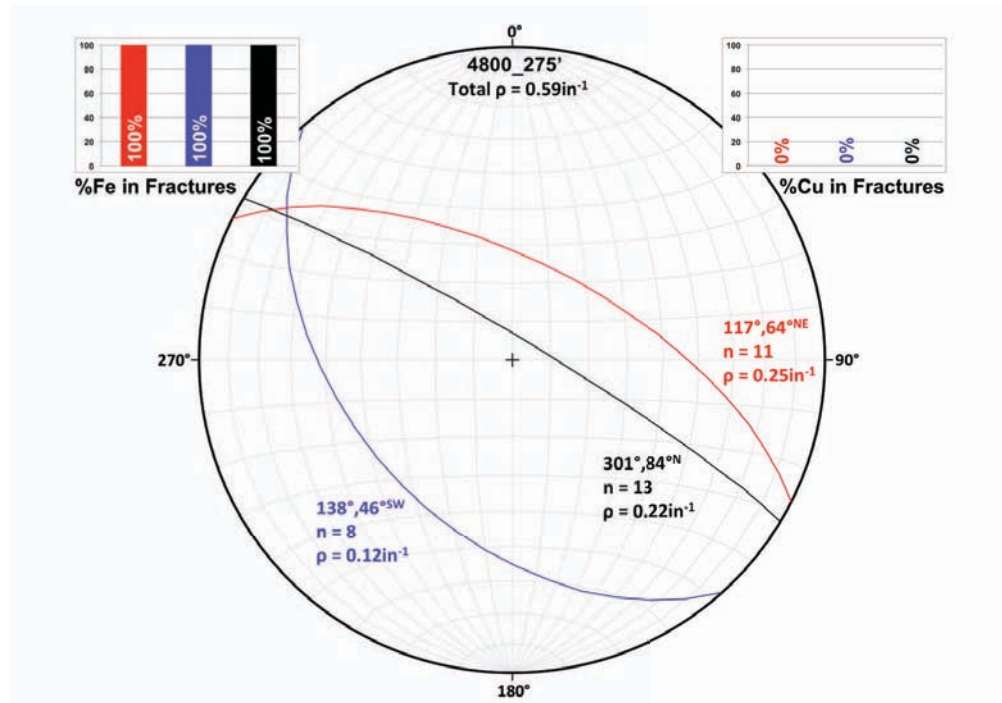


**Figure 5.49.** Stereonet of interval 4800\_275 showing orientation, number of fractures, and fracture density per fracture family. Bar charts are color coordinated and show percent copper and iron occurring in each fracture family.

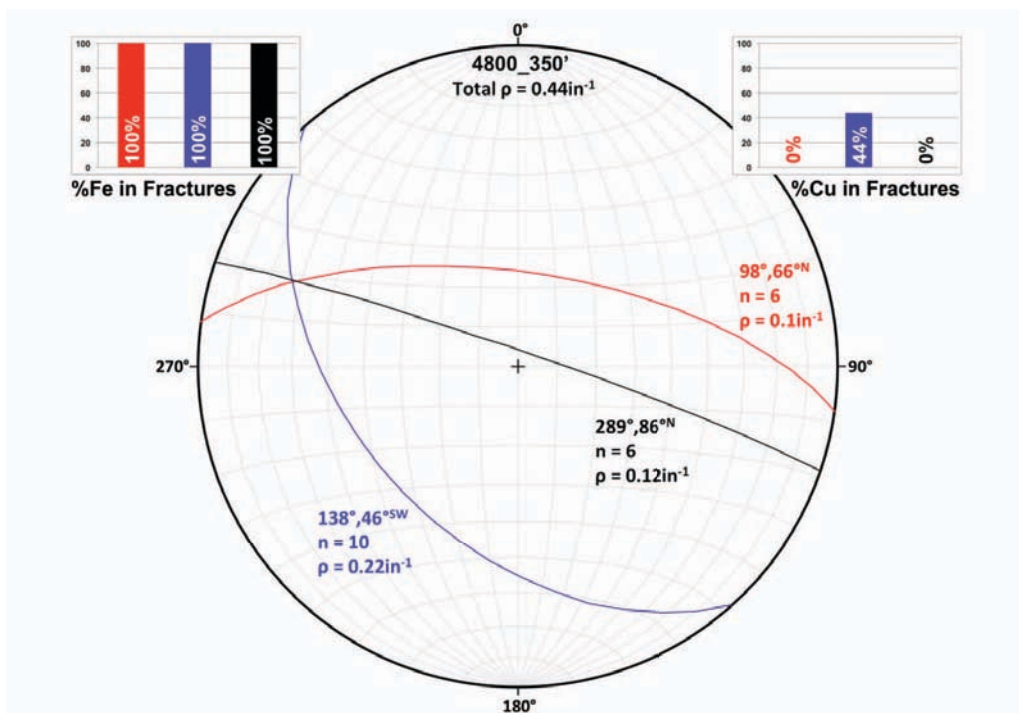


**Figure 5.50.** Stereonet of interval 4800\_350 showing orientation, number of fractures, and fracture density per fracture family. Bar charts are color coordinated and show percent copper and iron occurring in each fracture family.

## 19.4. Appendix 5.4. Fracture Density Bivariate Analysis

**Table 5.10.** Correlation coefficient matrix from bivariate analysis of fracture density data.

Row	F1 CuOx	F1 FeOx	F1 t-Ox	F1 n	F1 Density	F2 CuOx	F2 FeOx	F2 t-Ox	F2 n
F1 CuOx	1								
F1 FeOx	0.442343	1							
F1 t-Ox	0.446479	0.99909	1						
F1 n	0.350478	0.83208	0.83272	1					
F1 Density	0.444265	0.99338	0.99412	0.83097	1				
F2 CuOx	0.639423	0.0666	0.07021	0.07049	0.06319	1			
F2 FeOx	0.112728	0.19981	0.19985	0.20148	0.19119	0.50826	1		
F2 t-Ox	0.116129	0.19534	0.19933	0.21016	0.19014	0.5573	0.97684	1	
F2 n	0.057495	0.12334	0.12833	0.09168	0.12283	0.4053	0.75342	0.77809	1
F2 Density	0.091131	0.20064	0.20499	0.22623	0.20432	0.52417	0.96482	0.98683	0.77475
F3 CuOx	0.502721	0.06485	0.06792	0.05504	0.05312	0.58847	0.02543	0.07878	0.05441
F3 FeOx	-0.07651	0.11564	0.11195	0.04263	0.08652	-0.02411	-0.0011	0.00941	-0.0882
F3 t-Ox	-0.07651	0.11564	0.11195	0.04263	0.08652	-0.02411	-0.0011	0.00941	-0.0882
F3 n	-0.12643	0.09246	0.09051	0.08229	0.07849	-0.0785	0.04514	0.0482	0.01946
F3 Density	-0.07687	0.12361	0.12039	0.05176	0.09956	-0.03717	-0.0058	0.00396	-0.095
T-CuOx	0.865848	0.24444	0.24874	0.20184	0.23992	0.87602	0.25677	0.29578	0.20216
T-FeOx	0.251466	0.72215	0.71941	0.58158	0.69759	0.21158	0.48401	0.47922	0.29625
T-Ox	0.255139	0.71805	0.71788	0.58424	0.69581	0.23679	0.48384	0.4986	0.31542
T-n	0.195742	0.66277	0.66415	0.75944	0.65459	0.16622	0.45586	0.47302	0.46446
T-Density	0.254858	0.74221	0.74243	0.61286	0.73344	0.21627	0.47953	0.49307	0.31369



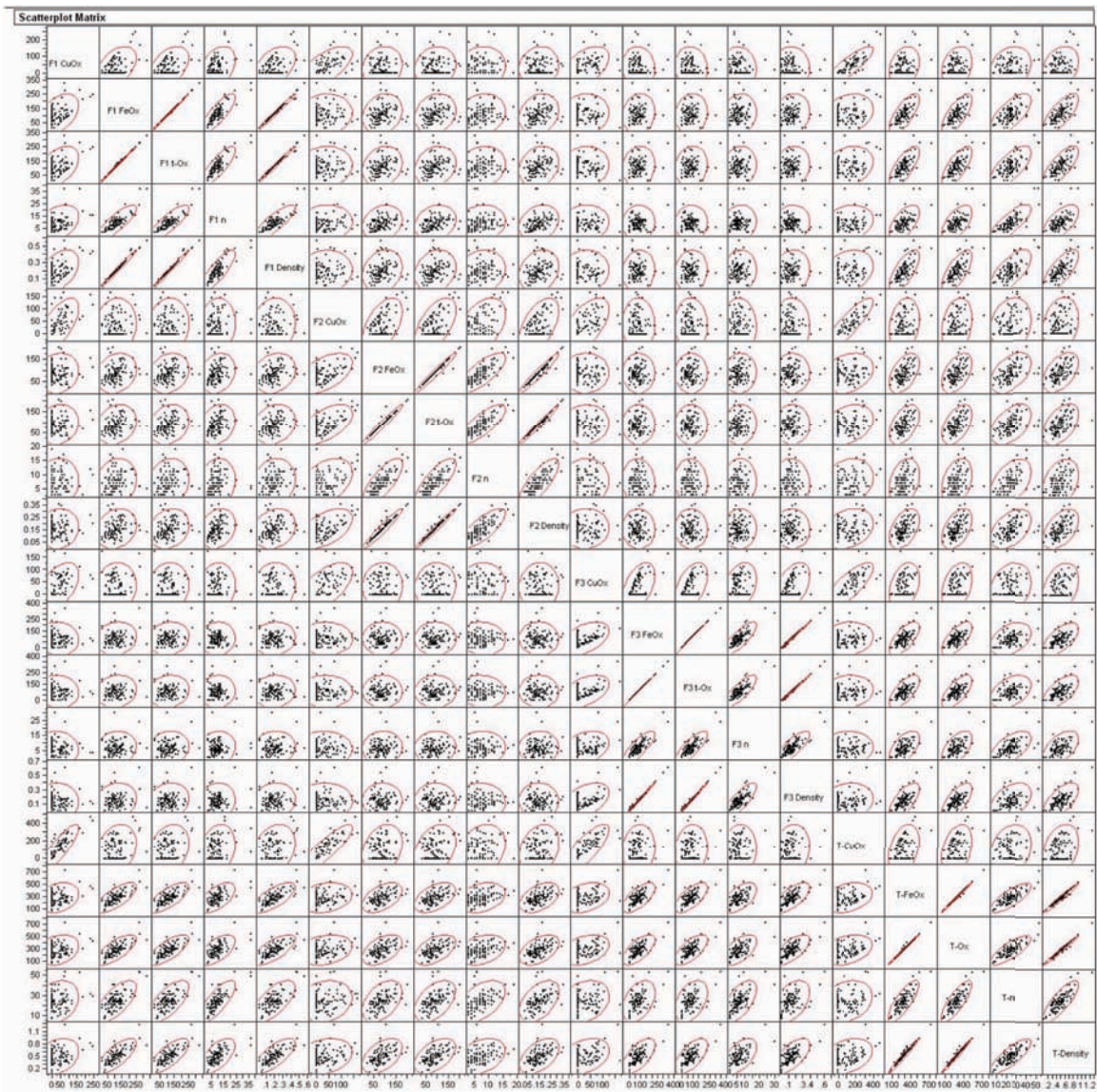


**Figure 5.51.** Scatter plot matrix from bivariate analysis of fracture density data.

## 19.5. Appendix 5.5. Spatial Distribution of Fracture Density Data

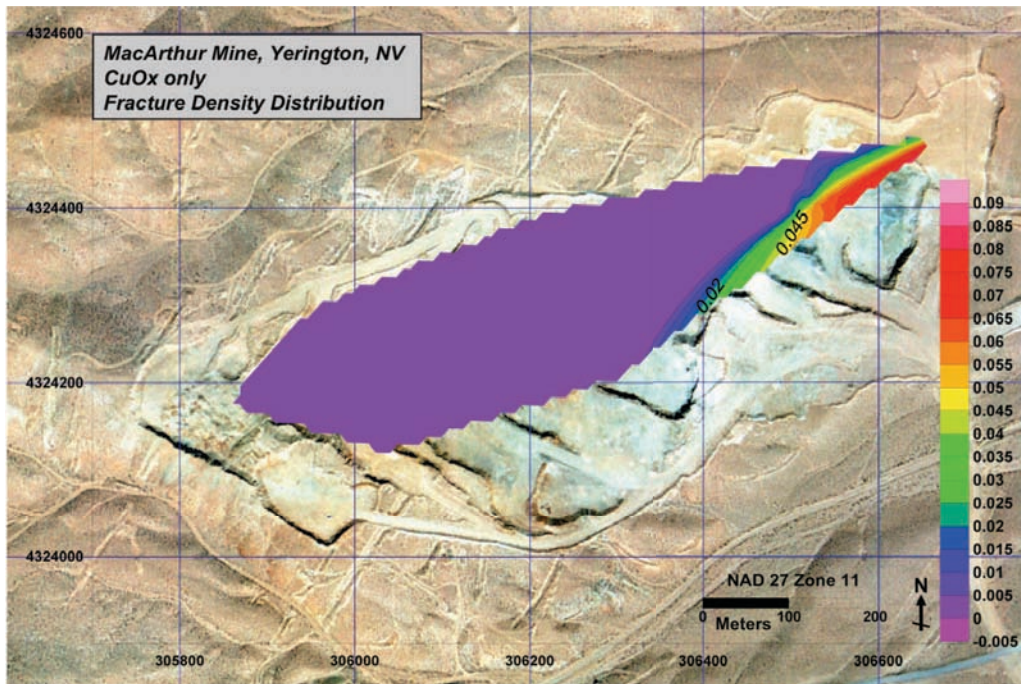


**Figure 5.52.** Contour map showing density distribution of CuOx only fractures in the MacArthur pit, Yerington, Nevada.

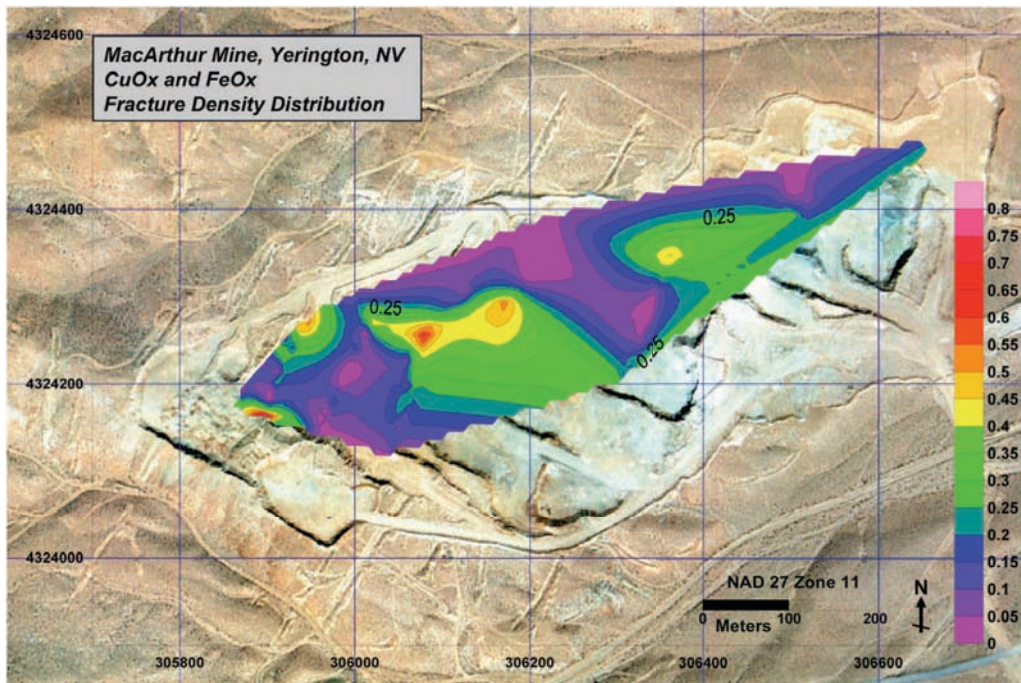


**Figure 5.53.** Contour map showing density distribution of CuOx and FeOx mixed fractures in the MacArthur pit, Yerington, Nevada.

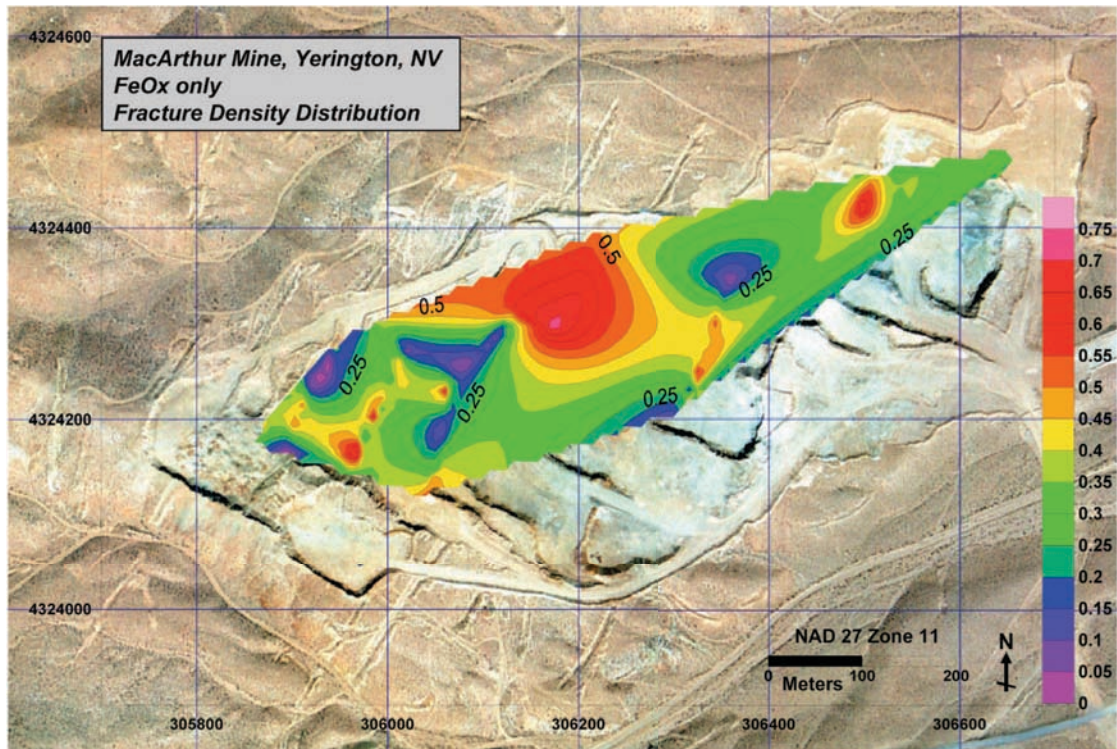


**Figure 5.54.** Contour map showing density distribution of FeOx only fractures in the MacArthur pit, Yerington, Nevada.

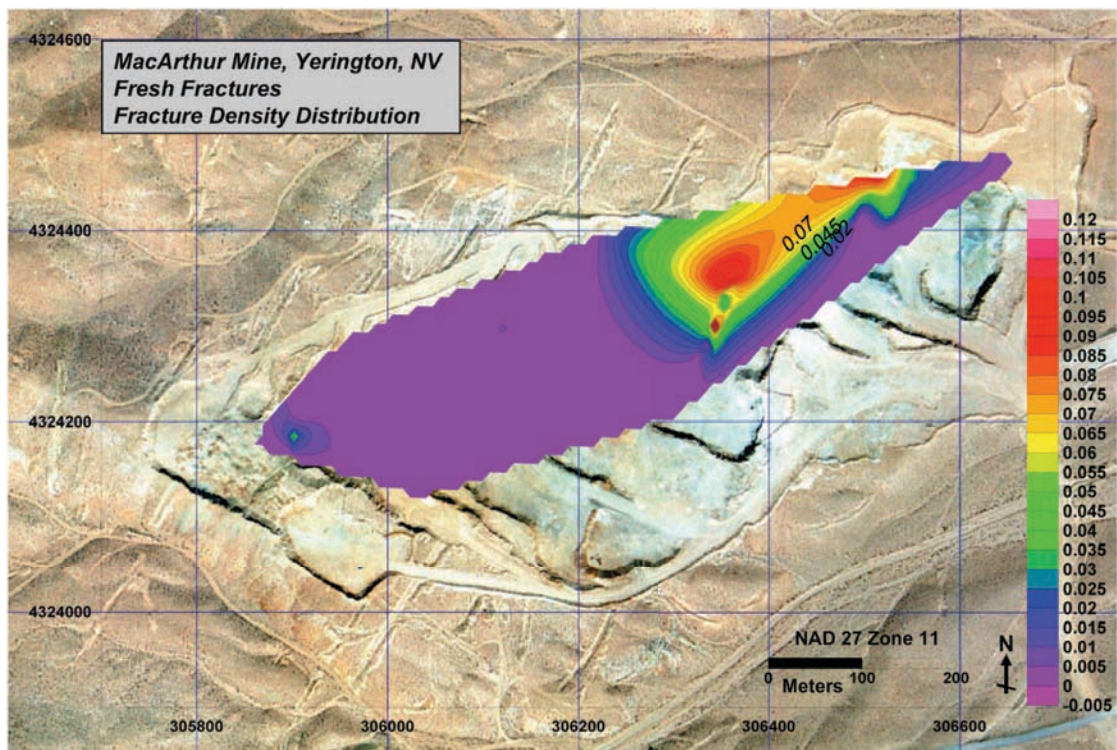


**Figure 5.55.** Contour map showing density distribution of Fresh fractures in the MacArthur pit, Yerington, Nevada.

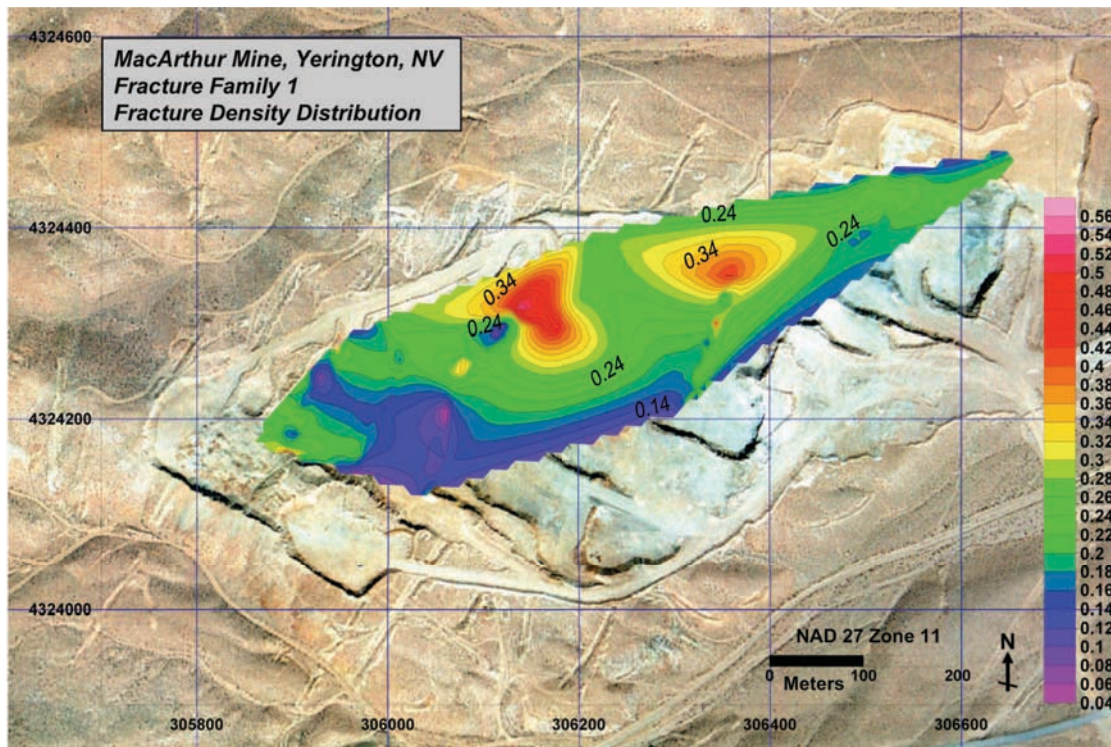


**Figure 5.56.** Contour map showing density distribution of Fracture Family 1 (F1) in the MacArthur pit, Yerington, Nevada.

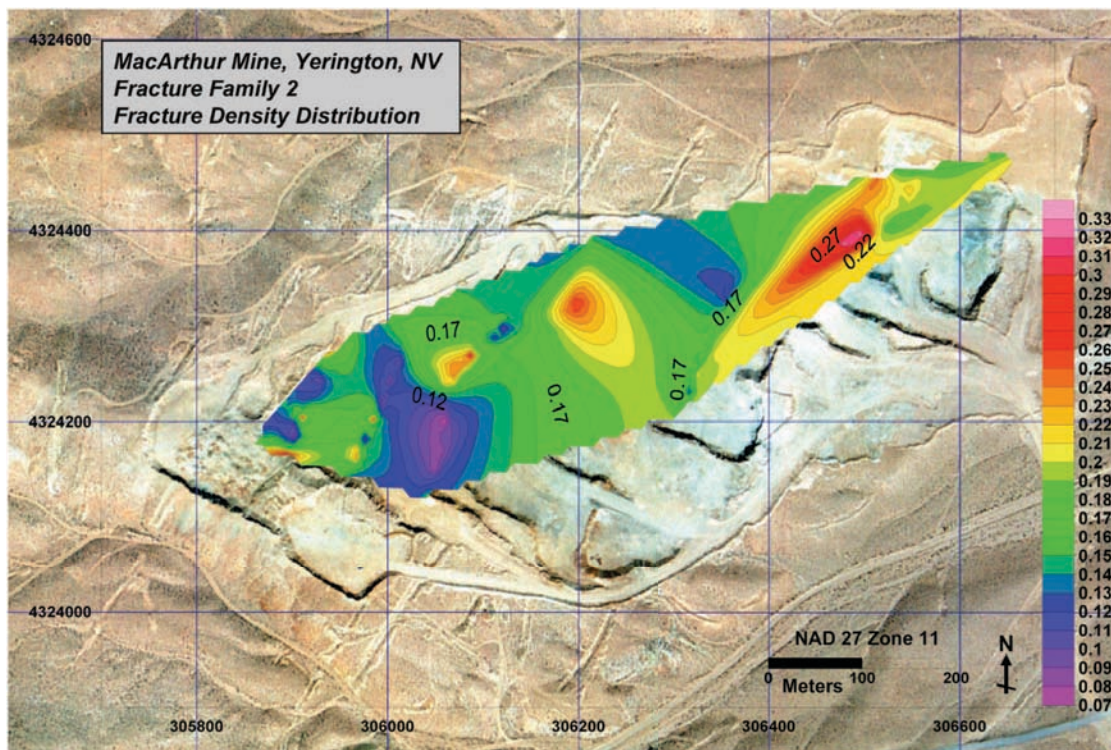


**Figure 5.57.** Contour map showing density distribution of Fracture Family 2 (F2) in the MacArthur pit, Yerington, Nevada.

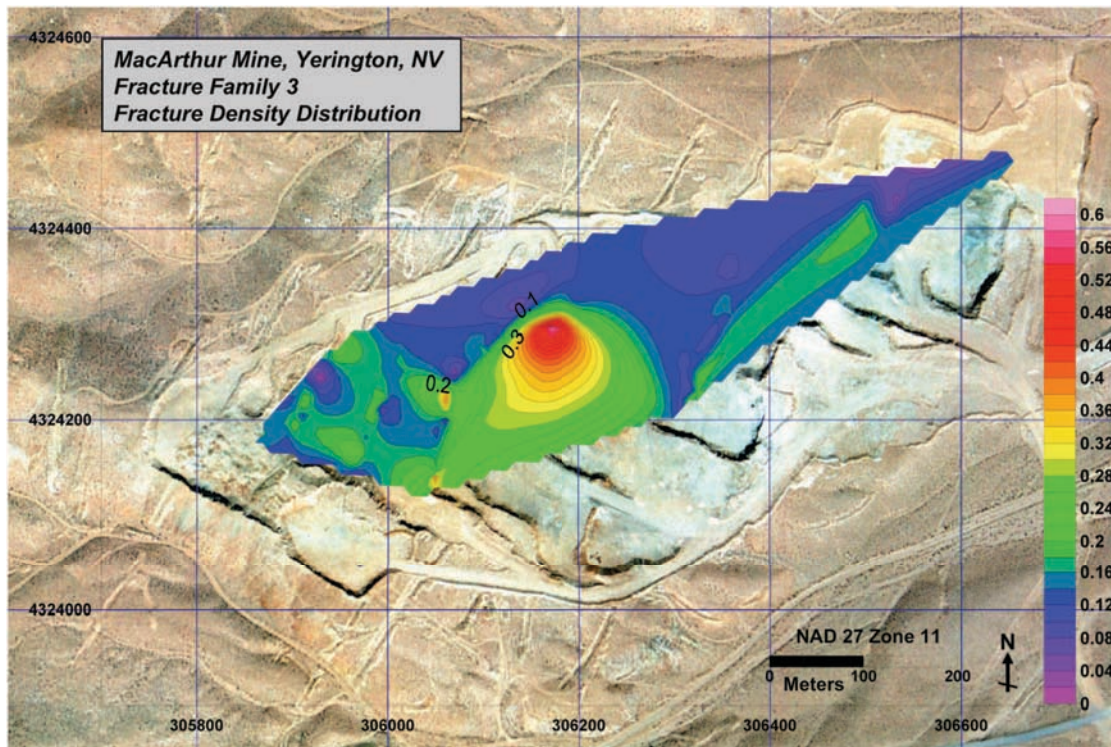


**Figure 5.58.** Contour map showing density distribution of Fracture Family 3 (F3) in the MacArthur pit, Yerington, Nevada.

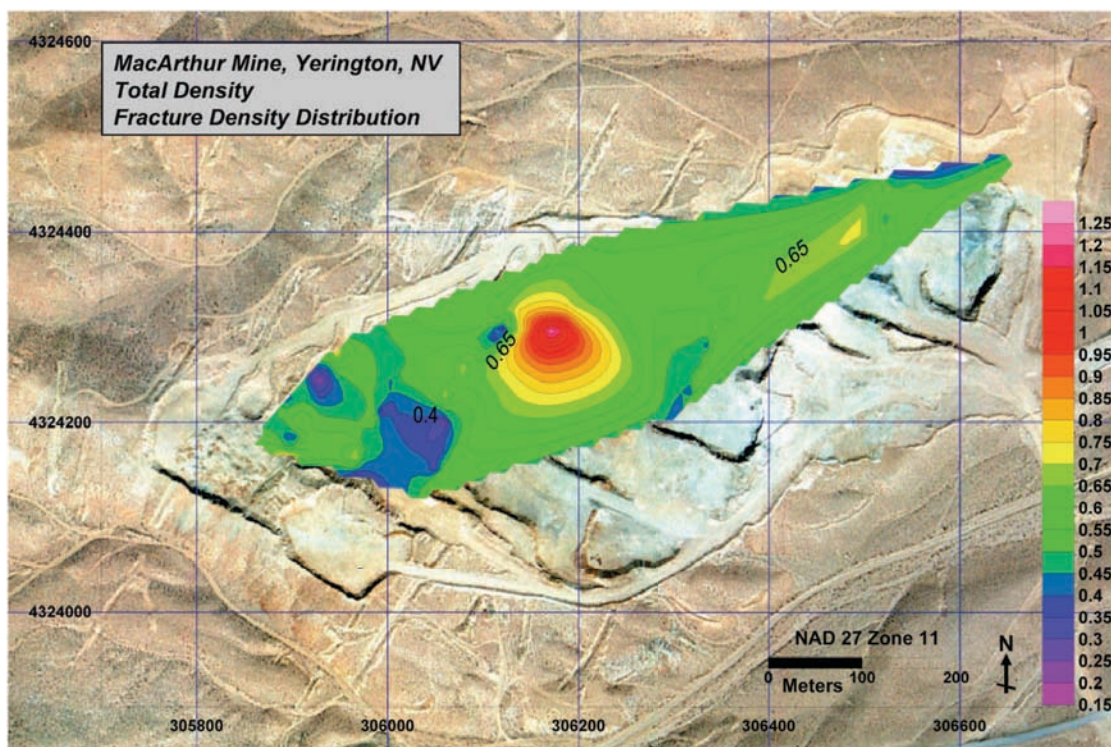


**Figure 5.59.** Contour map showing density distribution of Total Fracture Density in the MacArthur pit, Yerington, Nevada.

## 20. APPENDIX 6 – DATA INTEGRATION FIGURES

Appendix 6 shows four figures of data integration. Panorama photos are used to show two bench intervals with fracture density, geochemistry, and spectral radiometry test sites with spectral profiles.

PAGE

### 20.1. Appendix 6.1 – Data Integration Figures

Figures 6.1 – 6.4. .... 332

## 20.1. Appendix 6.1. Data Integration Pictures

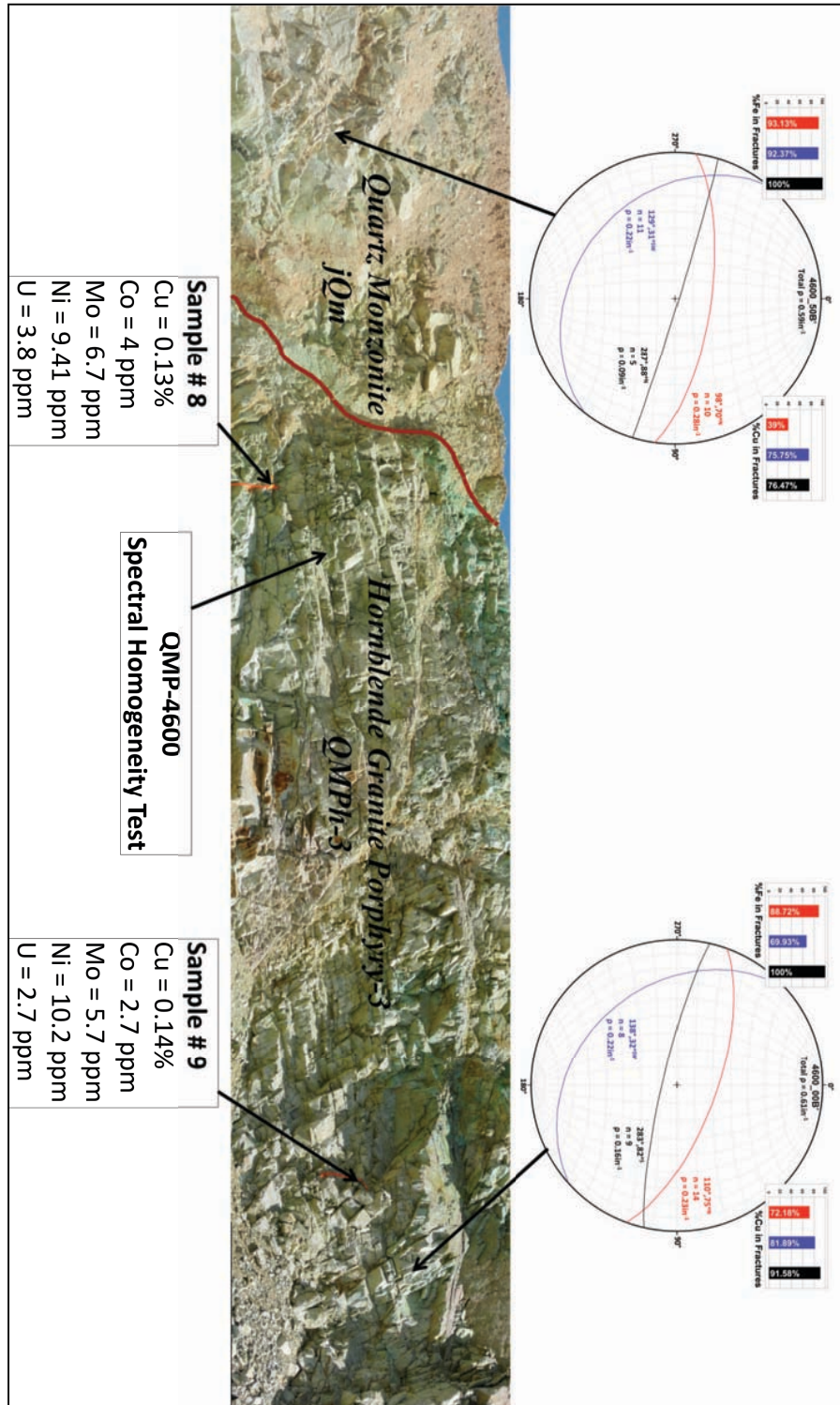


**Figure 6.1.** Bench 4600 B. Figure incorporates geochemistry, fracture density, and location of spectral radiometry homogeneity test site QMP-4600.

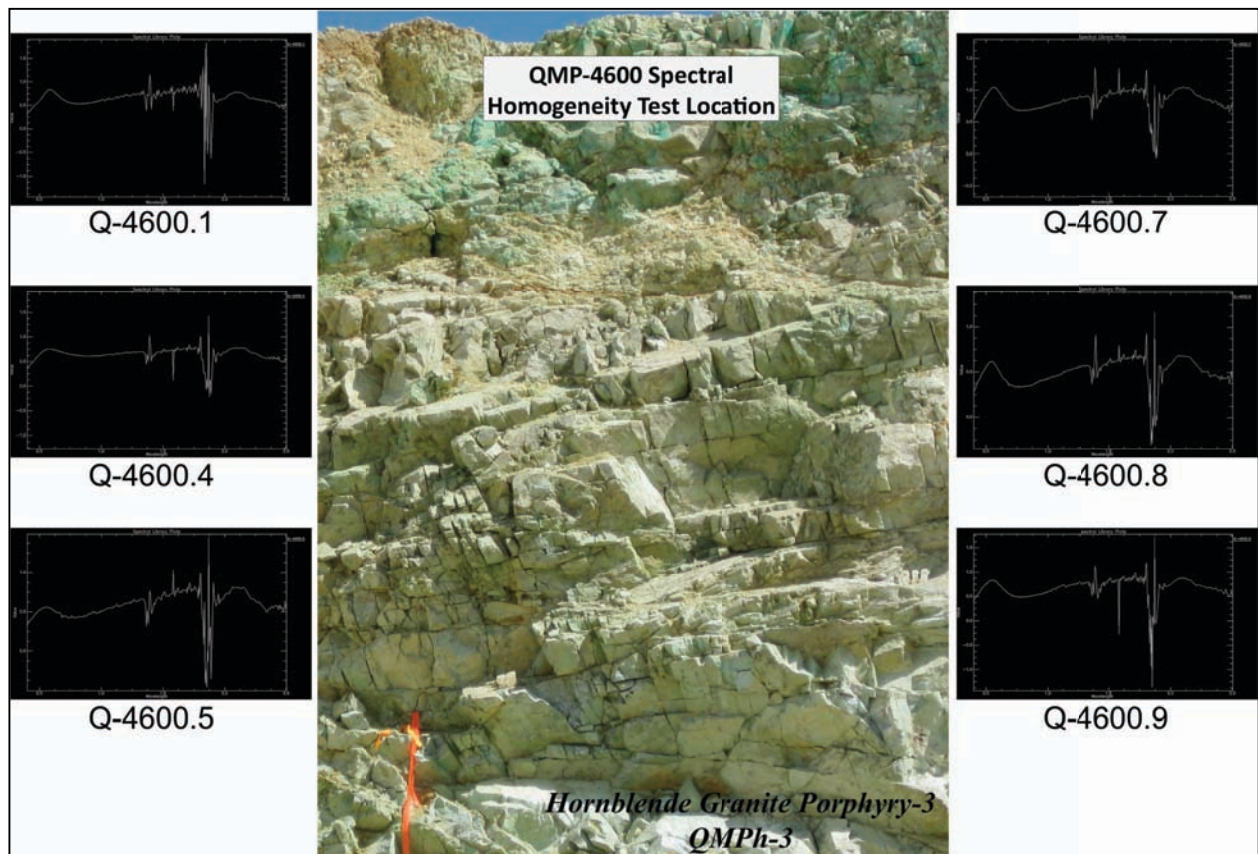


**Figure 6.2.** Spectral homogeneity test site QMP-4600.

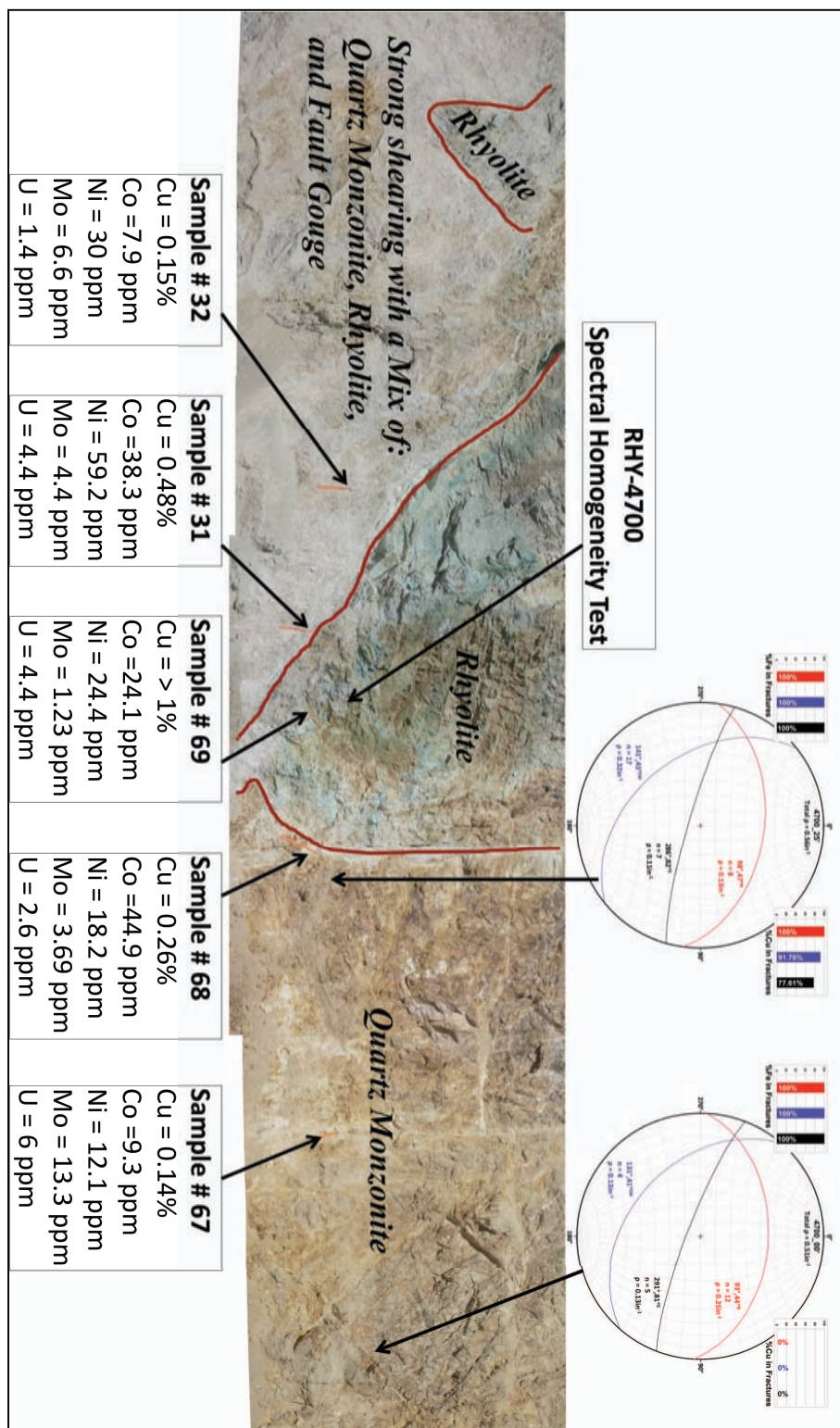


**Figure 6.3.** Bench 7000. Figure incorporates geochemistry, fracture density, and location of spectral radiometry homogeneity test site RHY-4700.

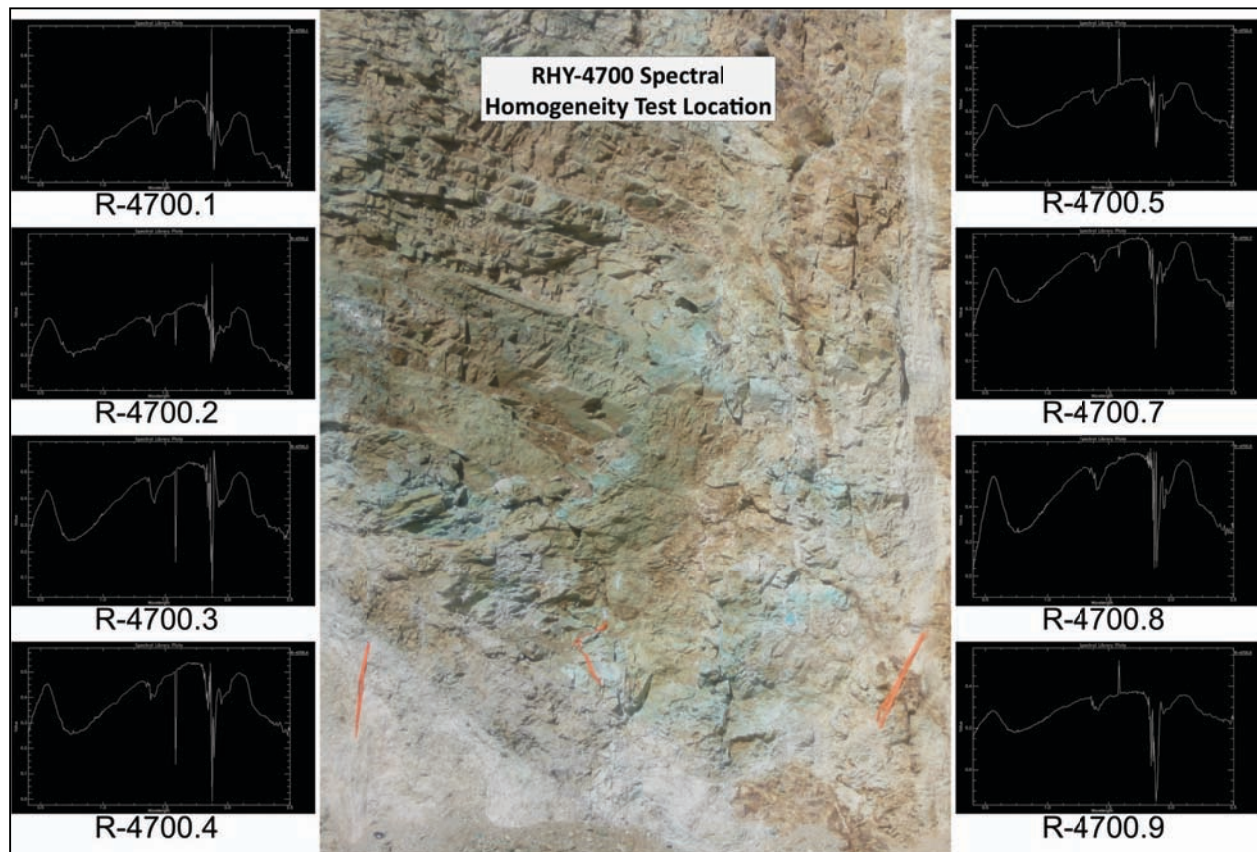


**Figure 6.4.** Spectral homogeneity test site RHY-4700.

## **CURRICULUM VITA**

Joseph Lori was born in Iron Mountain, Michigan to parents Dan and Nancy Lori. Attending Iron Mountain High School through the tenth grade, he graduated from Kingsford High School in 1998 and moved on to study tree care and sports turf. Returning to school in 2002 at Lake Superior State University (LSSU) he studied as an education major with a science minor and quickly realized his love for geology and graduated from LSSU in 2007 receiving a bachelor's of science degree in geology. With an interest in uranium and economic geology he choose to attend Graduate School at the University of Texas at El Paso (UTEP) under advisor Dr. Philip Goodell, a worldwide known uranium geologist. During his first year at UTEP Joseph was hired by Quaterra Resources Inc. to intern in the historic Yerington Nevada mining district at the MacArthur Mine. Here he learned about porphyry copper deposits and returned to UTEP in the fall of 2008 with funding and salary from Quaterra Resources Inc. as well as a new thesis topic. After receiving a master's of science in geology in the fall of 2010 from UTEP, Joseph Lori returned to work in the Yerington District as a full time geologist for Quaterra Resources Inc.